Lecture Notes in Electrical Engineering 177

David Jin
Sally Lin
Editors

Advances in Mechanical and Electronic Engineering

Volume 2

Springer

For further volumes:
http://www.springer.com/series/7818

David Jin and Sally Lin (Eds.)

Advances in Mechanical and Electronic Engineering

Volume 2

Springer

Editors
David Jin
Wuhan Section of ISER Association
Wuhan
China

Sally Lin
Wuhan Section of ISER Association
Wuhan
China

ISSN 1876-1100
ISBN 978-3-642-31515-2
DOI 10.1007/978-3-642-31516-9
Springer Heidelberg New York Dordrecht London

e-ISSN 1876-1119
e-ISBN 978-3-642-31516-9

Library of Congress Control Number: 2012940780

Preface

In the proceeding of Volume 1 of ICMEE2012, you can learn much more knowledge about Mechanical Engineering and Automation; Vehicle Engineering and Technology all around the world. The main role of the proceeding is to be used as an exchange pillar for researchers who are working in the mentioned field. In order to meet high standard of Springer, the organization committee has made their efforts to do the following things. Firstly, poor quality paper has been refused after reviewing course by anonymous referee experts. Secondly, periodically review meetings have been held around the reviewers about five times for exchanging reviewing suggestions. Finally, the conference organization had several preliminary sessions before the conference. Through efforts of different people and departments, the conference will be successful and fruitful.

During the organization course, we have got help from different people, different departments, different institutions. Here, we would like to show our first sincere thanks to publishers of Springer, LNEE series for their kind and enthusiastic help and best support for our conference.

In a word, it is the different team efforts that they make our conference be successful on June 23–24, 2012, Hefei, China. We hope that all of participants can give us good suggestions to improve our working efficiency and service in the future. And we also hope to get your supporting all the way. Next year, In 2013, we look forward to seeing all of you at ICMEE2013.

April 2012 ICMEE2012 Committee

Committee

Honor Chairs

Prof. Chen Bin	Beijing Normal University, China
Prof. Hu Chen	Peking University, China
Chunhua Tan	Beijing Normal University, China
Helen Zhang	University of Munich, China

Program Committee Chairs

Xiong Huang	International Science & Education Researcher Association, China
LiDing	International Science & Education Researcher Association, China
Zhihua Xu	International Science & Education Researcher Association, China

Organizing Chair

ZongMing Tu	Beijing Gireida Education Co.Ltd, China
Jijun Wang	Beijing Spon Technology Research Institution, China
Quanxiang	Beijing Prophet Science and Education Research Center, China

Publication Chair

Song Lin	International Science & Education Researcher Association, China
Xionghuang	International Science & Education Researcher Association, China

International Committees

Sally Wang	Beijing Normal University, China
LiLi	Dongguan University of Technology, China
BingXiao	Anhui University, China
Z.L. Wang	Wuhan University, China
Moon Seho	Hoseo University, Korea
Kongel Arearak	Suranaree University of Technology, Thailand
Zhihua Xu	International Science & Education Researcher Association, China

Co-sponsored by

International Science & Education Researcher Association, China
VIP Information Conference Center, China
Beijing Gireda Research Center, China

Reviewers of ICMEE2012

Z.P. Lv	Huazhong University of Science and Technology
Q. Huang	Huazhong University of Science and Technology
Helen Li	Yangtze University
Sara He	Wuhan Textile University
Jack Ma	Wuhan Textile University
George Liu	Huaxia College Wuhan Polytechnic University
Hanley Wang	Wuchang University of Technology
Diana Yu	Huazhong University of Science and Technology
Anna Tian	Wuchang University of Technology
Fitch Chen	Zhongshan University
David Bai	Nanjing University of Technology
Y. Li	South China Normal University
Harry Song	Guangzhou Univeristy
Lida Cai	Jinan University
Kelly Huang	Jinan University
Zelle Guo	Guangzhou Medical College
Gelen Huang	Guangzhou University
David Miao	Tongji University
Charles Wei	Nanjing University of Technology
Carl Wu	Jiangsu University of Science and Technology
Senon Gao	Jiangsu University of Science and Technology
X.H Zhan	Nanjing University of Aeronautics
Tab Li	Dalian University of Technology (City College)
J.G Cao	Beijing University of Science and Technology
Gabriel Liu	Southwest University
Garry Li	Zhengzhou University
Aaron Ma	North China Electric Power University
Torry Yu	Shenyang Polytechnic University
Navy Hu	Qingdao University of Science and Technology
Jacob Shen	Hebei University of Engineering

Contents

Section I: Mechatronic Engineering and Technology

The Design of Control System for Low-Power Photovoltaic Grid-Connected Inverter

Ruilan Wang

School of Information and Control Enginerring,
Weifang University
Weifang, Sandong, China
wrl2836@163.com

Abstract. This paper introduces the 200W solar PV grid-connected inverter that can directly converted DC that is generated by solar panels to 220V/50Hz of power frequency AC and output to the grid. This system consists of DC / DC converter and DC / AC inverter. The topology of the DC / DC controller with push-pull circuit, the control chip is SG3525; DC / AC inverter with full-bridge inverter circuit that is controlled with DSP.

Keywords: photovoltaic grid, DC-DC converter, DC-AC Inverter, DSP.

1 Introduction

21st century, mankind will be faced with major challenges to achieve sustainable economic and social development. The dual constraints of limited resources and environmental protection, energy issues will become more prominent, which is mainly reflected in: ① energy shortage; ② environmental pollution; ③ greenhouse effect. Therefore, human beings in solving the energy problem and achieve sustainable development, can only rely on scientific and technological progress, large-scale development and utilization of renewable and clean energy. Solar has large reserves, the widespread use of economic, clean environment, etc., so the use of solar energy more and more widespread attention, and become an ideal alternative energy. power 200W solar PV grid-connected inverter is elaborated in this paper, it can directly convert DC that is generated by solar panels to 220V/50Hz of power frequency AC and output to the grid.

2 The Circuit Structure and Working Principle of Photovoltaic Grid-Connected Inverter

The circuit structure of solar photovoltaic grid-connected inverter is shown in Fig. 1. In this system, the 62V DC that is the output of solar panels is converted to 400V DC through DC / DC converter, and then is converted to 220V/50Hz AC through the DC / AC inverter. And this system to ensure that 220V/50Hz sinusoidal voltage the grid-connected inverter output synchronized with the grid voltage.

D. Jin and S. Lin (Eds.): Advances in Mechanical and Electronic Engineering, LNEE 177, pp. 1–5.
springerlink.com

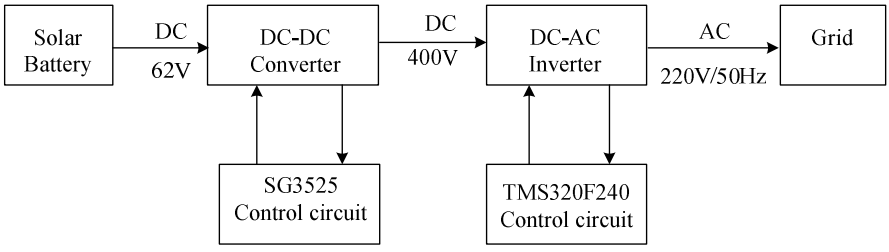

Fig. 1. The circuit block diagram

3 The Control Program of the System

The main circuit topology of photovoltaic grid-connected inverter is shown in Fig. 2. This system consists of DC / DC converter and DC / AC inverter. The inverter circuit of the DC / DC converter with push-pull circuit, it will convert 62V DC voltage of solar panels output into a DC voltage of 400V. The main circuit of the DC / AC inverter adopts full-bridge structures, it consists of four MOS tube, and will convert 400V DC to 220V/50Hz AC voltage.

3.1 The Control Program of DC / DC Inverter

The control block diagram of DC / DC converter is shown in Fig. 3. Control circuit based on IC SG3525 as the core, two 50kHz drive signal of the SG3525 output connect to the gate in the push-pull circuit switch Q1 and Q2 by the gate drive circuit. In order to maintain the stability of the DC / DC converter output voltage, the detected output voltage was compared with the command voltage, the error voltage by the PI regulator to control the duty cycle of SG3525 output drive signal. The control circuit also has protection function to limit over-current and over-voltage output. When the detected output current of DC / DC converter is too large, SG3525 will reduce the width of the gate pulse, and reduce the output voltage, thus reduce the output current. When the output voltage is too high, stop the work of the DC / DC converter.

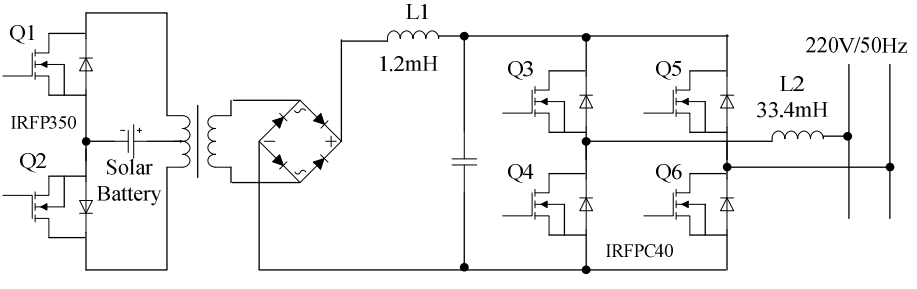

Fig. 2. The main circuit topology

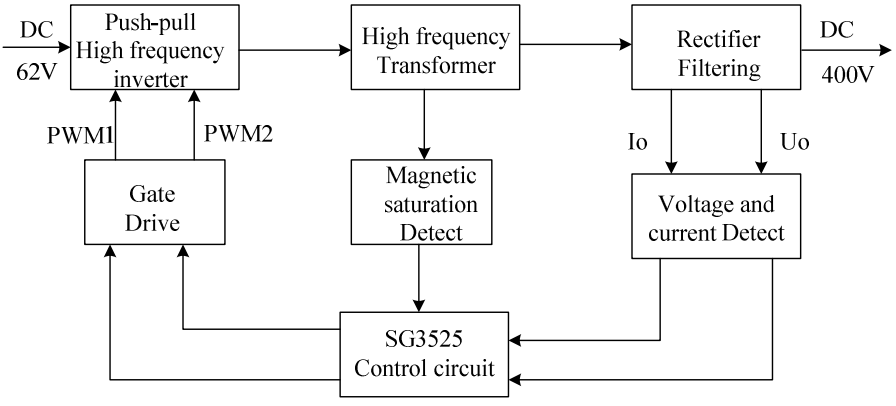

Fig. 3. The control block diagram of DC / DC converter

3.2 The Control Program of DC / AC Inverter

DC / AC inverter is the key and difficult points of photovoltaic grid and its control block diagram is shown in Fig. 4. The core control chip uses DSP TMS320F240. Because the real-time processing capability of DSP is very powerful, thus ensuring that the system has a higher switching frequency.

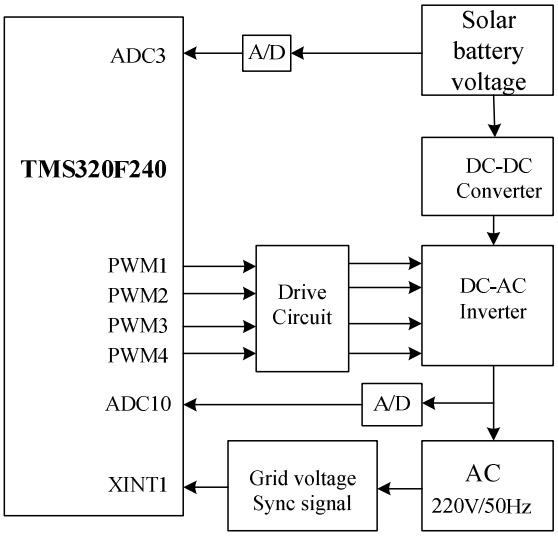

Fig. 4. The control block diagram of D C / AC inverter

3.3 The Control Program of DSP

The control program of DSP is shown in Fig. 5. the reference voltage was compared to actual voltage of the solar cell, its error after the PI regulator will be the current

instruction IREF and multiplied by the sine table value in ROM, produce alternating output current instruction iref, then it is compared with the actual output current value, the error after the proportional (P) links will get the instruction negated, and plus the AC side voltage Us ,the resulting waveform is then compared with the triangular wave, to produce 4-channel PWM modulation signal (triangular wave frequency is 20kHz).

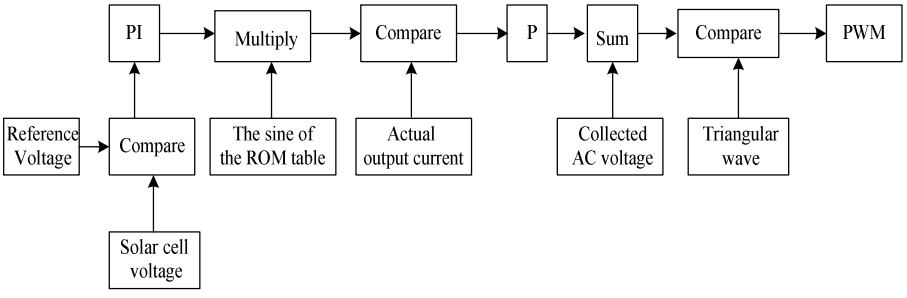

Fig. 5. The control program of DSP

3.4 The Software Control Flow of TMS320F240

The software is divided into four parts, namely, the main program, the T1 underflow interrupt, the T2 underflow interrupt, and synchronous interrupts. Flowchart is show in Fig. 6. T1 underflow interrupt occurs once every 50μs, the procedures used to

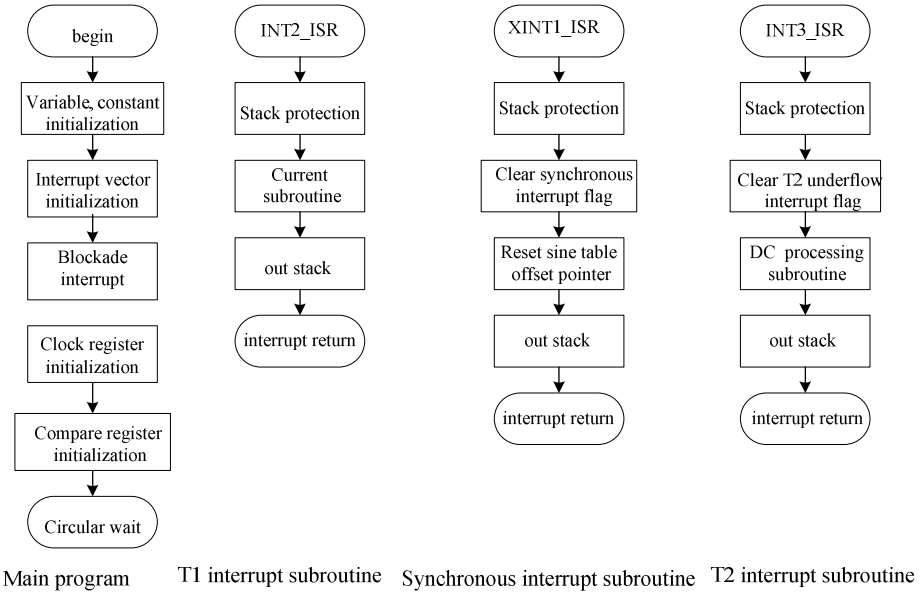

Fig. 6. The software flow chart

generate the PWM wave; T2 underflow interrupt occurs once every 10ms, the program is mainly used to produce the current command; synchronous interrupt approximately occurs once every 20ms.

4 Summary

This paper describes a control system of low power PV grid-connected inverter. Circuit topology of the DC / DC controller with push-pull control chip SG3525, the circuit is effective in preventing the magnetic bias; DC / AC inverter full-bridge inverter circuit with DSP control, due to the relatively high speed of operation of the DSP, so the inverter output current can well track the grid voltage waveform. The effectiveness of the Photovoltaic Inverter control program has be verified in the laboratory. The control system ensures that the output of the inverter power supply power factor close to 1, the output current is sinusoidal waveform.

References

1. Wang, S., Jin, X., Yang, H.: Design for A Low- Power Photovoltaic Inverter Interconnected with Electric Utility Lines with the Improved Current Control Strategy. Electric Age 3 (2006)
2. Feng, Z., Wang, G.: Research and Experiments on a Three-phase ZCT Grid-connected Photovoltaic Inverter. Electric Drive 39 (2009)
3. Xue, M., Yang, G.: Modeling and Simulation of an Improved Current Control Strategy for Three-Phase Grid-Connected Inverter. Computer Simulation 28 (2011)
4. Liu, D., Chen, G.: Development of Single-phase Two-stage Non-isolated Grid-connected Photovoltaic Inverter. Journal of Power Supply 2 (2011)
5. Zeng, Y., Cai, P.: Application of One-cycle Single-stage Control Method in Grid-connected Photovoltaic Inverter. Journal of Power Supply 3 (2011)

Process Development and Simulation Analysis of Power Generation and Refrigeration Technology Using Natural Gas Pressure Energy with Electronic Gas Alarm Processor

HongPing Shen[1], QiuXiong Chen[1,2], Han Lu[1], and WenDong Xu[1,2]

[1] Key Laboratory of Enhanced Heat Transfer & Energy Conservation of the Ministry of Education, School of Chemistry and Chemical Engineering, South China University of Technology, Guangzhou 510640, Guangdong, China
[2] ShenZhen Gas Corporation Ltd, Shenzhen 518040, Guangdong, China
hongpings@163.com

Abstract. With the development of China's natural gas industry and the improvement in the construction of medium,high pressure natural gas pipeline network,large scale utilization of pressure energy of natural gas with electronic gas alarm processors from pipeline network is possible.This paper developed a new process using pressure energy to produce cold water ,analyzed the energy and electricity saving benefit of this process,and pointed out the optimization direction of this process.The results of the study show that: with this process,income of the natural gas station of 1950000 Nm3/d is 24000 yuan,amounts to support cold water for 161000m2 for 8 hours everyday and the energy efficiency of the total process is 62.49%.This process will have a broad application prospects with the further development of China's natural gas industry.

Keywords: Natural gas, Pressure energy utilization, Energy analysis, electronic gas alarm processors.

1 Introduction

It's needed to throttle and regulate pressure with electronic gas alarm processors before natural gas sent to the terminal users via pipeline, and enormous pressure energy is recoverable in this process. For example, ecyclable pressure energy of 25℃,4 MP natural gas expanded to 0.4 MPa is about 322 kJ/kg in theory, while it's rarely recycled in the actual process.

At present, the researchers proposed several recycling way, the main two ways to use pressure energy of natural gas are power generation[1,2] and refrigeration [3,4,5].The domestic industry widely used the latter to produce cold energy for city gas peak-shaving.

In order to improve the pressure energy utilization efficiency, This paper develops a power generation and refrigeration technology using natural gas pressure energy which uses the electric energy Outputed by natural gas turbine to drive ammonia

D. Jin and S. Lin (Eds.): Advances in Mechanical and Electronic Engineering, LNEE 177, pp. 7–12.
springerlink.com

refrigerating compressor, then let the low temperature natural gas after expansion exchanges heat with water to produce air conditioning cold water, thus can greatly reduce electricity consumption[6,7].

2 Simulation of Power Generation and Refrigeration Technology Using Natural Gas Pressure Energy with Electronic Gas Alarm Processor

2.1 Streams and Parameters Setting

This paper is based on 1950000 Nm^3/d (62326.875kg/h) of natural gas as the calculation benchmark,,the compositions of natural gas are shown in table 1. Natural gas of 15℃, 9MPa is from high pressure gas network,and its temperature turns to 5℃ after utilization.

In this article, the ASPEN software is used to calculate, Peng-Robison equation of state is chosen as thermodynamics method,the isentropic efficiency of gas turbine is 80% and its mechanical efficiency is 90%,the mechanical efficiency of pump is 90%,maximum pressure drop of heat exchanger is 0.3atm.ammonia is choosen in the Cold media circulation system.

Table 1. Natural gas composition of high pressure pipeline

composition	CH_4	C_2H_6	C_3H_8	i C_4H_{10}	n C_4H_{10}	CO_2	N_2	total
Mole fraction[%]	89.39	5.76	3.30	0.78	0.66	0.0	0.11	100

2.2 Process Simulation

The process of power generation and refrigeration Technology using natural gas pressure energy proposed in this paper can be seen in figure 1. As can be seen in figure 1, natural gas of 15℃, 9.0MPa, 62326.875kg/h is divided into three shares by splitter, NH3 is divided into five shares.

A stream of the natural gas expands to 2.5 MPa ,its temperature is lowered to - 49.1℃, then heated to 5℃ by NH_3 and transported to the gas users, NH_3 is cooled to - 15 ℃.

A stream of the natural gas expands to 4 MPa, its temperature is lowered to - 31℃, then heated to 5℃ by NH_3 and transported to the gas user ,NH_3 is cooled to -15 ℃.

A stream of the natural gas expands to 4 MPa, its temperature is lowered to - 14℃, then heated to 5℃ by NH_3 and transported to the gas users,NH_3 is cooled to -8 ℃.

A stream of the natural gas is divided into two streams by splitter,one is transported to the gas users directly ,the other expands to 1.0 MPa ,its temperature is lowered to - 56℃, then heated to 5℃ by NH_3 and goes into the next stage of expansion,NH_3 is cooled to -25 ℃;the 1.0MPa natural gas continue expands to 3.0 MPa,,its temperature is lowered to - 50℃, then heated to 5℃ by NH_3 and transported to the gas user, NH3 is cooled to -15 ℃

5 shares of ammonia flow are combined for heat exchange with water to produce air conditioning cold water.

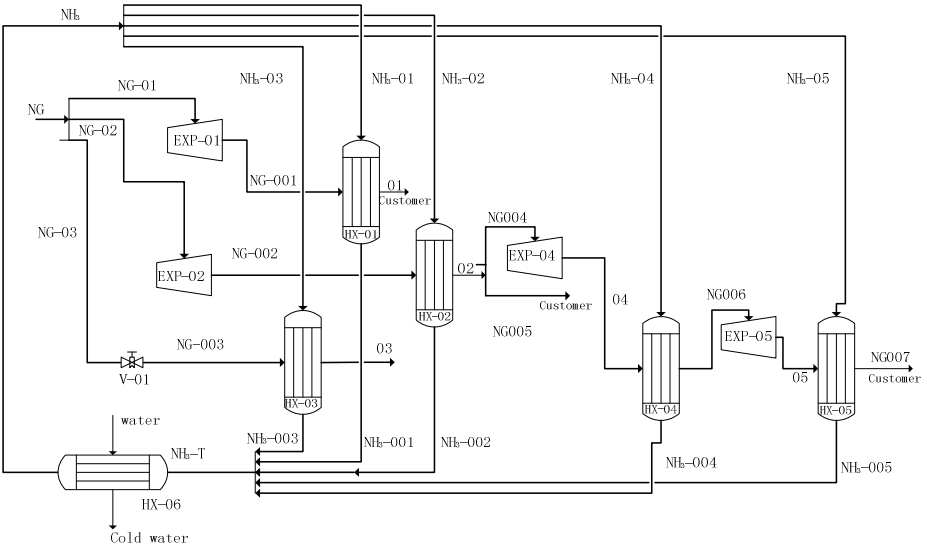

Fig. 1. Process of power generation and refrigeration technology using natural gas pressure energy with electronic gas alarm processor

3 Results and Discussions

3.1 Power Saving Benefit Analysis

From the simulation results ,it's clear that ammonia refrigerant can offer 2360kW cold energy using the cold from -15 ℃ to 10 ℃ which can produce 400t/h , 7℃ air conditioning cold water(leaving water temperature is 12℃). It's calculated that this process can support cold for 61000m^2 area for 8 hours eeverday (The cooling demand is 116W/m^2), if COP(Coefficient Of Performance) of -15℃ is calculated by 3.3 ,electricity price is calculated by 0.85yuan / kwh ,then this cold energy equivalent to save electricity of 15000 yuan.

At the same time, the natural gas pressure energy can generate electricity 1166KW, the income is 24000 yuan Everyday ,electricity is used to drive the refrigeration compressor to produce cold energy which can support cold for 100000m^2 area for 8 hours everday (The cooling demand is116W/m^2) as the electricity can't be incorporated into the grid.

Thus the income of the natural gas station of 1950000 Nm^3/d is 24000 yuan everyday , amounts to support cold for 161000m^2 for 8 hours everday.

3.2 Energy Analysis

The energy Method, also known as "availability analysis," is a technique of thermodynamic analysis which uses the "Second Law of Thermodynamics" as its assessment basis[8].energy is energy that out of equilibrium with its environment, It represents the maximum work can hope to harvest from energy[9].

The energy of a substance is composed of physical energy and chemical energy[10] which is Expressed in Eq.1.

$$E_X = E_{X,\,phys} + E_{X,\,chem} \tag{1}$$

For steady flow system, it has neglected potential energy and kinetic energy of the working fluid, thus the energy of the working fluid in a certain state can be represented in Eq.2.

$$E_X = H - H_0 - T_0(S - S_0) \tag{2}$$

The T_0, H_0, S_0 mean temperature, enthalpy and entropy in reference state, which is 25℃, 1atm in this paper.

Because it is a steady flow of physical process ,does not involve chemical reaction, so only physical energy is calculated in this paper.Eq.2 is used to calculate the energy of each stream, the results can be seen in Table 2.

Table 2. Energy Calculation Results

stream	flow [kg/hr]	temperature [℃]	enthalpy [kJ/kg]	entropy [kJ/kg·K]	energy [MJ/hr]
1	23971.88	5	-4251.2	-6.7127836	10170.75
2	22373.75	5	-4273.51	-6.981261	10784.45
3	15981.25	5	-4273.88	-6.9826128	7703.611
4	6392.5	-55	-4378.55	-6.8583802	2175.625
5	6392.5	-50	-4330.82	-6.1276374	1087.952
NG	62326.88	15	-4321.1	-7.4440343	35676.02
NG01	23971.88	15	-4407.5	-7.3464229	10952.73
NG001	23971.88	-50	-4321.1	-7.4440343	13721.55
NG002	22373.75	-30	-4377.7	-7.3851123	11147.39
NG02	22373.75	15	-4321.1	-7.4440343	12806.78
NG003	15981.25	-13	-4321.1	-7.1583686	7786.588
NG03	15981.25	15	-4321.1	-7.4440343	9147.698
NG004	6392.5	5	-4273.51	-6.981261	3081.273
NG005	15981.25	5	-4273.51	-6.981261	7703.181
NG006	6392.5	5	-4229.38	-6.2446054	1959.33
NG007	6392.5	5	-4219.69	-5.6829188	950.7361
NH_3	6155	10	-2749.1	-6.8433133	1572.2
NH_3-T	6155	-15	-4129.49	-11.738555	2059.221
NH_3-01	2720	10	-2749.1	-6.8433133	694.7821
NH_3-02	1690	10	-2749.1	-6.8433133	431.6845
NH_3-03	560	10	-2749.1	-6.8433133	143.0434
NH_3-04	670	10	-2749.1	-6.8433133	171.1412
NH_3-05	515	10	-2749.1	-6.8433133	131.5488
NH_3-001	2720	-15	-4126.57	-11.727286	908.7822
NH_3-002	1690	-15	-4128.48	-11.734657	565.1434
NH_3-003	560	-8	-4096.41	-11.612096	184.7607
NH_3-004	670	-25	-4172.25	-11.907477	229.2456
NH_3-005	515	-15	-4128.48	-11.734657	172.2183
H_2O	75000	30	-15949.2	-9.2446395	225.075

Commonly used energy analysis models are black box model and grey box model. black box model is a technology studying internal energy utilization process of the subsystem with the help of energy information of the input, output subsystem. Grey box model is the system that all the equipment are regarded as black boxes ,Black boxes are connected together to form network by main energy flow ,that is a black box network model.

For black box model, the total energy of input, output systems is constant, total energy of input system includes support energy $E^S_{X,\sup}$ and bring-in energy of stream $E^S_{X,br}$;total energy of output system includes effective energy $E^S_{X,eff}$ and loss energy of system $E^S_{X,loss}$; loss energy of system includes ineffective energy $E^S_{X,ineff}$ of output system and internal loss energy $E^S_{X,irr}$.

Energy balance relationship can be seen in Eq.3. energy efficiency is defined as the ratio of the effective energy of output system to the total energy of input system which can be calculated by Eq.4,by calculating, energy efficiency and energy loss of each units are shown in Table 3

$$E^S_{X,\sup} + E^S_{X,br} - E^S_{X,eff} - E^S_{X,loss} = 0 \tag{3}$$

$$\eta = \frac{E^S_{X,eff}}{E^S_{X,\sup} + E^S_{X,br}} \tag{4}$$

Table 3. Energy efficiency and energy loss of each unit

Operation unit	energy loss [MJ/hr]	effective energy [MJ/hr]	energy efficiency [%]
EXP-01	2770	1864	67.29
EXP-02	1660	1140	68.66
EXP-03	905	604	66.74
EXP-04	871	583	66.96
HX-01	13027	9263	71.10
HX-02	10716	10219	95.36
HX-03	7644	7519	98.37
HX-04	1730	2004	86.30
HX-05	418	956	45
HX-06	1347	1834	73.45
Total process		62.49	

It can be seen from Table 3 that energy efficiency of total process is 62.49%, energy efficiency of HX-05 is the lowest, only 45% ,This may due to the larger temperature difference between hot and cold streams in HX-05,the temperature distribution of each streams in HX-05 is shown in Figure 2.

It's obvious in figure 2 that The maximum temperature difference between hot and cold streams is 55℃, larger temperature difference results in lower energy efficiency of HX-05.

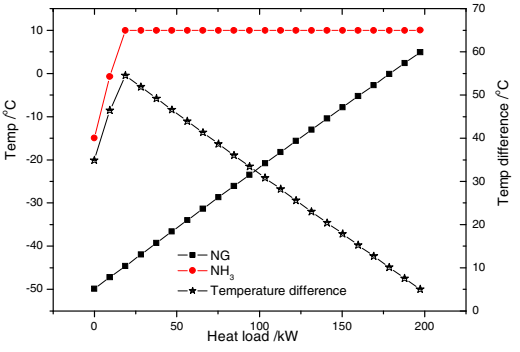

Fig. 2. Temperature distribution of each streams in HX-05

4 Conclusions

This paper develops a new process using pressure energy to produce cold water, analyses the energy and electricity saving benefit of this process. Through above analysis, it's concluded as follows:

1) the income of the natural gas station of 1950000 Nm^3/d is 24000 yuan Everyday , amounts to support cold for 161000m2 for 8 hours everday.
2) energy efficiency of total process is 62.49%,energy efficiency of HX-05 is the lowest, only 45%, HX-05 unit is the main energy saving optimization unit of this process.

Along with the development of China's natural gas industry and the improvement in the construction of medium,high pressure gas pipeline network,pressure energy Available for recycling can be also more and more,thus the power generation and refrigeration Technology using natural gas pressure energy proposed in This paper will have a broad application prospects.

References

1. Chen, S.K., Li, Z.L., Gao, Z.: Oil & Gas Storage and Transportion 28(2), 51 (2009)
2. Shen, D.M., Fernandes, F., Simões-Moreira, J.R.: Hydrocarbon Processing 85(1), 47–50 (2006)
3. Lawrence Kimble, E.: U.S.Patent: 6209350B1 (2001)
4. Lun, L.Y., Xie, Y.B., Yang, X.L.: Natural Gas Industry 26(6), 114 (2006)
5. Escobar, R.F., Juarez, D., Siqueiros, J.: Desalination 222(1/3), 666 (2008)
6. Xu, W.D., Zheng, H.P., Lang, X.M., Chen, Y.J., Fan, S.S.: Chemical Industry and Enreering Progress 29(12), 2385 (2010)
7. Peng, L.: Public Utilities 24(3), 35 (2010)
8. Gord, M.F., Maghrebi, M.J.: International Journal of Energy 6(1), 131 (2009)
9. Zheng, Z., Wang, S.L., Wang, B.H.: Natural Gas Industry 5(7), 104 (2006)
10. Hinderink, A.P., Kerkhof, F.J.: Chemical Engineering Science 51(5), 4693 (1996)

Application of PLC in the Electroplating Automation Manufacture

Tao Wu

Faculty of Mechanical and Electrical Engineering,
Kunming University of Science & Technology,
Kunming, China
Kmwutao13@126.com

Abstract. The waste liquid, gas and residue produced in the electroplating production will do harm to the environment and the human body, so it is essential to realize automatic electroplating manufacture. The technological process of automatic electroplating manufacture and the overall arrangement of plating tanks are discussed in this paper. MITSUBISHI FX PLC is used to control the automatic electroplating reciprocate production line. PLC I/O terminals configuration, control flowchart and corresponding ladder program is discussed at the same time. Thus could improve working condition and raise working efficiency.

Keywords: electroplating, automation, PLC, circulation.

1 Introduction

Electroplating is widely used in manufacture, electronics and national defense industry. The surface property of solid materials could be changed through electroplating. In mechanical products, the part number that needs to be electroplated is amount to 80~90%. With the rapid social development, the part quantity of ferrous metal, nonferrous metal and other nonmetals will be increased. This will put forward arduous task to electroplating industry. But the waste gas, waste liquid and residue does harm to the environment and human beings. To realize automatic electroplating is imperative.

2 Technological Process

The total length of this electroplating production line is about 20 meters. There are 17 plating tanks in this production line such as copper plating tanks, rinse tanks and so on. The production mode adopts reciprocate mode. The motion sequence is shown in Fig.1 [1]. In Fig.1, the vertical real line, the vertical broken line and the horizontal real line represents right hook, left hook and traveling crane respectively. There are 31 technological steps. The 31steps could be merged into one circulation.

D. Jin and S. Lin (Eds.): Advances in Mechanical and Electronic Engineering, LNEE 177, pp. 13–18.
springerlink.com

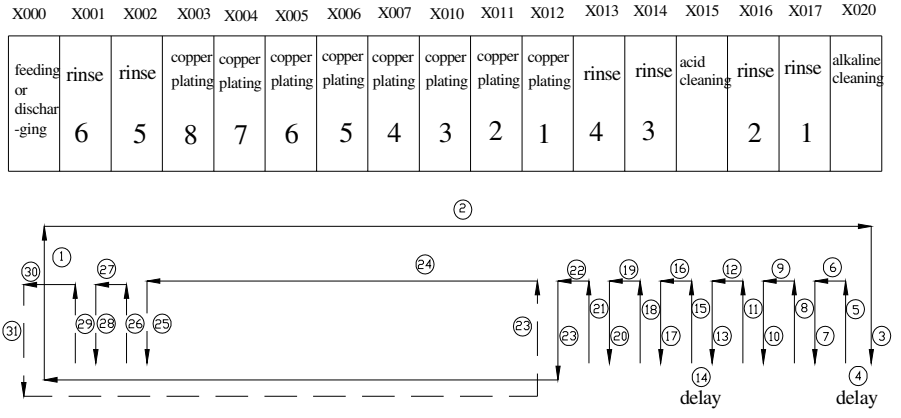

Fig. 1. Electroplating process flow diagram

According to different technological demands, the electroplating time could be calculated by Eq. (1) [2].

$$t = \frac{60\rho d}{100KD_k\eta_k} \tag{1}$$

Where: t-electroplating time, min;
d-coat mean thickness, μm;
K-electrochemical equivalent of the metal to be plated, g/(A·h);
D_k-cathode current intensity, A/dm^2;
η_k-cathode current efficiency, %;
ρ-density of the metal to be plated, g/cm^3;

The traveling crane motion speed should be controlled between 12 and 20m/min. The up and down speed of the hook should be controlled between 8m/min and 12m/min. With calculation, the copper-plating time of some part is about an hour. To make full use of this time, 8 copper-plating tanks are set. In every copper-plating tank there are 2 places on the left or right side respectively to put the parts.

During this hour, the parts to be plated are put successively in the 8 tanks by the right hook and the plated parts are fetched by the left hook. This is called a cycle. There are 8 circulations in a cycle. So in the next cycle, it must be that the left hook put the parts to be plated, and the right hook fetch the plated parts. In this cycle, there are also 8 circulations. There are 31 technological steps in every circulation. The cycle that right hook put the parts to be plated and the left hook fetch the plated parts is called single cycle. The conversely cycle is called double cycle.

3 PLC Control System Design

3.1 Hardware Design

The left hook, right hook and the traveling crane are driven by 3 motors respectively. Each motor could rotate clockwise or counterclockwise to realize the up and down motion of the hook, the left and right motion of the traveling crane. The motor power is chosen according to load weight.

A Programmable Logic Controller (PLC) is microprocessor based control system that can be programmed to sense, activate and control industrial equipment and therefore incorporates a number of input/output terminals for interfacing to an industrial process [3]. A control program stored in the PLC memory determines the relationship between the inputs and outputs of the PLC. PLC is an intelligent automation station that possesses highly useful and desirable features such as: robustness, high degree of scalability, extensibility, sophisticated communication capabilities, powerful development environment.

Among so many kinds of PLC, MITSUBISHI FX PLC is selected. The tank position proximity switch numbers are shown in Fig.1. Other main I/O relay numbers are shown in table 1 and table 2 respectively.

Table 1. PLC input relay number and function

function	PLC input relay number	function	PLC input relay number
left hook up limit proximity switch	X021	feeding photo detector	X033
left hook low limit proximity switch	X022	discharging photo detector	X034
right hook up limit proximity switch	X023	start button	X035
right hook low limit proximity switch	X024	stop button	X036

Table 2. PLC output relay number and function

function	PLC output relay number	function	PLC output relay number
left hook up	Y000	right hook down	Y003
left hook down	Y001	traveling crane left motion	Y004
right hook up	Y002	raveling crane right motion	Y005

3.2 Software Design

This system is a typical step control. The step control relay represents program state step. The step function flowchart could be worked out. Thus the ladder diagram and statement list could also be got. A segment of step function flowchart is shown in Fig.2a). The corresponding ladder is shown in Fig.2b) [4, 5].

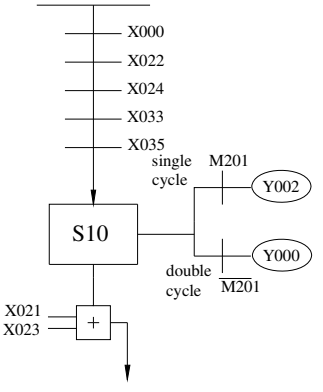

a) Segment of step function flowchart

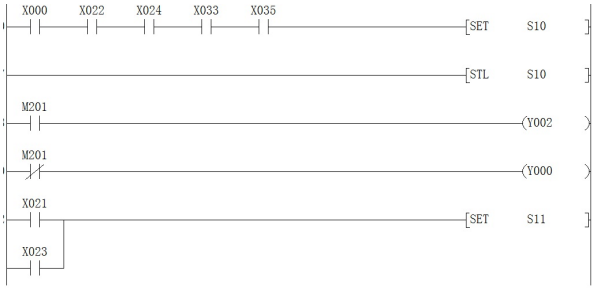

b) Corresponding ladder diagram

Fig. 2. Segment of step function flowchart and corresponding ladder diagram

Seen from Fig.1, the third to sixth, thirteenth to sixteenth technological steps are all down, delay, up, left. Moreover, the seventh to ninth, tenth to twelfth, seventeenth to nineteenth, twentieth to twenty-second technological steps are all down, up, left. The above 2 programs are different only one step—delay. Thus they could be synthesized into one circulation control, as shown in Fig.3. The concrete way is that the latter program leaps the delay step.

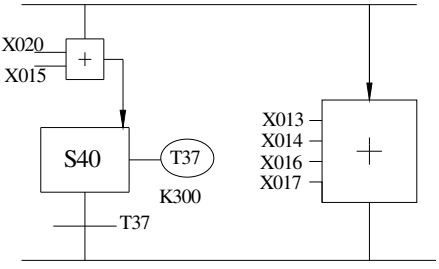

Fig. 3. Circulation control step function flowchart

Copper plating tank position is controlled by the shift register.

The single-double cycle change is realized by binary prescaler. The work principle is shown in Fig.4a). The corresponding ladder diagram is shown in Fig.4b).

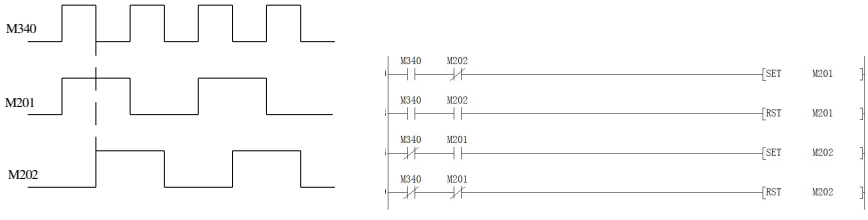

a) Work principle of binary prescaler b) Corresponding ladder diagram

Fig. 4. Work principle and corresponding ladder diagram of the binary prescaler

4 Summary

In the light of electroplating procedures, the plating tanks, ascension transfer device, control device PLC and other devices are put together to constitute the automatic electroplating production line. By contrast with manual operation, this automatic production could improve the production greatly, reduce labor intensity, ensure production quality stability, ameliorate workshop environment.

Acknowledgments. This work is supported by the Yunnan Province Education Department Scientific Research Foundation (Grant No. 2011Y366).

References

1. Subaı, C., Baptiste, P., Niel, E.: Scheduling issues for environmentally responsible manufacturing: The case of hoist scheduling in an electroplating line. Production Economics 99, 74–87 (2006)
2. Feng, L.-M.: Electroplating process and equipment. Chemical Industry Press, Beijing (2005) (in Chinese)

3. Da'na, S., Sagahyroon, A., Elrayes, A., Al-Ali, A.R., Al-Aydi, R.: Development of a monitoring and control platform for PLC-based applications. Computer Standards & Interfaces 30, 157–166 (2008)
4. Huang, M.-Q., Feng, J.-Y., Wang, F.-P.: Programmable Logic Controller. ChongQin University Press, ChongQin (2003) (in Chinese)
5. Fu, J.: Application of PLC in Electroplating Product Line Traveling Crane Control System. Electrical Automation 28(2), 64–67 (2006) (in Chinese)

Key Technologies Research on Collaborative Virtual Maintenance of Large-Scale Electromechanical Equipments

Wenliang Guan, Qinhe Gao, Yihong Li, and Xiangyang Li

Xi'an Research Inst. of Hi-Tech,
Hong Qing Town,
Xi'an, P.R. China
gwlz2000@126.com

Abstract. Aiming at the complexity of large-scale electromechanical equipments and the difficulty of actual equipment training, key technologies of collaborative virtual maintenance of large-scale electromechanical equipments were researched according to complex systems modeling, distributed interactive simulation virtual maintenance and other aspects of advanced technology. The key technologies can be used in the design and implementation of collaborative virtual maintenance training system of large-scale electromechanical equipments, which can provide the technical support and solution for more immersion, perceivable and informational collaborative virtual maintenance training system.

Keywords: collaborative virtual maintenance, simulation model, electromechanical equipments.

1 Introduction

Large-scale electromechanical equipments usually use the technology of mechanical, hydraulic, electric and optical system in one form, the system is complex and highly integrated, the working principle and repair operation of the system is more complex. Excessive wear and accidental damage will caused by real equipment training which lead to additional costs, equipment maintenance training and collaborative research will be restricted greatly, so a new advanced simulation technology must be seeked to its development. However, in advanced simulation technology and its applied research, China has been using the method of tracking foreign technology. Virtual maintenance technology, known as the cutting-edge of the field, is started late in domestic research, and has remained mostly theoretical research in the laboratory level, simulation application development is less. To this end, virtual maintenance technology can be used in the equipment maintenance on teaching and training of large-scale electromechanical equipments though theoretical and technical research around the fields related. Training costs can be reduced, new simulation application based on military development can be explored at the same time, it is with good economic and important military significance.

D. Jin and S. Lin (Eds.): Advances in Mechanical and Electronic Engineering, LNEE 177, pp. 19–23.
springerlink.com

2 Collaborative Maintenance Task and Process Modeling Based on Simulation Model of Large-scale and Complex Equipments

After the analysis of multi-level hierarchy structure and functional characteristics of each hierarchy of large complex systems, optimized design and reasonable selection were done to temporal and spatial resolution of each sub-system, different resolution model and model between sub-systems interconnection were established, so that the aggregation model of overall system has fine granularity and high points of accuracy. Meanwhile, according to the static properties, dynamic properties and failure mode, the effectiveness and impact of each major components were analyzed based on different failure mode to identify the decision of its main performance parameters of the physical state and to study its variation, hybrid modeling method were used to create different types of faults simulation model.

Collaborative maintenance task model was established according to maintenance tasks and specific implementation procedures of large-scale and complex equipments, task can be distributed based on operating personnel of different station. Maintenance operational model was established according to maintenance operational processes and implement steps of each station to the specification and testing of operating personnel.Maintenance expert system and maintenance guidance model were established based on the technical specifications and empirical knowledge of the maintenance operations of large-scale and complex equipments to guide the current operations of maintenance personnel. Collaborative virtual maintenance process is shown in Fig.1:

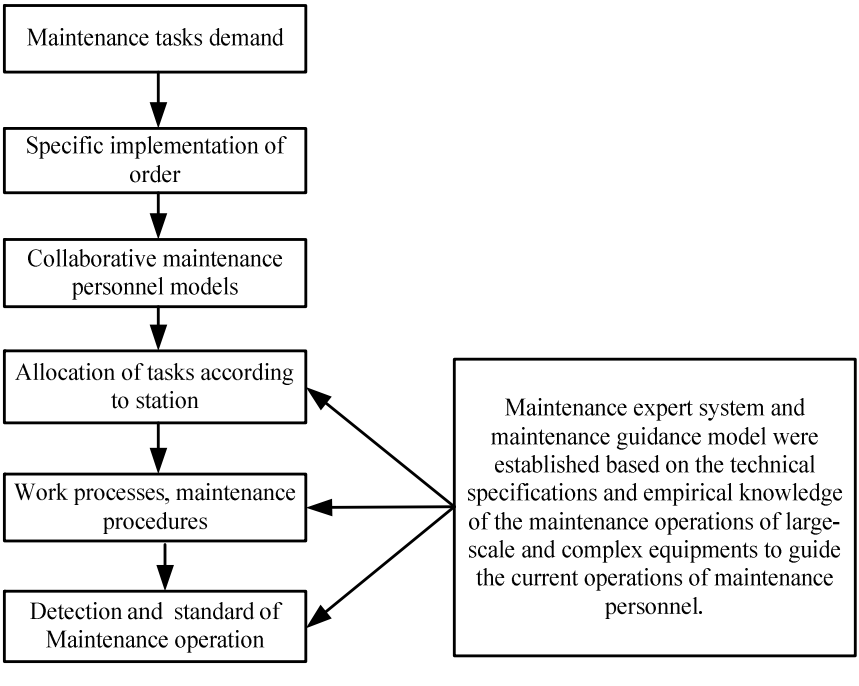

Fig. 1. Collaborative virtual maintenance process

3 Heterogeneous Data Communication and Co-treatment Interaction of Collaborative Virtual Maintenance Process

The heterogeneous data of collaborative virtual maintenance of large-scale and complex equipments, including not only the three-dimensional solid model of different data structures, mathematical models, physical models, motion simulation model and the human-computer interaction models, and also involving the data of different types of content structure and knowledge representation, the underlying heterogeneous databases, interactive information of different data formats.

The data interaction communication and co-processing between the models is realized by the following steps. Firstly, the interoperability of the heterogeneous data is ensured by mapping the template data or model to transform the data information and dynamic call by the use of extensible markup language XML. Secondly, interactive communication and distribution management strategies of data information of the models is created to insure the data information can be interacted reliably and orderly by the use of high-level architecture on HLA / RTI object management, time management and data distribution management services. Thirdly, the parameter value of the current time is calculated and assigned by using digital signal processing theory and calculation methods, by using interpolation and extrapolation methods for asynchronous state parameters of each node to receive compensation for information. Finally, status parameters assigned are simultaneous calculated and co-processed using time synchronization mechanism, the status parameters updated the time synchronization mechanism for the assignment the state after the simultaneous calculation of parameters and co-processing, the updated status data is feedback to the appropriate node for further processing, to ensure the data accurate and reliable, to ensure the data interactive communication synergy too.The data interaction communication and co-processing between the models is shown in Fig.2:

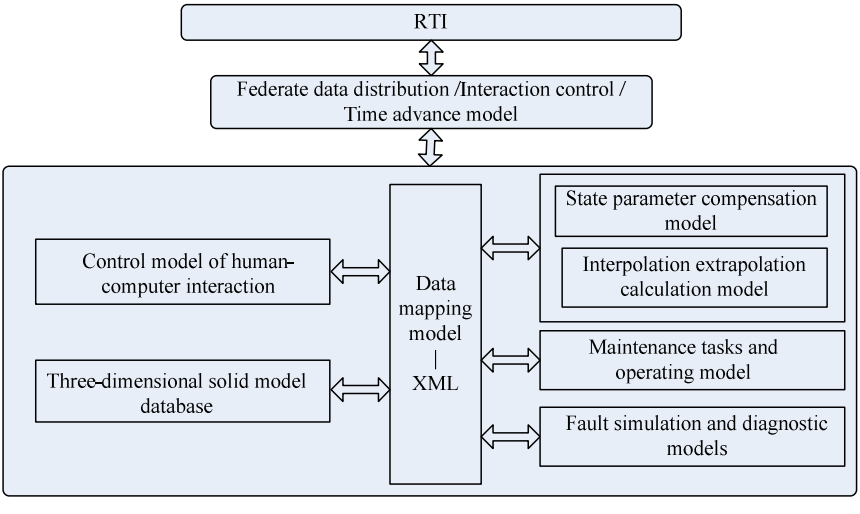

Fig. 2. The data interaction communication and co-processing between the models

4 Human-computer Interaction Control and Co-motion Simulation of Collaborative Virtual Maintenance Operations

The process of Collaborative virtual maintenance operation is that, the spatial position, body posture, hand movements and operating instructions and other data of maintenance personnel are transmitted to human-computer interaction model by spatial location tracking systems, data gloves and VR interactive peripherals, three-dimensional mouse and API function with standardized interface protocol, calculation, analysis and decision-making process are done by the human-computer interaction model to realize real-time control to the motion simulation and interactive operation of virtual maintenance personnel.

Interactive communications, data distribution management strategies and time synchronization mechanism of the data information are used to achieve status information of other maintenance training personnel operation module timely. Unreasonably operation requests of maintenance personnel are restricted by human-computer interaction control policy to ensure the accuracy, reliability and real-time of co-motion simulation in collaborative virtual maintenance operations. Finally, operation input control and motor coordination control of different station maintenance training personnel are realized, operation with each other, motor coordination and co-motion simulation of virtual maintenance personnel are achieved too.

Virtual reality technology and virtual maintenance theory are used to analyze and design the interactions mode of operation, exercise restraint and physical response relationship of the virtual human and equipment components / maintenance tools to create high fidelity and realistic virtual environment to provide technical support service. Human-computer Interaction Control process is shown in Fig.3:

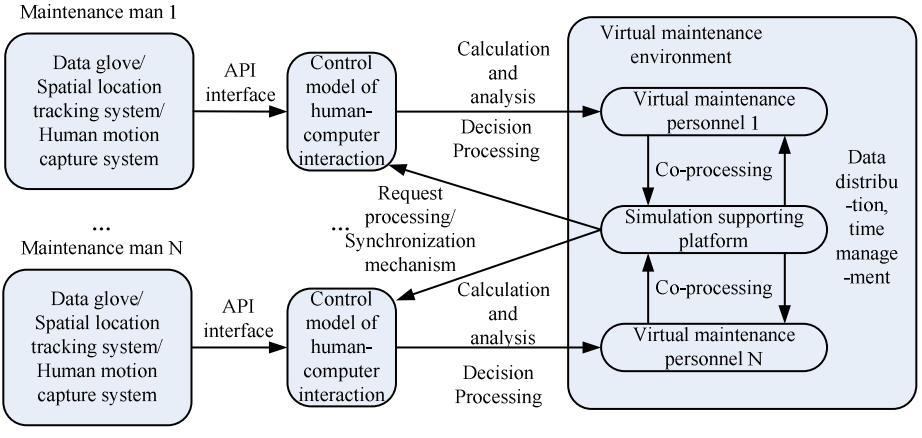

Fig. 3. Human-computer Interaction Control process

5 Conclusion

Optimization design and simulation development of maintenance task model, maintenance operating model, maintenance expert systems and maintenance guide model are researched according to hierarchical structure, dynamic characteristics and failure modes of electromechanical-hydraulic integrated system based on analysis of collaborative maintenance training requirements. Mapping conversion and interactive communication mechanisms of heterogeneous data information between models are researched, information compensation, synchronous computing and collaborative processing method of state parameters are researched too.Interactive communications and data distribution management strategies of all kinds of data information are created. Time synchronization mechanism of operation input control and motor coordination control of different station maintenance training personnel are researched, operation with each other, motor coordination and co-motion simulation of virtual maintenance personnel are achieved too. Simulation models and data support can be provide to the formation of large-scale collaborative virtual electromechanical equipments maintenance training system, and then to carry out research on virtual maintenance, maintenance analysis and maintenance program development by the research results.

References

1. Li, X.: Research on Fault Diagnosis of Hydraulic System in Missile Armament Simulation System Based on HLA. In: Proceedings of 2008 Asia Simulation Conference, pp. 358–361. Research Publishing Services, Singapore (2008)
2. Li, X.: Research on Simulation and Development of Fault Diagnosis Training System of Large–scale Armament Equipment. Journal of System Simulation 21(21), 6770–6773 (2009)
3. Liang, F.: Research on Development of Virtual Assembly Simulation Platform of Large-scale Armament Equipments. Journal of System Simulation 21(suppl. 2), 136–139 (2009)
4. Fang, C.: General Platform for Virtual Maintenance Training System of Missile Equipment. Computer Engineering 35(3), 274–276 (2009)
5. Wang, Q.: Complex Equipment Virtual Maintenance Training Technology. Ordnance Industry Automation 28(12), 1–3 (2009)
6. Yang, Y.: Missile Maintenance Training System Based on Virtual Reality Technology. Acta Armamentarh 27(2), 297–300 (2006)
7. Chang, G.: Application of Database to Virtual Maintenance Training System. Journal of Englneering Graphlcs (5), 157–162 (2010)

Design of IC Card Fast Switching Device

LiGuo Tian, BeiBei Guan, Meng Li, and ZhiLiang Chen

Tianjin Key Laboratory of Information Sensing & Intelligent Control,
Tianjin University of Technology and Education,
Tianjin, 300222, China
{tlg1234,limeng-3260711}@163.com,
bei199022@126.com,
czl_tj@sina.com

Abstract. Along with the automation industry's rapid development, miniature embedded control system has been more and more widely used in modern production. Aiming at the IC card manufacturing industry, it designed a set of automatic IC card fast switching device, used to replace the workers of the factory to write procedures before leaving factory. The device with the control core of ATmega8 Single-chip Microcomputer (SCM), directly drives 4 electronic switches to switch on 4 IC cards in time division, and finishes writing program into IC card. The results show that, the IC card fast switching device is simple for operation and works well.

Keywords: Automation, IC Card, ATmega8 SCM, Fast Switching Device.

1 Introduction

The rapid development of modern science technology, especially great progress in micro-electronics, computer and SCM technology, made the automatic control widely being used in modern production. As a kind of automatic device, the IC card fast switching device proposed in the paper is an automation device which has strong pertinence, replaces manual operation to accomplish the IC card switching process in the process of the traditional production, which not only improves work efficiency, but also saves the manpower and material resources.

2 Overall Project of the System

The function realized by the IC card fast switching device is to replace manual operation to switch 4 IC cards rapidly in proper order, switching sequence is enable card, initialized card, parameter-setting card and exfactory closed card, the switching time is 2s,3s,2s and 2s successively; after switching is completed, the alarm module informs operator the process is finished, which also includes the checkout process, testing process and so on, finally, implementation of series of program written work for IC card will be finished before leaving factory[1]. The overall block diagram of system is shown in Fig.1.

D. Jin and S. Lin (Eds.): Advances in Mechanical and Electronic Engineering, LNEE 177, pp. 25–29.
springerlink.com

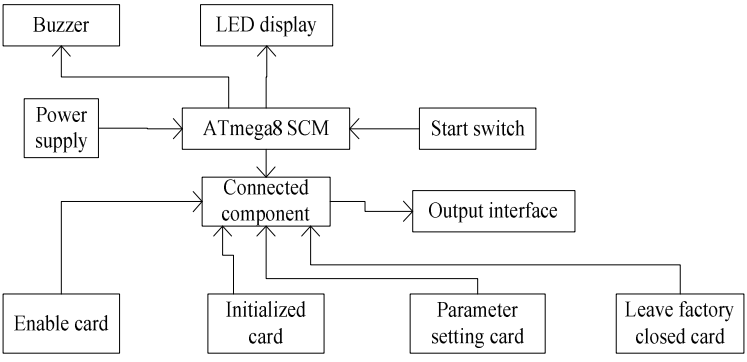

Fig. 1. The overall block diagram of the system

3 Hardware System

IC card fast switching device used ATmega8 single chip microcomputer as the control center, is mainly composed of a microcontroller module, power supply circuit module, connected component module (electronic switch) and alarm module.

3.1 Microcontroller Module

The microcontroller uses ATMEL's ATmega8 single chip microcomputer, which is a high performance, low power consumption microcontroller, with 8MHz frequency and 5 kinds of sleep modes, can work by the low power mode under the control of low voltage; it integrates on-chip1K SRAM, 8K FLASH; besides, ATmega8 SCM also has a wealth of peripherals, such as: 23 programmable I/O ports,8 ten-bit A/D converter, 1 serial peripheral interface SPI and 1 USART, can completely meet the design requirements. As a powerful microcontroller, ATmega8 provides many embedded control applications with flexible and low cost solutions [2].

3.2 Power Supply Circuit Module

In the IC card fast switching device, working voltage of ATmega8 microcontroller SCM is 4.5V~5.5V, so the power supply circuit adopts a typical DC stabilized power supply to provide ATmega8 SCM and other module with voltage. Power supply circuit diagram as shown in Fig.2, external power supply uses 220V AC signal, which could be transforms into 12V pulsating DC through the transformer and the bridge rectifier circuit, after 7805 integrated chip and capacitance filter, the final output of 5V DC voltage is obtained [3]. This kind of power supply mode is a very common, which is safe and reliable, economical and practical, could meet the ATmega8 SCM requirements for voltage.

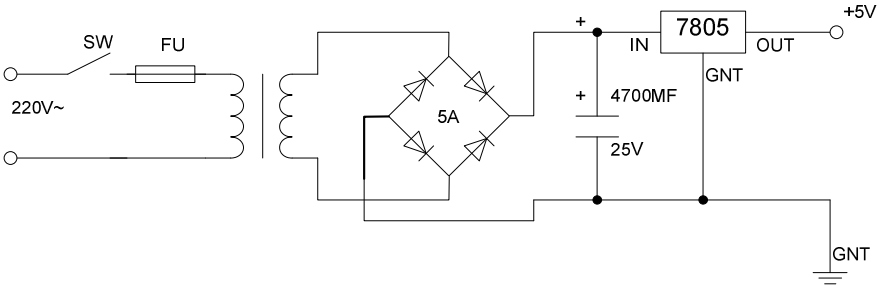

Fig. 2. The power supply circuit

3.3 Connected Components Module

The Connected components module is mainly responsible for the completion of the four IC cards switching work, using an electronic switch to achieve. The drive current of electronic switch is very small, which can be better matched up with single chip microcomputer, without the need of external circuit, and the price is very low. Considering economy and safety performance of the equipment, the IC card fast switching device selects 74HTC4066 integrated electronic switch, which is driven by the ATmega8 single-chip microcomputer to complete 4 IC cards switching [4].

74HCT4066 adopts high-speed CMOS technology; it is an IC chip which has independent four sets of logic switch and strong anti-interference ability and low power consumption etc. Each switch has two terminals as input or output (1Y~4Y, 1Z ~4Z), and four enable signal terminal 1E~4E, when the enabling end gets the enable signal (i.e. when the enable signal is high level), the corresponding switch from nY to nZ is switched on.

4 Software System

4.1 The Main Program

Software design of the IC card fast switching device uses C language, and adopts the modular idea. The program is divided into several subprograms, and then it is called by the main function [5]. The main program mainly includes the initialization subprogram, system detection subprogram and error processing subprogram etc. the flow chart of the main program is shown in Fig.3.

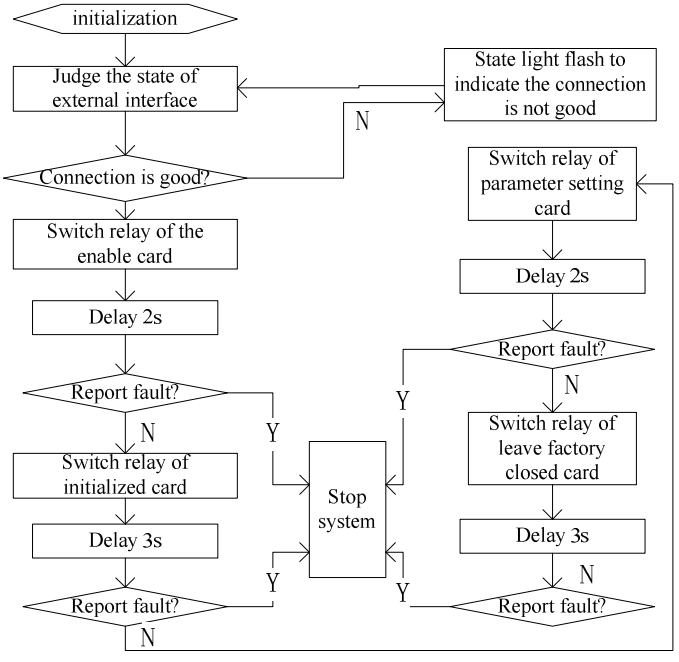

Fig. 3. The flow chart of the main program

4.2 The System Detection Subprogram

The function of system detection subroutine is to test connection of SCM power supply and I/O port, and ensure the normal work of SCM, program flow chart as shown in Fig.4. The main principle is to read the relative status register, and register contents could reflect if the connection between ATmega8 SCM interface and the external is good, then through comparison and analysis, if the connection is good the next operation will be done, or else, the fault light is lightened and the program will go back to the judging procedure until the connection is good.

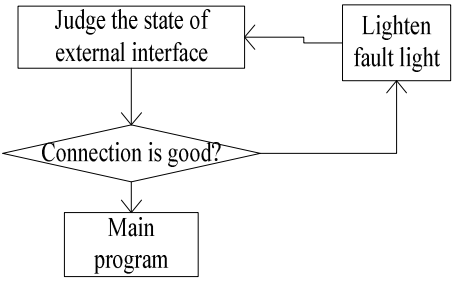

Fig. 4. The flow chart of system detection subroutine

5 Conclusion

Automation device represents the high-degree automation of the modern production; it can replace manual operation to complete a series of operations, to realize the automatic production, thereby improving the production efficiency and economic benefit. According to the control requirements and performance index of the IC card fast switching device, the paper selected and designed the hardware circuit, and completed the design, writing and debugging of the software program, finally finished the whole design process, and achieved the control requirement. After tested, the IC card fast switching device is running well, safe, reliable, worthy of promotion.

References

1. Zheng, Y., Xu, H.: Design of Station Data Writing Device for IC card. Meter Technology and Sensor 4, 61–62 (2006)
2. Ma, C., Zhan, W., Geng, D.: Atmega8 Principle & Application Handbook. Tsinghua University Press, Beijing (2003)
3. Sun, Y.: Regulated Power Supply Design and Skill Training. Electronics Industry Press, Beijing (2007)
4. Xie, Z.: Design, Experiment and Test of Electronic Circuit, 3rd edn. Huazhong University of Science and Technology Press, Wuhan (2006)
5. Yuan, T.: Advanced C Language Program Design and Application for SCM. Beijing University of Aeronautics and Astronautics Press, Beijing (2002)

Design of Test Device for Double-Rate Counter

ZhiLiang Chen, Meng Li, LiGuo Tian, and JiePing Zhang

Tianjin Key Laboratory of Information Sensing & Intelligent Control,
Tianjin University of Technology and Education,
Tianjin, 300222, China
czl_tj@sina.com,
{tlg1234,limeng-3260711}@163.com

Abstract. Along with rapid development of microelectronic technology and single-chip microcomputer technology, the market appears more and more electronic rate counter, the counting accuracy testing device also subsequently grow in quantity. Aiming at the double-rate counter, it designed a testing device used for double-rate counter accuracy test. The testing device used low-power microprocessor ATmega8 SCM(single-chip microcomputer) as the control core, collocated with a pulse output circuit, the LED digital tube display circuit and alarm circuit to implement count accuracy test together. After tested, the test device works well, and has the advantages of simple structure, convenient to use.

Keywords: Test device, Counter, ATmega8, LED Nixie Tube, microelectronic technology.

1 Introduction

Counting accuracy is the most important performance index for rate counter, and it concerns if the counter can get the final application. Therefore, before marketed the product needs to undergo strict counting accuracy test. The paper proposed and designed a kind of test device combined with the SCM and electronic technology, aiming at the double-rate counter, used to test their counting accuracy. The test device for double-rate counter used ATmega8 SCM as the core, inputs the pulse to the input end of double-rate counter through the pulse output circuit, then contrast number of pulses to complete the test work [1], it has simple operation, low cost, and certain application value.

2 Overall Design of the System

2.1 Analyses of System Requirements

Double-rate counter is a kind of cumulative counting device for metering occasions. The device has two input ends, one is rate selection end, and another is rate input end.

D. Jin and S. Lin (Eds.): Advances in Mechanical and Electronic Engineering, LNEE 177, pp. 31–36.
springerlink.com

Its work is as follows: when the input signal in the rate selection end is low level (0.3V), the number of pulses inputted from rate input end is included into rate A, and when the rate selection end is high level(above 3.6V, not to exceed the maximum12V), the inputted pulses is included into rate B. The rate A count plus rate B is equal to the total number of pulses. When the level of rate selection end is in the range of 0.3V~3.6V, the results is included into A or B randomly, so the counting to pulse should be avoided in the process of testing.

2.2 Overall Block Diagram of the System

Double-rate counter test device is composed of a control module (ATmega8 SCM), parameter setting and manual operation module (keyboard operation), display module (LED digital tube) and power supply module. The control module is the core of double-rate counter test device, using ATmega8 microcontroller to complete the function of each module. Keyboard part adopts a single-key keyboard equipped with a starting key, the stop key and the setting key, which are used for operating personnel to control the test device. LED digital tube display module which employs LED dynamic display mode to display the setting number of pulses. Power supply module is used to provide the test device with a stable DC power; a single-phase alternating current is converted into the stable DC voltage through the power transformer, rectifier circuit, filter circuit and a voltage stabilizing circuit. The system overall structure diagram is shown in Fig.1.

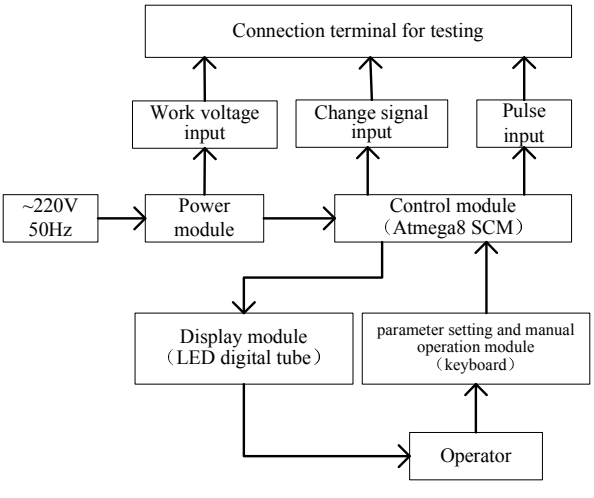

Fig. 1. The overall structure diagram of the system

3 Hardware System

3.1 Microcontroller Module

The microcontroller adopts Atmega8 SCM made by ATMEL Company. Atmega8 is a high performance, low power microcontroller, under the 4MHz working frequency, power consumption is about 10mW, it can use the battery to run, and the range of power supply voltage is from 2.7V to 5.5V; it has 5 kinds of sleep mode, without the need for data acquisition it can be set to idle mode, current is only 1.0mA; it has 512K E2PORM, which can be used to store small amounts of data; besides above, Atmega8 also has two programmable serial USART, 8 ways of 10-bit A/D converter and 23 programmable I/O ports [2].

3.2 LED Digital Tube Display Module

The principle of LED digital tube display as follows: every chip is composed of 7 light emitting diodes, known as the 7-section LED display. The connection of seven light emitting diodes has two kinds: one is to connect all the anode of light emitting diodes together, called common anode connection; another is to connect all the cathode of 7 light emitting diodes together, called common cathode connection. LED digital display has two ways: one is a static display, using the I/O interface circuit provided with latch, SCM sends the new font code while data needs to be updated; another is a dynamic scanning display, using a time division method to lighten every displayer one by one circularly [3]. The test device designed in the paper adopts dynamic scanning mode. LED digital display circuit is shown in Fig.2.

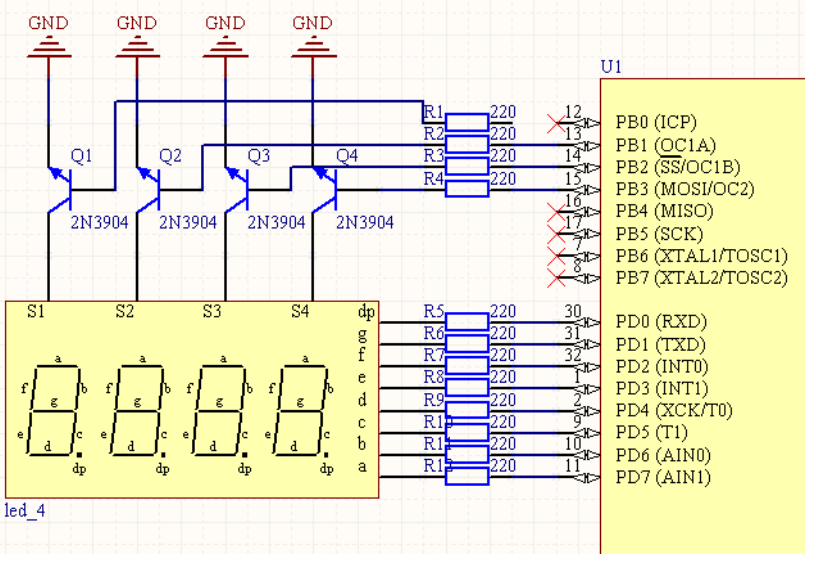

Fig. 2. The LED digital display circuit

3.3 Keyboard Module

According to different connection mode, Keyboard can be divided into non-matrix keyboard and matrix keyboard. The non-matrix keyboard has the advantages of simple structure and convenient to use, but occupies many I/O ports and applicable to the occasion which needs a fewer number of button; matrix keyboard programming is more complex, in order to reduce the system I/O occupancy, the matrix keyboard is generally used while the number of key needs more.

The test device for double-rate counter uses a matrix keyboard, is provided with the S1(start key), S2(stop key) and S3(set key), each key owns a I/O line alone, the working condition of the key connected to each I/O line does not affect the other I/O lines condition. Hardware circuit as shown in Fig.3, three resisters connected to the keyboard in series is to protect the SCM port pin.

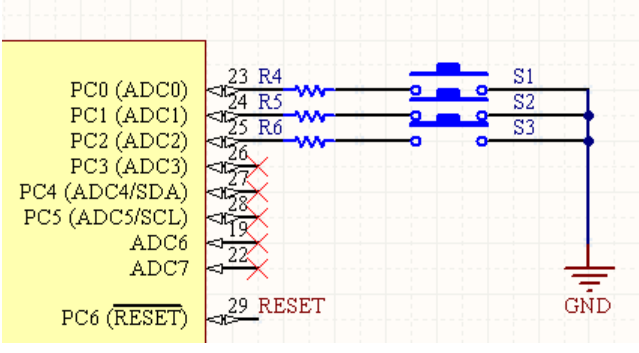

Fig. 3. The keyboard circuit

3.4 Power Supply Module

The test device for double-rate counter adopts stable DC power supply, which is converted from AC voltage. The task of single-phase small power DC power supply is to convert 50Hz, 220V single-phase AC voltage to a stable DC voltage (for example, several volts or tens of volts), at the same time can provide a certain output current (for example, from tens of mA to several A). Single-phase small power DC power supply is generally composed of power transformer, rectifier, filtering and voltage stabilizing circuit, totally 4 parts [4], and the composition diagram as shown in Fig.4.

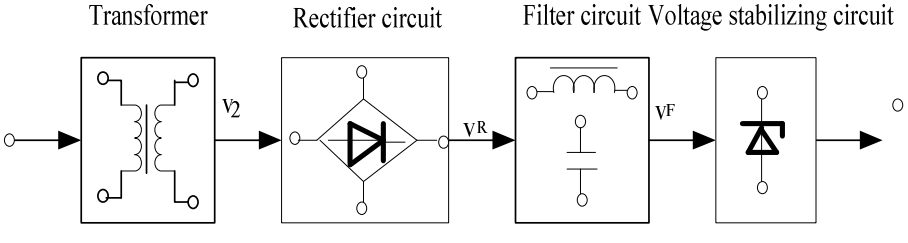

Fig. 4. The block diagram of single phase small power DC power supply

4 Software System

Software system uses C language to program; program design mainly adopts module structural idea to divide the whole program into several subroutines, which will be called in the main function [5], flow chart of the main program as shown in figure 5. When tested, at first the test device need to be set the number, then the counter is electrified, transmit pulse. When sending the number of pulse reaches the set value, the buzzer will remind the pulse has been finished to send out, and then read the display values of double-rate counter, and compare setting value with the display value, to judge if the double-rate counter is accurate.

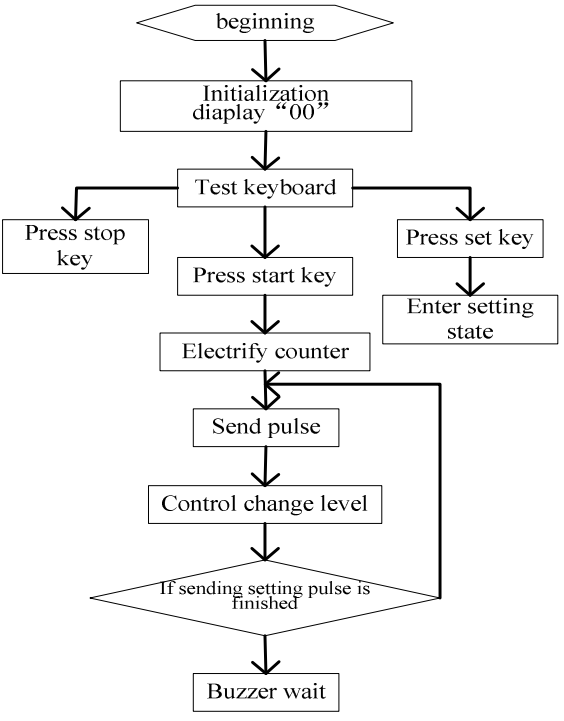

Fig. 5. The flow chart of the main program

5 Conclusion

Various counter products have been applied in modern life and industrial production, the device to test the counter accuracy is also more and more produced. The test device for double-rate counter based on ATmega8 single-chip microcomputer designed in the paper, provided with the corresponding hardware and software, to complete the counting accuracy test together. The results show that, the test device has reliable performance, simple circuit, and low cost, strong practicability.

References

1. Lv, X., Jiang, X., Duan, H.: Design of Multi-route Arbitrary Waveform Signal Generator Based on ATmega8. Applied Science and Technology 32(8), 23–25 (2005)
2. Ma, C., Zhan, W., Geng, D.: Atmega8 Principle & Application Handbook. Tsinghua University Press, Beijing (2003)
3. Li, S.: SCM LED display Interface Technology. Journal of Yangtze Staff University 20(4), 47–49 (2003)
4. Xie, Z.: Design, Experiment and Test of Electronic Circuit, 3rd edn. Huazhong University of Science and Technology Press, Wuhan (2006)
5. Shen, W., Zhan, W.: Introduction to C Language Development for AVR Single-chip Microcomputer. Tsinghua University Press, Beijing (2003)

Weapon Scheduling Method for Cooperative Air-Defense Operation

Liang Yu, Changfeng Xing, and Zhangsong Shi

Electronic Engineering College,
Naval University of Engineering,
Wuhan 430033,
China
falcon1980@sina.com

Abstract. By defining the weapon scheduling plan and weapon combat action, the mathematical formulation of weapon scheduling problem for cooperative air-defense operation is introduced. On the basis of discussing the primary constraints of weapon scheduling process, the regulation constraint model and resource constraint model are established. Then the evaluation criteria for weapon scheduling plan are analyzed. Finally, the weapon scheduling methods for single-target and multi-target are presented respectively by employing the definitions and models proposed in the paper.

Keywords: Cooperative air-defense operation, Weapon scheduling method, Combat action, Operational resource.

1 Introduction

As cooperative air-defense operations involve multiple various anti-air weapons installed in multiple geographically distributed tactical platforms, the air-defense coverage can be greatly extended and the operation flexibility can be enormously promoted. However, the complexity of weapon application in a cooperative air-defense operation is correspondingly increased. Exclusive problems of cooperative operations, such as overlapping trajectories, mutual weapon effects, and intersected platform routes, make it much more complicated to use weapons in a safe and effective way.

Weapon scheduling is a process of determining the specific action plans of the weapons on cooperative platforms. It's the key to appropriately apply weapons in cooperative operations. An operation with a proper weapon scheduling can not only avoid mutual weapon negative effects and eliminate operational resource conflicts, but also maximize weapon functional performance and generate systematic defense predominance. Therefore, the research on weapon scheduling methods for cooperative air-defense operations is very practical and significant.

D. Jin and S. Lin (Eds.): Advances in Mechanical and Electronic Engineering, LNEE 177, pp. 37–42.
springerlink.com

2 Mathematical Formation of Weapon Scheduling Problem

The core of weapon scheduling problem is to seek out the optimal (or a satisfactory) weapon scheduling plan (WSP), namely, to arrange a series of weapon combat actions achieving the integral air-defense operational effectiveness to the maximum (or a satisfactory level). Therefore, the weapon scheduling problem can be defined as: For a given function $f(x)$ representing the fleet integral air-defense operational effectiveness, to formulate a weapon scheduling plan P_0 subjecting to formula $f(P_0) \geq f(x)$ (or $f(P_0) \geq C_0$), where variable x is a valid weapon scheduling plan, constant C_0 is the operational effectiveness value of the referenced plan, and eligible plan P_0 can be called as the weapon scheduling solution.

2.1 Weapon Scheduling Plan

A WSP for cooperative air-defense operation is constituted by combat action sequence function (CASF) of each anti-air weapon unit. Assuming that n anti-air weapons are involved in an air-defense operation, a WSP $P(t)$ formulated by the battlefield situation at time t, can be expressed by a CASF set of the n weapons:

$$P(t) = \{\alpha_1(t), \alpha_2(t), \cdots, \alpha_n(t)\} \tag{1}$$

where $\alpha_i(t)$ is the CASF of the i th weapon ($i = 1,2,\cdots,n$).

Actually, the CASF $\alpha_i(t)$ is an ordered set of weapon combat actions, in which all the elements are ordered in time sequence. It can be expressed by:

$$\alpha_i(t) = \{A_1(t,i), A_2(t,i), \cdots, A_r(t,i)\} \tag{2}$$

where $A_j(t,i)$ is the j th combat action executed by the i th weapon ($j = 1,2,\cdots,r$).

The combat action $A_j(t,i)$ is a quaternion, which can be expressed by:

$$A_j(t,i) = \langle A_{TYPE}, T_k, t_s, t_d \rangle \tag{3}$$

where A_{TYPE} is type of the combat action, T_k is target of the combat action ($k = 1,2,\cdots,m$, k is target sequence number, m is total number of targets), t_s is starting time of the combat action, t_d is execution time of the combat action.

As all the anti-air weapons are known and their combat actions' average execution time $\bar{t}_d$ can be measured in advance, we can replace t_d with $\bar{t}_d$ in the equation above, namely, regard the period of a given weapon executing a given type of combat action as a constant. Then, combat action $A_j(t,i)$ can be simplified to a triple:

$$A_j(t,i) = \langle A_{TYPE}, T_k, t_s \rangle \tag{4}$$

2.2 Weapon Combat Actions

In terms of tactical procedures, typical anti-air weapon systems have many characteristics in common. For this reason, we can use a universal model to describe the behaviors of anti-air weapons in air-defense operations. Here, weapon operational behaviors are classified into three types of combat actions: firing preparation, firing initiation and firing retaining.

Firing preparation action refers to a series of tactical actions executed by an anti-air weapon from the moment when it acquires target information to the moment when it accomplishes all the preparation work before firing.

Firing initiation action refers to a series of tactical actions executed by an anti-air weapon from the moment when the "FIRE" button is pressed down to the moment when it shoots the first ammunition off the bore or launcher.

Firing retaining action refers to a series of tactical actions executed by an anti-air weapon during a continuous firing of a certain unit of ammunition. And when the quantity of ammunition consumed in a continuous firing is more than one unit, it can be considered as the firing retaining action having been executed for several times.

3 Constraints of Weapon Scheduling Process

In a cooperative air-defense operation, the application of anti-air weapons will be restricted by many factors, such as weapon technical performances, fleet combat regulations, weapon tactical compatibilities, and operational resource availabilities. Therefore, during the process of weapon scheduling, the influence of these constraints must be fully considered. A weapon scheduling plan can be a valid plan, only if the arrangement of all its combat actions is carried out under all these constraint conditions.

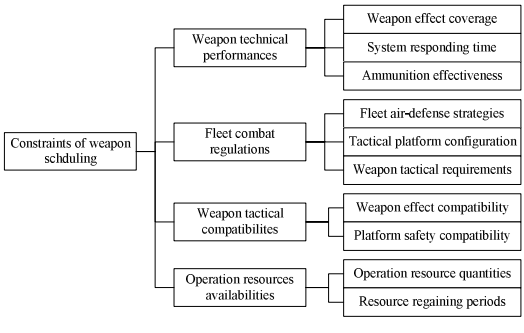

Fig. 1. The constraints of weapon scheduling process

As shown in Fig. 1, there are many different constraints affecting the weapon scheduling process. However, they can be generally divided into two types by the different mechanisms of production: the regulation constraint and the resource constraint.

The regulation constraint is a set of conditions constrained by action logical relations and tactical requirements. Assuming the combat actions of anti-air weapons

are $A_1, A_2, \cdots, A_n$ (n is a natural number), their corresponding action starting times are $t_1, t_2, \cdots, t_n$, and a regulation constraint is expressed by inequality $f(t_1, t_2, \cdots, t_n) \geq 0$. Then, when the values of $t_1, t_2, \cdots, t_n$ satisfy the inequality, all the combat actions can be executed; otherwise, it means there are one or more regulation conflicts among these combat actions, and none of them can be executed.

The resource constraint is a set of conditions constrained by operational resource limitations. Assuming the operational resource status at time t is $R(t)$, the request resource of combat action A is $R_A(t)$, and the resource constraint is expressed by equation $R_A(t) \cap R_A(t) = R_A(t)$. Then, when the equation is true, it means the request resource of combat action A can be obtained, and A can be executed at time t; otherwise, it means part of the request resource of A cannot be satisfied, and A cannot be executed at time t.

4 Evaluation of Weapon Scheduling Plan

Evaluation of weapon scheduling plan, as a critical procedure of solving weapon scheduling problems, is a process of ascertaining the qualities of valid plans and determining which plan can be chosen as the solution.

The evaluation criterion contains two important aspects: the air-defense combat capability and the operational resource consumption. Ordinarily, the fist aspect is the primary factor. More specifically, the higher the air-defense combat capability is, the better the plan is. When two plans have equivalent capability, the less the resource consumption is, the better the plan is.

As to the air-defense combat capability, it can also be divided into two parts: the active combat capability and the passive combat capability. The active combat capability indicates a WSP's ability of striking and intercepting targets, and the passive combat capability indicates a WSP's ability of jamming and deceiving targets. In other words, the active combat capability reflects the combat capability of hard-weapons, such as ship-to-air missile, naval gun, CIWS, and etc; the passive combat capability reflects the combat capability of soft-weapons, such as radar jamming, IR jamming, chaff, and etc.

In fact, the mathematical model of evaluation is the very air-defense operational effectiveness function $f(x)$ mentioned above.

5 Weapon Scheduling Method for Single-Target

The weapon scheduling method for single-target is a conditional ergodic process of searching valid WSP for single-target. The method, aiming at a single target, applies regulation constraints and resource constraints to builds all possible combination of weapon combat actions, and finally formulates valid WSPs.

The flow chart of weapon scheduling method for single-target is presented in the Fig. 2. (FRDT is short of the firing result determining time.)

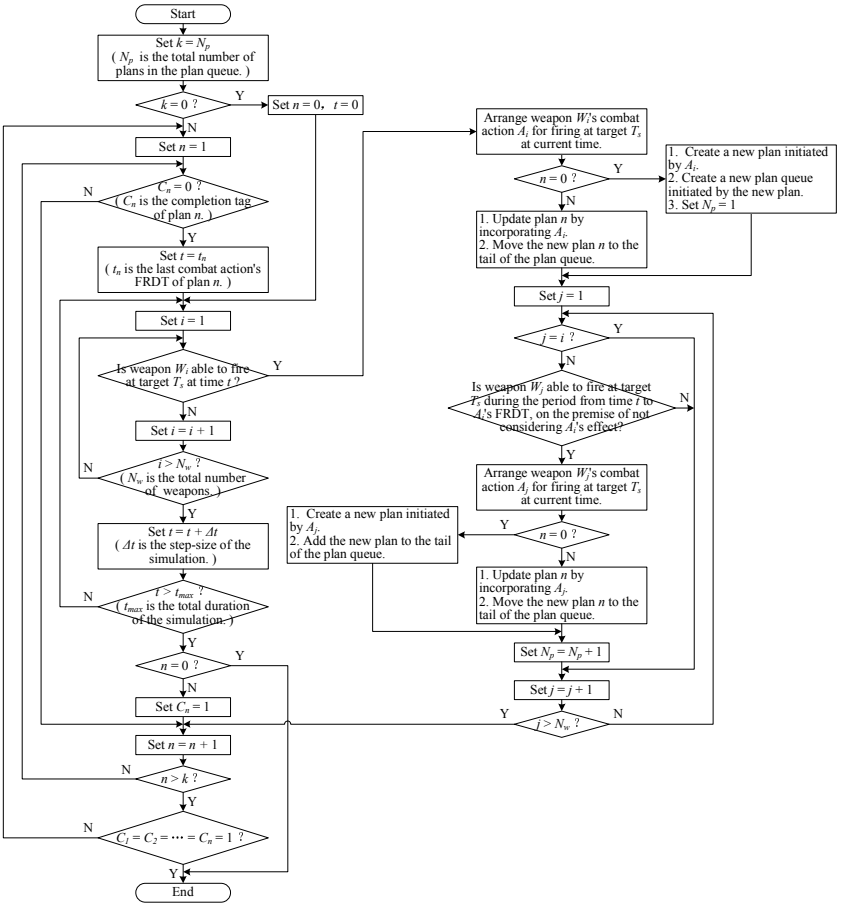

Fig. 2. The weapon scheduling method for single-target

6 Weapon Scheduling Method for Multi-Target

The weapon scheduling method for multi-target is based on the weapon scheduling method for single-target, which decomposes a multi-target problem into multiple single-target problems. The method completes weapon scheduling processes of each target in descending order of target threat level, and formulates the final solution by integrating these single-target plans.

The flow chart of weapon scheduling method for multi-target is presented in the Fig. 3.

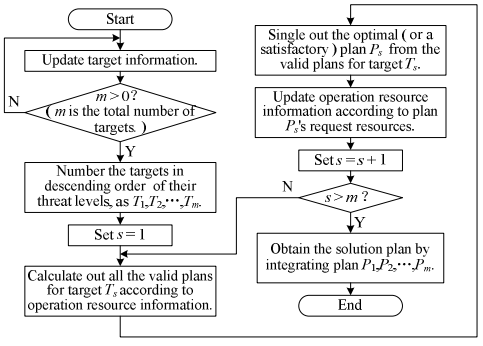

Fig. 3. The weapon scheduling method for multi-target

7 Conclusion

On the basis of defining the weapon scheduling problem, modeling the constraints of weapon scheduling process and analyzing the evaluation criterion of weapon scheduling plan, the weapon scheduling methods for single-target and multi-target are proposed in the paper. The proposed methods provide an effective way of solving the cooperative operation problem of multiple weapons, and the research approach can be use for reference to scheduling problems in other fields.

References

1. Yu, L., Xing, C.F., Shi, Z.S.: A Research on Modeling of the Weapon Scheduling Problem in Multi-platform Cooperative Air-Defense Operations. In: 4th International Workshop on Advanced Computational Intelligence, pp. 783–787. IEEE Press, Wuhan (2011)
2. Ghallab, M., Nau, D., Traverso, P.: Automatic Planning: Theory and Practice. Tsinghua University Press, Beijing (2008)
3. Maheswaran, R.T., Tambe, M., Bowring, E.: Taking DCOP to the Real World: Efficient Complete Solutions for Distributed Multi-Event Scheduling. In: 3rd International Joint Conference on Autonomous Agents and Multiagent Systems, pp. 310–317. IEEE Press, New York (2004)
4. Gintner, V., Kliewer, N., Suhl, L.: Solving Large Multiple-Depot Multiple-Vehicle-Type Bus Scheduling Problem in Practice. OR Spectrum 27, 507–523 (2005)
5. Sultanik, E.A., Modi, P.J., Regli, W.C.: On Modeling Multiagent Task Scheduling as a Distributed Constraint Optimization Problem. In: 20th International Joint Conference on Artificial Intelligence, pp. 1531–1536. AAAI Press, Hyderabad (2007)
6. Wu, L.: A Research on Real-Time Intelligence Algorithms for Dynamic Weapon Target Allocation. Tsinghua University Press, Beijing (2008)

Online Monitoring System for Fault Diagnostics of High-Pressure Piston Diaphragm Pump Based on Acoustic Emission

Yu Gong[1], Weidong Geng[1], Li Zhang[2], Chunlei Pan[3], and Xiaodong Wang[4]

[1] Productivity Promotion Center of Kunming, Kunming, 650000, China
[2] Yunnan Academy of Scientific and Technical Information, Kunming, 650051, China
[3] Yunnan Da Hong Shan Pipeline Co., Ltd., Kunming, 650302, China
[4] Faculty of Information Engineering and Automation, Kunming University of Science and Technology, Kunming, 650500, China
gy@kmtm.org.cn

Abstract. The high-pressure piston diaphragm is the croe of slurry pipeline implementing agencies ,need to focus on monitoring and maintenance. Because of its working conditions is extremely complex, the common means of detection can't get the fault information. Based on the acoustic emission technique, sound signals, indirect monitoring of diaphragm pumps. This paper presents an on-line monitoring idea, which is a fault diagnosis of the high-pressure piston diaphragm pump based on acoustic emission. It is technically feasible, and has the considerable propagableness.

Keywords: Acoustic emission, High-pressure piston diaphragm pump, Fault diagnosis, On-line monitoring system.

1 Introduction

Dahongshan pipeline is the present domestic the longest, control technology, the most complicated terrain of iron concentrate pipeline. It's from the Dahongshan mining area to the KunSteel plant needs across the mountains, large U-shaped terrain, through the tunnels and pipelines length is 171km;the slurry was sent to the height difference is 1520m, which is the largest in the international arena. Thus the slurry transportation pressure has reached the highest in the 24.44Mpa in the international. All these require technology and management of the pipeline transportation to achieve new and higher requirements. According to the characteristics of the Dahongshan iron concentrate pipeline, in order to ensure the slurry pipeline safety, smooth, economy and environmental protection runs to the new faulty equipment management information system has become particularly important. According to the characteristics of the Dahongshan iron concentrate pipeline, in order to ensure the slurry pipeline safety, smooth, economical, environmentally friendly to run, which research the new faulty equipment management information system has become particularly important[1,2].

D. Jin and S. Lin (Eds.): Advances in Mechanical and Electronic Engineering, LNEE 177, pp. 43–46.
springerlink.com

High pressure piston diaphragm pump is the driving force of slurry transportation, timely diagnosis fault is very important; in order to improve the reliability of its use, reduce downtime brings direct and indirect economic loss. At present, in China the solid materials in the pipeline industry is still in its infancy, and fault diagnosis of whose power source - the high-pressure piston diaphragm pumps is still in the exploratory stage. Among them, the focus of the piston pump fault detection is valves and diaphragm, of whose tightness is an important performance indexes, system security and economy of the equipment has a very large influence. Leakage of the valve and diaphragm are often the major accident risks, but also a waste of resources and environmental pollution. Enterprises in the past common practice is regularly big overhaul, each valve diaphragm demolition, repair, due to lack of specificity, this approach is not scientific. According to statistics, in fact, only less than 50% of the valves and diaphragm need to be demolished repairs would have resulted in a waste of human, financial and material resources in the demolition of the repair process may cause some artificial damage. Therefore, to carry out research in this area which health monitoring and fault diagnosis of the high-pressure piston diaphragm pump has important theoretical and practical significance [3].

This paper using acoustic emission technique for fault detection of the piston pump, acoustic emission technology in the online detection of the piston pump main advantages: no effect of the valve and diaphragm integrity without dismantling ,the layout of the high sensitivity of the sensor in the valve body external, determine valve diaphragm for leaks; detection, does not affect the normal production; the results intuitive, direct quantitative measure valve leakage; close to not ask for much of the check valves and diaphragm can be used for difficult or not detected close to the environment, such as the environment of the high and low temperature, nuclear radiation, flammable, explosive or toxic, etc.; to ensure the safe operation of equipment, reducing environmental pollution and reduce the cost of inspection and maintenance[4].

2 The Overall Design of the System

Acoustic emission is the high frequency stress wave signal of the fault structure, not easy by the surrounding environment noise interference, so acoustic emission detection method has been more and more applications in fault diagnosis.

2.1 The Principle of Acoustic Emission Detection Technology

Acoustic emission source is divided into two categories: directly related to the deformation and fracture mechanisms under stress elastic wave emission source of acoustic emission source in the usual sense; fluid leakage, friction, impact, burning no direct relation with the deformation and fracture mechanisms the elastic wave emission source is called the secondary acoustic emission source, valves and diaphragm leakage belongs to the secondary acoustic emission source.

The acoustic emission signals, including the burst type and continuous type. Burst-type acoustic emission signals from the pulse different from the background noise, and can be separated in time; a single pulse of continuous acoustic emission signals

can't be distinguished. In fact, the continuous acoustic emission signal by the large number of small burst signal, but too dense and can't distinguish .At present, the acoustic emission signal analysis methods including parametric analysis and waveform analysis.

2.2 The Hardware Structure of Acoustic Emission System

Acoustic emission system is made up of parallel detection channel. Each channel consists of similar measurement component, digital signal measurement handling procedures and calculator program, namely the powerful computer, matched again with complete peripheral parts. Here every channel referred measuring components including acoustic emission sensors, the preamplifier and acquisition card, shown in figure 1.

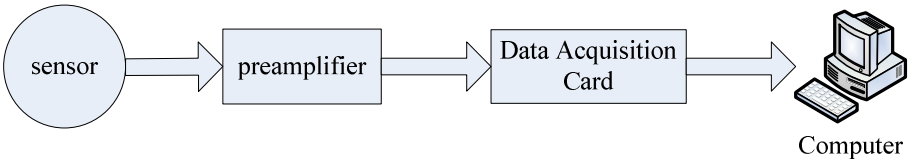

Fig. 1. The basic composition of acoustic emission system

The core technology is acoustic emission system based on PCI special data acquisition card. Acoustic emission acquisition card attached to the computer through the PCI bus, share a chassis with the computer system, and provide electricity through the computer power supply, matched to the basic sensor and preamplifier, and then formed the PCI acoustic emission system. The key point is the acquisition card inserted directly in the PCI slots, connected with computer through the PCI bus; and it saves the hardware cost, because of power supplied by the computer system, high integration and simple structure.

3 The Principles for the System Design

In system design, in a pragmatic manner, and strive in the investment capacity to advanced technology, and considering the future cost of operation management system, data security and reliability at the same time, as well as to the future of the system extension adaptability.

The design should follow the principles:

1) The principle of progressiveness

Taking the future development into account, to avoid the waste of the investment, the system do not use products and technologies, which has been eliminated; and to achieve the advanced level of the domestic industry in the design.

2) The principle of economy

The scheme design should take full account of the system development costs and the operation of the system management fees in the future. In the design phase, data

processing, the transmission way and storage to be thorough analysis, carefully arranged and carefully calculated, it will lay a good foundation for saving costs.

3) The principle of practicality

Only practical system can bring convenience、fast and can be accepted by users. In the design, not blindly pursuing high、large, and full, but striving to simple、convenient and effective operation.

4) The principle of security

The design will take full account of the various levels of security needs, and take strong safety precautions.

5) The principle of adaptability

The necessary method should be used in the technology, make the system adapt to the needs of different changing environmental, and establish a set of parameters system that can be adjusted.

6) The principle of scalability

To connect conveniently with other systems in the future, the system should stay enough and sufficient interface.

4 Conclusions

The pipeline has become one of the important modes of transport of iron ore concentrate. The high-pressure piston diaphragm pump is the core of the pipeline transportation, and needed focus on monitoring and maintenance. Taking the advantage of the acoustic emission technique, indirectly monitor of the diaphragm. This paper gives the fault diagnosis method based on acoustic emission signals. The method is feasible, and has better popularization.

References

1. Wu, J., Wang, H., Fan, Y., Wang, X.: Intelligent Plant Design of Complex Landform Long Distance Pipeline Transport of Iron concentrate. Applied Mechanics and Materials 48, 632–636 (2011)
2. Zhenyu, J., Wu, J.: Design of Pipeline Displacement Detection System based on MEMS accelerometer. Sensor and Micro System 31(1), 140–142 (2012)
3. Pu, G., Wu, J., An, J., et al.: The Design and Application of the Ore Pulp Water Treatment in Pipeline Transport of Refined Iron Ore. In: The 3rd International Symposium on Knowledge Acquisition and Modeling, pp. 192–195 (2010)
4. An, J., Wu, J., Pu, G., et al.: A Kind of Pressure Detection Method in Long Distance Ore Slurry Pipeline. In: The 3rd International Symposium on Knowledge Acquisition and Modeling, pp. 196–198 (2010)

Surface Profile Evaluation and Redesign Method for Reverse Engineering

Zheng Liu and Bo Sun

School of Mechatronic Engineering,
Xi'an Technological University,
Xi'an China
zheng.liumail@gmail.com
sunbomm@163.com

Abstract. Based on OpenGL technology, the 3D surface evaluation and redesign system is constructed. Above all, the compensating procedure for the radius of probe ball is performed with the data from coordinate measuring machine. The B-spline surfaces are reconstructed with the pretreated point array. After establishing the mathematical model of profile error evaluation, the OpenGL-based 3D evaluating environment is developed. In addition, the evaluating process is real-time controlled and displayed. It is more intuitive and convenient to show the results with combination of data report and 3D model. It makes benefits to improve the flexibility and intuitive of the reverse engineering system.

Keywords: Surface profile, OpenGL, Surface reconstruction, Knot control.

1 Introduction

Many CAD systems are developed to support the inverse engineering. The data processing and model optimization are important sections. Especially for free form surface, the profile error evaluation and 3D design environment development take up a significant position in these systems. For reverse engineering, to digitize the surface profile, the measurement data must be evaluated and treated to support the following optimal design procedure. The coordinate measuring machine is the most widely used contact measurement equipment, which acquire the signal by moving the probe along with the surface and translate the point coordinate into computer through the sensors for the following analysis [1].

A key point is the method dealing with point cloud data to reconstruct the surface model and regulate the parameters of the model. Among the data processing procedure, the profile evaluation of freeform surface is a very important section. If the coordinate system is not uniform to result in systematic error, the free-form surface matching method is used to eliminate the error [2]. The profile evaluation involves many aspects including the algorithm to calculate point-to-surface distance [3], surface matching method [4] and the optimization of evaluating method [5,6]. Currently, most evaluating system is affiliated with the commercial equipment as auxiliary software. Such fixed system may not meet the specific requirements of

D. Jin and S. Lin (Eds.): Advances in Mechanical and Electronic Engineering, LNEE 177, pp. 47–51.
springerlink.com

users. Especially for free surface, the measurement is more complex than other features [7]. Problem on finding the effective way to combine the result with the 3D environment is still need for further study. The cubic B-spline is used to reconstruct the surface, which has good attributes to fit and adjust [8]. Instead of secondary development method of commercial system, OpenGL is adopted to construct the 3D environment to provide a more flexible system [9]. The whole evaluating system involves many modules. This paper emphasizes on the profile evaluation that is the key point of data treatment aspect.

2 The Framework of the System

The profile evaluating system realizes the surface fitting, normal vector calculation of points and profile evaluation in 3D environment to improve the efficiency and intuitiveness. The system is mainly composed of six modules as shown in Figure 1.

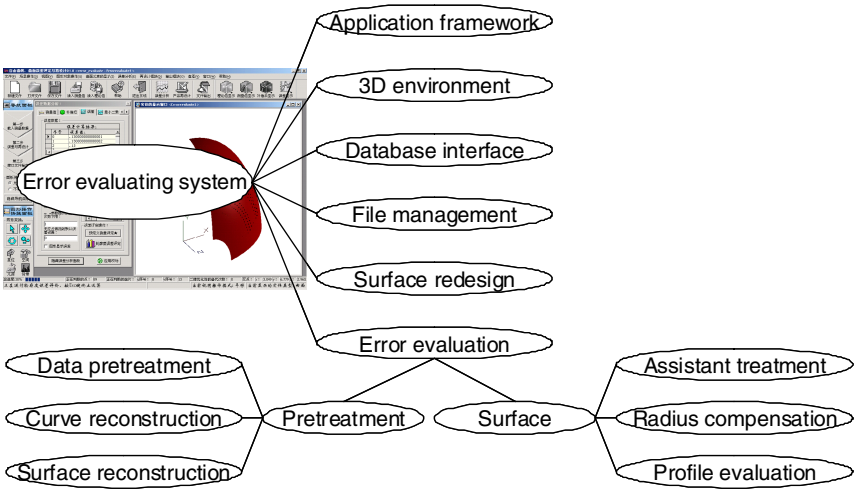

Fig. 1. Framework of the system

The application framework deals with relationship between documents and views as well as the conversion of system files to internal data structures. The system uses the mechanism of multi-document multi-view, which permits observing the same model from different viewpoints. The 3D environment is developed based on OpenGL technology. The navigating panel is provided to give the user a navigating guide.

The error evaluation module involves two parts of the pretreatment and freeform surface. The pretreatment part deals with the reading of the lattice information and converting them. The control points of the surface are calculated. The surface module consists of the assistant treatment, radius compensation and profile evaluation. It also involves the matrix calculation, optimizing calculation, tangent vector calculation and normal vector calculation. The surface redesign module provides the function of

adjusting the shape of curve and surface based on the control points. In order to exchange information with commercial CAD systems, the system provides the STEP format file exchange interface.

3 OpenGL Based 3D Environment Construction

The 3D scene operating module involves the view settings, clip space, background settings, light settings and graphics transform operations. The solid display module deals with the display of point, freeform curve and freeform surface object. The procedure is shown in Figure 2.

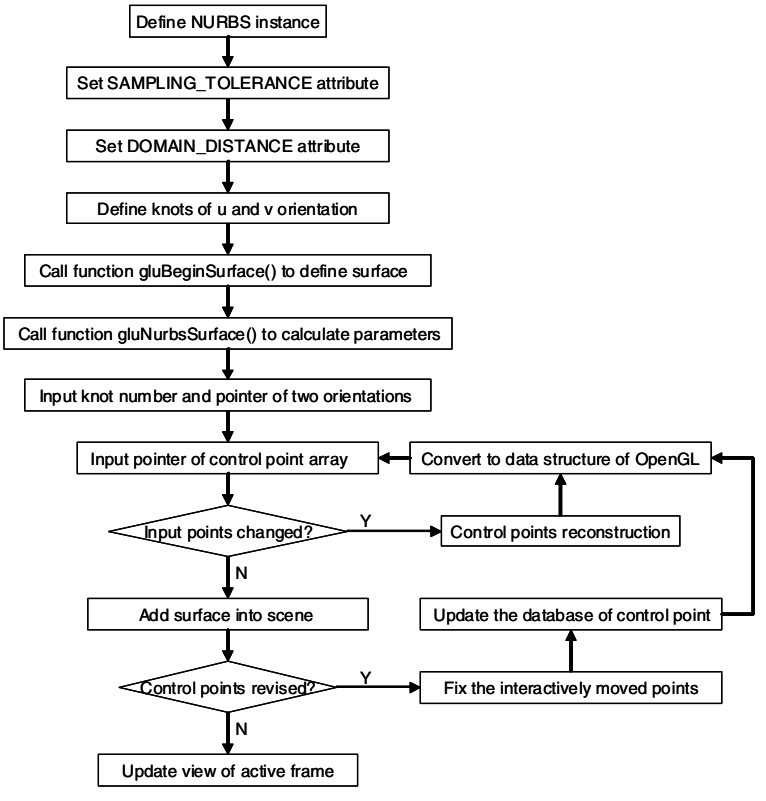

Fig. 2. The procedure of 3D model construction

Firstly, the NRUBS object is declared with the pointer of GLUnurbsObj. Then, the properties are set. After the definition of the nodes, the surface is defined with parameters such as the array of knot in two directions, the order in two directions and the control points array.

4 Surface Profile Evaluation and Redesign

The surface evaluation is the basis of shape redesign procedure. After the radius compensation and surface reconstruction, the profile evaluating procedure is performed. With the evaluating result, the corresponding control points are fixed, which provide the foundation for the adjusting perform.

4.1 The Main Procedure of Evaluation

The main procedure of evaluation is as follows:

- The coordinates of the probe center are measured.
- The probe center surface is fitted with dual cubic B-spline surface.
- The normal vector of points is calculated.
- The radius of the probe is compensated.
- The surface is reconstructed with the real contacted points.
- The theoretical surface is reconstructed.
- The profile of freeform surface is evaluated.

4.2 The Radius Compensation

Because the probe of coordinate measuring machine is spherical, the actual measured data is the coordinates of the probe center. The desired data is the contact point of the probe with the measured surface. Therefore, the trajectory of the probe center should be converted into that of the contact points. These two surfaces are offset surface. The normal vector is calculated as follows.

$$\vec{N}_{(i,j)} = \frac{\vec{P}^{u}_{(i,j)} \times \vec{P}^{v}_{(i,j)}}{\left| \vec{P}^{u}_{(i,j)} \times \vec{P}^{v}_{(i,j)} \right|} \tag{1}$$

The direction of the vector is the compensating direction. The compensating relationship is as follows.

$$\vec{P}_{(i,j)} = \vec{P}*_{(i,j)} \pm r\vec{N}_{(i,j)} \tag{2}$$

The positive sign means the compensating direction is the same with the vector. Whereas, the negative sign means the probe is along the inside part of surface. For the convenient 3D display of the vector, the compensating direction is intuitive to determine.

4.3 Control Points Based Surface Profile Design

The evaluating operations are integrated within one property sheet that involves six single property pages. Each property page corresponding to a kind of functions involving the theoretical data, measured data, compensation data, error evaluation, least square method and the adjusting of control point. The profile evaluation is presented with both report form and 3D form. After the profile analysis, the attractive points can be located on the property page and highlighted on the 3D surface model. By dragging the corresponding control point, the profile of the surface is evolved.

5 Conclusion

In this paper, method for evaluating surface profile and according 3D result report system is explored and proposed. Compared with the traditional calculating procedure, the parameter judgment based optimal method for point-to-surface distance is presented to improve the efficiency. The three-dimensional surface profile evaluating environment, which is more intuitive to show the result, combines the data report with the 3D model. Moreover, it makes exploration for the 3D evaluating system of reverse engineering. Future work will be emphasized on the comprehensive evaluating method to expand the application scope of the system.

Acknowledgments. This work was financially supported by the Science and Technology Development Plan Foundation of Shaanxi Province (No. 2011K07-11), Scientific Research Program Funded by Shaanxi Provincial Education Department (Program No. 11JK0864), President Fund of Xi'an Technological University (No. XAGDXJJ1007) and Shaanxi Major Subject Construction Project.

References

1. Li, D., Cui, Y.: Application of coordinate measuring machine in reverse engineering. Machinery Design & Manufacture 7, 72–74 (2007)
2. Gao, D., Kong, L., Yao, X., Du, X.: An algorithm for evaluating form errors of optical freeform surfaces. Journal of Harbin Institute of Technology 38, 1630–1632 (2006)
3. Dai, N., Liao, P., Wang, J., Liu, X.: Calculating of Complex Surface Form Error Based on Matlab. Measurement & Control Technocgy 29, 95–101 (2010)
4. Yu, Y., Lu, J., Wang, X.: Modeling and Analysis of the Best Match in Free-form Surface Measuring. Mechanical Science and Technology for Aerospace Engineering 20, 19–20 (2001)
5. Yang, H., Tu, D., Wu, R., Huang, Z.: A Method for Evaluating Complicated Conicoid Profile Error. Mechanical Science and Technology for Aerospace Engineering 27, 1155–1158 (2008)
6. Yang, H., Tu, D., Wu, R., Huang, Z.: Detection of profile error of ship hull plate processing surface. Journal of Harbin Engineering University 27, 635–638 (2006)
7. Li, Y., Gu, P.: Free-form surface inspection techniques state of the art review. Computer-Aided Design 36, 1395–1417 (2004)
8. Chen, X., Ma, W., Paul, J.: Cubic B-spline curve approximation by curve unclamping. Computer-Aided Design 24, 523–534 (2010)
9. Bourdot, P., Convard, T., Picon, F.: VR-CAD integration: Multimodal immersive interaction and advanced haptic paradigms for implicit edition of CAD models. Computer-Aided Design 42, 445–461 (2010)

Computational Tool for the Efficiency Forecasting of Grid-Connected Photovoltaic Systems

Javier Saumell-Ocáriz[1], Rodolfo Dufo-López[1],
Ismael Aso[2], and José L. Bernal-Agustín[1]

[1] Department of Electrical Engineering, University of Zaragoza,
Zaragoza, 50018, Spain
[2] National Centre on Hydrogen and Fuel Cell Technology Experimentation,
Puertollano, 13500, Spain
javiersaumell@gmail.com, {rdufo,jlbernal}@unizar.es,
ismael.aso@cnethpc.es

Abstract. In this paper, the factors affecting the electric production of grid-connected photovoltaic systems are reviewed. Not only are the main parameters considered but also the minor ones, which altogether might create important variations in the final results. The theoretical base of each element has been utilized to develop a computer tool called PVEF. Using time series historical data of many weather stations and some other parameters that are specific from each location or technology, PVEF forecasts the production and efficiency of a grid-connected installation. The results show that the efficiency of an installation can be predicted with a very high accuracy if the input parameters are known with a high or medium precision.

Keywords: Photovoltaic Energy, Efficiency Forecasting.

1 Introduction

Medium and long-term photovoltaic power prediction is important for the appropriate planning of a photovoltaic installation. However, due to the great number of factors affecting the final value of production, it is very difficult to make an accurate forecasting. Meral and Dinçer [1] talk about materials band gap as the main barrier in making the most of solar energy. They also mention the temperature effect as well as system equipments and dirt. In her thesis, Caamaño [2] adds the tilt angle and shading as important factors affecting cell efficiency. A research made by the Electronic Enginery Department of the Jaen University [3] states that there are other sources of power losses, such as mismatch or low irradiance. There are many studies specialized in each single element – and even of all the main ones – but it is hard to find an article explaining the whole, and none of the more extended computer tools takes all of them into account.

This paper shows all factors, and the developed tool PVEF takes all of them into account to make fine predictions of power production and efficiency that a PV power station is going to provide. The results show that it is possible to make good forecasts of the future production of a photovoltaic station.

D. Jin and S. Lin (Eds.): Advances in Mechanical and Electronic Engineering, LNEE 177, pp. 53–59.
springerlink.com

2 Factors Affecting Production and Efficiency

2.1 Materials

Each material has a wide rank of possible efficiencies [1] [4], depending on the way they have been manufactured, their crystalline structure, etc. The silicon is the most popular and widely extended material due to its relatively low price and good properties. However, its average efficiency is around 15%. Much higher efficiencies can be achieved by combining the band gap of different materials.

2.2 Temperature

The temperature of a PV cell affects directly to the amount of energy it generates.

The mathematical formulation that allows calculating the temperature efficiency of a PV cell [3] is:

$$T_{cell} = T_{air} + \frac{G_{total}}{800}(NOCT - 20) \tag{1}$$

$$\eta_{temp} = 1 - \gamma(T_{cell} - 25) \tag{2}$$

Where G_{total} is the total hourly irradiance in W/m^2; T_{cell} is the cell temperature in ºC; T_{air} is the air temperature in ºC; NOCT is the *Nominal Operating Cell Temperature* in ºC, η_{temp} is the cell temperature efficiency, taking the standard conditions as a reference; and γ is the power temperature coefficient in absolute value. The *NOCT* is the value the cell would reach with an irradiance of 800 W/m^2 and 20ºC of air temperature.

2.3 Tilt Angle

Every component of the solar irradiance over a PV panel strongly depends on the angles, as shown in the formulas 3-5 [5-6].

$$G_{direct,total} = G_{direct,horizontal}\frac{\max[0,\cos\theta_s]}{\sin\gamma} \tag{3}$$

$$G_{diffuse,total} = G_{diffuse,horizontal}\left((1-K_2)\frac{1+\cos\beta}{2} + K_2\frac{\max(0,\cos\theta_s)}{\sin\gamma}\right) \tag{4}$$

$$G_{reflected,total} = G_{global,horizontal}\cdot\rho_{albedo}\frac{1-\cos(\beta)}{2} \tag{5}$$

Where G is the irradiance in W/m^2; θ_s is the incidence angle of the sun; γ is the sun height angle; K_2 is the anisotropic index of the Hay and Davies method; β is the panel inclination angle; and ρ_{albedo} is the ground reflectivity coefficient. The incidence angle θ_s depends on both panel tilt angles, as well as on the solar angles.

The higher irradiance over the cells, the more power they produce, although there is also more temperature loss. An improvement in the final generated power can be achieved by installing a sun-tracking system in one or both axis.

2.4 Dirt and Dust

According to research by the Hong Kong Polytechnic University [7], the relationship between the dust layer density and the power losses is linear and independent of the cell material. They state that 22 g/m^2 lead to a 26% efficiency decrease. Mani [8] says that a daily cleaning of the panels would delete this source of power losses. Therefore, the resulting formula for dirt efficiency is:

$$\eta_{dirt} = x_{dust} \cdot \frac{26}{22} \tag{6}$$

Where η_{dirt} is the dirt efficiency in %; and x_{dust} is the amount of dust over the panel surface in /m^2.

As the results are calculated with hourly values, the increase of the dust amount in time has been considered as linear, as the program uses only the final value and the cleaning frequency.

2.5 Electric Losses

Power losses in the wires will be determined not only by their length and width but also by the amount of current through them. The disposition of the panels in series and parallel groups will also have influence in the lost energy due to this concept. The series stretch can be as long as necessary because the current running through it is the same that generates a single cell, and the resulting losses will be very small. In contrast, the parallel stretch length should be minimized because all the current will go through it. These losses can be calculated by first obtaining the wire resistance and then multiplying it by the current in the wire. This current must be calculated hourly because it varies with the sun's irradiance. The way of doing this (approximately) is by simply dividing the hourly power by the voltage in the maximum power point, which is similar to the one in normal working.

Electric losses also include the ones caused by electric devices, mainly by the inverter.

2.6 Degradation

A PV cell does not always generate the same power. As the years pass, the material gradually loses its properties. At the end of its useful life, the material degradation is the most important source of power losses.

2.7 Other Losses

Shading. An accurate study of this phenomenon requires a shadow contour of the place [2], and the decrease in efficiency due to this factor does not usually go over 5% [3].

Mismatch. A little difference between a group of panels connected in series or parallel leads to a limitation in the output power [9]. This factor can lead to losses up to 4% [3].

Low Irradiance. The irradiance over a surface changes from one year to another. This might cause differences in the global efficiency of a PV station, although these differences are not usually greater than 3% at the end of the year [3].

3 Results

The developed program PVEF has been used to calculate the efficiency and production of a PV power station in Larrés (Aragón, Spain). The real data of power generation in this installation are shown in Tables 1 and 2. The real results have been calculated using the irradiance and power data in Table 1 along with some of the station parameters. With the data in Table 2, PVEF has calculated the production and efficiency. The real efficiency of the installation is 11.88%, while the value given by the program rises to 11.79%. Comparing both, there's a difference of only 0.76% between the real result and the predicted one. This means that the efficiency of a PV power station can be predicted with a very high accuracy if the installation data are adequately obtained.

Table 1. Power and irradiance data of the Larrés station

Month	Irradiance (W/m2)	Power (W)
January	190.53	20950.38
February	247.98	27555.9
March	355.52	39821.67
April	343.11	39348.16
May	315.26	38802.74
June	305.09	38710.88
July	379.09	47919.12
August	436.78	49908.47
September	356.92	39600.23
October	294.38	34290.73
November	285.84	31187.16
December	270.92	31162.5

Table 2. Panel *Atersa A-180P* and station properties

Power Station Properties	
Maximum Power	180 W
Voltage in the max. power point	35.52 V
Efficiency	13.67 %
Voltage Temp. Coefficient	-0.32 %/ºC
Power Temp. Coefficient	-0.43%/ºC
Surface	1,63 m^2
Material	Polycrystalline silicon
Wire diameter series/parallel	2.26 mm/3.57 mm
NOCT	47±2 ºC
Number of panels	600 W
Cleaning frequency	Every 7 days
Dirt level reached	7 g/m^2
Series panels	30
Stretch length series/parallel	800 m/40 m
Inverter efficiency	98%
Mismatch losses	1 %
Tracking	2-axis

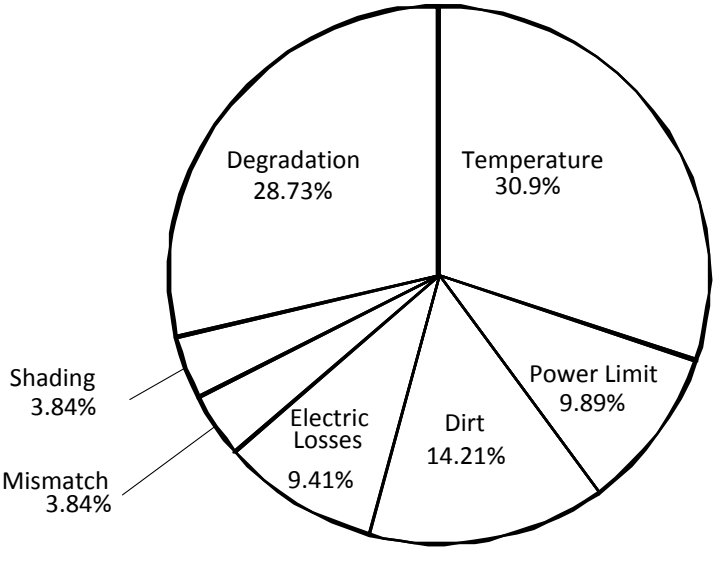

Fig. 1. Losses distribution in the Larrés station

As for the production, the error is much higher, being the predicted value at 17.8% lower than the real one. The problem in this case has been that the irradiance data used by the program corresponds to the three meteorological stations that are closest to Larrés. As the distance between the locations is big, so is the error.

The tool also allows comparing the percentage that represents each source of losses from the whole, by representing in a circle plot the fraction corresponding to each factor, as seen in Figure 1.

4 Conclusion

In this paper, the parameters that affect the efficiency and power provided by a PV power station have been carefully reviewed. Material band gap, temperature, tilt angle, dirt, and degradation are the main sources of a decrease in power output, although there are other factors such as electric losses, shading, mismatch, and low irradiance, which can also be important causes of decrease in output. All these parameters have been introduced in PVEF, a program that calculates the production and efficiency of a PV station. The program has been used to predict the production and efficiency of a real power station, obtaining an efficiency result that digresses from the real one only by 0.76%. The difference between the power generation forecast and the real results has been greater, due mainly to low availability of solar irradiance data. The results show that it is possible to forecast performance of a photovoltaic installation with great accuracy, provided that the best irradiance data are available. A greater database might already reduce the error in power prediction to values below 5%.

Acknowledgements. This work was supported by the "Ministerio de Ciencia e Innovación" of the Spanish Government, under Project ENE2009-14582-C02-01.

References

1. Meral, M.E., et al.: A Review of the Factors Affecting Operation and Efficiency of Photovoltaic-Based Electricity Generation Systems. Renewable and Sustainable Energy Reviews 15, 2176–2184 (2011), doi:10.1016/j.rser.2011.01.010
2. Caamaño Martín, S.: Estefanía, Edificios Fotovoltaicos conectados a la Red Eléctrica: Caracterización y Análisis (PV Buildings Connected to the Electric Grid: Characterization and Analysis). Thesis. Madrid Polytechnic University (March 1998)
3. Almonacid, F., et al.: Calculation of the Energy Provided by a PV Generator. Comparative Study: Conventional Methods vs. Artificial Neural Networks. Energy 36, 375–384 (2011), doi:10.1016/j.energy.2010.10.028
4. El Chaar, L., et al.: Review of Photovoltaic Technologies. Renewable and Sustainable Energy Reviews 15, 2165–2175 (2011), doi:10.1016/j.rser.2011.01.004
5. Dufo-López, R.: Dimensionado y control óptimos de sistemas híbridos aplicando Algoritmos Evolutivos (Sizing and Optimal Control of Hybrid Systems Using Evolutionary Algorithms). Doctoral thesis. Zaragoza University (2007)

6. Quaschning, V., Hanitsch, R.: Irradiance Calculation on Shaded Surfaces. Berlin University of Technology, Institute of Electrical Power Engineering, Renewable Energy Section, Secr. EM 4, Einsteinufer 11, D-10587 Berlin, Germany (August. 1997)
7. Jiang, H., et al.: Experimental Investigation of the Impact of Airborne Dust Deposition on the Performance of Solar Photovoltaic (PV) Modules. Atmospheric Environment 45(25), 4299–4304 (2011), doi:10.1016/j.atmosenv.2011.04.084
8. Mani, M., et al.: Impact of Dust on Solar Photovoltaic (PV) Performance: Research Status, Challenges and Recommendations. Renewable and Sustainable Energy Reviews 14, 3124–3131 (2010), doi:10.1016/j.rser.2010.07.065
9. Kaushika, N.D., Rai, A.K.: An Investigation of Mismatch Losses in Solar Photovoltaic Cell Networks. Energy 32(5), 755–759 (2007), doi:10.1016/j.energy.2006.06.017

Stepping Motor Control Device Design in Fiber Positioning System

Xuepeng Liu and Dongmei Zhao

Zhongshan Polytechnic, P.R. China
liuxuepeng1026@yahoo.com.cn, zdmeihn@163.com

Abstract. Positioning stepping motor control device in LAMOST fiber positioning system is studied. Single-chip microcomputer system I/O scheme of the stepping motor control device and interface circuit design and all kinds of motion control and serial communication module of software design is analyzed. The multiple motor driver circuit under Double power mode is designed. The circuit and driving motor are tested.

Keywords: LAMOST, fiber positioning system, I/O, Double power mode.

1 Introduction

In LAMOST fiber positioning system, to find the star in the accuracy and reliability is undoubtedly an important index, and the system is reliable and accurate, the premise is the star search positioning unit to the stable, reliable working.

So many of the optical fiber, how to accurately and reliably complete their orientation, so it can achieve and observation 4000 star request, is the whole project in the difficulty. Many stepping motor parallel control device for controllable optical fiber positioning unit system, it is very important to the quality of the design, safe, reliable and effective can, high speed work, will directly related to the success or failure of LAMOST project, so we must carry on the research.

This article mainly on SCM control principle, software and hardware design of parallel; Stepping motor driver control circuit of the double power, and many road work in the way of the circuit board design; drive For main controlling computer instruction under the control of the control device driver motor testing[1-4].

2 I/O Design

The whole device control amplifier circuit can be divided into two parts. Among them was a single chip board, this a piece of a communication module and single chip microcomputer, including minimum model system some used for I/O control, choose the pulse output and back to zero signal input chips; Part of it is five pieces of drive circuit boards, each pulse and back to zero on signal of I/O chip, 0, 1 logic will signals into 1, 1 logic signals before the class amplifier, and can drive the four units were eight step motor power amplifier circuit. Between two parts will be connected to a power line, ground, address/data bus and some necessary control signal.

D. Jin and S. Lin (Eds.): Advances in Mechanical and Electronic Engineering, LNEE 177, pp. 61–64.
springerlink.com

This system driver is a bipolar type two phase stepping motor. Motor excitation winding for A, B two phase, each motor only need A, B two way signal can drive, the eight data bus, one can drive the four motor, 20 units have 40 motor, need 10 gigabytes of interface address. Each motor and one of the zero state signals, 40 motor all five bytes. Of the 15 address decoder with two pieces of 74 LS138 can complete address to interface with the selected communication, conversion between. The I/O interface can choose eight latches 74 LS373.

3 System Software Design

The main program including are turning, reverse and back to a sports module and send, accept two communication module. Among them are turning and the reversal of the module, because only the direction of the pulse sequence hair is different, can be combined into a module, as long as that add a direction of motion parameters.

Motor control needs to adopt a parallel. A pulse is four motor a group, and points out the ten times to go to. So save the overall orientation of time. Because motor pulse time interval of about 1 milliseconds, microcontroller to execute a instructions about 1 time in the motor microseconds, needed a pulse before, a lot of the time to deal with other motor pulse sequence, control efficiency is greatly increased.

Pulse count. To make the operation speed up will count to reduce the count. A pulse count is used Specific means is bad minus pulse count, count the motor according to their respective go for the steps, then each order motor and its front steps sent between motor calculated. So, in my parallel control motor sports, when the number of motor sports less when ending, other motor have been gone for so many steps, as long as continue to move, after the end of the motor than stopped that part of the steps. Step motor to turn around the total number of more than 100000 steps, if count for 2 bytes, length counting can be at most 65535 step; If you use 4 bytes count, on the one hand, waste of space, on the other hand also can make computing time extended. Will eventually and sent more than 65535 steps in front of motor step motor split into two motor processing, and is the first completed a 65535 steps count, continue to control the motor operates, of the remaining steps. Do still have an advantage, is to use a bad minus pulse count, at most only a motor sent more than 65535 steps reduce pulse, as long as additional storage a motor data space can solve problems. Long count

Secondly and control pulse. The spacing of each motor pulse interval must be even, also can continuously adjust. A little before is to make the motor operates smoothly, later to start motor to realize smooth acceleration process. In order to control the time interval, use timer. Will a cycle of instructions on program waiting for sending pulse before, when the timer overflow instructions by disruptions, the interrupt service procedure will end circulation, and to wait for timing, positive &negative control program is will immediately send out a pulse of the motor. Because of the motor is continuous, each pulse sent a pulse synthesis and send the instructions are certain, so different address of the motor pulse interval is the same. And every time is just start timer in before sending pulse, the timer interrupt service procedure the operation instructions did not change, time is fixed, so as long as the timer initial value must be, motor pulse of the time interval is uniform. So, change the time

interval pulse and easy. In order to realize the motor speed of the motor of the smooth, start frequency for 600 Hz ac, and then change the timer for initial value, until the motor to 1000 Hz ac frequency stability and accelerate the process will need 615 steps. It has been determined that such control time interval work under the pulse of the motor speed up and running are very stable.

The motor running in place must be kept in the current pulse. Two arrays, and an array of mark has stalled motor position, and the other array record has stalled when the motor stopped the pulse information. In sending pulse, before a array will have stalled motor position clear after the pulse, an array of pulse fill in will keep in, and then the generation to meet the requirements of new pulse sending to the motor.

Finally there is a judge. The end of the mission There is a record number of variables has stopped motor, so long as it with the total number of equal, motor could finish the are turning (or reverse) to the task.

4 Motor Back to Zero Control Function Design

The function of the problem to be solved in the new main is already arrived at zero motor mark the end of the task and judgment. From the front I/O interface design can know, all 40 motor zero signal can be read from five consecutive addresses, and 40 motor pulse signals from 10 consecutive addresses send out, in both address exist between a mapping relationships. Specifically, 10 send motor pulse address, each address control four motor, the motor of the turn, stop state there are 24 = 16 kinds of combination, the 16 kinds of combination and zero address data on low four (or high four) corresponds. Will the mapping relationship existing in tabular form area of storage, program every time read all the zero signal, the zero signal look-up table can be motor state of array value, and then send pulse, every state with this step motor array of pulse signal and it. Judging the end of the mission is that all the zero signals with or operation, result to zero, that means all the motor back to zero, the task could come to an end.

5 Driving Circuit Board Design

TDA1521 reverse input and between the series a 2.35 k Ω resistance, so reducing the TDA1521 amplification, and thus reduce the influence of the input clutter. In TDA1521 output termination has a 4.7 u F insulation of straight capacitance and diode composed of bridge type circuit. Due to the motor as a sensitive device, so on and off in will be the versa electricity back to a circuit, the disturbance, therefore, the bridge type circuit filter out the interference. TDA1521 power part is connected to the 2200 u F the electrolytic capacitor, the capacitance can filter out the power, ensure that the exchange of dc power supply, remove exchange interference. Fig.1 is pulse figure after TDA1521 amplification.

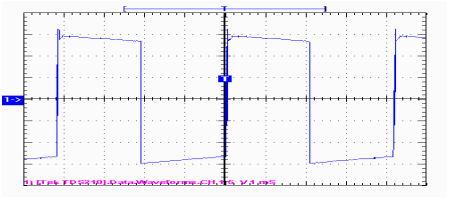

Fig. 1. Pulse figure after amplification

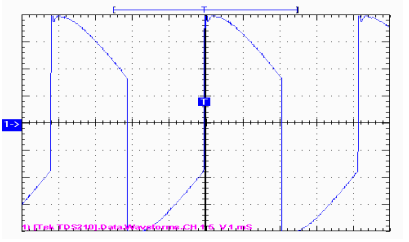

Fig. 2. Direct drive motor pulse waveforms

The Fig.2 is a capacitor direct drive motor pulse waveform figure. Because after the capacitance, level of jumping in front is not overshoot the diode bridge type circuit to eliminate. But the overshoot can increase the drive motor voltage and current of the motor, increase load capacity is good, and experiments have not found it on the motor running smoothness to have what not good effects. Other aspects of this waveform, such as impulsive intervals evenness, pulse jump to change the quickness of, etc. Are all very good, to meet the requirements of our drive motor.

References

[1] Tuanshan, Z., Na, Z.: Study of driving bipolar stepper motors based on enhanced STM32. Electronic Measurement Technology 33(10) (2010)
[2] Chi, X.-X., Zhao, K.-Q.: A Microcontroller-centered Stepping Motor Control and Drive Apparatus. Journal of Southwest Forestry College 25(2) (2005)
[3] Masia, C.G.: DSP-based stepping motor drivers for the lhc collimators. IEEE Transactions on Nuclear Science (01) (2008)
[4] Wang, C., Sun, Y.: Analyze and design of stepping motor control based on MCU. Foreign Electronic Measurement Technology 27(9) (2008)

Maximum Power Point Tracking Method for Experiment System of Single-Phase Single-Stage Photovoltaic Inverter

Jingrong Yu, Jian Yang, Yijun Wang, and Weibiao Wu

School of Information Science and Engineering,
Central South University, Changsha, China
fish2bear@gmail.com

Abstract. In this paper, the model of experiment system for single-phase single-stage photovoltaic (PV) inverter is analyzed, and a novel Maximum Power Point Tracking (MPPT) method based on extremum seeking algorithm is established to satisfy the specific requirement of this topology. Experimental results demonstrate that the single-phase single-stage photovoltaic inverter with this proposed MPPT method can avoid the employment of extra external disturbance signal, and track the maximum power point quickly and precisely.

Keywords: Maximum power point tracking, Extremum seeking algorithm, Single-phase single-stage photovoltaic inverter, optimal design of experiment system.

1 Introduction

Recently, power generation technology with renewable energy source is developing rapidly, among which photovoltaic (PV) technology is considered to be the most promising one[1]. PV roof is deemed to be the main form of being popularized in the future, and single-phase single-stage inverter is the most promising topological structure for the large-scale adoption of PV systems[2].

In PV system, the most widely used MPPT methods are the Perturbation and Observation (P&O) method and Incremental Conductance (IncCond) method. The former one will cause the output power of the PV battery fluctuating around Maximum Power Point (MPP), and the longer the perturbation step is, the more fluctuation there will be. The IncCond method has the problem of choosing the length of step either, and its threshold value is restricted by the accuracy of sensors. Extremum Seeking Algorithm (ESA) is able to achieve the best matching of estimated value. A periodic signal with small amplitude is utilized as an interference signal, and ESA searches the optimal value by means of modulation and demodulation[3].

In this paper, the ripple voltage of the DC voltage in experiment system for single-phase single stage inverter is utilized, and it is treated as the interference signal of ESA. A MPPT method based on ESA is proposed. To further optimize the MPPT method, an optimal design method is presented, and the controller based on the proposed MPPT method is designed for the single-phase single-stage inverter. Experimental results prove that the MPPT method possess good steady state and dynamic performance.

D. Jin and S. Lin (Eds.): Advances in Mechanical and Electronic Engineering, LNEE 177, pp. 65–70.
springerlink.com

2 The Model and Characteristics of Single-Phase Single Stage PV System

The I-V characteristic curves of PV array is a single-peak curve if not shaded, the output power will reach the maximum value at a particular voltage. Therefore, to improve the efficiency of PV system, the output voltage of PV array is controlled to operate near the maximum power point by MPPT method.

Fig. 1 is the schematic of PV system. Single-phase single-stage PV inverter is composed of capacitor C of DC side, single-phase voltage inverter, bridge and an output filter. where four IGBTs constitute the voltage source inverter bridge, the output filter inductor consists of L_{f1}, L_{f2}, capacitor C_f and resistance R_c, and R_l is equivalent load.

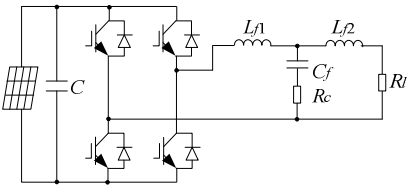

Fig. 1. Topology of single-stage single-phase PV system

Suppose the voltage of ac side for PV inverter is $v_g=v_m\sin\omega t$, where v_m is the peak voltage, ω is the angular frequency. The ac current is $i_g=i_m\sin\omega t$, where i_m is the peak current. The power output p of the PV system is

$$p = v_g i_g = \frac{v_m i_m}{2}(1-\cos 2\omega t) \tag{1}$$

According to Equation(1), DC component and the second order harmonic component comprise the output power of PV system.

Under steady state condition, the output power of PV array provides the DC component as shown in Equation(1), this component is actually the active power output from inverter. The ac part of Equation(1) adds a ripple component to the average voltage of capacitor C, and this ripple component is the approximate second order harmonic wave with the amplitude ΔU_c as

$$\Delta U_c \approx \frac{P_{PV}}{2\omega U_0 C} \tag{2}$$

Where P_{PV} is the output power of PV array under standard condition, U_0 is rated voltage, C is the capacitance of capacitor paralleled to PV array[4]. Generally, the amplitude ΔU_c is 1% and 3% of the rated voltage.

3 Optimial Design for MPPPT Method Based on ESA

3.1 MPPPT Method Based on Basic ESA

ESA is essentially a modulation process. That is, a smaller amplitude or periodic disturbance signal is added to the optimal target, and some objects or performances will change with it. Then, the derivative of target is estimated by high-pass filter and demodulation process, and the local optimal solution will be obtained by the utilization of gradient method[5].

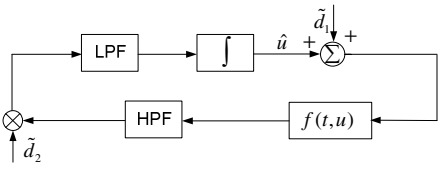

Fig. 2. Block diagram of MPPT method based on ESA

The principle of MPPT method based on ESA is shown in Fig.2. where, *f(t,u)* is the power function of PV array, $\tilde{d}_1(s), \tilde{d}_2(s)$ are external disturbance signals, $\hat{u}$ is the optimal value for DC voltage in PV system.

Since the changing speed of power function *f(t,u)* is far slower than the rate of external disturbance, the optimal estimation can be realized with gradient $\frac{\partial f}{\partial u}(\hat{u})$.

The key point of ESA is to extract useful information during the demodulation process and eventually gets the optimal value. Assume the disturbance signal $\tilde{d}_1(s)$ and demodulation signal $\tilde{d}_2(s)$ are of sine signals with the same frequency, that is

$$\begin{cases} \tilde{d}_1(t) = a\sin\omega_n t \\ \tilde{d}_2(t) = b\sin(\omega_n t + \beta) \end{cases} \tag{3}$$

Where a and b are the amplitudes of the disturbance signals, ω_n is the angular frequency of disturbance signals, β is the phase difference between the two signals.

3.2 The Proposed MPPT Method Based on ESA

In this paper, the ripple voltage with frequency of twice fundamental voltage and amplitude of ΔU_c is extracted to be the disturbance signal for MPPT method.

The proposed MPPT method based on ESA is shown in Fig.3. Where *f(t,u)* is the current-voltage function of PV array, it is actually shown the *I-V* curve in Fig.1, I_{pv} is the output value of PV cells current, $K(s)$ is the compensator used to optimize ESA, $F_1(s)$ and $F_2(s)$ are equivalent transfer functions of current and voltage sampling circuit.

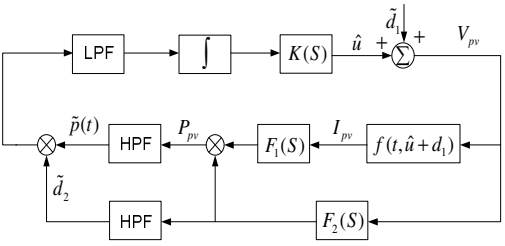

Fig. 3. Block diagram of MPPT method based on ESA

In the proposed MPPT method, the ripple voltage of capacitor is used as the disturbance signals of ESA, and the output of ESA is the ectimate value of the maximum power point for PV arrey.In Fig.3, $F_1(s)$ and $F_2(s)$ are realized by LPF, and the second order Butterworth LPF is utilized to filter the sampling signals. Since the cut-off frequency of LPF is 10 times of the harmonic frequency in PV system, the influence of phase shift caused by LPF can be ignored. Suppose G_2 is the comprehensive transfer function of LPF, integrator and compensator $K(s)$; G_1 is the transfer function of HPF, $\ell(t,\hat{u}+\tilde{d}_1)$ is the output power function of PV array, P_{pv} is the output power, the closed-loop function can be deduced by average model, that is

$$\hat{u} = G_2[\tilde{d}_2 G_1(\ell(t,\hat{u}+\tilde{d}_1))] \tag{4}$$

With high order ignored, expanded by the second order Taylor expansion at the MPPT voltage is written as

$$P_{pv} = P_{opt} + \frac{1}{2}Q(u-u^*)^2 \tag{5}$$

Where P_{opt} is the maximum power for PV array, Q is the second order derivatives of function $\ell(t,\hat{u}+\tilde{d}_1)$ at the voltage for MPP.

Substituting Eqation(5) into Eqation (4) leads to

$$\begin{aligned}\hat{u} &= G_2[\tilde{d}_2 G_1(\ell(t,\hat{u}+\tilde{d}_1))] \\ &= G_2[\tilde{d}_2 G_1(P_{opt}+\frac{1}{2}Q(\hat{d}_1+\hat{u}-u_{otp})^2)] \\ &= G_2[\tilde{d}_2 G_1(P_{opt}+\frac{1}{2}Q(\hat{d}_1^2+2\hat{d}_1(\hat{u}-u_{opt})+(\hat{u}-u_{opt})^2))]\end{aligned} \tag{6}$$

Suppose the amplitude gain of HPF function nearby the second order harmonic angular frequency is g_1, Equation(6) is simplified as

$$\hat{u} = G_2[g_1(\frac{1}{2}Q(d_2\hat{d}_1^{\,2}+2d_2\hat{d}_1(\hat{u}-u_{opt}))] \tag{7}$$

Recall the conception of the average model to get the following:

$$r_1 = \lim_{T\to\infty} \frac{1}{T} \int_0^T \frac{1}{2} Q \tilde{d}_2 \tilde{d}_1^{\,2} dt \tag{8}$$

$$r_2 = \lim_{T\to\infty} \frac{1}{T} \int_0^T \tilde{d}_2 \tilde{d}_1 dt \tag{9}$$

Substitute Equation(8) and (9) into Equation(7) to get new expression as

$$\hat{u} = G_2 g_1 [r_1 + Q r_2 (\hat{u} - u_{opt})] \tag{10}$$

According to the Equation(10), the characteristic equation of closed-loop system is

$$1 - G_2 g_1 Q r_2 = 0 \tag{11}$$

3.3 Optimization Design of Compensator *K*(*s*)

The convergence of ESA based on the ripple voltage is too slow to be controlled. In order to control the dynamic performance of MPPT method, an extra freedom control is added to the proposed MPPT method. The compensator *K(s)* is the introduced extra freedom of control, and it benefits to optimize the performance of MPPT method by controlling the convergence of ESA.

In Fig.3, LPF is the second order Butterworth filter, and the transfer function $G_2(s)$ composed of LPF and integrator becomes the third order system. For high order system, proportion integral differential (PID) control is the most popular control method. To make good tradeoff between the complexity and effectiveness of the system, proportional control is employed to be the compensator $K(s)$.

The closed-loop system shown in Fig.3 is a three-order system. In engineering practice, it can be simplified to a two-order system approximately, and the parameter k_P of $K(s)$ can be regulated for the best performance of a two- order system.

4 Experimental Results

In order to validate the effectiveness of the proposed MPPT method, a test platform of single-phase single stage PV system has been built in the laboratory of Central South University. Under the condition of a sunny day, the open voltage of PV is about 36 to 38 V, while short current is roughly 4 to 6 A. The output voltage for the maximum power is approximately 29 to 30V. However, the value would be altered with different temperature. When the weather is fine, the actual maximum power is between 140 and 150 W, and ripple voltage of capacitor is about 1V.

The waveforms of output power for PV array under different conditions are shown in Fig.4. When a compensator $K(s)$ is designed as k_P=9.5, the output power of PV array with different initial voltages are shown as waveform 1 and 2, When no compensator is employed, the output power with different initial voltages are shown as waveform 3 and 4.

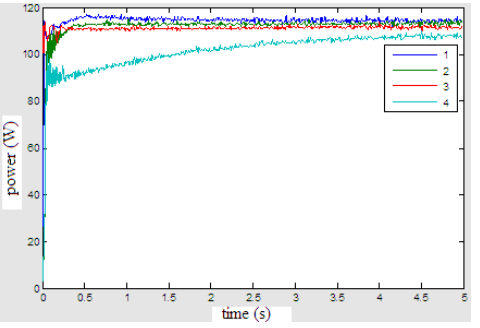

Fig. 4. Comparisons of output power of PV array

Obviously, the introduction of compensator $K(s)$ greatly improved the dynamic performance and efficiency of the PV system.

5 Conclusion

To improve the performance of experiment system for single-phase single-stage PV inverter, a novel MPPT method based on ESA and inherent ripple voltage is proposed. The ripple voltage of capacitor is analyzed in details, and its second order component is utilized as the disturbance signals in ESA. Through the introduction of optimal compensator in ESA, the convergence of ESA and the dynamic performance of MPPT are soundly improved.

Acknowledgments. This work was supported by the National Science Foundation Foundation under Grant 61104047 and Research Fund for the Doctoral Program of Higher Education of China under Grant 20100162120014.

References

1. Ren, J.B., Li, Z.W., Wang, Y.P.: The Interaction between Solar PV Roofs and Loads of the Building. Solar Journal 29(7), 849–855 (2008)
2. Casadei, D., Grandi, G., Rossi, C.: Single-phase Single-stage PV Generation System Based on A Ripple Correlation Control Maximum Power Point Tracking. IEEE Transactions on Energy Conversion 21(2), 562–568 (2006)
3. Leyva, R., Alonso, C., Queinnec, I.: MPPT of PV Systems Using Extremum-Seeking Control. IEEE Transactions on Aerospace and Electronic Systems 42(1), 249–258 (2006)
4. Ho, B.M.T., Chung, H.S.-H.: An Integrated Inverter with Maximum Power Tracking for Grid-Connected PV Systems. IEEE Transaction on Power Electronics 20(4), 953–962 (2005)
5. Li, Y.G., Shen, J.: On-line Combustion Optimization of a Utility Boiler Based on an Extremum-search Control. Thermal Energy and Power Engineering 4, 466–469 (2009)

Analysis on Power Battery Performance Test and Consistency in Packing Process

Xiaoliang Li[1], Bizhong Xia[1], and Weiwei Zheng[2]

[1] Graduate School at Shenzhen,
Tsinghua University, Shenzhen 518055
[2] Sunwoda Electronics Co., LTD, Shenzhen 518108
lxl19870719@163.com,
xiabz@sz.tsinghua.edu.cn,
zhww@sunwoda.com

Abstract. In order to solve the application of the battery consistency group problem, a new type of power Li-ion battery consistency assemblying method is proposed and analysed through testing the DC resistance, capacity, self-discharge of the battery, which ensures not only maximum utilization rate of monomer battery in the samples but also makes certain battery does not occur over charge/discharge and improves battery life and safety.

Keywords: lithium ion power battery, consistency, resistance, capacity, self-discharge.

1 Introduction

With the advantage of large capacity, high specific energy, high operating voltage, stable discharge voltage, wide operating temperature range, low self-discharge, long cycle life, no memory effect, small size, light weight and green environmental protection etc, lithium ion battery becomes the first choice for secondary batteries. At present the voltage of electric car is about 300 V, which makes it necessary to use multiple lithium ion battery monomers in series to form a battery pack; but a large-scale, high reliability and long-lasting lithium battery pack is a very complicated issue. The differences between each monomer will inevitably lead to inconsistency of the battery charge and discharge; therefore, in the process of charging and discharging it is need to solve the problem of balance and safety protection. Lithium battery is very sensitive for excessive charging or excessive discharge, so how to ensure the consistency of the group is the key problem of lithium ion battery groups [1].

Single battery performance difference is mainly composed of the two following aspects: the performance differences before packing, differences in the cycle and stored procedure. The inconsistent performance between the single battery makes some single battery capacity accelerate attenuation and shorten the battery life, so it is necessary to match the battery before into a group.

It is generally believed that the mainly inconsistencies of the battery include resistance, voltage and capacity[2]. The resistance inconsistency, especially ohmic

D. Jin and S. Lin (Eds.): Advances in Mechanical and Electronic Engineering, LNEE 177, pp. 71–76.
springerlink.com

resistance inconsistency will seriously affect the change of voltage in the battery charge and discharge process; and when the current flows, the battery temperature change would be inconsistent and some of the single battery may exceed the applicable temperature range, which results in performance degradation and security risks. Due to the differences between the monomer battery capacities, it is prone to happen battery overcharge or over discharge in the process of charging and discharging; which affect the battery life, even happen fires and explosions. When the batteries are in parallel and voltage difference between monomers will make the battery charge each other. And, the above factors are not independent among each other, but mutual coupling and influence.

2 Power Battery Performance Testing

2.1 DC Resistance Test

The lithium-ion battery internal resistance refers to the resistance of the current through the battery, including ohmic resistance and polarization resistance[3].

Ohmic resistance includes the electrode material, electrolyte, separator resistance and contact resistance of some components. The polarization resistance is caused during the electrochemical reaction; it includes the electrochemical polarization resistance and concentration polarization resistance.

As shown in Fig.1, when the battery begin discharge, a transient voltage drop is caused by the ohmic resistance of the battery, this part of the internal resistance is the DC resistance. Similarly, when the battery end discharge, a transient voltage rise is caused. Power battery test is more concerned about the DC resistance.

Voltage changes caused by ohmic resistance happens in a very short period of time, after which the cell polarization effect will be effective; therefore, the measurement of voltage changes must be within a very short time (usually in 1-2s or less), which requires the test system has high test accuracy and shorter response time. DC resistance test typically requires the application of current pulses to charge and discharge, at the same time testing the battery terminal voltage changes, then divided by the corresponding current value, which can obtain the DC internal resistance of the battery. The formula shown as follows:

$$R_D = \frac{\Delta U}{I} \tag{1}$$

DC resistance test consists of two parts: the pulse discharge test and pulse charge test.

According to the Fig.1 and Fig.2, the calculated battery DC internal resistance as follows:

$$R_{\mathrm{DC}} = \frac{R_{\mathrm{charge}} + R_{\mathrm{discharge}}}{2} \tag{2}$$

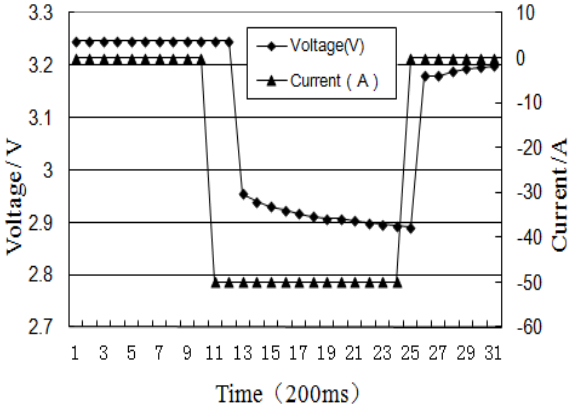

Fig. 1. Pulse discharge test

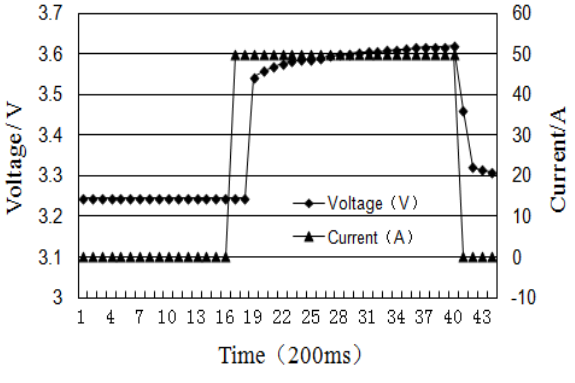

Fig. 2. Pulse charge test

2.2 Battery Capacity Test

The battery capacity is an important performance parameters of the lithium-ion battery. Therefore, the battery capacity test is very important for battery consistency group and must be carried out[4, 5]. The battery capacity test uses the constant current discharge method; due to the stability of the current in the discharge process, it is easy to calculate the battery capacity value. Capacity of the battery is influenced by discharge mode, charging mode and stalling time, it must provide the same charge and discharge mode and stalling time, which makes the measured data is comparable.

The standard capacity test is under 25^0C, the discharge current is 1I3; stop the discharge process when the battery voltage reaches the limits of the voltage (2.0V), the battery capacity value is equal to current multiplied by the battery discharge time. Capacity test steps shown as follows: constant current discharge to 2.0V, put it aside for 60min, constant current and constant voltage charge to full, put it aside for 60min, 1I3 constant current discharge to 2.0V, calculate battery capacity. It can be seen from Fig.3, the maximum gap between the capacity of the battery is 180mAH, which indicates that battery capacity test is important.

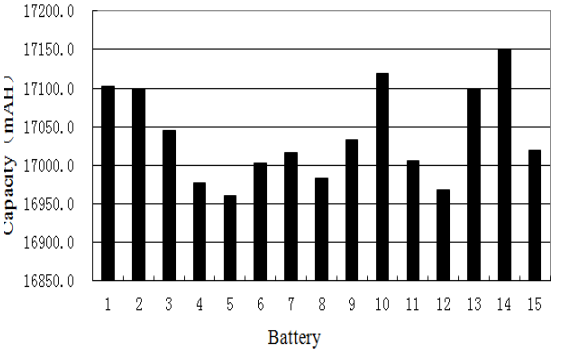

Fig. 3. Standard capacity contrast

2.3 Self-discharge Test

Self-discharge of the battery causes voltage drops in the process of stalling, this is inevitable when the electrode is $LiMn_2O_4$, $LiCoO_2$ and $LiNiO_2$. The scale of self-discharge depends on the manufacturing process of cell, the nature and concentration of the electrolyte, the storage temperature and storage time, etc.

Calculation of battery self-discharge can be achieved by calculating the battery open circuit voltage drop; first charge the battery, then put it aside for 12-24 hours, then measure OCV1; put it aside for 48-120 hours, measure the battery OCV2; battery open circuit voltage drop calculated as follows:

$$\Delta OCV = OCV1 - OCV2 \tag{3}$$

Different storage time corresponds to different battery self-discharge and the battery OCV drop is different, this is detrimental to online measurement and control. In order to facilitate comparing and screening, it must provide the same stalling time and environment. And lithium-ion battery self-discharge is very weak, so high-precision voltage test equipment must be used.

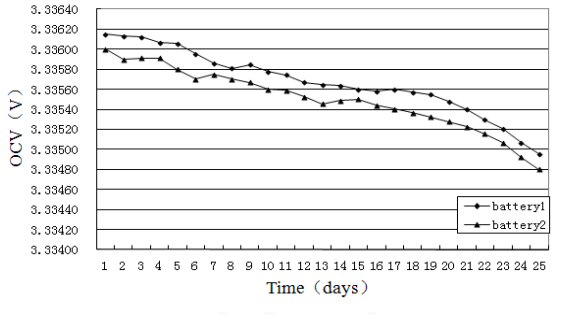

Fig. 4. Self-discharge test

3 Algorithms of Into Group

In order to meet the capacity and voltage requirements of the electric vehicle, the battery must group in series-parallel. Parallel to increase the capacity of the battery, the series used to meet the requirements of the battery voltage, lithium-ion battery into a group usually adopts the mode of series after parallel.

Cells in parallel modules must meet the requirements of the consistency of capacity, because the current value through the parallel modules in charge and discharge process is equal, if the capacities of the battery in parallel modules are inconsistent, and then it is bound to result in overcharge and over discharge or charge and discharge not fully in charge-discharge process.

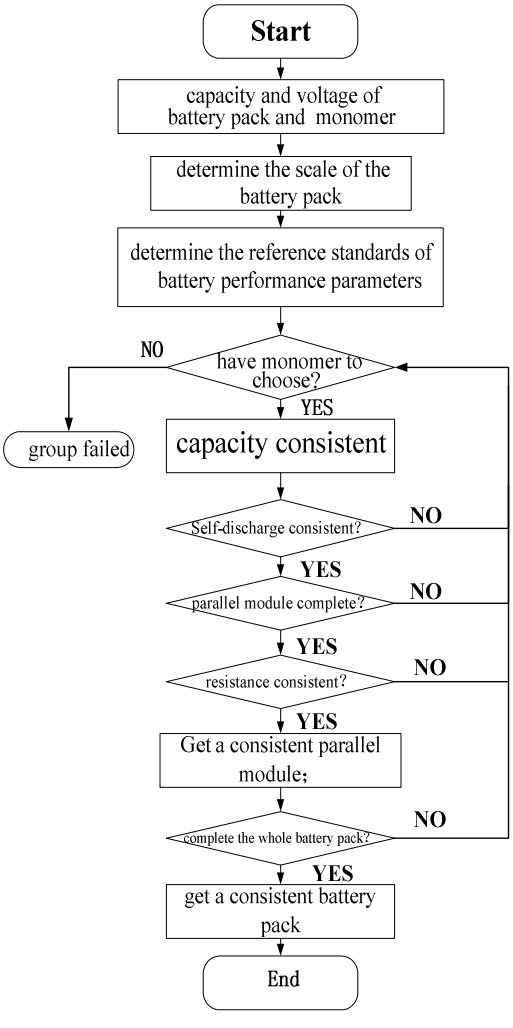

Fig. 5. Algorithm flow chart

The self-discharge rate of the modules is also required to be consistent; if the self-discharge is inconsistent, even if the battery capacity meet the requirements, battery self-discharge can also make the same battery capacity become inconsistent after standing for some time, it will result in overcharge and over discharge or charge less and discharge not fully.

In order to make the battery fever consistently in the charge-discharge process, it must ensure consistent with the internal resistance between the parallel modules. In summary, the diagram of the algorithm of consistency into group is shown as in Fig.5.

4 Conclusions

Experiment used iron phosphate lithium-ion battery, the battery rated capacity is 16.5Ah, after 1500 standard charge and discharge cycles the capacity decreased to 80%. A single battery standard charge mode is as follows: under conditions of ambient temperature 25±2°C, charge the battery with constant current to constant voltage mode. Constant current is 1I3(A), the constant voltage is 3.65V, charge termination current in the constant voltage process is 825mA, then put the battery aside for 1 hour. Experiment adopted two battery packs that were used respectively the consistency group algorithms and random group to compose, the battery packs is two parallel monomers and four series monomers, test the two battery packs with standard charge and discharge cycle; the 1I3 constant current charging to the battery voltage up to 14.6V, then adopt constant voltage charging to the end, put aside for 60min, and then discharge to 8.0V with 1I3 constant current, repeat the cycle 200 times. The result is that the average capacity decay rate of the consistent battery pack is 0.0152%; the other battery pack average capacity decay rate is 0.0305%. As can be seen from the above data, the consistent group algorithm proposes cycle life of the battery pack, which makes it clear that the algorithm is valuable.

References

1. Wang, Z., Sun, F., Lin, C.: An analysis on the influence of inconsistencies upon the service life of power battery packs. Beijing University of Science and Technology Journal (July 2006)
2. Yi, S.: Research on uniformity of Lithium Ion battery. China Academy of Science and Technology and Shanghai Microsystems Institute (June 2008)
3. Xu, K., Qiu, T., Chen, J., Gui, C.: Ohm internal resistance test for power battery. Chinese Battery Industry (February 2011)
4. Bai, Z., Cao, L., Yang, J.: Study on methods for assessing performance of power batteries used in pure electric vehicle. Journal of Hunan University (October 2006)
5. He, P., Yue, Q.: The consistency and safety of multi-cell Li-ion batteries. Battery Bimonthly (June 2010)

The Research of Mechanical and Electrical Integration Linear Output Transmission System with Sensor Function

Yuwang Liu[1], Yuquan Leng[1,2], Haitao Luo[1,2], and Weijia Zhou[1]

[1] State Key Laboratory of Robotics, Shenyang Institute of Automation
Chinese Academy of Sciences, Shenyang 110016, China
[2] Graduate School of the Chinese Academy of Sciences, Beijing 100039, China
{Liuyuwang,Lengyuquan,Luohaitao,Zwj}@sia.com

Abstract. With the further theory research and engineering application, the study of the small electro-mechanical systems, with movement conversion, motion transmission, force/torque transmission and sensor function, becomes popular. The new highly integrated mechanical and electrical integration linear output sensor system is designed in this paper, to solve the problems of movement conversion/transmission, force transmission/measurement etc, and further theory study is also presented. The function of sensing parameters and transmission parameters is deduced and the key parameters of system design and the constrained conditions are shown. Then, the result of simulated experiment that made in allusion to the model was compared with the theory speculation, accordingly, validated the accuracy of the theory.

Keywords: Integration, Linear Output, Mechanical, Electrical, Parameter, Simulation.

1 Introduction

Transmission system is the intermediate structure or system which transfers the energy of driving source to the drive mechanism. The main functions are movement conversion, motion transmission, force/torque transmission [1~4]. Due to the restriction of the size of components, space of structure and energy of driving source etc, the driving source couldn't be fixed on the driven mechanism to release the energy directly, but placed in certain distance away and the transmission system transfers the energy of driving source to the movement of driven mechanism. There are four types of transmission systems: 1) rotation to rotation; 2) rotation to linear motion; 3) linear to linear; 4) linear to rotation. So far, the applications of the rotation motor transmission systems are more popular than the linear motor. The technology has been quite mature that transfer the rotation from motor to driven organization, which is mainly carried out by gear-driven mechanism and turbine and worm driving. The system which transfer the rotation motion of motor to the linear motion of driven mechanism is complex, and the mainly transmission methods are ball screws and worm gears, gear and rack mechanism, the crank and slider mechanism. Usually, the

D. Jin and S. Lin (Eds.): Advances in Mechanical and Electronic Engineering, LNEE 177, pp. 77–82.
springerlink.com

size of latter is too big to be settled in small space meeting the special requirements. Consequently, the mechanisms mentioned in the paper are all screw nut-driven.

Due to the increasing requirements of control systems, sensing systems become the significant research area in automation. The dynamic and operating precision of automatic equipments could be raised by accurate measurement of force/torque, and the force/torque sensing system, as an essential component of accurate drivers, is very popular[5]. So far, the measurement of force/torque is implemented by external force/torque sensors, which cannot meet the requirements of small accurate drivers because of the complex structures and components and the big size and mass[1, 2].
Nowadays, transmission systems are made of two parts: transmission system and sensing system and these two parts have independent structures and functions, which leads to the increasing of the complexity of the whole system and the size and mass [1, 2]. The miniaturization and integration of the transmission systems are the main study direction in automation research, and are used widely, especially on robot studies. In this paper a unique electro-mechanical system is presented to meet application requirements and developments. This system could transfer the rotation motion of the driving source to linear motion, and also can test the force/torque of system. Motion conversions, motion transferring, force/torque transferring and force/torque measurement are all achieved in a suit of components which realize miniaturization and integration of the transmission systems.

Based on this system, further theory study was presented. The function of sensing and transmission parameters was deduced through theory computation, which is the key of sensing system research. Then, made finite-element analysis according to the specific given parameters, and calculate the simulated transmission parameters by taking the output force as the independent variable, and confirmed the accuracy of the theory by comparing the result and the value.

2 Mechanism and Principles of Integration System

Regarding to the requirements and restrictions;

a) Transferring the rotation motion to linear motion and output;
b) Driving force transmission and measurement;
c) Long distance transmission;
d) Small spatial arrangement.

Considering the functional distribution, spatial arrangement and structural design and other factors, integrate features such as the motion conversion motion transmission, force transmission and measurement, in a small sensor system. This system does not only have all functions of transmission system, but also integrated measurement of transferring force, without additional components. The functional design of the system block diagram is shown in Figure1.

In the design, precision movement and high force transmission are realized by screw, and the measurements of the force/torque are achieved based on specially designed components. The mechanical structure of new transmission sensor system, shown in Figure 2, is composed of coupling joint, screw, slotted nut, pin, thin-walled shell and strain gauge. Motor passes the motion to screw, and nut moves on the axial direction because it is fixed by pin, which realizes the transfer from rotation motion to

linear motion and the transmission of driving force. The realization of sensor function is achieved by the specially designed shell, as shown in figure 2, the interaction force between the screw and nut is passed to shell by the pin, which leads to the deformation of shell. The transmission force could be measured indirectly by measuring the deformation. The shell is designed to the structure of thin in the middle and thick on both sides, to obtain the high rigidity of driving system and sufficient torsion deformation of the shell.

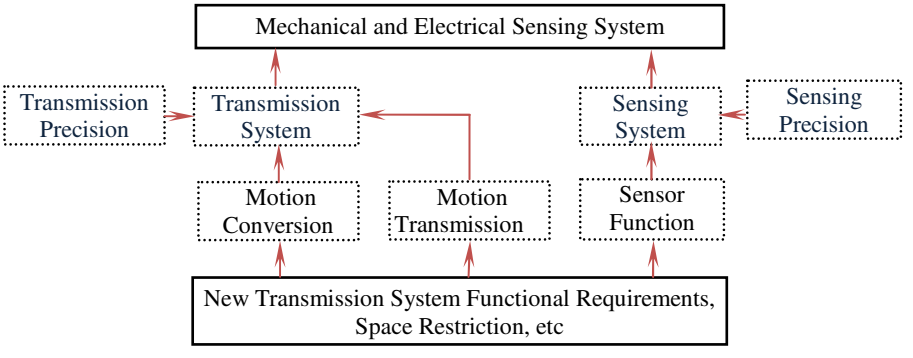

Fig. 1. Mechanical and Electrical transmission and sensing system function block diagram

The highly integration and miniaturization are achieved which can be seen from the system function design and detailed structure design. But the structure makes the factors of transmission and the factors of sensor couple, which means transmit parts are sensor measuring parts at the same time. In order to ensure transmission accuracy, the stiffness of the transmission parts should be higher, in the other side, the measurement of sensor factors ask for more deformation. Since the system is designed to share the transmission components and sensor components, it is a big challenge that ensures the transmission accuracy and the sensing precision at the same time. The following sections focus on solving this challenge.

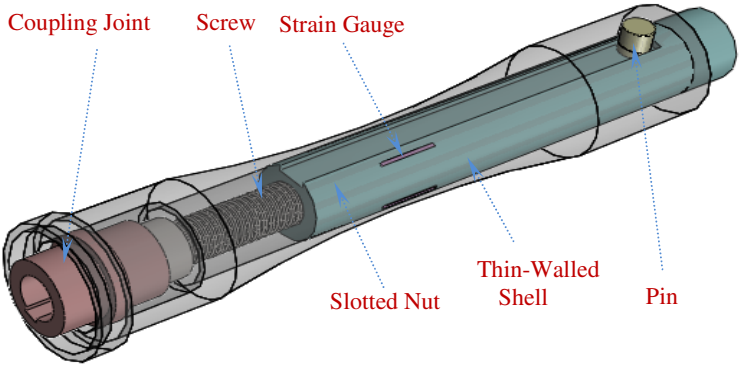

Fig. 2. Mechanical and Electrical transmission and sensing system

3 Verifying the Function of Transmission and Sensing Parameters

Transmission parameters are mainly transmission power and transmission speed, and sensor parameters are mainly shell torsion deformation. Since the system is designed in low speed, the system dynamic performance can be ignored, therefore, the relationship between transmission parameters and sensor parameters is considered only. Firstly, in screw transmission system, the torque can be acquired under given output by solving the spiral transmission statics, then calculate the shell deformation of the system, to determine the function of output force and shell deformation.

3.1 The Analysis of Spiral Transmission Statics

Figure 3.a) shows the spiral pairs of designed model. Torque Tn is exerted in the screw, and same force with opposite direction and load W are exerted on nut. When the screw rotates, the nut moves up and down along the axial direction. Rectangle screw pairs can be simplified to a block slides along the inclined plane, shown in figure 3, an inclined plane with angle λ can be get by stretching rectangle screw along d2. When the moving direction of nut is same to W, the force is shown in figure 3.b), otherwise see figure 3.c).

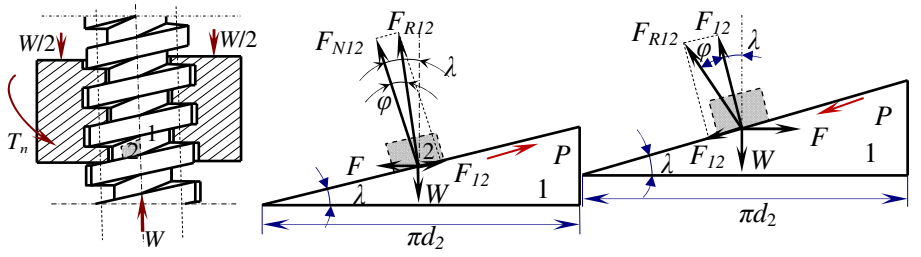

a) Force of helical pair b) The same direction c) Reverse direction

Fig. 3. Force analyses of helical pair

When the screw rotates related nut, the inclined plane applies to the slider normal reaction FN12, frictional force F12, and then get total force about FN12 and F12, called FR12. The angle between FR12 and FN12 is φ called friction angle. Horizontal force F can be calculated based on F, W and FR12 three force balance about slider.

$$F = W\tan(\lambda \pm \varphi)$$

In equation, $\lambda=P/\pi d_2$, $\varphi=\arctan f$, f means the frictional coefficient.

Torque applied on nut is $T_n=d_2F/2=d_2W\tan(\lambda\pm\varphi)/2$, "+" means the moving direction of nut is opposite to W, "-" means otherwise.

For non-rectangular thread,

$$\begin{cases} F = W\tan(\lambda \pm \varphi_v) \\ T_n = d_2 W\tan(\lambda \pm \varphi_v)/2 \end{cases}$$

In equation, f_v means equivalent coefficient of friction, $f_v=f/\cos\beta$ (β means friction angle); φ_v means equivalent angle of friction, $\varphi_v=\arctan f_v$.

3.2 The Stress-Strain Analysis of Thin-Walled Shell

Based on the structural characteristics of the system, thin-walled shell is under torque and axial friction, but the contact surface between shell and pin is after special treatment, so the friction is small and can be ignored. Therefore torsion is only considered when we analyses the shell torsion. According to mechanical properties, the maximum stress and the maximum relative deformation of strain gauge can be shown as:

$$\begin{cases} \tau_R = 2T_n R_s / \pi\left(R_s^4 - r_s^4\right) \\ \varphi_R = 2T_n R_s l / G_s \pi\left(R_s^4 - r_s^4\right) \end{cases}$$

In equation, G_s means modulus in shear; τ_R means shearing stress about surface of radius R; l means the effective length of the strain gauge, φ_R means the relative deformation of the both side of the strain gauge.

4 Simulation

The integrative transmission system consists of the motion transmission and force/torque transmission. Moreover, the transmission parameters in the system are achieved based on the deformation of the thin-walled shell. The finite-element analysis is also necessary. The subordinate factors such as the axial attrition of the system are unconsidered in the simulated analysis, and all the components are supposed to be in good condition. The specific nonobjective model is shown in Figure1 (the dimensions have been defined).Take 100N,120N,140N, 160N,180N,200N as the output force from the notch nut for example, the finite-element analysis is shown in Figure 4, which is contrasted in Table 1.

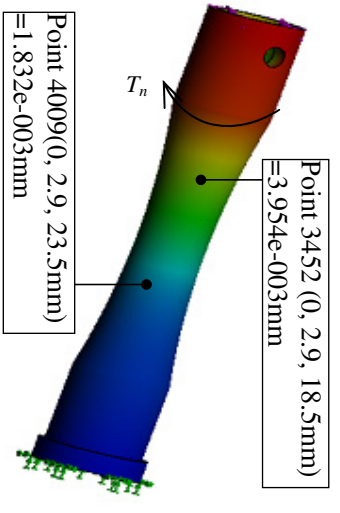

Fig. 4. Finite-Element Analysis

Table 1. The comparison of date between theory and analyze

Type / Force(N)	Theory Date (mm)	Analyze Date (mm)	Deviation (%)
100	2.318×10^{-3}	2.122×10^{-3}	9.24%
120	2.782×10^{-3}	2.516×10^{-3}	10.57%
140	3.246×10^{-3}	2.939×10^{-3}	10.44%
160	3.709×10^{-3}	3.342×10^{-3}	10.98%
180	4.173×10^{-3}	3.825×10^{-3}	9.09%
200	4.637×10^{-3}	4.228×10^{-3}	9.67%

5 Conclusion

Present a new mechanical and electrical system for small space, which integrated motion conversion, motion transmission, force/torque delivery and sensor function. Because of the integration and the miniaturization, the system could be used in small complex robot or other equipments, to solve difficult problems in engineering area. The function of the output force and transmission parameters was established, and validated the accuracy of the theory and the feasibility of the system through simulated analysis.

References

1. Bishop, R.H.: Mechatronics: an introduction. CalTech (2006)
2. Onwubolu, G.C.: Mechatronics: principles and applications, Heidelberg (2005)
3. Yang, B., Tan, U.X., McMillan, A.B., Gullapalli, R., Desai, J.P.: Design and Control of a 1-DOF MRI-Compatible Pneumatically Actuated Robot With Long Transmission Lines. Mechatronics 16, 1040–1048 (2011)
4. Kesner, S.B., Howe, R.D.: Design Principles for Rapid Prototyping Forces Sensors Using 3-D Printing. Mechatronics 16, 866–870 (2011)
5. Wu, B., Shen, F., Luo, J., Wu, Z.: Design and Application of Six-Axis Force Sensor Integrated in Perceptual Foot System of Humanoid Robot. Sensor Lett., 1436–1442 (2011)

The Application of Method on Centroid Recognition and Fuzzy Judgment in Indoor Monitoring System Based on Electronic Equipments

Yunhai Hou*, Wanxin Gao, and Dehua Sun

Changchun University of Technology,
130012 Changchun, China
houyunhai@mail.ccut.edu.cn, wanxingao@126.com

Abstract. In the paper,the arithmetic of detection and recognition to video movement was discussed and the technology on disposal and recognition for electronic images in the simple condition, which are based on the technology of video recognition. At the same time a fuzzy judgment algorithm based on the minimum distance is presented combined with the all kinds of disturb factors in indoor monitoring. According to the feature parameters such as the area of moving objects and the distance of moving objects, the method will make an identification, give an alarm and make a judgment toward the target so as to capture and store the abnormal phenomena and finally sound the alarm signal. The experiments show that the method may help to detect and identify the moving objects in video sequence.

Keywords: gentroid identifying, fuzzy judgment, monitoring system, identifying to moving objects, electronic equipments.

1 Introduction

Visual dynamic recognition surveillance technology is an important applications class in modern IT technology. Visual dynamic recognition surveillance technology not only has a very wide range applications in society daily life and work,but also plays an increasingly important role in energy, defense, transportation and other fields. Making effective treatment to the rapid changed environment is one of the problems in visual dynamic recognition.The common methods of extracting the change area from the background in sequences image are: 1) background subtraction method: a technology of using the differential of the current image and background image to detect movement zone.2) the time difference method: If a location in an image object changes, then the gray-scale corresponds to the location will changes, but the gray of the part of the object which has not changed does not change or occurrences a small change. This method only compare corresponding pixel grayscale differences of two adjacent images in the sequence images.3): the optical flow method: Gibson proposed the optical flow concept firstly in 1950. The so-called optical flow is the model velocity in the image, that is the vector field of process of change in optical

* Corresponding author.

D. Jin and S. Lin (Eds.): Advances in Mechanical and Electronic Engineering, LNEE 177, pp. 83–88.
springerlink.com

information.Optical flow field is a two-dimensional instantaneous velocity field, is the projection of the two-dimensional velocity vector in the imaging surface of three-dimensional velocity vector.Optical flow not only contains movement information on the object being observed, and carry information on the movement of objects and features three-dimensional structure,it plays an important role in several branches of the field of computer vision research.

Using the above method will have a false alarm to fluorescent strobe light, shadows of some movement and region interference caused by local small disturbances, reduces the reliability of the monitoring system greatly.

1.1 Analysis of Object Motion Distance

When it has detected and extracted the moving object, gets into the motion object tracking process, oversees the moves of centroid (geometric center) of the movement object in a certain time frame to,if the object tracked over a predetermined time, or centroid change of material exceeds the threshold,then ends distance analysis of the object motion and records the maximum distance the object moves and the image of the object.Object centroid is defined as

$$x_c = \sum_{x=0}^{w-1} \sum_{y=0}^{H-1} xM(x, y) \ . \tag{1}$$

$$y_c = \sum_{x=0}^{w-1} \sum_{y=0}^{H-1} yM(x, y) \ . \tag{2}$$

Among them, $M_n(x, y)$ is the mapping table for the mask, W, H are the width and height of $M(x, y)$ respectively. Movement distance of the object is defined as

$$d = |x_{c1} - x_{c0}| + |y_{c1} - y_{c0}| \ . \tag{3}$$

In which, $(x_{c0} - y_{c0})$, $(y_{c1} - y_{c0})$ are the centroid of movement object at the beginning and the end of the tracking respectively.

The distance analysis is one of the conditions be used to determine whether the object is the human,the movement of people is generally larger, and some vibration (such as leaves, curtains, etc.) in background objects and switch to night lights suddenly near the building tenants is relatively small, therefore, the movement distance analysis can be used to eliminate some false alarms.

1.2 Detection of Light Switch Event

Switch lamp is more frequent occurrenced event, switch lights should not cause alarm system.The easiest way of detecting switch lights is to measure the brightness of each

pixel in the current frame have increased or reduced.we consider the ordinary USB camera adjust the gain automatically here, when the color contrast and larger size objects gets into the background, will result in an increase or decrease of the average brightness about the current frame.

It was found that: when the brightness larger objects get into the background, the pixels in addition to the current frame pixel motion reduces the brightness; the other hand, when the light dark objects get into the background, the pixels in addition to the current frame pixel motion reduces the increase; If the switch light events has occured, all of the current frame pixel brightness will increase or decrease.Through these features, the switch light incident detection can combine with moving objects detecting.

First, calculate the average luminance of change in pixel block between the current context and the current frame difference

$$\overline{Y}_{bn} - \overline{Y}_{cn} = \frac{\sum_{x=0}^{W-1}\sum_{y=0}^{H-1}\left(Y_{bn}(x,y) - Y_{cn}(x,y)\right)\times M_n(x,y)}{N_{bn}} \quad . \tag{4}$$

In which

$$N_{bn} = \sum_{x=0}^{W-!}\sum_{y=0}^{H-1} M_n(x,y) \quad . \tag{5}$$

W, H are frame width and frame high respectively, N_{bn} is the number of change pixels block, $\overline{Y}_{cn}$ is the average brightness in the current frame block, $\overline{Y}_{bn}$ is the average brightness in the current context, $M_n(x,y)$ is the mask map.

Then re-calculate the average brightness of pixels between outside the current frame and the current context in addition to the change in pixel block

$$\overline{Y}_{bn1} - \overline{Y}_{cn1} = \frac{\sum_{x=0}^{W-1}\sum_{y=0}^{H-1}\left(Y_{bn}(x,y) - Y_{cn}(x,y)\right)\times\left(1 - M_n(x,y)\right)}{WH - N_{bn}} \quad . \tag{6}$$

In which, $\overline{Y}_{bn1}, \overline{Y}_{cn1}$ are the average brightness of pixels between outside the current frame and the current context in addition to the change in pixel block respectively.

Through $\overline{Y}_{bn}$, $\overline{Y}_{cn}$, $\overline{Y}_{bn1}$ and $\overline{Y}_{cn1}$ can identify the switch lights event.

Switch lights event:

$$\begin{cases} \left(\overline{Y}_{cn} - \overline{Y}_{bn} > T_1\right) \\ \left(\overline{Y}_{cn1} - \overline{Y}_{bn1} > T_2\right) \end{cases} . \tag{7}$$

Turn off lights event:

$$\begin{cases} \left(\overline{Y}_{cn} - \overline{Y}_{bn} < T_1\right) \\ \left(\overline{Y}_{cn1} - \overline{Y}_{bn1} < T_2\right) \end{cases}. \tag{8}$$

Moving Target:

$$\begin{cases} \left(\overline{Y}_{cn} - \overline{Y}_{bn} > T_1\right) \\ \left(\overline{Y}_{cn1} - \overline{Y}_{bn1} < T_2\right) \end{cases}. \tag{9}$$

Or

$$\begin{cases} \left(\overline{Y}_{cn} - \overline{Y}_{bn} < T_1\right) \\ \left(\overline{Y}_{cn1} - \overline{Y}_{bn1} > T_2\right) \end{cases}. \tag{10}$$

In which, T_1, T_2 are the measured threshold of the brightness variations.

The light intensity of input signal often encounter changes suddenly in monitoring system in the actual, such as when the light switch, the gain of USB camera adjust automatically and so on.When the system detects that the light mutation, the system will speed up extraction rate of video frame (sampling rate), while increasing speed up the replacement rate of distribution model, until the background model adapts to this mutation.

2 Alarm Target Recognition and Processing

By the previous algorithm, we get the largest area of before and after in moving objects and the dist moving distance before and after in moving objects.When it detected movement distance and target size which meets the certain alarm conditions, then it creats an alarm signal.

This paper uses a fuzzy identification method to size area and moving distance to get fuzzy decision, it is shown in Fig. 1.

The decision formula is:

$$alarm = \begin{cases} 1 \quad (\text{alarm}) & if\ (S_1 + S_2) \geq temp \\ 0 \quad (\text{no alarm}) & if\ (S_1 + S_2) < temp \end{cases}. \tag{11}$$

In which

$$S_1 = \begin{cases} area/Area, & if \quad area \le Area \\ 1 \quad , & if \quad area > Area \end{cases} . \tag{12}$$

$$S_2 = \begin{cases} dis/Dis, & if \quad dist \le Dist \\ 1 \quad , & if \quad dist > Dist \end{cases} . \tag{13}$$

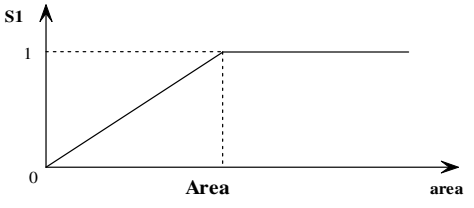

(a) The ruling curve of moving object area

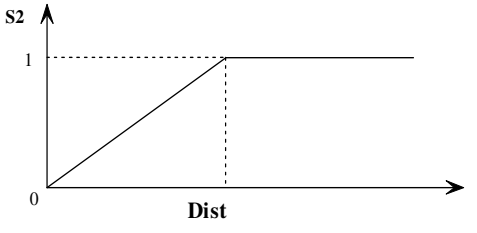

(b) The ruling curve of moving distance from objects

Fig. 1. Alarm decision-table of moving object

In which, Area is the maximum of the reference area, D1 is the maximum of reference movement distance of moving objects, S1 and S2 are the judgment coefficients of the moving object size and the distance judgments factor.When the detected moving objects the summation $S_1 + S_2$ of the size decision factor S1 and the movement ruling factor S2 of moving objects is greater than the detection threshold temp, then there are anomalies that need to alarm, and record the image information of current frame and current moving objects identify.

Because the specific application of the scene monitor may be different, such as the relative distance of camera and the the scene subjected, capture the size and speed of unusual moving objects and so on will change with the different application background and requirements.

Therefore, in fuzzy decision, the area reference value Area and move distance reference value Dist and detection alarm threshold temp are variable, it adjustments according to the specific situation used,In the implementation of specific computer software, it can revise decision parameters in the scene through the dialog box.

The specific processes is shown in Fig. 2 and 3:

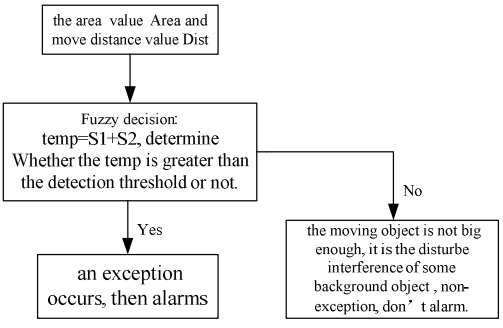

Fig. 2. The identification process of moving objects

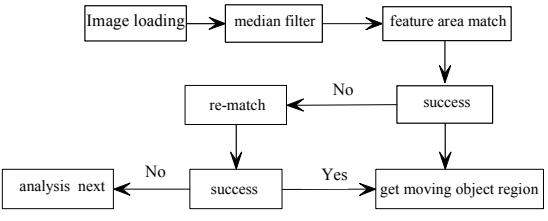

Fig. 3. Alarm decision-table of moving object

3 Conclusions

In this paper, we use the fuzzy decision algorithm, it is based on the size of moving objects and movement distance of moving objects such as the characteristic parameters, determines an alarm identification to the targe, captures and storages anomalies, alarms at last.

References

1. Kenneth, U.S., Castlemal, R.: Digital Image Processing. Electronics Industry Press
2. Feng, D.: VC + + programming-based. Tsinghua University Press
3. He, B., et al.: VC + + digital image processing. People Post Press
4. Cohen, I., Medioni, G.: Detecting and tracking moving objects For video surveillance. In: IEEE Proc. Computer Vision and Pattern Recongnition, pp. 2319–2325 (1999)
5. Zhang, Y.-J.: Image and Computer Vision. Tsinghua University Press

The Research of Efficiency and Quality on Graphic Interpolation Algorithm for LCD Display

Xiancheng Fu, Chuan Wu, and Guojun Wen*

School of Mechanical & Electronic Information, China University of Geosciences, Wuhan
xcfuwh@yahoo.com.cn, 804902891@qq.com, wenguojun@126.com

Abstract. LCD has being used for displaying characters, pictures, and graphs in every industry. One difficult point is to display the graphs plotted real time with high efficiency and good quality. There are four kinds of main plotting algorithms, i.e., pointwise comparison interpolation method, digital differential interpolation method, midpoint interpolation method, and Bresenham interpolation method, for interpolating the straightline and arc while plotting graphs. Based on the contrast studies for the principles of four algorithms, this paper compared the interpolating efficiency while they are used to interpolate straightline and circle. Then a LCD display system with drive circuit was designed and manufactured for comparing the plotting quality and display effect. Finally, the optimized algorithms with highest efficiency and best quality for plotting were achieved for interpolating the straightline and circle with these four algorithms on the LCD. The research result will be helpful to selecting a best interpolation algorithm for LCD display.

Keywords: LCD, Interpolation Algorithm, Graph Plotting, Interpolating Efficiency, Plotting Quality.

1 Introduction

The graph on the LCD is usually made up of geometric elements and non-geometric elements. The geometric elements include dot, line, face, body. The non-geometric elements include gradation, color, line type, line width [1]. The straightline and arc are basic element of graph, so, the interpolation algorithm about straightline and circle are very important to the graphic efficiency on a LCD.

The interpolation algorithms at present within computer graphics field are pointwise comparison interpolation method, digital differential interpolation method, midpoint interpolation method, and Bresenham interpolation method, time-sharing interpolation method, spline interpolation method and so on. The first four algorithms are mainstream interpolation methods.

The key about the graphic display on LCD is how to exactly select a right interpolation algorithm to perform the interpolation operation real time and with high precision [2]. The general rules to select a good algorithm are as follows: (1) The

* Corresponding author. Tel: +862767883277.

D. Jin and S. Lin (Eds.): Advances in Mechanical and Electronic Engineering, LNEE 177, pp. 89–94.
springerlink.com

straight line should be straight (The arc should be smooth); (2) Line or arc's brightness and color should be uniformity; (3) The speed of plotting should be fast [3].

2 Introduction to Interpolation Algorithms

2.1 Pointwise Comparison Interpolation Method (A)

Pointwise comparison method is also known as regional judging method, algebra operation method, or drunken step type approximation method. After each forward step, this method will compare the current coordinate value with that of the given profile to determine the next step direction, thus ensuring the actual profile matching the given profile. As it approximates the straight line, arc, or all kinds of curve by using the fold line, the maximum allowable error is not more than a pulse equivalent [4]. As a result, as long as the pulse equivalent is small enough, the accuracy of plotting graph will be able to be ensured.

2.2 Middle Point Interpolation Method (B)

The basic principle of middle point interpolation method for interpolating a line is illustrated in Fig. 1. If the current pixel point is assumed to be point $P(x_p, y_p)$, the next pixel point will be point $E(x_p+1, y_p)$ or $NE(x_p+1, y_p+1)$. Point $M(x_p+1, y_p+0.5)$ is the middle point between points E and NE while point Q is the ideal pixel point. If ordinate value y of point M is smaller than that of point Q, the next pixel point will be point NE. On the contrary, the next pixel point will be point E.

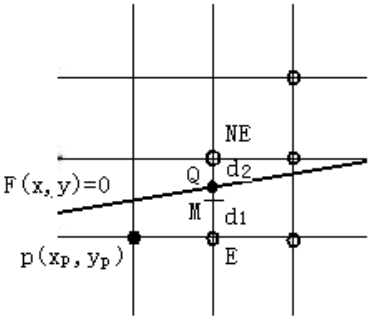

Fig. 1. Interpolating line by using middle point interpolation method

2.3 DDA Interpolation Method (C)

Digital differential analyzer (DDA) interpolation method solves equations by numerical methods. It is also a kind of increment algorithm. The value of x and y in next step will be figured out after x and y in previous step adds a small increment simultaneously and respectively. The value of y and gradient k should be indicated as float number and y should be rounded in each step.

2.4 Bresenham Interpolation Method (D)

The basic idea of Bresenham method is that the point with minimum error value will be next pixel point illustrated in Fig. 2. If given that the current column is $x=x_i$ and the pixels point in x_i column that is most closer to the arc (or straight line) is point $P(x_i, y_i)$, the most closer pixels point in next x column ($x=x_{i+1}$) will be point $H(x_{i+1}, y_i)$ or point $L(x_{i+1}, y_{i-1})$[1]. Point H is on the right of point P and L is on the bottom right of point P. For an arc, the distance between optimized next point and center of the arc will be shortest. For a straightline, the distance between optimized next point and the intersectional point of the straighline and HL will be shortest.

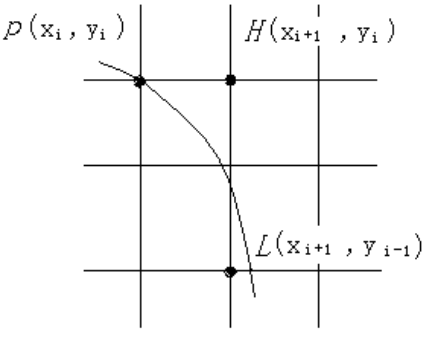

Fig. 2. Plotting arc by using Bresenham interpolation method

3 Contrast and Analysis on Interpolation Efficiency and Plotting Quality for Four Algorithms

The interpolation efficiency for four algorithms will be compared by program simulation in KEIL C51 while the plotting quality will be compared by displaying the straightline and circle on a LCD driven by same circuit. The less time to run the program, the higher efficiency of the interpolation algorithm. The more smoother and thinner of the graph's line, the higher quality of the interpolation algorithm. For an arc, it also need to compare the roundness.

3.1 Comparison on Interpolation Efficiency by Using Four Interpolation Algorithms

3.1.1 Comparison on Interpolation Efficiency for Plotting Straightine

For a straightline between points (50, 140) and (160, 50), the running results for four interpolation algorithms programs are illustrated in Fig. 3 (legend: the "sec" stands for time).

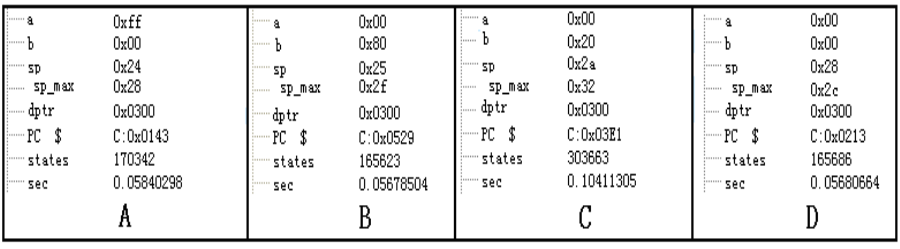

Fig. 3. Running Results of four interpolation algorithms programs for plotting straightline

According to abovementioned results, the running time for interpolating a straightline of four interpolation algorithms can be extracted and listed in table 1. For plotting a straightline, DDA interpolation method used the longest running time for the interpolation program. Pointwise comparison interpolation method, middle point interpolation method and Bresenham interpolation method nearly have similar running time. As a result, DDA interpolation method is the lowest efficient method for plotting a straightline.

Table 1. Running time for interpolating a straightline

Interpolation algorithm	Time
Pointwise comparison interpolation method	0.058403s
Middle point interpolation method	0.056785s
DDA interpolation method	0.104113s
Bresenham interpolation method	0.056807s

3.1.2 Comparison on Interpolation Efficiency for Plotting Circle

For a circle with the center of （150,120） and the diameter of 240mm, the running results for four interpolation algorithms are illustrated in Fig. 4.

According to abovementioned results, the running time for interpolating a circle of four interpolation algorithms can be extracted and listed in table 2. For plotting a circle, pointwise comparison interpolation method and Bresenham interpolation method are the highest efficient algorithms with less time for running program.

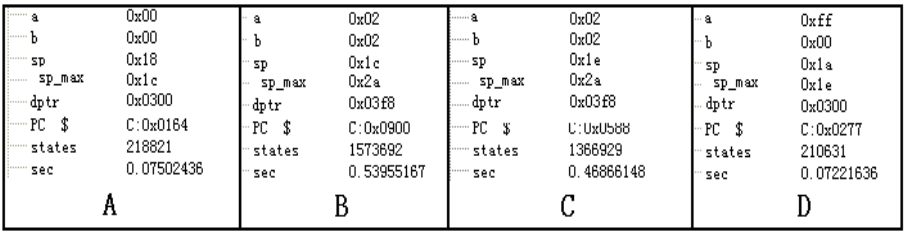

Fig. 4. Running Results of four interpolation algorithms for plotting circle

Table 2. Running time for interpolating a circle

Interpolation algorithm	Time
Pointwise comparison interpolation method	0.075024s
Middle point interpolation method	0.539551s
DDA interpolation method	0.468661s
Bresenham interpolation method	0.072216s

3.2 Comparison on Plotting Quality by Using Four Interpolation Algorithms

3.2.1 Comparison on Plotting Quality for Plotting Straightline

For a straightline, the display results of four interpolation algorithms on a LCD driven by same circuit are illustrated in Fig. 5.

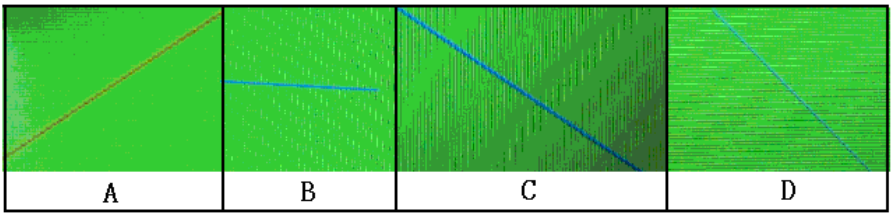

Fig. 5. Display Results of four interpolation algorithms for plotting line

The straightlines plotted by both pointwise comparison interpolation method and Bresenham interpolation method are thinner and smooth. The straightlines plotted by other interpolation algorithm are coarse and zigzag. Consequently, the higher quality algorithms for plotting a line are pointwise comparison interpolation method and Bresenham interpolation method.

3.2.2 Comparison on Plotting Quality for Plotting Circle

For a circle, the display results of four interpolation algorithms on a LCD driven by same circuit are illustrated in Fig. 6.

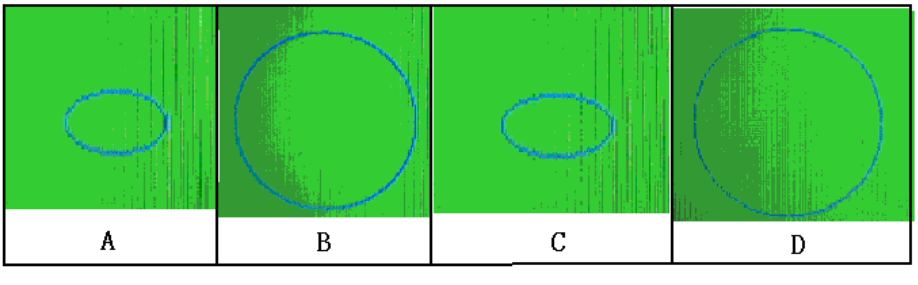

Fig. 6. Display Results of four interpolation algorithms for plotting circle

Circles plotted by middle point interpolation method and Bresenham interpolation method are smooth. Circles plotted by other algorithms are ellipse and the line is not smooth. Consequently, the higher quality algorithms for plotting a circle are middle point interpolation method and Bresenham interpolation method.

4 Conclusions

Based on the analyses for the principles of four kinds of algorithms, pointwise comparison interpolation method, digital differential interpolation method, midpoint interpolation method, and Bresenham interpolation method, the relevant programs are edited and compiled for interpolating straightline and circle with them and then the contrast studies on interpolating efficiency are performed by comparing their running time. After the hardware circuit is designed and manufactured, the plotting quality is compared by displaying the straigntlines and circle plotted by four interpolation algorithms on the same LCD driven by the same circuit.

The contrast studies results provide an optimized interpolating scheme for plotting graph on intelligent LCD display. The pointwise comparison interpolation method and Bresenham interpolation method are best choices for interpolating a straightline while Bresenham interpolation method is a best choice for interpolating a circle.

References

1. Wang, J., Wang, S., Liao, Z.: Virtues and defects analysis of three methods of draw circle. Journal of Xinyang Normal University 18(4), 486–488 (2005)
2. Dong, W., Gao, G., Sun, D., et al.: Study on the errors and real-time interpolation methods. Machine Building & Automation 35(6), 18–20 (2006)
3. Ma, Z.: The demand of drawing line on display & several arithmetic methods. Journal of Gansu Radio & TV University 11(4), 48–51 (2001)
4. Zhang, Z.: CNC applied technology. Chemical Industry Press, Beijing (2004)

Deducing on Rotation Compliance of Single-notch Right Circular Flexure Hinge

Jianying Shen*

College of Mechanical & Electrical Engineering, Jiaxing University,
314001 Jiaxing, China
zjjxsjy@163.com

Abstract. In the paper, the rotation compliance equation of flexure hinge is detailedly deduced. Then, the relationship between the rotation compliance and the ratio t/R is calculated by using the software Matlab. The conclusions can be drawn that the rotation compliance reduces rapidly as the ratio t/R is increased when t/R <0.1 while the rotation compliance reduces slightly as the ratio t/R is increased when t/R >0.1. The result has an important significance to design flexure hinge.

Keywords: Single-notch Right Circular flexure hinge; Rotation Compliance Equation; Deducing.

1 Introduction

Flexure hinge has been widely used in high precision micro-positioning mechanism and the most common type is right circular flexure hinge. Flexure hinge mechanisms have been found wide application in fields like nano-positioning stage[1] and precision displacement system [2]. They have many advantages. They have no stick-slip friction, no clearance, smooth and continuous displacement, and have no need of lubrication and inherently infinite resolution. There are two types of right circular flexure hinge, which are double-notch and single-notch right circular flexure hinges[3,4], respectively. The paper focuses on single-notch right circular flexure hinge.

2 Construction Parameters of Single-notch Right Circular Flexure Hinge

The basic construction parameters of single-notch right circular flexure hinge include the width *b*, the minimum hinge thickness *t*, the cutting radius *R* and the height b, as shown in Fig.1. The notched part of flexure hinge is weak, where a small angular displacement around the rotation axis under the application of the moment *M*.

In actual application its angular displacement is used, so a bigger rotation compliance of flexure hinge around the rotation axis is required. So deformations of flexure hinge come from the necked-down section.

* Corresponding author: College of mechanical & electrical engineering, Jiaxing University, NO.118, Jiahang Road, Jiaxing, China.

D. Jin and S. Lin (Eds.): Advances in Mechanical and Electronic Engineering, LNEE 177, pp. 95–100.
springerlink.com

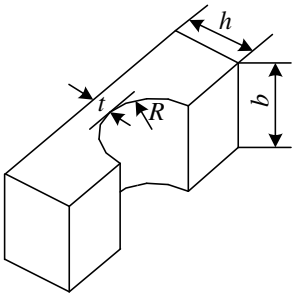

Fig. 1. Single-notch right circular flexure hinge

Through the interface circuit, D/A converter the digital signal from computer is amplified by driving power to produce a control DC voltage to control piezoelectric actuator and the micro stage produces the output of micro displacement driven by piezoelectric actuator. The micro displacement from micro stage is detected by a displacement sensor and it is returned to the computer through A/D data acquisition circuit. Then the closed-loop control for micro stage can be fulfilled by computer according to the deviation.

3 Calculation of Rotation Compliance

The cutting part of flexure hinge is redrawn alone, as shown in Fig.2. According to the integral calculus the slope of a curve is expressed as:

$$\tan\theta = \frac{dy}{dx} \tag{1}$$

Actually, the angular displacement of flexure hinge is very small, therefore, the rotation angle of flexure hinge can be given:

$$\theta \approx \tan\theta = \frac{dy}{dx} \cdot \tag{2}$$

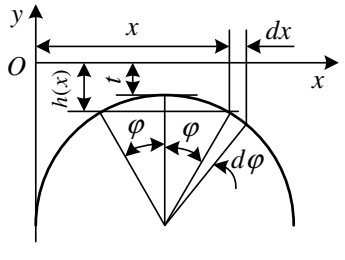

Fig. 2. Calculation of rotation compliance for flexure hinge

According to the simple bending theory of mechanics of materials, the bending equation of flexure hinge can be expressed as:

$$\frac{M(x)}{EI(x)}=\frac{\frac{d^2y}{dx^2}}{\left[1+\left(\frac{dy}{dx}\right)^2\right]^{3/2}}. \tag{3}$$

where, E is the elastic modulus of flexure hinge, $I(x)$ is the rotational inertia of the cross-section on dx, and $M(x)$ is the moment applied on dx.

The rotation angle θ of flexure hinge is very small, so $\left(\frac{dy}{dx}\right)^2 \le 1$. Then Eq.3 can be simplified as:

$$\frac{M(x)}{EI(x)}=\frac{d^2y}{dx^2}. \tag{4}$$

Generally, the length of the notch-part is far less than the other dimensions of flexure hinge. Thus, the bending moment $M(x)$ can be considered as a constant. Integrating Eq.4, the expression of angular deformation can be obtained:

$$\theta=\frac{dy}{dx}=\int_x\frac{d^2y}{dx^2}dx=\int_x\frac{M}{EI(x)}dx. \tag{5}$$

Substituting the rotational inertia $I(x)=\frac{bh^3(x)}{12}$ into Eq.5, the following formula can be given:

$$\theta=\int_x\frac{12M}{Ebh^3(x)}dx. \tag{6}$$

By introducing the central angle as the integral variable for the notch-part shown in Fig.2, we know that the $h(\varphi)$ at an angle φ on the hinge can be expressed as:

$$h(\varphi)=R+t-R\cos\varphi,-\frac{\pi}{2}\le\varphi\le\frac{\pi}{2}. \tag{7}$$

From $x=R+R\sin\varphi$ to give

$$dx=R\cos\varphi d\varphi. \tag{8}$$

Substituting Eqs.7 and 8 into Eq.6, the following formula can be given:

$$\theta=\frac{12M}{Eb}\int_{-\frac{\pi}{2}}^{\frac{\pi}{2}}\frac{R\cos\varphi}{(R+t-R\cos\varphi)^3}d\varphi. \tag{9}$$

From Eq.9, the rotation compliance equation of single-notch right circular flexure hinge can be written as:

$$C=\frac{\theta}{M}=\frac{12}{Eb}\int_{-\frac{\pi}{2}}^{\frac{\pi}{2}}\frac{R\cos\varphi}{(R+t-R\cos\varphi)^3}d\varphi=\frac{12}{Eb}\frac{1}{R^2}\int_{-\frac{\pi}{2}}^{\frac{\pi}{2}}\frac{\cos\varphi}{(1+\frac{t}{R}-\cos\varphi)^3}d\varphi$$
$$=\frac{12}{EbR^2}\int_{-\frac{\pi}{2}}^{\frac{\pi}{2}}\frac{\cos\varphi}{(1+\frac{t}{R}-\cos\varphi)^3}d\varphi \quad (10)$$

Let $n=1+t/R$, the following formula can be obtained as:

$$C=\frac{12}{EbR^2}\int_{-\frac{\pi}{2}}^{\frac{\pi}{2}}\frac{\cos\varphi}{(n-\cos\varphi)^3}d\varphi. \quad (11)$$

Let $P=\tan\frac{\varphi}{2}$, the following formulas can be obtained as:

$$\cos\varphi=\frac{1-\tan^2\frac{\varphi}{2}}{1+\tan^2\frac{\varphi}{2}}=\frac{1-P^2}{1+P^2}. \quad (12)$$

$$d\varphi=\frac{2}{1+P^2}dP. \quad (13)$$

Substituting Eqs.12 and 13 into Eq.11, the following formula can be given:

$$C=\frac{12}{EbR^2}\int_{-\frac{\pi}{2}}^{\frac{\pi}{2}}\frac{\cos\varphi}{(n-\cos\varphi)^3}d\varphi=\frac{12}{EbR^2}\int_{-1}^{1}\frac{2(1-P^4)}{\left[(n-1)+(n+1)P^2\right]^3}dP. \quad (14)$$

Solving the indefinite integral, it can be given:

$$\int\frac{2(1-P^4)}{\left[(n-1)+(n+1)P^2\right]^3}dP$$
$$=\frac{2P}{(n+1)^2\left[(n-1)+(n+1)P^2\right]}+\frac{2nP}{(n+1)^2(n-1)\left[(n-1)+(n+1)P^2\right]^2} \quad (15)$$
$$+\frac{3nP}{(n+1)^2(n-1)^2\left[(n-1)+(n+1)P^2\right]}+\frac{3n}{(n+1)^2(n-1)^2}\frac{a\tan(P\sqrt{\frac{n+1}{n-1}})}{\sqrt{(n-1)(n+1)}}+C_0$$

Then, we get

$$\int_{-1}^{1}\frac{2(1-P^4)}{\left[(n-1)+(n+1)P^2\right]^3}dP=\frac{2(n-1)^2+4n-1}{(n+1)^2(n-1)^2n}+\frac{6n}{(n+1)^2(n-1)^2}\frac{a\tan\sqrt{\frac{n+1}{n-1}}}{\sqrt{(n-1)(n+1)}}. \quad (16)$$

So the rotation compliance equation is obtained by

$$C=\frac{12}{EbR^2}\left[\frac{2(n-1)^2+4n-1}{(n+1)^2(n-1)^2n}+\frac{6n}{(n+1)^{5/2}(n-1)^{5/2}}a\tan\sqrt{\frac{n+1}{n-1}}\right]. \quad (17)$$

The Matlab software is used to calculated the value of the rotation compliance with respect to t/R due to $n=1+t/R$ and the results are shown in Fig. 3. The geometric basic parameters of computational model have a minimum hinge thickness t of 1 mm, a cutting radius R of 3 mm and a width b of 10 mm. 45 steel is selected as the material of flexure hinge, and its elastic modulus E is 206 GPa.

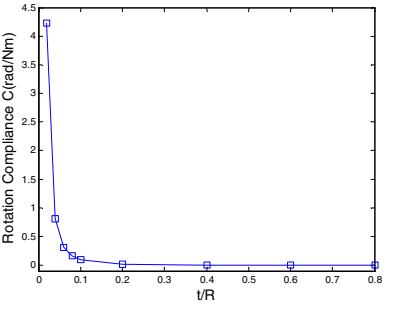

Fig. 3. The value of the rotation compliance with respect to t/R

From Fig.3, we know that the rotation compliance reduces as the ratio t/R is increased. Moreover, there are two cases divided by the boundary line corresponding to the ratio $t/R=0.1$. One case is that the rotation compliance reduces rapidly as the ratio t/R is increased when t/R <0.1. For example, the rotation compliance reduces from 4.22 rad/Nm to 0.15 rad/Nm as the ratio t/R is increased from 0.02 to 0.08. Another case is that the rotation compliance reduces slightly as the ratio t/R is increased when t/R >0.1. For example, the rotation compliance reduces from 0.0178 rad/Nm to 0.0013 rad/Nm as the ratio t/R is increased from 0.2 to 0.6.

4 Conclusions

The In the paper, single-notch right circular flexure hinge has been put forward. The rotation compliance equation of flexure hinge is deduced. Then, the relationship

between the rotation compliance and the ratio t/R is calculated by using the software Matlab. The conclusions can be drawn that the rotation compliance reduces rapidly as the ratio t/R is increased when t/R <0.1 while the rotation compliance reduces slightly as the ratio t/R is increased when t/R >0.1.

Acknowledgements. This work was supported by Science and Technology Bureau of Jiaxing, Zhejiang Province of China, No. 2010AY1087 and by Key Foundation of Jiaxing University, No. 70110X06BL.

References

1. Liu, C.H., Jywe, W.Y., Jeng, Y.R., et al.: Design and control of a long-traveling nano-positioning stage. Precision Engineering 34(3), 497–506 (2010)
2. Wang, S.-H., Chen, Y.-R., Wang, S.-Z., et al.: Design of 3D precision displacement system. Opt. Precision Eng. 18(1), 175–182 (2010) (in Chinese)
3. Wu, Y., Zhou, Z.: Deduct ion of Design Equation of Flexure Hinge. Chinese Journal of Scientific Instrument 25(1), 125–128 (2004)
4. Yang, R., Jouaneh, M., Schweizert, R.: Design and characterization of a low-profile micropositioning stage. Precision Engineering 18(1), 20–29 (1996)

Research on Evaluation and Sensor Modeling for Wireless Channel around Launch Area

Minqiang Dai[1,2], Wei Cai[2], and Shengdun Zhao[1]

[1] School of Mechanical Engineering, Xi'an Jiao tong University, Xi'an, 710049, China
[2] Xi'an Research Inst. of Hi-Tech, Hongqing Town, X'an, P.R. China
dmq0739@163.com

Abstract. The paper constructed a radio frequency signal monitoring platform based on N1918A power analysis soft, N9340B radio frequency spectrum analyzer and several U2000 series power sensor. The spectrum and power of electromagnetic noise of more than 20 observation position around the missile launcher during the whole launching process were measured. And the co-channel interference and adjacent-channel interference data of the wireless monitoring network were obtained. The interference statistical characteristics of main electromagnetic interference sources in different observation position were obtained. The quantitative analysis of electromagnetic interference level in every important position of the whole system during the whole process was implemented. And the bases for modeling of wireless channel and optimization designing of wireless monitoring network were obtained.

Keywords: Launch Area, Electromagnetic Environment, Wireless Channel, Spectrum, Self-organization Wireless Micro Network.

1 Introduction

Wireless intelligent monitoring is a focus research direction of monitoring and diagnosing fields and has wide application prospect in large complex equipments and weapon system. Reliable data transmission which is depended on the wireless data sending and receiving units and wireless channel between them is the basic guarantee of wireless monitoring system [1]. Around launch area of weapon system the electromagnetic environment and wireless channel have important influence on security and fighting efficiency of weapon, and also have important meaning to information-based war [2]. Wireless channel is closely related with space electromagnetic environment and the transmission distance.

In this paper, the accurate evaluation and modeling of wireless channel around launch area were built through full measuring of the electromagnetic environment of the whole weapon system during the process of launching, and the wireless data transmission units and communication protocol were designed according to analysis of the wireless channel characteristics.

D. Jin and S. Lin (Eds.): Advances in Mechanical and Electronic Engineering, LNEE 177, pp. 101–105.
springerlink.com

2 Complex Electromagnetic Environment Sensor Modeling

The number and kind of electromagnetic interference sources were rich around the missile launcher in the launch area, but the major electromagnetic interference sources were determined [3]. Take a launch area for example, the missile launcher and power supply vehicle were the major hosts of electromagnetic interference sources which were mainly consisted of a 40 kW diesel generating set, a 22 kW vehicular diesel generating set, motor, power controller of leveling and erecting, hydraulic pump, hydraulic electromagnetic valves, engine of tractor, 500 ultra shortwave radio and 154 shortwave radio of command automation system, circuit of electronic control system and wireless interphone in launch area etc.

We constructed a radio frequency signal monitoring platform based on N1918A power analysis soft, N9340B high sensitivity radio frequency spectrum analyzer and several U2000 series power sensor. The spectrum and power of electromagnetic noise of more than 20 observation position around the missile launcher during the whole launching process were measured. And the co-channel interference and adjacent-channel interference data of the wireless monitoring network were obtained. The interference statistical characteristics of main electromagnetic interference sources in different observation position were obtained through structuring samples by measurement results. The quantitative analysis of electromagnetic interference level in every important position of the whole system during the whole process was implemented. And the bases for modeling of wireless channel and optimization designing of wireless monitoring network were obtained [4].

According to the above spectrum and power measure method, more than 10 field tests which were aimed at the whole operating process of the missile launcher in the launch area were completed. The power trace diagram of a typical moment and the backgrounds noise spectrum measured nearby power controller of leveling and erecting were shown in Fig. 1.

The following features can be seen from Fig. 1.

(1) All kinds of electromagnetic interference around launch area were shown as pulsations and intermittent.

(2) The interferences were centralized on frequency point or frequency band such as 104.36 MHz, 182.62 MHz, 469.57 MHz, 521.75 MHz, 873.92 MHz, 945.66 MHz, 1402.17 MHz and 1806.52 MHz etc. The noises nearby 873.92 MHz, 945.66 MHz and 1806.52 MHz should be wireless public network which were continuous, and the noise nearby 1806.52 MHz frequency point should be signal of wireless interphone in launch area which was discontinuous but was high signal intensity.

(3) Transient interference with high signal intensity was detected through three dimensions spectrum diagram. Fig. 2 shows the noise spectrum trace diagram obtained by locating in time axis.

As can be seen from Fig. 2, some serious double frequency noises were appeared when the wireless interphone were working nearby the radio frequency observation position.

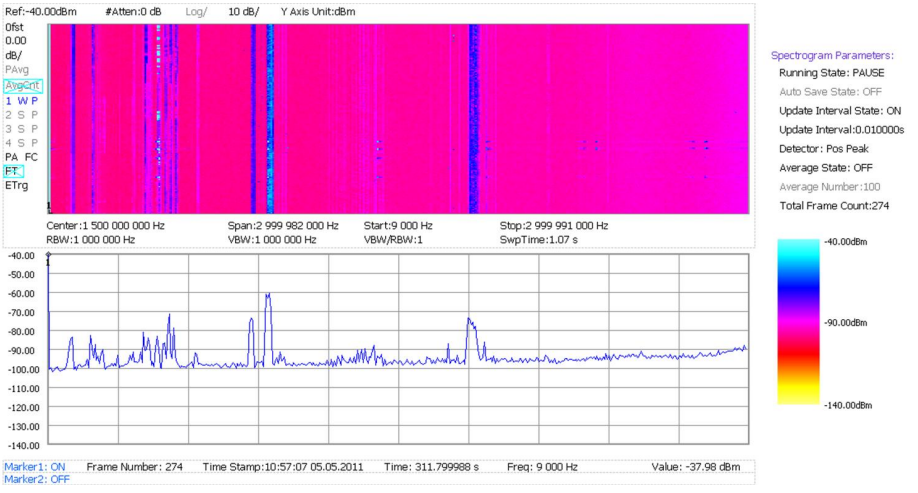

Fig. 1. The power trace and backgrounds electromagnetic noise spectrum diagram measured nearby power controller of leveling and erecting

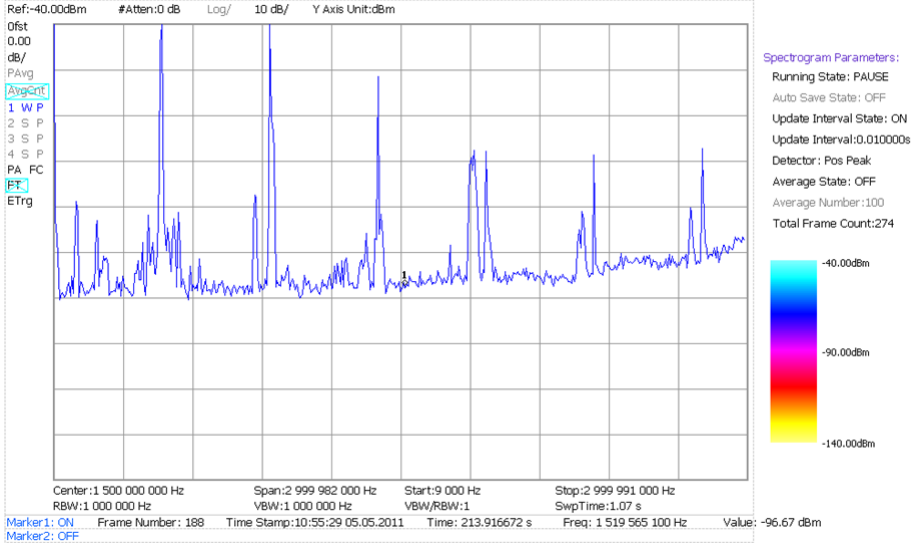

Fig. 2. The backgrounds electromagnetic noise spectrum trace diagram when the wireless interphone were working in launch area

3 Evaluation and Sensor Modeling for Wireless Channel

The interference signal intensity of every main interference frequency point in different moments and different observation position nearby missile launcher can be further accurately measured using the function of N9340B high sensitivity radio frequency spectrum analyzer based on broadband spectrum scanning. According to the measurement results of interference signal intensity, the accurate wireless channel model was built and the basis for optimum seeking and improving of wireless monitoring units was provided.

According to the above measurement results, the system selected two kinds wireless network which were the 2.4 GHz 802.11 b/g backbone network and the 431.41 MHz self-organization wireless micro network based on principle of frequency isolation. As for the later, it is difficult to find an existing suitable model to describe the channel considering the particularity of the application environment. Based on the theoretical analysis, we built a channel model according to noise analysis and radio frequency spectrum measurement of the field and evaluated the loss and fading.

Take the ultimate transmission distance d=30 m for example, the transmission path loss of the self-organization wireless micro network is approximately given as follow.

$$P_L=-10\log_{10}[\lambda^2/(4\pi)^2 d^2] =54.7 \text{ dB}. \quad (1)$$

The interference signal intensity nearby the self-organization wireless micro network working frequency point was approximate 20 dB according to the foregoing backgrounds electromagnetic noise spectrum. In addition, the passive interference, the loss caused by shadow effect, the fading caused by multi-path propagation, the climate effect and the loss of antenna feed line were must be considered, which caused the whole channel loss as 55 dB according to the common channel loss empirical value. In summary, the receiving power was calculated as -89.7 dBm which was more than the receiving sensitivity of the wireless units and had about 30 dB margin [5].

In order to study the practical transmission effects and the signal noise ratio characteristics when all the transmission units of the self-organization wireless micro network were working, the electromagnetic spectrum and power curve in launch area of it during the working process were measured and the results were shown in Fig. 3.

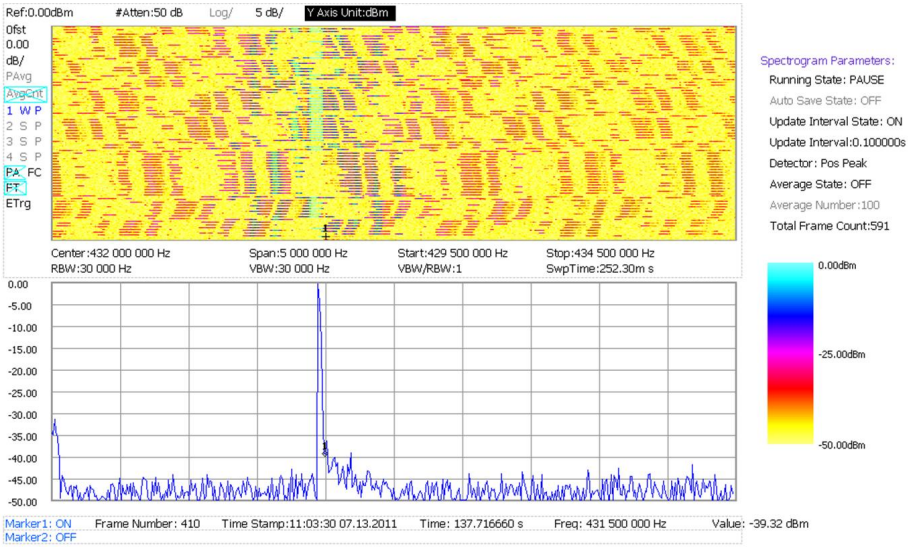

Fig. 3. The electromagnetic spectrum and power curve diagram in launch area when the self-organization wireless micro network was working

4 Summary

Plenty of measurement results shown that noise level differences were reached 20 dB with differences of the time which was meant the operator states of equipment and the space which was meant the location of the monitoring equipments.

According to contrast tests, the best location of the monitoring equipments were determined, which the measurement results by N9340B radio frequency spectrum analyzer shown that the signal noise ratio in effective frequency band was more than 30 dB. At the same time, the bandwidth usage and the ratio of co-channel and adjacent-channel of the wireless monitoring units were can be accurately measured by the N9340B. The data transmission reliability can be determined close to 99.99% based on the empirical comparison relationship among signal noise ratio, data transmission reliability and receiving level margin.

References

1. Dai, M., Zhao, S., Yuan, X.: In: Yang, Y., Ma, Y. (eds.) Advanced Materials Research, vol. 323, Publications/Trans. Tech. Publications (2011)
2. Ding, X., Chen, Y.: Equipment Environmental Engineering 8(1) (February 2011)
3. Li, N., Zhang, X.: Equipment Environmental Engineering 5(1) (February 2008)
4. Xie, J., Fann, P.: Journal of Southwest Jiaotong University 8(1) (May 2000)
5. Wang, D., Shang, S., Dong, J., Lu, M.: Journal of Harbin Institute of Technology 7(4) (2000)

Multiunit Synchronization Control System of Dyeing Mechanical and Electronic Equipment Based on PROFIBUS-DP

Lian Yang, Xiujie Dong, and Kai Fu

The School of Electronic Information, Zhongyuan University of Technology, China

Abstract. This paper sets up a multi-level network composed by Siemens S7-300 PLC and Ac motor of mechanical equipment synchronization control system. It is based on PROFIBUS-DP fieldbus, designs a multiunit synchronization control system of dyeing mechanical equipment specifically introduces control strategy and algorithm of the mechanical electronic synchronization control system in the transmission, electronic control system integration programs, realization of PLC and MicroMaster 440 communication. The paper proves that: the operation of control system is stable and reliable, static control precision can reach 0.05%, when a given order mechanical no-load speed step change the dynamic response of the system is 10% less than 200 ms, all the technical indexes can meet the requirements of the printing and dyeing machinery and electronic process.

Keywords: mechanical and electronic engineering, synchronization control, data communication, network structure.

1 Introduction

In dyeing industry, the jigger is a of the more varieties of small batch dyeing equipment, the production process through the fabric in jigger several times back and forth winding, uniform dyeing of the fabric. Jigger is main made up of received unwinding unit, draw roll 1, 2, before and after the pressure volume, dye tank unit. Among the unwinding and rewinding units 1, 2, draw roll 1,2 is driven by an independent of AC induction motor. To ensure uniform dyeing and winding evenly, it is necessary to achieve the synchronization control of multi-unit, making the fabric between each unit, a constant tension[1][2]. But jigger in the process of winding and rewinding, the diameter of the winding roller and the unwinding roll is constantly changing. How to ensure that the jigger received any speed, and change in diameter of the winding, unwinding tension stability, coordination and control of each unit is the core of the machine control. This paper use PROFIBUS-DP field total to build the entire transmission network control system, synchronization of multi-unit motor control with PLC.

D. Jin and S. Lin (Eds.): Advances in Mechanical and Electronic Engineering, LNEE 177, pp. 107–112.
springerlink.com

2 System Architecture and Control Strategy

The jigger AC motor synchronous control systems architecture is shown in Figure 1.

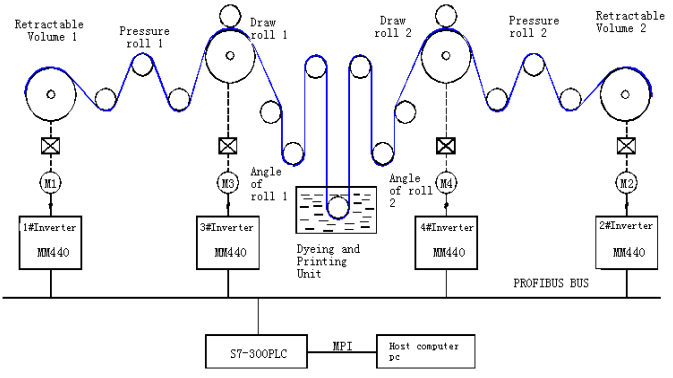

Fig. 1. PROFIBUS-DP based dyeing machine control system architecture diagram

2.1 Control System Structure

Control system is divided into three. The first level the field level by the four inverters, the jigger four independent drag unit drive control respectively, by Siemens the MicroMaster 440 series vector control (FOC) of general purpose inverter. Inverter with pulse encoder and counter module for the detection of the motor running speed. Each inverter plug PROFIBUS-DP communication module, the inverter via PROFIBUS communication template is connected to the PROFIBUS-DP bus, makes up network with the host PLC. Second-level control system for the PLC, PLC as the master, use SEMIENS the S7-300 series, with the inverter via PROFIBUS-DP bus high-speed communication to complete the site status signal and run data collection, draw roll speed control the speed of the unwinding and rewinding to follow as well as closed-loop tension control, realization of the entire printing and dyeing system synchronization control of the transmission. S7-300 PLC via the DP interface attached to the PROFIBUS-DP fieldbus, control and monitoring of the inverter via PROFIBUS, such as sending a control word, the main the given value, and so on, the inverter status word and actual value. The third level is the upper optimal control system, DELL company's industrial control computer, connected via the CP5611 card and MPI cable PLC's MPI interface. The host computer using the Siemens configuration software WinCC, through Industrial Ethernet communication with the PLC, implement control system monitoring and management and human intervention.

2.2 Control Strategy

Use closed loop tension control with speed mode, through the tension sensor feedback and draw roll linear velocity input to control the constant tension.

2.2.1 Drafting Rollers 1, 2 Motor Control Strategy

Set directly on the drafting rollers 1, 2, two inverter speed (frequency f_q) converted into a run, with a floating roll angle roller 1,2, for the indirect detection of tension, floating roller piston with low friction cylinder is connected [3] [4]. It works when the fabric tension to the desired settings, the floating roller in a vertical position, but once due to various disturbances of fabric tension changes, the floating roller to deviate from the vertical position, have a certain swing angle θ, do PID operation for the swing angle feedback and main settings ,the output of the PID regulator as the operating frequency compensation amount Δf_q , final two inverter operating frequency settings $f = f_q + \Delta f_q$. The system according to the draw roll 1,2 tension change, real-time adjustment of the two inverter operating frequency settings, so that the tension throughout the winding process, two draw roll 1,2 remained in the settings to allow range, in order to achieve the draw roll 1,2 between the fabric of a constant linear velocity, then the linear velocity of the whole system also will be constant.

2.2.2 Unwinding and Rewinding of the Motor Control Strategy

Retractable volumes 1 and 2 must follow the speed of drawing roller motor running, the control method of the unwinding and rewinding one motor:

Draw roll to one inverter output frequency f_{qy} of collection into the PLC, and translated into linear velocity V conversion formula:

$$V = \pi \cdot D_q \cdot f_{qy} \cdot 60 \cdot (1 - s_q) / (i_q \cdot p_q) \tag{1}$$

Equation (1), D_q : Diameter of Draw roll one; i_q : Mechanical Transmission Ratio of Draw roll; p_q : Pole Pairs of Draw roll one motor; s_q : Slip of Draw roll one motor.

Unwinding and rewinding a motor running line speed for the V ,PLC according to the unwinding and rewinding roll a drum roll diameter D_s calculation to match the frequency of the motor settings f_s :

$$f_s = V \cdot p_s \cdot i_s / 60 \cdot \pi \cdot D_s \cdot (1 - s_s) \tag{2}$$

i_s : The Mechanical Transmission Ratio of Retractable roll p_s : The Pole Logarithmic of Retractable Volume one motor; s_s :Slip of Retractable Volume one motor.

Equation (2), actual operating speed n_s of the unwinding and rewinding a motor, drum roll diameter :

$$D_s = V \cdot i_s / \pi \cdot n_s \tag{3}$$

PID regulator, the regulator's output Δf_s matches the frequency compensation as a motor rewind and unwind, unwinding and rewinding motors operating frequency settings:

$$f_3 = f_s + \Delta f_s \tag{4}$$

This retractable volume motor will follow the draw roll speed, and in accordance with the rewind and unwind at the size of the actual tension and coil diameter changes in real-time change its operating speed, constant tension control system.

3 Control System Integration and Configuration

Function of the control system requirements, I / O points and control characteristics, complete to the control system hardware integration, and then the programming software STEP 7 V5.5,complete system configuration . Configuration master, the hardware configuration window of the "synchronization control" projects in accordance with the item number of the hardware, firmware version and the actual connection order to add rack, CPU module, the switch I / O modules and analog I / O modules, configure the properties of the PROFIBUS network. Configuration slave, the four sets of the MicroMaster 440 inverter (slave device) attached to the PROFIBUS-DP network, station address distribution of each inverter is respectively 3, 4, 5, 6, confirm that the communication of PPO type PPO3, the system will automatically assign the communication area of the four drives. PZD data such as # 1 inverter PIW256 PQW256 ~ 259 ~ 259. Control system configuration results shown in Figure 2.

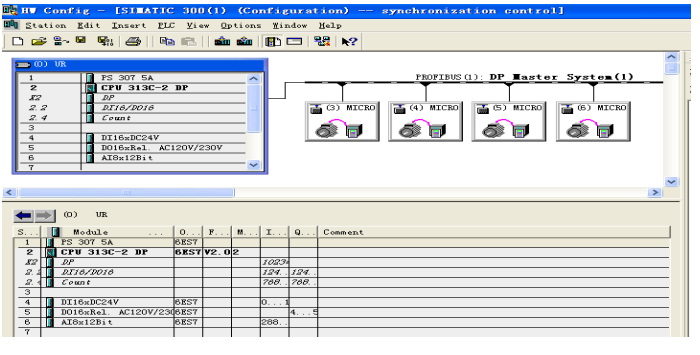

Fig. 2. Dyeing machine multi-camera control system hardware configuration

4 The Communication of S7-300PLC and MicroMaster 440

In the synchronous control system, PLC as grade a DP host connects PROFIBUS . It is used in data communication with a bus from 4 sets standing (MM440), releasing control command, sending position, speed, tension set data and etc.

PROFIBUS- DP protocol exchange data with message, and the structure of the MM440 cyclic data communication message coding is shown in fig.3.

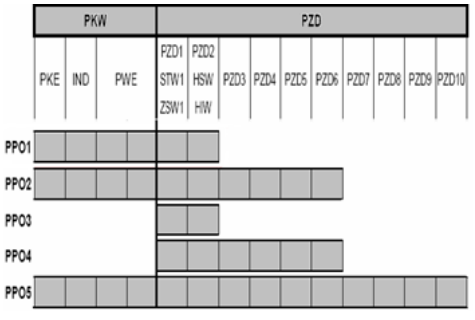

Address	Name	Type	Initial value	Comment
0.0		STRUCT		
+0.0	PKE_R	WORD	W#16#0	READ PKW-PKE
+2.0	IND_R	WORD	W#16#0	READ PKW-IND
+4.0	PWE1_R	WORD	W#16#0	READ PKW-PWE1
+6.0	PWE2_R	WORD	W#16#0	READ PKW-PWE2
+8.0	PZD1_R	WORD	W#16#0	READ PZD-ZSW
+10.0	PZD2_R	WORD	W#16#0	READ PZD-HIW
+12.0	PKE_W	WORD	W#16#0	WRITE PKW-PKE
+14.0	IND_W	WORD	W#16#0	WRITE PKW-1ND
+16.0	PWE1_W	WORD	W#16#0	WRITE PKW-PWE1
+18.0	PWE2_W	WORD	W#16#0	WRITE PKW-PWE2
+20.0	PZD1_W	WORD	W#16#0	WRITE PZD-ZSW
+22.0	PZD2_W	WORD	W#16#0	WRITE PZD-HIW
=24.0		END_STRUCT		

Fig. 3. packet structure of data communication , packet structure of the PLC data buffer

In order to realize the periodic data communication between PLC and inverter MM440, The packet structure of the data buffer is shown in fig3.As the system running, in the PLC communication program, according to call the system function block SFC14/SFC15 , read each inverter status words and the master actual value and send the control word and the lord given value to each inverter, each call of the system function block could read and modify a set of parameters.

With inverter 1# for example, insert data block DB1 into the program block, then according to call the system function block SFC14(DPRD_DAT) in the organization block S7-300PLC read the status word and the main actual value from the 1# inverter output start address of W # 16 # 100 . Call SFC15 （DPWR_DAT） to write out control word and master given value into1# inverter output start address of W # 16 # 100 (256). Communication program is as follows:

```
Network 1:
A     M    5.1
=     L    20.0
A     L    20.0
JNB   _001
CALL "DPRD_DAT"
LADDR : = W#16#100
RET_VAL : = MW12
RECORD: =P#DB1.DBX8.0 BYTE 4
_001  NOP  0
JNB   _002
CALL "DPWR_DAT"
LADDR: =W#16#100
```

```
RECORD: =P#DB1.DBX20.0  BYTE 4
RET_VAL:=MW14
_002  NOP  0
```

So MM440 through the method of PROFIBUS communication and realize the synchronous control.

5 Conclusion

This dyeing and printing equipment employ the Siemens S7-300 PLC and vector control inverter MM440, and the PROFIBUS-DP fieldbus is applied to constitute multi-level network for realizing the coordination control of multiple independent unit , thus the cost of the hardware connection is greatly reduced; Optimized control strategy improved the mechanical and electronic system speed and tension control accuracy; The process data transmitted from the master station to passive station through PROFIBUS fieldbus has ensured the real-time and reliability of the mechanical electronic system control and greatly reduced the cost of hardware connection. Practice has proved that this mechanical and electronic control system is stable and reliable, the static control precision can reach 0.05%, in the case of mechanical and electronic system on-load when given a speed step change of 10% the time of the mechanical and electronic system dynamic response will be less than 200 ms, all technical indicators can meet the requirements of dyeing machinery and electronic process.

References

1. Cui, J.: The Siemens Industry Network Communications Guid. Mechanical Industry Press (2005)
2. Zhu, T.: The VVVF tension control method and its application. Electrical Drive Automation (2010)
3. Zhang, X., Yang, K., Zhang, C.: Intelligent Detection System Tension. In: Proceedings of the 2010 International Conference on Information Technology and Scientific Management, vol. 2 (2010)
4. Yau, H.-T., Li, S.C.: Implementation of Optimal PID Control for Chaos Synchronization by FPGA Chip. In: Proceedings of the 2011 International Conference on Fluid Power and Mechatronics (2011)

Injection Mold Running System Optimal Design of Lampshade Part Based on Moldflow

Shuhui Ding[1], Zhenyun Chu[2], Xueyi Li[1], and Peisi Zhong[1]

[1] College of Mechanical and Electronic Engineering, Shandong University of Science and Technology, 579 Qianwangang Road, Qingdao, China
[2] Engineering Training Center, Shandong University of Science and Technology, 579 Qianwangang Road, Qingdao, China
{shding,czy,xueyi_1,pszhong}@sdust.edu.cn

Abstract. In order to solve the questions of long cycle, high cost, one time success rate and etc during the mold design, polymer rhelolgy theory is introduced. Power-law equation is used to describe the rheological behavior of pseudoplastic fluid. The location of gate is optimized in Moldflow and several modeling schemes are listed. With the help of the filling time analysis, cavity pressure analysis, injection mouth pressure curve analysis and flow front temperature analysis, scheme with best gate location and runner system is confirmed.

Keywords: Gate location optimizing, Runner system optimizing, Pseudoplastic fluid, Moldflow.

1 Introduction

In traditional design process of injection mold, only after many times of mold test and repair, qualified products can be produced. The cycle of traditional mold design process is long and cost, and at the same time, the inner character of mold will changed, which can lead to the reduction of mold performance[1].

Injection process simulation is a professional CAE technology[2]. Under the circumstance of injection process simulation, according to the basic theory of plastic processing rheology and heat transfer[3,4], the mathematical model of flow and heat transfer of melted plastic in mold cavity is built. With the help of numerical calculation theory, the phases of filling, holding and cooling of thermoplastic injecting process are simulated. Through the forecast of plastic melt's flow in runner, gate and cavity, and the calculation of distribution of pressure field, temperature field and shear stress field, the gate location and injection technology parameters are optimized, and the possible defects of short shot, burns, unreasonable weld line location and cavitation are found timely.

2 The Rhelolgy Theory of Polymer

Rheology is the subject of material deformation and flow research, which is the basis of plastic injection. The injection molding process of melted polymer is a

D. Jin and S. Lin (Eds.): Advances in Mechanical and Electronic Engineering, LNEE 177, pp. 113–118.
springerlink.com

non-isothermal, unsteady non-Newtonian fluid flow and heat transfer process. The flow behavior changes of melted plastic along with pressure, temperature, shearing rate and other physical quantity directly affect the inner structure, residual stress and final shape.

Incompressible perfect fluid will flow with very small shear stress, which is the pure viscous flow. When the external force is released, the flow stops immediately, but the viscous yielding cannot be recovered. The shear stress generated within the layers of fluid is in proportion to the normal velocity, and has nothing to do with the press. The shear stress of perfect fluid follows the Newton law of viscosity, which is expressed as follows:

$$\tau = \mu \frac{du}{dy} \tag{1}$$

where τ stands for shear stress, du/dy is the shear velocity, μ stands for Newtonian viscosity, which is a material constant having nothing to do with time and shear velocity.

But polymer fluid has the characteristics of non-Newtonian viscosity, elastic recovery and molecule orientation, which is not possessed by ordinary simple fluid. Its flow behavior presents as pseudoplastic[5]. When the fluid velocity rises step by step, its shear stress decreases. There is not a linear relationship between shear stress and velocity, which is shown as Fig.1.

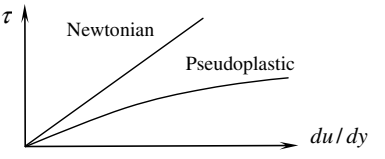

Fig. 1. The shear velocity-shear stress graph between Newtonian fluid and pseudoplastic fluid

At present, there is not a precise rheology definition which can reflect the essence of Newtonian melted plastic fluid. But some simplified models, such as power-law equation, can express some of its characters[6]. Power-law equation is used to describe the rheological behavior of pseudoplastic fluid. There is not gelstrength when the fluid holds still. So, when there is a very small force, the fluid can flow. With the increase of shear stress, pseudoplastic fluid appears thinner gradually. The power-law equation is shown as follows:

$$\tau = k(du/dy)^n \tag{2}$$

where τ is shear stress, du/dy stands for shear velocity, k is consistency coefficient and n is power law index which stands for the level of non-Newtonian. When $n=1$, the fluid is . When $n<1$, the fluid is pseudoplastic.

3 Part Modeling and Moldflow Preferences

Moldflow is the leading product of plastic molding flow simulation software. With the help of Moldflow, the times of mold test are reduced, the product cost is decreased, the product development cycle is shortened and the product quality is improved[7].

The parts of lampshade have complicated profile, so it is difficult to model lampshade parts in Moldflow directly. The 3D model of lampshade is created in Pro/Engineer software and saved as IGES format, which can be opened in Moldflow. The lampshade is shown in Fig.2.

Fig. 2. The 3D model of lampshade part

The material of this part is ABS and its coefficient of heat conductivity, density, specific heat, modulus of elasticity, coefficient of thermal expansion, limit of yielding and other parameters are shown in Fig.3-6.

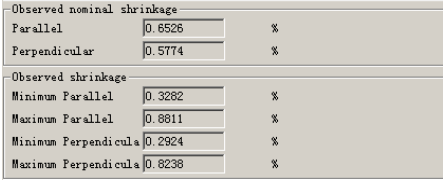

Fig. 3. Shrinkage characteristic of the part

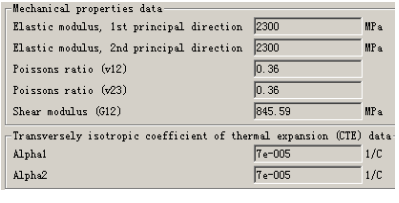

Fig. 4. Mechanical characteristic of the part

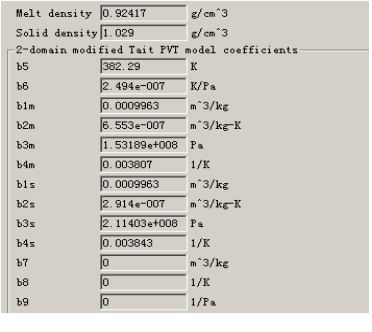

Fig. 5. Other characters of the part

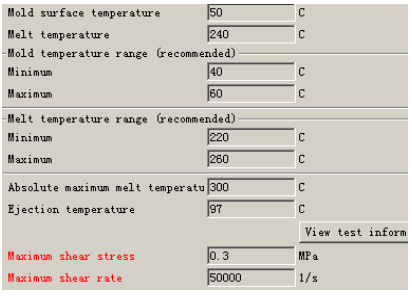

Fig. 6. Recommended process condition

4 Gate Location Analyses

With the help of optimization in Moldflow, the best gate location can be analyzed according to the part's geometry and other technological parameters, which can avoid the possible defect caused by improper gate location. The analysis result of gate location is shown as Fig.7.

Fig. 7. Result of the best gate location analysis

The gate location analysis result figures show the layout of optimal gate and there are three places where the scheme is feasible. The first scheme is to use the point of factor 0.9136 as the gate location and submarine single gate is used. The factor 0.8369 point is used as gate location, which is the second scheme and edge double gate is used. At the third scheme, the point of factor 0.776 is the gate location and edge single gate is adopted.

Because the performance of runner system can affect the filling of product, the filling result can be used to analyze the runner system further. At the next part of this thesis, the flow behavior of different scheme is compared, and then the best gas location, gate number and the layout of runner system are determined.

5 Filling Analysis

The stage of filling starts from the entrance of melted plastic into cavity to the arriving of fluid to the cavity bottom. The melt fluid front positions at different time are shown by the calculation of filling analysis, which is used to forecast the filling behavior under the circumstance of relative technology preferences.

The important parameters during filling process include melt temperature, injection pressure and filling time. The technology condition settings of filling include the control of filling, the transfer between velocity and pressure and pressure maintaining. The filling result consists of filling time, molecular orientation, shear velocity, cavitation and welding line.

Take the third scheme as example, and its filling time result is shown in Fig.8. The following conclusions can be drawn. (1) Filling time at two sides of the gate is mainly symmetrical. (2) The velocity of melt fluid front is equal in the two sides of the gate. (3) All the far-end of the cavity is filled at the same time.

At every time of filling, the pressure value of every node is recorded. The pressure distribution during filling should be balanced, and in pressure stage there should be a balanced pressure distribution. In the third scheme, when the filling finishes at 1.182

seconds, the peak value of cavity pressure is 76.19MPa, which is shown as Fig.9. In the first scheme, the peak value is 66.88MPa, and the second is 56.73MPa.

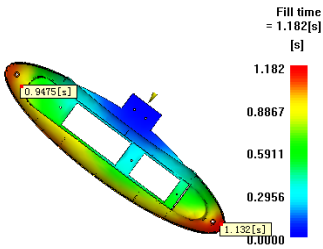

Fig. 8. Filling time of the third gate location scheme

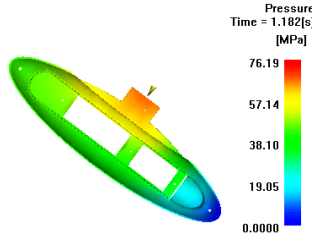

Fig. 9. The cavity pressure at 1.18 seconds of the third scheme

Because the pressure when the filling ends is very sensitive to pressure balance, the balanced filling of workpiece will be achieved, if the pressure distribution graph shows the pressure is in equilibrium at the end of filling. In the first scheme, there is a little nonequilibrium, which is mainly manifested in the obvious pressure difference at both ends of the symmetrical region. In the second scheme, the pressure distribution is almost balanced. In the third scheme, the deviation of mean value is a little large.

The injection pressure is important parameter in molding, and it determines the pressure limit value that the injection molding machine should provide. The pressure curve of injection mouth in the third scheme is shown in Fig.10, and its injection pressure limit value is about 80MPa. The design pressure limit of mold is about 70% of injection molding machine. So the machine with pressure limit of 140MPa can meet demands. But there is a peak on the pressure curve at about 1.1 second, which indicates that the filling pressure of workpiece is nonequilibrium, or the filling velocity increases because of the obvious decrease of the frontier fluid. The injection mouth pressure of the first scheme is 48MPa and the second is 68MPa. The pressure curves of the first and second scheme is smooth, which indicates there is very little or no undercurrent in these schemes.

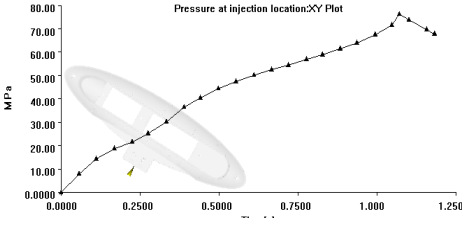

Fig. 10. The injection mouth pressure curve of the third scheme

Temperature at flow front is a mid-stream nodal result generated from a mid plane, Fusion and 3D flow analysis, and shows the temperature of the polymer when the flow front reached a specified node. If the flow front temperature is too low in a thin

area of the part, hesitation or short shot may occur. In areas where the flow front temperature is too high, material degradation and surface defects may occur. Rational flow front temperature distribution should be uniform, otherwise hesitation may occur. The flow front temperature graph of the third scheme is shown in Fig.11 and the temperature difference is 4.7°C. In the first scheme, the difference is also 4.7°C and the second scheme is 2.5°C.

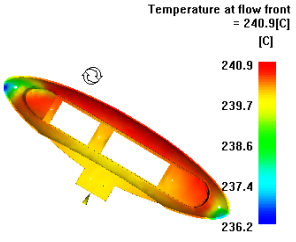

Fig. 11. The flow front temperature graph in the third scheme

6 Conclusions

With the help of 3D modeling technology and rhelolgy theory of polymer, the location of workpiece gate is optimized in Moldflow and there modeling schemes are listed. With the help of the filling time analysis, cavity pressure analysis, injection mouth pressure curve analysis, flow front temperature analysis, conclusion can be reached that the gate location and runner system of the third scheme is the best.

Acknowledgement. This research is financially supported by Shandong Province Natural Science Foundation, China (No. ZR2011EEM014 and ZR2010EM013) and Science and Technology Development Program of Shandong Province, China (No. 2010GGX10408).

References

1. Liu, X.F., Zhang, F.: CAD/CAE Technology for Injection Mould Based on Pro/E and moldflow. Machinery Design & Manufacture 4, 239–241 (2011) (in Chinese)
2. Qian, P., Zhu, H.J., Zhu, L.: Application of CAE Technology in Optimum Design of the Injection Mold Filling System. Mechanical Engineer 4, 84–86 (2010) (in Chinese)
3. Kaminoyama, M., Nishi, K., Misumi, R.: A Method for Determining the Representative Apparent Viscosity of Highly Viscous Pseudoplastic Liquids in a Stirred Vessel by Numerical Simulation. Journal of Chemical Engineering of Japan 44, 868–875 (2011)
4. Mitsoulis, E.: Fountain Flow of Pseudoplastic and Viscoplastic Fluids. Journal of Non-Newtonian Fluid Mechanics 165, 45–55 (2010)
5. Guedda, M., Kersner, R.: Non-Newtonian Pseudoplastic Fluids: Analytical Results and Exact Solutions. International Journal of Non-Linear Mechanics 46, 949–957 (2011)
6. Yu, X.R.: Study and Application of Design Optimization for Injection Molding. Zhengzhou University, Zhengzhou (2004) (in Chinese)
7. Cao, J.D., Lu, L.X.: Optimum Design of Injection Mould of Hairdryer Shell Based on Moldflow. Plastics 39, 122–125 (2010) (in Chinese)

Springback Analysis and Bending Process Numerical Simulation of Inserted Slice

Shuhui Ding, Xueyi Li, Peisi Zhong, and BinBing Huang

College of Mechanical and Electronic Engineering, Shandong University of Science and Technology, 579 Qianwangang Road, Qingdao, China
{shding,xueyi_1,pszhong}@sdust.edu.cn, kinghuang1990@163.com

Abstract. In order to solve the problem of springback control difficulty in the bending process of stamping parts, on the base of the mechanism introduction of the springback, the algorithms of dynamic explicit and static implicit are analyzed. Dynamic explicit is used to analyze the forming process and its result is taken as the initial condition which is provided to the springback analysis with the algorithms of static implicit. Through the analysis of the calculation results, the thinning and springback is allowable and the forming process can meet production requirement.

Keywords: Springback, dynaform, dynamic explicit, static implicit.

1 Introduction

A variety of complex physical phenomena are contained in the bending process of stamping parts, which mainly includes contact and impact, friction and wear, large displacement, large rotation and large deformation and elastic-plastic deformation[1]. The complexity of these phenomena makes it very difficult to design and control, resulting in the defects in the forming process, and it is difficult to correct. The most important quality of the defects in the bending process is wrinkling, rupture and springback of the parts, and the springback is the most difficult to control, which involves accurately predict of it, and the law of springback vary greatly for the different materials and different shapes of stamping[2].

The springback is a key factor to consider in mold design for sheet metal forming, and the final shape of the parts depends on the springback after forming[3]. It turns to be the forming defects when the springback exceeds the allowable tolerance, and affects the parts of the geometric accuracy.

2 The Mechanism of the Springback

Any kinds of plastic deformation of the sheet metal under outside loads consists of the plastic deformation and elastic deformation. When the external load is removed, the plastic deformation of materials save the residual deformation and make the parts deform. However, size deformation changes in the opposite direction when the load changes due to elastic deformation elastic recovery and plastic deformation of elastic

D. Jin and S. Lin (Eds.): Advances in Mechanical and Electronic Engineering, LNEE 177, pp. 119–124.
springerlink.com

deformation part of the elastic recovery of its shape, this phenomenon is known as springback, which in all kinds of the stamping process are likely to occur. Classification in accordance with the traditional stamping forming, sheet metal forming includes bending, drawing, flanging, local shape, bulging, flaring and necking, etc. The most typical is the springback after unloading in the bending process and the springback is the most serious[4].

Pure plastic bending occurs under plastic moment in sheet metal, the tangential stress distribution on the cross section is shown in Fig.1. Assuming a hypothetical elastic bending moment M applied in sheet metal, which equal to the plastic bending moment in numerical , but in the opposite direction when unloading. At this time the outside torque of sheet metal suffered is zero. The resultant stress of plastic moment and the hypothetical elastic moment in the cross section of sheet, that is, the residual stress at free state on the cross section of bending part after unloading, which changes in the order of pulling, pressure, pulling, pressure within the cross-section of the deformation zone from the inner to the outer layer . Fig.2 shows the tangential stress changes in cross-section of the sheet when the elastic-plastic bending is unloaded.

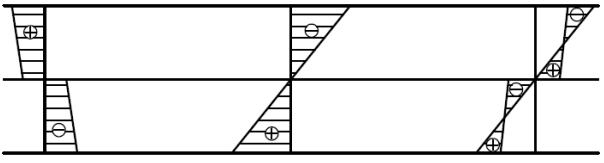

(a) Elastic bending (b) Elasto plastic bending (c) Plastic bending

Fig. 1. Shear stress change of plates section during the plastic bending unload

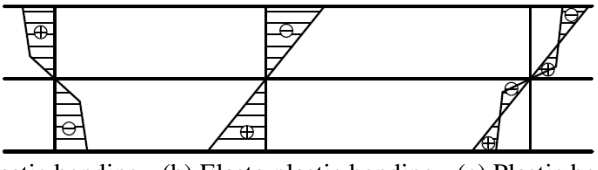

(a) Elastic bending (b) Elasto plastic bending (c) Plastic bending

Fig. 2. Shear stress change of plates section during the elastic bending unload

From the analysis above we can see that, the inner and outer stress and strain is on the contrary in nature in the loading process on the bending deformation zone, and the direction of springback deformation is opposite when unloading. The result is that the shape and size change is very significant in bending parts, and seriously influence the size precision.

3 Algorithm Analysis of Sheet Metal Forming Numerical Simulation

Sheet metal forming numerical simulation solution mainly includes dynamic explicit and static implicit algorithm[5-6]. Accurate inserted slice numerical simulation

includes forming process and the springback after forming, these contents use dynamic explicit algorithm and static implicit algorithm combined methods to solve.

Constructing and solving the large sparse stiffness matrix are consisted in the solving process of static implicit algorithm, and each step of the iteration requires contact detection. With large amount of calculation and high precision of calculation, it can solve the springback problem of high efficiency. The dynamic explicit algorithm uses explicit time integration, which is usually based on dynamic time difference scheme, and is characterized by its explicit finite element equation, avoids iterative algorithm in static implicit integration algorithm, so it is suitable for calculating all kinds of complex molding problem with the high calculation efficiency and good stability.

In this thesis, during the numerical simulation of the bending and springback of inserted slice, dynamic explicit algorithm is used to compute the forming process, and then static implicit algorithm is taken for the springback analysis, using the forming result.

Its process is as follows. (1) Import the geometry model of forming parts and take finite element mesh of it. (2) Define the forming tool. (3) Define blank. (4) Define forming parameters. (5) Solving. (6) Post processing. stress, strain and thickness isoline map analysis; stress, strain and thickness of the cloud image analysis; forming limit diagram analysis; deformation animation; section stress, strain and other display of physical quantity changes, etc. According to the calculation results, modifications to the parameters in the forming process of sheet metal and guide the actual die design are proposed.(7) Springback analysis. Import the above calculated model, complete the springback analysis parameter settings and analyse the springback results.

4 Numerical Simulation and Springback Analysis of Inserted Slice

4.1 Modeling

The bending model of inserted slice is shown in Fig.3. The symmetrical structure of parts is benefit of improving the bending springback, so the die for bending is designed in a cap-shaped pieces at first, then cut it off to the inserted slice body. Low alloy steel plate of 09MnV is selected as the material. The material model selected is the 3-parameter Barlat material model, which takes both the influence of thick anisotropic of the material and the anisotropy in the plane of the sheet on the yield surface into account, the model can well reflect the influence by anisotropy in stamping.

Fig. 3. Solid model of inserted slice

4.2 The Selection of Element Type

The selection of element type is one of the main factors affecting the precision of forming simulation. We should choose the appropriate element type according to the different situations in the finite element numerical simulation. For sheet metal forming simulation analysis, the most commonly used element types are the Hughes-Liu shell element and Belytschko-Tsay shell element. But in the analysis of springback, we should use the FULL INTEGRATED element (the element of integration) with a lot of time, but it is accurate for the springback analysis, also appears less convergence problem. Therefore, this paper uses the FULL INTEGRATED element.

4.3 Analysis and Calculation

(1) Analysis and solution. Submit the forming job and finish the analysis. Open the "Post-processor" and observe the preliminary analysis of sheet metal forming, which defects more obvious affect the subsequent operation, can not correctly calculate the springback angle and springback radius of curvature. Thinning examination, through the thin volume changes can find the rupture and wrinkling defect in process of blank forming. The thinning of this analysis is shown in Fig.4. The forming limit diagram(FLD) can be a very good description of the stamping process of the blank forming conditions,which is shown in Fig.5.

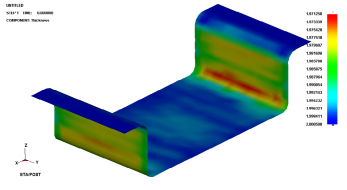

Fig. 4. The thinning condition before springback

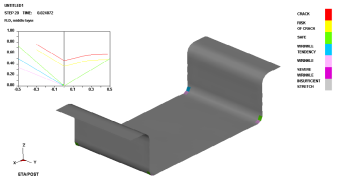

Fig. 5. The FLD before springback

(2) Calculation of springback and analysis of springback result. Import the earlier calculated model, and analyze the springback of part. The "LS-DYAN3D" calculation module completes the computation and generates data files including node coordinates, stress, strain and the complete information of the workpiece and some machining process simulation result, these files can build next model for simulation analysis. The thinning condition after springback is shown in Fig.6. The FLD after springback is shown in Fig.7.

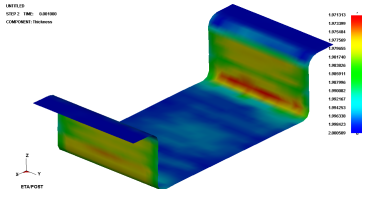

Fig. 6. The thinning condition after springback

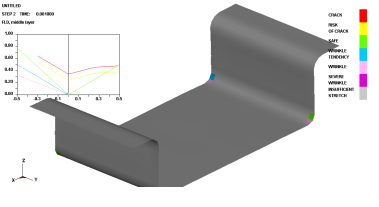

Fig. 7. The FLD after springback

The contrast of thinning degree shown in Figure.4 and Figure.6 show that the thinning rate change is not big by springback, the bottom and binder ring basically have no thinning tendency, thickness increased a little, it is 2.001238mm before the bringback and 2.000509mm later. But in the side wall thinning degree is unequal in size, the red region is the maximum, the thickness is 1.971016mm before and 1.971313mm after the bringback. in the area of the side wall and bottom corner above, yellow for thinning serious region, the thickness is 1.979651mm and 1.977569mm respectively. As can be seen from the figure in the whole process of bending, the parts become thinner, but there is almost no effect on the whole parts for the later forming. So we can continue to follow the original process plan.

The forming limit diagram shown in Fig.5 and Fig.7, which can discriminate complex stamping process design is appropriate or not and improve the technology. Take some points from the forming part and measure its long, short axis strain according to the circle of coordinate grid method, and compare with the forming limit diagram. From the chart we can judge, forming parts in the bending process have no crack or fracture risk after bending, only in the bottom corner have some wrinkling risk, which can be achieved by increasing the blank width direction dimension or the blank holder force. In mold design this can be ignored since the wrinkling is not particularly serious.

The simulation results is shown in Fig.8 to Fig.11. Compare Fig.8 with Fig.9, through the measurement in corresponding multiple element, it can be concluded that springback occurred in the cap bending after unloading due to residual stress, the bending angle between bottom and sidewalls becomes larger, the side wall outwardly inclined. In this case the springback is 1.717°. Take contrast to Fig.10 and Fig.11.Calculating the changes of radius of curvature between bottom surface and the side surface of the cap-shaped part is another kind of springback analysis method. The springback of radius of curvature is 2.239163mm.

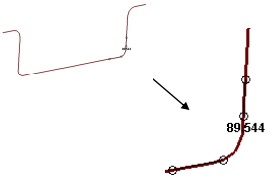

Fig. 8. The angle of formed analysis

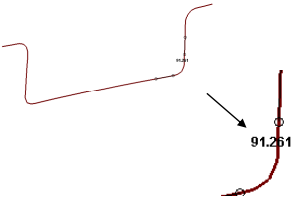

Fig. 9. The angle of springback analysis

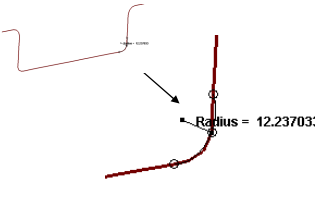

Fig. 10. The curvature of formed analysis

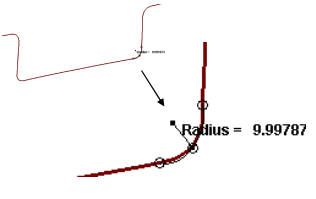

Fig. 11. The curvature of springback analysis

5 Conclusion

The following conclusions can be drawn from the results by computer simulation analysis of stamping process obtained in this study.

(1) More accurate description of workpiece and die interaction relations, complex loading process and other factors in cap bending forming process made the model actually reflects the deformation process.

(2) The calculation results agree well with the experimental data, which shows that it is feasible to simulate cap-shaped parts process and determine the reasonable technological parameters using this method.

(3) The springback of cap-shaped parts is not very serious through Dynaform numerical simulation, so make an appropriate changes to punch and die can improve the springback.

Acknowledgement. This research is financially supported by Shandong Province Natural Science Foundation, China (No. ZR2011EEM014 and ZR2010EM013) and Science and Technology Development Program of Shandong Province, China (No. 2010GGX10408).

References

1. Wang, J.W., Fu, Z.C., Hu, P., Xu, Y.W.: Experiment on the springback of auto body panel parts and CAE analytical method based on universal formability technology. Journal of Plasticity Engineering 17, 41–45 (2010) (in Chinese)
2. Panthi, S.K., Ramakrishnan, N., Ahmed, M., et al.: Finite Element Analysis of Sheet Metal Bending Process to Predict the Springback. Materials & Design 31, 657–662 (2010)
3. Tang, S.H., Chen, G.R.: Simulation Research on Automotive Body Panels Stamping and Spring-back. Manufacturing Technology & Machine Tool 9, 25–28 (2008) (in Chinese)
4. Xue, F.: Analysis and Springback Study of Car Body Panel Stamping. Nanjing University of Science and Technology, Nanjing (2009) (in Chinese)
5. Tang, Y., Xue, S.: Springback analysis and control of forming process for automobile front bumper reinforcing plate. Die & Mould Industry 36, 30–32 (2010) (in Chinese)
6. Schwarze, M., Vladimirov, I.N., Reese, S.: Sheet Metal Forming and Springback Simulation by Means of a New Reduced Integration Solid-Shell Finite Element Technology. Computer Methods in Applied Mechanics and Engineering 200, 454–476 (2011)

Advanced Control Method for Photovoltaic Inverter Experiment System

Mi Dong[1], Jian Yang[1,*], and Yan Tang[2]

[1] College of Information Science and Engineering,
Central South University
Changsha 410083, China
[2] Department of Mechanical Engineering,
Embry-Riddle Aeronautical University
Daytona Beach, FL 32114
mailofyang@qq.com

Abstract. An advanced control method for a photovoltaic inverter experiment system is proposed in this paper. It is introduced that a new linear cycle discrete control algorithm, realizing linear control for the DC-bus voltage and getting the reference current for the inner current loop with a little calculation synchronously. Then, to assure a good immunity to noise and model uncertainty, the output current control method is chosen to be an auto-disturbance rejection control. The output current of PV inverter to the grid is with low harmonic distortion and unity power factor. Simulation and experiment results show the inverter is of excellent robustness and effective. The experiment system becomes a good education platform for students.

Keywords: photovoltaic inverter experiment system, cycle discrete control, auto-disturbance rejection control.

1 Introduction

Electricity production from photovoltaic (PV) power has become less costly and more efficient in recent years[1]. This paper develops an advanced control method for photovoltaic inverter experiment system. It is controlled by two closed-loops. First, a new linear cycle discrete control method is proposed in voltage control, which realizes linear control for DC-bus voltage and gets the reference current amplitude synchronously with a little calculation[2]. Then, for PV inverter's output current control, presented is a nonlinear controller, so called Auto-Disturbance Rejection Controller (ADRC)[3][4], not relying on mathematical model of the controlled plant and compensating the internal and external disturbances dynamically. Therefore, this advanced control method brings new methodology to ensure robustness and conduct disturbance rejection. The PV experiment system becomes a good education tool for students.

* Corresponding author.

D. Jin and S. Lin (Eds.): Advances in Mechanical and Electronic Engineering, LNEE 177, pp. 125–130.
springerlink.com

2 Control Method

Fig. 1 shows the photovoltaic inverter's structure and the control scheme. Cycle discrete control is advanced in DC-bus voltage control. ADRC is employed in output current control. Such control algorithms will be shown in details in the following subsections.

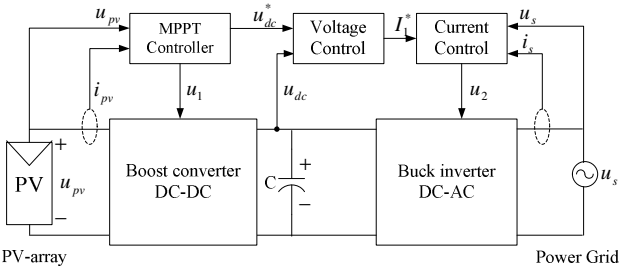

Fig. 1. The circuit of photovoltaic inverter and control scheme

2.1 Cycle Discrete Control for DC-Bus Voltage

For each cycle, the discrete model of capacitor is rewritten as

$$G(z) = \frac{T}{C} \cdot \frac{1}{z-1} \tag{1}$$

According to the discrete control law, for DC side capacitor, the current ($i_{dc}(t)$) integral of each cycle is

$$\int_{kT}^{(k+1)T} i_{dc}(t)dt = \int_{kT}^{(k+1)T} [I_1(k) - I_2(k)]dt = T[I_1(k) - I_2(k)] = \Delta u_{dc} \cdot C \tag{2}$$

That is,

$$I_1(k) - I_2(k) = \Delta u_{dc} \cdot C / T = C \cdot (u_{dc}(k) - u_{dc}(k-1)) / T = u(k) \tag{3}$$

where $I_1(k)$ and $I_2(k)$ are the average values of current $i_1(t)$ and $i_2(t)$ in cycle $[(k-1)T, \quad kT]$, respectively. Then, the expected current value can be obtained as

$$I_2(k) = I_2(k-1) + u(k) \tag{4}$$

Therefore, one cycle discrete PI control is applied in voltage control, which is shown in Fig. 2. Where K_P and K_I represent proportion and integral parameters.

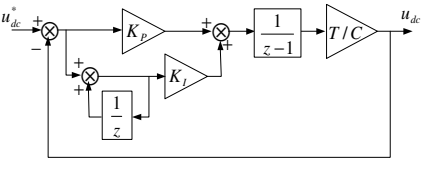

Fig. 2. Voltage control model using cycle discrete PI controller

2.2 ADRC Control for Output Current

ADRC is applied in the output current control. The state function of buck inverter is

$$\begin{bmatrix} \dot{u}_{dc} \\ \dot{i}_s \end{bmatrix} = \begin{bmatrix} 0 & \frac{1}{C} \\ -\frac{1}{L_2} & -\frac{R}{L_2} \end{bmatrix} \begin{bmatrix} u_{dc} \\ i_s \end{bmatrix} + \begin{bmatrix} \frac{1}{C} i_{pv} u_1 \\ -\frac{1}{L_2} u_s \end{bmatrix} + u_2 \begin{bmatrix} -\frac{2}{C} i_s \\ \frac{2}{L_2} u_{dc} \end{bmatrix} \tag{5}$$

where $u_2 \in \{0, \quad 1\}$. It is the control signal that ensures the output current i_s to track the reference current i_s^*. Assuming $\omega(t) = -u_s / L_2$, and treating it as the system's unknown disturbance, compensated by NLSEF, we design ADRC as follows[5]

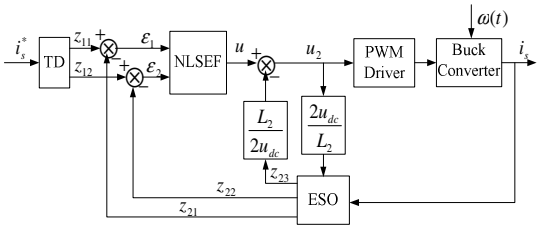

Fig. 3. Structure block diagram of ADRC current control

- TD:

$$\begin{cases} z_{11}(k) = z_{11}(k-1) + h z_{12}(k-1) \\ z_{12}(k) = z_{12}(k-1) - hMsat[z_{11}(k-1) - i_s^* + |z_{12}(k-1)| * z_{12}(k-1)/2M, \quad \delta_0] \end{cases} \tag{6}$$

where M refers the maximum acceleration which this system can reach. Here

$$sat(A, \quad \delta) = \begin{cases} sign(A), & |A| > \delta \\ A/\delta, & |A| \le \delta, \delta > 0 \end{cases} \tag{7}$$

The output $i_s = z_{11}$ tracks the reference input i_s^* in the shortest time possible without overshoot, while z_{12} converges to generalized derivation of i_s^*.

- ESO:

$$\begin{cases} z_{21}(k) = z_{21}(k-1) + h\{z_{22}(k-1) - \beta_{01} fal[\varepsilon(k), \quad \alpha_1, \quad \delta_1]\} \\ z_{22}(k) = z_{22}(k-1) + h\{z_{23}(k-1) - \beta_{02} fal[\varepsilon(k), \quad \alpha_1, \quad \delta_1] + \frac{2u_{dc}}{L_2} u_2(k-1)\} \\ z_{23}(k) = z_{23}(k-1) + h\beta_{03} fal[\varepsilon(k), \quad \alpha_1, \quad \delta_1] \end{cases} \tag{8}$$

where $\varepsilon(k) = z_{21}(k-1) - i_s(k)$. β_{01}, β_{02} and β_{03} are coefficients of ESO. The nonlinear function fal is defined as

$$fal(\varepsilon_i, \quad \alpha, \quad \delta) = \begin{cases} |\varepsilon_i|^{\alpha} \operatorname{sgn}(\varepsilon_i) & |\varepsilon_i| > \delta \\ \varepsilon_i / \delta^{1-\alpha} & |\varepsilon_i| \le \delta \end{cases} \tag{9}$$

- NLSEF:

$$\begin{cases} u(k) = \beta_1 fal(\varepsilon_1(k), \quad \alpha, \quad \delta) + \beta_2 fal(\varepsilon_2(k), \quad \alpha, \quad \delta) \\ u_2(k) = u(k) - \dfrac{2u_{dc}}{L_2} \cdot z_{23}(k) \end{cases} \tag{10}$$

where $\varepsilon_1(k) = z_{11}(k) - z_{21}(k)$, $\varepsilon_2(k) = z_{12}(k) - z_{22}(k)$, β_1 and β_2 are gains.

3 Simulation and Experiment Results

The simulation results show in Fig. 4 and Fig. 5 with the parameters in system described in Fig. 1: $L_1 = 1mH$, $L_2 = 750\mu H$, $C = 2mF$, $R = 1\Omega$. And the parameters of ADRC controller are $M = 6000$, $\delta_0 = 0.01$, $\alpha = 0.5$, $\delta = 0.001$, $\beta_1 = 7$, $\beta_2 = 2$, $\alpha_1 = 0.5$, $\delta_1 = 0.0001$, $\beta_{01} = 0.1$, $\beta_{02} = 0.5$, and $\beta_{03} = 0.4$.

From these results, it is shown that the harmonic and current distortions of output current are small when they are in steady state shown as Fig. 5. There are no overshoot and surge obtained for the dynamic response.

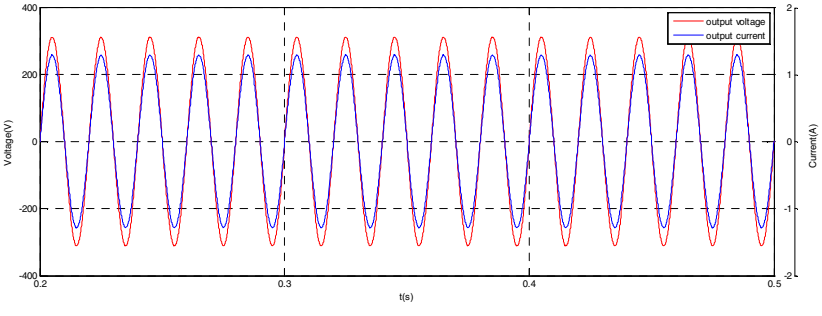

Fig. 4. Simulation results of system's steady state

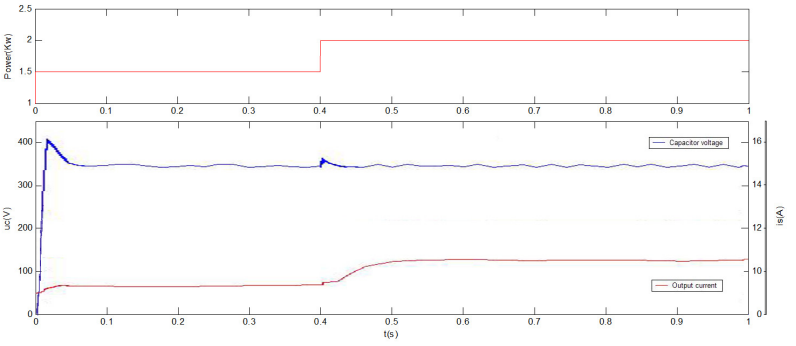

Fig. 5. Simulation results of system's dynamic response

Furthermore, a prototype of experiment system is built in our lab. The parameters of the experiment controller are chosen according to the simulation data. Fig. 6 shows the results of the experimental inverter when the solar radiation changes. Noticing that the output current has no overshoot, and the dynamic current dash is reduced greatly.

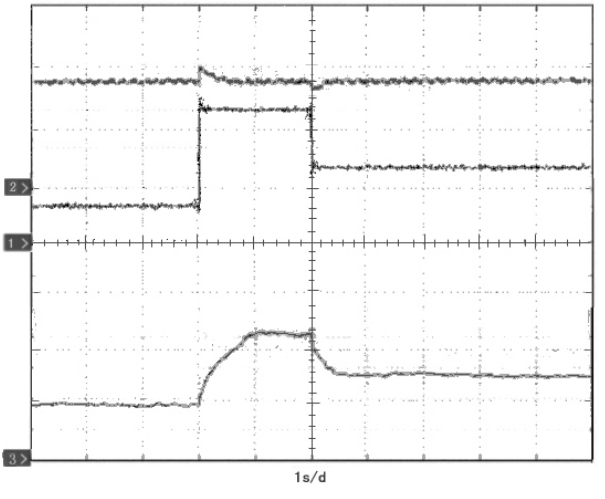

Fig. 6. Experiment results.(channel 1 is PV power; channel 2 is capacitor voltage; channel 3 is output current)

4 Conclusions

An advanced control method for photovoltaic inverter experiment system is proposed in this paper. A linear cycle discrete control method for DC-bus voltage is introduced. The control method realizes linear control for DC-bus voltage and gets the fundamental component of the load current synchronously with a little of calculation. Meanwhile, ADRC control is employed for PV inverter's output current. This control possesses

good performance of the anti-interference for internal and external perturbation. It doesn't depend on the mathematics model of the system, and achieves better robustness and adaptability. Both the simulation and the experiment validate the effectiveness of the control method. The experiment system becomes a good education platform for students.

Acknowledgments. This work was supported by the National Young Teacher Foundation under Grant 2011QNZT037.

References

1. Myrzik, J.M.A., Calais, M.: String and module integrated inverters for single-phase grid connected photovoltaic systems - a review. In: Power Tech Conference Proceedings, vol. 2, p. 8 (2003)
2. Ji, F., Mansoor, Xie, D.: A single-phase shunt active filter based on cycle discrete control for DC-side voltage. In: Proceedings of the CSEE, vol. 25, pp. 37–43 (2005)
3. Han, J.: From PID technique to active disturbances rejection control technique. Control Engineering of China 9, 13–18 (2002)
4. Gao, L., Han, J., Li, C.: Nonlinear robust auto-disturbance rejection controller for power systems. Journal of Tsinghua University 40(3), 59–63 (2000)
5. Han, J.: Nonlinear state error feedback control law – NLSEF. Control and Decision 10, 221–225 (1995)

Characteristic Analysis of the PWM Speed Control High-Speed Switching Valve

Hong Ji, WeiGuo Zhu, and MinXue Luo

School of Mechanical and Electrical Engineering,
Anhui University of Architecture, 230601 Hefei, China
jdautozwg@aiai.edu.cn

Abstract. The characteristic analysis of the PWM speed control High-speed Switching Valve in mechanical and electronic engineering is investigated in this paper. First the structure and working principle of the high speed switching valve is introduced, and according to theoretical calculation the static characteristics of the high-speed switching valve is obtained, then using the Simulink Module of MATLAB software the dynamic characteristics of control cavity pressure in the high-speed valve is simulated. The simulation results reflect the system have better dynamic characteristics.

Keywords: High-speed switching valve, Dynamic Characteristic, Static Characteristic, Simulink simulation, Mechanical and electronic engineering.

1 Introduction

The high-speed switching valve is a new digital electro-hydraulic conversion control element, which use pulse flow control means to realize switching action and widely used in engineering machinery. It can largely improve the engineering machinery driving performance, operation, safety and comfort, which is the trend of future development of engineering machinery.

At present, the research on the high speed switching valve mainly is concentrated on the valve design and simulation, application characteristics etc. The document [1] introduces the working principle of high-speed switching valve and its application in automobile automatic transmission, hydraulic actuator velocity and displacement digital control, but the theoretical research on the high-speed switching valve characteristics is less. Hu Xueqing studied the design and digital simulation of the high-speed switching valve [2]. But only the model creation method of the high-speed switching valve is given, and didn't introduce the detailed simulation process. The document [3] introduces the application of High Speed Switch Valve in Speed Control System. It mainly studies how to use single chip to control the high-speed switching valve.

The digital high-speed switching valve is introduced in this paper, in which the static and dynamic performance of the high-speed switching valve is studied. The high-speed valve has the advantages of low price, simple structure, reliable work, easy to repair, long service life, strong ability to resist pollution, so that it is suitable for the digital multi-way directional valve in engineering machinery.

D. Jin and S. Lin (Eds.): Advances in Mechanical and Electronic Engineering, LNEE 177, pp. 131–136.
springerlink.com

2 Structure of High-Speed Switching Valve

According to the work position and pass number, the high-speed switching valve can be classified into 3/4- way, 2/3-way and 2/2-way, in which the most common is 2/2 way high-speed switching valve [4]. The 2/3-way high speed switching valve is illustrated in Figure 1. When the solenoid valve is energized, the armature 1 can generate the electromagnetic thrust which by the ejector and separation pin 6 can drive the return oil ball valve 5 and supply oil ball valve 6 to move right together. At the same time the return oil ball 5 is closed, the supply oil ball valve 6 is opened, and then the control port is high-pressure. When the solenoid valve is power, the supply Oil port and control port is disconnected, then the control port and return oil port is connected, so the control port is low-pressure.

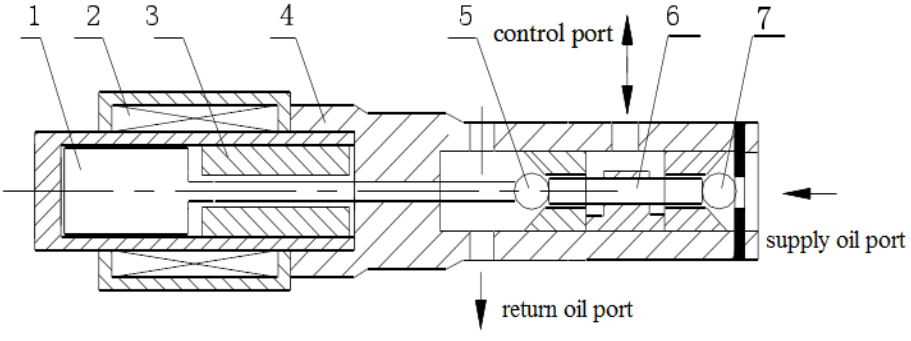

1-Armature 2- Coil 3- Pole shoe 4-valve body 5- return Oil Ball valve
6-Seperation pin 7-supply oil ball valve

Fig. 1. Schematic diagram of the high-speed switching valve

3 Static Characteristic Analysis of High-Speed Switching Valve

The high-speed switching valve performance characteristics include the static and dynamic performance [5]. The static characteristics refer to the no load flow characteristics and load flow characteristics. The no load flow characteristics is the relationship between the average flow rate and the duty ratio of the input signal pulse width, and the load flow characteristics is the relationship between the average output flow and load pressure. Usually dynamic performances of the high-speed switching valve are the frequency characteristics and step characteristics. Since the frequency characteristics of the pulse width modulation switching valve varies with pulse modulation frequency and duty cycle varies, its dynamic performances can only serve as reference. Therefore, the following discussion is focused on the static characteristics.

The no load Flow characteristics is one of the important static performances of high-speed switching valve, which can essentially reflect the ability of the valve to control system. At present, the no load flow is relatively small (<20L/min), so it is mainly used for small power control or pilot valve.

3.1 Ideal No Load Flow Characteristics

Assuming the switching valve is a theoretical high-speed switching valve, it can response transiently the rise side and fall side of pulse signal. The transient flow of the switching valve can be expressed as:

$$Q=\begin{cases}0 & t=0\\ C_d\omega x_x\sqrt{\dfrac{2}{\rho}(p_p-p_1)} & 0<t\le t_p\\ 0 & t_p<t\le T\end{cases}. \tag{1}$$

Where ω is the area gradient of the switching valve, x_m is the maximum opening of valve core, t_p is the pulse time, and T is the pulse cycle.

Therefore, in the carrier cycle the average flow $\overline{Q}$ is

$$\overline{Q}=QT_p/T=C_d\omega x_x\sqrt{\frac{2}{\rho}(p_p-p_1)}\cdot\tau. \tag{2}$$

From Equation (2) it can clearly be seen that when the pressure difference (p_p-p_1) before and after the switching valve is constant, in a carrier period the average output flow of the switching valve is proportional to the duty cycle.

3.2 Actual No Load Flow Characteristics

Due to the influence of the solenoid response lag time and spool movement time, the average flow of the high-speed valve can be calculated by the average opening quantity. Therefore:

$$\overline{Q}=C_d\omega x_x\overline{X_v}\sqrt{\frac{2}{\rho}(p_p-p_1)}\ . \tag{3}$$

Where X_v is the dimensionless average displacement of the valve core.

According to Equation (3), it can be found that the average flow is independent of the carrier cycle. Experimental results also show that if the carrier cycle is reasonably selected, it is correct. However the high carrier (modulation) frequency will smooth flow curve and accurate flow control, so the carrier frequency should be as high as possible.

3.3 Load Flow Characteristics of the High-Speed Switching Valve

The hydraulic circuit used for the load flow characteristics of the two-position, three-way high speed switching valve is illustrated in Figure 2[6]. The supply oil pressure is P_s, and the outlet port is connected to a variable orifice flow and a flow meter. The return oil port is connected with the oil tank

Assuming the duty cycle, of the pulse width modulation τ and modulation period T, the average flow which flow from the supply port to the valve cavity is

$$\overline{Q} = \tau T C_d A \sqrt{(2/\rho)(P_s - \overline{P_L})} \quad . \tag{4}$$

where C_d is the Valve orifice flow coefficient, A is the maximum opening of the high-speed switching valve （m^2）, P_s is the system oil pressure(MPa), $\overline{P_L}$ is the average pressure of control port(MPa), ρ is the density of hydraulic oil(kg/m^3).

The average flow which flow from the valve cavity to return port is

$$\overline{Q}_D = (1-\tau) T C_d A \sqrt{(2/\rho)\overline{P_L}} \quad . \tag{5}$$

Therefore, the average flow of the return oil port can be given:

$$\overline{Q_L} = \overline{Q_S} - \overline{Q_D} = \tau T C_d A \sqrt{(2/\rho)(P_s - \overline{P_L})} - (1-\tau) T C_d A \sqrt{(2/\rho)\overline{P_L}} \quad . \tag{6}$$

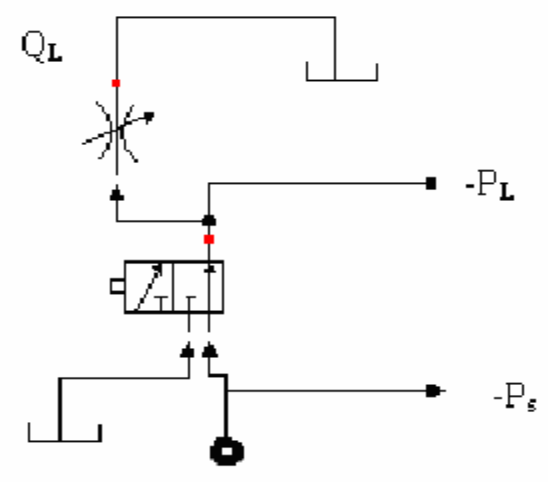

Fig. 2. Hydraulic circuit used for the load flow characteristics of the high speed switching valve

4 Pressure Dynamic Characteristics of the High-Speed Switching Valve

The flow continuity equation in the pilot control cavity of High-speed switching valve is

$$Q_0 = \frac{V_1}{E} p_{s1} \quad . \tag{7}$$

Where V_1 is the control volume of the high-speed switching valve, E is the oil bulk modulus of elasticity, and p_{s1} is the pressure of the control cavity.

At Zero operating point the linear flow equation of the high-speed switching valve is

$$Q_0 = C_d w x_m \sin\varphi \sqrt{\frac{2}{\rho} p_i \tau} - \frac{\pi C_r^2 w}{32\mu} p_{s1} \quad . \tag{8}$$

Substituting Equation(8) into Equation （7）, we can obtained:

$$k_{q0}\tau - k_{c0} p_{s1} = \frac{V_1}{E} p_{s1} \quad . \tag{9}$$

Applied the Laplace transform for (9), the relationship between the duty ratio τ and the control cavity pressure p_{s1} can be obtained.

In a cycle the transfer function is given by:

$$G_1(S) = \frac{p_s(S)}{\tau(S)} = \frac{k_{q0}}{\frac{V_1}{E} S + k_{c0}} = \frac{k_{p0}}{T_d S + 1} \quad . \tag{10}$$

By means of the Simulink Module of MATLAB software[8] the simulation curves of pressure response is obtained, as shown in Figure 3.

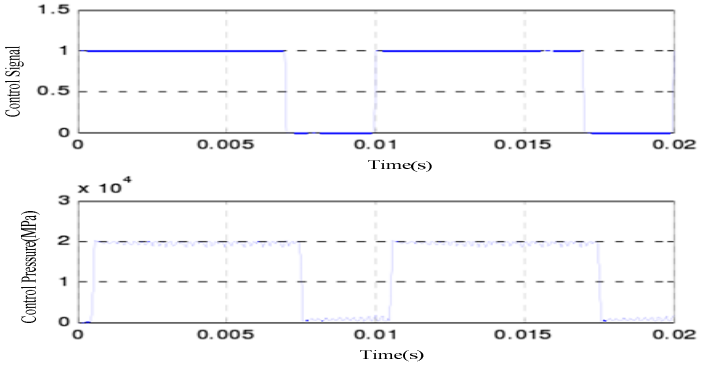

Fig. 3. Simulation curve of pressure response

It can be seen from Figure 3 that using the high-speed valve in a very short period of time the system pressure can set up, and the pressure in the control cavity can reach steady state with smaller fluctuations, which shows that the system has good dynamic characteristics.

5 Conclusions

The structure, characteristics, control mode, control loop form and the movement principle of the high speed switch valve is investigated. In most cases the high speed switch valve studied in this paper is used as a pilot valve to form a new digital electro-hydraulic proportional directional valve. The opening of the multi-channel directional valve is controlled by its valve core position, and the relationship between valve core displacement and its control flow is certain. Next, the control law of the high-speed switching valve used as a pilot valve in the multi-valve will further study.

Acknowledgment. This work has been supported by Foundation of Anhui Educational Committee, project number KJ2011Z048, KJ2011A066, KJ2012A059.

References

1. Du, Q., Chen, X., Wu, W., et al.: PWM High Speed Switch Valve Performance and Its Application. Hydraulics Pneumatics and Seals 6, 10–11 (2002)
2. Hu, X., Cao, J., Wang, H.: Design and digital simulation of the high-speed switching valve. Digital Technology and Application 7, 55 (2011)
3. Li, D., Shen, J., Xu, Y.: Application of High Speed Switch Valve in Speed Control System. Light Industry Machinery 29, 50–53 (2011)
4. Jing, B., Yin, Y., Liu, S., et al.: Simulation of Digital Electro-hydraulic Proportional Control System of Working Device for Loader. Transactions of the Chinese Society for Agricultural Machinery 2, 47–50 (2005)
5. Liu, Z.: Application Research of Pulse Width Modulation Technology on Hydraulic System. Machinery & Electronics 4, 13–15 (2006)
6. Feng, Z.: The research of a new type digital proportional pilot operated electron-hydraulic valve for the loader. Jilin University. master's thesis (2004)
7. Fu, Y., Qi, X.: AMESim system modeling and Simulation - from entry to the master. Beijing University of Aeronautics & Astronautics Press, Beijing (2006)
8. Cheng, W.: MATLAB5.3 Application Guide. The People's Posts and Telecommunications Press, Beijing (2000)

Malfunction Analysis on Reverse-Flighted Screw Automatic Cable Layer Based on Fault Tree

Kegang Zhu[1], ZhaoGang Zhang[1], and Qingfu Zeng[2]

[1] Liao Ning Institute of Science and Technology,
117004, China
chhyrabbit@126.com
[2] Shandong Iron and Steel Group Logistics Center, Jinan,
250132, China
zqf978@126.com

Abstract. By comprehensive analysis of the factors that affect the operation of automatic cable layer and the establishment of fault tree through deduction, the factors that affect have been quantified, and a fault tree mode of automatic cable layer (main components) has been established. A reliability analysis has been conducted, the major problems that cause breakdowns have been found, and the directions to make improvements have been pointed out.

Keywords: Malfunction Analysis, Fault Tree, Reverse-Flighted Screw Automatic Cable.

1 Introduction

This Underground electric carry scraper (the carry scraper) is the major equipment for carrying, transporting, unloading in underground mine trackless excavation operation, it is a new high-efficient underground carrier, transporter and unload equipment that cause no air pollution. The carry scraper moves in two opposite directions, and power cables are needed to move with it. Frequent operation needs automatic cable layer to insure efficiency. Meanwhile, all kinds of equipment have to endure miserable working environment. According to actual observation, underground engineering plant without automatic cable layer would suffer from the extrusion and pull tension imposed on the cable, these forces are easily result in unexpected tight and snarling which will cause bumping, discarding and abruption. It has been estimated that the expense on damaged cable accounts for one third of the total operation expense for the carry scrapers[1-3].

According to the research during recent decades, if a cable layer equipment could put the cables away; the damage probability of the carry scrapers would be largely reduced[4]. Institutions from home and abroad have developed mechanical turning cable layer, numerical control servo driven cable layer and hydraulic pressure cable layer in succession[5-7]. Reverse-flighted screw mechanically automatic cable layer has simple structure, and cable could be carried on the roll from two different

D. Jin and S. Lin (Eds.): Advances in Mechanical and Electronic Engineering, LNEE 177, pp. 137–143.
springerlink.com

directions and in many layers, which makes it popular on electric carry scrapers. But reverse-flighted screw mechanically automatic cable layer has easily-fretted link slide blocks and so on, which makes it hard to fit the frequent inverting and turning of electric carry scrapers, therefore, this problem limits its popularization on electric carry scrapers[8-10]. In this essay, a fault tree for automatic cable layer has been established, quantitatively analyzed, which has provided basis for the fault resolution of reverse-flighted screw automatic cable layer.

2 Failure Mode of Automatic Cable Layer

The cable layer for the carry scrapers lies in rear end on one side (Fig. 1). Automatic cable layers arrange the cables on rolls in a good order, and it is between the roll and the set of driving rolls (Fig. 2). Tugging the cables through tunnels would bring silts, sewage and grease contamination to cable layer, therefore, the working environment for the automatic cable layer is wretched, which leads to high hazard rates.

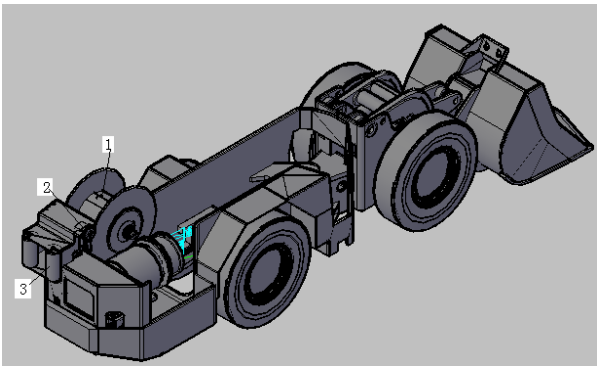

Fig. 1. The schematic drawing of electric carry scraper
1. Toll 2. Automatic cable layer 3 driving rolls (cable edging roll and cable carrier roller)

According to the maintenance records and the content of maintenance handbook, the factors that affect the equipment have been decided.

2.1 Transmission Malfunctions of Automatic Cable Layer

Transmission malfunction of automatic cable layer (represented by M_1) mainly refers to no cable arrangement (represented by M_4) and out-of-order cable arrangement (represented by M_5); no cable arrangement is usually caused by oil hydraulic motor malfunction (represented by M_8) or chain sticking (represented by X_4), oil hydraulic motor malfunction is caused by low pressure of fuel feed pump(represented by X_1), clogged overflow valve (represented by X_2) or motor internal leakage(represented by X3); out-of-order cable arrangement is usually caused by bearing system malfunction

(represented by M_9), low rotate speed (represented by X_7) or high rotate speed (represented by X_8); the bearing system malfunction is caused by bearing factors (represented by X_5) or shaft block problems (represented by X_6).

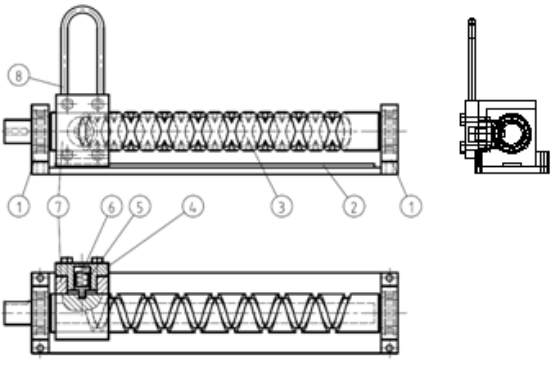

Fig. 2. Reverse-flighted screw mechanically automatic cable layer
1. Shaft block 2.dump rail 3. Reverse-flighted screw 4.Gland bush 5.Link slide block
6. Hold-down spring 7. Cable guildway8. Cable guider

2.2 Spares Abrasion and Component Abrasion of Automatic Cable Layer

Spares abrasion and component abrasion of automatic cable layer (represented by M_2) usually appears as the abrasion of cable guiders (represented by X_9) or malfunctions caused by link slide block abrasion (represented by M_6); link slide block abrasion is usually caused by the muddy water in screw groove (represented by M_{10}), mismatch of friction auxiliary materials (represented by X_{12}) or the reverse-flighted screw (represented by M_{11}); muddy water in screw groove is affected by the factors of guilders in the top of screw (represented by X_{10}) and the lack of screw seal protection (represented by M_{11}) jointly; the factor of reverse-flighted screw is caused by unqualified installation of screw (represented by X_{13}) or unqualified screw (represented by X_{14}).

2.3 Electric Fault of Automatic Cable Layer

Electric fault of automatic cable layer (represented by M_3) is usually caused by burnout of the fuse (represented by X_{15}), burnout of control transformer (represented by X_{16}), poor contact of slip-ring brush (represented by X_{17}) or the cut off by leakage protector (represented by M_7); cut off by leakage protector is mainly caused by short-circuit because of cable damage (represented by X_{18}), short-circuit between electrical apparatus elements (represented by X_{19}), shedding of slip ring (represented by X_{20}) or earth leakage because of cable damage and electrical apparatus damage (represented by X_{21}).

3 The Establishment of Fault Tree for Automatic Cable Layer and the Qualitative Analysis

3.1 The Establishment of Fault Tree

Based on the principles of fault tree establishment, the malfunction of automatic cable layer is the top event (represented by T), transmission malfunctions of automatic cable layer, spares abrasion and component abrasion of automatic cable layer and electric fault of automatic cable layer are intermediate event, after levels of analyses finally comes to the bottom events, the final fault tree has been made after simplifying the original one, the final fault tree is shown in Fig. 3.

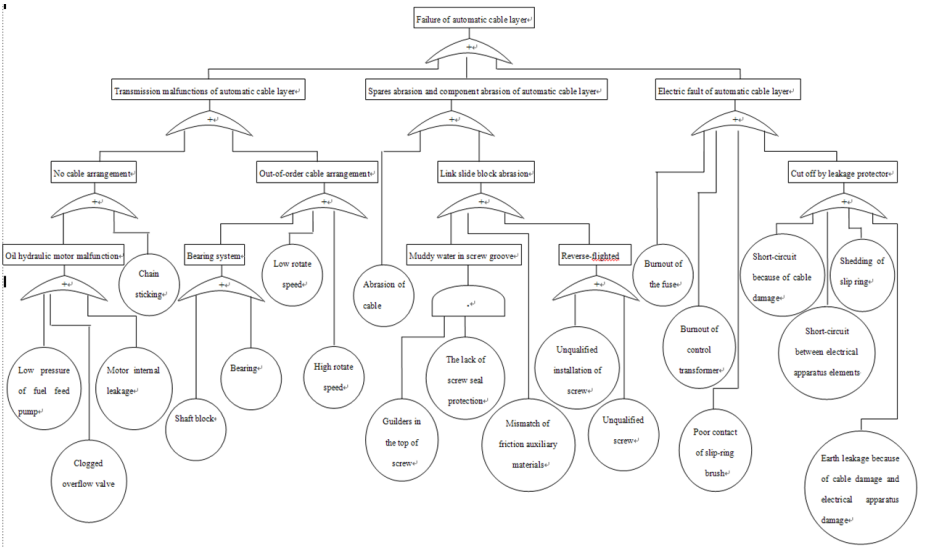

Fig. 3. The fault tree of reverse-flighted screw cable layer

3.2 The Qualitative Analysis of the Fault Tree

Suppose if M_1、M_2……M_{11} are intermediate events transmission malfunctions of automatic cable layer, spares abrasion and component abrasion of automatic cable layer, electric fault of automatic cable layer and so on; suppose if X_1、X_2……X_{21} are probability of happening of low pressure of fuel feed pump, clogged overflow valve, earth leakage because of cable damage and electrical apparatus damage, etc. With descending method, the minimal cut set solved is shown in Table 1.

Table 1. Minimal cut set

Top event	The first step	The second step	The third step	Minimal cut set
T	M_1	M_4	M_8	X_1
				X_2
				X_3
			X_4	X_4
		M_5	M_9	X_5
				X_6
			X_7	X_7
			X_8	X_8
	M_2	X_9	X_9	X_9
		M_6	M_{10}	$X_{10}X_{11}$
			X_{12}	X_{12}
			M_{11}	X_{13}
				X_{14}
	M_3	X_{15}	X_{15}	X_{15}
		X_{16}	X_{16}	X_{16}
		X_{17}	X_{17}	X_{17}
		M_7	X_{18}	X_{18}
			X_{19}	X_{19}
			X_{20}	X_{20}
			X_{21}	X_{21}

The top event shows as

$$T = X_1 + X_2 + X_3 + X_4 + X_5 + X_6 + X_7 + X_8 + X_9 + X_{10}X_{11} + X_{12} + X_{13} + X_{14} + X_{15} + X_{16} + X_{17} + X_{18} + X_{19} + X_{20} + X_{21} \quad (1)$$

T ——top event

X_i ——the ith bottom event

The above formula shows that there are at least 20 factors that could lead to malfunction of automatic cable layer.

4 Experiment Analysis

The qualitative analysis is based on the fault tree, by analyzing the incident rate of the top event and the probability importance degree of bottom events to lay the foundation for automatic cable layer improvement.

4.1 The Incidence Rate of the Top Event

Keeping bottom events as independent event and according to the respective incidence rate of bottom events known from the maintenance records and maintenance handbook of the automatic cable layer, the formula is as follow:

$$g(P) = P(T) = 1 - \prod_{X_1=1}^{20} (1 - P_{X_i}) \tag{2}$$

$$= 1 - (1 - P_{X_1})(1 - P_{X_2})(1 - P_{X_3})(1 - P_{X_4})(1 - P_{X_5})(1 - P_{X_6})(1 - P_{X_7})(1 - P_{X_8})(1 - P_{X_9})$$
$$(1 - P_{X_{10}} P_{X_{11}})(1 - P_{X_{12}})(1 - P_{X_{13}})(1 - P_{X_{14}})(1 - P_{X_{15}})(1 - P_{X_{16}})(1 - P_{X_{17}})(1 - P_{X_{18}})(1 - P_{X_{19}})$$
$$(1 - P_{X_{20}})(1 - P_{X_{21}}) = 1 - (1 - 0.002)(1 - 0.001)(1 - 0.002)(1 - 0.002)(1 - 0.002)(1 - 0.002)$$
$$(1 - 0.002)(1 - 0.002)(1 - 0.005)(1 - 0.002 \times 1)(1 - 0.002)(1 - 0.002)(1 - 0.005)(1 - 0.001)$$
$$(1 - 0.001)(1 - 0.002)(1 - 0.001)(1 - 0.001)(1 - 0.001)(1 - 0.001) = 0.03836$$

where, $g(p)$ is the incidence rate of the top event.

4.2 The Calculation of the Probability Importance Degree

The probability importance degree is the change scope of top event caused by the difference in incidence rate of bottom event Xi. According to the formula of top event incidence rate, the incidence rate of bottom events could be classified as little probability bottom event (the hazard rate is 0.001), medium probability bottom event (the hazard rate is 0.002), and high probability bottom event (the hazard rate is 0.01). This essay mainly emphasizes on the effects of the changes in the incidence rate of these bottom events have on the incidence rate of the top event. The formula of the probability importance degree:

$$\Delta g(t) = \frac{\partial g[P(t)]}{\partial P_{X_i}} = \frac{\partial F_S(t)}{\partial F_i(t)} \tag{3}$$

$\Delta g(t)$ ——he probability importance degree;

$F_i(t)$ ——the unreliability of the ith bottom event, $F(t) = 1 - e^{-\lambda t}$;

P_{X_i} ——the incidence rate of the ith bottom event;

$g[P(t)]$——the incidence rate of the top event, $g[P(t)] = F_S(t)$;

$F_S(t)$ ——the unreliability of the system;

From the fault tree it could be known:

$$\begin{aligned} F_S(t) &= 1 - [1 - F_1(t)][1 - F_2(t)][1 - F_3(t)][1 - F_4(t)][1 - F_5(t)][1 - F_6(t)] \\ &[1 - F_7(t)][1 - F_8(t)][1 - F_9(t)][1 - F_{10 \bullet 11}(t)][1 - F_{12}(t)][1 - F_{14}(t)][1 - F_{15}(t)] \\ &[1 - F_{16}(t)][1 - F_{17}(t)][1 - F_{18}(t)][1 - F_{19}(t)][1 - F_{20}(t)][1 - F_{21}(t)] \end{aligned} \tag{4}$$

Put formula 4 into formula 3, the probability importance degree of little probability bottom event (the hazard rate is 0.001), medium probability bottom event (the hazard rate is 0.002), and high probability bottom event are as the following Table (suppose the working hour is 100 hours).

Table 2. The probability importance degree of bottom event

Bottom event	Little probability bottom event	Medium probability bottom event	High probability bottom event
The probability importance degree	0.0224	0.0247	0.0334

5 Conclusions

In this essay, the hazard rate of automatic cable layer has been calculated, which is 3.836%, but taking other affecting factors into consideration, the rate calculated is 4%. In practice, the cable layer should be maintained every 25 days, the accuracy of fault tree of automatic cable layer has been proved, and the incidence rate of each bottom event is in accordance with the reality. The importance of each event calculated by this fault tree could be used as the basis for improving the cable layer, according to the calculation, eliminating guider abrasion; changing unqualified abrasion auxiliary materials and some other issues are the most important ones.

Acknowledgments. This work is supported by the Planned LiaoNing Science and Technology Project(NO. 2011220037).

References

1. Jacob, C., Dubois, D., Cardoso, J.: Uncertainty handling in quantitative BDD-based fault-tree analysis by interval computation. Scalable Uncertainty Management 6929, 202–218 (2011)
2. Ramesh, V., Saravannan, R.: Reliability Assessment of a Co-Generation Power Plant in a Sugar Mill Using Fault Tree Analysis. Energy Sources, Part A: Recovery, Utilization and Environmental Effects 33(12), 1168–1183 (2011)
3. Huang, H.Z., Zhang, H., Li, Y.: A New Ordering Method of Basic Events in Fault Tree Analysis. Quality and Reliability Engineering International 28, 297–305 (2012)
4. Han, S.H., Lim, H.G.: Top event probability evaluation of a fault tree having circular logics by using Monte Carlo method. Nuclear Engineering and Design 243, 336–340 (2012)
5. Lindhe, A., Rosén, L., Norberg, T., Bergstedt, O.: Fault tree analysis for integrated and probabilistic risk analysis of drinking water systems. Water Research 43(6), 1641–1653 (2009)
6. Volkanovski, A., Cepin, M., Mavko, B.: Application of the fault tree analysis for assessment of power system reliability. Reliability Engineering & System Safety 94(6), 1116–1127 (2009)
7. Durga Rao, K., Gopika, V., Sanyasi Rao, V.V.S., Kushwaha, H.S., Verma, A.K., Srividya, A.: Dynamic fault tree analysis using Monte Carlo simulation in probabilistic safety assessment. Reliability Engineering & System Safety 94(4), 872–883 (2009)
8. Majdara, A., Wakabayashi, T.: Component-based modeling of systems for automated fault tree generation. Reliability Engineering & System Safety 94(6), 1076–1086 (2009)
9. Park, A., Lee, S.J.: Fault tree analysis on handwashing for hygiene management. Food Control 20(3), 223–229 (2009)
10. Shalev, D.M., Tiran, J.: Condition-based fault tree analysis (CBFTA): A new method for improved fault tree analysis (FTA), reliability and safety calculations. Reliability Engineering & System Safety 92(9), 1231–1241 (2007)

Temperature Field Distribution Analysis for High-Speed Motorized Spindle of Vertical and Horizontal Machining Center

Peng Wang, Baocheng Zhou, and Chunli Lei

School of Mechanical and Electronically Engineering,
Lanzhou University of Technology, Lanzhou, 730050, China

Abstract. For High-speed motorized spindle of vertical and horizontal machining center, two main heat sources: motor and bearing are analyzed in details. After get the heat generation rate of the heat source and coefficient of heat transfer between each part of motorized spindle, a thermal model of the motorized spindle is set up by ANSYS software. The system steady temperature field distribution and the transient temperature variation curve of the bearing are obtained respectively. The results show that the existing cooling system can control the temperature rising of the bearing and the spindle. Meanwhile, some suggestions are also offered for further improvement in the future.

Keywords: Motorized spindle, Temperature Field Distribution, ANSYS.

Foundation item: Major national science and technology projects (2009 ZX04001-015).

1 Introduction

High-speed motorized spindle is the key component of high-speed machine tools in the process of high-speed spindle operation. Experiments show that: during the precision machining process, manufacturing errors caused by the spindle thermal deformation account for 40%-70% of the total manufacturing errors [1].So the study on temperature distribution of the motorized spindle is very important. The structure of the motorized spindle is shown in figure 1.

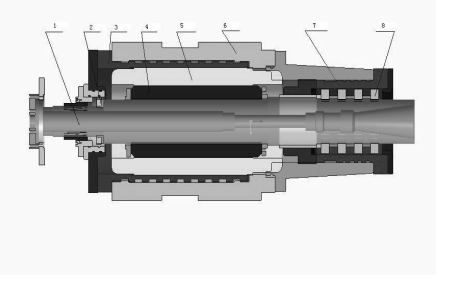

Fig. 1.
1. main shaft 2.rear bearings 3.cooling jacket 4.motor rotor
5. motor stator 6.housing 7.cooling jacket 8. Fore bearing

D. Jin and S. Lin (Eds.): Advances in Mechanical and Electronic Engineering, LNEE 177, pp. 145–151.
springerlink.com

2 The Main Heat Source of the High-Speed Motorized Spindle

2.1 The Heat Production Rates of Stator and Rotor

Study finds that nearly 1/3 of the motor heat is produced by motor rotor during the high-speed operation of the motor. 2/3 of the heat is produced by the motor stator [2-3].The power rating loss of the motor (P_{vn}=3.8KW) is completely transformed into heat Q_m . 2/3 is produced by the stator. (Q_s=2.53KW), 1/3 is produced by the rotor(Q_r=1.27KW).Iron cores of the stator and rotor, Length L=0.4m.The diameter of the inner iron core to the stator D_{di}=0.16m . External diameter D_{do}=0.24m .The diameter of the inner iron core to the rotor D_{zi}=0.102m . external diameter D_{zo}=0.158m .The heat production rates of stator and rotor are as following:

$$q_s = \frac{Q_s}{V_s} = \frac{Q_s}{\frac{\pi}{4}\left(D_{\mathrm{do}}{}^2 - D_{\mathrm{di}}{}^2\right)L} = 251791\left(W/\mathrm{m}^3\right) \tag{1}$$

$$q_r = \frac{Q_r}{V_r} = \frac{Q_r}{\frac{\pi}{4}(D_{zo}{}^2 - D_{zi}{}^2)L} = 277787\left(W/m^3\right) \tag{2}$$

2.2 Heat Production Rate of the Bearing

Friction between various components of the angle contact ball bearing is the main reason of the bearing heat. we can get the heat of the fore bearing c 1568 W. Rear bearing is 166W. So the heat production rates of the fore bearing and rear bearing are:

$$q_f = \frac{Q_f}{V_f} = \frac{Q_f}{\pi^2 d_m (D_b/2)^2} = \frac{1568}{\pi^2 \times 0.125 \times (0.0055/2)^2} = 168062543(\mathrm{W/m^3}) \tag{3}$$

$$q_r = \frac{Q_r}{V_r} = \frac{Q_r}{\pi^2 d_m (D_b/2)^2} = \frac{166}{\pi^2 \times 0.09 \times (0.00695/2)^2} = 15475980(\mathrm{W/m^3}) \tag{4}$$

3 Boundary Conditions of the High-Speed Motorized Spindle

3.1 The Convective Heat Transfer Coefficient of Lubrication Gas

$$\alpha = (C_0 + C_1 u^{C_2}) \tag{5}$$

In the formula: μ - the average gas speed in the bearing. Unit: m/s. C_0、C_1、C_2: The values measured by experiment constantly [4] are:9.7、5.33、0.8. heat transfer coefficients of the bearing lubrication gas are resulted in table 1.

3.2 The Convective Heat Transfer Coefficient of Air Gap to the Stator and Rotor

$$\alpha_t = 28\left[1 + \sqrt{0.45 u_t}\right] \tag{6}$$

In the formula: u_t -peripheral speed, The convective heat transfer coefficients of air gap to the stator and rotor are resulted in table 1.

3.3 The Convective Heat Transfer Coefficients of the Outside Surface and the Surrounding Environment (Active Surface) to Motorized Spindle

We approximately take the temperature of the bearing thermal equilibrium T_{av} =50°C as the average air temperature of the end of the rotor. The average diameter of the end to the rotor is $D_t = 0.158$m . The speed of end to the rotor is $v_t = \pi n D_t / 60$ .So $\alpha_t = 182W / (m^2 \cdot {}^0c)$.

3.4 The Convective Heat Transfer Coefficients of the Outside Surface and the Surrounding Environment (Stationary Surface) to Motorized Spindle

The shell and air heat transfer is a composite heat transfer. According to the literature [5], we take composite heat transfer coefficient9.7.

3.5 The Convective Heat Transfer Coefficient between the Motorized Spindle Cooling Jacket and Circulating Cooling Oil

The cooling system to the stator of motorized spindle adopts oil-water system. Convective heat transfer coefficient of cooling oil

$$\alpha = \frac{N_\mu \cdot \lambda}{h_{gap}} \tag{7}$$

In the formula: N_μ -Nusselt numbers, $N_\mu = 0.0225 \cdot \mathrm{Re}^{0.8} \cdot Pr^N$ when heating fluid N=0.4 , cooling fluid N=0.3. Re -Reynolds number. Pr -Prandtl number. $0.7 < \mathrm{Pr} < 120$. λ —coefficient of heat conductivity. h_{gap} —the design scale of gap. Convective heat transfer coefficients of cooling oil are resulted in table 1.

4 Character Analysis of the Thermal State to High-Speed Motorized Spindle

4.1 Analysis of Steady Temperature Field to the High-Speed Motorized Spindle Are as Following

Environment temperature $T = 20^oC$ .Inlet temperature $T_{in} = 20^oC$ .export temperature $T_o = 30$ ℃. spindle revolving speed $n = 15000 rad/\min$.

Table 1. Heat production rate of each heat source and the convective heat transfer coefficients of each part

Parameter name	Calculation result
the rotor heat production rate w/m^3	241320
the stator heat production rate w/m^3	222930
rear bearing heat production rate w/m^3	15492301
fore bearing heat production rate w/m^3	13950178
The heat transfer coefficient of air gap of stator and rotor $\mathrm{m}^2 \cdot {}^oC$	167
the heat transfer coefficient lubrication gas $\mathrm{m}^2 \cdot {}^oC$	260
The heat transfer coefficient of motorized spindle outside surface and the surrounding environment (active surface) $\mathrm{m}^2 \cdot {}^oC$	182
The heat transfer coefficient of motorized spindle outside surface and the surrounding environment (stationary surface) $\mathrm{m}^2 \cdot {}^oC$	9.7
The heat transfer coefficient of between the motorized spindle cooling jacket and circulating cooling oil $\mathrm{m}^2 \cdot {}^oC$	180

4.2 Building 2 d ANSYS Thermal Model of the Motorized Spindle

Build half of spindle profile ANSYS model. Threaded hole, vents, chamfering have little effects to temperature field distribution, so can be ignored [6].Using PLANE55 grid division, the structure is shown in figure 2.

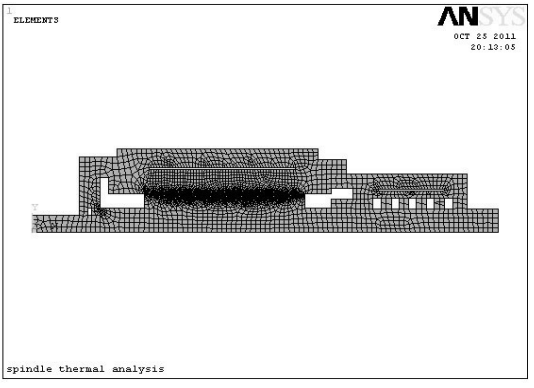

Fig. 2. Motorized spindle finite element model

4.3 The Steady-State Temperature Field Analysis to the Motorized Spindle

Parameters in table 1 are loaded on the model in ANSYS software. The steady temperature field distribution is as shows in figure 3:

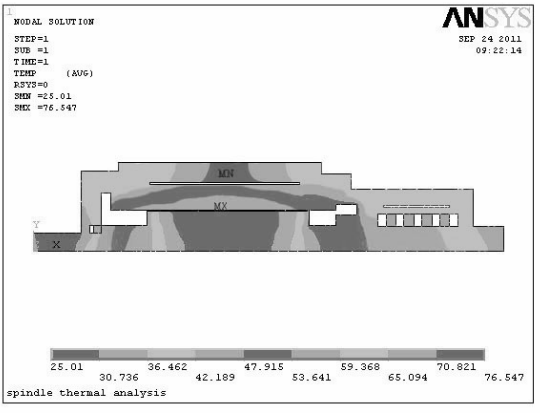

Fig. 3. Motorized spindle temperature field distribution

4.2.2 Motorized Spindle Transient Analysis

If the transient analysis time is 5000 s, take the three node temperature of the second, the third and the fourth bearing outer ring as the research object. the temperature rise is as shown in figure 4.

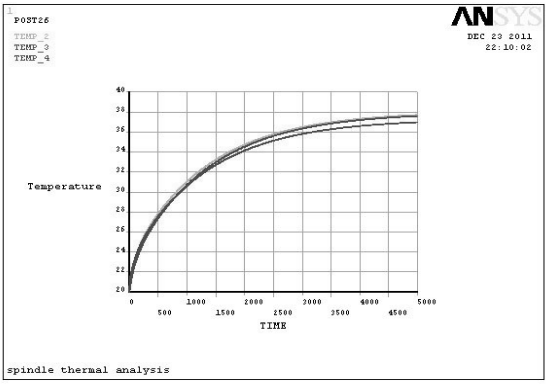

Fig. 4. The bearing temperature rise figure

5 The Measures of Improve Temperature Field Distribution

(1) From the steady temperature field distribution of motorized spindle, it is known that the rotor heating has a big effect on spindle temperature rise. We can improve the structure and change heat transfer measures such as increasing the motor and main supporting of axial compression air, force convective heat transfer in the condition of not replace the motor model.

(2) Because of the highest temperature at spindle center through analysis, so the improving cold air cooling in spindle center can be considered.

6 Conclusion

(1) Motorized spindle has two internal main heat sources, one is built-in motor heating, and the other is the bearing heating. Both heats can cause the temperature increasing of motorized spindle, which produces the uneven temperature field.

(2) According to the actual working condition, calculating load and boundary conditions of motorized spindle, analysis the temperature field distribution that we provides theory basis for effective temperature control of motorized spindle.

References

1. Zhang, B.L., Yang, Q.D., Chen, C.: High speed cutting technology and application, vol. (9). Mechanical Industry Press, Beijing (2002)
2. Borisenko, V.E., Danke, B., YaKe, A.H., Fu, L.: Motor of air dynamics and heat transfer, vol. 17. Mechanical Industry Press, Beijing (1985)
3. Ding, S.N.: Large mechanical heat and cooling. Science and Technology Press, Beijing (1991)

4. Wu, N.X.: High speed, high precision CNC lathe structural dynamic characteristics and simulation technology research: [Ph.D. Thesis]. Southeast University, Nanjing (2004)
5. Chen, Z., Chen, Z.C.: Machine hot modal study of the basic. Beijing Industry Press, Beijing (1989)
6. Zhang, M.H., Yuan, S.M., Liu, Q.: Based on the finite element analysis method of high-speed electric spindle thermal modal. Manufacturing Technology and Machine Tool (4), 29–32 (2008)

Design of the New Generation Airborne Electro-optical Dynamic Harmonization System

LiangFa Xu and FanJun Hu

The First Aeronautical Institute, Xinyang, Henan Province, China, 464000
ps20021119@qq.com

Abstract. The harmonization course of current airborne weapon system is very complex, also need many special equipments and skilled maintenance crews, so the weapon system can't get enough support under depth and near-battlefield conditions. The new airborne electro-optical dynamic boresight system for future has been designed, which is composed of automatic alignment system, misalignment assessment system, adjuster and positioner system, also the components and its operation principle of subsystem, and the procedure of harmonization are introduced in detail, then the boresight harmonization of airborne weapon system has no longer depended on peculiar ground support equipment and maintenance crews, the harmonization has been improved into automatization and dynamic representation, which help to improve the harmonization accuracy well, to meet the need of future fight,is also helpful to design and make future fighters.

Keywords: boresight, fire control computer, target acquisition and designation system.

1 Introduction

At present, attack helicopters and fighter jets designed and manufactured are mounted with weapon systems, its harmonization work usually need to be completed by specialized technical personnels in factory or on airport, and with abundant optical, mechanical special harmonizing equipments to finish on the ground. On the one hand,the harmonization process need to be cooperated by many people, which are slow and arduous task with multifarious steps, trouble operation, its technical requirements for calibration operators is high, and the differences of the operator's technical level has big influence on the accuracy of the hamonization; On the other hand, with harmonization and uing of weapon systems are disjointed, if in the air the pilot founds weapons accuracy is problem,he cannot harmonize immediately. But the future battle will be unfolded in great depth complex environment, attack helicopters and fighter jets are demanded with sufficient and timely support, but existing harmonization equipment and means for weapon system obviously can't meet the needs of the future battle. For this reason, this paper puts forward the future airborne photoelectric dynamic harmonization system planning, by the system pilot can timely realize the static harmonization on the ground and the dynamic harmonization in the air through simple operation, and no longer need ground harmonizing equipments and personnels, which will provide powerful guarantee for operations and training tasks.

D. Jin and S. Lin (Eds.): Advances in Mechanical and Electronic Engineering, LNEE 177, pp. 153–157.
springerlink.com

2 Components and Operating Principle of the Airborne Photoelectric Dynamic Harmonization System

In order to match with the airborne photoelectric dynamic harmonization system, on the basis of the full use of electronic equipment, helmet-mounted sight and weapons in aircraft, need to add three turreted systems respectively for gun, electronic- optical system and aiming devices like antenna, which are controlled by electronic-optical aiming system installed in the helmet, so as to realize the relevant devices' angle adjustment in harmonization. And airborne photoelectric dynamic harmonization system's main function is to automaticly input timely flying states to the fire control computer , then the fire control computer provides the instantaneous adjustment parameters about weapon pylons' position, and permit the aircrew one by one to adjust aviation weapon system, target acquisition and designation system, lord installed aiming subsystem without ground support equipment or ground crew, and make them quickly be adjusted well [1, 2]. This system is mainly composed by the automatic adjusting system, automatic misalignment evaluation system and the accurate positioning system:

2.1 The Automatic Adjusting System

This system consists of a pair of optical transmitter and receiver installed in the pylon and fuselage,respectivcly, as shown in Figure l. The optical transmitter with compact structure is installed in the pylon, which launches three pencil sized infrared beams to the antenna array installed under the fuselage envelope, each two beams are between about 33 mm. The antenna array consists of three solid detectors installed in the fuselage,they detect through three windows [3].The center array is radially sensitive detectors,which can accurately detect the elevation and azimuth angle variations in the incoming beam. On both sides of the center array are vertically oriented linear detectors. Simultaneous illumination of the linear delectors by two of the projected beams of fight defines a plane, and can be read via signal processing as a roll.

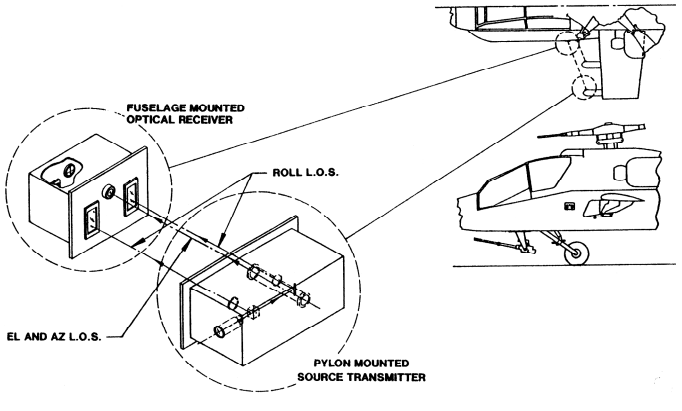

Fig. 1. Optical transceivers mounted in pylon and fuselage

The system is used to automatically timely measure the three axials' position or angle information of the wing pylon relative to the fuselage. They will timely monitor every pylon in its monitoring range, and automatic provide position or measurement results of actual angle deviation zero line with digital form to fire control computer, then the fire control computer provides the instantaneous adjusting information of the wing pylon position after the logic operation[4]. Thus not only meets to timely proofread the wing hang point, and in the condition of load variations, record the whole process of the wing migration, and the load variations and the information of the flight path graph are consistent. Flexure of the wing stores' stations not only meet weapons calibration under static state, and requires to timely monitor to weapon system in various flight paths, including hovering state. Special low power consumption and long-lived parts chosen can ensure its continuous use, after the airplane engine starts, the system can always keep in work state.

2.2 The Automatic Misalignment Evaluation System

To make the harmonization no longer rely on special ground support equipment, the system directly uses TV imaging technology compatible with existing display device aboard the plane, and its output information can be used directly by the fire control computer. It doesn't need ground staff or aircrew to input the offset information through the keyboard. When TV images overlaps or aircrew want to adjust a subsystem to the content, just click the information input switch.

The automatic misalignment evaluation system first calculate angle degree of the view splitter balance ring for the weapons subsystems, then use which to update information for computer. For example, when aviation weapon system TV camera aims at the target acquisition/designation system TV, at three corresponding points requested to match, operator presses servo switch one by one, whenever instant angles of aviation weapon system and the target acquisition/designation system phase splitters are consistent, the angle will into the fire control computer to replace the previous aiming information. At the input port of consistent point, there will be enough information for fire control computer to compute any intermediary deviators between weapon aiming goal and the target acquisition system aiming goal [5].

2.3 The Accurate Positioning System

At civil time, a small adjustment positioning system is rarely used, but after hard landing, system repairment, parts replacement, in order to make the subsystems connected by three universal joints coordinate with the fuselage information, this system is put in handy. The prospective locator of the system was first attached to the baseline, and close to installation frame of flight attitude reference system and doppler measurement system, as shown in figure 2.

Helmet display aiming system is used as actuator and display, at first the operator aligns gun camera to the target aiming instrument mounted on the fixator. When gun camera graticule marker and the designated target overlap, so suggest that the computer switchs on the control switch [6]. The angle of the gun gimbal is automaticly recorded. If the gun camera aims at the left side, and the image in the target positionerwill turn to

the right side, these informations are fed into the computer. Thus, a channel is established between the movable subsystem and the corresponding system of the determination baseline.

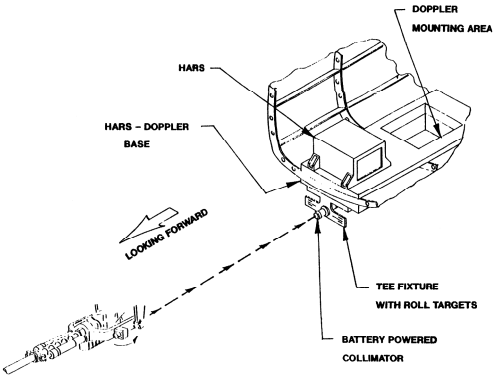

Fig. 2. Adjuster and positioner

3 Airborne Photoelectric Dynamic Harmonization System Use

Co-pilot or front seat striker's vision in the front of the plane is rarely blocked in general, the assumption is that the harmonization will be operated by him. When he operates, using the target acquisition and designation system visual TV and helmet aiming display system will be utilized as display, the first make the target acquisition and designation systemaimed aim at some appropriate fixed reference points within $\pm 10^{o}$from the plane center line, and the system will be locked in this direction[7]. The selected goal should be at least 500 m distance, may be arbitrary object. Then, disconnect the control from helmet aiming display system to the target acquisition and designation system, the target acquisition and designation system is changed from

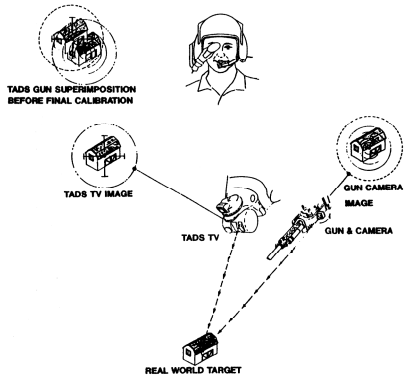

Fig. 3. HMDASS controls gun and target acquisition and designation system

locked condition to searching state; Garnish with helmet aiming display system to control aircraft gun to turn to the reference goal. In the harmonization process, the role of the helmet aiming display system is to join the the operator's head movement with several universal driving motors of the gun, again lead gun camera view (about 26^{o}) to target with enough accuracy . With the help of operater's head tiny, accurate move to make the graticule marker of gun camera and target superposition [8]. This is the real "best aiming point", as shown in figure 3.

4 Conclusions

After the airborne photoelectric dynamic harmonization systemis adopted, through simple operation the pilot can timely realize the static harmonization on the ground and the dynamic harmonization in the air, and no longer need ground harmonizing equipments and personnels, in the plane life,the costs used in maintenance will be greatly reduced, but for the cost and weight of the plane itself without too big change, this will bring high economic significance and military benefits. Therefore, the most attractive dynamic harmonization system is what the crew are eagerly looking forward to have.

References

[1] Lu, Y.: Aircraft fire control technology, pp. 156–157. National Defense Industry Press, Beijing (2004)
[2] Gu, Y.-F.: Aircraft integral design. Beijing Airspace University Press, Beijing (2001)
[3] Zha, G.-Y., Ni, Q.-M., Xu, L.-F., et al.: Military laser technology and application, p. 271. Blue Sky Press, Beijing (2003)
[4] Vawter, G.A.: Semiconductor laser with tapered-rib adiabatic-following fiber coupler for expanded output-mode diameter. IEEE Photonics Tech. Lett. 9(4), 425–427 (2007)
[5] Wang, Y., Yu, H.-K.: Airborne computing system, pp. 158–161. National Defense Industry Press, Beijing (2008)
[6] Wang, Y.-N., Zhu, L.-S., Sun, L.-H.: Helmet mounted display and sighting system, pp. 167–178. National Defense Industry Press, Beijing (1994)
[7] Courten, H.C., Neill, T.E.O.: Weapon system harmonization. Vertiflite 46(16), 11–12 (2006)
[8] Dai, Z.-D.: Automatic control technology base, pp. 182–183. Tsinghua University Press, Beijing (2007)

Analysis and Forecast of Hydrodynamic Simulation for Small Autonomous Underwater Vehicle

GuiJie Liu*, Ru Yan**, NaiLong Wu, and YongKai Yao

College of Engineering,
Ocean University of China,
Qingdao 266100, China
liuguijie@ouc.edu.cn
weiyada68@sina.com

Abstract. According to the high cost and tedious work of model test method for fluid's velocity issue around Autonomous Underwater Vehicle (AUV), this paper has found out the convenient simulation way by building the relationship of simulation results for AUV with rotating propeller and that with stationary propeller. Under different flow velocity and propeller speed conditions, hydrodynamic simulation for a small AUV model has been carried out to establish the relationship of drag coefficient for the two conditions mentioned above. The result demonstrates that margin of drag coefficient under the two conditions tends to be a fixed value. The analysis of actual running resistance of small AUV can be obtained only by studying that of stationary one base on the result. Numerical simulation method can be well used in the fluid's velocity analysis instead of the model test method.

Keywords: Small AUV, Hydrodynamic simulation, Numerical simulation.

1 Introduction

In recent years, research on hydrodynamic characteristics of small Autonomous Underwater Vehicle (AUV) is deserved to study the stability and rapidity of small AUV from the perspective of maneuverability. Computational fluid dynamics (CFD) technique has got a great development with the rapid promote of computer hardware. The use of CFD to AUV's maneuverability simulation is introduced in [1].

However, model test method is needed for massive practical problems on flow resistance problem because of the various model shape of AUV and the complicated flow around the shell. A practical model test method is used for the investigation on hydrodynamic characteristics of an ocean current power turbine by RuiJun Fan[2] as an example. The result is accurate but higher cost is needed especially for underwater experiments.

* Corresponding author. Professor of Marine Electromechanical Equipment Technology, Ocean University of China, Qingdao, China.
** Postgraduate of Autonomous Underwater Vehicle.

D. Jin and S. Lin (Eds.): Advances in Mechanical and Electronic Engineering, LNEE 177, pp. 159–164.
springerlink.com

In this context, an existing small AUV model has been regarded as the research object to conduct hydrodynamic simulation under different flow velocity and propeller speed for the relationship of drag coefficient. The result demonstrates that it can be used for the study of simplifying the velocity issue for small AUV.

2 AUV Model

2.1 Establishment of AUVhysical Mod's Pel

Figure 1 shows the essential mechanical components of the robot. Its inside diameter is 325mm, outside diameter 355mm,total length 2796mm, length of cylindrical section 1732mm, tail length 620mm,span 388.5mm, flat diameter 203.2mm and tail diameter is 37.9mm, with only one propeller.

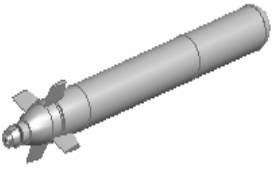

Fig. 1. Physical model of AUV

2.2 Model for Thrust System

The Navier-Stokes[3] Equation of AUV is:

$$\rho \bullet \frac{du_i}{dt} = -\frac{\partial\left(p + \frac{2}{3\mu\nabla\cdot\boldsymbol{u}}\right)}{\partial x_i} + \frac{\partial\left[\mu\left(\frac{\partial u_i}{\partial x_j} + \frac{\partial u_j}{\partial x_i}\right)\right]}{\partial x_i} + \rho f_i \tag{1}$$

where μ is viscosity and $\boldsymbol{u}$ is velocity vector.

The propeller can be simplified by the following mathematical simplified model[4]

$$\dot{\omega} = \alpha\left(\frac{T_d}{C_T} - \omega|\omega|\right) \tag{2}$$

$$T_a = C_T\omega|\omega| \tag{3}$$

where ω is the propeller's angle, C_T and α are constant. T_d is anticipant thrust and T_a is the actual thrust.

3 Simulation Analysis

3.1 Simulation Model

In our case, the boundary conditions [5] was settled as follows:

Fluid Density, ρ=1000kg/m^3. Water depth, h=200m;

Inlet conditions: The rectangular water was 2.402m×4.116m ×2.402m around AUV. As shown in Fig.2, give velocity as $u = U_\infty$ or give velocity and the corresponding propeller speed.

Outlet: The pressure gradient was given as $p = \partial p / \partial x = \partial p / \partial n = 0$ according to the outflow's free flow boundary conditions.

Wall: A condition of boundary with non-slip is supposed for the velocity boundary and normal velocity is given as $V_n = 0$.

3.2 Hydrodynamic Simulation Analysis of Small AUV

The parameters of propeller model[6] is assumed as C_T=0.17, α=0.10.Then the relationship between fluid velocity U and propeller speed n turned to be $U \propto n^3$ according to equation 1 to 3. Different value of U and n had been taken as input to conduct hydrodynamic simulation of AUV. The values and curves are represented as follows [7~10]:

Table 1. Value of resistance coefficient by calculating

U(m·s^{-1})	N(r·min^{-1})	Frictional resistance coefficient C_{Df}		Form resistance coefficient C_{Dp}		Total resistance coefficient C_D	
		Not rotate	Rotate	Not rotate	Rotate	Not rotate	Rotate
0.5	69	0.22363	0.24763	0.19007	0.31164	0.41370	0.55927
0.8	81	0.19940	0.18691	0.18799	0.30403	0.38739	0.49094
1.0	87	0.18849	0.16524	0.18790	0.30123	0.37639	0.46600
1.2	93	0.17987	0.16099	0.18755	0.30501	0.36742	0.46800
1.5	100	0.16989	0.14809	0.18648	0.30131	0.35673	0.44935
1.8	106	0.16280	0.14666	0.18576	0.29995	0.34856	0.44661
2.0	110	0.15871	0.14143	0.18589	0.29953	0.34459	0.44097

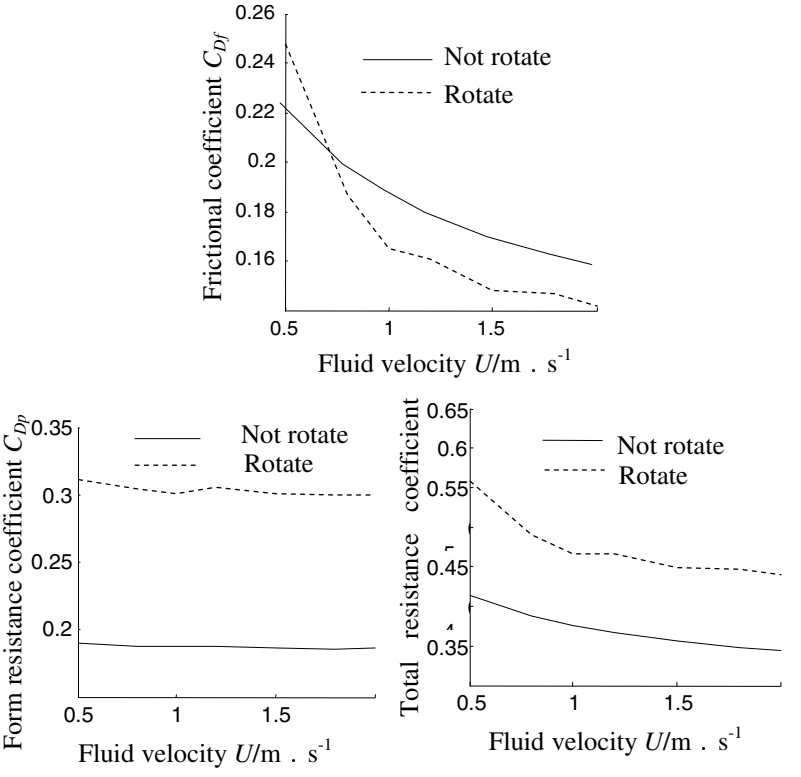

Fig. 2. Simulating curve of resistance coefficient of AUV

It can be shown in Fig. 2 that friction resistance coefficient decreased while form resistance coefficient increased a lot with the propeller rotating. Water tends to concentrate with propeller rotating and clings to the hell of small AUV. As a result velocity in vitro has been decreased and bigger vortex occurred, which make form resistance coefficient take the major position of friction coefficient. The simulation result shows fluid velocity has little effect on form resistance coefficient in Figure 2.

Take C_{D2} for the resistance coefficient under rotating condition while C_{D1} for that under stationary condition, the value of C_{D2}/C_{D1} and $(C_{D2}-C_{D1})$ can be calculated as shown in Table 3 and simulated the relation curve as shown in Fig.3.

Table 3. Contrastive results

U/m·s^{-1}	C_{D2}/C_{D1}	$(C_{D2}-C_{D1})$
0.5	1.3518672	0.1455674
0.8	1.2672926	0.1035476
1	1.2393609	0.090092
1.2	1.2683085	0.0985821
1.5	1.2596339	0.0926197
1.8	1.2813109	0.0980538
2	1.2796654	0.0963711

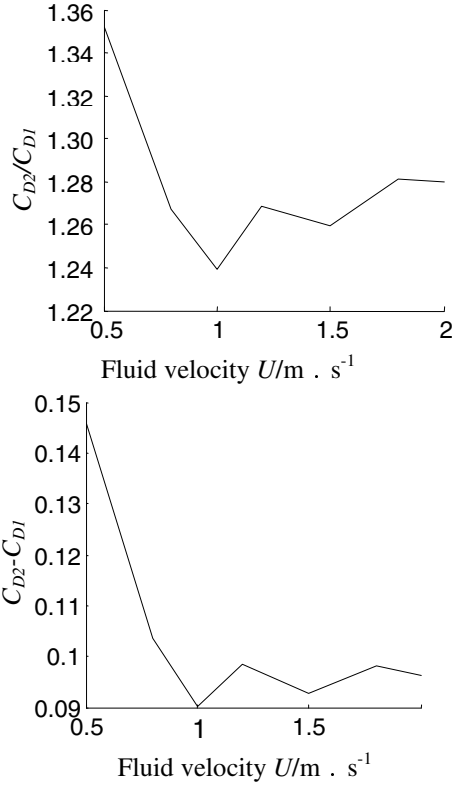

Fig. 3. Curve of contrastive results

Obviously resistance coefficient ratio of the two conditions keeps at 1.24~1.28 while the difference fluctuates slightly around 0.095. It can be conjectured that the difference of resistance coefficient under these two conditions will approach to a constant with the fluid velocity changing.

4 Conclusions

1) A small AUV model was used to conduct hydrodynamic simulation under different flow velocities and propeller speed, then the resistance as well as the relationship of drag coefficient is obtained.

2) The parameters of propeller model is assumed as C_T=0.16, α=0.10.Then the relationship between fluid velocity U and propeller speed was inferred as : $U \propto n^3$.

3) The relationship between resistance coefficient C_{D2} under rotating condition and C_{D1} under stationary condition has been found, which demonstrate the feasibility of this method to simplify research on AUV's rapidity problem. The analysis of actual running resistance of small AUV with one or even more boosters can be obtained only by studying that under the propeller stationary state.

Acknowledgments. This paper was supported by grants from State Key Laboratory of Ocean Engineering, Shanghai Jiao Tong University(1004).

References

1. Fan, R.J., Zhou, Z., Chaplin, J.R.: Investigation of Hydrodynamic Performance for Horizontal Axis Marine Current Turbine. J. Robot (2010)
2. Wen, L., Fan, Z., Wang, T.M., et al.: Fuzzy Control of Biomimetic Propulsion Using Flapping Foil. J. Robot 32(3), 307–313 (2010)
3. Kim, J., Chung, W.K.: Accurate and Practical Thruster Modeling for Underwater Vehicles. J. Ocean Engineering 33(5-6), 566–586 (2006)
4. Zhang, W.J.: Simulation of Power System for Warship. Shanghai Jiao Tong University Press, Shanghai (2006)
5. Cao, H.J.: Numerical Simulation Calculation for Hydroplane Direct Route motion Based on Fluent. Journal of Dalian Maritime University 37(1) (2011)
6. Liu, Y., Zhao, M.: The Derivation of Submarine Simulation Math Model. Journal of Harbin Engineering University 20(2) (1999)
7. McHyman, J.: Numerical Methods for Tracking Interfaces. Physics D 12, 296–407 (1984)
8. Hopfield, J.J., Tank, D.W.: Neural Computation of Decision in Optimization Problems. Biological Cybernetics 52, 141–152 (1985)
9. Fan, J., Liu, S.J.: Applications and Examples of MATLAB Control System. Tinghua University Press, Beijing (2008)
10. Huang, Y., Ma, L., Liu, H.M.: Development of Modeling and Simulation and Applications of Advanced Engineering by MATLAB7.0/Simulink6.0. Tinghua University Press, Beijing (2005)

Design of Test Equipment for Electronic Module Sampling Accuracy

LiGuo Tian, BeiBei Guan, Meng Li, and ZhiLiang Chen

Tianjin Key Laboratory of Information Sensing & Intelligent Control,
Tianjin University of Technology and Education,
Tianjin, 300222, China
{tlg1234,limeng-3260711}@163.com,
bei199022@126.com,
czl_tj@sina.com

Abstract. Along with rapid development of the electronic, sensor and SCM technology, the market appeared more and more intelligent products; product performance is improving gradually, so the test requirements and approach aiming at product performance also need further improvement. Aiming at the electronic sampling module it designed a sampling accuracy testing device used to test the sampling accuracy. The testing device used ATmega16 single-chip microcomputer (SCM) as the control core, periphery is collocated with a corresponding signal acquisition circuit, the LED digital tube display circuit, relay control circuit and alarm circuit to complete electronic module sampling accuracy test. The results showed that, the device is convenient to use, and works well.

Keywords: Electronic Sample, Accuracy Test, ATmega16 SCM, Photoelectric Sensor.

1 Introduction

With the rapid development of scientific technology and social progress, all kinds of intelligent measuring instrument have also appeared, therefore, aiming at the product performance, accuracy testing device has received more and more attention. Accuracy testing device is the basic means and equipment to test and control the information of the material world, was the source and component of the information industry [1]. This paper combined with SCM, sensor and mechanical technology, designed a kind of test device for sampling accuracy aiming at the electronic module.

2 Development and Key Technology of Modern Accuracy Test Device

In order to meet the general requirements for product development, product performance and accuracy testing device is also continually being developed,

D. Jin and S. Lin (Eds.): Advances in Mechanical and Electronic Engineering, LNEE 177, pp. 165–170.
springerlink.com

according to the international development trend of accuracy test device, we can see the development of modern accuracy test device has the following main features: technical index continues to improve; individual accuracy test device develops towards miniaturization, intelligentization and beautification; it can be used independently, embeddedly or networkly; range of measurement and control develops towards three-dimensionalization and globalization; the function of measurement and control develops towards the systematization and networking.

Key technologies of modern accuracy testing device are: sensor technology, system integration technology, intelligent control technology, human-computer interaction technology, reliability technology.

3 Overall Design of the System

In fact, electronic module sampling accuracy testing device is an automatic detection system, it integrated electronic, mechanical and automatic knowledge, which mainly is composed of a needle bed and fixture, control and centralized processing module (ATmega16 SCM) [2], the input signal generating module, output signal collecting module, intermediate variables acquisition module (photoelectric sensor), parameter setting and artificial control module (keyboard) and inspection report (digital tube) display module, system structure diagram as shown in Fig.1.

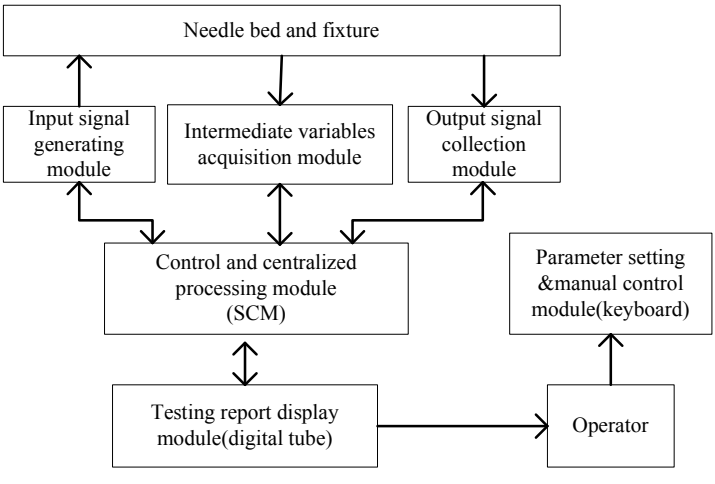

Fig. 1. The structural diagram of the system

4 Hardware Design

The hardware design of electronic module sampling accuracy testing device mainly includes: alarm circuit design, signal acquisition circuit design, the key acquisition circuit design, LED digital display circuit design, relay-controlled DC motor circuit design and power circuit design.

4.1 Design of Signal Acquisition Circuit

In order to collect data from the electronic module conveniently and accurately, the testing device uses EE-SPY302 type photoelectric sensor, which can convert the collected signal directly into the high or low level and transmit to ATmega16 SCM [3].

In order that the SCM can get accurate high or low level signals, the testing device filter the high and low level signal acquired by photoelectric sensors through RC-π type circuit, thereby effectively eliminates interference generated by the outside environment, and ensure the single-chip microcomputer can receive good pulse signal. Signal acquisition circuit as shown in Fig.2: for circuit, D1is the reference signal acquisition sensor, D2 is the tested signal acquisition sensor.

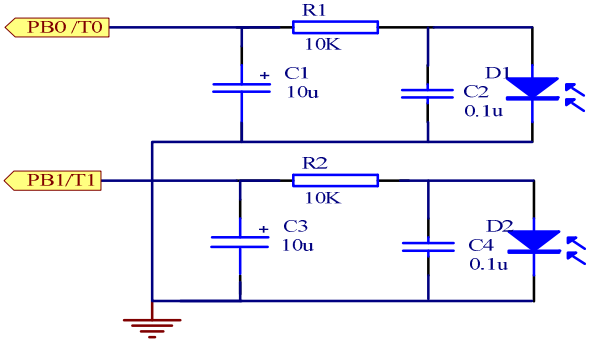

Fig. 2. The signal acquisition circuit

4.2 Design of Relay-Controlled Circuit for DC Motor

The test device adopts a relay to control the DC motor's starting and stopping, and then the DC motor drives the reduction gear to rotate, so as to obtain the required speed. Relay-controlled circuit for DC motor is shown in Fig.3.

When the output of PC3 port is high level, transistor switches into conduction, so signal is amplified to drive the relay being electrified, thereby enabling the relay to control the DC motor to start; conversely, when the output of PC3 port is low level, DC motor is stopped. D3 is a freewheeling diode used to avoid mis-conducting; DS5 is a light-emitting diode, when the transistor is conducted and the relay is electrified, that DS5 is lighted shows the relay works normally.

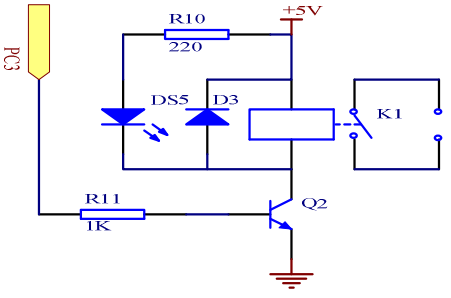

Fig. 3. The relay-controlled circuit for DC motor

4.3 Design of Power Supply Circuit e

The structure of power supply circuit for the testing device as shown in Fig.4: transformer and the bridge rectifier circuit transform 220V AC into the 12V DC, which input the Vin end of 7805 through D4 diode used to prevent current oppositely and capacitor filter; after Integrated voltage stabilizing chip 78L5, +5V DC voltage could be gotten; through the capacitor filtering, at last, the power supply circuit can provide SCM with +5V DC power supply. The branch composed of a resister and a light-emitting diode is to show if the power circuit works normally in parallel with output end [4].

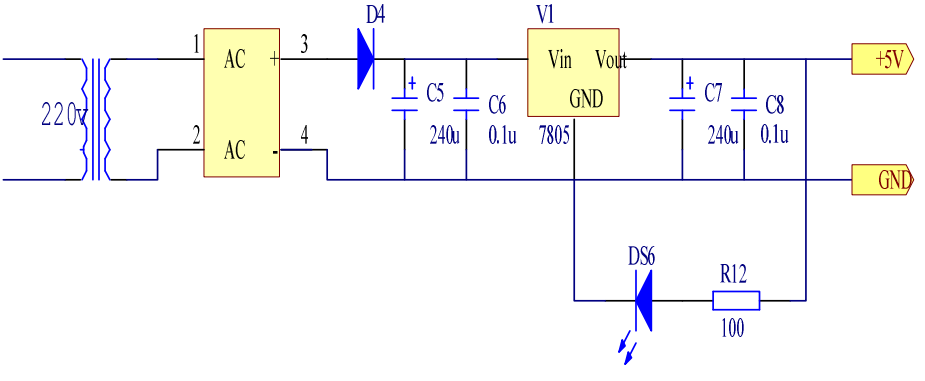

Fig. 4. The power supply circuit

5 Software Design

Software design for electronic module sampling accuracy test device adopts the structuralized idea, it is divided into several different modules to achieve different functions, which not only increases the readability of the program, but also is conducive to the joint debugging for the hardware and software in future [5-6], the main program diagram as shown in Fig.5.

The main program from the overall diagram can be seen, the system software is composed of the system initialization module, keyboard function design, signal acquisition and process design, display function, the motor control module, the error handling process and so on.

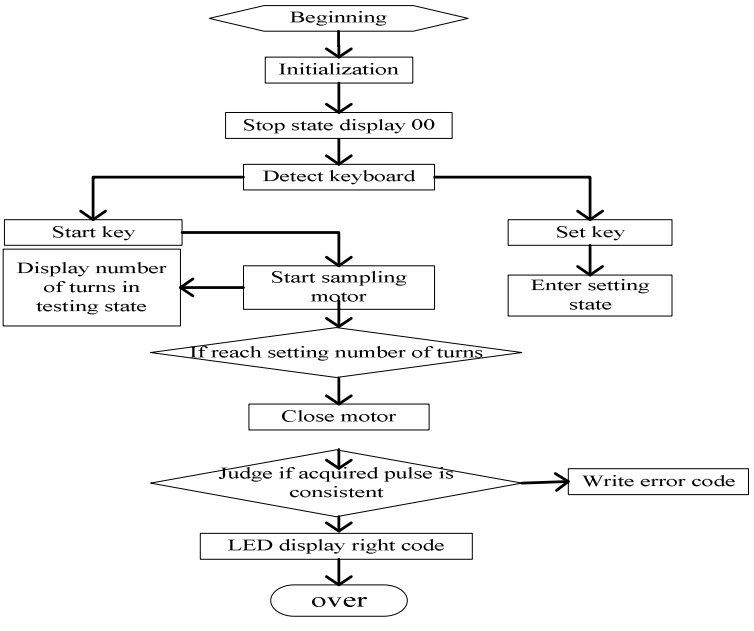

Fig. 5. The overall block diagram of the main program

6 Conclusion

An intelligent product performance should be tested before application, modern accuracy testing device is used to test product accuracy. Based on ATmega16 SCM, the electronic module sampling accuracy test device proposed in the paper realized to test sampling accuracy for the electronic module through overall design of the hardware and software. After tested, the test device works well, has achieved the design requirements. The electronic module sampling accuracy testing device has the advantages of convenient use, low cost, low power consumption, high stability, strong anti-interference ability and so on.

References

1. Guo, Z.F.: Measurement Accuracy and Measurement Instrument Accuracy. Gansu Environmental Study and Monitoring 16(4), 468–469 (2003)
2. Song, H.N., Zou, Q.P.: Design and Implementation of Object-counting Device Based on ATmega16. Machinery & Electronics 33, 496–497 (2010)

3. Xie, W.: New Development and Application of Photoelectric Sensor Technology. Instrument and Meter User 12(5), 1–2 (2005)
4. Xie, Z.M.: Design, Experiment and Test of Electronic Circuit, 3rd edn. Huazhong University of Science and Technology Press, Wuhan (2006)
5. Yuan, T.: Advanced C Language Program Design and Application for SCM. Beijing University of Aeronautics and Astronautics Press, Beijing (2002)
6. Shen, W., Zhan, W.: Introduction to C Language Development for AVR Single-chip Microcomputer. Tsinghua University Press, Beijing (2003)

Design and Research on Fuzzy Controller in Digital Speed Control System

Hongying Wang and Wei Zhou

Henan Polytechnic Institute,
Nanyang Henan, China
Ying09200@163.com

Abstract. Based on fuzzy control theory, Fuzzy controller is designed in this paper. And a combination of PID control and fuzzy control is used for DC double closed-loop speed control system. Compared with the traditional PID control, fuzzy control in many aspects has more advantages, such as control effect on system, immunity performance, speed of response, dynamic performance, etc.

Keywords: Fuzzy controller, control system, design, algorithm, simulation.

1 The Design Process of Fuzzy Controller

In control engineering, when the object is very complex, which is difficult to use the existing law of general performance to explain and describe, its mathematical model is hard to establish, the application of traditional control theory, including modern control theory can not obtain satisfactory control effect, but the people in the manual operation at present but can obtain the normal operation, and achieved certain expected results. The manual control strategy is adopted to operator learning, experiment and long-term accumulated a wealth of experience, it can make use of some qualitative inaccurate statements to describe the expression. Because natural language is ambiguous, so the control language called fuzzy language control, fuzzy control.

In order to realize fuzzy control, linguistic variable concept can be described as a manual control strategy based, and on the basis of the development of a new controller, fuzzy controller. Its role is through the computer according to the precise amount of transformation from fuzzy input information, according to the summary of manual control strategy to achieve language control rules fuzzy inference, fuzzy judgment, and converted into a precise amount as a control volume.

Design of fuzzy controller mainly solves the following three problems:

(1) will the control variable of the system with fuzzy linguistic variables, the appropriate language value into the fuzzy set of domain.

(2) the design of fuzzy control algorithm, and fuzzy control rules and fuzzy decision.

(3) by the control rules of fuzzy quantity output of fuzzy decision, fuzzy weight to a precise amount of conversion.

D. Jin and S. Lin (Eds.): Advances in Mechanical and Electronic Engineering, LNEE 177, pp. 171–176.
springerlink.com

Following the fuzzy controller system block diagram, as shown in figure 1:

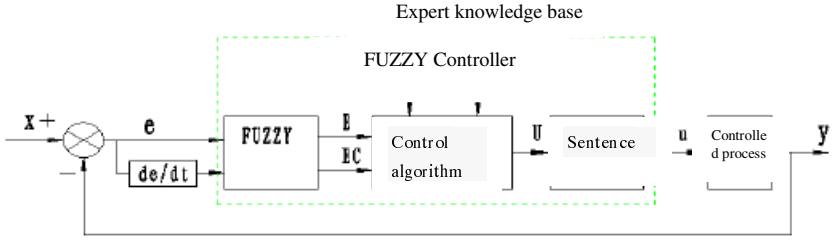

Fig. 1. Arithmetic frame chart of blur controller

CNC machine tool is very important in applied mutation load condition can maintain a constant speed, the system of immunity, robustness is largely embodied in the machine speed can be quickly with the given value and stability, so in the design of fuzzy controller to replace the ASR control, the input is a speed control voltage and speed feedback error E and e error rate of change e ', the deviation and deviation rate fuzzy processing, fuzzy input, fuzzy controller based on input fuzzy variables, according to the fuzzy reasoning rules, calculated by fuzzy control volume. The fuzzy control quantity to blur into the exact amount as a current loop input value.

2 The Design of Fuzzy Controller Algorithm

2.1 Fuzzy Variable Assignment and Control System

Set input speed deviation and deviation change rate of e e ' basic universe as [X, X], fuzzy quantization level of the fuzzy set theory as [n + n], so the exact amount of quantification factor: K = n / X. Error E quantization level domain for E = [- 3, - 2, - 1, 0, 1, 2, 3], the discretization usually after divided into several files," big" (PB) and + 3 near; "in the middle" (PM) and + 2 is near;" small" (PS) and + 1 near;" zero" (Z0) and 0 near;" negative small" (NS) and nearby - 1;" negative" (NM) and nearby - 2;" negative" (NB) and nearby - 3 a total of 7 linguistic variables to describe. Fuzzy mathematics, often with real R as the domain of membership function of fuzzy set, called the fuzzy distribution, commonly used fuzzy distribution of triangle distribution, trapezoidal distribution, normal distribution, then use a triangular distribution method as shown in figure 2:

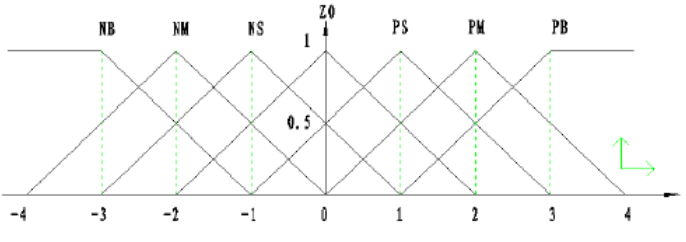

Fig. 2. Trigon chart of blur distribution

In this paper, the speed deviation E assignment table as shown in table 1:

Table 1. Value of rotate speed warp E

	-3	-2	-1	0	1	2	3
NB	1	0.5					
NM	0.5	1	0.5				
NS		0.5	1	0.5			
ZO			0.5	1	0.5		
PS				0.5	1	0.5	
PM					0.5	1	0.5
PB						0.5	1

According to the same rules are given speed EC error rate of change of the membership function table as shown in table 2:

Table 2. Value of rotate speed rate warp EC

	-3	-2	-1	0	1	2	3
NB	1	0.5					
NM	0.5	1	0.5				
NS		0.5	1	0.5			
ZO			0.5	1	0.5		
PS				0.5	1	0.5	
PM					0.5	1	0.5
PB						0.5	1

In order to improve the control precision of fuzzy decision making theory expansion for U: U = [- 6, - 5, - 4, - 3, - 2, - 1, 0, 1, 2, 3, 4, 5, 6], linguistic variable value is" big" (PB)," median" (PM), is " small" (PS)," zero" (Z0)," negative small" (NS)," negative" (NM)," negative" (NB), to

A typical variable assignment table as shown in table 3:

Table 3. Value of blur decision-making U

	NB	NM	NS	ZO	PS	PM	PB
-6	1	0.2					
-5	0.8	0.7	0.1				
-4	0.4	1	0.4				
-3	0.1	0.7	0.8				
-2		0.2	1				
-1			0.4	0.5			
0				1			
+1				0.5	0.4		
+2					1	0.2	
+3					0.8	0.7	0.1
+4					0.4	1	0.4
+5					0.1	0.7	0.8
+6						0.2	1

The fuzzy control rules to establish the principle is: when the error of E becomes larger, higher volume control U to eliminate the error; when E is small, controlled amount of U cannot choose too large, to prevent the appearance of input overshoot, ensure the stable operation of the system; when the E is negative in EC, and honorable, control measure is zero, in order to prevent overshoot. Similarly, when E is big, EC is negative when the amount of control, selection of zero. According to the above principles, fuzzy control rules are shown in table 4:

Table 4. Control rule of blur controller

	NB	NM	NS	ZO	PS	PM	PB
NB	NB	NB	NB	NM	NM	NS	ZO
NM	NB	NB	NB	NM	NS	ZO	PS
NS	NB	NM	NM	NS	ZO	PS	PM
ZO	NB	NS	NS	ZO	PS	PM	PB
PS	NM	NS	ZO	PS	PM	PB	PB
PM	NS	ZO	PS	PM	PB	PB	PB
PB	ZO	PS	PM	PB	PB	PB	PB

2.2 Fuzzy Control Mechanism Agorithm

Fuzzy control rule table determines a two input and single output of the Fuzzy controller as shown in figure 3:

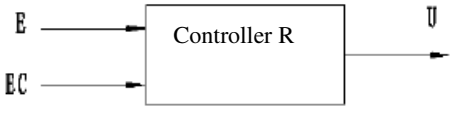

Fig. 3. Fuzzy controller of two input and one output

The design of Fuzzy controller is derived from human control process. In the reality of industrial control process, the operator usually observe the output and its changes or the combination to determine the control amount. The fuzzy control determines the input amount to the controller on this basis. in the control system, the number of independent variables of Fuzzy controller is called system dimension. Single-input and single-output controller is generally designed as one-dimensional or two-dimensional, but occasionally three dimensional fuzzy controller .

3 Fuzzy Controller Used in Composite Control Simulation

From the establishment of fuzzy controller process controller can be seen, to the error and error change as input variables, with fuzzy proportional derivative control action,

but the lack of fuzzy integral control, steady state performance is poor, and the integral control to eliminate the steady state error, but slow dynamic response, proportional integral control action can obtain higher steady-state precision, with fast dynamic response, therefore the PI control and fuzzy control nodes and together, constitute fuzzy PI compound control.

This combined control strategy is in big deviation range using fuzzy control, in the small deviation range conversion for PI control. The main point is that fuzzy controller to eliminate the steady-state error of the system itself is weak, it is difficult to achieve high control precision. The PI regulator integral regulation theoretically can make the system steady error control for zero. When the error of E at a certain threshold outside, fuzzy control, in order to obtain good transient performance, when the error in

Threshold when using PI control, in order to obtain good steady-state performance.

The inner current loop still use PI regulator, speed regulator using fuzzy PI compound control, the use of Switch module as the changeover switch. Process control requirements for control system transformation, i.e. from fuzzy control is converted to PI control, need to set the Switch threshold, fuzzy control and PI control of the switching point, the system threshold setting too premature entry into PI control mode and affects the response speed of the system, if the selection is too small it may appear to oscillate, or fuzzy controller to control the properties of rough, can not reach the threshold, which can not be converted to PI control mode. In this case the step input setting Switch value is 0.15, namely the error is less than 0.15 when entering the PI control state, the composite control of velocity response curve, the same parameters and the original pure PI under the control of the velocity response curve compared with fast dynamic response, small steady state error,Results as shown in figure4.

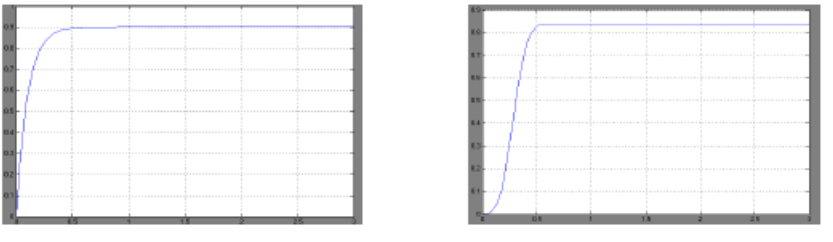

a) Fuzzy PI compound control b) The conventional PI controller

Fig. 4. Compare curve of general pi controller and fuzzy-pi complex controler

References

1. Roopaei, M., Zolghadri, M., Meshksar, S.: Enhanced adaptive fuzzy sliding mode control for uncertain nonlinear systems. Communications in Nonlinear Science and Numerical Simulation 14(9-10), 3670–3681 (2009)
2. Martinez, J.J., Sename, O., Voda, A.: Modeling and robust control of Blu-ray disc servo-mechanisms. Mechatronics 19(5), 715–725 (2009)

3. Nassirharand, A.: Matlab software for inversion of describing functions. Advances in Engineering Software 40(8), 600–606 (2009)
4. Zheng, X.: The NC Transmission Servo System Modeling And Simulation Based On The Bldcm, pp. 66–76. Taiyuan University of Technology (2010)
5. Wang, Z.Y., Ming, Z.X., Feng, H.Y.: The adaptive fuzzy neural network control of electro-hydraulic servo system. China Mechanical Engineering (4), 681–684 (2004)
6. Prakash, J., Srinivasan, K.: Design of nonlinear PID controller and nonlinear model predictive controller for a continuous stirred tank reactor. ISA Transactions 48(3), 273–282 (2009)
7. Noroozi, N., Roopaei, M., Zolghadri Jahromi, M.: Adaptive fuzzy sliding mode control scheme for uncertain systems. Communications in Nonlinear Science and Numerical Simulation 14(11), 3978–3992 (2009)

Design of Power Transformer Fault Measuring Model Based on Relevance Vector Machine

KaiQi Sun

School of Electrical Engineering,
Shandong University, Jinan, China
sunkq@mail.sdu.edu.cn

Abstract. Recently, condition monitoring of power transformer has become global due to the potential advantages to be gained from reduced maintenance costs, improved productivity and increased machine availability. In this paper, a novel fault measuring method base on relevance vector machine (RVM) is proposed for power transformer condition monitoring. Empirical results demonstrated that using, using similar training time, the RVM model has shown comparable generalization performance to the popular and state-of-the-art support vector machine (SVM), while the RVM requires dramatically fewer kernel functions and needs much less testing time. The results lead us to believe that the RVM is more powerful tool for on-line fault measuring method than the SVM.

Keywords: power transformer, fault measuring, relevance vector machine.

1 Introduction

Power transformers are essential devices in supplying power energy to electrical equipments. An unexpected transformer failure can cause a long halt of processes, costly repairs and significant environmental damages. Therefore, it is desirable to instantly dter equipment. Data mining is a effective tool to discover valuable and non obvious information embedded in a large collection of data. The methods of data mining include Grey Cluster, Fuzzy Cluster, Neutral Network, Bayesian Network Classifier, Support Vector Machine (SVM), and so on. However, because of the structural complexity and the diversity of the faults mechanisms, the effectiveness of the fault diagnosis method needs to be improved; therefore further research is needed in this area. Relevance vector machine is a new learning method is statistical learning theory. Compared to SVM, RVM is greater sparseness and accuracy. RVM is based on a probabilistic Bayesian learning framework, and as a feature it can yield a decision function that depends on only a very fewer number of so-called relevance vectors. In this paper, the proposed method is tested and compared with a state-of-the-art 'support vector machine' classifier. It is demonstrated that the RVM classifier can yield a decision function that is much sparser than the SVM classifier while providing higher classification accuracy. Consequently, the RVM classifier greatly reduces the computational complexity, making it more suitable for real-time implementation.

D. Jin and S. Lin (Eds.): Advances in Mechanical and Electronic Engineering, LNEE 177, pp. 177–181.
springerlink.com

2 Support Vector Machines (SVM)

Support Vector Machines belongs to the classifier group called large margin classifiers [1]. As being a binary classifier, SVM uses the following formula to classify given test data:

$$f(\mathbf{x}) = y = \operatorname{sgn}\left(\sum_{i=1}^{k} \alpha_i y_i K(\mathbf{x}, \mathbf{x}_i) + b \right) \tag{1}$$

where α_i is nonzero Lagrange multiplier for each support vector x_i, k the support vector number, $y_i \in \{-1, +1\}$ the class label, b the bias value for the hyperplane and $K(\mathbf{x}, \mathbf{x}_i)$ the kernel function. Polynomial kernel can be given as an example kernel function:

$$K(\mathbf{x}, \mathbf{x}_i) = ((\mathbf{x}, \mathbf{x}_i) + 1)^d \tag{2}$$

where d is the polynomial degree, which we select as one resulting in a linear SVM in this study based on our preliminary studies with other kernel. The dual problem for SVM can be solved by finding the α_i valued by maximizing the cost function $Q(\alpha)$:

$$Q(\alpha) = \sum_{i=1}^{N} \alpha_i - \frac{1}{2} \sum_{i=1}^{n} \sum_{j=1}^{n} \alpha_i \alpha_j y_i y_j K(\mathrm{x_i}, \mathrm{x_j}) \tag{3}$$

subject to $\sum_{i=1}^{n} \alpha_i y_i = 0$ and $C \geq \alpha_i \geq 0$.

The $\mathrm{x_i}$ input (training) vectors with the nonzero Lagrange multiplier α_i are called support vectors.

3 Relevance Vector Machines (RVM)

RVM assumes that the targets are noisy observations of the actual values [2]:

$$t = y + \varepsilon \tag{4}$$

where t is the noisy observed output, ε the noise value and y the actual target output. RVM can learn the noise variance along the training procedure as well. Because of its several advantages, RVM is getting more attention in today's machine learning applications. While SVM assumes -1 or +1 values for class labels, RVM classification assumes that the label values for t to be 0 or 1 for each class.

In this sparse Bayesian probabilistic model, for a given test vector x, the class label y can be found as:

$$f(\mathbf{x},\mathbf{w}) = y = \sum_{i=1}^{n} w_i K(\mathbf{x}, \mathbf{x}_i) + w_0 \tag{5}$$

where the w_i is the i^{th} weight for the i^{th} training input, $\mathrm{w} = [w_1, w_2, \cdots\cdots, w_n]^{\mathrm{T}}$, and n the training sample number.

In this Bayesian approach, each w is assumed to have a Gaussian distribution parameterized by a hyperparameter α ,whose most probable value is calculated iteratively through the RVM algorithm with the expectation maximization algorithm. The hyperparameter α for RVM differs from the one defined for SVM.

$$p(\mathbf{w}|\alpha_1, \cdots\cdots, \alpha_n) = (2\pi)^{-n/2} \prod_{i=0}^{N} \alpha_i^{1/2} \exp(-\frac{1}{2} \sum_{i=1}^{n} \alpha_i w_i^2) \tag{6}$$

where α_i is the hyperparameter corresponding the w_i, and is related to the inverse variance. The training vectors that have finite α value are called relevance vector. Therefore, in general, the RVs do not lie on the margin as opposed to SVs for SVM, and generally number RVs is much smaller than the number of SVs providing a more efficient clsssifier.

4 Feature Extraction

4.1 Signal Characteristics

The analytical base of diagnosis is some diagnostic gas obtained by DGA. The content information reflects the states of transformer. The diagnostic gases include hydrogen (H_2), methane (CH_4), ethane (C_2H_6), ethylene (C_2H_4), acetylene (C_2H_2), et al. So in this paper we chose these 5 gases as input features.

Based on analyzing the characteristic of transformer fault, the transformer fault diagnosis which is identified relying on the effective information provided by DGA is divided into six types of transformer state. The six types as follows: partial discharge (PD), discharges of low energy (D_1), discharges of high energy (D_2), thermal fault (T_1), thermal fault (T_2), thermal fault (T_3).

4.2 Normalization

The normalization procedure is applied to minimize possible bias due to different ranges in different feature dimensions. Normalization is a process of scaling the predictor data to improve the accuracy of the subsequent numeric computations. The method, used in this work, to normalize a data set is to center it at zero mean and scale it to unit standard deviation. If the data set of any feature is denoted as E, the normalized value e' can be obtained by computing[3-5]:

$$e' = \frac{e - m_E}{\sigma_E} \tag{7}$$

where m_E is the mean of data set E and σ_E is the standard deviation of data set E. Thus, the feature vectors are extracted from the raw signals and the feature space is obtained.

4.3 Feature Selection

Too many features can cause curses of dimensionality and also can be a burden as it requires a large amount of time to calculate. Thus feature selection is necessary to remove garbage features and pick up the significant one for fault diagnosis. In order to solve this problem, Fisher criterion is adopted as the feature selection method. The Fisher criterion for one single feature is defined to be the ration of the between-class variance to the within-class variance and is given by

$$J_F(y_j) = \frac{S_{B,j}}{S_{W,j}} \tag{8}$$

where y_j is the j th feature dimension vector, $S_{B,j}$ is the between-class variance of y_j, given by

$$S_{B,j} = (m_{1j} - m_{2j})^2 \tag{9}$$

where $S_{W,j}$ is the total within-class variance of y_j, given by

$$S_{W,j} = \sigma_{1j}^2 + \sigma_{2j}^2 \tag{10}$$

where $m_{ij}(i = 1, 2)$ is the mean of class i, and σ_{1j}^2 is the within-class variance of class i.

5 Experiment Result

The continuous input vectors are consisted of the volume fraction of gases, H_2, CH_4, C_2H_6, C_2H_4, and C_2H_2[6]. There are 120 training samples and 37 testing samples. These training samples are used to determine the parameters of diagnosis model and testing samples are used to verify the diagnosis accuracy of diagnosis model. In order to judge the accuracy of fault diagnosis, we compared the diagnosis using RVM and using SVM. The prediction performance results are shown in Table 1.

Table 1. Performance comparisons of SVM and RVM

INDEX	SVM	RVM
Training time(s)	0.9688	0.9531
Test time(s)	0.0156	0.0011
Number of SVs/RVs	31	6
Training accuracy (%)	95.39	95.41
Test accuracy (%)	92.11	92.76
Total accuracy (%)	93.75	94.08

6 Conclusions

In this paper, we have presented a novel fault measuring method for power transformer condition monitoring, based on relevance vector machine. Statistical characteristics were extracted as feature vectors, and the Fisher criterion was adopted as a feature selection tool. The RVM and the SVM were compared using the same Kernel function and the same parameters, over the same training and test data sets. Empirical results demonstrated that the RVM has the similar high classification performance to the SVM while consumes close training time. Furthermore, the RVM utilizes dramatically fewer kernel functions, needs much less testing time, offers smooth predictive probability distribution. The results lead us to believe that the RVM is a more powerful tool for on-line fault detection than the SVM.

References

1. Moulin, L.S.: Support vector machines for transient stability analysis of large-scale power systems. IEEE Transactions on Power Systems 19(2), 818–825 (2004)
2. Kaplowicz, N.: Learning from imbalanced data sets: a comparison of various strategies. In: Proceeding of Learning from Imbalanced Data Sets, pp. 10–15. AAAI Press, Menlo Park (2000), Tech.Rep. WS-00-05
3. Browne, M.W.: Cross-validation methods. Journal of the Mathematical Psychology 44, 108–132 (2000)
4. Kaplowicz, N.: Learning from imbalanced data sets: a comparison of various strategies. In: Proceeding of Learning from Imbalanced Data Sets, pp. 10–15. AAAI Press, Menlo Park (2000), Tech.Rep. WS-00-05
5. Tipping, M.E.: Sparse Bayesian learning and the relevance vector machine. Mach. Learning 1, 211–244 (2001)
6. Shang, Y.: Synthetic insulation fault diagnose model of oil-immersed power transformers utilizing information fusion. Elec. Eng. (2002)

EPS Central Monitoring System Based on Virtual Instrument

Lei Chen[1,*], Shuang Chen[2], and BaoRu Han[3,*]

[1] Northeast Petroleum University at Qinhuangdao,
Qinhuangdao, Hebei 066004, China
[2] Institute of Math and Information Technology,
Hebei Normal University of Science and Technology,
Qinhuangdao, Hebei 066004, China
[3] Department of Electronic Engineering,
Hainan Software Profession Institute, Qionghai, Hainan, 571400, China

Abstract. In order to realize the central monitoring to the voltage, current and the relative alarming state of emergency power supply, the system design scheme based on virtual instrument was presented. The MCU STC11F04E was used as the control core of the slave device, combining with the voltage or current transformer, true RMS voltage measurement circuit, high precision amplifier and the 10-bit resolution A/D conversion circuit, to accomplish the acquisition, processing and display of multi-channel signals in the slave device, which mainly includes city power voltage, inverting voltage, output current and storage battery voltage. The MODBUS protocol was used to realize the RS-485 communication between the master computer and the slave device. The graphical programming environment LabVIEW was adopted to realize the function of monitoring, communication, data storage and query in master computer. The practical application shows that this system design scheme is feasible and reliable.

Keywords: Emergency Power Supply, Data Acquisition, MODBUS Protocol, LabVIEW.

1 Introduction

Emergency Power Supply (EPS) can provide emergency power in the situation of breaking off or abnormity of the city power, which is a important part of the modern building safety guarantee facility, and has been widely used in many public places such as marketplace, hospital, library and so on. There are usually many EPS facilities scattered in different position or floor of these places, so it is necessary to monitor these EPS facilities centrally with computer [1].

2 Hardware Design of Slave Device

The block diagram of the slave device is shown in Fig .1.

* Corresponding author.

D. Jin and S. Lin (Eds.): Advances in Mechanical and Electronic Engineering, LNEE 177, pp. 183–188.
springerlink.com

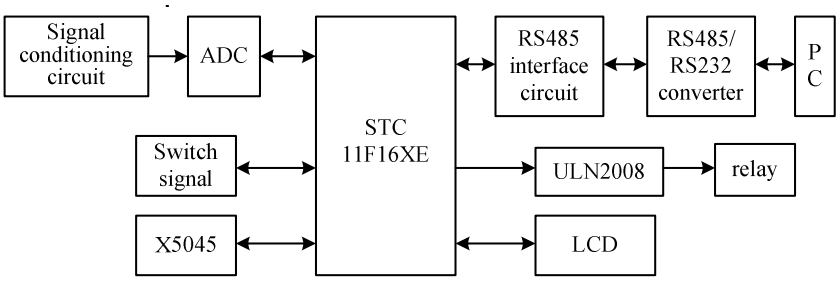

Fig. 1. Block diagram of the slave device

2.1 Signal Conditioning Circuit

The signal processing circuit of AC current consists of current transformer, voltage sampling circuit, true RMS voltage measurement circuit and high precision amplifier circuit, as shown in Fig.2. When measuring the alternating current, the current transformer transform the 0-25A alternating current effective value to 0-5mA in proportion. A 0~200mV AC voltage was obtained by a 40 Ω sampling resistor, and the true RMS of this voltage is measured by AD736. The DC output voltage range of AD736 is 0~200mV, which should be strengthened for sampling by an analog-to-digital converter. The analog-to-digital converter that sensing it has a fixed input range of 0~5V. To take full advantage of the input range, it is desirable to apply a gain of 25 to the AD736 output voltage by instrumentation amplifier AD620, so that it swings from 0~5V. The MCU program can calculate the final ac current value according to above transform relation. Fig. 3 shows the true RMS conversion circuit based on AD736 and the amplifying circuit based on AD620.

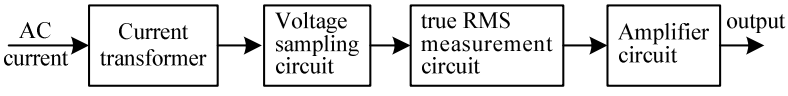

Fig. 2. AC current measurement scheme

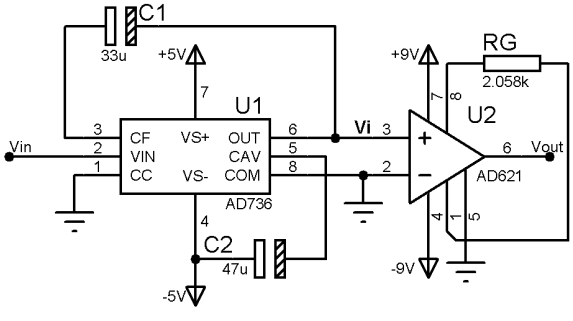

Fig. 3. True RMS conversion and amplifying circuit

The AC voltage measurement circuit is similar as the AC current.

2.2 Analog to Digital Conversion

TLC1543, a Successive Approximation Register analog-to-digital converter, is used to accomplish the A/D conversion. TLC1543 has 10-bit resolution and 11 analog input channels, which can satisfy the demand of multi-channel acquisition and high resolution. In addition, the integrated reference circuit based on LM336 is used to provide 5V voltage reference for TLC1543.

2.3 Collection and Control of Switch Signal

MCU measures the switch signals on the spot such as overheating, fog and short circuit, and output the corresponding control signals. The photo-couplers are used to realize the electrical isolation between MCU and the input-output devices, and darlington arrays IC ULN2008 is used to drive relays.

2.4 RS485 Interface Circuit

The information is displayed by LCD on the slave device, which facilitates the field debugging. And at the same time the RS-485 bus is used to realize the centralized monitoring on multi-fields by computer. The host computer acquires the terminal information from slave machines by polling method. The slave machine uses RS485 port, while the host computer uses the RS232 port, and they are non-compatible with each other, so the conversion between RS485 and RS232 is necessary.

RS-485 bus has the advantages of low cost, easy operation, far transmission distance etc. The engineering practice shows that when some details are disposed improperly or one node on the bus is failure, the communication failure and system paralysis will happen. So it is necessary to improve the reliability of RS-485 bus, and some measures are introduced as follows [2].

In the situation of long distance communication or high electromagnetic interference routing environment, the differential transceiver with transient voltage suppression SN75LBC184 should be used, which can withstand the lightening impulse and endure electrostatic discharge as high as about 8kV. SN75LBC184's input resistance is as high as 2 times the normal, and 64 devices are allowed to connect on the bus, built-in protection against high-energy noise transients. These features provide a substantial increase in reliability for better immunity to noise transients coupled to the data cable over most existing devices. And SN75LBC184 provides a reliable low-cost direct-coupled data line interface without requiring any external components.

The high speed photocoupler is suggested to be used in the connection between MCU and the RS-485 communication IC.

The RS485 bus operates in half-duplex communication mode. In order to avoid the reflection phenomenon, the RS485 transceivers should be connected in daisy chain rather than star topology.

The pull-up resistor connected with A pin and power, the pull-down resistor connected with B pin and ground are used to provide the network failure protection and improve the reliability of RS-485 bus. A resistor between A and B is adopted to realize terminal matching.

Even if only one communication IC is in failure, the bus may be in trouble, so the resistors about 4~20Ω are needed to connect to the bus, thus the whole bus communication can not be affected by the slave machine, the TVS diodes between the communication port and ground are needed to eliminate the surge interference.

If the communication distance exceeds 1km, the communication reliability should be improved by increasing the relay module or reducing the communication speed. The relay has the function of the signal amplifying and photoelectric isolation, which can increase the communication distance and improve the communication quality.

3 Program Design of Slave Device

The programs of slave device mainly include analog-digital conversion, digital filter, MODBUS RTU communication and LCD display subprogram. The digital filter program and communication scheme are described in detail as follows.

3.1 Digital Filter

Analog filter can not reduce noises with in bandwidth remarkably, so the appropriate software digital filter is necessary. The median-average filter is adopted here, sampling N data continuously, eliminate the maximum and the minimum, then calculate the average value of the other (N-2) data. This method can eliminate the errors caused by random impulse interference. The filter effect is favorable for the slow change parameter such as temperature, liquid level, pressure and so on. The program is given as follows.

```
unsigned char filter()
{  unsigned char k,i,j,temp,buf[N];
 unsigned int sum;
 for (k=0;k<N;k++)
   { //calling analog-digital conversion subprogram
    buf[k]=AD1543(0);
     delay(10);   // calling  delay subprogram
   }
 for (j=0;j<N-1;j++)
   { for (i=0;i<N-j;i++)
      { if ( buf[i]> buf[i+1] )
         { temp=buf[i];buf[i]=buf[i+1];
          buf[i+1] = temp; }
       }
    }
 for(k=1;k<N-1;k++) sum+= buf[k];
 return (unsigned char)(sum/(N-2));
}
```

3.2 MODBUS RTU Communication Program

MODBUS is a request-reply protocol and offers services specified by function codes, slave nodes will not typically transmit data without a request from the master node, and do not communicate with other slaves. This system adopted the RTU mode of MODBUS protocol, and realized the communication between master and slave node on the bus. MODBUS RTU is a mainstream protocol used by intelligent instruments, which is widely applied in industrial field combined with RS485 bus.

The function code 03 is used to read the contents of a contiguous block of holding registers in a remote slave device in this system. The master device sends the hexadecimal request frame as 01 03 00 00 00 07 04 08 based on MODBUS RTU, where the first byte represents the slave address 01, the second byte is the function code 03, 04 08 is the CRC value calculated by the sending device, and 00 00 00 07 specifies the starting register address 00 00 and indicates that the master device will read the contents of registers from 0 to 7, amount to 14 bytes.

If the slave devices on the bus receive the above request, the serial interrupt is used to receive the first byte. This byte is analyzed to determine if the frame is for the device. If not, the frame will be discarded. The slave address is unique on a MODBUS serial bus, and only the slave device whose address is 01 will continue to receive the other 7 bytes. After all the 8 bytes are received by the slave device, the CRC of the fore 6 bytes will be calculated. Then the receiving device compares the calculated value to the actual value it received. If the two values are equal, the slave will respond according to the frame shown in Table. 1. Other wise an error results.

Table 1. Respond message frame

Slave address	Function code	Byte count	Register value	CRC value
01 (hex)	03 (hex)	0E (hex)	14 bytes	2 bytes

4 Program Design of Slave Device

Graphical programming environment LabVIEW was used to exploit the computer centralized monitoring system for EPS. LabVIEW provides powerful graphical control, unprecedented hardware integration and compatibility, which make it very convenient and rapid to create and deploy measurement and control systems [3].

The master computer acquires information from the slave device based on MODBUS protocol. The information includes city power voltage, inverting voltage, output current, storage battery voltage, field temperature and switch signal state.

The NI Modbus Library for LabVIEW is a free, downloadable set of VI function blocks that provide Modbus communication from any standard ethernet or serial port. It implements the Modbus protocol in software and offers both master and slave functionality. Copying the NI Modbus.llb file to the vi.lib folder under LabVIEW installation program, and the nimodbus.mnu file to the user.lib folder, then open LabVIEW, we can find all NI Modbus sub-VI in the user library of function panel, here

the MB Serial Init.vi and MB Serial Query(poly).vi are used to realize the communication program based on MODBUS. The communication program code is shown in Fig. 4, where "Data" is the register values acquired from the slave device.

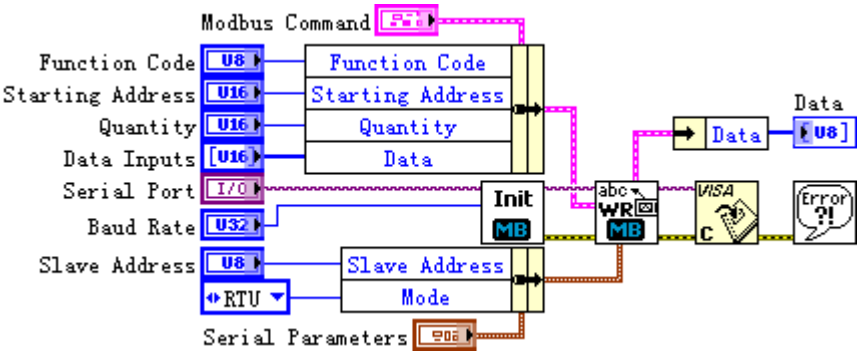

Fig. 4. MODBUS communication program code

LabVIEW itself does not have the function of database accessing, so the test and measurement system based on LabVIEW needs other assistant tools to access database. Here the free LabSQL toolkit was used to realize the data storage and the history data query. The implementation scheme can reference related literature [4, 5].

5 Conclusion

The virtual instrument technology was used to realize the EPS computer centralized monitoring system based on LabVIEW. Practice shows that the scheme discussed in the paper is feasible, and the good application result was obtained.

Acknowledgement. This work is supported by the Natural Science Foundation of Hainan Province (No.611127).

References

1. Wu, L., Zhao, C.Y.: Development of a kind of novel single-phase Emergency Power System (EPS). Electronic Measurement Technology 30(8), 141–142 (2007)
2. http://www.com-tcp.cn/jishu/485buxianguifan.html
3. http://www.ni.com
4. Li, W.T., Cao, Y.H., Bo, X.F.: Implementation of Database Accessing Technique of Labview and Its Application. Industry and Mine Automation 30(3), 69–71 (2012)
5. Zhou, H., Mo, J., Li, D.S.: Using LabSQL Tools to Access Database in Labview. Chinese Journal of Scientific Instrument 30(6), 321–324 (2009)

Study on the Continuous Running Automation Control Mode of the Double-Layer Subsurface-Flow Snow Melting System Based on the Interaction Mechanism of Electronic Sensor

Binxia Xue[1], Weiguang Li[1], and Xiaofei Kang[2]

[1] School of Architecture, Harbin Institute of Technology,
No. 66 West Dazhi Str. Nangang Dist. Harbin, China
[2] Urban Planning and Design Institute, Harbin Institute of Technology,
No. 66 West Dazhi Str. Nangang Dist. Harbin, China
binxia68@126.com, lwg0605@163.com,
kxf999999@sina.com

Abstract. Generally, there are quite amounts of cities in our country meeting the problems of snow covering, which would have impacts on the urban transportation, if the snow is not cleaned up immediately. This paper proposed the double-layer subsurface-flow constructed tanks and the snow melting well system to deal with the problem of snow cover on the urban roads, in order to forming new routines of ecological disposal and utilization of the urban ice and snow. Thus, it would also help with enhancing the efficiency of protecting and utilizing the fresh water resources. At the meanwhile, for the purpose of proving the practice meaning of this system, this paper also demonstrated the possibility of this automation operating system based on the electronic sensor, and it proposed the prospect of applying this system in practice as well.

Keywords: Snow Melting Techniques, Automation, Snow Cover on the Ground, Double-Layer Subsurface-Flow Filtering Tank, Electronic sensor.

1 Introduction

It is well known that the northern cities of China would face the problem of snow cover in winters widely. It is because that the snowfall in northern cities is always concentrated; moreover, its intensity is quite huge. For instance, the city of Harbin, the capital city of Heilongjiang Province, has about 33 days of snowing yearly, which would cause high snow covering ratio. As a result, the average cover thickness would reach around 20cm, and the duration of snow cover could reach 105 days. [1] Therefore, dilatory snow removal would have influence on the urban transportation and daily life. However, the common approach of dealing with the covering snow is piling up that snow beside the green belts. Once the weather turns warm and the snow would begin to melt, which would resulting the sewage in transverse flowing. Such results would have impacts on the urban landscape and the travel safety of the urban residents. Furthermore, it also would damage the urban grounds due to the

D. Jin and S. Lin (Eds.): Advances in Mechanical and Electronic Engineering, LNEE 177, pp. 189–195.
springerlink.com

freezing-thawing alternation, which would result in the cracks on the ground need quite amounts of governmental funding and energy to maintaining the urban roads.

On the other hand, the covering snow has been identified as a kind of advantaged ice and snow resources, which could help achieve the purpose of making good use of fresh water resources and maintaining the ecological balance of the urban. Therefore, the utilization of the covering snow has been recognized as a meaningful research subject. So far, in our country, there are quite less the researching subjects on the ice and snow resources. And the engaged techniques of snow removal generally have their limited conditions or their specific operating conditions, such as the cable heat storage, solar thermal accumulation, geothermal resource, underground pipes, mechanical operation and ice removal with chemical agents.[2] Consequently, based on the specific rainwater treatment technology in winter cities including double-layer subsurface-flow constructed wetland system, the ice and snow accumulated in the urban areas is storage and applied in public water and landscape construction with the broad development prospect when the spring comes. At the same time, the perfect economic, environmental and social benefits are reflected.

2 The Structure of the Ground Snow Melting System

As a new ecological method of disposing the ground accumulated snow, the main body of the double-layer subsurface-flow tanks snow melting system is making use of two kinds of functional constructions to making use of the urban underground space adequately. After taking the actions of melting the snow, degradation and resources recovery, those melt water would be used as municipal water such as city greening water, road cleaning and fire fighting water. Either, after a further up deepen treatment, it can also be used as reclaimed water for the residents' daily life.

3 The Operating Principles of Snow Melting Unite

The urban melting snow can be treated as the potential original water resource for the double-layer subsurface-flow constructed tanks, providing the winter complementary water resource. Moreover, a good routine of disposing the accumulating snow would be good for the safety of urban transportation. Otherwise, the squeezing accumulated snow on different grounds by the cars and pedestrians, or full of dust would result in the great pollution. So collecting and disposing those accumulating snow is going to be recognized as the premise of guaranteeing the quality of the water.

The heating snow melting well plays the role in collecting and melting snow. The heating and melting assemblies are only running in the winters, but in summers, collecting wells are just simply running as rainwater collecting tanks. While the road snow collecting is taken the actions of manual collecting and dumping to make the snow come together at the heat preservation wells. And their locations are beneath the street green areas including the ends of the street green belts and the outer edge of the landscape green areas. The collecting wells are designed in the trapezoid shape, which could be good for the large-scale snow falling down. The heat preservation covers make the snow melting wells separated from inside and outside, enhancing the

working efficiency of the heating assemblies inside and reducing the heat loss of the well inside. After the snow collecting and closing the heat preservation cover, the system starts the assembly of heating snow, and then the melted snow goes through the network filtering assembly into the system of the double-layer subsurface-flow tanks. There is a must of installing the snow melting assemblies at the bottom, outside and inside of the heat preservation well, in order to make the collected ice and snow melted into water and put into the subsequent dispose and utilization.

4 The Operating Principles of the Double-Layer Subsurface-Flow Tanks

It is known that the main body of completing the process of purification and utilization has been identified as the double subsurface-flow tanks. The system of double-layer subsurface-flow constructed wetland landscape tanks is divided into upper and under parts. The upper part is the constructed wetland landscape system and the under part is the horizontal undercurrent tanks.(Figure 1) The upper constructed wetland system is made up of four parties that water body, wetland matrix, upper vegetation and microorganism. The process of degradation and purification for the pollution is mainly conducted by those four assemblies. However, in the winter, the upper landscape tanks would lose its function of water purification due to the low temperature and the vegetation withered.

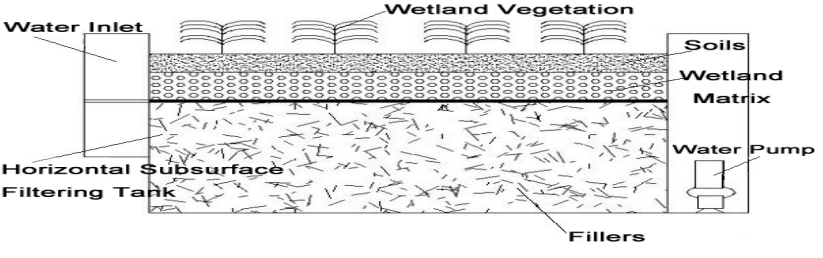

Fig. 1. The Structure Diagram of the Double-layer Subsurface-flow Filtering Tank

While the under horizontal tanks would take full advantage of the urban underground space to disposing the rainwater further. Putting fillers into the horizontal undercurrent tanks, the microorganism could adhere to those fillers forming a biological film, making use of organics in the running rainwater as the nutritious materials to achieve the goal of purification thoroughly. Comparing to the general activated sludge process, this method shows better running effects under the low impact condition. Because the biological film could adhere to the fillers for quite a long time, so it is good for some microorganism with long generation time such as nitrobacteria. So the more kinds of microorganism are in the biological film, the longer the food chain in this tiny environment is, which would help with reducing the production of the sludge amount. When the snow water is stored in the subsurface-flow tanks for a long time, not only it plays a role of storage and adjustment, but also

guarantee the water quality, avoiding the secondary pollution. As the undercurrent tanks are located beneath the tundra, even if in the freezing winter, the microorganism in the tanks would also work normally that would guarantee the purifying efficiency. More than that, the undercurrent tanks can also work as adjustment assembly storing the snow for a short time. Thus different season working mode would improve the operating efficiency of the holistic system making it continuously running, which would decrease the times of start and stop and save huge amount of time and investment.

5 The Operation of Road Snow Melting System

If the double-layer subsurface-flow tanks-the snow melting well system wants to be applied in the real-time snow removal technique, there should be a combination with the urban comprehensive design and planning ideas and couple with the urban construction process to form a wholesome construction system. The application of this kind of technique should not only maintain the disposing effect but also take its cost and management into account. If there is a need of great amount of labor and material resources to maintain the normal operation, such system is obvious not suitable for the economic demand. However, along with the development of various sensors and automation technologies, this technique would have increasing wider development space.

6 The Arrangement and Operation Process of the System

There is a must of arranging the snow melting system reasonably according to the urban spatial character. The arrangement of this system should follow the principle that separating snow collection and deal with them according to their characteristics, in order to decrease the input of techniques and enhance the efficiency.

This kind of snow melting system could be located along with the both sides of the urban pedestrian green belts or the landscape yards and green space of the architecture or resident areas. Combining with dispose and storage system of the living areas, they can not only be used as the independent rainwater recycling facility and urban prevent waterlogged system but also as a part of the urban drainage system. Consequently, the infrastructure planning should take the nearby civic drainage layout into account as well as refer to the locations and distance of the block and yard to arrange the snow melting wells. For the small capacity of the snow melting wells and their dispersive arrangement, there is a need of choosing optimal transforming routines by considering the realistic conditions.

7 The Automation Equipment

Simply, the melted snow in the snow melting well would turn into snow water after heated, and would go through the syphon equipment or lifting pump into the sub-layer undercurrent tanks. After a while of stay in the tanks, the pollution in the snow water would be digested. A part of the disposed well water would be stored in the tanks and

the rest would be discharged into the water storage structures of the residential communities. Taking the huge snow capacity into consideration, the instantaneous discharge into the tanks would increase dramatically. Thus, the capacity of the undercurrent tanks would not satisfy the demand of adjustment. So there is a need of installing a overflow equipment to guarantee the safety of this technique. Hence, in the running process, there is a must of reasonable control from various aspects, which we hope to achieve by the automation equipment. (Figure 2)

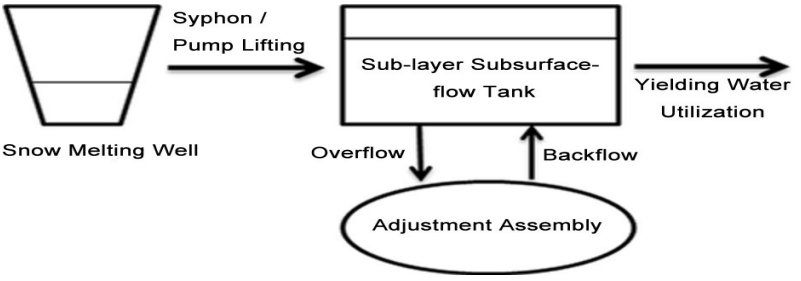

Fig. 2. Technological Process of the Snow Melting System

For the snow melting wells, owing to the different rate of snow melting, it is difficult to estimate their working schedule after close the heat preservation cover, which is not adverse for the reasonable arranging the snow disposal. As a result, we hope to know the working schedule of the snow melting wells by the sensor equipment. In the industrial practice, the pressure sensor is the most common sensor utilizing in different industries widely, such as industrial self-control environment, hydropower engineering, railway transportation, smart architecture, production auto control, shipping and pipes. The piezoelectric effect is the main working principle of the pressure sensor. It shows up the changes of pressure decline of the snow through the change of electrostatic capacity that installing the pressure sensor at the boundary between the water and ice, which would be transferred into electric signal. These electric signals would be connected with the indicator light and dealt by the relay, and finally, they would be shown up in the form of photoelectric signal. The electronic signal is connected with the indicator and ultimately, after the process of relay, is manifested in the form of optical signals, which is able to outs put the voltage information completely due to its wide transmission and high reliability, avoiding the loss of data signals. The collected information is changed into optical information by the typical photoelectric information system. The optical information, as the carrier of the tested information, reaches the photoelectric converter through the optical transmission, turning the optical signals into electrical signals. The conventional electronic device conducts operation processing on the signals to realize the detection and control, following by the computing to compose the automated photoelectric system. Meanwhile, through the indication of the indicator light, the urban managers and sanitation personnel would know the working schedule of the snow melting wells to arranging the snow removal reasonably. Beyond that, those electric signals could be coupled with the remote sensing to be managed by the computer platform center.

Thus, we can supervisor the working schedule of the system to control and adjust the networked system from a macro perspective.

For the sub-layer undercurrent tanks, as their limited capacity, if the amount of the melting snow increases, the instantaneous discharge would also grow. In order to resist this impact, there is a need of overflow equipment to make it guided into other adjustment structures. At the same time, for the purpose of maintain the regular life actions of the microorganisms in the tanks, there is a need keeping the height of the snow water in the tanks, not only for making enough space for the microorganism to provide necessary Dissolved Oxygen (DO), but also providing a water environment for the microorganism. For the purpose of steady operation, the system needs multiple strobes cooperating with each other to realize the connection among various structures of the system. As such system with multiple strobes needs to be controlled and managed flexibly and restructured immediately, so it could utilize the quick response water level monitor. The water level monitor is operated through the engineering or electric method to monitor and control the water level, which equipment could control the magnetic valve and water pump, developing into the water level auto-controller or water level alerter. Thus, there would be achievement of semi-automation or automation in this snow melting system. Furthermore, the electric water level button could monitor the water level through the electric probe, and then water level text chip disposes the acquired signals. When the tested liquid reaches the safe water level or the lowest level, the test chip would export high and low level signals and cooperate with the relay to control the strobe's switch. Thus, the auto-equipment would realize the control to the water level. This controller could immerse in the water for a long time and has been utilized widely and identified as high safety. Through this water level controller, the sub-layer undercurrent tanks would run under the most optimal working conditions.

To sum up, by applying these modern automation controllers, the management of the operating process of the double-layer subsurface-flow snow melting system would be simplified dramatically, reduce the labor input and realize the auto management of the system operation.

8 Conclusion

As a particular fresh water resource, the ice and snow resources would change and improve the situation of lacking fresh water in urban area, if only we make good use of them. Nevertheless, the double-layer subsurface-flow snow melting system would solve the road snow problems in an ecology friendly means. By reasonable operation and adjustment with the help of the modern automation controlling techniques, this snow melting system would be made to meet the functional and economic demand with a widespread development prospect.

Acknowledgment. This work belongs to Ministry of Housing and Urban-rural Development of the People's Republic of China (2011-K7-15) under grant of Ministry of Architecture Energy-saving and Scientific Research of the People's Republic of China.

References

1. Zhang, Y., Hou, J.: Study on the Development of Ice and Snow and Its Culture in Harbin. Harbin School Journal (4), 1–3 (1994) (in Chinese)
2. Yu, W., Li, S., Feng, W., Yi, X.: The Analysis on the Status Quo and Development Tendency of the Technique of Road Melting Snow Removal. Journal of Glaciology and Geocryology 33(4), 933–940 (2011) (in Chinese)

A Cooperative Design Approach of Fault-Tolerant Controller and Observer for Networked Control Systems with Long Time-Delays

Xuan Li, Hai-bing Pan*, and Yun Gao

College of Engineering, Huazhong Agricultural University, Wuhan 430070, China
Lx334@hotmail.com,
{phb,dongshan}@mail.hzau.edu.cn

Abstract. Focusing on networked control systems with long time-delays, a control method based on observer for integrity against sensor failures is proposed. The state observer of the system is designed according to the time-delay compensation strategy and an augmented mathematic model for the networked control systems based on the state observer is developed, then the cooperative design approach of the controller and the observer is given and the existence conditions of guaranteed cost fault-tolerant control law are testified in terms of the Lyapunov stability theory combined with bilinear matrix inequalities. Furthermore, the designs for fault-tolerant control law and the state observer are presented.

Keywords: networked control systems, fault-tolerant control, state observer, long time-delays.

1 Introduction

Networked Control Systems are feedback control system wherein the control loops are closed through a real-time network(NCS)[1-3]. Compared with traditional point-to-point control, networked control systems have more advantages such as shared resources, long range manipulation, low cost and easy of system maintenance. Hence, it has good application prospect. However, because of insertion of the communication network in the feedback control loop, problems of time-delay, data packet dropout and disordered time sequence arise, which can degrade performance of the systems and even breakdown the systems. So it is significant to do research on the fault-tolerant control for the networked Control Systems.

When time-delay is longer than one sampling period, it is called long time-delay. At present, more and more attentions have been to the study on fault-tolerant control. A kind of networked control systems with random time-delays are modeled as a discrete-time jump linear system with Markov delay characteristics and the actuator failures of networked control systems are analyzed based on jump linear system theory and fault-tolerant control theory in [4]. For a class of networked control

* Corresponding author.

D. Jin and S. Lin (Eds.): Advances in Mechanical and Electronic Engineering, LNEE 177, pp. 197–202.
springerlink.com

systems with time-varying delays, based on the integrity fault-tolerant control theory and the time-delay-dependent stability criteria, the sufficient conditions for systems with integrity against actuator failures are given, and the robust fault-tolerant cont roller is designed in [5]. A procedure is proposed for controlling a system over a network using the concept of an NCS-Information-Packet which is an augmented vector comprising control moves and fault flags, then the problem of fault-tolerant control for networked control systems is studied in [6]. The conclusions of these references are based on state feedback. However, in actual systems, as the complexity of network, the all states of the system are not convenience enough to be obtained. Then the state observer is prone to be used. Therefore it is essential to do research on networked control systems with state observer.

In this paper, we aim at solving the problem of integrity against sensor failures for networked control systems with long time-delays. According to the time-delay compensation strategy, the state observer of the system is designed and an augmented mathematic model based on state observer is developed. Then the cooperative design approach of the controller and the observer is given and the existence conditions of fault-tolerant control law are testified in terms of the Lyapunov stability theory combined with bilinear matrix inequalities. Furthermore, the designs for fault-tolerant control law and the state observer are presented.

2 Problem Formulation

Networked control systems studied in this paper is shown in Fig.1. Network exists between sensor and controller and as well as controller and actuator, so the system have output time-delay τ_k^{sc} and control time-delay τ_k^{ca}.

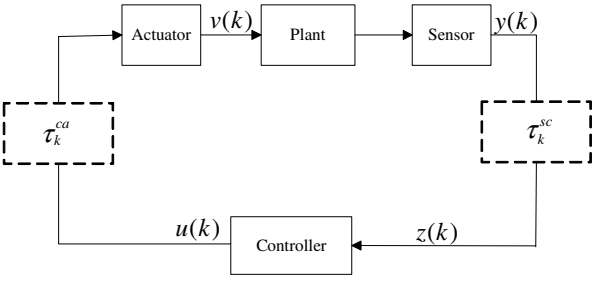

Fig. 1. Structure diagram of the networked control systems

We assume:

(1) The sensor is driven by time, which is sampled with known fixed T. The controller and the actuator are also time-driven;

(2) $\tau_k^{sc} \in (0, \bar{d}_{sc}T]$, $\tau_k^{ca} \in (0, \bar{d}_{ca}T]$, where $\bar{d}_{sc} \in Z^+$ and $\bar{d}_{ca} \in Z^+$;

Assume that the process to be monitored is an LTI (Linear Time Invariant) system described by:

$$\begin{cases} x(k+1)=Ax(k)+Bv(k) \\ y(k)=Cx(k) \\ v(k)=u(k-\tau_k^{ca}) \\ z(k)=y(k-\tau_k^{sc}) \end{cases} \tag{1}$$

Where $x(k)\in R^n$, $v(k)\in R^r$, $u(k)\in R^r$, $z(k)\in R^l$ and $y(k)\in R^l$ are state vector, input vector ,control output vector , control input vector , measure output vector respectively. A, B and C are known matrices of compatible dimensions.

The buffer is added into the acceptance port of the actuator so that the control time delay is changed into constant delay, which means that $\tau_k^{ca}=\bar{d}_{ca}T$. For the output time-delay, the state observer with the time-delay compensation can be designed. So according to the time-delay compensation strategy[7], the observer is designed:

$$\hat{x}(k+1)=A\hat{x}(k)+Bu(k-\bar{d}_{ca})+L_{d_{sc}}(z(k)-CA^{-d_{sc}}(\hat{x}(k)-\sum_{i=1}^{d_{sc}}A^{i-1}Bu(k-\bar{d}_{ca}-i))) \tag{2}$$

Where $L_{d_{sc}}\in R^{n\times l}$ and $\hat{x}(k)\in R^n$ denote the state observer gain matrix and the state estimate respectively, $d_{sc}=\tau_k^{sc}/T$ and $d_{sc}\in\{1,2,...,\bar{d}_{sc}\}$.

According to (1), we can obtain:

$$z(k)=Cx(k-d_{sc})=CA^{-d_{sc}}(x(k)-\sum_{i=1}^{d_{sc}}A^{i-1}Bu(k-\bar{d}_{ca}-i)) \tag{3}$$

In order to formulate the possible sensor failure faults, the fault model must be established first. Considering possible sensor failure faults, we can introduce a switched matrix H to the system (2), and lay the matrix H before the control input vector $z(k)$, where $H=diag(h_1,h_2,\cdots,h_m)$ and for $i=1,2,\cdots,m$

$$h_i=\begin{cases}1 & \text{the } i\text{th sensor normal} \\ 0 & \text{the } i\text{th sensor failure}\end{cases}$$

Let

$$e_k=x_k-\hat{x}_k \tag{4}$$

Aiming at system (1), using state feedback control law based on observer

$$u(k)=K\hat{x}(k) \tag{5}$$

where $K\in R^{r\times n}$.

Let an augmented vector

$$\theta(k)=\left[e^T(k)\quad x^T(k)\quad u^T(k-\bar{d}_{ca}-\bar{d}_{sc})\quad\cdots\quad u^T(k-1)\right]^T$$

From (1), (3), (4) and (5), the augmented system r can be represented by:

$$\theta(k+1)=\sum_{d_{sc}=1}^{\bar{d}_{sc}}\xi(d_{sc})(\bar{A}+\bar{L}_{d_{sc}}F\tilde{A}_{d_{sc}})\theta(k) \tag{6}$$

Where , $\xi(d_{sc}):R\to\{0,1\}$, $\sum_{i=1}^{\bar{d}_{sc}+1}\xi(d_{sc})=1, \hat{d}=\bar{d}_{ca}+\bar{d}_{sc}+2$

$$\tilde{A}_{d_{sc}}=diag(CA^{-d_{sc}},CA^{-d_{sc}},\overbrace{0\ \cdots\ 0}^{(\bar{d}_{sc}-d_{sc})},\overbrace{CA^{-1}B\ \cdots\ CA^{-d_{sc}}B}^{d_{sc}},\overbrace{0\ \cdots\ 0}^{\bar{d}_{ca}})$$

$$\bar{A}=\begin{bmatrix}\overbrace{\begin{matrix}A&0&0&0&\cdots&0\\0&A&0&0&\cdots&0\\0&0&0&I&\ddots&0\\\vdots&\vdots&\vdots&\ddots&\ddots&0\\0&0&0&0&0&I\\0&0&0&0&0&0\\0&0&0&0&0&0\\\vdots&\vdots&\vdots&\vdots&\vdots&\vdots\\0&0&0&0&0&0\\-K&K&0&0&0&0\end{matrix}}^{(\bar{d}_{sc}+2)} & \overbrace{\begin{matrix}0&0&0&0\\B&0&0&0\\0&0&0&0\\0&0&0&0\\0&0&0&0\\I&0&0&0\\0&I&\ddots&0\\\ddots&\ddots&\ddots&0\\0&0&0&I\\0&0&0&0\end{matrix}}^{\bar{d}_{ca}}\end{bmatrix}_{\hat{d}\times\hat{d}},$$

$$\bar{L}_{d_{sc}}=\begin{bmatrix}-L_{d_{sc}}&L_{d_{sc}}&-L_{d_{sc}}&\cdots&-L_{d_{sc}}\\0&0&0&\cdots&0\\0&0&0&\cdots&0\\\vdots&\vdots&\vdots&\ddots&\vdots\\0&0&0&\cdots&0\end{bmatrix}_{\hat{d}\times\hat{d}},\ F=diag(\overbrace{I,I-H,\cdots,I-H}^{(\bar{d}_{ca}+\bar{d}_{sc}+2)})$$

Obviously, the system described by (6) is equivalent to an automatically switched discrete linear system with $(\bar{d}_{sc}+1)$ subsystems.

3 Main Results

Lemma 1[8]**.** Given matrices W,M,N of appropriate dimensions and with W symmetric, $W+N^TF^T(k)M^T+MF(k)N<0$, then for all $F(k)$ satisfying $F^T(k)F(k)\le I$, if and only if there exists a scalar $\varepsilon>0$ such that

$$W+\varepsilon MM^T+\varepsilon^{-1}N^TN<0$$

Lemma 2 [9]. Given a linear discrete switched system as follows

$$x(k+1)=\sum_{i=1}^{l}\mu_i A_i x(k)$$

Here $i=1,2,\cdots,r$, $r<\infty$ denotes the number of subsystems, $\mu_i \to \{0,1\}$, $\sum_{i=1}^{r}\mu_i=1$, if there exits a symmetry positive-definite matrix P and a constant scalar, such that $A_i^T PA_i - P<0$ （$i=1,\cdots,r$）, then the switched system is asymptotically stable.

***Theorem 1*:** Consider the system (6), if there exist symmetry positive-definite matrices $P>0$, matrices K , $L_{d_{sc}}$, and scalars $\delta_{d_{sc}}>0$, such that

$$\begin{bmatrix} -P & \bar{A}^T & 0 & \delta_{d_{sc}}\tilde{A}_{d_{sc}}^T \\ * & -P^{-1} & \bar{L}_{d_{sc}} & 0 \\ * & * & -\delta_{d_{sc}} I & 0 \\ * & * & * & -\delta_{d_{sc}} I \end{bmatrix}<0 \tag{7}$$

then the system (6) is asymptotically stable, where $d_{sc}\in\left\{1,2,\ldots,\bar{d}_{s_{sc}}\right\}$, $\bar{A}$, F and $\tilde{A}_{d_{sc}}$ have been defined above, (*) is denoted as an ellipsis for terms that are induced by symmetry.

Proof: Defining the Lyapunov function

$$V(k)=V(\theta(k))=\theta^T(k+1)P\theta(k)$$

$\Delta V(k)<0$ means $(\bar{A}+\bar{L}_{d_{sc}}F\tilde{A}_{d_{sc}})^T P(\bar{A}+\bar{L}_{d_{sc}}F\tilde{A}_{d_{sc}})-P<0$

Based on *Schur mend theorem*, the above inequality can be rewritten as

$$\begin{bmatrix} -P & \bar{A}^T \\ * & -P^{-1} \end{bmatrix}+\bar{\delta}_{d_{sc}}\begin{bmatrix} 0 \\ \bar{L}_{d_{sc}} \end{bmatrix}\begin{bmatrix} 0 \\ \bar{L}_{d_{sc}} \end{bmatrix}^T+\bar{\delta}_{d_{sc}}^{-1}\begin{bmatrix} \tilde{A}_{d_{sc}}^T \\ 0 \end{bmatrix}\begin{bmatrix} \tilde{A}_{d_{sc}}^T \\ 0 \end{bmatrix}^T<0 \tag{8}$$

In light of *Schur mend theorem* and using the *Lemma* 1, the inequality (8) can be equivalently obtained from (13). So based on *Lemma 3*, when inequality (7) is satisfied, the observers system (6) remains asymptotically stable.

For the inequalities of theorem 1 contain P^{-1} and P , which again yield linear matrix inequality, Pre-and post-multiplying both sides of (7) with $diag\left\{I,P,I,I,I\right\}$ and inequality (7) can be transformed to bilinear matrix inequality, which can be solved with MATLAB and PENBMI[10].

4 Conclusion

The problem of fault-tolerant control for the networked control systems with long time-delays based on state observer against sensor failures is investigated in this paper. The state observer of the system is designed and an augmented mathematic model based on state observer is developed. Based on Lyapunove stability theory and bilinear matrix inequality, fault-tolerant controller and observer are designed. The advantage of the presented fault-tolerant control method is considering the case that all states of the system are not convenience enough to be obtained, so it has practical significance to the application of the networked control systems.

Acknowledgments. This work was supported by the "Fundamental Research Funds for the Central Universities" (52902-0900201080 and 52902-0900201159). Authors are thankful to the anonymous referees for the constructive comments in enhancing the content and structure of the manuscript.

References

1. Zhang, W., Branicky, M.S., Phillips, S.M.: Stability of networked control systems. IEEE Control Systems Magazine 21(1), 85–99 (2001)
2. Hespanha, J.P., Naghshtabrizi, P., Xu, Y.G.: A Survey of Recent Results in Networked Control Systems. Proceedings of the IEEE 95(1), 138–162 (2007)
3. Antsaklis, P., Baillieul, J.: Special Issue on Technology of Networked Control Systems. Proceedings of the IEEE 95(1), 5–8 (2007)
4. Huo, Z.H., Fang, H.J.: Fault-tolerant Control of Networked Control System s with Random Time-delays. Information and Control 35(5), 584–588 (2006)
5. Guo, Y.N., Zhang, Q.Y., Gong, D.W., et al.: Robust fault-tolerant control of networked control systems with Time-varying delays. Control and Decision 23(6), 689–692 (2008)
6. Klinkhieo, S., Kambhampati, C., Patton, R.J.: Information Packets and MPC Enable Fault-tolerance in Network Control. In: IEEE Conference on Emerging Technologies and Factory Automation, ETFA 2006, September 20-22, pp. 689–694 (2006)
7. Yu, Z.X., Jing, P., Chen, H.T., et al.: Design of Statusobserver for Networked Control Systems with Transfer Delay. Information and Control 29(2), 125–130 (2000)
8. Yu, L.: Robust control-dealing with Linear Matrix Inequalities. Tsinghua University Press, Beijing (2002)
9. Zhang, M.J., Tarn, T.J.: A switching control strategy for nonlinear dynamic systems. In: Proceeding of the 2003 IEEE International Conference on Robotics & Automation, Taipei, Taiwan, pp. 1476–1481 (2003)
10. Kočvara, M., Stingl, M.: PENBMI, Version 2.0 (2004), free developer version, `http://www.penopt.com`

Research on the System of Three-Phase VSR PWM Rectifier Based on SVPWM Control

YingZhan Hu

Department of Electrical Engineering,
Henan Polytechnic Institute, Nanyang, 473009, China
huyz168@163.com

Abstract. The pulse-width modulated (PWM) is the key technology to acquire the high power factor. In 1980s, the PWM control technology was presented on the basis of voltage space-vector, which had the higher efficiency than the SPWM. This paper firstly introduces the fundamental principle of Space-Vector Pulse Width Modulation(SVPWM). Then, the system structure of three-phase VSR PWM rectifier was designed based on SVPWM control,and also set up the parameters of the voltage-current double-loop control, and implemented the SVPWM control algorithm. Finally, the system simulation results were given by MATLAB simulation software, and the circuit was constructed by designating DSP TMS320LF2407A as the control core. The results proves that the control system is correct and feasible, and the performance is acceptable.

Keywords: SVPWM, rectifier, three-phase VSR, DSP.

1 Introduction

The conventional rectifier unit widely consists of diode-rectifier circuit and phase-control thyristor rectifier, which injects large amounts of harmonics into the power networks and produces much contamination. With the fast developing technology of green energy, an ever-enhanced attention has been focused to the PWM rectifier in the field of power electronics. PWM rectifier technology owns such features as constant output voltage, running under unit power factor. Space vector pulse-with modulation (SVPWM) also is known as the method of the sine PWM of magnetic flux, The main idea is to generate the effect of the whole three-phase waveform as a precondition, approximating the idea circular track of the magnetic flux of the electric motor air-gap for the purpose, using the actual magnetic flux generated from the different switch modes of the inverter to approximate circular flux, the rectifier switches based on the results of their comparison, form a PWM waveform. The control idea to be used in three-phase rectifier can also obtain the satisfied rectification effect.

2 The Topology of Three-Phase Voltage PWM Rectifier

The topology diagram of three-phase voltage PWM rectifier is shown in Figure.1.

D. Jin and S. Lin (Eds.): Advances in Mechanical and Electronic Engineering, LNEE 177, pp. 203–208.
springerlink.com

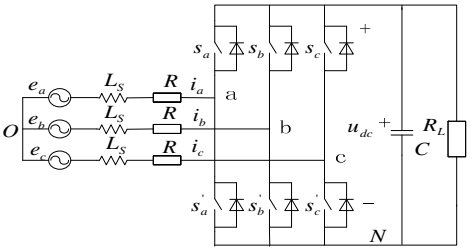

Fig. 1. The topology diagram of three-phase voltage PWM rectifier

The three-phase bridge is composed of six switching devices with an anti-parallel diode, and it constitutes a symmetrical two-way switch. e_a、e_b、e_c are the three phase voltages of AC power source.L_s is the equivalent inductance of AC side. u_{dc} is the voltage of DC side. R_L is the load of the DC side. Because of the using of DC energy storage capacitor C in the side of DC, the most notable feature of three-phase voltage PWM rectifier is to have a low impedance voltage source.

3 The Principle of SVPWM

SVPWM control obtains the voltage vector instructions U* mainly by the calculation of current loop regulation, and it realizes the vector U*of the tracking control by vector U_x (x=1, 2, 3, 4, 5, 6) composition, as a result, the current control of VSR is achieved. Eight space vectors,which are formed by the different rectifier switch states, form SVPWM trigger waves.The location and size of the eight basic voltage space vectors are shown in Figure 2, and it includes six nonzero voltage vectors U_x (x=1,2,3,4,5,6) and two zero voltage vectors (U_0、U_7). Each of the six nonzero voltage vectors magnitude is $2U_d/3$, and their phase angle difference is π/3.The complex plane is divided into six fan-shaped regions. In any fan-shaped region, the voltage vector U*can be made up of the adjacent space voltage vectors(U_x、$U_{x\pm60}$). The corresponding basic space vector constituting instantaneous command is the purpose of voltage space vector technology. The average input voltage is made equal to the command voltage during the pulse period T that the space voltage vector trajectory approaches a round.

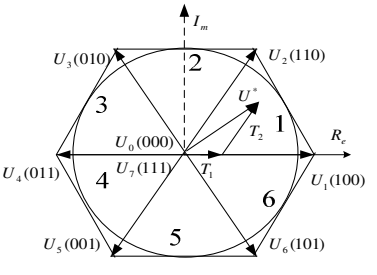

Fig. 2. The space vector and switch state

In other words, considering any small cycle time T, during which the output of the rectifier is the same as the average command voltage, such as the equation (1):

$$\frac{1}{T}\int_{nT}^{(n+1)T} U^{*}(t)dt = \frac{1}{T}(T_1 U_x + T_2 U_{X\pm 60}) \tag{1}$$

T_1、T_2 respectively are the action time of U_x、$U_{x\pm 60}$.

If the sum of T1 and T2 is less than the pulse period T, then it use the zero vector (U_0、U_7) fills up the remaining time of period T.

4 The System Architecture of Three-Phase Voltage PWM Rectifier Based on SVPWM Control

The paper designs a system of three-phase voltages PWM rectifier for capacity of 8KW and it's based on space voltage vector control. System block diagram is shown in Figure 3.

The main circuit used the intelligent power modules PM20CSJ060 of Mitsubishi Corporation IPM products. The whole system adopts two-closed-loop control that is composed by the inner current loop and the outer voltage loop. The role of the outer voltage loop is to control the DC voltage u_{dc} of three-phase PWM rectifier, the size and the direction of the rectifier output power with a given signal of the three-phase current can be determined according to the size of u_{dc}. The role of the inner current loop is to control the current based on the command current of outer output voltage, the actual input current of rectifier can follow the given current, and realize current control of sinusoidal of unity power actor.

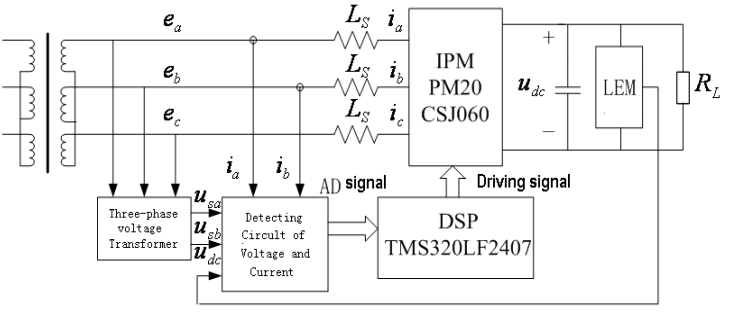

Fig. 3. System block diagram of three-phase voltages PWM rectifier based on SVPWM control

4.1 Design of the Inner Current Loop

The importance of current loop is to obtain faster following performance and restrain the overshoot. Following the second order optimal designed system, it is ξ=0.707, overshoot $\sigma\% \leq 5\%$. It is assumed that a given voltage in the linear modulation region of the PWM is not saturated and completely decoupled. According to the approach of small-inertia element, the simplified current inner structure is shown in Figure 4.

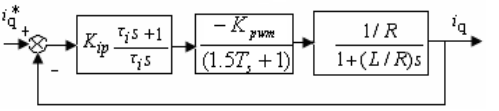

Fig. 4. A simplified block diagram of the inner current loop

In the figure 4,T_s is the sampling period of current of the inner current loop (PWM switching period), K_{pwm} is the equivalent gain of the PWM bridges, in this paper, K_{pwm}=20. R=0.5Ω, L=3mH,f=10KHz.By using the second-order optimal design, the current loop PI regulator parameters by calculation is Equation (2) :

$$\begin{cases} K_{ip} = 0.5 \\ \tau_i = \dfrac{L}{R} = 6ms \end{cases} . \tag{2}$$

4.2 Design of the Outer Voltage Loop

When the switching frequency is far higher than fundamental frequency of grid voltage, PWM harmonics components can be ignored to simplify the design of control system. Considering the anti-jamming performance of the voltage loop, the simplified voltage loop structure is designed according to the typical II system as shown in Figure 5.

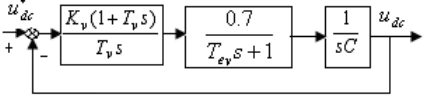

Fig. 5. The simplified control structure diagram of outer voltage loop

In the figure 5, τ_v is time constant of small-inertia element of voltage sampling. $T_{ev}=\tau_v+3T_s$. According to the optimum design principle of third order and considering the system requirements for the immunity and following performance in engineering, IF is selected, $\tau_v=T_s$, and the value of capacitor C is 1.1mF, so that the voltage loop PI regulator parameters is equation (3):

$$\begin{cases} T_v = 5T_{ev} = 20T_s = 2ms \\ K_v = \dfrac{4C}{(\tau_v + 3T_s)} = 11 \end{cases} \tag{3}$$

5 The Simulation of the System Based on Matlab/Simulink

According to the design of the system mentioned above, the simulation model of the system is built based on Matlab/Simulink as shown in Figure 6. Three-phase input voltage is set to 311V/50Hz, the given DC voltage is 620V, the given reactive current is

set to 0A, the switching frequency is 10KHz, the AC side filter reactor is 3mH, the input side equivalent resistance is 0.5Ω, the DC side capacitor is 1100μF, and the DC side resistance is 50Ω.

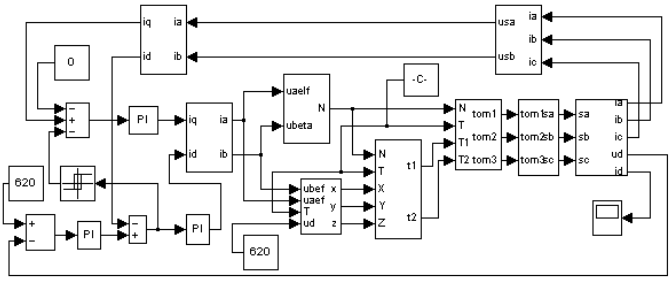

Fig. 6. Simulation model of the system

The simulation results show the waveforms of A phase input voltage and current are shown in Figure 7, and the waveforms of DC voltage and current are shown in Figure 8.

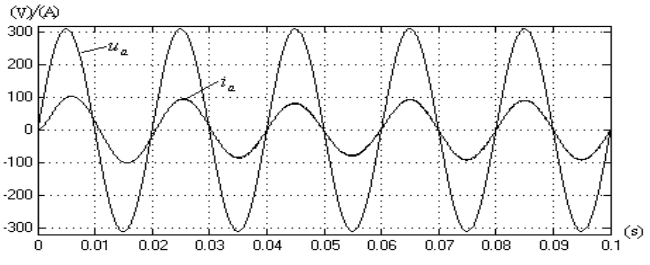

Fig. 7. The waveforms of A phase input voltage and current

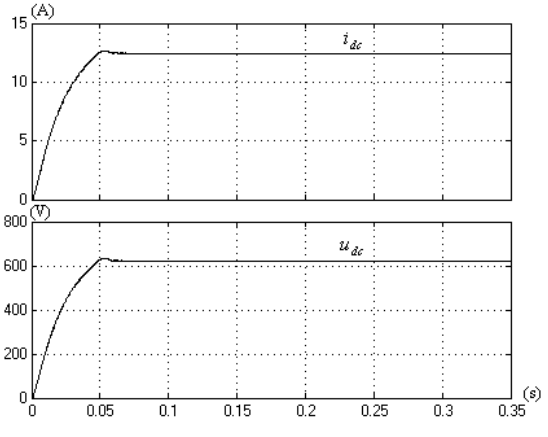

Fig. 8. The waveforms of DC voltage and current

6 Conclusion

From the above, we know AC side current lags behind the voltage slightly when it just starting, but voltage and current will satisfy in-phase and in the same direction after a cycle. This shows that the designed system owns the characteristics of high starting speed, high current tracing speed, and running in the rectification mode with the power factor near to 1. As Figure 8 shows, control system only needs 0.05s to reach steady state, DC voltage and current rise faster, and the system has a better starting performance. It also shows that the voltage and current wave little after reaching steady state, which confirms its excellence of the steady state performance of the system.

Experiments are carried out by using evaluation board TCETEK-LF-2407-A, hall current sensor TBC10LX and hall voltage sensor TBC10/25A to collect three-phase voltage and using TBC5/25A DC to collect output voltage, the synchronous trigger module and some other circuit-formed. The results show the control algorithm proposed by author is correct and available.

References

1. Liu, F.J.: Modern inversion technology and application. Electronic Industry Press, Beijing (2006)
2. Zhang, C.W., Zhang, X.: PWM rectifier and control. Beijing Mechanical Industry Press, Beijing (2003)
3. Zheng, Z., Tian, J.X.: The direct current control for PWM converters. Techniques of Automation and Application 26, 76–78 (2007)
4. Zheng, Z., Tao, H.J.: Studying of Control Algorithm for Fast Space Vector PWM. Electrical Applications 25, 38–40 (2006)
5. Zhang, Y.G., Zhang, G.Q., Sun, N.: Development and application of TMS320LF240x DSP. Harbin Institute of Technology Press, Harbin (2006)
6. Liu, H.P., Wang, W.J.: TMS320LF240x DSP C language development and application. Beijing Aerospace University Press, Beijing (2003)
7. Wang, C.W., Li, H.: Simulation on Three Phase PWM Rectifier Using Space Vector Pulse Width Modulation (SVPWM). Torpedo Technology 18, 146–151 (2010)

The Chromatic Aberration Estimation of TP Film with Two Layers Coating for Electronic Appliance

Huang-Chi Chen[1,4], Yu-Ju Chen[2], Chuo-Yean Chang[3], Yu-An Lin[1], Jui-Chen Chien[1], and Rey-Chue Hwang[1,*]

[1] Electrical Engineering Department, I-Shou University, Kaohsiung, Taiwan
rchwang@isu.edu.tw
[2] Information Management Department, Cheng Shiu University, Kaohsiung, Taiwan
[3] Electrical Engineering Department, Cheng Shiu University, Kaohsiung, Taiwan
[4] Management Information System Department, Far East University, Kaohsiung, Taiwan

Abstract. This paper presents the chromatic aberration estimations of touch panel (TP) film with two layers coating for electronic appliance in human's daily life. The data of TP film with Cr and Cr2O3 coats were studied and simulated. The complex relationship between the chromatic aberration, i.e. L, a, b values, and the relevant evaporation parameters of TP film could be developed through the neural network's (NN) training. The well-trained NN model then can be used to estimate the chromatic aberration. In other words, an artificial intelligent (AI) mechanism for the estimation of the optical properties of TP film is possibly to be created. Thus, the technician is able to set the control parameters of evaporation process in advance to make the quality of TP film meet the customer's request.

Keywords: chromatic, aberration, estimation, touch, panel.

1 Introduction

Recently, TP has become an important part of the electronic appliance in human's daily life. It has been widely used in many products such as the mobile phone, electronic dictionary, GPS navigation system, MP3 and TV screen etc. In the manufacturing process of TP, a thin plate with coating film will be stuck on TP for the specific function. The coating process is to deposit one or more layers of material onto the substrate and it is usually done by evaporator [1-4]. The evaporation is generally processed in the vacuum condition. Fig. 1 shows the principle of coating process. The number of layers of coating will depend on the special function of TP needed.

Basically, the chromatic aberration is one of measurements used to judge the optical quality of TP film. It includes the values of *L*, *a*, *b*. The *Lab* is a color space with lightness *L* and the colors *a* and *b*. Undoubtedly, in the coating process, these values are highly correlated with all possible influencing factors such as the target composition, the layers of coating, the thickness of film and the speed of evaporation

* Corresponding author.

D. Jin and S. Lin (Eds.): Advances in Mechanical and Electronic Engineering, LNEE 177, pp. 209–214.
springerlink.com

etc. These possible factors play an important role in determining the optical properties of TP film. However, due to the relationship between chromatic aberration and its possible influencing factors are very complex, nonlinear and ill defined, the trial-and-error method for setting the control parameters of evaporation process is usually taken by the technician. Definitely, many trials not only affect the work efficiency, but also increase the cost of company. Thus, how to find a sufficient way to accomplish the evaporation work precisely is the aim of this research.

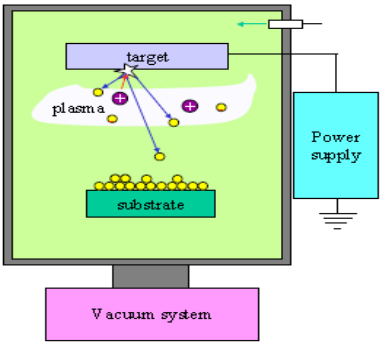

Fig. 1. The evaporation principle (provided by Mildex Optical Inc.)

It is well known that NN technique has been widely employed into many applications due to its powerful nonlinear learning ability [5-7]. Through the simple training process of NN, the mathematic mapping model between input and output signals could be developed automatically. Such a well-trained NN then can be used to execute the specific work designed by the user. In our previous studies, the chromatic aberration estimation for TP film with one layer coating has been studied and proposed [8-9]. The research results show that the estimation of chromatic aberration by using NN model is quite promising. In this research, the chromatic aberration estimation of TP with two layers coating were studied. The NN model was used to find the mapping relationship between TP's chromatic aberration and its all possible influencing factors.

2 Neural Network

In our study, the multi-layer feed-forward NN was used to be the learning model. The size of NN model is m-h_1-h_2-1. The network consists of one input layer with m nodes, two hidden layers with h_1 and h_2 nodes respectively, and one output layer with one node. A reliable and superior intelligent chromatic aberration estimator of TP decoration film is expected to be obtained. Newton's method is a learning algorithm for solving the optimization problem. In order to produce a significant improvement in the convergence performance of NN's training, the higher-order information is used in NN's training process. The quadratic approximation of the error surface

versus the synaptic weight vector is involved in the weight adjustment. Generally, the weight's adjustment $\Delta\omega_k$ applied to the synaptic weight vector ω_k is given by

$$\Delta\omega_k \propto A_k^{-1} g_k, \ \omega_{k+1} = \omega_k - A_k^{-1} g_k \tag{1}$$

where A_k is Hessian matrix. It is the second-order differential term of the cost function with respect to the weight ω_k. g_k is the local gradient vector. Both terms can be expressed by the following equations.

$$A_k \equiv \partial^2 E(\omega)/\partial\omega^2, \omega = \omega_k; \ g_k \equiv \partial E(\omega)/\partial\omega, \omega = \omega_k \tag{2}$$

However, if A_k^{-1} is computable, A_k must be nonsingular. Unfortunately, there is no guarantee that the Hessian matrix of the error surface will always meet this condition. Thus, the modified Newton's method, named quasi-Newton method, is used for NN's training. The learning steps of quasi-Newton method can be summarized as follows [10].

Step 1: For *k*=0, initialize all weights, $\omega_k = 0$, *k*=0 and $A_k = I$, *I* is the unit matrix.

Step 2: If $g_k = 0$, then stop the calculation. Otherwise, $d_k = -A_k g_k$.

Step 3: Compute

$$\alpha_k = \arg\min f(\omega_k + \alpha d_k), \alpha \geq 0; \ \omega_{k+1} = \omega_k + \alpha_k d_k \tag{3}$$

Step 4: Compute

$$\Delta\omega_k = \alpha_k d_k; \ \Delta g_k = g_{k+1} - g_k \tag{4}$$

$$\begin{aligned} A_{k+1} = A_k &+ [(\Delta\omega_k \Delta\omega_k^T)/(\Delta\omega_k^T \Delta g_k)] - [(([A_k \Delta g_k][A_k \Delta g_k]^T)/(\Delta g_k^T A_k \Delta g_k)] \\ &+ \Delta g_k{}^T [A_k \Delta g_k]^T \left[(\Delta\omega_k /(\Delta\omega_k^T \Delta g_k)) - (A_k \Delta g_k /(\Delta g_k^T A_k \Delta g_k))\right] \end{aligned} \tag{5}$$

Step 5: Let *k*=*k*+*1* and go back to Step 2.

3 Simulations

In this study, the data provided by Mildex Optical Inc. were analyzed and simulated. Table 1 lists the example of data collected. The information includes the value of quartz crystal deposition monitor, the rotation speed of holder, the position number of substrate placed, Cr thickness, Cr_2O_3 thickness and *Lab* values of chromatic aberration. The complex mapping relationship between *Lab* values and the possible influencing factors is expected to be obtained. In order to demonstrate the feasibility of NN technique and get a fair research result, four different data sets; named Set-1, Set-2, Set-3 and Set-4, were randomly re-organized from the original data. Different

combinations of inputs were simulated for searching the best influencing factors of the chromatic aberration estimation. In each data set, 100 points were used for NN's training and 44 points were used for testing. The mean absolute error (MAE) and mean absolute percentage error (MAPE) are used as the measures of estimation results.

Table 2 shows the error statistics of *L* value's estimation by using different input sets. The best average estimation accuracy can reach to 1.54%. Table 3 lists the error statistics of *a* value's estimation by using different inputs. The best average estimation accuracy can reach to 1.539%. Table 4 is the report of error statistics of *b* value's estimation by using different inputs. The best average estimation accuracy can reach to 5.48%.

Table 1. The example of data collected

Inputs					Outputs		
Quartz crystal	Holder speed	Substrate position	Cr thickness	Cr_2O_3 thickness	Chromatic aberration		
					L	*a*	*b*
621	15	7	50	30	62.23	3.77	4.40
621	20	9	50	30	63.21	3.51	3.91
631	15	7	150	130	33.03	3.46	3.75
631	5	2	150	130	30.58	3.39	3.41

Table 2. The error statistics of L estimation by using different input combinations

Inputs : quartz crystal, the rotation speed of holder, the position of substrate, Cr thickness and Cr_2O_3 thickness										
L value	Set-1		Set-2		Set-3		Set-4		Avg.	
	MAE	MAPE	MAE	MAPE	MAE	MAPE	MAE	MAPE	MAE	MAPE
Training	0.6027	1.5287	0.6007	1.4917	0.5816	1.4976	0.5809	1.4937	0.5915	1.5029
Test	0.6651	1.6922	0.6424	1.7469	0.6588	1.6270	0.7113	1.7805	0.6694	1.7117
Inputs : quartz crystal, the position of substrate, Cr thickness and Cr_2O_3 thickness										
Training	1.2621	3.3849	0.8794	2.3890	1.3411	3.7008	1.8921	5.2018	1.3437	3.6691
Test	1.4809	3.9780	1.0523	3.0194	1.5822	4.0479	1.8231	4.8793	1.4846	3.9812
Inputs : quartz crystal, the rotation speed of holder, Cr thickness and Cr_2O_3 thickness										
Training	0.6206	1.5638	0.7135	1.7079	0.5909	1.5205	0.6077	1.5741	0.6332	1.5916
Test	0.6006	1.5615	0.6388	1.5934	0.6228	1.5330	0.6066	1.4728	0.6172	1.5402
Inputs : the rotation speed of holder, the position of substrate, Cr thickness and Cr_2O_3 thickness										
Training	0.6735	1.7547	0.9067	2.4615	0.6833	1.8182	0.5865	1.5202	0.7125	1.8887
Test	0.7484	1.9791	1.0079	2.8960	0.7004	1.7821	0.6863	1.6873	0.7858	2.0861
Inputs : quartz crystal, Cr thickness and Cr_2O_3 thickness										
Training	0.9172	2.5113	0.9021	2.4545	0.9602	2.7258	0.9025	2.5380	0.9205	2.5574
Test	0.9101	2.5952	0.9022	2.6213	0.8111	2.1118	0.8936	2.408	0.8793	2.4341
Inputs : the rotation speed of holder, Cr thickness and Cr_2O_3 thickness										
Training	0.8434	2.2866	0.6211	1.5554	0.5909	1.5205	0.6869	1.7040	0.6856	1.7666
Test	0.9304	2.6243	0.5351	1.4212	0.6228	1.5330	0.675	1.5852	0.6908	1.7909
Inputs : the position of substrate, Cr thickness and Cr_2O_3 thickness										
Training	1.7699	4.7397	1.8564	4.9552	1.8103	4.9102	2.0235	5.4633	1.8650	5.0171
Test	2.1116	5.8643	1.9214	5.3930	2.1558	5.7007	1.6427	4.4238	1.9579	5.3455

Table 3. The error statistics of *a* estimation by using different input combinations

Inputs : quartz crystal, the rotation speed of holder, the position of substrate, Cr thickness and Cr_2O_3 thickness										
a value	Set-1		Set-2		Set-3		Set-4		Avg.	
	MAE	MAPE	MAE	MAPE	MAE	MAPE	MAE	MAPE	MAE	MAPE
Training	0.0463	1.3892	0.0518	1.5555	0.0484	1.4587	0.0501	1.4857	0.0492	1.4723
Test	0.0606	1.7999	0.0506	1.5145	0.0534	1.5755	0.0552	1.6672	0.0550	1.6393
Inputs : quartz crystal, the position of substrate, Cr thickness and Cr_2O_3 thickness										
Training	0.0488	1.475	0.0527	1.5797	0.0501	1.5232	0.0501	1.4902	0.0504	1.5170
Test	0.0547	1.637	0.0497	1.4837	0.0667	1.9224	0.0527	1.5953	0.0560	1.6596
Inputs : quartz crystal, the rotation speed of holder, Cr thickness and Cr_2O_3 thickness										
Training	0.0487	1.4614	0.0528	1.5890	0.0546	1.6517	0.0513	1.5222	0.0519	1.5561
Test	0.058	1.7185	0.0547	1.6211	0.0516	1.5148	0.0499	1.5085	0.0536	1.5907
Inputs : the rotation speed of holder, the position of substrate, Cr thickness and Cr_2O_3 thickness										
Training	0.0438	1.3187	0.0455	1.3708	0.0466	1.4056	0.0466	1.3890	0.0457	1.3710
Test	0.0511	1.5188	0.0604	1.7861	0.0488	1.4352	0.0463	1.4030	0.0517	1.5358
Inputs : quartz crystal, Cr thickness and Cr_2O_3 thickness										
Training	0.0483	1.4521	0.0509	1.5274	0.0500	1.5071	0.0555	1.6585	0.0512	1.5363
Test	0.0552	1.6348	0.0523	1.5479	0.0542	1.5970	0.0520	1.5761	0.0534	1.5890
Inputs : the rotation speed of holder, Cr thickness and Cr_2O_3 thickness										
Training	0.0522	1.5607	0.0489	1.4749	0.0531	1.5916	0.0474	1.4091	0.0504	1.5091
Test	0.0595	1.7597	0.0541	1.6050	0.056	1.6436	0.0465	1.4099	0.0540	1.6046
Inputs : the position of substrate, Cr thickness and Cr_2O_3 thickness										
Training	0.0643	1.9023	0.0684	2.0186	0.0687	2.0444	0.0638	1.8777	0.0663	1.9608
Test	0.0761	2.2316	0.071	2.089	0.0670	1.9332	0.0793	2.3606	0.0733	2.1536

Table 4. The error statistics of *a* estimation by using different input combinations

Inputs : quartz crystal, the rotation speed of holder, the position of substrate, Cr thickness and Cr_2O_3 thickness										
b value	Set-1		Set-2		Set-3		Set-4		Avg.	
	MAE	MAPE	MAE	MAPE	MAE	MAPE	MAE	MAPE	MAE	MAPE
Training	0.1476	4.3451	0.1622	4.7460	0.1811	5.3248	0.1423	4.0616	0.1583	4.6194
Test	0.2032	6.0336	0.2501	7.4049	0.1894	5.7674	0.1935	6.0963	0.2091	6.3256
Inputs : quartz crystal, the position of substrate, Cr thickness and Cr_2O_3 thickness										
Training	0.1738	4.9052	0.1720	5.0477	0.1793	5.2329	0.1747	4.8868	0.1750	5.0182
Test	0.2022	6.1788	0.2024	5.8248	0.1919	5.6119	0.2899	9.8268	0.2216	6.8606
Inputs : quartz crystal, the rotation speed of holder, Cr thickness and Cr_2O_3 thickness										
Training	0.1494	4.4535	0.1610	4.9039	0.1693	5.0529	0.1585	4.6612	0.15955	4.7679
Test	0.2032	6.0799	0.1616	4.9003	0.1912	5.8127	0.1830	5.6801	0.18475	5.6183
Inputs : the rotation speed of holder, the position of substrate, Cr thickness and Cr_2O_3 thickness										
Training	0.1914	6.1563	0.2098	6.2076	0.1788	5.2598	0.1547	4.5253	0.1837	5.5370
Test	0.2507	8.1053	0.2026	6.0929	0.1678	5.0302	0.1885	5.8669	0.2024	6.2738
Inputs : quartz crystal, Cr thickness and Cr_2O_3 thickness										
Training	0.1977	5.8116	0.1875	5.6568	0.2035	5.9710	0.1925	5.5913	0.1953	5.7577
Test	0.1967	5.8299	0.1790	5.3628	0.1925	5.8771	0.2050	6.2576	0.1933	5.8319
Inputs : the rotation speed of holder, Cr thickness and Cr_2O_3 thickness										
Training	0.1794	5.3141	0.1848	5.5780	0.1802	5.3488	0.2215	6.4538	0.1915	5.6737
Test	0.1845	5.5025	0.1615	4.8937	0.1684	5.2061	0.2028	6.3332	0.1793	5.4839
Inputs : the position of substrate, Cr thickness and Cr_2O_3 thickness										
Training	0.2824	9.0637	0.3165	10.2499	0.2951	9.3115	0.2612	8.3540	0.2888	9.2448
Test	0.3422	11.2826	0.2991	9.2947	0.3487	11.2421	0.3754	13.0608	0.3414	11.2201

4 Conclusion

In this research, the chromatic aberration estimations of TP with two layers coating are presented. The mapping relationship between chromatic aberration and its possible influencing factors can be obtained automatically by NN model. The simulation results show that the NN technique is quite promising to be used as the intelligent estimator for chromatic aberration of TP. The study shows that the estimations of *L* and *a* values are very accurate. Both MAPEs can reach to around

1.5%. But, the estimations of *b* value are not as good as what we expect. The reason is the colors of TP film experimented and collected are all near black or grey. These films lack the characteristics of blue or yellow color. Thus, the measurement error caused by man-made or instrument's inaccuracy might be easily included in the *b* data. Besides, from the simulations shown, we found that the value of quartz crystal deposition monitor, the rotation speed of holder, Cr thickness and Cr_2O_3 thickness are four most important influencing factors for TP film's chromatic aberration. Thus, in our future study, the TP film with large *a* and *b* values will be experimented and collected. The completed chromatic aberration estimation of TP decoration film will be continuously studied.

Acknowledgments. This work was supported by the National Science Council of Republic of China under contract No. NSC-99-2221-E-022-004.

References

1. Dmitruk, N.L., Korovin, A.V.: Generalized analytical model for the calculation of light transmittance through a thin conducting film. Thin Solid Films 484(1-2), 382–388 (2005)
2. Wu, Y.T., Weng, X.L., Deng, L.J.: Transmittance and electromagnetic shielding of ITO films deposited at low temperature. Zhenkong Kexue yu Jishu Xuebao/Journal of Vacuum Science and Technology 26(5), 372–376 (2006), Language: Chinese
3. Wang, K., Jia, H.Z., Xia, G.Z.: Determination of optical parameters in thin films by transmittance spectra. Spectroscopy and Spectral Analysis 28(11), 2713–2716 (2008), Language: Chinese
4. He, G.Z., Yao, X.L.: Properties of ITO thin films prepared by APS assisted EB Evaporation. Proceedings of the International Society for Optical Engineering 6831 (2008)
5. Khotanzad, A., Hwang, R.C., Abaye, A., Maratukulam, D.: An adaptive modular artificial neural network: Hourly load forecaster and its implementation at electric utilities. IEEE Transactions on Power Systems 10, 1716–1722 (1995)
6. Wohler, C., Anlauf, J.K.: An adaptive time-delay neural-network algorithm for image sequence analysis. IEEE Transactions on Neural Networks 10, 1531–1536 (1999)
7. Chen, Y.J., Huang, T.C., Hwang, R.C.: An effective learning of neural network by using RFBP learning algorithm. Information Sciences 167(1-4), 77–86 (2004)
8. Huang, C.C., Huang, D.J., Chen, Y.J., Wang, S.M.T., Hwang, R.C.: The identification of TP chromatic aberration by using nearly equivalent NN model. Advanced Materials Research 211-212, 275–279 (2011)
9. Huang, D.J., Liu, F.T., Chuang, S.J., Huang, H.C., Hwang, R.C.: The estimation of TP chromatic aberration by using neural network. Advanced Materials Research 189-193, 2211–2214 (2011)
10. Simon, H.: Neural Networks: A comprehensive foundation, 2nd edn. Prentice-Hall International, Inc. (1999)

The QNN Transmittance Estimator of TP Film with Two Layers Coating for Electronic Appliance

Huang-Chi Chen[1,4], Yu-Ju Chen[2], Chuo-Yean Chang[3], Pu-Ten Hsu[1], Shuming T. Wang[1], and Rey-Chue Hwang[1,*]

[1] Electrical Engineering Department, I-Shou University, Kaohsiung, Taiwan
rchwang@isu.edu.tw
[2] Information Management Department, Cheng Shiu University, Kaohsiung, Taiwan
[3] Electrical Engineering Department, Cheng Shiu University, Kaohsiung, Taiwan
[4] Management Information System Department, Far East University, Kaohsiung, Taiwan

Abstract. This paper presents the transmittance estimation of touch panel (TP) film with two layers coating by using quantum neural network (QNN) model. Due to the capability of classifying the features of signals, QNN model was used to catch the complex relationship between TP transmittance and its all possible influencing factors. An artificial intelligence (AI) evaporation decision mechanism is expected to be developed. Such an AI system could help the technician to set the control parameters before the TP film's evaporation process is taken. This smart system can not only help technician to improve the work efficiency, but also reduce the company's cost. In order to demonstrate the possibility and superiority of the research, several QNN models with different input combinations were simulated and reported. The simulation results are shown as a comparison.

Keywords: transmittance, estimation, touch panel, quantum neural network.

1 Introduction

Recently, TP has become an important part of electronic appliance in our daily life. It is widely used in many products such as the mobile phone, electronic dictionary, GPS navigation system, MP3, digital photo frame and TV screen, etc. Usually, a thin plate with coating will be stuck on TP screen as the decoration film. Such film can not only protect the screen of TP, but also provide the specific optical function. In the manufacturing process, the coating is to deposit one or more layers of material onto the plate and it is usually done by evaporator [1-6]. In fact, the decoration film has become a necessary and indispensable part of TP.

As mentioned, the process of film's decoration is usually done by the vacuum evaporator. However, before the evaporation process is started, the control parameters of evaporator need to be set by the full experienced technician to ensure the whole coating process could be accomplished successfully. In fact, the success of evaporation process might be affected by many factors, including the coating target

* Corresponding author.

D. Jin and S. Lin (Eds.): Advances in Mechanical and Electronic Engineering, LNEE 177, pp. 215–220.
springerlink.com

composition, the layers of evaporation, the thickness of film, the position of plate placed and the rotation speed of evaporator's holder, etc. All these factors could possibly determine if the quality of decoration film meets the customer's request or not. The transmittance is an important and common measure used for judging the quality of decoration film. And, in our previous studies, the nonlinear relationship indeed exists between the transmittance and the influencing factors mentioned above [7-8]. However, these studies only focused on the TP film with one layer coating. They might not exactly show the real condition of evaporation process. Thus, in this study, the transmittance estimation of TP film with two layers coating was studied. Cr and Cr_2O_3 are used to be the coating targets. The complex relationship between TP transmittance and its all possible influencing factors is expected to be obtained.

In the past three decades, NN has been widely employed in different areas such as pattern recognition, signal processing and system identification due to its powerful learning and mapping properties [9-11]. The nonlinear and complex relationship between input and output pairs of historical data could be automatically developed by NN through a simple training process. But, many signal processing applications do have the problem that the environment of signal information is complex, uncertain and ill defined. Such a phenomenon makes NN have the ill learning condition sometimes.

QNN has been used to deal with the signals with fuzziness and uncertainty. Its hidden units have various graded levels that are capable of classifying the features of signals [8, 12]. In this study, QNN model was used to catch the relationship between transmittance and its possible influencing factors. QNN and its learning algorithm are described in Section 2. Section 3 shows some experiments of QNN model. The conclusion is given in Section 4.

2 Quantum Neural Network

In this paper, QNN model is used for all experiments. The n_s-level sigmoid function is taken as the transfer function by the units in the first hidden layer. Its math form is expressed as

$$sgm(x) = (1/n_s)\sum_{r=1}^{n_s}(1/(1+\exp(-(x-\theta^r)))) \tag{1}$$

Except the units of first hidden layer, one-level sigmoid function is adopted by all the units in other layers. Its form is given by

$$sgm(x) = 1/(1+\exp(-(x-\theta))) \tag{2}$$

The major steps of QNN learning algorithm can be summarized and presented as following [8, 12]. The weight's adjustment are computed by,

$$\omega(k+1) = \omega(\mathrm{k}) + \Delta\omega(k) \tag{3}$$

$$\Delta\omega(k) \propto ((1/n_s)\sum_{r=1}^{n_s} y^r(k)(1-y^r(k))) * \sum_l \delta_l(k)\omega(k) \tag{4}$$

where, n_s is the number of levels and r is the number of jump points.

The quantum interval adjustment in each training epoch can be calculated by the following equations. For each hidden node,

$$\bar{h} = \sum_{i=0}^{n_i} \omega X_i \tag{5}$$

n_i is the number of input signals.

$$h^r = \sum_{r=1}^{n_s} sgm(\bar{h} - \theta^r), \quad \tilde{h} = \frac{1}{n_s}\sum_{r=1}^{n_s} h^r, \quad v^r = h^r(1-h^r) \tag{6}$$

Take the average values for each class, $\langle \tilde{h}_{Cm} \rangle$ and $\langle v^r_{Cm} \rangle$.

For m-th class C_m,

$$\langle \tilde{h}_{Cm} \rangle = \frac{1}{|C_m|}\sum_{x_m, x_m \in C_m} \tilde{h}_m, \quad \langle v^r_{Cm} \rangle = \frac{1}{|C_m|}\sum_{x_m, x_m \in Cm} v^r{}_m \tag{7}$$

where, $|C_m|$ denotes the cardinality of C_m.

Then, the quantum interval can be adjusted by,

$$\Delta\theta^r = \alpha_\theta \frac{1}{n_s} * \sum_{m=1}^{C_{mo}} \sum_{x_m \in Cm} \left(\langle \tilde{h}_{Cm} \rangle - \tilde{h}\right) \times \left(\langle v^r_{Cm} \rangle - v^r\right) \tag{8}$$

where, α_θ is the learning rate.

$$\theta^r = \theta^r + \Delta\theta^r \tag{9}$$

3 Simulations

It is known that the evaporation process of TP film coating is a very complex work. Many control parameters need to be set before the process is taken. This work is usually executed by the technician with full experiences. And, trial-and-error is the common method adopted by the technician. Thus, if a well-designed AI decision mechanism for the manufacturing control parameters setting could be developed, this mechanism certainly can help the junior technician to do the evaporation work easily.

In this study, the data of decoration film provided by Mildex Optical Inc. were analyzed and simulated. Table 1 shows the example of data collected. The information includes the value of quartz crystal deposition monitor, the rotation speed

of holder, the substrate position, Cr thickness, Cr_2O_3 thickness and transmittance. The complex relationship between transmittance and its possible influencing factors is expected to be obtained by QNN model. For demonstrating the feasibility of QNN model used, four different data sets named Set-1, Set-2, Set-3 and Set-4, were randomly re-organized from the original data. For each data set, 100 points were used for QNN's training and 44 points were used for testing. The mean absolute error (MAE) and the mean absolute percentage error (MAPE) are taken as the measurements of performance.

Table 1. The example of data collected

Item	Quartz crystal	Holder's rotation speed	Substrate position	Cr thickness	Cr_2O_3 thickness	Transmittance (T%)
1	625	10	6	50	30	59
2	632	15	11	100	80	32
3	631	10	6	150	130	25
4	631	10	5	150	130	23
5	632	15	8	100	80	31
:	:	:	:	:	:	:

Several simulations were carried out by using the different input combinations. Two coating targets, Cr thickness and Cr_2O_3 thickness are important influencing factors highly correlated with the transmittance. Thus, these two variables are inevitable inputs for all simulations. Table 2 to Table 9 show the statistic errors of the simulations by QNN model with different input sets. From the simulation results shown, we can obviously find that a well-trained NN indeed is able to estimate the transmittance according to the proper input variables. In other words, the accurate transmittance of decoration film is possibly to be predicted before the evaporation process is taken.

Table 2. The error statistics performed by NN with five inputs. (Inputs: quartz crystal deposition monitor's value, holder's rotation speed, substrate position of panel, Cr thickness and Cr_2O_3 thickness).

Data Set	MAE		MAPE (%)	
	Training	Test	Training	Test
Set-1	0.68444	0.74370	2.04189	2.14170
Set-2	0.66424	0.67887	1.87562	1.91438
Set-3	0.69538	0.71907	1.91485	2.02893
Set-4	0.66954	0.78510	1.99822	1.99773
Avg.	0.67840	0.73169	1.95765	2.02069

Table 3. The error statistics performed by NN with four inputs. (Inputs: holder's rotation speed, substrate position of panel, Cr thickness and Cr_2O_3 thickness).

Data Set	MAE		MAPE (%)	
	Training	Test	Training	Test
Set-1	0.86881	0.81912	2.73790	2.41201
Set-2	0.69259	0.67383	1.97600	1.89707
Set-3	0.89531	0.82219	2.76752	2.52959
Set-4	0.84383	0.79691	2.66760	2.04264
Avg.	0.82513	0.77801	2.53726	2.22049

Table 4. The error statistics performed by NN with four inputs. (Inputs: quartz crystal deposition monitor's value, substrate position of panel, Cr thickness and Cr_2O_3 thickness).

Data Set	MAE		MAPE (%)	
	Training	Test	Training	Test
Set-1	0.96058	0.84898	3.02530	2.54711
Set-2	0.93855	0.88146	2.95641	2.72103
Set-3	0.89539	0.98620	2.78187	3.03919
Set-4	0.95214	0.91810	3.08998	2.58563
Avg.	0.93667	0.90869	2.96339	2.72324

Table 5. The error statistics performed by NN with four inputs.(Inputs: quartz crystal deposition monitor's value, holder's rotation speed, Cr thickness and Cr_2O_3 thickness).

Data Set	MAE		MAPE (%)	
	Training	Test	Training	Test
Set-1	0.72056	0.75121	2.08853	2.01120
Set-2	0.74836	0.69817	2.12258	1.96769
Set-3	0.70695	0.78246	1.95385	2.20404
Set-4	0.87135	0.93542	2.77856	2.61158
Avg.	0.76180	0.79181	2.23588	2.19863

Table 6. The error statistics performed by NN with three inputs. (Inputs: quartz crystal deposition monitor's value, Cr thickness and Cr_2O_3 thickness).

Data Set	MAE		MAPE (%)	
	Training	Test	Training	Test
Set-1	0.97140	0.82352	3.06674	2.47221
Set-2	0.97174	0.91485	3.04479	2.80339
Set-3	0.91690	1.00877	2.83172	3.12003
Set-4	1.03339	0.93625	3.29998	2.62863
Avg.	0.97336	0.92085	3.06081	2.75607

Table 7. The error statistics performed by NN with three inputs. (Inputs: substrate position of panel, Cr thickness and Cr_2O_3 thickness).

Data Set	MAE		MAPE (%)	
	Training	Test	Training	Test
Set-1	1.85902	1.89471	5.58237	5.29566
Set-2	1.95678	1.76855	5.76814	5.01275
Set-3	1.79428	2.06238	5.23304	6.38934
Set-4	1.94263	1.69998	5.79642	4.64223
Avg.	1.88818	1.85641	5.59499	5.33450

Table 8. The error statistics performed by NN with three inputs. (Inputs: holder's rotation speed, Cr thickness and Cr_2O_3 thickness).

Data Set	MAE		MAPE (%)	
	Training	Test	Training	Test
Set-1	0.89054	0.84210	2.79483	2.46460
Set-2	0.86118	0.77825	2.61874	2.29371
Set-3	0.70524	0.74817	2.02124	2.22100
Set-4	0.87575	0.93508	2.78823	2.58824
Avg.	0.83318	0.82590	2.55576	2.39189

Table 9. The error statistics performed by NN with two inputs. (Inputs: Cr thickness and Cr_2O_3 thickness).

Data Set	MAE		MAPE (%)	
	Training	Test	Training	Test
Set-1	1.92342	1.77223	5.71371	5.07052
Set-2	1.91956	1.77737	5.69732	5.11501
Set-3	1.80539	2.05468	5.27047	6.36017
Set-4	1.97375	1.69616	5.86544	4.64060
Avg.	1.90553	1.82511	5.63674	5.29658

4 Conclusion

This paper presents the transmittance estimation of TP decoration film with two layers coating. The complex and nonlinear relationship between the transmittance and its possible influencing factors is expected to be obtained by using QNN technique. From the simulation results shown, the average MAPE can reach around 2%. That means QNN model is a quite suitable tool for creating an AI transmittance estimator for TP evaporation process. In this research, we only focused on the possibility of QNN

model to be the transmittance estimator. We did not put many efforts in searching the best parameters of QNN. The appropriate QNN size, the initial weights and the learning rate were not considered too much in our simulations. All studies are not the best results which can be achieved by QNN model used. We believe that the best accuracy of transmittance estimation could be obtained if all possible conditions are considered.

Acknowledgments. This work was supported by the National Science Council of Republic of China under contract No. NSC-100-2622-E-214-007-CC3.

References

1. Dmitruk, N.L., Korovin, A.V.: Generalized analytical model for the calculation of light transmittance through a thin conducting film. Thin Solid Films 484(1-2), 382–388 (2005)
2. Wu, Y.T., Weng, X.L., Deng, L.J.: Transmittance and electromagnetic shielding of ITO films deposited at low temperature. Journal of Vacuum Science and Technology 26(5), 372–376 (2006)
3. Wang, K., Jia, H.Z., Xia, G.Z.: Determination of optical parameters in thin films by transmittance spectra. Spectroscopy and Spectral Analysis 28(11), 2713–2716 (2008) Language: Chinese
4. Kim, D.H., Yoon, H.K., Shih, D.H., Murakami, R.I.: Electromagnetic wave shielding properties of ITO/PET thin film by film thickness. In: The Proceedings of 10th International Conference on the Mechanical Behaviour of Materials, vol. 345-346(II), pp. 1585–1588 (2007)
5. Gupta, R.K., Ghosh, K., Mishra, S.R., Kahol, P.K.: Electrical and optical properties of high mobility W-doped In2O3 thin films. In: 2008 Materials Research Society Symposium, Large-Area Processing and Patterning for Active Optical and Electronic Devices, vol. 1030, pp. 34–39 (2008)
6. Feng, C., Liu, K., Wu, J.S., Liu, L., Cheng, J.S., Zhang, Y.Y., Sun, Y.H., Li, Q.Q., Fan, S.S., Jiang, K.: Flexible, stretchable, transparent conducting films made from superaligned carbon nanotubes. Advanced Functional Materials 20(6), 885–891 (2010)
7. Huang, D.J., Huang, C.C., Chen, Y.J., Huang, H.C., Chen, S.W., Hwang, R.C.: System identification of TP film evaporation by using nearly equivalent NN model. In: The Fourth International Conference on Genetic and Evolutionary Computing, pp. 118–121 (2010)
8. Huang, D.J., Yang, J.P., Chen, Y.J., Liu, F.T., Chang, C.Y., Hwang, R.C.: Transmittance estimation of TP decoration film by QNN. In: The Fourth International Conference on Genetic and Evolutionary Computing, pp. 122–125 (2010)
9. Chen, S., Billings, S., Grant, P.: Non-linear system identification using neural networks. International Journal of Control 51, 1191–1214 (1990)
10. Khotanzad, A., Hwang, R.C., Abaye, A., Maratukulam, D.: An adaptive modular artificial neural network: Hourly load forecaster and its implementation at electric utilities. IEEE Transactions on Power Systems 10, 1716–1722 (1995)
11. Hwang, R.C., Chen, Y.J., Huang, H.C.: Artificial intelligent analyzer for mechanical properties of rolled steel bar by using neural networks. Expert Systems With Applications 37(4), 3136–3139 (2010)
12. Purushothaman, Karayiannis: Quantum neural networks (QNN's): Inherently fuzzy feed-forward neural networks. IEEE Transactions on Neural Network 8(3), 679–693 (1997)

An Improved SAR Controller for Fast Locking and Relocking All Digital DLL

TaiLong Xu[1], Chao Xu[1], ChangYong Zheng[2], LiLi Wang[2], Jian Meng[1], DaoMing Ke[1], and JunNing Chen[1]

[1] Anhui Provincial IC Design Laboratory,
School of Electronic and Information Engineering,
Anhui University, 230601 Hefei, China
[2] School of Electronic and Information Engineering,
Anhui University of Architecture, 230601 Hefei, China
xutailong@ahu.edu.cn

Abstract. All digital delay-locked loops are widely used to solve the clock skew in modern day VLSI. However, the conventional SARDLL has the dead-lock problem, which limits its applications. So an improved SAR controller without dead-lock is proposed by embedding a restarting module into the conventional SAR controller. Using the improved SAR controller, a fast locking and relocking all digital SARDLL is implemented in 0.18μm CMOS . Post-layout transistor-level simulation results show that the lock-in and relock-in time are both within N cycles of input clock for N-bit SAR controller.

Keywords: SARDLL, dead-lock, fast-locking, PVTL.

1 Introduction

With the rapid advances in deep-submicron CMOS technology and guideline of the concept of system-on-chip (SOC), there are more and more functional blocks integrated on the same chip. As a result, the clock-skew problem becomes one of the bottlenecks in realizing high-speed and high-performance digital systems. So the delay-locked loops (DLLs) have been widely adopted to solve the clock-skew problems [1, 8].

The design of DLLs can be classified into two types: analog DLLs (ADLL) and all digital DLLs (ADDLL) [2]. Currently, more attention is paid to the ADDLLs, which are more suitable for system-on-a-chip. At present, there are three most conventional ADDLLs: the register-controlled DLL (RDLL), the counter- controlled DLL (CDLL) and the successive approximation register-controlled DLL (SARDLL) [1, 3]. Due to adopting the binary search algorithm (BSA), the SARDLL has the shortest locking time among the three ADDLLs [3]. However, as [4] and [5] point out, the conventional SARDLL proposed in [3] will be dead locked because of the open-loop characteristic after stopping the searching operation. Therefore, the conventional SARDLL will not track the process, voltage, temperature, loading (PVTL) and operating frequency variations after the first lock-in, especially for low power designs that adopt the dynamic voltage and frequency scaling (DVFS) [9].

D. Jin and S. Lin (Eds.): Advances in Mechanical and Electronic Engineering, LNEE 177, pp. 221–227.
springerlink.com

Based on the previous work, an improved SAR controller without dead-lock is presented. And using it, a fast locking and relocking SAR DLL is designed in this paper to track the PVTL and operating frequency variations after the first lock-in.

2 The Dead-Lock Problem of the SAR Controller and Improved Solutions

The block diagram of the conventional 6-bit SARDLL is depicted in Fig.1. (a) [3]. It consists of a phase comparator (PC), a digital-controlled binary weighted delay line, a divide-by-four frequency divider, an initialization circuit (IC) and a 6-bit SAR controller to provide the control word for the delay line. The PC gives phase information between input clock and output clock. If it is locked, the lock detect signal LD will become "1". If it is out of lock, LD will be "0". The signal Comp tells the phase of output clock lags or leads the input clock. The control word b[5:0] of the delay line comes from the 6-bit SAR controller.

Based on the output of the PC, the value of each bit of the output b[5:0] of the SAR controller in the DLL is determined in a sequential and irreversible manner [7]. The conventional 6-bit SAR controller and internal structure of the kth flip-flop with truth table are illustrated in Fig.1. (b) and (c) respectively. Whenever the flip-flip's are triggered, the kth flip-flop will have three different data inputs coming from: 1) the output of the (k+1)th flip-flop (shift right); 2) the output of the PC, Comp (data load); 3) the outputs of the kth flip-flop itself (memorization).

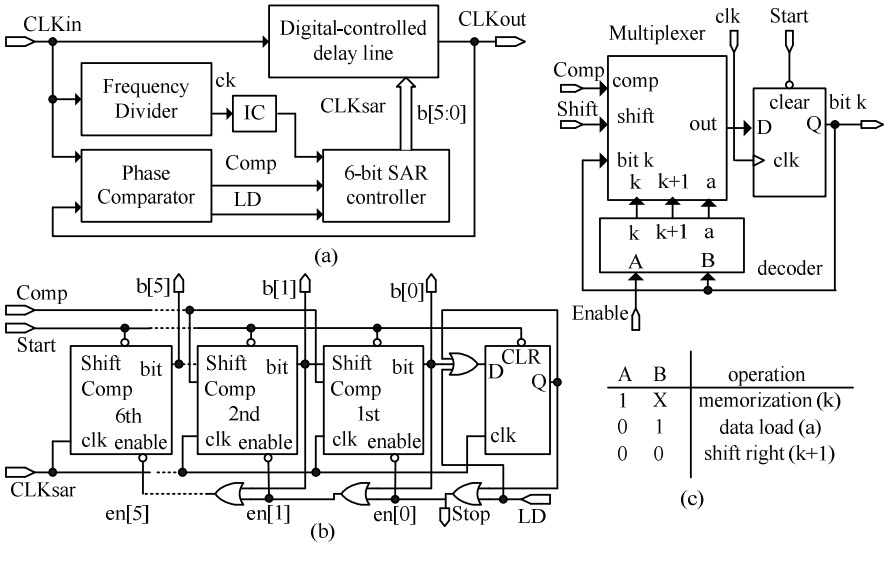

Fig. 1. (a)The diagram of the conventional 6-bit SARDLL, (b) the conventional 6-bit SAR circuit and (c) the internal structure of the kth flip-flop

In the beginning, the signal Start sets the 6th flip-flop and clears the others. Therefore, the control word b[5:0] equals to be 100 000 initially. Now the delay time is half of the whole delay line. When the SAR process begins, the signal Comp will decide the "1" of b[5] to remain or change to "0". In the delay time perspective of view, this "1" will be reserved if the delay time is not enough and will not if the delay time is sufficient. Likewise, b[4] will be "1" (shifted from the 6th flip-flop). Then the signal Comp will examine this "1" of b[4] in the same way as b[5]. This SAR process will go on to b[0], until the SARDLL is locked (the signal LD is up).

However, the conventional SAR DLL has a dead-lock problem. When the signal LD changes to "1", the signal Stop will be activated, through the OR gate feeding back to the flip-flop's, it forces the SAR controller to be in memorization mode. Due to the output of the additional DFF in the right end of Fig.1. (b) is fed back to its input through an OR gate, when the operation is stopped, the logic "1" output of this DFF will prohibit any possibility of re-starting the operation even the signal LD is pulled down again when the PC detects a large phase error for the operation condition variations. This denotes that relock-in process will never perform again even the PVTL and frequency variations are unacceptable. Then the SARDLL is useless.

To overcome the dead-lock drawback, [5] loads the output of the SAR controller to an up/down counter. This problem is free at the cost of an extra counter, and the SAR controller is out of use after the first lock-in process. A variable successive approximation register-controlled (VSAR) algorithm is proposed in [4]. When the binary search is over, this VSAR controller can be transformed into a counter to avoid the open-loop nature without any extra counter. But the relock-in processes are counter-controlled, not SAR-controlled, i.e. the fast-locking characteristic of SAR is not kept in the relock-in processes. As a result, in the worst case, both of them will take 2N-1 steps to be in the locked state again. So an improved SAR controller whose relock-in process is also SAR-controlled is proposed in this paper.

3 The Improved SAR Controller

From the description of section 2, the feedback of the DFF in the right end of Fig. 1. (b) from output to input is indeed the source of the dead-lock problem. So, in the improved SAR controller depicted in the Fig.2 (a), a restarting module is added to break the feedback in the conventional SAR controller. During the initialization state, the signals *Start* and *LD* are logic "0", so the outputs of DFF1 and DFF2, and the signals *Start_in* and *Stop* are all also logic "0". The outputs *b[5:0]* of SAR controller are forced to be "100 000". When the signal *Start* is changed to be logic "1", the fist lock-in process begins and it is the same as the operation of the conventional SAR controller. When the output of PC, *LD* transforms to be logic "1", i.e. the SAR DLL is locked, the SAR controller goes into memorization mode.

According to the schematic of Fig.2 (a), different from the conventional SAR controller, after the SARDLL first lock-in, if the PVTL and operating frequency variations result in lock-out, the signal *LD* will transit from "1"to "0". And then, when the rising edge of *CLKsar* comes, the output of the D flip-flop DFF2, i.e. the signal *q2* changes to be logic "1". On the next rising edge of *CLKsar*, the output of the D flip-flop DFF1, i.e. the signal *q1* changes to be logic "0". On the third rising edge of

CLKsar, the signal *q2* changes to be logic "0" and the signal *q1* keeps logic "0". So the pulse width of the singal *q2* equals to two cycles of the *CLKsar*, and in this period, the signal *Start_in* is forced to be in the logic "0", the SAR controller exits from the memorization mode, the outputs of SAR controller *b[5:0]* are initialized to be "100 000" again. And then the relock-in process begins likewise the first lock-in process. The timing diagram is depicted in Fig.2 (b) to illustrate how the improved SAR controller works.

Compared to [4] [5], the improved SAR controller in this paper reserves the SAR characteristic after the first lock-in, meanwhile, the first lock-in and relock-in process both only need N steps in the worst case.

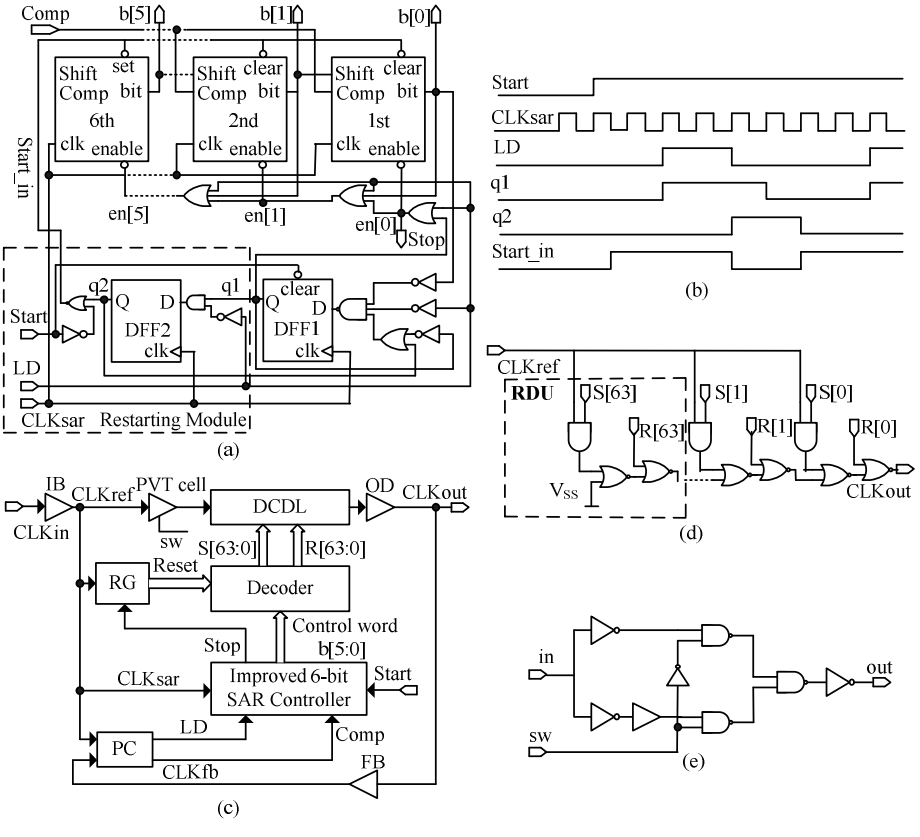

Fig. 2. (a) the schematic of the improved SAR controller, (b) the operating timing diagram of the improved SAR controller, (c) the diagram of the fast-locking and relocking SAR DLL using the improved SAR controller, (d) the schematic of the DCDL proposed in [6] and (e) the schematic of the PVT cell

4 Simulation Results

In order to validate the improved SAR controller proposed in this paper, as described in Fig. 2 (c), an all digital SAR DLL using the improved SAR controller is designed, which comprises input buffer (IB), PVT cell, digital-controlled delay line (DCDL), output driver (OD), reset signal generator (RG), decoder, clock driver (CD), improved SAR controller, phase comparator (PC) and feedback buffer (FB). As shown in the Fig. 2 (d), the scheme of DCDL proposed in [6] is adopted for its fast-locking and harmonic-free characteristic, which consists of resettable delay units (RDU). The SARDLL using the scheme of DCDL can lock-in within N cycles of input clock [6]. The signals *CLKin* and *CLKout* denote the input and output clocks respectively.

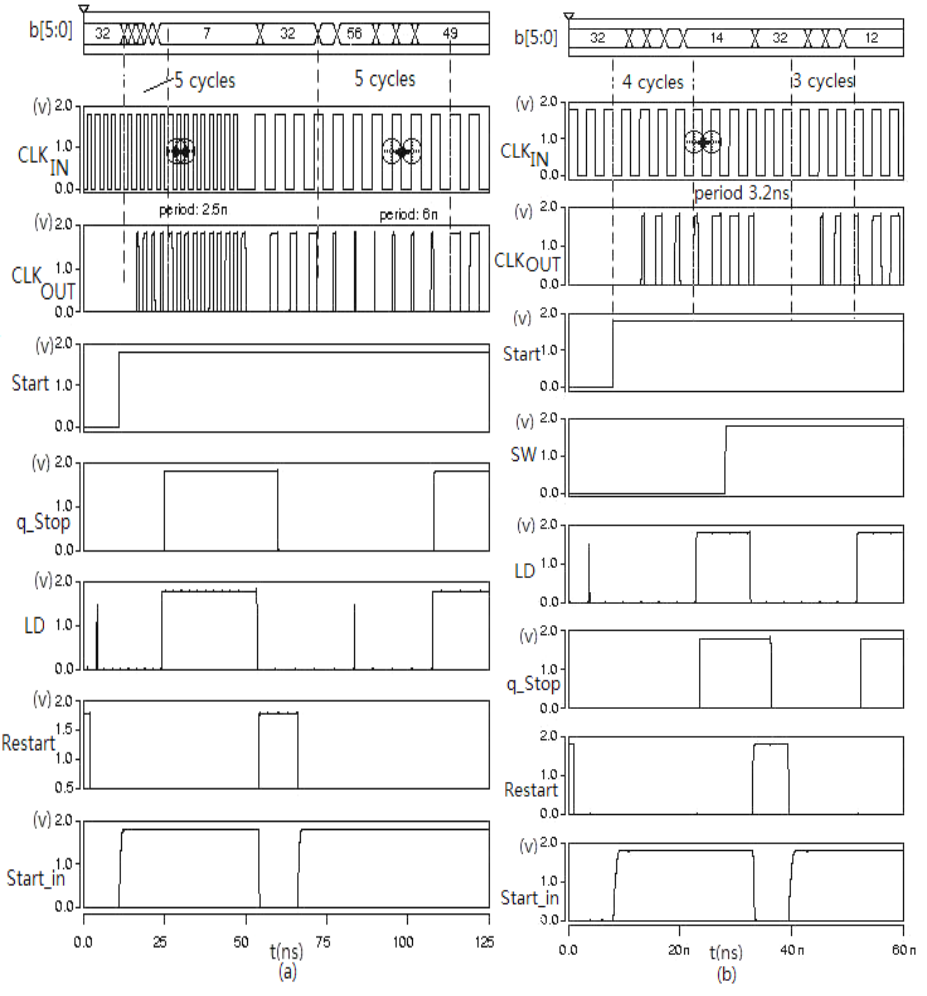

Fig. 3. The relock-in process (a) when the period of the input clock is transited from 2. 5 ns to 6 ns and, (b) when the PVTL variations result in lock-out

In order to simulate the impact of PVTL variations, a PVT cell is added into the clock path, because of the impact of PVTL variations can be equivalently represented as a variable delay element to be added in the clock path [5]. The circuit of the PVT cell is shown in Fig. 2 (e), during the normal operation, the control signal *sw* for the cell is set to "0", and the PVT cell provides an intrinsic delay to the clock path. This extra delay will be considered automatically in the locking process and will not affect the function of the SAR DLL. After lock-in, *sw* can be pulled high intentionally at a particular time. Now, the PVT cell will provide a much larger delay.

The all digital SARDLL with the improved 6-bit SAR controller is implemented in CMOS 0.18μm. HSIM is chosen as the simulator. The post-layout transistor level simulation results, which are based on SPICE models, TT corner at 1.8V/25℃and the load is 0.005pf, are in Fig. 3. The signal *sw* of PVTL cell is set to logic "0", Fig.3 (a) shows that the SARDLL can track the operation frequency variation. In the Fig. 3 (b), when the signal *sw* is set "0", the DLL can get locked, and the signal *LD* goes high. And then, the signal *sw* is set "1" to turn on the PVT cell intentionally, as a result, the DLL becomes unlocked, and the signal *LD* is pulled low. Now the restarting module is activated, the control word *b[5:0]* is fine tuned continuously, finally, the DLL gets locked again, and the signal *LD* goes high again. Both the first lock-in and the relock-in time are within 6 cycles of input clock, i.e. the dead-lock issue of conventional SARDLL is eliminated and the advantages of the SAR algorithm are kept after the first lock-in. The values of *b[5:0]* in the Fig.3 are all decimal.

5 Conclusion

An improved SAR controller that eliminates the dead-lock problem is presented in this paper, using it an all digital SARDLL is implemented. Compared to the previous work, the all digital SARDLL using the improved SAR controller can fast lock-in and relock-in within N cycles of input clock, and the characteristic of SAR algorithm is kept in the relock-in process.

Acknowledgments. The authors would like to thanks the support of the youth research fund of Anhui University (No.KJQN1011), the Anhui provincial excellent youth research fund (No. 2012SQRL013ZD) and the NSFC (No. 61076086).

References

1. Dehng, G.-K., Lin, J.-W., Liu, S.-I.: A fast-lock mixed-mode DLL using a 2-b SAR algorithm. IEEE J. Solid-State Circuits 36(10), 1464–1471 (2001)
2. Okajima, Y., Taguchi, M., Yanagawa, M., er al.: Digital delay-locked loop and design technique for high-speed synchronous interface. IEICE Trans. Electron. E79-C(6), 798–807 (1996)
3. Dehng, G.-K., Hsu, J.-M., Yang, C.-Y., et al. : Clock-deskew buffer using a SAR-controlled delay-locked loop. IEEE J. Solid-State Circuits 35(8) (August 2000)
4. Yang, R.-J., Liu, S.-I.: A 40-550MHz harmonic-free all-digital delay-locked loop using a variable SAR algorithm. IEEE J. Solid-State Circuits 42(2) (February 2007)

5. Wang, J.-S., Wang, Y.-M., Cheng, C.-Y., et al.: An improved SAR controller for DLL applications. In: ISCAS, pp. 3898–3901 (2006)
6. Huang, K., Cai, Z.K., Chen, X., et al.: A harmonic-free all digital delay-locked loop using an improved fast-locking successive approximation register- controlled scheme. IEICE Trans. Electron. E92-C(12) (December 2009)
7. Wang, L., Liu, L.B., Chen, H.Y.: An implementation of fast-locking and wide-rang 11-bit reversible SAR DLL. IEEE Trans. on Circuits and Systems–II 57(6), (June 2010)
8. Moorthi, S., Meganathan, D., Krishna, N., et al.: A Novel 14~170 MHz All Digital Delay Locked Loop with Ultra Fast Locking for SOC Applications. In: IEEE Recent Advances in Intelligent Computational Systems (RAICS), pp. 76–80 (2011)
9. Chung, C.C., Chang, C.L.: A wide-range all-digital delay-locked loop in 65nm CMOS technology. In: IEEE International Symposium on VLSI Design Automation and Test (VSLI-DAT), pp. 66–69 (2010)

Tool Path Design and Cutting Condition Optimization of Thin and Hard-to-Cut Material in Mechatronic Engineering

Dong-Mei Xu[1], Jinn-Jong Sheu[2], and Chin-Wei Liu[2]

[1] Fujian Polytechnic of Information Technology, 106, Fu Fei Road, Gu Lou District, Fuzhou 350003, Fujian Province, P.R.C.
[2] National Kaohsiung Univsersity of Applied Sciences, 405, Chien Kung Road, Kaohsiung 80778, Taiwan, R.O.C.
xdm33@163.com, jjsheu@kuas.edu.tw, jinnwoel@hotmail.com

Abstract. The thin stainless plate is not only a hard-to-cut material but also easy to lose flatness during high speed machining. Poor tool life and bad flatness of workpiece are the major concern of such type material cutting. The issues of tool life and flatness requirements were divided and conquered. Better cutting path designs were proposed to obtain good cutting tool life. The cutting conditions were optimized using DOE method to avoid deformation of the thin plate cutting and obtain better surface flatness of cut work-piece. The cutting experiments had shown the tool wearing is strongly depends on the tool path design. The proposed tool path design and cutting conditions were able to cut the thin stainless plate with good surface flatness and reasonable tool life.

Keywords: Hard-to-cut material, tool path design, thin plate cutting, stainless cutting, cutting optimization, Mechatronic Engineering.

1 Introduction

The temperature rise for stainless cutting results in the quick wearing of cutter. EDM process is usually adopted to make stainless products but the efficiency is poor. High speed machining (HSM) is an alternative to make stainless part cutting with reasonable efficiency and tool life. Ozel et al.[1] adopted FEM simulation to analyze the cutting force, chip flow and temperature distribution of workpiece. The proper cutting condition and tool path can be selected based on the predicted cutting force and tool stress. Malalis et al.[2] used MARC to study the chip formation of orthogonal cutting. Chip-separation criterion was proposed to find the steady state cutting of AISI-1045 and WC. Chiou et al.[3] had developed dynamic cutting force model based on instantaneous shear plane of end milling. The helical angle is the most important parameter of the cutting force. Gologlu et al.[4] had studied the surface roughness of pocket milling. Different cutting conditions and tool path designs were arranged using Taguchi method to obtain optimum combination. The spiral tool path has better surface roughness than the two-way or one-way tool designs. Lim et al.[5] had cut the turbine blade with a five-axis CNC machine considering the lead in angle and the different cutting directions. The vibration effect

D. Jin and S. Lin (Eds.): Advances in Mechanical and Electronic Engineering, LNEE 177, pp. 229–234.
springerlink.com

can be minimized with proper cutting direction and lead in angle. The surface roughness of workpiece can be decreased with decreasing of vibration. In this paper, the cutting conditions and the tool path were designed to minimize the tool wearing and surface roughness of workpiece. A fixture was also designed to avoid vibration and deflection of thin stainless plate milling.

2 Tool Path Designs for Pocket and Holes

The stainless product adopted in this study and the measurement points of cutting deformation are shown in Fig. 1. The original circular workpiece is 2.6 mm in thickness and 108 mm in outer diameter. The blank center has a small hole with 7 mm in diameter. Two cutting stages are required to make the upper layer of circular pocket (1.5 mm in depth and 99 mm in diameter) and the other nine rectangular holes, perceptively.

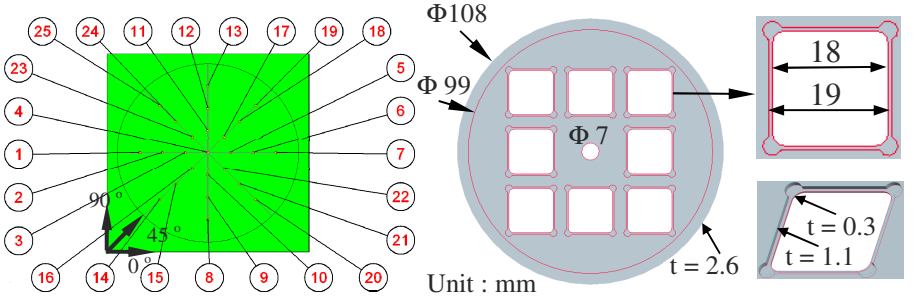

Fig. 1. The measurement points (left), geometry and dimensions (right) of the stainless product

2.1 Tool Path Designs for Circular Pocket

Two issues are considered in this stage: tool wearing and flatness of the pocket. The cutting experiments using parallel (zero and ninety degrees), circular, and spiral tool path designs were carried out to evaluate the tool wearing and find the better cutter path design. The cutting conditions are: spindle speed 10000 rpm, feed 2000 mm/min, step distance 3 mm, and depth of cut 0.1 mm, respective. The 4-flute end mill cutter 6 mm in diameter was used in all cutting tests.

2.2 Optimum Design of Cutting Conditions for Circular Pocketing

The better tool path design found in the tool wearing evaluation experiments was adopted to determine the optimum cutting conditions using Taguchi method with orthogonal array L9 (4^3). The objective is to minimize the average flatness deviation of the 25 measurement points (the-smaller-the better) shown in Fig. 1. There are four 3-level condition factors considered: spindle speed (10000, 15000, 20000 rpm), feed (2000, 2500, 3000 mm/min), step distance (0.5, 1, 1.5 mm), and depth of cut (0.05, 0.1, 0.15 mm), respective. The arrangement of the cutting conditions for the carried out 9 experiments according to the L9 orthogonal array (O.A.) is given in Table 1.

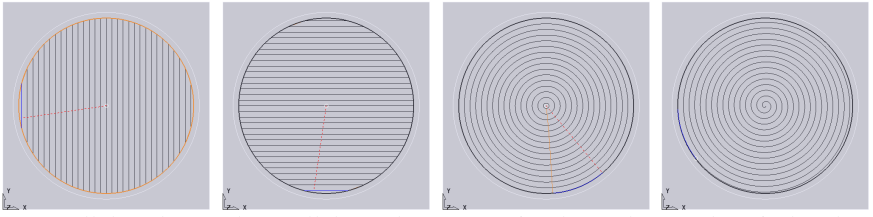

(a)Parallel (0 deg.) (b)Parallel (90 deg.) (c) Circular path (d) Spiral path

Fig. 2. Four cutting path designs for tool wear evaluation (parallel, circular, and spiral)

Table 1. The O.A. of cutting conditions and the average deformation of workpiece

Exp. No	*A*, Spindle speed(rpm)	*B*, Feed (mm/min)	*C*, Step distance (mm)	*D* ,Depth of Cut (mm)	Deviation (mm)	S/N ratio
1	10000	2000	0.5	0.05	0.110	19.18
2	10000	2500	1	0.1	0.109	19.25
3	10000	3000	1.5	0.15	0.182	14.82
4	15000	2000	1	0.15	0.172	15.31
5	15000	2500	1.5	0.05	0.065	23.69
6	15000	3000	0.5	0.1	0.135	17.39
7	20000	2000	1.5	0.1	0.075	22.48
8	20000	2500	0.5	0.15	0.207	13.69
9	20000	3000	1	0.05	0.089	20.99
optimum	20000	2000	1.5	0.05	Doe0.057 **exp.0.046**	24.06

2.3 Tool Path Designs for Rectangular Holes

There are 8 rectangular through holes (1.1 mm in depths) to be made at the bottom of the circular pocket as shown in Fig. 1. The circular and the parallel tool path designs are shown in shown in Fig. 3.

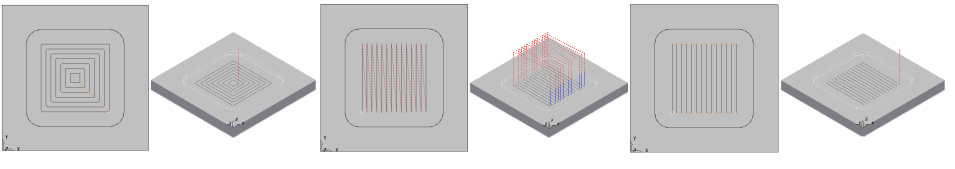

(a)Circular path (b)One-way parallel path (c) Two-way parallel path

Fig. 3. Cutting path designs for the pocketing of the rectangular through holes

3 Results and Discussion

3.1 Cutting Results of Circular Pocket

The rough machining of the circular pocket was carried out to evaluate the tool wearing and find the better cutting strategies. The cut workpieces of different tool path designs and the corresponding tool wearing were shown in Fig. 4. The cutting patterns are shown clearly on the top by using a large step distance (3 mm). The wearing measurement of the tool edge (on the bottom) had revealed that circular path design is better than the others. The circular path with ramped lead in cutting was adopted to find the optimum cutting conditions for all cutting steps.

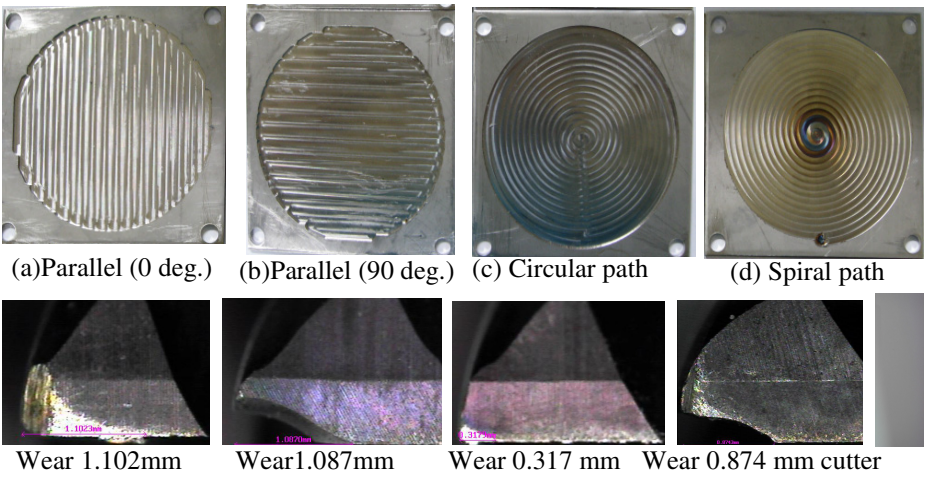

Fig. 4. Cutting results of 4 tool path designs (top) and wearing of tools (bottom)

3.2 Optimum Design of Cutting Conditions

The response chart of the average flatness deviation of the 25 measurement points and the cutting workpieces are shown in Fig. 5. The effect of depth of cut and step distance are ranking 1 and 2, respectively. The smaller the depth of cut and the larger the step distance is going to reduce the deviation of cutting surface (improve the flatness of product). The effect of the spindle speed and feed rate are smaller than the depth of cut and the step distance. The predicted deviation is 0.057 mm and the measured cutting result is 0.046 mm which is in good agreement with the theoretical prediction. The results of the adopted design of experiment method are good and feasible.

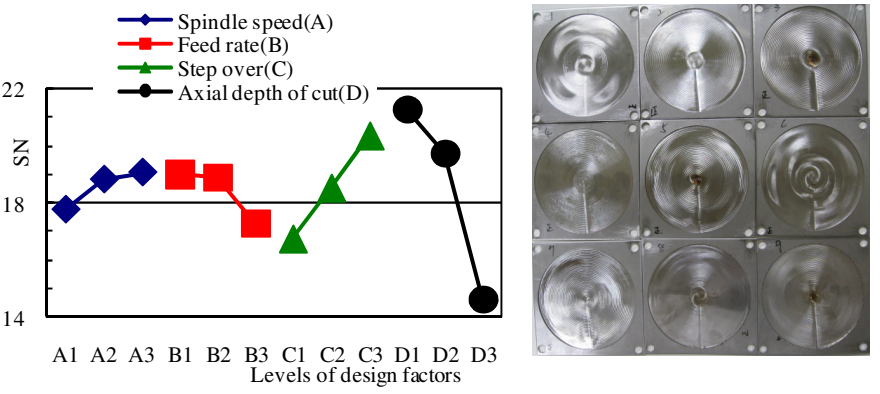

Fig. 5. Response chart of the four design factors (left) and the cutting results (right)

3.3 Validation of the Optimum Design of Cutting Conditions

The obtained better tool path and the cutting conditions were adopted to test the complete cutting process. Since the effect of the spindle speed and feed rate are no significant, the spindle speed and feed rate were increased to 30000 rpm and 3600 mm/min to speed up the cutting efficiency. The cut product and the measured surface roughness were shown in Fig. 6. The maximum surface roughness is less than 1.8μm and the Ra is only 0.1μm.

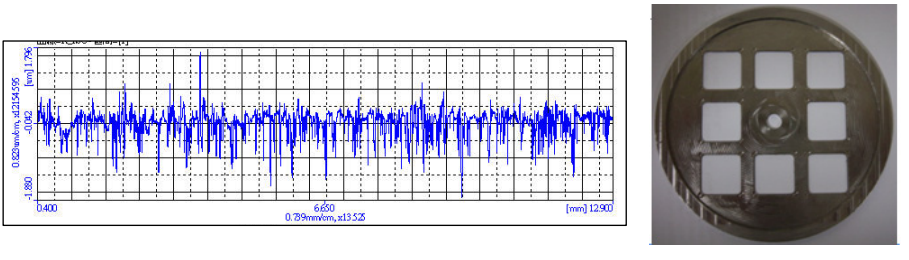

Fig. 6. Response chart of the four design factors (left) and the cutting results (right)

4 Conclusions

The authors proposed tool path design methods and coped with the optimum cutting conditions to machine a thin stainless plate with circular pocket and rectangular through holes. The effects of the cutting conditions shown this hard-to-cut material can be made by using good cutting conditions to prevent tool wearing and obtain good surface condition.

References

1. Ozel, T., Altan, T.: Process simulation using finite element method- prediction of cutting forces, tool stresses and temperatures in high-speed flat end milling. Int. J. Mach. Tools Manufact. 40, 713–738 (2000)
2. Mamalis, A.G., Horvath, M., Branis, A.S., Manolakos, D.E.: Finite element simulation of chip formation in orthogonal metal cutting. J. Mat. Process. Tech. 110, 19–27 (2001)
3. Chiou, C.H., Hong, M.S., Ehmann, K.F.: Instantaneous shear plane based cutting force model for end milling. J. Mat. Process. Tech. 170, 164–180 (2005)
4. Gologlu, C., Sakarya, N.: The effects of cutter path strategies on surface roughness of pocket milling of 1.2738 steel based on Taguchi method. J. Mat. Process. Tech. 206, 7–15 (2008)
5. Lim, T.S., Lee, C.M., Kim, S.W.: Evaluation of cutter orientations in 5-axis high speed milling of turbine blade. J. Mat. Process. Tech. 130-131, 401–406 (2002)

Design of Dust Removal Device for Electric Meter

ZhiLiang Chen, LiGuo Tian, Meng Li, JiePing Zhang, and BeiBei Guan

Tianjin Key Laboratory of Information Sensing & Intelligent Control,
Tianjin University of Technology and Education,
Tianjin, 300222, China
czl_tj@sina.com,
{tlg1234,limeng-3260711}@163.com

Abstract. With the development of automation industry, more and more manufacture depends on automation to improve production efficiency. After welded the electric meter, it is necessary to clean up dust in the dial plate. At present, there have been some manufacturers began to design automatic dust removal equipment in order to improve the efficiency of the industry. Because of these reasons, it designed a set of meter dust removal device, the device used the SCM ATmega16 as the control core, through the selection of components, and hardware and software design, to achieve the automatic dust removing function for electric meter. After tested, the dust removal device runs stably and reliably, the result of dust removal is clean, so as to avoid polluting the air.

Keywords: Automation, Electric Meter, Dust Removal Device, Single-chip Microcomputer (SCM).

1 Introduction

With the development of modern science and technology, automated production equipment is more and more widely applied in the field of intelligent control. Good automated production equipment is important to improve production efficiency and then improve product value. This paper designed the automatic dust removal device used the ATmega16 SCM as the control core for electric meter[1], which completes the dust removal work well in the production process of electric meter, eliminates the manual cleaning time, greatly improves the work efficiency, reduces manpower, material resources, thereby reducing the cost of product development.

2 Overall Design of the System

In the paper the dust removal device for electric meter used ATmega16 single-chip microcomputer as the core, adopting gas air dust removal method, is mainly composed of control unit(SCM), electromagnetic shaker, product positioning fixture, high-pressure gas electromagnetic valve, negative pressure motor and spiral dust remover[2-3]. After judging electric meter in its place, the system will start electromagnetic shaker and begin to shake, and then open the electromagnetic valve

D. Jin and S. Lin (Eds.): Advances in Mechanical and Electronic Engineering, LNEE 177, pp. 235–239.
springerlink.com

used to control high-pressure gas, high-pressure gas is blown into the barrel, using spiral precipitator on barrel to carry out all-round dusting. After the electromagnetic shaker and high-pressure gas electromagnetic valve are running for a period of time, the negative pressure motor will be started, gases mixed with impurity will be inhaled from the barrel to the dust removing barrel, after working for a period of time, the single-chip microcomputer will control to close all the work, at the same time, a buzzer sweet to indicate the dust removal work is finished. The overall system structure chart is shown in Fig.1.

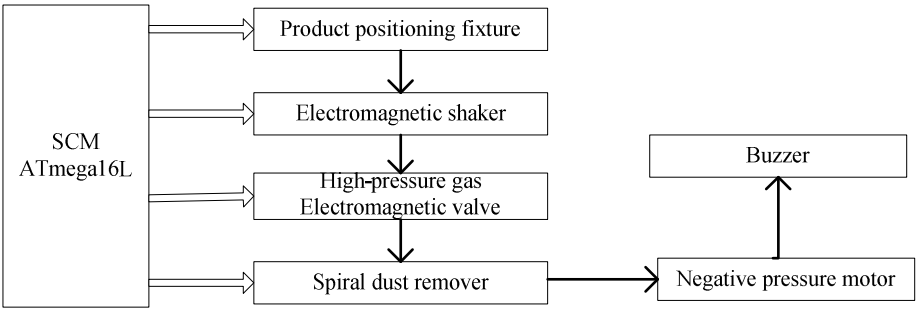

Fig. 1. The overall structure of the system

3 Hardware Design

3.1 Product Positioning Fixture Module

The function of the product positioning fixture module is to fix the electric meter on the dust removal device, also control the device to start. After the electric meter is positioned, SCM will judge if the electric meter is already in place. If it is ready, the system will wait for the SCM to give orders to execute the next step, if it is not in place, then the SCM will not perform any commands until the product is in place.

3.2 Electromagnetic Shaker Module

The function of electromagnetic shaker module is to shake off the welding slag in the electric meter which is placed on the automatic dust removing device. The shaking motor startup control circuit is shown in Fig.2. After the dust removal device for electric meter is started, the control unit, namely SCM ATmega16 will energize the relay KM1; the shaking motor will be electrified and begin to work. The shaking motor adopts the ZG series of inertia vibrator, which is a new type shaking device provided with the shaking force by the eccentric block arranged in both ends of rotor of a special double shaft three-phase asynchronous motor. Compared with other shaking device, it has the advantages of small volume, simple structure, low power, large shaking force and low noise.

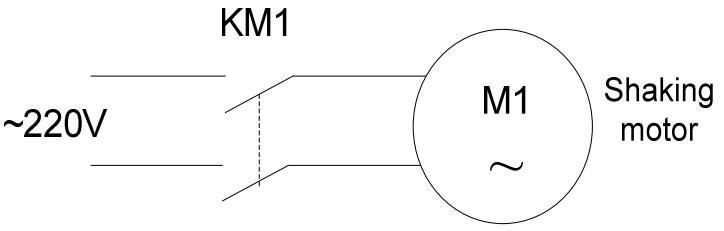

Fig. 2. The startup control circuit for shaking motor

3.3 High-pressure Gas Electromagnetic Valve Module

The main function of high-pressure gas electromagnetic valve is to control the flow of high pressure gas. After the control unit ATmega16 judge the product is already in place, the control unit will start the shaking motor to shake at first, while the control unit electrifies the relay KM2, and open the high-pressure gas electromagnetic valve, high-pressure gas is blown into the barrel to carry out all-round spiral gas dusting.

3.4 Negative Pressure Motor Module

The function of negative pressure fan is to use the principle of cross-ventilation, and negative pressure ventilation to inhale air with large amounts of impurities from the barrel to the dust collecting barrel. After the electromagnetic shaker and high-pressure air electromagnetic valve works for a certain period of time, the negative pressure motor will be started, and inhale gases mixed with impurity from the barrel to dust removing barrel, after working for a period of time, the control unit will close the device. While the control unit ATmega16 energizes relay KM3, the negative pressure motor begins to work.

3.5 Spiral Dust Remover Module

The main work process of spiral dust remover is as follows: after impurities pass into the dust removing barrel under the suction of the negative pressure motor, it will rotate in a spiral, at the same time flow upwards under the force of the barrel wall, the light dust is moved to the top of dust removal barrel, heavy impurities fall into the bottom of dust barrel relying on gravity. After stopping, the heavy impurities gathered on the bottom of the dust removal barrel could be cleared through opening the impurity cleanout of the barrel, and lightweight impurities is sucked out from the top of the dust barrel through fan; then the air mixed with impurities will be filtrated and become clean air, and then let out into the indoor space, so as to realize air cycle, while not affecting the indoor air cleanness.

3.6 DC Power Supply Module

In the dust removal device for electric meter, power supply module design is as follows: at first, use the transformer to transfer the AC 220V voltage into desired AC voltage, and then use the rectifier circuit to convert the AC voltage into one-way

pulsating DC current, and then use the filter circuit to filter out the ripple of the one-way pulsating DC voltage as far as possible and make it become smooth DC voltage, at last, use voltage stabilizing circuit to stabilize the output DC voltage at the desired voltage values [4]. DC power supply circuit diagram is shown in Fig.3.

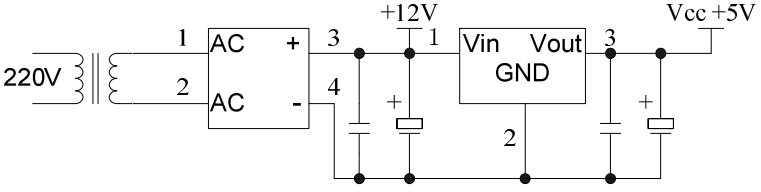

Fig. 2. The DC stabilized power supply circuit

4 Software Design

According to the specific requirements of the dust removal device for electric meter, program flow chart as shown in Fig.4. The program mainly adopts the module structure method, including system initialization module, starting module of electromagnetic shaker and the high-pressure gas electromagnetic valve, a negative pressure motor starting module, the work module of spiral dust catcher, a time-delay module as well as the end module [5-6].

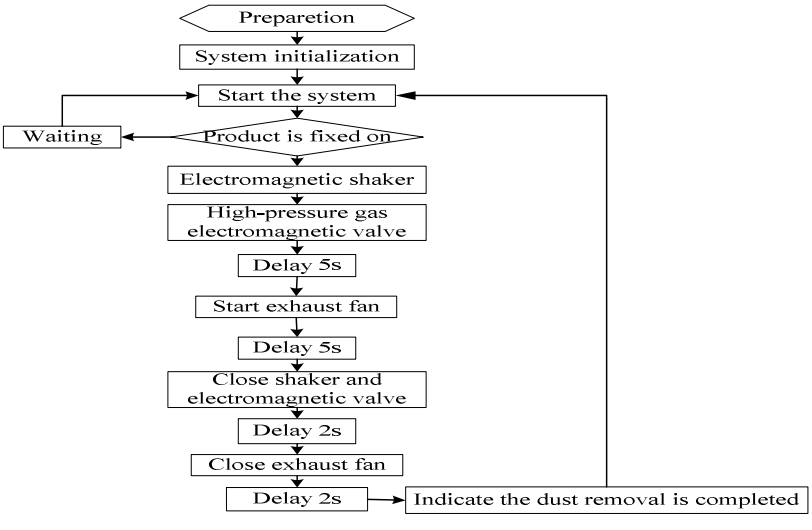

Fig. 4. The flow chart of the main program

5 Conclusion

Various production design of automation equipment is mainly designed in order to improve the production efficiency which plays a very important role for the development of enterprises. The paper designed the hardware and software of the dust removal device based on the ATmega16 single-chip microcomputer for the electric meter, and realized the dust removal efficiently in the process of meter production. After tested repeatedly, the equipment is stable and reliable, has a certain practical value.

References

1. Li, W., Lv, J., Wang, L.: The Utility Model Dust Removal Device—Ring-bar Power Dirt Catcher. Heat Energy Power Engineering 17(4), 420–422 (2002)
2. Chen, D.: Principle and Development Guidance of ATmega16 SCM. Mechanical Industry Press, Beijing (2006)
3. Yang, Q.J., Li, G.H.: Dust Controller Design based on Single-chip Microcomputer. Instrument Technique 3, 56–57 (2006)
4. Xie, Z.M.: Design, Experiment and Test of Electronic Circuit. Huazhong University of Science and Technology Press, Wuhan (2006)
5. Yuan, T.: Advanced C Language Program Design and Application for SCM. Beijing University of Aeronautics and Astronautics Press, Beijing (2002)
6. Shen, W., Zhan, W.Q.: Introduction to C Language Development for AVR Single-chip Microcomputer. Tsinghua University Press, Beijing (2003)

Analysis on the Form of Electronic Product's Finger Manipulator

Canqun He* and Xiujie Wei

School of Art, Jiangsu University, Zhenjiang, Jiangsu, China
hecq@163.com

Abstract. Using finger has become an essential part of human's activities when operating all kinds of electronic products with the improvement of electronic technology. To understand human's operating habits better, our study focused on how to use our fingers properly. Based on the experience and habits of operation, the types of finger manipulation are classified in this paper. Then seek the links between the modes and forms of operation by analyzing the forms of finger manipulators in order to provide a strong basis for inproving electronic product operator's designs.

Keywords: electronic product, finger manipulation, types of actions, movement forms, visual forms, tactual forms.

Introduction

Since we human walk upright, our hands get free and we can engage in all kinds of complex work. As the fingers are the most sensitive parts of our hands, we can't live without them. With the extensive use of touch screen, the universality and flexibility of finger manipulation are brought into fuller play. In one word, finger manipulation has become an essential action in people's lives.

Different forms make people generate different associations and then induce users' behaviors. Good form not only give people the visual beauty, but also convey correct information, improve the ease in use and reduce the misusage so as to give users a physical and psychological pleasure.

Finger operators mentioned in the article refer to related keys, buttons, switches, knobs, handles and etc. The reasonableness, comfort, ease of these objects can be reflected through which if the operation is clear or not.

1 Finger Manipulation Overview

1.1 The Importance of Finger Manipulation

Since childhood, we have started to learn a variety of finger songs and games to practice using our hands flexibly. Eating, dressing, housing, driving, using can't be

* Corresponding author.

D. Jin and S. Lin (Eds.): Advances in Mechanical and Electronic Engineering, LNEE 177, pp. 241–247.
springerlink.com

realized without finger manipulation in our daily life. If the tool is an extension of the hand, then the hands are the most complex and smart tools. As modern electronic products become increasingly abundant, the finger manipulation has become an important link between people and electronic products.

1.2 Main Types of Finger Manipulation

The finger movements are accurate and flexible. Table 1 is the main types of finger manipulation based on the definitions in Chinese dictionary and people's using habits.

Table 1. Main types of finger manipulation

Name	Similar type	Usage situation	Finger usage
raise	hoist uncover	open the water faucet; take off the lid of electric apparatus; operate the joystick	mostly four other finger(except thumb) to operate
press	push	the operation of keystroke or button on control panel of keyboard, refrigerator, washer, induction cookers and so on	mostly use thumb or forefinger to operate
push	shove	to operate the pulled switch, the wind pushing button in hair dryer, the microphone switch and so on	mostly use thumb to operate
wrench	turn	move the lever; tighten up a screw; the steering wheel and so on	mostly use five fingers to operate at the same time
turn	revolve rotate; turn swivel	to operate the volume pot of audio-visual equipment such as acoustics, radio, the fire-control knob of microwave oven and the faucet etc.	mostly use thumb, forefinger and the middle finger at the same time
lift	carry, raise	carry a basket or kettle or barrel or other things with handle	mostly use five fingers to operate at the same time
hold	grasp	grasp the phone, the camera or remote control; to operate hand-held electric such as coffee pot; to use pens or chopsticks	mostly use five fingers to operate at the same time
draw	pluck; draw move; uncork	to use some electronic products with USB interface or lift the stopper from a carafe	mostly use thumb, forefinger and the middle finger at the same time
support	brace	open [put up; unfurl; unfold; spread] an umbrella	mostly use five fingers at the same time
rock	Shake wave; turn vacillate	operate the rocker to charge up rocker-flashlight or manipulate the joystick	mostly thumb work in close with the forefinger or use five fingers at the same time

1.3 Force Direction and Movement Forms

Given that finger manipulation has many types, it is classified based on force direction and movement forms (see table2).

(1) Vertical Type: Change the amount of controlling by moving the controller up and down. The trail of movement is a straight line. It mainly refers to vertical interaction between fingers and contacted surface, such as button operation.

(2) Translational Type: Change the amount of controlling by moving the controller front and behind or left and right[1]. The trail of movement is also a straight line. It mainly refers to which the force direction and the contact surface are in the same plane, such as the operation of pushing buttons.

(3) Tilting Type: Change the amount of controlling by tilting the controller. The main movement form is swing. This mainly refers to which there is an angle (not including vertical angle) between the force direction and the contact surface, such as the operation of rocker switchs and wall switchs.

(4) Centripetal Type: Change the amount of controlling by turning the controller. The trail of movement is rotation and circular motion, such as the operation of knobs and rockers.

Table 2. Main types of finger manipulation according to force direction and movement forms

Force direction	Trail of movement	Main types of finger manipulation
perpendicularity	straight line	press; push down; carry; lift; hold;grasp; pluck; pull; drag; haul; tear
translation	straight line	push; shove; dial
tilt	wiggle	wrench; uncover; tear off; raise; take off; hoist; press
centripetal direction	circular motion	turn; revolve; circle; spin; twist; wrench; wring; shake; wave; rock

2 The Form Analysis of Finger Operators

Form design is expanded and spreaded by a variety of expression patterns in such an explosive era of knowledge economy. Form can convey human information accurately and turn into intermediary in service. Form can show the indicative use of the electronic product, implying the ways by which people use and operate the product. For example, tactile slot on the side of knob implies its mode of operation is rotation. Meanwhile the numbers of tactile slot, thickness and other visual or tactile forms convey the accuracy in adjusting. Therefore, the analysis of form can indicate the connection between form and mode of operation, enrich our cognition and provide designers with the design principles.

From the perspective of product semantics, form can express function because the form itself is a symbol system that hase meaning, expression and conveying functions like language [2].

Due to the human perception, people would always make the appropriate response in some forms. For instance, all kinds of operating keys in electronic product interface convey semantic. These reactions depend on our experience gained from practice. We can accurately identify the semantics in forms because of the familiar shadows found in real life.

2.1 Visual Form Analysis

Product's usage, working principle and operation reflect the relationship between the product form and human physiology. In additional, it also includes some psychological aspect related with people's awareness, habits, memory, imagination and emotion. Based on these the product morphology design methods start from the symbol meanings of human visual communication, so that the product tells the purpose of operation and accurate methods of operation through its own external visual images [3].

2.1.1 Vertical Operator: Pressing Type

The smooth operation of pressing down or inward will produce linear motion, which requires a certain process. It is reflected in the form of button on a certain degree of uplift.

Keys and buttons are usually rectangular or circular among which the majority is circular (including oval). From a cognitive perspective, it should be designed with a little sinking in the center at best. The designed concave can lead the finger to put into the center of button and ensure the accuracy of operation.

However, it's better for some important keys such as the start switch, brake button to be designed with a convex in the center to strengthen the tactile feeling and then ensure safe operation.

2.1.2 Translational Operator: Pushing Type

The smooth operation of translating will produce a parallel straight line motion, which requires a certain process. It is reflected in the form of button that the location of pushing button has been left a certain distance. The wind pushing button in hair dryer as shown in fig. 1a and gear switch pushing button as shown in fig.1b can both run a certain distance in a parallel direction.

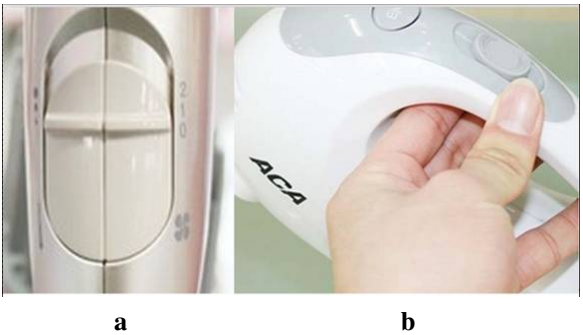

a **b**

Fig. 1. Pulled Manipulator

2.1.3 Tilting Operator: Turning Type

The smooth operation of turning will produce tilt motion, which requires a certain process on the slant. It is reflected in the form of switch on a certain degree of tilt.

As shown in Figure 2, rocker switch and toggle switch have the same structures. There is a similar structure like the seesaw inside using knob handle instead of rocker switch. Once one side of the seesaw fall, the seesaw contacts with touch spot to accomplish controlling. Completion of this process is reflected in the form of a side on the tilt.

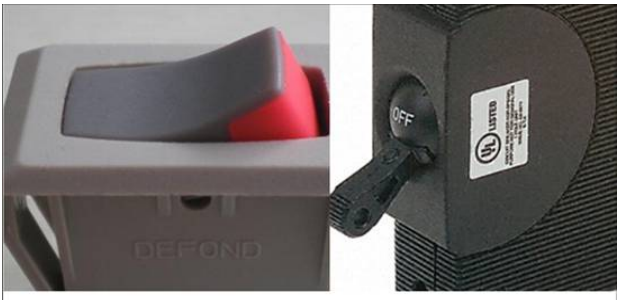

Fig. 2. Toggle Switches

2.1.4 Centripetal Operator: Rotating Type

Continuous smooth rotating operation requires consistency with the form of knob. So the knobs are mostly made into cylindrical, cone-shaped, nearly cylindrical polygon or pointer with positioning instructions forms. In order to facilitate the fingers holding and forcing to ensure the speed and accuracy of the operation, the size of the knob needs to ensure the fingers and the knob rim have sufficient contact surface.

2.2 Tactual Form Analysis

As an independent entrance for sense organs, the tactual sensation has the ability to convey information. Generally, for the common product which the design is not aimed for the particular users, the function of tactual sensation is mainly to cooperate with forms [4]. For instance, the groove on the edge of a knob indicates the accuracy of rotation operations, which puts the user's tactual experience on a dominant level.

People's tactual experience can be gained by the knowledge learned and accumulated from daily life. The design of shape or texture originates from identical or similar tactual experience, which can evoke potential experience. In this way, users can gain the tactual experience of the product. A concave surface on button transmits that operation is required by vision and tactile organ.

For operational products, user's tactile perception is one of the essential elements of function design [5]. These factors have manifested themselves mainly in the consideration and adjustment of shape, resistance and skin texture. Table 3 is the analysis on tactual form of finger manipulator.

Table 3. Analysis on tactual form of finger manipulator

name	visual form	tactual form	
		resistance	skin texture
vertical operator	a concave on the surface; important buttons designed with arc-shaped surface	there is vertical interaction between fingers and contact surface when pressing the button; the forefinger's resistance is 2.8~10N, yet thumb's operation is 2.8~22N	rough surface can prevent the fingers sliping(except those very important buttons such as power switch)
translational operator	a concave or a ribbed raised design on the interface	there is force feedback in the translational direction when pushing.	furrows on the interface can increase the friction force; the bulge has fixed function which can prevent the thumb sliping
tilting operator	a clear transition on the connection of two incline	the mutual force produced between inclined plane and the finger	rough surface can prevent the fingers slips
centripetal operator	groove designed on the interface	feel resistance at a tangent when turning the knob	the knob with ridges around the edge in order to increase the friction force

2.3 Morphological Information Analysis

Morphological information includes indicative words and graphics, different psychological colors, and feedback information, such as sound, light. Particular words, symbol or color can stir up our memory about the knowledge and experience of morphological information. Reminded of the scenes and incidents in daily life, users can gain more information about the electronic product in an effective and accurate way. Melt into auditory feeling，Morphological information is an effective complement of visual information, which makes the operation more effective.

2.3.1 Indicative Information

Lucid indicative information such as particular words or symbols can allow users to understand the structure and performance of electronic product very easily. Furthermore, the information can send the correct method of operation to the users. The calibrations or words around knob and the information of wind level on hairdryer can show users the proper operation and direction. However, operational states are be showed by the word "on-off" on microphone switch as well as some indicative information which includes the words on toggle switches and the icons on knobs.

2.3.2 Color Information

During the long period of social practice, people have different understandings for and emotional sympathetic response to different colors, which are endowed with emblematic meanings. For instance, red button mainly means "stop", "cut-off" or "accident" [1], and most indicator lights are also red. The reason is that red can easily

attract people's attention. As a symbol of danger and terror, red can be used as warning marks. On the other hand, green button, as a symbol of freedom and comfort, mainly shows "action".

Mastering the information and psychological feeling communicated by colors can bring the expression of color and the function of vision into full play, then the linguistic expression capability of electronic product design will get twice the result with half the effort.

2.3.3 Feedback Information

The success of finger manipulation or not ought to be judged from corresponding feedback information. Clicks, the change of resistance as well as indicator lights can provide effective feedback to users.

In our actual operating process, three types of factors including visual factors such as the form of operator and indicative information, tactual sensation such as force feedback and skin texture, and sonic feedback, all play an important role. In other words, the whole operation process integrates multiple sensory organ passage such as visual, auditory and tactile sense.

3 Conclusion

According to the previous experience, different forms have different imaginations and symbolic significances. Based on the analysis of main types and forms of finger manipulation, the connection between form and mode of operation is gained, which enrich our knowledge and make forms to be certain symbols. The designer successfully encodes the visual or tactile symbols during product shape design. It is possible to remind users of the memory and imagination of certain visual symbol when they see the same shape in real life [6]. As a kind of symbolic language, the shape and usage scenarios also can communicate with users.

Acknowledgments. This work was financially supported by the MOE Humanities and Social Sciences Youth Fund (10YJCZH036).

References

[1] Canqun, H.: Ergonomics of Product Design. Chemical Industry Press, Beijing (2006)
[2] Duan, D.: Study Assimilation of Morphological Semantics and Symbol Language. J. Forum on Art and Design 09, 124–125 (2004)
[3] Wang, B., Long, J., Yan, X.: Application of Morphological Semantics to Ergonomics Design. J. Chinese Journal of Ergonomics 11, 27–28 (2005)
[4] Zhou, R.: Tentative Study of the Product Design Based on the Tactile Experience. J. Arts Exploration 23, 119–122 (2009)
[5] Chen, S.: Application of human's haptic experience on product design innovation. Journal of Zhengzhou Light Industial Institute 2, 72–74 (2008)
[6] Zhang, J., Xie, Q.: The Emotional Symbols Design Study of Product Form Symbols Based on Product Semantics. J. Art and Design 2009(12), 191–193 (2009)

A High-Rate and High-Diversity Scheme of Space-Frequency Coding

ZhenChao Wang and YaLi Wu

College of Electronic & Informational Engineering,
Hebei University,
Hebei Baoding, China
wangzhenchaohbdx@163.com,
arlyarly@126.com

Abstract. This paper proposes a space-frequency coding scheme of combining phase shift diversity with subcarrier group (SFBC-PSD-SG) for OFDM system. This scheme can obtain frequency diversity gain effectively and reduce the complexity of decoding. It also solves the problem that the code rate can't reach one when the transmit antenna increases(more than two). It's a scheme of high diversity and high rate. The nice bit error rate performance of the improved scheme is confirmed by numerical simulations.

Keywords: MIMO, OFDM, SFBC, PSD, SG, SFBC-PSD-SG.

1 Introduction

Multiple-input multiple-output(MIMO) uses multiple antennas at the transmitter and receiver to obtain space diversity gain without extra power and bandwidth; Orthogonal frequency division multiplexing(OFDM) transforms high-speed information flow into multiple low-speed flows. With cyclic prefix(CP) of length greater than channel order inserted per OFDM symbol, we can overcome intersymbol interference and get multipath diversity gain. By encoding between transmit antennas and subcarriers, we can obtain space and frequency diversity. This is space frequency block coding(SFBC).

Although the theoretical design standard of SFBC is given in [1], the complexity of decoding on all subcarriers is high. In [2], the code rate of SFBC can't reach one as transmit antenna increases (more than two). With phase shift diversity(PSD), it can be solved in [3]. However, the drawback in [3] is that the frequency diversity gain can't be achieved effectively. This paper proposes a SFBC scheme combining PSD and subcarryier group (SFBC-PSD-SG) , which presents high rate, high diversity and low complexity. With SG, the correlation between subcarriers is diminished. Encoding in each group independently reduces the decoding complexity. To achieve less correlation, PSD is applied owing to the virtual multipath channel created , and the code rate can reach one with any transmit antennas.

D. Jin and S. Lin (Eds.): Advances in Mechanical and Electronic Engineering, LNEE 177, pp. 249–253.
springerlink.com

2 System Model

The block diagram of the scheme with four transmit antennas is showed in Fig.1.

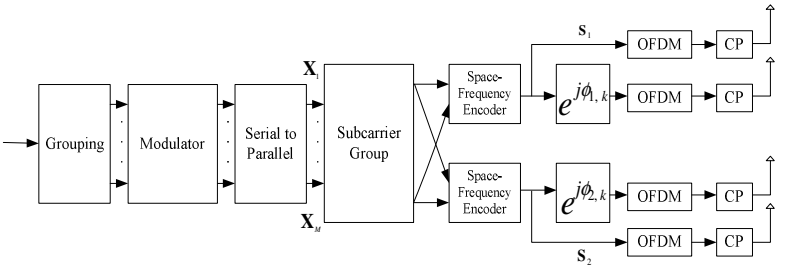

Fig. 1. Diagram of transmission system for the proposed scheme

The input serial binary information bits are expressed as follows:

$$a_1 \ , a_2 \ , a_3 \ , \ \cdots \ , a_M \ , a_{M+1} \ , a_{M+2} \ , a_{M+3} \ , \ \cdots \ , a_{2M} \ , a_{2M+1} \ , \ \cdots$$

After grouping, the above bits are divided into several groups as follows:

$$a_1 \ , a_{M+1} \ , a_{2M+1} \ , \ \cdots ; a_2 \ , a_{M+2} \ , a_{2M+2} \ , \ \cdots ; a_3 \ , a_{M+3} \ , a_{2M+3} \ , \ \cdots ; \ \cdots ; a_M \ , a_{2M} \ , a_{3M} \ , \cdots$$

Each sequence end in semicolon is modulated as a group into complex symbol sequence by mary phase shift keying(MPSK) independently. The serial to parallel converter collects L_0 serial symbols in each group into a data vector. $\mathbf{X}_n$ denotes the n-th vector: $\mathbf{X}_n = \left[X_n(0), X_n(1), \ \cdots , X_n(L_0-2), X_n(L_0-1) \right]^{\mathrm{T}}$. where n=1,2,$\cdots$,M. Let K denote the subcarriers number in an OFDM symbol, which meets $ML_0 = K$. $(\cdot)^{\mathrm{T}}$ represents the complex transpose. With SG in [4], we can get: $X_n(i) = s_1(iM+n-1), X_n(i+1) = s_2(iM+n-1)$, where $s_1(iM+n-1)$ $s_2(iM+n-1)$ represent the symbol on the $iM+n-1$ -th subcarrier of data vector $\mathbf{s}_1, \mathbf{s}_2$ respectively, and i=0,2,$\cdots$, L_0-2. The encoding matrix by coding on the subcarriers which separated at a distance of M subcarriers is given as follows:

$$\begin{bmatrix} s_1(iM+n-1) & -s_2^*(iM+n-1) \\ s_2(iM+n-1) & s_1^*(iM+n-1) \end{bmatrix}. \tag{1}$$

where Superscripts $(\cdot)^*$ represents the complex conjugate, making

$$-s_2^*(iM+n-1) = s_1((i+1)M+n-1), \ s_1^*(iM+n-1) = s_2((i+1)M+n-1) \ . \tag{2}$$

i.e., $-s_2^*(iM+n-1)$, $s_1^*(iM+n-1)$ represent the symbol on the $(i+1)M+n-1$-th subcarrier of $\mathbf{S}_1$, $\mathbf{S}_2$ respectively. $\mathbf{S}_1$, $\mathbf{S}_2$ will be modulated by the *K*-point Inverse Fast Fourier Transform(IFFT) , inserted CP , and transmitted from the first and third antenna respectively. The symbol on the *k*-th subcarrier of $\mathbf{S}_d$ multiplies phase rotation $\exp(j\phi_{d,k})$ as new data is transmitted from the second antenna as *d*=1 and the fourth as *d*=2 .

Let $\tau_{\max}$ denote the maximum delay spread, *T* serial data symbol period. The wireless channel will present frequency selective fading when $\tau_{\max} > T$. Let $L = \lfloor \tau_{\max} / T \rfloor$ denote channel order. The serial data symbol is modulated by IFFT into an OFDM symbol with symbol period *KT*. If $KT \gg \tau_{\max}$, i.e., the coherent bandwidth is far greater than subcarrier interval, which guarantee the maximum diversity gain for SFBC. For simplifying model, the channel is assumed quasi-static, i.e., constant during the transmission of one OFDM symbol. From transmit antenna *i* to the receive antenna *j*, we assume there is a multipath fading channel with *L* independent propagation paths and channel impulse response(CIR) can be expressed: $h_{j,i}(t) = \sum_{l=1}^{L} \alpha_{j,i}(l)\delta(t-\tau_l)$, τ_l denotes the delay on the *l*-th path with the same power delay, $\alpha_{j,i}(l)$ the *l*-th path amplitude of CIR with zero-mean, variance δ_l^2 and complex Gaussion distribution between the *i*-th transmit antenna and the *j*-th receive antenna, where $\delta_l^2 = 1/L$, i.e., the power delay is evenly distributed on the whole channel. Using IFFT, the frequency response function is given by: $\mathbf{H}_{j,i} = \left[H_{j,i}(1), \cdots, H_{j,i}(K)\right]^{\mathrm{T}}$, where $H_{j,i}(k) = \sum_{l=1}^{L} \alpha_{j,i}(l) e^{-j2\pi kl/K}$, $k=1, \cdots, K$. $H_{j,i}(k)$ represents the channel gain on the *k*-th subcarrier from transmit antenna *i* to receive antenna *j*. In [5], there is $L-1$ uncorrelated subcarriers for any the *k*-th subcarrier in the Rayleigh fading channel with *L* paths. In the section of 2.1, $L_0 = L$.

We assume a receive antenna and the knowed channel state information at the receiver. With ideal synchronization and sampling, CP removal and Fast Fourier Transform(FFT), the received signal on the *k*-th subcarrier can be expressed as:

$$\begin{aligned} r_k &= H_{1,1}(k)s_1(k) + H_{1,2}(k)s_1(k)e^{j\phi_{1,k}} + H_{1,3}(k)s_2(k) + H_{1,4}(k)s_2(k)e^{j\phi_{2,k}} + \eta_k \\ &= s_1(k)\left(H_{1,1}(k) + H_{1,2}(k)e^{j\phi_{1,k}}\right) + s_2(k)\left(H_{1,3}(k) + H_{1,4}(k)e^{j\phi_{2,k}}\right) + \eta_k \\ &= \left[H_1(k) \quad H_2(k)\right]\left[s_1(k) \quad s_2(k)\right]^{\mathrm{T}} + \eta_k \end{aligned} \tag{3}$$

where η_k denotes addtitive white Gaussion noise(AWGN) on the *k*-th subcarrier and is modeled as independent identically distributed complex Gaussian random variable. Based on the formula (1)、(2)、(3), we can get the following equation:

$$\begin{bmatrix} r_k \\ r_{k+M}^* \end{bmatrix} = \begin{bmatrix} H_1(k) & H_2(k) \\ H_2^*(k+M) & -H_1^*(k+M) \end{bmatrix} \begin{bmatrix} s_1(k) \\ s_2(k) \end{bmatrix} + \begin{bmatrix} \eta_k \\ \eta_{k+M}^* \end{bmatrix} . \tag{4}$$

where r_{k+M} , η_{k+M} represent the received signal and AWGN on the k+M-th subcarrier. Above equation can be simplified as: $\mathbf{R} = \mathbf{HS} + \boldsymbol{\eta}$. We define the channel matrix $\mathbf{H}$. $\mathbf{H}$ is now a virtual MIMO matrix with space (columns) and frequency (rows) dimensions. With a diagonalized space frequency decoder Γ, we can get• $\Gamma\mathbf{R} = \Gamma\mathbf{HS} + \Gamma\boldsymbol{\eta}$, where $\Gamma = \begin{bmatrix} H_1^*(k+M) & H_2(k) \\ H_2^*(k+M) & -H_1(k) \end{bmatrix}$, the resulting $\Gamma\mathbf{H}$ is orthogonal, i.e., $\Gamma\mathbf{H} = \left(H_1^*(k+M)H_1(k) + H_2^*(k+M)H_2(k)\right)\mathbf{I}_2$. $\mathbf{I}_2$ is the 2×2 identity matrix. We can get the following equation:

$$\begin{bmatrix} \tilde{s}_1(k) & \tilde{s}_2(k) \end{bmatrix}^{\mathrm{T}} = \left(H_1^*(k+M)H_1(k) + H_2^*(k+M)H_2(k)\right)\begin{bmatrix} s_1(k) & s_2(k) \end{bmatrix}^{\mathrm{T}} + \begin{bmatrix} \bar{\eta}_k & \bar{\eta}_{k+M}^* \end{bmatrix}^{\mathrm{T}} . \tag{5}$$

The symbols are estimated by the Maximum-Likelihood(ML) approach, i.e.,

$$\hat{s}_d(k) = \arg\min_{\hat{s}_d(k) \in S_n} \left(H_1^*(k+M)H_1(k) + H_2^*(k+M)H_2(k) - 1\right)\left|\hat{s}_d(k)\right|^2 + d^2\left(\tilde{s}_d(k), \hat{s}_d(k)\right). \tag{6}$$

where $k = iM + n - 1$, d=1,2. S_n represents constellation with size 2^b of the n-th group, and b is the number of bits per symbol which can be choosed based on transmission rate and quality. The transmitted data vector $\hat{\mathbf{x}}_n$ is decoded independently based on the n-th signal constellation as $n = 1, 2, \cdots, M$, $i = 0, 2, \cdots, L_0 - 2$. After demodulating,, we can get the following symbols:

$$\hat{a}_1, \hat{a}_2, \hat{a}_3, \cdots, \hat{a}_M, \hat{a}_{M+1}, \hat{a}_{M+2}, \hat{a}_{M+3}, \cdots, \hat{a}_{2M}, \hat{a}_{2M+1}, \cdots$$

3 Simulation Result

The entire bandwidth is 20MHZ and is divided into 2048 subcarriers. The CP time is 256T where $T = 0.05\mu s$. The channel model is Jakes model with two-path. Each path with same delay and exponential distributed power .

The BER performance of SFBC-PSD and SFBC-PSD-SG with 0.05 μs and 0.1 μs delay in each path is given by Fig.2. The difference isn't obvious during the range of low Signal to Noise Ratio (SNR). SFBC-PSD-SG has better performance than SFBC-PSD after 15dB, expecially when the delay is large.

4 Summary

In this paper, we highlight the improved scheme of SFBC-PSD-SG in OFDM. Expecially, this paper gives a model using four transmit antennas. The complexity has a exponential relationship with L_0 subcarriers in group and a linear relationship with M groups rather than a exponential relationship with K subcarriers. This scheme achieves high diversity by using PSD and SG compared with single SFBC, which can be suggested by the simulation.

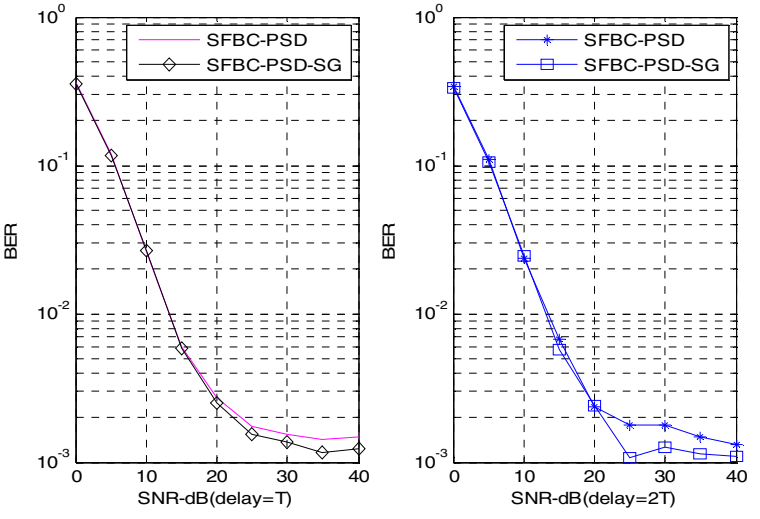

Fig. 2. The BER performance of SFBC-PSD and SFBC-PSD-SG

References

1. Bolcskei, H., Paulraj, A.J.: Space-Frequency Coded Broadband OFDM Systems. In: Proc. IEEE WCNC 2000, Chicago, pp. 1–6 (2000)
2. Bai, W., Fu, J.X., Younghak, K.: A Full Diversity Rate 4-Antenna Alamouti Code. In: 16th IEEE International Symposium on Personal, Indoor and Mobile Radio Communications, pp. 72–76 (2005)
3. Zhang, J., Fan, Y.Y., Wang, Y.W.: A Space-Frequency Coding Technique Combined with Phase Shift Diversity. J. Computer Simulation, 104–106 (2008)
4. Liu, Z., Xin, Y., Giannakis, G.B.: Space-Time-Frequency Coded OFDM over Frequency-Selective Fading Channels. J. Trans. Signal Processing, 2465–2476 (2002)
5. Luo, W., Wu, S.Q.: Space-Time-Frequency Block Coding for OFDM Systems. Journal of Systems Engineering and Electronics 27, 391–394 (2005)

Multiband Wireless Channel Measurements and Models in Various Typical Indoor Scenes

Shan Zhu[1], Bang Wang[1], Wenyu Liu[1], and Xuanli Zhang[2]

[1] Department of Electronics and Information Engineering,
Huazhong University of Science and Technology, Wuhan, P.R. China
[2] Library, Huazhong University of Science and Technology, Wuhan, P.R. China
luckz@126.com, {wangbang,liuwy}@mail.hust.edu.cn,
43015496@qq.com

Abstract. This paper presents some corrected empirical indoor propagation model and PDP parameters for various typical indoor scenes based on our extensive field measurements. We choose some classical models for calibration, using channel power measurements at multiband. Our calibration results can be used for wireless transmission planning and wireless optimization, forecasting and quality control as reference model parameters in indoor scenarios.

Keywords: propagation model, PDP, indoor coverage, empirical model.

1 Introduction

The data statistics from NTT DOCOMO show that 70% of the mobile data traffic produced indoor and the data statistics from China Mobile Communication Corporation also show that 70% of the voice services and 90% of the data services came from indoor environment [1]. To solve the problems in wireless communication system planning, coverage and quality control, it is a important problem to research the wireless channel of wideband in various indoor scenes [2].

These kinds of channel measurements indoor are still not well explored. Measurements from 2.3 to 10GHz have been carried out in Beijing, China. We also make simulations to validate the proposed models and got a desirable outcome.

2 Measurement Setup

2.1 Measurement Site

The measurement sites are typical indoor scenes in Beijing city, China. (Fig. 1).The type of sites is typical indoor scenes just like office or meeting room shown in table 1 below. There are glass or wood walls surrounded these sites and also wood furniture just like tables and chairs inside. The average height of the sites is 3m. Most of them have no people inside during testing period. In the underground garage there are cars and typical barriers in this kind of indoor scene just like walls and stand columns. The figures 1 and 2 show testing blueprint and actual environment of one site.

D. Jin and S. Lin (Eds.): Advances in Mechanical and Electronic Engineering, LNEE 177, pp. 255–261.
springerlink.com

Table 1. Test Scenario

ID	Name	Transmitter No.	Receiver No.
1	Meeting Room 1	2	10
2	Office1	2	40
3	Office2	2	40
4	Meeting Room 2	2	20
5	Hallway	3	20
6	Lab 1	2	30
7	Lab 2	2	40
8	Apartment	3	30
9	Underground garage	1	40

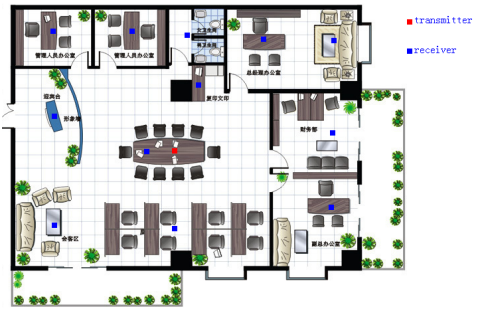

Fig. 1. The blue print

Fig. 2. Measurement environment

2.2 Equipment

The measurement equipment is a N5242A PNA-X microwave network analyzer from Agilent. The working frequency is from 10 MHz to 26.5 GHz and it has high output power (+18 dBm), low harmonics (-60 dBc) and a wide power sweep range (38 dB). It also has the best dynamic accuracy: 0.1 dB compression with +13 dBm input power at the receiver and low noise floor of -114 dBm at 10 Hz IFBW. It radiated a continuously oscillating signal at the surveyed frequencies: 2.3G to 10GHz during the test.

2.3 Equipment Calibration

In the beginning of whole measurement, we perform an antenna calibration in a fully anechoic chamber (Fig 3) to avoid interference to channel from antenna in order to get the pure characteristics of the channel. The fully anechoic chamber is a dark room with wave-absorbing material on all six sides inside and the radio wave can only propagate directly without reflection and diffraction. In this antenna calibration, the height of the transmit and receive antenna is 1.5m, and the distance from each other is

1m ,2m and 4.7m. We spin around the antenna each time to test the difference in directions[3]. We perform the test 10 times in each distance and a spectral scan was performed in the 2.3G to 10G bands.

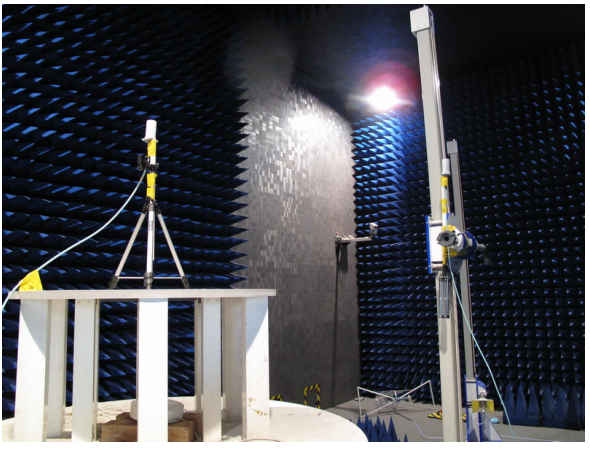

Fig. 3. Fully anechoic chamber

2.4 Measurements Procedure

In each site, we determine the testing area first and draw each testing points on the blueprint. A group of testing points contains few transmit antenna points and each transmit antenna point has dozens of receive antenna points while the number determined by the size of the area. In the field test, we fix the transmit antenna and move the receive antenna according to the blueprint, a spectral scan will be performed in the bands of interest on each point. We perform the test repeatedly on each point to avoid interference.

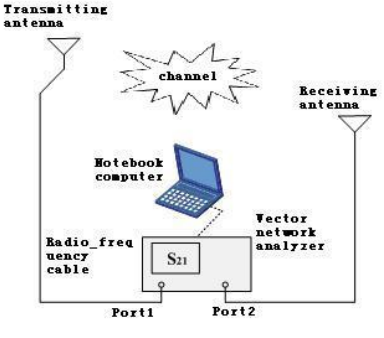

Fig. 4. System block diagram

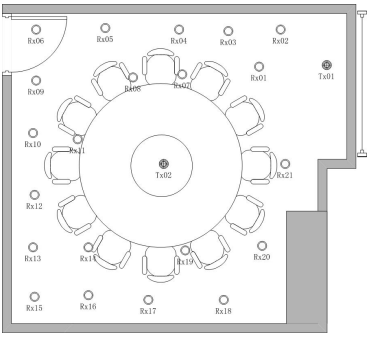

Fig. 5. Testing points

3 Model Calibration

The propagation model and power delay profile(PDP) are two key factors to represent the indoor coverage. The path loss of propagation model is defined as the difference between the effective transmit power and the received power (all in dB representation). It represents the signal attenuation during transmission and is an important factor to determine the link budget analysis. The PDP gives the intensity of a signal received through a multipath channel as a function of time delay. The time delay is the difference in travel time between multipath arrivals.

3.1 Propagation Model

The method to build-up a indoor wireless propagation model is similar as the way outdoors. The standard path loss model is expressed as the following formula [4,5]:

$$PL(d) = PL(d_0) + 10n\lg(\frac{d}{d_0}) + X_\sigma \quad (1)$$

The path loss *PL(d)* is a related function of d which means the distance between the transmitter and receiver. *PL(d)* is always divided into three parts, $PL(d_0)$ the first part is the free space propagation path loss of the reference distance. The reference distance is always valued for 1m

After the measurement, we use the least square method to fit the data. So we can get $PL(d_0)$ and the path loss index *n* [6]. In this way we can last get the parameter of the calibrated model.

We use formula (1) to calculate the model parameters in all these sites.. We can see the result below in (Table. 2).

Table 2. Result of measurement

Room ID	Room Type	PL_0	*n*
1	Meeting Room 1	47.3	1.5
2	Office1	45.2	1.6
3	Office2	42.1	1.2
4	Meeting Room 2	43.5	1.3
5	Hallway	42.3	1.1
6	Lab 1	46.6	1.6
7	Lab 2	42.7	1.8
8	Apartment	32.3	1.0
9	Underground garage	40.3	2.1

3.2 Power Delay Profile(PDP)

In designing wireless telecommunication systems, it is crucial to control the intersymbol interference (ISI) and more importantly the bit error rate (BER). The ISI

is directly related to the multipath phenomena resulting from objects (such as walls, furniture, and people) in the propagation path between the transmitter and receiver. The delay spread of the radio propagation channel is a measure of the multipath effects which are a detriment to system performance

The PDP gives the intensity of the received signal as a function of time delay. In our measurements, the resolution that could be achieved is 1ns. When we get the PDP below(Fig. 6), we can calculate the results with the least squares method. And the correctional parameters of PDP are shown below.

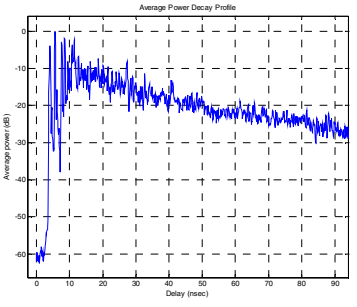

Fig. 6. PDP

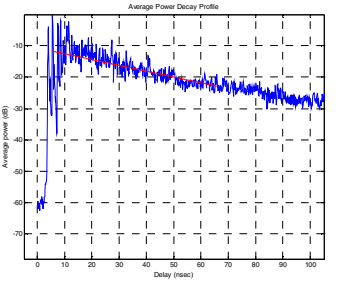

Fig. 7. Parameter Calculate

Table 3. Result of measurement

PDP calculating result:

Scene Numbers	Tx Numbers	PDP Attenuation Parameters（dB/ns）	PDP Parameters
1	1	0.1853	23.4332
	2	0.1327	32.7241
2	1	0.1406	30.8830
	2	0.1232	35.2446
3	1	0.1448	29.9952
	2	0.1806	24.0518
4	1	0.1971	22.0349
	2	0.1234	35.2033
5	1	0.1269	34.2331
	2	0.1508	28.7971
	3	0. 1869	23.2317
6	1	0.4096	10.6028
	2	0. 3176	13.6729
7	1	0. 6721	6.4619
	2	0.5434	7.9915
8	1	0. 2590	16.7708
	2	0. 3520	12.3384
	3	0. 2823	15.3854
9	1	0.3921	11.0767

4 Simulaion and Measurement Results Comparison

We use a simplified PDP predicting model [7] as the formula (2,3) below, join attenuation parameters and PDP parameters from Table 3 compare with the origin parameters.

$$PDPo = 1 \quad \tau = 0 \quad for\ n = 0 \tag{2}$$

$$PDPn = \frac{1}{4}\frac{r^n}{n^2} \quad \tau_n = \frac{t_c}{2}(2n-1) \ \ for\ n \neq 0 \tag{3}$$

The results of the comparison are shown below, we can see from the figurations that the correctional parameters are more close to the measurement data than original model parameters, which will be more conducive to PDP predict work.

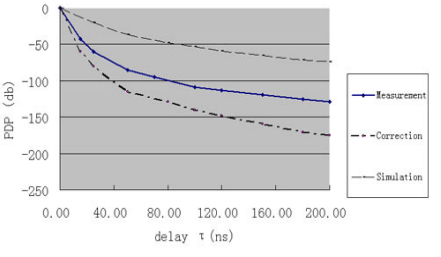

Fig. 8. PDP for Measurement and Simulation in Scene 1

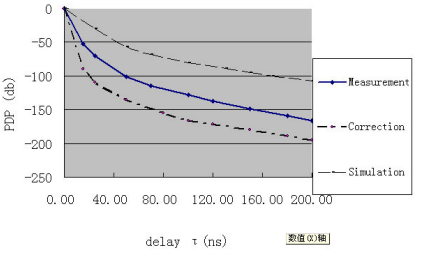

Fig. 9. PDP for Measurement and Simulation in Scene 3

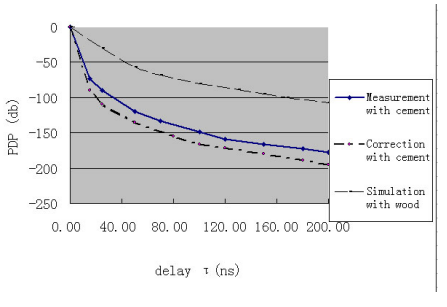

Fig. 10. PDP for Measurement and Simulation in Scene 5

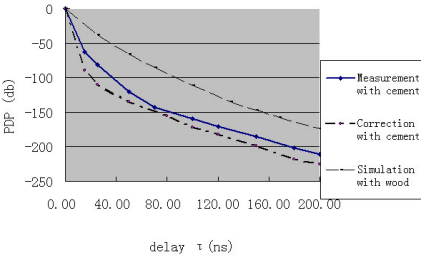

Fig. 11. PDP for Measurement and Simulation in Scene 9

5 Concluding Remarks

In this paper, indoor channel models at 2.3-10 GHz for office environments have been proposed. The proposed models involve different office areas, and both LOS and NLOS scenarios. The proposed channel models reveal important multipath effects, resulting in large path loss deviations around its mean value in many of the situations observed. Wireless devices have a strong impact, as it can be observed from the power delay profiles obtained in the office room and meeting room case. In addition, we provide experimental performance results and simulation performance results, which incorporate the proposed channel models. The match of these results further validates the proposed channel models.

Acknowledgement. In this paper, the research is sponsored by the National High-Tech R & D Program (863) of China "Research on generic technology and verification system R&D of UWB"(Nos. 2009AA011202).

References

1. Campos, D., et al.: Satellite-Indoor Mobile Communications Path Propagation Losses. In: Proceedings of the 16th IEEE International Conference on Electronics, Communications and Computers (CONIELECOMP 2006) (2006)
2. Andersen, J.B., Rappaport, T.S., Yoshida, S.: Propagation measurements and models for wireless communications channels. IEEE Communications Magazine 33(1), 42–49 (1995)
3. Damosso, E., Paraboni, A., Protto, F.: Indoor propagation measurements: Application to mobile channel modelling. CSELT Technical Reports 23(2), 173–182 (1995)
4. Phaiboon, S.: Propagation Path Loss Models for Parking Buildings. In: 2005 Fifth International Conference on Information, Communications and Signal Processing, Bangkok, pp. 1348–1351 (2005)
5. Seker, S.S., Oc, Y., Kunter, F.: Multi-components mobile propagation model of park environment. In: SIU 2010 - IEEE 18th Signal Processing and Communications Applications Conference, Diyarbakir, Turkey, pp. 320–323 (2010)
6. Motley, A.J., Keenan, J.M.M.: Personal communication radio coverage in buildings at 900mhz and 1700mhz. Electronics Letters 24(12), 763 (1988)
7. Holloway, C.L., Cotton, M.G., Mckenna, P.: A Simplified Model for Predicting the Power Delay Profile Characteristics of an Indoor Radio Propagation Channel (1998)

One Hybrid-Parallel Weighted Bit-Flipping Algorithm for Low-Density Parity-Check Codes*

Zhongxun Wang and Fangqiang Zhu

School of Opto-electronic Information Science and Technology,
Yantai University, Yantai 264005, China
ytwzx3@tom.com ,zhufangqiang1111@163.com

Abstract. In this paper, in order to reduce the performance loss due to loop oscillation in weighted bit-flipping algorithm, one hybrid-parallel WBF algorithm for low-density parity-check codes is presented. This algorithm uses one random disturbance switching to another multi-bits flipping rule by changing the target function while the loop oscillation is discovered. This will be out of the inherent errors due to loop oscillation. Simulation and complexity analysis show that this new decoding offer excellent performance with lower complexity compared with the known best kinds of bit-flipping algorithms.

Keywords: Low-density parity-check codes, decoding algorithm, loop oscillation, hybrid parallel.

1 Introduction

Low-density parity-check (LDPC) codes was first invented by Gallager in 1962 [1]and was rediscovered by the Mackay and Neal in the 20th nineties[2], which showed better performance over Turbo codes.The main decoding methods include bit-flipping decoding based on hard-decision and BP algorithm based on soft-decision, the improved algorithm (LP-WBF[3] ,MP-WBF [4]) based on these.

In this paper, a new decoding algorithm is presented. The problems of [3][4] based on loop detection is that flipping bits are changed back again after some steps, it affected the convergence speed of decoding and performance. Referred to the paper [5][6],we proposed a reduced loop-oscillation algorithm which solve the above problems well.

2 Modified Parallel Weighted Bit-Flipping Algorithm

$(N, K)LDPC$ code is completely defined by parity-check matrix H .The column weight and row weight of H are respectively expressed as w_c and w_r .Choose

* This work is supported by Shandong Province Natural Science Foundation of China (ZR2009GM026)

D. Jin and S. Lin (Eds.): Advances in Mechanical and Electronic Engineering, LNEE 177, pp. 263–268.
springerlink.com

codeword $c=(c_1,c_2,...,c_N)$, which is mapped to $x=(x_1,x_2,...,x_N)$ according to $x_i=2c_i-1$.Let assume information transmission through AWGN channel by BPSK modulation. For $0\le i<N$, $y_i=x_i+n_i$.The output of the receiver is assumed $y=(y_1,y_2,...,y_N)$ Let $z=(z_1,z_2,...,z_N)$ be the hard decision sequence vector obtained from y.

$$z_i = \mathrm{sgn}(y_i) = \begin{cases} 1, & y_i \ge 0 \\ 0, & y_i < 0 \end{cases} \tag{1}$$

We denote the set of bits which participate in the m-th check equation and the set of checks where symbol n involves respectively by:

$$\begin{aligned} N(m) &= \{n : H_{mn} = 1\} \\ M(n) &= \{m : H_{mn} = 1\} \end{aligned} \tag{2}$$

The flipping function of this algorithm: Where $l_m=\min_{n\in N(m)}|y_n|, u_m=\max_{n\in N(m)}|y_n|$.

$$E_n^{(k)} = \sum_{m\in M(n)}\left[(2s_m-1)\frac{u_m}{2}+\frac{u_m+l_m}{2}-|y_n|\right] \tag{3}$$

Let $n^{(k')}=(n_0^{(k')},n_1^{(k')},...,n_{N-1}^{(k')})$ and $n_j^{(k')}$ denotes the modulus of occurrences in the sets $D^{(k')}=(D^{(k'+1)},D^{(k'+1)},...,D^{(k)})$, where $0\le k'<k, 0\le j<N$.Let $\omega^{(k')}$ be the Hamming weight of $n^{(k')}$.For $0\le k'<k$, initial conditions are $n_j^{(k)}=1$ for $j\in D^{(k)}$; and $n_j^{(k)}=0$ for $j\notin D^{(k)}$.

$$n_j^{(k')} = \begin{cases} n_j^{(k'+1)} \oplus 1, & j = D^{(k')} \\ n_j^{(k'+1)}, & j \ne D^{(k')} \end{cases} \tag{4}$$

For $1\le k'<k$ $w^{(k')}=w^{(k'+1)}+p^{(k')}-2num(n_j^{(k')}=0,n_j^{(k'+1)}=1)$ Where $num(n_j^{(k')}=0,n_j^{(k'+1)}=1)$ expressing the number of $n_j^{(k')}=0,n_j^{(k'+1)}=1$ for the j bits position. The modified parallel weighted bit-flipping algorithm (MP-WBF) based on loop detection is as follows: Set iteration counter $k=0$, for $0\le m<M$, compute $u_m/2,(u_m+l_m)/2$.

Step 1: Compute syndrome vector $s^{(k)}$, If $s^{(k)}=0$,stop the decoding and return $s^{(k)}=0$.Otherwise, compute $P=\lfloor \omega_H(s^{(k)})/w_c \rfloor$, $\lfloor x \rfloor$ indicates that the largest integer is not more than x.

Step 2: $k \leftarrow k+1$, If $k > k_{\max}$ stop decoding. $k_{\max}$ is the maximum number of iterations.

Step 3: For $0 \le n < N$, compute $E_n^{(k)}$.

Step 4: Find out the p larger value in $E_n^{(k)}$ corresponded to set of bit $D^{(k)} = (j_1^{(k)}, j_2^{(k)}, ..., j_p^{(k)})$ $0 \le j_1^{(k)} < j_2^{(k)} < ... < j_p^{(k)} < N$.

Step 5: calculate $n^{(k')}$ and $\omega^{(k')}$.If $\omega^{(k')} = 0$,set $p \leftarrow p-1$ and return step4.

Step 6: Turn bit positions $z^{(k-1)}$ corresponded in $D^{(k)}$,get $z^{(k)}$ and return step1.

There is a problem: when $\omega^{(k')} = 0$, there will be the loops and execute $p \leftarrow p-1$. The corrected bits will be more likely again flipped, so it maybe generate error decoding within a limited iteration numbers. This will influence the convergence speed before reaching the maximum number of iterations.

3 The New Proposed Algorithm (NP-WBF algorithm)

To solve the above problem, we propose a new algorithm which is called hybrid weighted bit flipping decoding algorithm (referred to NP-WBF).we adopt one random disturbance switching to another multi-bits flipping rule, so it is out of the inherent error. NP-WBF as follows:

New symbols are as follows: λ_n is the flipped-accumulated value of variable node n, F_{th} is the flipped-threshold value, $\bmod e$ is the flipped-model.

Initialization: Set iteration counter $k = 0$, $\bmod e = 0$,for $0 \le m < M$, compute z^0, p^0, l_{mn}, $u_m / 2$, $(u_m + l_m)/2$.

Step 1: Compute syndrome vector $s^{(k)}$,If $s^{(k)} = 0$,stop decoding and return $z^{(k)}$.

Step 2: $k \leftarrow k+1$, If $k > k_{\max}$, stop decoding. If $\bmod e = 1$,turn step 6

Step 3: For $0 \le n < N$, compute $E_n^{(k)}$ and p.Find out the p larger value in $E_n^{(k)}$ corresponded to set of bit $D^{(k)} = (j_1^{(k)}, j_2^{(k)}, ..., j_p^{(k)})$ $0 \le j_1^{(k)} < j_2^{(k)} < ... < j_p^{(k)} < N$.

Step 4: calculate $n^{(k')}$ and $\omega^{(k')}$.If for any k', $\omega^{(k')} = 0$,set $\bmod e = 1$

Step 5: Turn bit positions $z^{(k-1)}$ corresponded in $D^{(k)}$, get $z^{(k)}$ and return step1.

Step 6: Compute syndrome vector $s^{(k)}$, and record the check node which is not satisfied check equation $u_m = \{ m \mid s_m = 1, 0 \le m < M \}$.

Step 7: calculate $EN_n^{(k)}$ .For any $m \in u_m$, Establish $n' = \arg\max_{n \in N_m} EN_n^{(k)}$, $\lambda_{n'} \leftarrow \lambda_{n'} + 1$, $F^{(k)} = \{ n \mid \lambda_n \ge F_{th}, 0 \le n < N, \}$,and flip all bits in $F^{(k)}$,set $\lambda_n \leftarrow 0$,return step 1. $EN_n^{(k)}$ can calculate in formula(5)

$$EN_n^{(k)} = \sum_{m \in M(n)} (2s_m - 1) l_{mn} - \alpha \mid y_n \mid \tag{5}$$

4 Simulation and Complexity Analysis

In this section we compares NP-WBF algorithm with the LP-WBF,MP-WBF and BP algorithms. The simulations use finite geometry $(1023,781)LDPC$ codes $w_c = 32$, where the computing of weighted factor α is in [4].We set $\alpha = 1.8$, $F_{th} = 10$, and the maximum number of iterations 40.

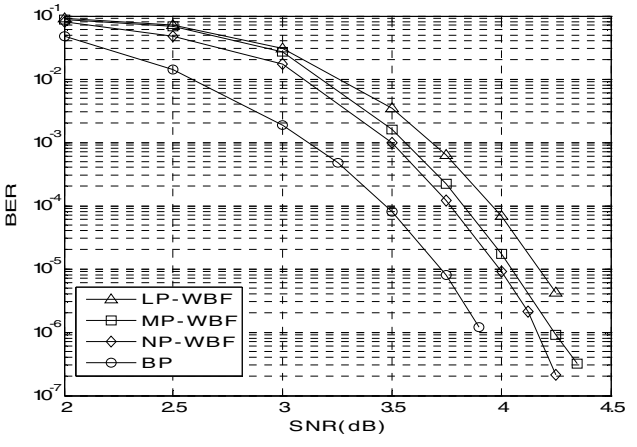

Fig. 1. BER performances of $(1023,781)LDPC$ codes in different algorithm

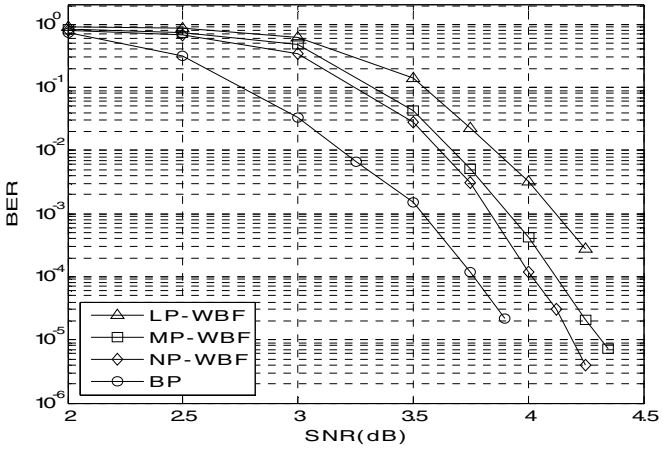

Fig. 2. FER performances of $(1023,781)LDPC$ codes in different algorithms

Fig 1 shows that ,at the BER of 10^{-6}, NP-WBF algorithm gets the gain of about 0.15 dB over M-PWBF algorithm. At the same time, it is only 0.35 dB worse than the BP algorithm. Fig 2 shows that when the FER is 10^{-5}, NP-WBF algorithm gets the gain of about 0.15 dB over M-PWBF algorithm .We select the frame 100000, Table 1 gave the statistics of convergence and FER performance at SNR=4.0 dB. When the frames falling into loop are similar, the percentage of correctly decoded frames into loop based on MP_WBF and NP_WBF is respectively 35.63% and 70.56%.

Table 1. The statistics of convergence and FER performance

Decoding algorithms	The average Num of iterations	The frames In loop	Correctly decoded frames in loop	Incorrectly decoded frames before kmax	The-percentage Of-correctly decoded-frames in loop/(%)
LP_WBF	29.432	13156	5122	917	38.93
MP_WBF	6.571	1698	605	124	35.63
NP_WBF	4.978	1678	1184	36	70.56
BP	2.1778	——	——	12	——

5 Conclusion

In this paper, NP_WBF algorithm belongs to the bit-flipping algorithms. Simulation shows that this algorithm is well for finite geometry codes, it can get coding gain about 0.15 dB over M-PWBF algorithm, the percentage of correctly decoded frames in loop increased to 70.56% with respect to M-PWBF can be only 35.63%.

References

1. Gallager, R.G.: Low -Density Parity -Check Codes. IRE Trans. Information Theory, 8 (1962)
2. MacKay, D.J.C.: Good error correcting codes based on very sparse matrices. IEEE Trans. on Inform Theory 45(2), 399–431 (1999)
3. Shan, M., Zhao, C.M., Jiang, M.: Improved Weighted Bit-flipping Algorithm for Decoding LDPC Codes. IEEE Communication 12(6), 919–923 (2005)
4. Jiang, M., Chun Ming, Z., Chen, Y.: An Improvement on the Modified Weighted Bit-flipping Decoding Algorithm for LDPC Codes 9(9), 814–817 (2005)
5. Liu, B., Gao, J., Dou, G.Q.: Hybrid weighted Bit-flipping Decoding Algorithm for LDPC Codes. Systems Engineering and Electronics 10(32), 2256–2259 (2010)

Labview-Based Design and Realization of Virtual Oscilloscope

Lixiao Zhang, Xin Li, and Yanshuang Li

Automation Department, Xiamen University, Xiamen, China, 36100
{zhanglixiao6733,wutongyu9345}@126.com,
liyanshuang0923@163.com

Abstract. Oscilloscope is an electronic measuring instrument which is used in production practice and scientific research widely. Ordinary oscilloscope have heavy exterior and single function, and we can't measure the signal amplitude and frequency characteristics accurately. This article uses the method of programming LabVIEW to design virtual oscilloscope. The virtual oscilloscope realized the real-time data acquisition, waveform display, and measuring parameters and other functions. Its various performance indicators are much better than that of a traditional oscilloscope.

Keywords: Virtual Instrument, Oscilloscope, LabVIEW.

1 Introduction

Oscilloscope is mainly used for observing the input and output signal waveform. The function and the structure of traditional instruments are fixed and users can't change their structure and function. Digital oscilloscopes have some functions of expansion, but the price and the cost of maintenance is high, it is difficult to popular in short time.

Along with the the development of electronic technology, computer technology, and information processing technology, there appears a new type of instrument based on computer and software virtual instrument. Virtual instruments are to make full use of strong graphic interface and data processing ability of computer to analyze and display the measurement data[1]. This paper developed a virtual oscilloscope based on the graphical programming language LabVIEW, which is the abbreviation of Laboratory Virtual Instrument Workbench.

The virtual oscilloscope is mainly composed of parameter measurement, spectrum analysis, and waveform display modules. It is mainly to realize waveform display, measuring parameters, and real-time collection and other functions. It has friendly interface, strong expansion and reliable dynamic characteristics and many other advantages.

1.1 The Structure of Virtual Instrument

The virtual instrument comprises a hardware platform and a software platform, the hardware platform completes the signal conditioning of a signal to be tested and the signal acquasition, the software platform completes the functions such as pretreatment, parameter measurement, waveform display and spectrum analysis and so on.

D. Jin and S. Lin (Eds.): Advances in Mechanical and Electronic Engineering, LNEE 177, pp. 269–274.
springerlink.com

The structure of virtual instrument is as the structure of traditional instrument, it is made up of the data acquisition, analysis of control data, and processing results show three parts. As for traditional instruments, three parts are almost completed by hardware. For virtual instrument, the last two parts are mainly realized by software. Compared with the traditional instruments, virtual instrument involved in the workload and complexity are greatly reduced. The structural diagram of the virtual instrument is shown in Fig.1.

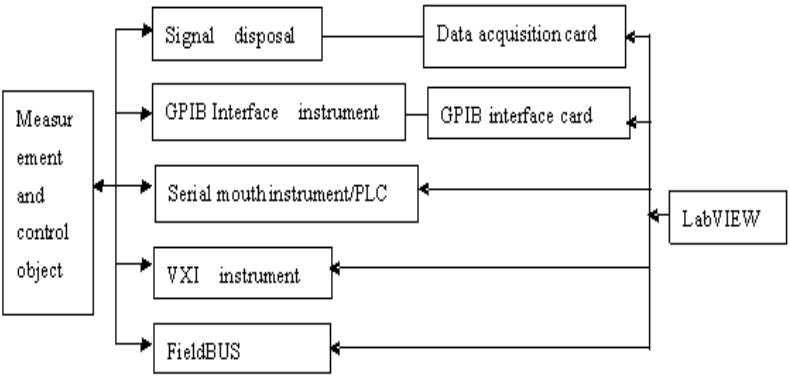

Fig. 1. Virtual instrument structure schematic drawing

A virtual instrument hardware platform includes two parts:

1) Computer: various types of computer are mainly used to manage the software and hardware resources of virtual instrument, it is the foundation of making the virtual instrument hardware.

2) An input/output interface equipment: is mainly used to complete the collection of signal measurement, amplification and D/A transformation. We can use different interface hardware equipment according to the actual condition.

A virtual instrument software has two parts:

1) An input/output interface drivers: is mainly used to accomplish the expanding, driving and communication of certain external hardware equipment.

2) Application software: is based on instrument driver, and directly faces the operation users. It completes testing tasks by providing friendly interface and rich data analysis.

1.2 The Introduction of Software Development Tools

Application software development environment is the software tools of designing. Application environment development environment need to provide users with a friendly interface and powerful application[2]. Software plays an important part in virtual instrument, it has been used to analyze data processing , such as digital filter, spectrum exchange, etc.

Usually, there are two ways in building virtual instrument software: one is the traditional programming methods, which uses advanced language, such as VC++ and

C++ Builder[3]. The other kind is to use popular graphical programming methods, such as LabVIEW of the NI company.

In short, as a graphical programming language environment, LabVIEW provides a fast, convenient and powerful software tool for virtual instrument development.

2 The Design of the Virtual Oscilloscope

Virtual oscilloscope are composed of hardware equipment, device driver software and virtual instrument panels. Hardware equipment includes instrument interface equipment and computer. Device driver software is driver, which directly controls all kinds of hardware interface[4]. Virtual instrument communicate through device driver software and real instrument system. In this paper, we developed a signal generator using software, the signal generator can produce two groups of signal. According to the need, we set up frequency and amplitude of the signal in the front panel and input a good signal to the oscilloscope, then adjust the control panel to observe the running situation of the oscilloscope.

2.1 Design for the Front Panel of Oscilloscope

The front panel is used to set the input value and observe the output value. Because virtual panel faces to users directly, the front panel is the core of the virtual oscilloscope[5]. So, the main consideration is interface aesthetics and simple operation in designing this part. Users can control the virtual oscilloscope through the various button and switch on the panel.

According to the functions of panel key of the traditional oscilloscope, we put display, the control key of channel selection, the control key of level and vertical gain and the control key of trigger options and switch on the designed panel by using the control template of LabVIEW. The realization of the front panel of virtual oscilloscope is shown in Fig.2.

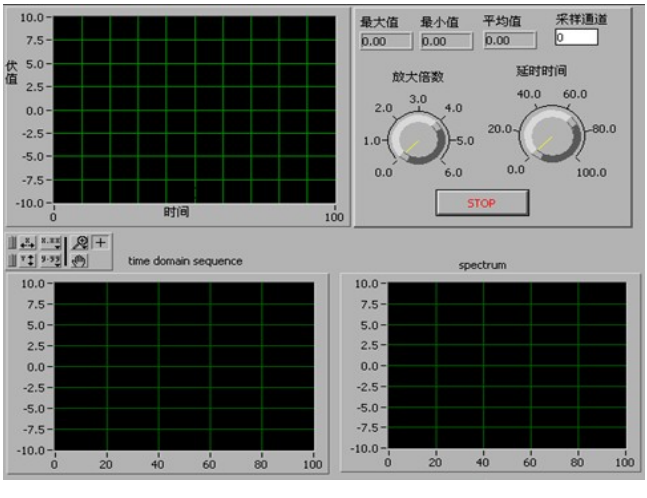

Fig. 2. The realization of the front panel of virtual oscilloscope

The front panel is used to display measurements and processing results, and users can also simulate the traditional equipment operation through the switch and button. We realized the control of the virtual oscilloscope through the keyboard and mouse. In Fig.2, the upper of the front panel is used to display acquisition of the waveform, the lower part is used to analyze the spectrum of the waveform.

2.2 Design for the Block Diagram of Virtual Oscilloscope

The front panel of each program is corresponding to a block diagram. We can carry out the design of the block diagram after the design of the front panel. Open *Windows >> Show Diagram* in the designing environment of LabVIEW, and enter the edit window of the flow chart. The port icon corresponding the control key of front panel automatically appears in the edit window of flowchart[6]. We placed each functional template in the panel flowchart by using the function of LabVIEW and the effect of control keys on the front panel of virtual oscilloscope. The block diagram of real-time waveform display is shown in Fig.3.

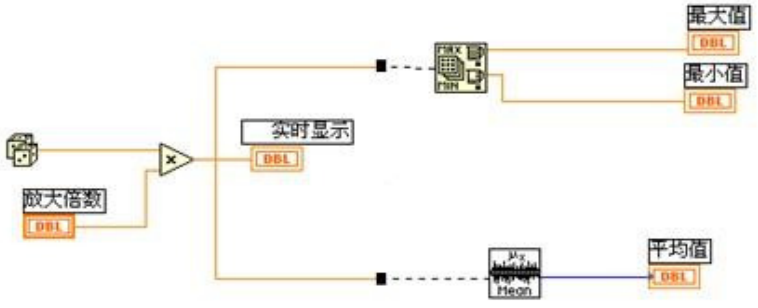

Fig. 3. The block diagram of real-time waveform display

3 The Realization of Virtual Oscilloscope

(1) We produced sine wave by signal generator, and used A/D transformation interface card PCL-812 PG to realize signal collection, so it can display in the hypothesized oscilloscope[7]. Fig.4 is to show waveform: we can choose magnification knob through the mouse, at this time, magnification is 2, so it is 2 times as the actual wave. Maximum, minimum, and average will have corresponding digital display. Because the choice of mouse is not accurate, so the maximum and the minimum display is not the number 2, it has certain error.

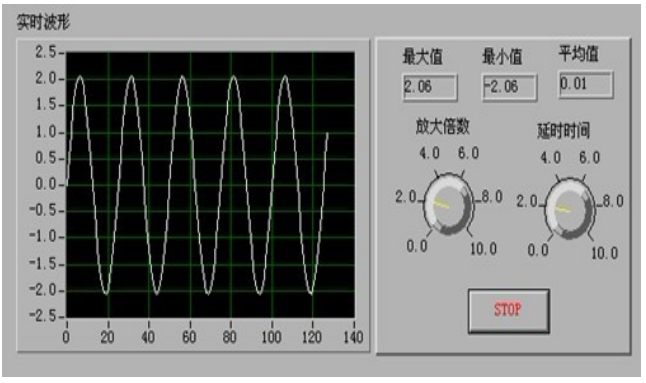

Fig. 4. Waveform after setting magnification

(2) The sampling signal getting from the board of DAQ is time signal. Get *N* sampling signal from DAQ board, the results will still *N* samples for this *N* samples after DAT transform, but it is the frequency domain representation[8].

Hypothesis the rate of signal sampling is fs, sampling interval is *t*, *t = 1 / fs*, sampling signal is expressed *Xi*, *0 < I < N-1* (*N* samples), the formula of Fourier transform is as follows:

$$X_k = X_1 * e^{(-j2*3.1415926*0\div N)} + X_2 * e^{(-j2*3.1415926*1\div N)} + \cdots\cdots Xi * e^{[-j2*3.1415926*(N-1)\div N]} \quad (1)$$

Pay attention to the *N* samples of time domain and frequency domain, at the same time, time intervals of time domain corresponding frequency is *f*, *f* is also called frequency resolution, increase the number of sampling *N* or decrease the sampling frequency *fs* can reduce *f* (improve the frequency resolution)[9].

Usually, what we need is the waveform display of frequency domain. We can get the waveform display of frequency domain by using the Fast Fourier Transform, if we choose the frequency of the waveform is 0.04, the waveform of time domain and frequency domain is shown in Fig.5.

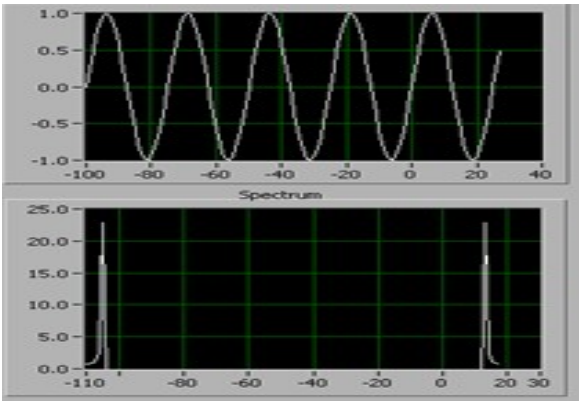

Fig. 5. Waveform of time domain and frequency domain

4 Summary

This article implemented the designing of the front panel and program diagram of virtual oscilloscope through the graphical programming language LabVIEW, including the simple processing of waveform. Compared with the traditional oscilloscope, the advantages of the virtual oscilloscope are as follows:

(1) Waveform can be stored and read.
(2) The measurement has high accuracy.
(3) Waveform is even, stable.
(4) Has the function of spectrum and filter.
(5) Capital investment is less.
(6) Can improve the performance of the instrument through upgrading hardware.

References

1. Jian, W.: Based on data collection and analysis of LabVIEW system development. Harbin Institute of Technology University, Harbin (2004)
2. National Instruments Corporation. Function and VI Reference Manual (1998)
3. National Instruments. LabVIEW User Manua. U.S.A (1996)
4. Liu, J.: LabVIEW virtual instrument design based on. Electronic Industry Press, Beijing (2003)
5. Yang, L., Xiao, X.: LabVIEW program design and application. Electronic Industry Press, Beijing (2001)
6. Naiguo, Z.: New electronic oscilloscope. China Metrology Press, Beijing (1990)
7. Yang, L., Li, H., Yang, L.: c3053. LabVIEW program design and application, 2nd edn. Electronic Industry Press, Beijing (2007)
8. Lu, L., Yao, J.: Virtual instrument overview. Electronic Technology (1), 44–47 (2000)
9. Data Acquisition Basic Manual.National Instruments Corporation (January 1998)

Multirate and Fast Parallel Implementation of 2-D DST-Kernel-Based Real-Valued Discrete Gabor Transform

JuanJuan Gu[1] and Liang Tao[2,*]

[1] Department of Electronic Engineering, Hefei University, Hefei, Anhui 230601, China
gujj@hfuu.edu.cn
[2] School of Computer Science and Technology, Anhui University, Hefei, Anhui 230039, China
taoliang@ahu.edu.cn

Abstract. A fast algorithm for the multirate and parallel implementation of the 2-D DST-kernel-based real-valued discrete Gabor transform (RDGT) is presented. Based on the multirate signal processing, a 2-D analysis convolver bank is designed for the 2-D RDGT. Each of the parallel channels in the convolver bank has a unified structure and can apply the 2-D fast discrete sine transform (DST) algorithm to reduce its computational load. The computational complexity of each parallel channel is very low and is independent of the oversampling rate. All the RDGT coefficients are computed in parallel during the analysis process. Thus, the proposed parallel algorithm is attractive for real time image processing.

Keywords: Real-valued discrete Gabor transform, Discrete sine transform (DST), Multirate.

1 Introduction

The Gabor transform has been recognized as being useful for image compression, texture analysis, image segmentation, and image recognition [1, 2]. However, the real-time applications of the Gabor transform encounter difficulties due to the complexity in the computation of the transform coefficients. Consequently, a number of approaches have been proposed to solve the problem [2]-[4], but each of those methods for computing the 2-D Gabor transform involves complex operations. Complex-valued Gabor transforms are complicated to be implemented in software or hardware. For real-valued images, real-valued discrete Gabor transform (RDGT) permits a computationally faster implementation. To overcome this deficiency, a 2-D DST-kernel-based RDGT is developed and one of the advantages of the RDGT is that it can utilize the fast DST algorithm for fast computation. To compute the 2-D RDGT even faster, in this paper, a multirate and DST-based fast parallel algorithm for the 2-D RDGT is presented. In terms of the similarity between the 2-D multirate-based analysis filterbank and the 2-D RDGT, a 2-D analysis convolver bank will be designed for the 2-D RDGT. Each of the parallel channels in the convolver bank has a unified structure and can apply the 2-D fast DST algorithm to reduce its

* Corresponding author.

D. Jin and S. Lin (Eds.): Advances in Mechanical and Electronic Engineering, LNEE 177, pp. 275–280.
springerlink.com

computational load. The computational complexity of each parallel channel of the convolver bank is independent of the oversampling rate. All the RDGT coefficients are computed in parallel during the analysis process. Thus, the proposed parallel algorithm is attractive for real time image processing.

2 2-D DST-Kernel-Based RDGT

Suppose a discrete image $I[x,y]$, x=0, 1, · · ·, X–1, y=0, 1, · · ·, Y–1, is partitioned into $\overline{K} \times \overline{L}$ nonoverlapping block matrices of dimensions $M \times N$ such that $X = K\overline{M}$ and $Y = L\overline{N}$. (K, L) and (M, N) are the numbers of 2-D Gabor sampling points in spatial and frequency domains, respectively. ($\overline{K}$, $\overline{L}$) and ($\overline{M}$, $\overline{N}$) are the 2-D Gabor frequency and spatial sampling intervals, respectively. The image $I[x,y]$ can be expressed by a real expansion form:

$$\begin{aligned} I[x,y] = & \sum_{k=0}^{K-1}\sum_{l=0}^{L-1}\sum_{m=0}^{M-1}\sum_{n=0}^{N-1} a[k,l,m,n]\, h[x-k\overline{M},\, y-l\overline{N}] \\ & \cdot d_m \sqrt{\frac{2}{M}} \sin\left\{\frac{\pi[\mathrm{mod}(x,M)+1/2]\mathrm{mod}(m,M)}{M}\right\} \\ & \cdot d_n \sqrt{\frac{2}{N}} \sin\left\{\frac{\pi[\mathrm{mod}(y,N)+1/2]\mathrm{mod}(n,N)}{N}\right\} \end{aligned} \tag{1}$$

where

$$d_m = \begin{cases} \sqrt{0.5} & m = 0, M \\ 1 & m = 1,2,\cdots,M-1 \end{cases} \quad \text{and} \quad d_n = \begin{cases} \sqrt{0.5} & n = 0, N \\ 1 & n = 1,2,\cdots,N-1 \end{cases}, \tag{2}$$

and the modulo operator mod(k,N) is defined to be the remainder when k is divided by N. The coefficients $a[k,l,m,n]$ can be obtained by

$$\begin{aligned} a[k,l,m,n] = & \sum_{x=0}^{X-1}\sum_{y=0}^{Y-1} I[x,y]\cdot\gamma[x-k\overline{M}, y-l\overline{N}] \\ & \cdot d_m \sqrt{\frac{2}{M}} \sin\left\{\frac{\pi[\mathrm{mod}(x,M)+1/2]\mathrm{mod}(m,M)}{M}\right\} \\ & \cdot d_n \sqrt{\frac{2}{N}} \sin\left\{\frac{\pi[\mathrm{mod}(y,N)+1/2]\mathrm{mod}(n,N)}{N}\right\}. \end{aligned} \tag{3}$$

Equation (3) is called as the 2-D DST-kernel-based RDGT and Equation (1) is called as its inverse RDGT. The RDGT is called DST-based because both (1) and (3) contain the 2-D DST kernel. The condition $KM \geq X$ and $LN \geq Y$ must be satisfied for a stable reconstruction. The critical sampling occurs when $\overline{K}\,\overline{M} = KM = X$ and $\overline{L}\,\overline{N} = LN = Y$, and the oversampling occurs when $KM > X$ and $LN > Y$. The RDGT coefficients

$a[k,l,m,n]$ are periodic in k, l, m, n, with periods K, L, M, N, respectively; and the synthesis window $h[x, y]$ or the analysis window $\gamma[x, y]$ is also real and periodic in both x and y, with periods X, Y, respectively. The biorthogonality relationship between $h[x,y]$ and $\gamma[x, y]$ is equivalent to the completeness condition of the 2-D DST-kernel-based RDGT, which takes the following form:

$$\begin{aligned}&\sum_{x=0}^{X-1}\sum_{y=0}^{Y-1} h[x+kM, y+lN]\ \gamma[x, y]\\ &\quad\cdot d_m\sqrt{\frac{2}{\overline{M}}}\sin\left\{\frac{\pi[\mathrm{mod}(x,\overline{M})+1/2]\mathrm{mod}(m,\overline{M})}{\overline{M}}\right\}\\ &\quad\cdot d_n\sqrt{\frac{2}{\overline{N}}}\sin\left\{\frac{\pi[\mathrm{mod}(y,\overline{N})+1/2]\mathrm{mod}(n,\overline{N})}{\overline{N}}\right\}\\ &=\sqrt{\overline{M}\,\overline{N}}\,\delta[k]\delta[l]\delta[m]\delta[n],\end{aligned} \tag{4}$$

where

$$0\le k\le \overline{K}-1,\ \ 0\le l\le \overline{L}-1,\ \ 0\le m\le \overline{M}-1,\ \ 0\le n\le \overline{N}-1.$$

3 DST-Kernel-Based RDGT Implemented by Convolver Bank

Because the computation of the RDGT coefficients of an image is similar to the analysis process of a 2-D analysis filterbank, we can design a 2-D analysis convolver bank for the multirate and parallel implementation of the DST-kernel-based RDGT. Let $I(x_c,y_c)$ denote a continuous and periodic image. After sampled uniformly with a sampling interval $(\Delta_{x1}, \Delta_{y1})$, $I(x_c,y_c)$ becomes a discrete image $I(x\Delta_{x1}, y\Delta_{y1})$, i.e, $I[x,y]$ with a period (X,Y). Rewrite (3) as follows:

$$\begin{aligned}A_{m,n}(k\Delta_{x2},l\Delta_{y2})=&\sum_{x=0}^{X-1}\sum_{y=0}^{Y-1} I(x\Delta_{x1}, y\Delta_{y1})\cdot\gamma([x-k\overline{M}]\Delta_{x1},[y-l\overline{N}]\Delta_{y1})\\ &\cdot d_m\sqrt{\frac{2}{M}}\sin\left\{\frac{\pi[\mathrm{mod}(x,M)+1/2]\mathrm{mod}(m,M)}{M}\right\}\\ &\cdot d_n\sqrt{\frac{2}{N}}\sin\left\{\frac{\pi[\mathrm{mod}(y,N)+1/2]\mathrm{mod}(n,N)}{N}\right\}\end{aligned} \tag{5}$$

where $\gamma[x-k\overline{M}, y-l\overline{N}]$ in (3) is rewritten as $\gamma([x-k\overline{M}]\Delta_{x1},[y-l\overline{N}]\Delta_{y1})$, $a[k,l,m,n]$ in (3) is rewritten as $A_{m,n}(k\Delta_{x2},l\Delta_{y2})$, $\Delta_{x2}=M\Delta_{x1}$, $\Delta_{y2}=N\Delta_{y1}$. Suppose that the oversampling rate $\beta=N/\overline{N}=M/\overline{M}$ is taken as an integer, $x=r_xM-\rho_x-1$, $y=r_yN-\rho_y-1$, $r_x=1,2,\cdots,\overline{K}$, $r_y=1,2,\cdots,\overline{L}$, $\rho_x=0,1,\cdots,M-1$, $\rho_y=0,1,\cdots,N-1$, and then (5) can be rewritten as

$$
\begin{aligned}
&A_{m,n}(k\Delta_{x2}, l\Delta_{y2}) \\
&\quad = \sum_{r_x=1}^{\overline{K}} \sum_{r_y=1}^{\overline{L}} \sum_{\rho_x=0}^{M-1} \sum_{\rho_y=0}^{N-1} I([r_x M - \rho_x - 1]\Delta_{x1}, [r_y N - \rho_y - 1]\Delta_{y1}) \\
&\qquad \cdot \gamma([r_x M - \rho_x - 1 - k\overline{M}]\Delta_{x1}, [r_y N - \rho_y - 1 - l\overline{N}]\Delta_{y1}) \\
&\qquad \cdot d_m \sqrt{\frac{2}{M}} \sin\left\{\frac{[(M-\rho_x-1)+1/2]m\pi}{M}\right\} \cdot d_n \sqrt{\frac{2}{N}} \sin\left\{\frac{[(N-\rho_y-1)+1/2]n\pi}{N}\right\}.
\end{aligned} \tag{6}
$$

Let $k = i_x + j_x\beta$, $l = i_y + j_y\beta$, $i_x, i_y = 0, 1, \cdots, \beta - 1$, $j_x = 0, 1, \cdots, \overline{K} - 1$, $j_y = 0, 1, \cdots, \overline{L} - 1$, the above equation becomes

$$
\begin{aligned}
&A_{m,n}([i_x + j_x\beta]\Delta_{x2}, [i_y + j_y\beta]\Delta_{y2}) \\
&\quad = \sum_{r_x=1}^{\overline{K}} \sum_{r_y=1}^{\overline{L}} \sum_{\rho_x=0}^{M-1} \sum_{\rho_y=0}^{N-1} I([r_x M - \rho_x - 1]\Delta_{x1}, [r_y N - \rho_y - 1]\Delta_{y1}) \\
&\qquad \cdot \gamma([r_x M - \rho_x - 1 - i_x\overline{M} - j_x M]\Delta_{x1}, [r_y N - \rho_y - 1 - i_y\overline{N} - j_y N]\Delta_{y1}) \\
&\qquad \cdot d_m \sqrt{\frac{2}{M}} \sin\left\{\frac{[(M-\rho_x-1)+1/2]m\pi}{M}\right\} \cdot d_n \sqrt{\frac{2}{N}} \sin\left\{\frac{[(N-\rho_y-1)+1/2]n\pi}{N}\right\}.
\end{aligned} \tag{7}
$$

Again let

$$
I_{\rho_x,\rho_y}(r_x\Delta_{x2},\ r_y\Delta_{y2}) = I([r_x M - \rho_x - 1]\Delta_{x1},\ \ [r_y N - \rho_y - 1]\Delta_{y1}), \tag{8}
$$

$$
\begin{aligned}
&g_{\rho_x,\rho_y}^{i_x,i_y}([j_x - r_x]\Delta_{x2}, [j_y - r_y]\Delta_{y2}) \\
&\quad = \gamma([r_x M - \rho_x - 1 - i_x\overline{M} - j_x M]\Delta_{x1},\ [r_y N - \rho_y - 1 - i_y\overline{N} - j_y N]\Delta_{y1}) \\
&\quad = \gamma([-(j_x - r_x)M - \rho_x - 1 - i_x\overline{M}]\Delta_{x1}, [-(j_y - r_y)N - \rho_y - 1 - i_y\overline{N}]\Delta_{y1})
\end{aligned} \tag{9}
$$

and then (7) becomes

$$
\begin{aligned}
&A_{m,n}([i_x + j_x\beta]\Delta_{x2}, [i_y + j_y\beta]\Delta_{y2}) \\
&\quad = \sum_{\rho_x=0}^{M-1} \sum_{\rho_y=0}^{N-1} \left[\sum_{r_x=1}^{\overline{K}} \sum_{r_y=1}^{\overline{L}} I_{\rho_x,\rho_y}(r_x\Delta_{x2},\ r_y\Delta_{y2})\ g_{\rho_x,\rho_y}^{i_x,i_y}([j_x - r_x]\Delta_{x2}, [j_y - r_y]\Delta_{y2}) \right] \\
&\qquad \cdot d_m \sqrt{\frac{2}{M}} \sin\left\{\frac{[(M-\rho_x-1)+1/2]m\pi}{M}\right\} \cdot d_n \sqrt{\frac{2}{N}} \sin\left\{\frac{[(N-\rho_y-1)+1/2]n\pi}{N}\right\}.
\end{aligned} \tag{10}
$$

Suppose

$$
u_{\rho_x,\rho_y}^{i_x,i_y}(j_x\Delta_{x2},\ \ j_y\Delta_{y2}) = \sum_{r_x=1}^{\overline{K}} \sum_{r_y=1}^{\overline{L}} I_{\rho_x,\rho_y}(r_x\Delta_{x2},\ r_y\Delta_{y2})\ g_{\rho_x,\rho_y}^{i_x,i_y}([j_x - r_x]\Delta_{x2}, [j_y - r_y]\Delta_{y2}) \tag{11}
$$

Let $\rho_x = M - q_x - 1$, $q_x = 0, 1, \cdots, M - 1$, $\rho_y = N - q_y - 1$, $q_y = 0, 1, \cdots, N - 1$, and then (10) becomes

$$A_{m,n}([i_x + j_x\beta]\Delta_{x2},[i_y + j_y\beta]\Delta_{y2}) = \sum_{q_x=0}^{M-1}\sum_{q_y=0}^{N-1} u_{M-q_x-1,N-q_y-1}^{i_x,i_y}(j_x\Delta_{x2},\quad j_y\Delta_{y2}) \cdot d_m\sqrt{\frac{2}{M}}\sin\left\{\frac{[q_x+1/2]m\pi}{M}\right\}\cdot d_n\sqrt{\frac{2}{N}}\sin\left\{\frac{[q_y+1/2]n\pi}{N}\right\}. \tag{12}$$

We can see from (12) that the RDGT coefficients $A_{m,n}([i_x + j_x\beta]\Delta_{x2},[i_y + j_y\beta]\Delta_{y2})$ can be obtained by taking an (M×N)-point fast 2-D discrete sine transform ((M×N)-point fast 2-D DST) of $u_{\rho_x,\rho_y}^{i_x,i_y}(j_x\Delta_{x2},\quad j_y\Delta_{y2})$ in the reverse order of (ρ_x, ρ_y). In terms of the above analysis process, a 2-D analysis convolver bank can be designed for the 2-D RDGT as shown in Fig.1, where the outputs of the analysis convolver bank are just the RDGT coefficients,

$$a[k,l,m,n] = A_{m,n}(k\Delta_{x2},l\Delta_{y2}) = A_{m,n}([i_x + j_x\beta]\Delta_{x2},[i_y + j_y\beta]\Delta_{y2}).$$

We see from (9) that the analysis function $\gamma(x\Delta_{x1},y\Delta_{y1})$ of the RDGT has the following relationship with the unit pulse responses $g_{\rho_x,\rho_y}^{i_x,i_y}(j_x\Delta_{x2},j_y\Delta_{y2})$ of the analysis convolver bank:

$$g_{m,n}^{i_x,i_y}(j_x\Delta_{x2},j_y\Delta_{y2}) = \gamma([-j_xM-m-1-i_x\overline{M}]\Delta_{x1},[-j_yN-n-1-i_y\overline{N}]\Delta_{y1}). \tag{13}$$

Note that $g_{m,n}^{i_x,i_y}(j_x\Delta_{x2},j_y\Delta_{y2})$ is periodic in (j_x, j_y) with a period ($\overline{K}$, $\overline{L}$) due to the periodicity of $\gamma(x\Delta_{x1},y\Delta_{y1})$.

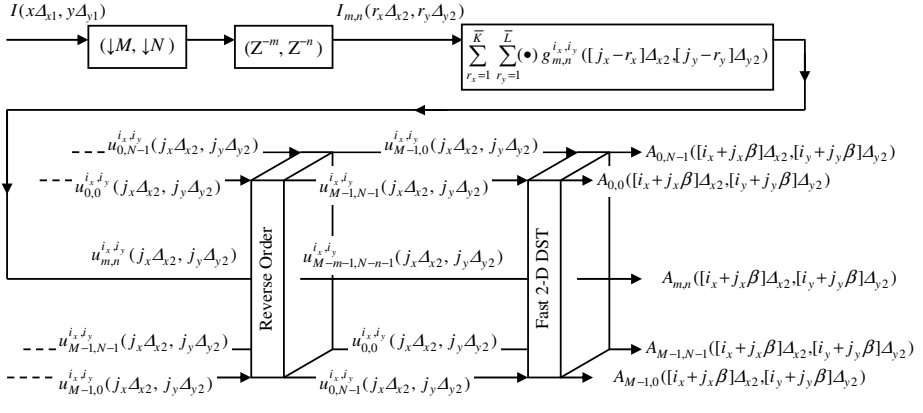

Fig. 1. 2-D analysis convolver bank designed for 2-D DST-kernel-based RDGT

3 Conclusion

This paper presented the novel and fast parallel algorithm for the multirate and parallel implementation of the 2-D DST-kernel-based RDGT. We designed a 2-D analysis convolver bank for the fast implementation of the 2-D RDGT. Each of the parallel channels in the convolver bank has a unified structure and can apply the fast 2-D DST algorithm to reduce its computational load. The computational complexity of each parallel channel of the convolver bank depends only on the size XY of the discrete input image and the number ($M \times N$) of the Gabor frequency sampling points, and is independent of the oversampling rate β. In fact, the bigger the oversampling rate β, the larger the parallel scale of the convolver bank. Therefore, the proposed parallel algorithm is very efficient and fast in computing the 2-D RDGT coefficients. Note that the proposed method can be also generalized to the reconstruction of the original image from the RDGT coefficients.

Acknowledgments. The authors would like to acknowledge the supports of the National Natural Science Foundation of China under Grant No. 61071169, the Key Project of the Natural Science Research in Anhui Provincial Higher Education Institutions under Grant No. KJ2010A290, and the Science Research Foundation of Hefei University under Grant No. 10RC01.

References

1. Gabor, D.: Theory of communication. J. Inst. Electr. Eng. 93, 429–457 (1946)
2. Daugman, J.: Complete discrete 2-D Gabor transform by neural networks for image analysis and compression. IEEE Trans. on Acoust, Speech, Signal Processing 36, 1169–1179 (1988)
3. Wang, L., Chen, C.-T., Lin, W.-C.: An efficient algorithm to compute the complete set of discrete Gabor coefficients. IEEE Trans. on Image Processing 3, 87–92 (1994)
4. Havlicek, J.P., Bovik, A.C., et al.: AM-FM Image modeling and Gabor analysis. In: Chen, C.W., Zhang, Y. (eds.) Visual Information Representation, Communication, and Image Processing. Optical Engineering Series, pp. 343–385. Marcel Dekker, Inc., New York (1999)

Distributed Collaborative Traceback Model against DDoS in Network Confrontation Based on Electronic Technology

Rong Luo, Junshan Li, and Lihui Sun

Xi'an Research Inst. of Hi-tech,
Hongqing Town
710025 Xi'an, China
db_workshop@163.com

Abstract. In order to effective tracing DDoS attacks in network confrontation, the autonomous system was regarded as a security unit in this paper. It constructed the distributed collaborative traceback model against DDoS based on the mobile agent technology and the deterministic packet marking method. It provides both domain tracking and remote tracking. Domain tracking applied the mobile agent technology to trace the attack path. Remote tracking used DPM method to directly reconstruct entrance address of the attack source. It provides a new scheme to solve the DDoS tracing problem in network confrontation.

Keywords: Distributed Denial-of-Service (DDoS), collaborative traceback, mobile agent, deterministic packet marking (DPM), electronic technology.

1 Introduction

In many of network attacks of network confrontation, DDoS attacks as the basic tactics of network warfare, is the most common, the most threatening, but also the most difficult to prevent. Attack source tracing technology is an important part of the defense process against DDoS attack. In the network confrontation, it will gain the upper hand with reasonable application of tracking technology. In this paper, regarding the autonomous system (AS) as a security unit, the distributed collaborative traceback model against DDoS is constructed based on the mobile agent technology and the deterministic packet marking method, which provides a new scheme for rapidly and effectively track attack sources in the network confrontation.

2 Basic Structure of the Distributed Collaborative Traceback Model against DDoS

The distributed collaborative defense model against DDoS is built on the network topology of multi-AS, which includes two defense nodes: the border defense node (BDN) and the domain defense node (DDN). The BDN which resides a monitor agent

D. Jin and S. Lin (Eds.): Advances in Mechanical and Electronic Engineering, LNEE 177, pp. 281–286.
springerlink.com

and an action agent, is responsible for the AS boundary critical node (router or key host). It mainly achieve network data collection, network security state monitoring and take corresponding defense measures. The DDN is responsible for any switching router or key host in the domain. There is one DDN that resides a decision agent in the AS within a certain time. Once the monitor agent discovered attack, the decision agent will activate action agents to defend.

In the distributed collaborative traceback model against DDoS, the AS which attacks are from is the source AS, and the AS which victim hosts are in is the destination AS, and all the AS between the source AS and the destination AS are the intermediate AS. All outside attacks come to the destination AS through border routers, and all inside attacks come to victim hosts through their access routers. Therefore, DDoS tracing will be divided into two kinds, one is domain tracking, the other is remote tracking. If the attacker comes from this domain, the decision agent will distribute a tracking agent to the access router of the victim host. The tracking agent will trace back in the domain until find the attacks entrance. If the attacker comes from the outside, the router will mark packets, and then the packets' initial marking address will be reconstructed.

3 Domain Tracing Scheme Based on Mobile Agent

3.1 Design of Trace Agent

Domain tracking is implemented through mobile agent technology. Based on the mobile agent components defined by Cubalesba [1][2], the domain-tracking agent of the traceback model is defined as follows.

$$T\_Agent = (M\_Agent, D\_Agent, GN, Result, p, vn, reply) \tag{1}$$

M_Agent is a mobile Agent, and its basic definition is as follows.

$$M\_Agent = (ID, DN, BC, LT, States) \tag{2}$$

ID is the legal identifier that can uniquely identify a mobile agent to ensure key nodes will accept it. *DN* is used to store the defense node information that generated the mobile agent, including its name, address, or digital signatures. *BC* is the binary code of a mobile agent. *LT* is lifetime of a mobile agent. *States* is used to record the current state of a mobile agent.

D_Agent is a detection agent carrying by the trace agent for detecting attacks. *GN* is the destination node distributed by the trace agent. *Result* is the result that trace agent completed the task. *p* is the migration path that trace agent will traverse, contains all nodes required access to. *vn* contains nodes that trace agent has visited on the attack path. When a node receives a trace agent, it will send *reply* to ensure the trace agent has reached the node.

3.2 Tracking Process

If the attacker is from the domain, the decision agent will first distribute an action agent to the key node nearest to the victim host. This key node will be a defense node, and the action agent will activate a domain-tracing agent to track.

Let *VDN* be the defense node of the victim host, and there are three adjacent switching nodes (R_1, R_2, R_3). The tracing process is as follows.

Step 1. *VDN* distributes detection agents to the adjacent nodes to detect whether they are under attack.

Step 2. If *VDN* receives an attacked reply from one node, it will generate a trace agent (T_Agent_0) and sent to the node (let it be R_1).

Step 3. After waiting some time, *VDN* has not received a confirmation back from one node, and then considered the node has been under attack and does not work. *VDN* will distribute detection agents to the node's adjacent nodes based on network topology.

Step 4. After R_1 received T_Agent_0, it distributes detection agents to its adjacent nodes (R_{11}, R_{12}, R_{13}) to detect whether they are under attack.

Step 5. If T_Agent_0 receives the attack response of a node (R_{12}), R_1 will be added to *vn*, and *GN* will be assigned. Then T_Agent_0 becomes T_Agent_1 through gaining this new information. R_1 will distribute T_Agent_1 to the next attacked node R_{12}.

Step 6. And so on, R_{12} will repeat the work of R_1. Until all of its adjacent nodes except been traversed have not been attacked, the node is the entrance of the attacker in the domain.

Step 7. Domain trace agent will inform decision agent to take measures to the node.

4 AS-level Remote Tracking Based on DPM Algorithm

The distributed collaborative traceback model against DDoS of network confrontation is suitable for deterministic packet marking algorithm(DPM)[3][4]. Each boundary router of the AS domain are border defense nodes, and they can mark each packet entering the AS. Therefore, in this paper DPM is applied to mark packets in border routers in order to get the initial marking entrance address of attack packets. Thereby we will get attacks source rapidly and accurately, and win opportunity of network confrontation.

4.1 Marking Information

In network confrontation, AS is a safety unit of the distributed collaborative traceback model against DDoS. Therefore, the marking information is not IP address of the edge router, but the AS number (ASN) and the entrance router number (ERN). ASN is currently a 16-bit integer, and ERN is a 12-bit hash value generated by 32-bit IP address of the border defense node.

It is the key of tracking DDoS attacks to trace back attacks ingress routers. There are two kinds of attacks ingress routers. One is the attack ingress router of the source AS, which is the entrance address of the first station that attack packets enter the network. The other is the attack ingress router of the destination AS, which is the

entrance address of the first station that attack packets enter the destination AS. With the aid of the DPM, the two attack entrance router addresses will be direct accessed in the distributed collaborative traceback model of network confrontation. Thus, the marking information needed includes three parts: ERN of the source AS (12 bits), the source AS number (16 bits) and ERN of the destination AS (12 bits), which is 40 bits in a total.

Based on literature analysis, marking fields in this paper as shown in Figure 1, includes ID field (16 bits), RF field (1 bit), offset field (13 bits) and TOS field (8 bits), which is 38 bits in a total. The RF field is a marked bit. If RF is 0, the packet is not marked, and if RF is 1, the packet has been marked. Address information is stored in ID field and the first 12 bits of offset field. The last bit of offset field is a flag bit that can identify the packet come from. If EF is 0, the packet is from the inside; if EF is 1, the packet is from the outside. The message authentication code (MAC) of marking information is stored in the TOS field.

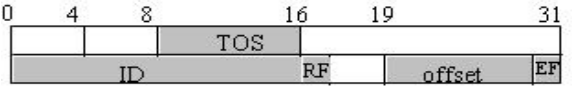

Fig. 1. Marking fields

4.2 Basic Idea

In DDoS co-tracing model, it is assumed that at least the border router of the destination AS have packet marking function. The basic idea of remote tracking is as follows.

When the attacker sent DDoS attack packets from the source AS, if border routers of the source AS are configured with packet marking, each attack packet will be first marked with the address information of the source AS and the border router. When attack packets are not marked, if there is an intermediate AS whose border routers are configured with packet marking, the packet will be first marked with the address information of the intermediate AS and the border router. When the attack packet reaches the border router of the destination AS, if it has been marked, it will be marked again. If it has not been marked, it will be first marked with the address information of the border router. When attack packets arrive at the victim host, the victim host will read the marked information to reconstruct the address information. The address information may be three types.

i) The source ASN and ERN of the source AS. It is the most ideal situation. Decision agent will inform the source AS' decision agent of the address and attack feature, in order to collaborative trace and defense.

ii) The intermediate ASN and ERN of the intermediate AS. Decision agent will inform the intermediate AS' decision agent of the address and attack feature, in order to collaborative trace and defense.

iii) ERN of the destination AS. Decision agent will inform all of the intermediate AS connected to the router.

4.3 Marking Operational Process

There are two phases of packet marking in remote tracking of the distributed collaborative traceback model against DDoS. In the first stage, packets are marked as close as possible to source entrance. In the second stage, packets are marked at the entrance of the destination AS. In this way, the attack entrance address of the destination AS is at least marked, if all router configuration is complete, the attack entrance of the source AS can be traced directly. The specific operation process is shown in figure 2.

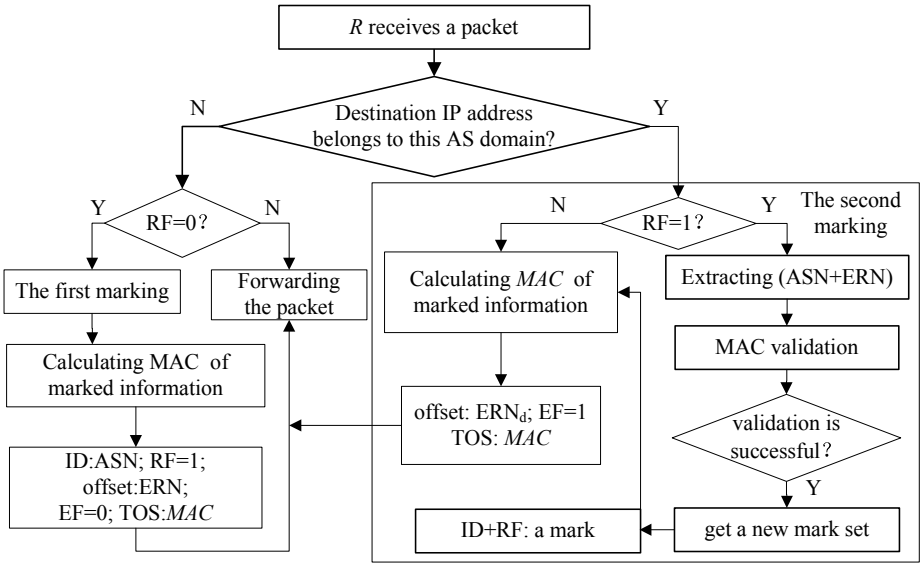

Fig. 2. Marking flow

Step 1. When a border router receives a packet, it will first determine whether the packet's destination IP address belongs to this AS. If it is, this AS is the destination AS, then goes to *Step*4; if not, this AS is the source AS or the intermediate AS, then goes to *Step*2.

Step 2. If RF is 0, the packet is not marked for the first time, and then goes to *Step*3 for the first marking, or the packet has been marked for the first time, then the router forwards the packet directly.

Step 3. The packet is first marked, then the packet is forwarded. The marked content includes: ID field is entered ASN of the domain (16 bits), offset field is credited to ERN of the domain (12 bits), EF is set to 0, RF is set to 1, and TOS field is recorded MAC of marked information.

Step 4. If the RF is 0, the packet is not marked for the first time, and then goes to *Step*9; otherwise, the packet has been marked for the first time.

Step 5. The information of ID field and the first 12 bits of offset field, which is extracted from the packet, combined into the address information of the first mark, that is ASN and ERN.

Step 6. First determines the packet transmission time, and then computes the MAC to MAC validation. If the validation is successful, the marked information is correct, and then goes to *Step*7; otherwise it is forged, and discarded.

Step 7. Using DPM-RD algorithm [5], the first marked address information (ASN + ERN) is compression transformed to get a new mark set.

Step 8. For each packet whose address selected is ASN and ERN, the router will randomly insert a mark with the same probability.

Step 9. The number of this border entrance router (ERN_d) is recorded in the offset field. EF is set to 1, which indicates that the attack packet is from the outside. The MAC of marked information is calculated and written to the TOS field, then the packet is forwarded.

5 Summary

In this paper, the distributed collaborative traceback model against DDoS, considering AS as a security unit, provides both domain tracking and remote tracking. When domain tracking is implemented in the destination AS, the mobile agent technology has been applied to trace the attack path. In the remote tracking, DPM method is used to directly reconstruct the ERN of the destination AS, the source ASN and its ERN, which is as close as possible to the attack source entrance. It is both direct and simple. Once the attack entrance address is obtained, AS decision agents will be able to complete the tracing and defense work through cooperation each other, also can maintain the privacy of AS.

References

1. Cubaleska, B., Schneider, M.: Detecting Dos attacks in mobile agent systems and using trust policies for their prevention. In: The 6th World Multi Conference on Systemics, Cybernetics and Informatics SCI (2002)
2. Tao, L.-M.: Integrated model for defending against DDoS attacks based on mobile Agent. Computer Engineering and Applications 44, 147–150 (2008)
3. Belenky, A., Ansari, N.: IP Traceback with Deterministic Packet Marking. IEEE Communication Letters 7(4), 162–164 (2003)
4. Belenky, A., Ansari, N.: On Deterministic Packet Marking. Computer Networks 51(10), 2677–2700 (2007)
5. Jin, G., Yang, J.: Deterministic Packet Marking based on Redundant Decomposition for IP Traceback. IEEE Communications Letters 10, 204–206 (2006)

DAC7615 Application in Embedded Controller for Adjusting Exhaust Throttle

Zhigang Lv and Peng Wang

School of Electronics and Information Engineering, Xi'an Technological University, Jinhua North Road, Xi'an, Shaanxi, China
gangji780807@sina.com

Abstract. During electrolyzing aluminum, in order to make blower run safely and energy-saving, opening degree of exhaust throttle is controlled according to blower's current, air temperature and other parameters, from which the efficiency of gasping air is developed. PXA270, a kind of ARM10 controller, equipped with DAC7615 which is a DA converter of 12 digits, is designed to control the two exhaust throttles. Based on hardware design of DAC7615, drive program and test program in Linux are introduced. From explaining the detailed code, general principle and concrete progress of developing driving program in embedded design was revealed.

Keywords: DAC7615, ARM10, Driving Program, Linux, Exhaust Throttle.

1 Introduction

During electrolyzing aluminum, embedded controller for exhausting smoke, based on the ARM10 controller of PAX270, controls the opening degree of exhaust throttle according to blower's current, blower's temperature, air's temperature and other parameters. If opening degree is too small, air out is limited. And a large quantity of smoke will be left into the factory. If it is too big, more energy is lost and a lot of dust will be thrown out. If the control voltage on exhaust throttle is 0V, the opening degree is 0°. If it is 2.5V, the opening degree is 180°.

According to above requirement, DAC7615 is chosen in the embedded controller to control two blowers. As a kind of device, the driving program for DAC7615 should be designed, or it can't work in Linux [1-2]. The performance of driving program will decide the total control precision of controller, which is common problem for embedded system design.

2 DAC7615

The DAC7615 is a quad, serial input, 12-bit, voltage output digital-to-analog converter (DAC) with guaranteed 12-bit monotonic performance. The device can be powered from a single +5V supply or from dual +5V and –5V supplies. It provides two output channels ranging from 0 V to +2.5 V or from -2.5 V to +2.5 V. DAC7615 is available in 16-led SOIC package. The function of every pin is given as the following [3].

D. Jin and S. Lin (Eds.): Advances in Mechanical and Electronic Engineering, LNEE 177, pp. 287–292.
springerlink.com

VOUTA~VOUTD: DAC A~D voltage output channel.
CS: Chip select input.
CLK: Serial data clock.
VDD: Positive analog supply voltage, +5V nominal.
VSS: Negative analog supply voltage, 0V or -5V nominal.
GND: Ground.
VREFL: Reference input voltage low. Set minimum output voltage for all DACs.
VREFH: Reference input voltage high. Set maximum output voltage for all DACs.
SDI: Serial data input.
LOADDACS: All DAC registers become transparent when it is low.
LOADREG: The selected input register becomes transparent when it is low.
RESET: Asynchronous reset input.
RESETSEL: When it is low, a low on RESET will cause the DAC and input registers to be set to code 000H. When it is high, a low on RESET will set the registers to code 8000H.

The hardware design for DAC7615 is very easy. RESET, LOADDACS, CS, CLK, SDI and LOADREG is connected to gpio19, gpio87, gpio86, gpio16, gpio17, gpio84 of PXA270 respectively. VOUTA and VOUTB is designed to control two exhaust throttles. VREFL is connected to ground and VREFH is connected to +2.5V, which is given as Fig.1.

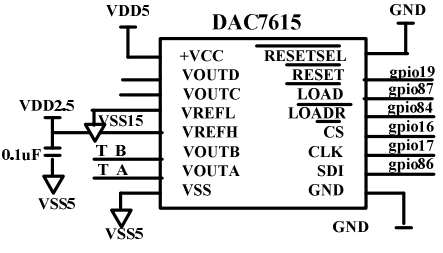

Fig. 1. Hardware design for DAC7615

3 Driving Program Design

The driving program of DAC7615 should be designed in the embedded system, which will be managed and executed by kernel as a kind of device node. DAC7615 belongs to serial DA converter. Consequently, the above pins of PXA270 should be controlled to simulate timing diagram of DAC7615 as the Fig.2.

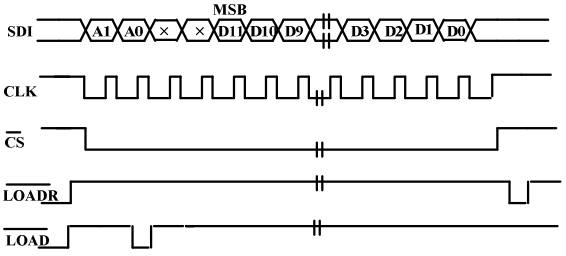

Fig. 2. DAC7615 Timing

From Fig.2, CS should be set low during converting. 16-bit data should be output from SDI at the positive edge of CLK. Among the 16-bit data, the front two bits decide the output channel of DAC7615 (00-Channel A 01-Channel B 10-Channel C 11-Channel D). The next two bits are invalid. The other 12 bits are the real data which is needed to convert.

For kernel, DAC7615 is a kind of chart device, which is named as "DAC7615drv". DAC7615 device is loaded into kernel by "insmod" command and unloaded by "rmmod" command [4-5]. In fact, the driving program of DAC7615 is separated into four functions. That is register-function, unregister-function, initializing-function and output-function.

When "insmod" command is used to load DAC7615 device, the following function is executed:

```
int __init DAC7615_init(void)
{
      misc_register(&misc_dac7615);//register DAC7615 device
}
```

When "rmmod" command is used to unload DAC7615 device, the following function is executed:

```
void __exit DAC7615_exit(void)
{
      misc_deregister(&misc_dac7615);//unregister DAC7615 device
}
```

When "open" function is used to open DAC7615 device, the following function following function is executed, in which initialization of pins is finished. Take RESET for example.

```
#define DAC7615_RESET 1<<19   //RESET is connected to gpio19
static int DAC7615_open(struct inode * s_node,struct file * s_file)
{
    ……
    pxa_gpio_mode((DAC7615_RESET | GPIO_OUT)); //set gpio19 as output pin
    clear_gpio_bit(DAC7615_RESET); //set gpio19 low
      set_gpio_bit(DAC7615_RESET);   //set gpio19 high
    ……
}
```

When "write" function is used to write DAC7615 device, DAC7615_write function is executed, in which the convert from digital to analog is finished.

```
static int DAC7615_write(struct file *led_file, const char *buf,int len,loff_t *loff)
{
    ……//code for simulating timing diagram of DAC7615
}
```

In DAC7615_write function, program flowchart for simulating timing diagram of DAC7615 is given as Fig.3.

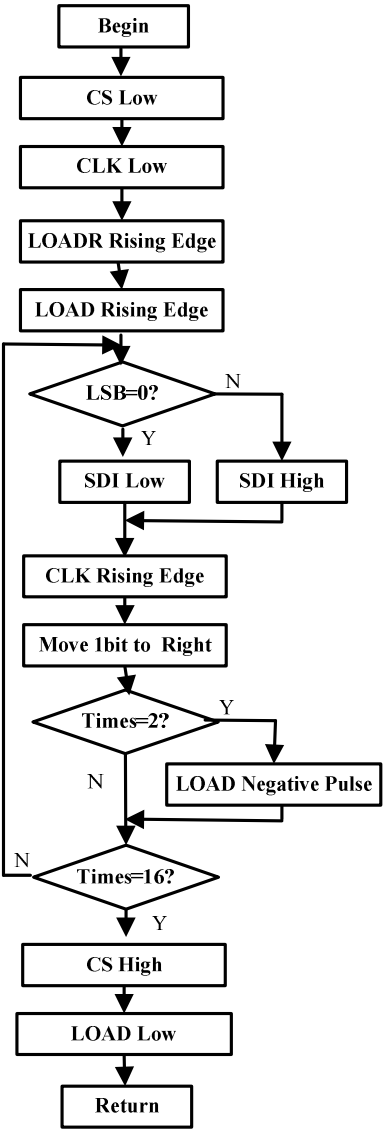

Fig. 3. Flow chart of DAC7615

4 Program Design

Every output channel of DAC7615 should be tested in testing program. For the specified data for one channel, multi-meter or oscilloscope is used to measure the real output voltage. If the real value is equal to the ideal value, which means that DAC7615 works well.

In testing program, "open" function is used to open DAC7615 device firstly [6]. DA data, increased step by step from 0 to 0xFFFh, and channel number is combined to generate a specified data which can be recognized by DAC7615. The specified data can be written into DAC7615 by "write" function. When DA data reached the max value (0xFFFh) on one channel, another channel is switched to test. The main code of testing program is given as the following.

```
int main(void)
{
  ……
  fd=open("/dev/DAC7615drv",O_RDWR); //open DAC7615 device
   while(1)
   {
     for(j=0;j<4;j++)
      {//test channel of A, B, C and D respectively
        Data=0;//the original value of DA data
        while(Data<=0xFFF)//max value of DA data is 0xFFF
        {
          fnGetDACData(j, Data,&rgcon); //DA data combined with channel No
          Data++;//DA data increase by 1
          write(fd,(char *)&rgcon,4) //finish convert operation
          delay();//delay for a while to measure the real output voltage
        }
     }
 }
```

5 Conclusions

Hardware design for DAC7615 is introduced in the paper. Based on the controller of PXA270, the driving program and testing program of DAC7615 is given in Linux, from which the common principle of embedded design is revealed. The test result shows that the maximum error between real output voltage and the real value of every channel is 0.1%, which can meet the requirement for controlling exhaust throttle.

Acknowledgement. Project Supported by the 2011 Special Funds of the Natural Science Foundation of Education Department of Shaanxi Provincial Government, China (Grant No. 11JK0896).

References

1. Viola, P., Jones, M.: International Journal of Computer Vision 57, 137–154 (2004)
2. Bradski, G., Kaebler, A.: Learning OpenCV-computervision with the OpenCV library, 3rd edn., New York, pp. 337–341 (2008)
3. Information on, http://www.ti.com/product/dac7615
4. Dalal, N., Triggs, D.: In: IEEE Conference on Computer Vision and Pattern Recognition, pp. 886–893 (2005)
5. Zhou, P., Hou, L.-G., Peng, X.-H., Chang, D.: Application of Electronic Technique 8, 30–32, 35 (2011) (in Chinese)
6. Luo, D.-H., Li, H.-G., Wang, Z.-M.: Journal of Shandong University of Technology (Natural Science Edition) 6, 98–100 (2011) (in Chinese)

An Electronic Technology Research on Architecture of P2P-CDN

Binjie Zhu, Meina Song, and Junde Song

School of Computer Science and Technology,
Beijing University of Posts and Telecommunications, Beijing, China
Zhubinjie1983@gmail.com

Abstract. With the development of electronic technology, electronic equipment interconnected to form a network. The data content access in the electronic devices is facing the problem of access speed, content distribution network is a technology used to solve this problem. The architecture of CDN is a key issue in the content distribution network research. Some researchers lead the P2P ideology into the CDN architecture to improve CDN performance. The P2P based CDN is called P2P-CDN. A new type of P2P-CDN architecture was proposed in this paper. This structure is divided into three levels: management layer, resource discovery layer and the server collaborative group layer. A simulation experiment was set up to analysis performance of this architecture. The results show that it has better performance than other architecture.

Keywords: content delivery, architecture, P2P, CDN.

1 Background and Related Work

With the development of electronic technology, electronic equipment interconnected to form a network. The data content access in the electronic devices is facing the problem of access speed, content distribution network is a technology used to solve this problem. The content delivery network architecture is a key issue in the content distribution network research. Now some researchers lead the P2P ideology into the CDN architecture to improve CDN performance [1]. The P2P based CDN is called P2P-CDN. Existing P2P- CDN architecture have three types: access based P2P-CDN, single core based P2P-CDN, peer-based P2P-CDN [4, 5].

Access-based P2P-CDN needs the users to form a P2P network as access network to share content[2]. It requires the user's participation, which is not benefit for the management and control of the whole delivery system [2]. All nodes in the peer-based P2P-CDN including resource management system are peers. It is not benefit for the management of the CDN system. Only the edge servers of the core-based P2P-CDN in the forms of peer to peer network, which can't only control the edge servers efficiently, but also share content between servers quickly, not need user participations [3].

There are some shortcomings in the core-based P2P-CDN. In the current core-based P2P-CDN, all the cache servers are peer-to-peer network. The servers of the P2P network are used to store both content objects and index table. There are some shortcomings in this architecture described as follows: First, long distance of logic

D. Jin and S. Lin (Eds.): Advances in Mechanical and Electronic Engineering, LNEE 177, pp. 293–298.
springerlink.com

layer lead the low efficiency. The index disperses in each of server, so in the processing of a hop of routing may map into a long distance in the physical layer, which increasing the delay. Secondly, the delay between servers may leading low efficiency and level in the content share. Thirdly, the structure of a server both store an index and content is unstable.

2 The Proposed Architecture

A new type of P2P-CDN architecture was proposed in this paper, shown as figure 1. This structure is divided into three levels: management layer, resource discovery layer, the server collaborative group layer.

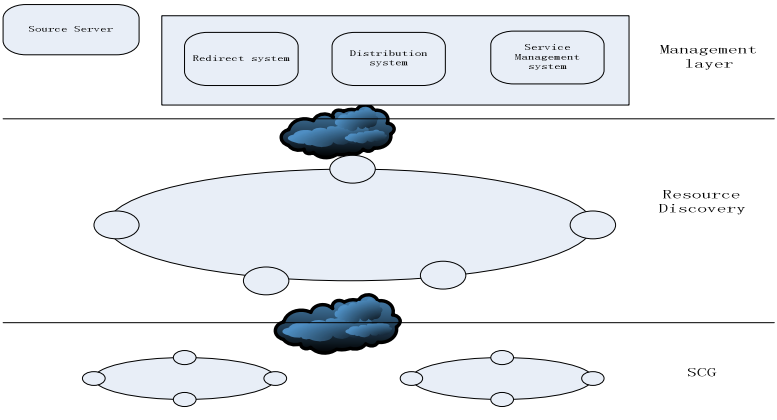

Fig. 1. The proposed architecture

The first layer is management layer, which responsible for the management of the whole CDN system. It includes content redirection subsystem, content distribution subsystem, and service quality management subsystem.

The second layer is global resource discovery layer, mainly responsible for finding the source in the global scope.

The third lay is local storage collaboration group layer, mainly responsible for the content storage, which serve for users in the local scope

We will explain the design in detail from request routing, content delivery and sharing.

2.1 Content Distribution and Sharing

CDN decrease user access delay and the bottleneck of server by distributing the content to the edge server in the network. It is a question that how to distribution the content to the edge server. A server recourse level distribution and sharing mechanism was designed in our architecture, which is called S-PUL, shown as figure 2.

Distribution and sharing mechanism is quite relative with architecture. In order to accomplish the collaboration in the server level, we proposed server collaboration group based on the P2P network. In the deployment stage, we judge whether add tracker node or not by measuring the distance, which must under a certain limit. If it lager than the limit, a new tracker node would be added into the network. The distance is the radius of server collaboration group.

In the server recourse level collaboration, when a server receives a content request, if none in the local server, it routes the request to the server which has the corresponded content in the group by local routing algorithm. The distance between the tracker node to each of the server is less than. So the distance between two servers is under controller and less than 2. Thus , by control the in the deployment stage to satisfy the need to the quality of collaboration in the group .

To achieve the share in the server level, we proposed server collaboration group (SCG). The content delivery pattern in the whole CDN system is based on SCG.

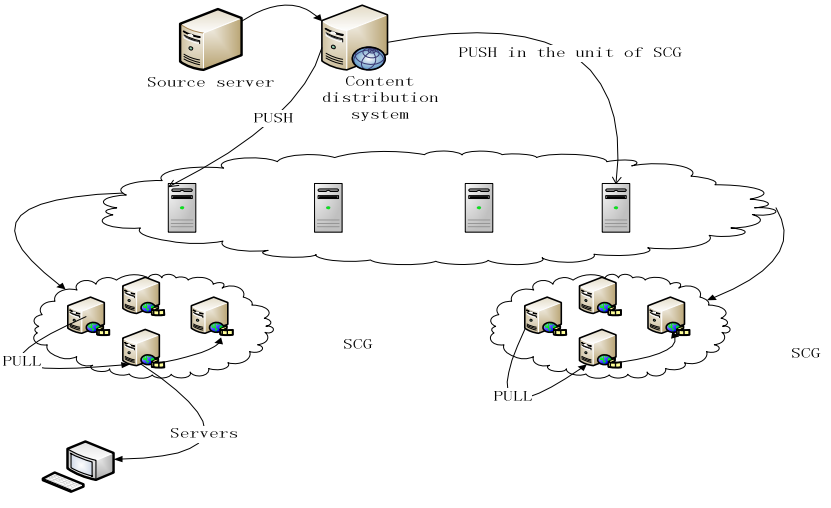

Fig. 2. Distribution and sharing mechanism

The push pattern of S-PUL is in unit of SCG. SCG as a caching collaboration group, inside the SCG is the content share pattern is pull and cache.

In this delivery pattern, active parts include CDN management server layer, SCG server group and single server. It is a combination of pull and push. This pattern share content in the server level based on SCG in order to achieve server recourse level sharing. Traditionally collaboration is in content level, but this pattern is in server level, benefit for sharing server recourse.

2.2 The Content Request Routing

The process redirects user’ s requests to the server that containing the required contents called content request routing. In the process of content request routing, if the selected server does not has the required content, it is necessary to propose a certain method to lookup the request content. The content object should be moved to the local server after finding out the required contents, so the local server can meet the user request. In such case, the process of searching resource is called resource discovery.

In this system, we proposed a content routing and searching mechanism with double layer DHT architecture, dividing the request routing into global resource detecting and content routing in the local caching group, shown as figure 3.

This system is divided into two layers: global resource discovery layer, and local routing layer. The first layer is formed by DHT-tracker. These DHT index servers are responsible for finding out the resource in global scope. The second layer is responsible for the local scope. All the nodes are equal in the storage collaboration group and each node includes functions such as content index and content storage service.

Each content object stores into the server, the system would generate a index pair at the same time, which would make up the index table and separate these index pairs into each server node by Hash function. Meanwhile, in the global layer, it would generate index pairs that take group as unit, and combine these index pair into index table. It also would separate these index pairs into each server node by some certain method.

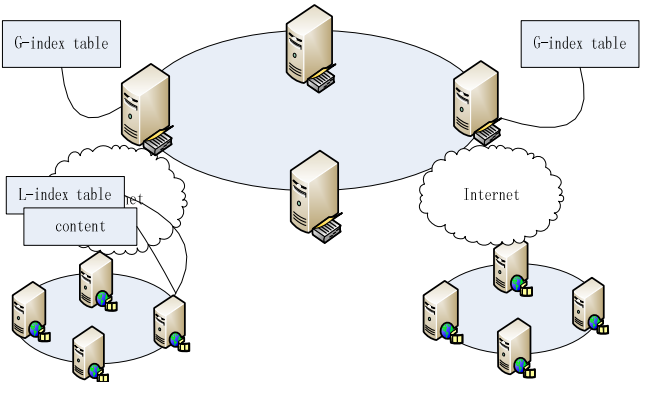

Fig. 3. The two layer DHT request routing system

The process for routing is as follows:

Step 1: Redirect the request to the nearest server.
Step 2: Find out whether the server contains the required content, if not, go to next step.

Step 3: Local routing and lookup the content, if not meet the request, go to step 4.
Step 4: Global resource discovery.
Step 5: Find out the SCG contains the required content.

3 Compared Analysis

Start delay is defined as the time from a user making a content request to the time that users start getting data. Start delay and the local hit rate in the single-layer core architecture related to the case of a local hit, the user access to services from the local server, so start delay is the redirected time and server to the user's time .

$$Sd_h = T_{Rd} + T_{SC} \tag{1}$$

If it is misses then it will start to find and pull the content to the local server. Therefore, the overall delay plus the global find time and pull time.

$$Sd_{Nh} = T_{Rd} + T_{S1} + T_P + T_{SC} \tag{2}$$

Hit rate is R_H, the average start-up delay is Sd_a.

$$Sd_a = Sd_h \cdot R_H + Sd_{Nh} \cdot (1 - R_H) \tag{3}$$

In the double-core architecture, start delay is not only related to a local hit but also the group hit. In local hit case, the user access to services from the local server. Startup delay is Dd_h.

$$Dd_h = T_{Rd} + T_{SC} \tag{4}$$

If the cases of the other servers in the group have the request content, known as the group hit. Content request was routing to the server that has the content through the local content routing system. Start delay including local content routing time T_{LR}.

$$Dd_{Nh1} = T_{Rd} + T_{LR} + T_{SC} \tag{5}$$

If group misses to find the requested content in the global scope and pull to the local group. In this case the start delay including global content discovery T_S and pull time T_P.

$$Dd_{Nh2} = T_{Rd} + T_{S2} + T_P + T_{SC} \tag{6}$$

The local hits rate R_H, the group hit rate is R_{Hg} ,the average start-up delay is Dd_a.

$$Dd_a = Sd_h \cdot R_H + Dd_{Nh1} \cdot (R_{Hg} - R_H) + \quad Dd_{Nh2} \cdot (1 - R_{Hg}) \tag{7}$$

In the case of a local hit, the startup delay in both architectures has no difference. So $Sd_h = Dd_h$. In the case of misses in the local but hit the group, the routing time is less than the global search time and pull time, $T_{LR} < T_S + T_P$, so $Dd_{Nh1} < Sd_{Nh}$. In the case of group not hit, $T_{S2} + T_P < T_{S1} + T_P$, so $Sd_a < Dd_a$.

The simulation result as figure 4. A1is the single-core base P2P-CDN, and A2 is the architecture designed in this paper. From the figure we can see that the start delay of two-layer-core P2P-CDN is lower.

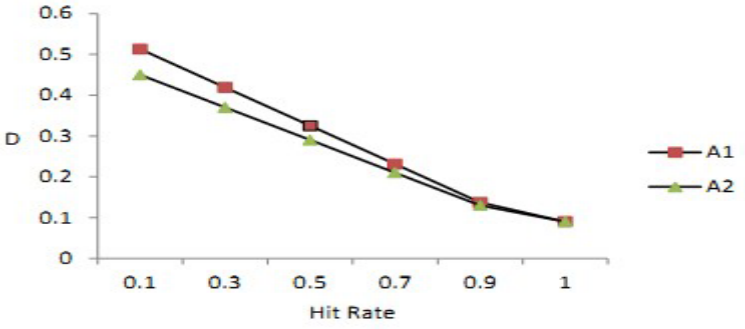

Fig. 4. The simulation results

Acknowledgments. This work is supported by the National Key project of Scientific and Technical Supporting Programs of China (Grant Nos.2008BAH24B04, 2008BAH21B03, 2009BAH39B03), the National Natural Science Foundation of China(Grant No.61072060), the Program for New Century Excellent Talents in University (No.NECET-08-0738), Engineering Research Center of Information Networks. Ministry of Education.

References

1. Sheu, S.-T., Huang, C.-H.: Mixed P2P-CDN System for Media Streaming in Mobile Environment. In: 2011 7th International on Wireless Communications and Mobile Computing Conference (IWCMC), July 4-8, pp. 657–660 (2011)
2. Jernberg, J., et al.: DOH: A Content Delivery Peer-to-Peer Network. In: European Conference on Parallel Computing, Germany, pp. 1026–1039 (2006)
3. Pakkala, D., Koivukoski, A., Paaso, T., Latvakoski, J.: P2P Middleware for Extending the Reach, Scale and Functionality of Content Delivery Networks. In: Pakkala, D. (ed.) Second International Conference on Internet and Web Applications and Services, ICIW 2007, May 13-19 (2007)
4. Turkmen, F., Mazzoleni, P., Crispo, B., Bertino, E.: P-CDN: Extending Access Control Capabilities of P2P Systems to provide CDN Services. In: IEEE Symposium on Computers and Communications, ISCC 2008, July 6-9, pp. 480–486 (2008)
5. Kim, T.N., Jeon, S., Kim, Y.: A CDN-P2P Hybrid Architecture with Content/Location Awareness for Live Streaming Service Networks. In: 2011 IEEE 15th International Symposium on Consumer Electronics (ISCE), June 14-17, pp. 438–441 (2011)

An Enhanced AODV Protocol Based on GIS Technology Applying in Electronic Engineering Area

Wei Li[1], MingMing Li[2], and WenQing Wang[1]

[1] School of Automation, Xi'an University of Posts & Telecommunications, WeiGuo Road, Chang'an District, 710121 Xi'an, China
liwei7728@yahoo.com.cn
[2] School of Communication, Xi'an University of Science & Technology, 58# YanTa Road, YanTa District, 710054 Xi'an, China
limmwork@yahoo.com.cn

Abstract. AODV is the most commonly used protocol in the Wireless Sensor Networks (WSN) of electronic engineering. because its performance is the best among all the Ad-Hoc improved protocols. But Ad-Hoc based protocols don't consider the limited energy characteristic of WSN, so the network life of AODV is not desirable. In order to improve the energy aware performance of AODV, this paper combined the GAF protocol with the AODV protocol and got an AODV_GAF protocol. Comparing AODV with AODV_GAF under NS2 simulator, the result shows the network life of AODV_GAF is at least 4 times of AODV and other network performance such as network delay, throughput etc. are close. Simulate result also shows the most suitable scenarios of AODV_GAF is when the load is heavy and the nodes are densely deployed.

Keywords: AODV, GAF, Energy Aware, WSN, NS2.

1 Introduction

Most of the WSN (Wireless Sensor Network) used in the military, chemical and forest field. The condition of those fields is so bad that it is difficult or impossible to support unlimited energy. Due to the energy constrain, the energy-aware must be set as the first rule for the system design in the WSN [1].

There are many Ad-Hoc improved routing protocols such as DSDV, CGSR, TORA and AODV. International research shows AODV has the best effect under high load condition [1].This paper equipped every sensor nodes with GPS (Global Position System) device, which enable GAF (Geographical Adaptive Fidelity)[3] could be combined with AODV to get an AODV_GAF protocol. Because the redundant nodes go to sleep periodically according to GAF, the energy efficiency of AODV_GAF is much better than AODV. NS2[4] Simulator is used to compare the difference of the two protocols. By changing the simulate scene, we found that AODV_GAF suit for the nodes denser and load heavier situation.

This paper is organized as following. In Sect. 2, the AODV and GAF protocol are briefly introduced; the AODV_GAF protocol is introduced and its performance is analyzed in Sects.3; The NS2 simulator is used to compare AODV and AODV_GAF protocols under different situation in section 4; Section 5 draws the conclusions.

D. Jin and S. Lin (Eds.): Advances in Mechanical and Electronic Engineering, LNEE 177, pp. 299–305.
springerlink.com

2 Brief Introduction of AODV and GAF

1). AODV Introduction

AODV (Ad Hoc On-demand Distance Vector routing)[2] is an improved distance vector routing protocol. It has the characteristic of on demand routing protocol: the node send route packet when it need to communicate. It will not exchange information periodically to get route of other nodes. It also has the characteristic of distance vector routing protocol: a node only maintain the route to other vicinity nodes, needn't to get the topology of whole network. Three types of route packet are used in AODV: RREQ, RREP and RERR. AODV keep route request and route reply in the middle nodes, use the extend circle search mechanism to restrict the destination nodes search range and adopt sequence number technology to ensure the circle route is not produced. For detail information of AODV, please refers to literature [2].

2). GAF Introduction

GAF[3] is an energy aware algorithm based on location information. Network area was divided into virtual grid and sensor nodes equipped with GPS card to get its location information and thus related with certain virtual grid. Please look at Fig.1. In which the max signal transmit distance is R, the d is the size of the grid. Select $R=\sqrt{5}d$, ensure the sensor in one grid communicate with any sensor in other neighbor grid directly. From the communication point of view, the nodes in one grid is the same, if one node work, the communication could work normally. So the other node is redundant. Let the redundant nodes go to sleep to save power could improve network life greatly. With the nodes number increase, the network life will also increase greatly. The aware node is the leader which takes charge of report data to the sink node. Leader will exchange periodically according to specific mechanism. Please refer to literature [3] for detail.

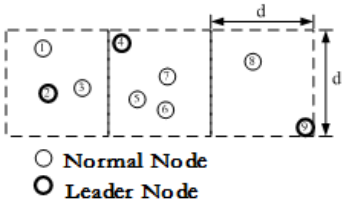

Fig. 1. GAF Grid

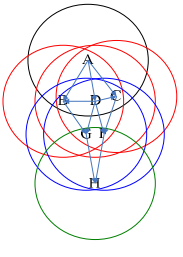

Fig. 2. AODV Route Request

3 Introduction of AODV_GAF

1). AODV Route Request Procedure Analyze

The route request packet RREQ is broadcast in AODV. Refer to Fig.2. Suppose node A need to transmit data to node H. The circle in Fig.2 is the max wireless communication range of every node. The route request procedure detailed as following: node A search its own route table to find if there is route entry to node H, if not found, A will broadcast a RREQ packet. Node B, C, D will all receive this

RREQ packet from node A. They will search their own route table to find if there is route entry to node H, if found, a RREP will send to node A, the route request will end; if not found, they will broadcast the RREQ packet. Here suppose D do not find the route entry to node H, D will broadcast the RREQ from A. and B,C,G,F,A will all receive the RREQ D broadcast. A will find that this RREQ is come from A itself, so A will discard it to avoid circle route. B and C receive it the second time and will rebroadcast it. G and F will receive the same RREQ from D,B,C, and they will broadcast it out. At last, H will receive the RREQ more than one time. H will reply a RREP to A. At the above procedure, there are more than one path exist from A to H:

(1):A->B->G->H (2):A->B->F->H (3):A->D->G->H (4):A->D->F->H
(5):A->C->G->H (6):A->C->F->H (7):A->D->B->G->H (8): A->D->B->F->H
(9):A->D->C->G->H (10): A->D->C->F->H

There probably be more, not list them out here.

2). The Disadvantage of AODV

To transmit data from node A to H need only one path, but more than one path appears in the above example, although there are only 6 nodes in total. By analyzing, we found that AODV has the following shortcomings:

(1) Because the RREQ packet is broadcasted in route request, the route packet will explode in the network.

(2) Node B, D, C will receive the RREQ packet from A at the same time and will re-broadcast it out almost at the same time, so the wireless signal conflict is unavoidable, this will lead to the result that node G can't receive the correct route request packet.

(3) More than one route path exist, it is a waste for information transmit.

(4) If one of the route paths such as A->B->G->H is selected as the data transmitting path, node C, D, F is redundant for data transmit. They do not work, so they are in idle state. Nodes in idle will expend power too. The proportion of transmit, receive, and idle power is: 1:1.05:1.4[1]. This idle power is wasted.

In short, a great deal of energy is wasted in AODV. There are so many transmit path in the above 6 nodes example. There are thousands upon thousands nodes in a real wireless sensor network, the phenomena listed above will be more serious. In essential, node B, C, D are equivalent for data transmit, node G, F are equivalent too. If we know this, we could let node D, C, F go to sleep to save idle power, and let only node B, G to work, the above problem will be solved. In this case, the RREQ transmit shows in Fig.3. The route request information explosion and the data conflict will be avoided. Furthermore, the nodes sleep power is far less than idle power, for an example based on MSP430, the idle current is 0.7mA/MHz but the sleep current is only 30uA/MHz, the proportion of sleep, idle power is:700:30, so many of the power will be saved.

3). Introduction of AODV_GAF Protocol

From the introduction to GAF in above section, we know that by equiping every node with GPS card, we could get the location of node; according to the location, the node could be related to a virtual grid; applying the state change mechanism make there is only one lead node awake and all other node sleep in one grid; so the problem

described in above could be solved. Improve AODV with GAF, we get AODV_GAF protocol.

In AODV_GAF, the node in every virtual grid change its state periodically to ensure there is only one node awake and the redundant nodes are sleep. The wake nodes transmit and receive data according to AODV protocol. To combine AODV and GAF protocol, the following measure should be taken:

(1) Because GAF protocol works in application layer and AODV works in route layer, the state change packet of GAF could be broadcast as load of route layer. So the states change of GAF does not need the route information of AODV.

(2) To ensure the AODV route table could not be lost when the leader node changed, when the leader node change, the route table in the old leader must be transmitted to new leader. This process will increase some energy spending, but avoid the new route request process. The energy spending of route table transmit from old table to new table is comparatively smaller than the new route request.

(3) The main limitation of GAF is that it does not consider the residual energy of node. The leader is elected randomly. But the reality is that the leader is responsible for the most of the data process and communication work which will consume a lot of energy. So randomly electing leader node is not reasonable. The less energy node is possible selected to be the leader and it will be invalidate quickly. This will lead the whole network invalidate quickly. To avoid change leader frequently, AODV_GAF change the leader changing mechanism. When the residual energy of current leader is less than 0.5W, the leader change procedure start and the node with most residual energy will be elected as the new leader.

(4)The Dimidiate Search Arithmetic of power selecting which is described in literature [5] is adopted to save more power in data transmitting.

(5) Suppose R is the maximum wireless signal transmitting distance, d is the size of the virtual grid. R= $\sqrt{5}d$ is selected in GAF protocol. Here we change it to R= $2\sqrt{2}d$ .So the node in one grid could communicate directly with the 8 neighbor grid.

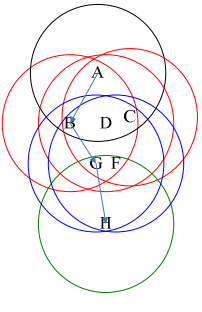

Fig. 3. Route Request when Redundant node sleep

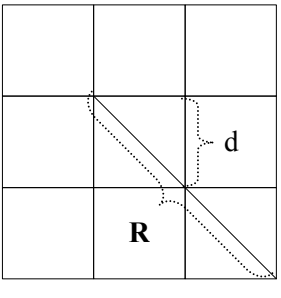

Fig. 4. The R selected in GAF

4 Simulation Result

The NS2[4] is used for simulation to validate AODV and AODV_GAF. It is presumed that there are N nodes distributed on a square of 1400×1400 meters, and the persistent time of a scenario is set as 2000s. Given all nodes fixed, the channel model is the TwoRayGround[4], the probability of the channel error is 0.0%. All nodes are 50 Joule in initial. The power model is default by NS: transmission: 0.66w/bit; receiving: 0.395w/bit; idle: 0.3w/s; sleeping: 0.013w/s. the maximum distance of wireless module is R=400 meters. Loads are randomly produced data flow by cbrgen tools. Each data flow produce 1package of 512 byte per second. The rate of wireless network is 2Mbit/s. Antenna both for transmitter and receiver is omini-directional antenna. The gains are equal of 1. Antenna height is 1.5 meter, the frequency is 914MHz, the diameter of a virtual network d=400/(2*sqrt(2))=140 meters. According to the above parameters, change the node number to evaluate the difference of AODV and AODV_GAF.

1). The Comparison of Node Number

Suppose all the nodes are static, change node number N from 50 to 300, the load is 0.4N, that is if there is 50 nodes, there will be 20 pairs of connection. Suppose the whole network is invalid if 80 percent nodes are invalid. The network life compare of AODV and AODV_GAF shows in Fig.5.

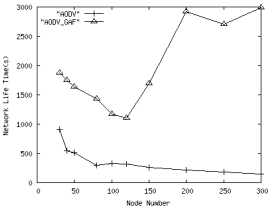

Fig. 5. Network Life Compare

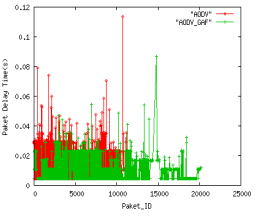

Fig. 6. Network Delay Compare

We can found from Fig. 5 that the network life of AODV_GAF is at least 4 times of AODV. Along with the increase of node number, the network life increase greatly. Because the area is the same, the more the node number, the more the node number in one virtual grid. The sleep node is more in AODV_GAF. The power saved is more. So we know that AODV_GAF is suit for the case that nodes are densely deployed..

2). The Comparison of the Network Delay

Fig.6 is the network delay compare of AODV and AODV_GAF when node number is 180. We can find from Fig.6 that the network delay of AODV and AODV_GAF have the same trend. The delay of AODV is a little longer than AODV_GAF. Because there is data conflict in AODV and the hop in AODV perhaps longer than AODV_GAF which will make the delay longer.

3). The Comparison of the Delay Jitter

Fig.7 is the delay jitter of AODV and AODV_GAF when node number is 180.We can see that the jitter of AODV is a bit longer than AODV_GAF. Because there is data conflict and the hop in AODV is greater than AODV_GAF, so the jitter is longer.

4). The Comparison of the Package Loss Rate Throughput
The package loss rate of AODV and AODV_GAF are all 0. Node 2 is selected to compare the throughput of AODV and AODV_GAF. The result shows in Fig.8. We can see from Fig.8 that throughput of the two protocols is always the same before 550 second, but after 550S, the throughput of AODV decreased rapidly to 0 because the energy of this node has been exhausted, but in AODV_GAF node2 still work to 720 second. This result also shows that the life of Node2 is longer in AODV_GAF.

5). Summary
From the simulation we found that the network life of AODV is much longer than AODV GAF. And the normal network performance such as delay, delay jitter and package loss rate of AODV_GAF is the same or is better than AODV. So AODV_GAF is a recommendable protocol for wireless sensor networks.

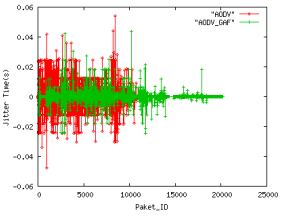

Fig. 7. Packet Delay Jitter Compare

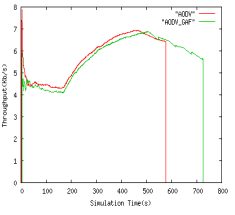

Fig. 8. Throughput Compare

5 Summary

This paper introduces an improved AODV protocol with the idea of GAF and gets a new AODV_GAF protocol. AODV_GAF could increase the network life at least 4 times when the normal performance is almost the same. Furthermore, the more the node number is, the better the performance of AODV_GAF. The shortage of AODV_GAF is that every node should be equipped with a GPS card to get its GIS information. But compared the improvement in network life, the expense is valuable. We also found that AODV_GAF is suitable for the case of large node density. This paper provides a good reference for network protocol design in electronic engineering.

Acknowledgments. This work was supported by the Youth Research Fund of Xi'an University of Posts & Telecommunications (grant # 1100405).

References

1. Callaway, E.H.: Wireless Sensor NetWork: Architechture and Protocal, pp. 41–62. CRC Press LLC (2004)
2. Perknsce, R.: Ad Hoc on-demand distance vector(AODV) routing. In: Proceedings of the 2nd IEEE Workshop on Mobile Computing Systems and Applications (WMCSA), New Orleans, LA, pp. 90–100 (1999)

3. Xu, Y., Heidemann, J., Estrin, D.: Geography informed energy conservation for Ad-hoc routing. In: Proceedings of the Seventh Annual ACM/IEEE International Conference on Mobile Computing and Networking, Rome, Italy, July16-21, pp. 70–84 (2001)
4. Fall, K., Varadhan, K.: The ns Manual (October 31, 2007)
5. Li, W., Chen, M., Li, M.M.: An Enhanced AODV Route Protocol applying in the wireless Sensor Networks. In: The 3rd International Conference on Fuzzy Information and Engineering, ICFIE 2009, ChengDu, China, pp. 441–446 (2009)

Workload-Awared HPC System Scalability Analysis Based on Electronic Technology Developing

Yufei Lin, Yuhua Tang, and Xin Zhang

National Laboratory for Parallel and Distributed Processing,
School of Computer, National University of Defense Technology, Changsha, China
linyufei@nudt.edu.cn

Abstract. As the electronic technology develops, the integration levels of CPUs and memories keep growing, and the speeds of communication devices are improved. The high-performance computing (HPC) systems consist of processing nodes and communication network, and their sizes are advanced by the development of electronic technology. Then the scalability of a large-scale parallel computing system, i.e. whether the computing performance is increased with the system size, becomes a major goal pursued by designers of parallel algorithms and high-performance parallel machines. Parallel speedup is a popular way to measure the scalability. This paper proposes the definition of HPC system scalability based on speedup first, and then analyzes the influence of function G(P), which describes how the workload changes with processor number, on the system scalability. Through case studies, we analyze some typical programs based on our scalability theorems and the results show that our analysis approach is correct.

Keywords: electronic technology, HPC system, system scalability, speedup, workload.

1 Introduction

The development of electronic technology, on the one hand, scales the performances of CPUs and memories, on the other hand, improves the speeds of communication devices. A high-performance computing (HPC) system, which is a parallel system, consists of processing nodes and communication network, and the development of electronic technology advances its scale. According to the data in TOP500, some experts say that the largest systems are growing exponentially in the number of processors [1]. The scalability of large-scale parallel system, i.e. whether the computing performance is increased with the system size becomes a major goal pursued by designers of parallel algorithms and high-performance parallel machines.

Parallel speedup is a popular way to measure the scalability [2–5]. In 1967, Amdahl's speedup model was proposed for a fixed-size problem [6], in which the workload of the problem doesn't change as the system size scales up. The system described by Amdahl's speedup model is unscalable [7], and it causes the appearance of Gustafson's speedup model [8]. Gustafson's speedup model is proposed for the fixed-time problem, which scales up the workload with the increasing number of

D. Jin and S. Lin (Eds.): Advances in Mechanical and Electronic Engineering, LNEE 177, pp. 307–313.
springerlink.com

processors. The system described by Gustafson's speedup model is scalable [7]. It is not difficult to find out that how the problem workload changes with the processor number will affect the system scalability. So how to increase the program workload with the processor number is a problem worth studying.

Furthermore, the latest TOP500 list shows that the number of the supercomputer's processor core reaches 10^5. When communicating on such a large-scale network, the communication overhead can't be ignored. So we should consider the influence of the communication while analyzing the system scalability. The communication overhead is the function of the program workload and processor number. Therefore, when considering communication overhead, analyzing the system scalability becomes more difficult. In this paper, we study the problem that how to increase the program workload to make sure the system is scalable, when the system size scales up. Our main contributions are as follows.

- Define the workload function *G(P)*, which describes how the program workload changes with processor number. Then quantify the influence of *G(P)* on system scalability in ideal case.
- Analyze the influence of *G(P)* on system scalability when considering communication overhead.
- Analyze the scalabilities of some typical programs through case studies.

The rest of the paper is organized as follows. Sect. 2 reviews the related works. Sect. 3 analyzes the system scalability in ideal case. Sect. 4 analyzes the general scalability that considering the communication overhead. The case studies are in Sect. 5.

2 Related Works

Scalability is a major goal pursued by the designers of parallel algorithms and high-performance parallel machine. Ananth Grama etc. proposed the definitions of a scalable parallel system and system scalability based on program efficiency in book [9]. The efficiency of a parallel program is $E=S/P$, where S is parallel speedup and P is processor number. In some parallel system, they have the ability to maintain efficiency at a fixed value by increasing the number of processing elements and the size of the problem. Such systems are called scalable parallel systems. The scalability of a parallel system is a measure of its capacity to increase speedup in proportion to the number of processing elements.

Xiaodong Yang proposed that the relative augment amount of the system performance (efficiency, speed, etc.) induced by the relative augment amount of parallelism degree can reflect the system scalability more comprehensive and more deeply [7]. They gave the definition of scalability as follows.

$$C(P) = \lim_{\Delta P \to 0} \left(\frac{\Delta S(P) / S(P)}{\Delta P / P} \right) = \lim_{\Delta P \to 0} \frac{\Delta S(P) / \Delta P}{S(P) / P}$$

$$= P \frac{\mathrm{d}S(P)}{\mathrm{d}P} / S(P) = P \frac{\mathrm{d}\ln S(P)}{\mathrm{d}P}$$

When $C(P) \le 0$, the system is unscalable; when $0 < C(P) < 1$, the system is scalable.

Scaled-speedup [9] is another metric to measure scalability. Scaled-speedup is defined as the speedup obtained when the program workload is increased linearly with the number of processing elements. If the scaled-speedup curve is close to linear with respect to the number of processing elements, then the parallel system is considered scalable.

3 Ideal Scalability Analysis

In this paper, what we concern about is the performance scalability, i.e. how the speedup changes, when the processor number is increased.

3.1 Defining the Ideal Scalability

When program scales, the serial workload won't change, so we define the *G(P)* ($G(P) \neq 0$) as the variation of the parallel workload while the processor number scales. In ideal case, system speedup is:

$$S = \frac{T_S}{T_P} = \frac{f_1 W + (1-f_1)WG(P)}{f_1 W + \frac{(1-f_1)WG(P)}{P}} = \frac{f_1 + (1-f_1)G(P)}{f_1 + \frac{(1-f_1)G(P)}{P}}$$

where P is the processor number, T_S is the execution time of the serial version of the program, T_P is the parallel execution time, f_1 is the serial part of the program, W is the total workload. When the processor number is increased, the serial workload, which is $f_1 W$, won't change, but the parallel workload is increased by *G(P)* times.

Definition 1: *If* $\lim_{P\to\infty} S = Q$ *(Q is a constant), then the system is unscalable; if* $\lim_{P\to\infty} S = \infty$, *then the system is scalable.*

3.2 Analyzing the Ideal Scalability

According to Definition 1, we can acquire Theorem 1, which is used to analyze the influence of *G(P)* on system scalability in ideal case.

Theorem 1: *In ideal case, the system is scalable, if and only if* $\Theta(G(P)) > \Theta(1)$.

Proof. $\Leftarrow$ If $\Theta(G(P)) > \Theta(1)$, then $\lim_{P\to\infty} S = \lim_{P\to\infty} \frac{f_1 + (1-f_1)G(P)}{f_1 + \frac{(1-f_1)G(P)}{P}} = \lim_{P\to\infty} P = \infty$.

According to Definition 1, the system is scalable.

$\Rightarrow$ If $\Theta(G(P)) \le \Theta(1)$, then $\lim_{P\to\infty} S = \lim_{P\to\infty} \frac{f_1 + (1-f_1)G(P)}{f_1 + \frac{(1-f_1)G(P)}{P}} = \lim_{P\to\infty} 1 = 1$.

According to Definition 1, the system is unscalable.

For the program described by Amdahl's speedup model, *G(P) = 1*, according to Theorem 1, the system is unscalable. For the program described by Gustafson's speedup model, *G(P) = P*, according to Theorem 1, the system is scalable. Fig. 1 shows the Amdahl's speedup and Gustafson's speedup.

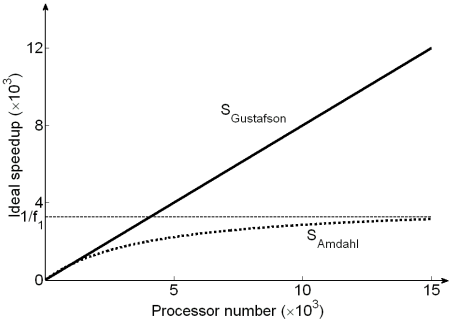

Fig. 1. Amdahl's speedup and Gustafson's speedup

4 General Scalability Analysis

4.1 Defining the General Scalability

The speedup in ideal case doesn't consider the communication overhead. However, as the system size keeps growing, the communication overhead shouldn't be ignored. So we consider the communication overhead to get a general speedup S^O. The communication overhead is the function of program size and processor number, and the program size decides its workload. Therefore, we denote the communication overhead as $O(G(P),P)$.

$$S^o = \frac{T_S}{T_P + O(G(P),P)} = \frac{T_S}{T_P}\frac{1}{1+\frac{O(G(P),P)}{T_P}} = S\frac{1}{1+\frac{O(G(P),P)}{T_P}}$$

Then we give the definition of the general scalability.

Definition 2: *If* $\lim_{P\to\infty} S^O = Q$ *(Q is a constant), then the system is unscalable; if* $\lim_{P\to\infty} S^O = \infty$*, then the system is scalable.*

4.2 Analyzing the General Scalability

According to Definition 2, we acquire the scalability theorem in general case.

Theorem 2: *In general case, the system is scalable if and only if* $\Theta(T_S) > \Theta(O(G(P),P))$.

Proof. $\Leftarrow$ If $\Theta(T_S) > \Theta(O(G(P),P))$, then $\Theta(\frac{T_S}{T_P}) > \Theta(\frac{O(G(P),P)}{T_P})$.

$S = \frac{T_S}{T_P}$, so $\Theta(S) > \Theta(\frac{O(G(P),P)}{T_P})$. Then $\lim_{P\to\infty} S^o = \lim_{P\to\infty} S \frac{1}{1+\frac{O(G(P),P)}{T_P}} = \infty$.

According to Definition 2, the system is scalable.

$\Rightarrow$ If $\Theta(T_S) \le \Theta(O(G(P),P))$, then $\Theta(\frac{T_S}{T_P}) \le \Theta(\frac{O(G(P),P)}{T_P})$, i.e. $\Theta(S) \le \Theta(\frac{O(G(P),P)}{T_P})$. Then $\lim_{P\to\infty} S^o = \lim_{P\to\infty} S \frac{1}{1+\frac{O(G(P),P)}{T_P}} = Q$ (Q is a constant).

According to Definition 2, the system is unscalable.

Corollary1: *In general case, the system is scalable if and only if* $\Theta(G(P)) > \Theta(O(G(P),P))$.

Proof. $T_S = f_1 W + (1-f_1)WG(P) = \Theta(G(P))$

From Theorem 2, the system is scalable if and only if $\Theta(G(P)) > \Theta(O(G(P),P))$

5 Case Studies

5.1 Matrix Addition

There are two matrixes *A* and *B* whose sizes are $n \times n$. At the beginning, they are on the root process, which divides them into *P* shares (supposing n^2 is divisible by *P*), and then it sends the (*P-1*) shares to the other (*P-1*) processes in the other nodes. Each process will compute the n^2/P elements of the result matrix. In this example, $G(P)=n^2$. Then we compute the communication overhead. If using packet routing, the overhead of each communication is $t_{comm} = t_s + mt_w$, where *m* is the message length, t_s is the startup time, t_w is the per-word transfer time. t_s and t_w are constants. Suppose the transfer of matrix A and B uses the scatter operation in minimum spanning tree algorithm [10]. The total communication overhead is:

$$O(G(P),P) = 2t_S \log_2 P + 2t_w m(P-1) = 2t_S \log_2 P + 2t_w \frac{n^2}{P}(P-1)$$

It is not difficult to find out that whatever the *n* is, $\Theta(G(P)) \le \Theta(O(G(P),P))$ always holds. According to Corollary 1, the system is unscalable. In this case, $T_S = \frac{n^2}{V}$, $T_P = \frac{n^2}{PV}$, $S^o = \frac{T_S}{T_P + O(G(P),P)} = \frac{n^2/V}{n^2/PV + 2t_s \log_2 P + 2t_w \frac{n^2}{P}(P-1)}$, where *V* is the computing speed. When *P* goes to infinite, the tendency of S^o is shown in Fig. 2. From Fig. 2 we can see that, the systems are always unscalable, but the values of V s influence the speedups.

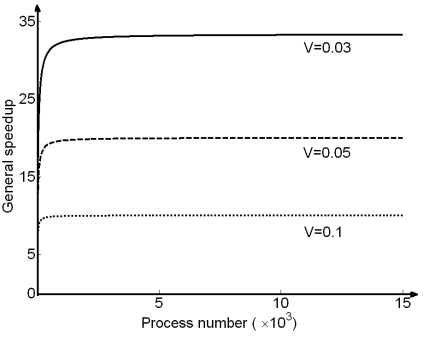

Fig. 2. General Speedup of Matrix Addition

5.2 Matrix Multiplication

Also take the matrix A and B in Sect. 5.1 for example to do the matrix multiplication. At the beginning, they are on the root process, which divides matrix A into *P* shares (supposing *n* is divisible by *P*), each of which contains *n/P* lines, and then sends the (*P-1*) shares of matrix A to the other (*P-1*) processes in the other nodes. Each process computes the *n/P* elements of the result matrix. In this example, $G(P)=n^3$. Suppose the transfer of matrix A uses the scatter operation in minimum spanning tree algorithm. The communication overhead of this operation is:

$$t_S \log_2 P + t_w m(P-1) = t_S \log_2 P + t_w \frac{n^2}{P}(P-1)$$

Suppose the transfer of matrix B uses the broadcast operation in minimum spanning tree algorithm. The communication overhead of this operation is:

$$t_S \log_2 P + t_w m(P-1) = t_S \log_2 P + t_w n^2 (P-1)$$

So the total communication overhead is $O(G(P), P) = 2t_S \log_2 P + t_w n^2 (P - \frac{1}{P})$.

According to Corollary 1, when $\Theta(G(P)) > \Theta(P^3)$, the system is scalable; when $\Theta(G(P)) \le \Theta(P^3)$, the system is unscalable. As shown in Fig. 3, when $G(P) = P^4$, the system is scalable; when $G(P) = P^3$, the system is unscalable.

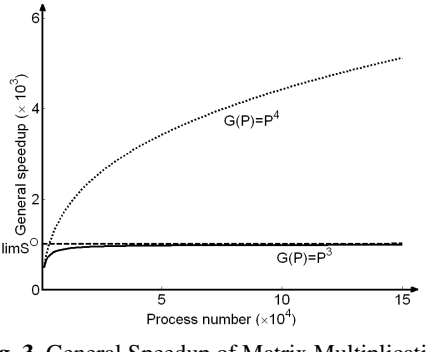

Fig. 3. General Speedup of Matrix Multiplication

6 Conclusion and Future Work

Development of electronic technology advances the scales of HPC systems. In this paper, we analyze the influence of the workload function *G(P)* on system scalability in ideal case. However, when the system scale is increased, the communication overhead should not be ignored. Therefore, we propose a way to analyze the system scalability in a general case which takes the communication into consideration. Besides communication, the major factors affect the system speedup also include overhead for fault-tolerance and memory access. We will deal with these factors in our future work.

Acknowledgments. This work is supported by the National Natural Science Foundation of China under Grant No. 60921062.

References

1. Geist, A.: Paving the Roadmap to Exascale. SciDAC Review 16(special issue) (2010)
2. Chen, J., Li, X.: A Practical Scalability Metric. In: Proceedings of the HPC Asia 2000, Singapore (2000)
3. Grama, A., Gupta, A., Kumar, U.: Isoefficiency Function: A Scalability Metric for Parallel Algorithms and Architectures. IEEE Parallel and Distributed Technique 1(3), 12–21 (1993)
4. Hwang, K., Xu, Z.: Scalable Parallel Computing: Technique, Architecture, Programming. McGraw-Hill Company, Boston (1998)
5. Sun, X., Rover, D.: Scalability of Parallel Algorithm Machine Combinations. IEEE Trans. Parallel and Distributed System 5(6), 99–613 (1994)
6. Amdahl, G.M.: Validity of the single processor approach to achieving large scale computing capabilities. In: AFIPS 1967 (Spring): Proceedings of the 1967 Spring Joint Computer Conference, pp. 483–485 (1967)
7. Yang, X.D., Lu, S., Mou, S.M.: Parallel Computer Architecture-Techniques and Analyses. Science Press (2009) (in Chinese)
8. Gustafson, J.L.: Reevaluating Amdahl's law. In: Multiprocessor Performance Measurement and Evaluation, pp. 92–93. IEEE Computer Society Press, Los Alamitos (1995)
9. Grama, G.K.A., Gupta, A., Kumar, V.: Introduction to parallel computing, 2nd edn. Pearson Education (2003)
10. Barnett, M., Payne, D.G., van de Geijn, R.A., Watts, J.: Broadcasting on meshes with wormhole routing. Journal of Parallel and Distributed Computing 35(2), 111–122 (1996)

A Novel AWG Demodulation System in Electronic Engineering

Zhihui Liu[1,*], Hongqiang Li[1], Changyun Miao[1], Haijing Yang[2], Honda Chen[3], Keqing Lu[1], Enbang Li[1,4], and Kejia Wei[1]

[1] School of Electronics and Information Engineering, Tianjin Polytechnic University, 300387 Tianjin, China
[2] School of Computer and Communication Engineering, Tianjin University of Technology, 300384 Tianjin, China
[3] Institute of Semiconductors, Chinese Academy of Sciences, 100083 Beijing, China
[4] School of Electrical, Computer and Telecommunications Engineering, University of Wollongong, NSW2522 Wollongong, Australia
88girllzh@sina.com, {lihongqiang,miaochuangyun,lukeqing,enbang}@tjpu.edu.cn, yhj126@tjut.edu.cn, hdchen@semi.ac.cn, weikejiaaa1988@163.com

Abstract. The fiber Bragg grating (FBG) sensor arrays are used in the civil engineer works, as well as in health signal monitoring of the human body in electronic engineering. In this paper, a new type of fiber Bragg grating demodulation system that employs an arrayed waveguide grating (AWG) is researched and realized. The principle of the demodulation method based on AWG is analyzed, and intensity-demodulating method is used to demodulate the wavelength of FBG sensors based on the building up of an experimental platform. The results show that the wavelength demodulation of the system has high linearity for fiber Bragg grating, the system gives a wavelength accuracy of 0.001nm. The demodulation error of human body temperature signal is ±0.16°C. It can be applied to the human body temperature measurement.

Keywords: FBG sensors, AWG, demodulation system, wavelength sensitivity, electronic engineering.

1 Introduction

Since 1978 K.O.Hill and his colleagues discovered photonic induced grating from the wrong fiber [1], people have been engaged in the work of the fiber Bragg grating wavelength demodulation [2]. Today the common demodulation methods are used as Fabry-Perot interferometer method [3, 4], Mach-Zehnder interferometer method [5], holographic grating based spectroscopic charge couple device method [6], tunable narrow-band light detection method [7] and so on. In order to ensure the accuracy of demodulation of body temperature signal in clinical medicine, ensure that patients receive timely and accurately diagnosis and treatment, arrayed waveguide grating

* Liu, Z.H. female, was born in 1988, postgraduate. She is engaged in the research on the demodulation of fiber Bragg grating and the optoelectronic integration system.

D. Jin and S. Lin (Eds.): Advances in Mechanical and Electronic Engineering, LNEE 177, pp. 315–319.
springerlink.com

wavelength division multiplexing/de-multiplexer becomes the first choice in the medical use of temperature signal demodulation system in electronic engineering [8].

This paper starts from the principle of demodulation method based on AWG. The paper also introduces the intensity-demodulating method to verify high-precision demodulation based on AWG demodulation and the feasibility of temperature signal demodulation system as electronic engineering.

2 The Principle of Demodulation Method Based on AWG

Take one FBG sensor demodulation for example, we propose two adjacent output channels of the AWG are channel *i*, channel *i+1* (*0≤i≤M*).

For the sake of the simplicity of mathematic analyses, we propose that the spectra reflectance of AWG is Gaussian, the transmission spectrum of the channel *i* can be approximately given by

$$T_{AWG}(i,\lambda) = T_O \exp\left[-4\ln 2\frac{(\lambda-\lambda_i)^2}{\Delta\lambda_i^2}\right] \tag{1}$$

Where T_0 and $\Delta\lambda_i$ are the peak transmittance and full-width at half maximum of the Gaussian component of channel *i*, λ and λ_i are the wavelength of the input light and the wavelength of the channel *i* of AWG.

We express the spectra reflectance of the FBG sensor as

$$R_{FBG}(\lambda) = R_0 \exp\left[-4\ln 2\frac{(\lambda-\lambda_{FBG})^2}{\Delta\lambda_{FBG}^2}\right] \tag{2}$$

Where R_0 and $\Delta\lambda_{FBG}$ are the peak transmittance, full-width at half maximum of the Gaussian profile of fiber Bragg grating, respectively. λ_{FBG} is the center wavelength of the FBG sensor.

In order to obtain values of optical power on individual AWG output channels, the product of functions described by (1) and (2) the light source intensity must be integrated across the source wavelengths. This can be expressed as follows:

$$P_i = (1-L)\cdot I_s \int_0^\infty R_{FBG}(\lambda)\cdot T_{AWG}(i,\lambda)d\lambda \tag{3}$$

$$P_{i+1} = (1-L)\cdot I_s \int_0^\infty R_{FBG}(\lambda)\cdot T_{AWG}(i+1,\lambda)d\lambda \tag{4}$$

In the condition that AWG's channel transmission coefficient is equal to the full-width at half maximum of fiber Bragg grating, combine (3) and (4), we have

$$\ln\left(\frac{p_{i+1}}{p_i}\right) = \frac{8(\ln 2)\Delta\lambda}{\Delta\lambda_i^2+\Delta\lambda_{FBG}^2}\lambda_{FBG} - \frac{4(\ln 2)\left(\lambda_{i+1}^2+\lambda_i^2\right)}{\Delta\lambda_i^2+\Delta\lambda_{FBG}^2} \tag{5}$$

According to the corresponding fiber Bragg grating wavelength getting from Equation (5), we can realize the simultaneous detection of the distributed FBG sensor array.

3 Experimental Results and Discussion

Based on the researches and analysis of the AWG demodulation principle, we built the fiber Bragg grating demodulation system by the method of the water bath method and the light intensity. We select the ZLS-1-545-010-1-2-D as SLED light source, two FBG sensors: FBG1 and FBG2, which center wavelengths are respectively 1552.834nm and 1550.111nm and eight adjacent channels whose central wavelengths range are from 1549.315nm to 1554.940nm as the output of AWG. The model number of the optical power meter we select is AV6334B, the optical power accuracy of which is ± 50pW. The AWG demodulation system we built is shown in Fig. 1. Considering it is used for human temperature measurement, and to ensure the stability of the experiment, we make the experimental temperature range between 30 and 44 degree. According to Fig. 1, we built an experimental platform as is shown in Fig. 2.

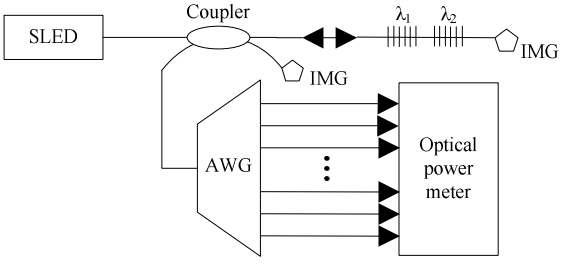

Fig. 1. Wavelength demodulation system based on AWG

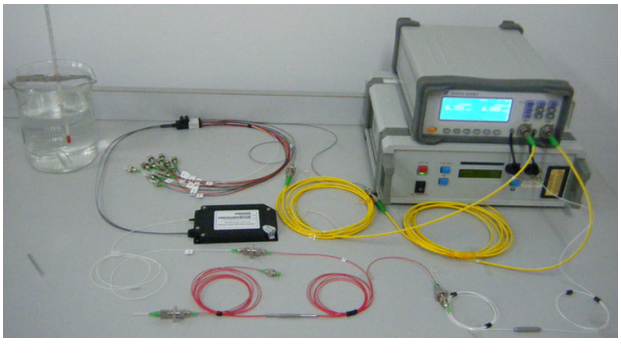

Fig. 2. Experimental platform of wavelength demodulation system based on AWG

In Fig. 2, a light beam form the broadband source come, sent to the FBG sensors through the isolator and the optical coupler. The reflected light from the FBG sensors are coupled into AWG. Then we connect the optical power meter to AWG's 31th channel, 30th channel, 33th channel and 34th channel. Considering the measurement range of the light power meter and the stability of the output light, the output power of light source is set for 7 mw. Observe the change of the light power with the temperature range from 30 to 44°C, and record the power of light of the channels every 1°C. Finally, we make analysis on the output data, getting the platform of the relationship between the light power and the central wavelength, as is shown in Fig. 3.

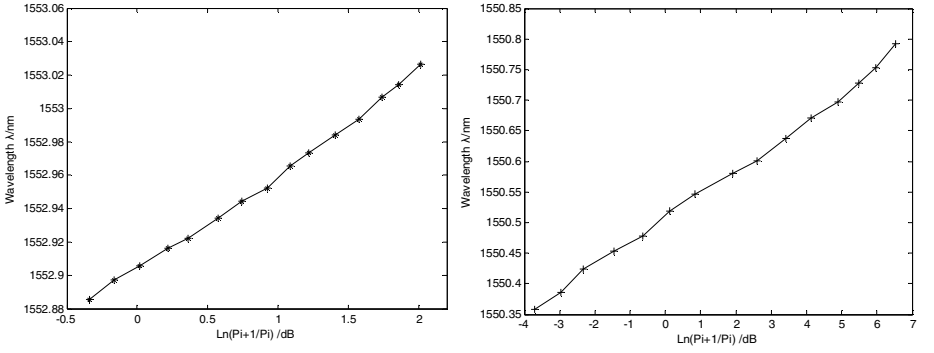

(a) (b)

Fig. 3. Relationship between the intensity ratio and the wavelength of the sensors, (a) Relationship between the intensity ratio and the wavelength of FBG1, (b) Relationship between the intensity ratio and the wavelength of FBG2

Fig. 3 shows that the relationship between temperature and the logarithm of the intensity ratio is linear, the wavelength detection sensitivity of FBG1 is 0.06nm/dB and the wavelength sensitivity of FBG2 is 0.04nm/dB. The range of the wavelength demodulation value is 1552.552~1553.356nm, 1550.121~1550.91nm respectively, which is consistent with the theoretical value of 1552.542~1553.347nm, 1550.116~1550.918nm.

Fig. 4 shows a cure of FBG1 sensitivity measured by MOI fiber-optic sensing instrument Si725, From Fig. 3(a) and Fig. 4, the intensity-demodulating can be used in fiber Bragg grating wavelength demodulation. Just as Fig. 3(a) shows, the wavelength standard deviation demodulated by intensity-demodulating is 0.001nm, which is half of wavelength standard deviation demodulated by the fiber optic sensing analyzer. The intensity-demodulation method has a high degree of demodulation accuracy.

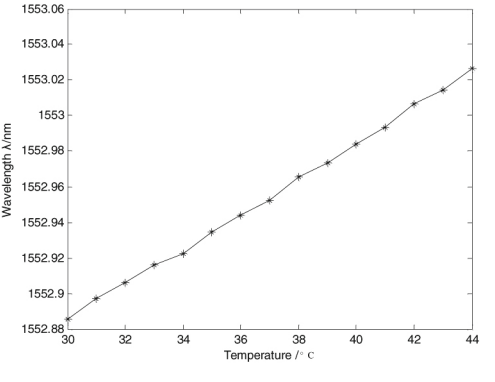

Fig. 4. Curve of FBG1 temperature sensitivity

After packaged by the unsaturated resin encapsulation polymers, FBG1 and FBG2 are put into intelligent clothes which are placed in the left and the right armpits. Then we get reflection wavelength data of FBG1 and FBG2, and compare calculated data with the mercury temperature data. The results show that the error of FBG sensors thermometer based on AWG demodulation and medical mercury thermometer is ± 0.16°C, the measurement accuracy of the body temperature is 0.1°C, which meets the human body temperature measurement.

4 Conclusion

This paper describes in detail human body temperature signal demodulation in electronic engineering based on AWG, builds a fiber Bragg grating temperature signal demodulation system in electronic engineering which can be used to demodulate the body temperature signal communication , and verify the feasibility of the system from the theory and practice. The experiments show that the system can demodulate multiple FBG sensors simultaneously in signal, the accuracy which is high. The system is compact, simple and low cost in the case of multiple FBG sensors demodulation, which has obvious advantages for multi-points temperature measurement in electronic engineering.

Acknowledgments. This work was supported by the National Natural Science Foundation of China (61177078, 60977059, 60877049), the Specialized Research Fund for the Doctoral Program of Higher Education of China (20101201120001) and the Tianjin City High School Science & Technology Fund Planning Project (20100710).

References

1. Hill, K.O., Fujii, Y., Johnson, D.C., et al.: Photosensitivity in optical fiber wavelength: application to reflection filter fabrication. J. Appl. Phys. Lett. 32, 649–847 (1978)
2. Jiang, D.S., He, W.: Review of Application for Fiber Bragg Sensors. J. Optoelectronics Laser 13, 420–431 (2002)
3. Mallinson, S.R.: Wavelength-selective filters for single-mode fiber WDM system using Fabry-Perot interferometors. J. Appl. Opt. 26, 430–436 (1987)
4. Zhang, L., Yin, Q.X.: An improved demodulation method for F-P and FBG multiplexing system. J. Optoelectronics Laser 08, 1008–1011 (2009)
5. Song, M., Yin, S., Ruffin, P.B.: Fiber Bragg grating strain sensor demodulation with quadrature sampling of Mach-Zehnder interferometer. J. Appl. Opt. 39, 1106–1111 (2000)
6. Usbeck, K., Ecke, W., Hagemanm, V., Mueller, R., Willsch., R.: Temperature referenced fiber Bragg grating refractometer sensor on-line quality control of petrol products. In: 13th OFS, Japan, pp. 163–166 (1999)
7. Yu, X.J., Yu, Y.L., Zhang, M., et al.: Study on the strain and temperature densing characteristics of FBG packaged by the copper slice. J. Acta Photonica Sinica 35, 1325–1328 (2006)
8. Yu, X.G., Miao, C.Y., Li, H.Q.: Research on human body temperature measurement models of intelligent clothing based on optical fiber Bragg grating. J. Opt. Technique 37, 704–708 (2011)

Study on Household Savings Prediction Based on Support Vector Machine

Xiang Li and Yuan-yuan Wang

College of Computer Engineering, Huaiyin Institute of Technology, Huai'an 223003, China
largepearstudio@gmail.com, 461044170@qq.com

Abstract. In this paper, we study on the prediction of household savings. Because the household savings are high nonlinear and redundancy, the household savings forecasting method has low accuracy. We proposed a household savings model based on support vector machine to improve the accuracy of the prediction. Firstly, build the sample of the historical data on household savings. Secondly, on the kind of the data pre-processing, it contains data normalized and PCA dimensionality reduction process. Then, using cross-validation to choose the best parameters c and g and using the best parameters to train the training set. Finally, forecast and analysis the test set. The household savings model is used to test and analyze the data in China for 2006 to 2009. Simulation results show that model predicts a higher accuracy and has good generalization ability. The household savings prediction based on support vector machine is an effective prediction method.

Keywords: support vector machine, household savings, prediction.

1 Introduction

Savings is an activity about deposit, household can put the currency that they unused temporary or surplus into bank or other financial institution .Savings is an important source of national capital accumulation. Harrod-Domar Model said that: the rate of economic growth equal to reserve ratio divide capital and subtract the output ratio, economic growth rate has a direct proportion with reserve ratio of this country. Since reforming and opening, our country keeps sustainable and healthy development, and household savings keep increase. The household savings of people live in the city and village reach 30.3302 trillion by the end of the December of 2010 in our country. We can offer the basis whit country to make a scientific guide about household savings because of the household saving prediction and tracking and reveal the changing regularity of savings, the household savings has became an important subject of society economic study.

Household savings is a classical set of the time series, it is trend and high nonlinear because of the economic、policy and so on, the key of the household savings is the arithmetic of prediction. The main prediction of economic field have time series model, Carl Mambo model, the neural network model at the current. This kind of the prediction has advantage and disadvantage: time series model is a forecast based on linear set, couldn't describe the nonlinear change and law of household savings so

D. Jin and S. Lin (Eds.): Advances in Mechanical and Electronic Engineering, LNEE 177, pp. 321–327.
springerlink.com

perfect and has low forecasting precision. Although Carl Mambo model is the improvement of multiple linear regressions with high predictor selectivity and high precision, this model needs to do great quantity arithmetic of array and vector and with complex algorithm and calculation. The neural network has better nonlinear approximation ability, and also is the main prediction of financial set at this moment, but this model needs based on a large number of study sample, less sample leads to low outcome.

SVM is the first proposed by Vapnik in 1995,it can used for pattern classification and nonlinear regression like multilayer perceptions net and radial basis function net .The main idea of SVM is build separating hyper plane as decision surface to maximize the peripheral isolate between positive and counter example .SVM has obvious advantages in dealing highly nonlinear classify and regression .In classify, it's classification accuracy、 generalization ability and modeling calculation are preceded than others and in regression, it has advantage with specific set. Because the household savings forecasting method has low precision, we proposed a household savings model based on SVM. Firstly, build the sample of the historical data on household savings and of the influencing factor. Secondly, pre-processing the training set and test set, using cross-validation to choose the best penalty parameters c and g. Finally, training and forecast with the best parameters.

2 The Principle of Household Savings Prediction

The household savings prediction means that analyze historical data on it and all kinds of index factor that affected it, and we can prediction the reserves in the future whit interrelated prediction theory、 means and model. The household savings are high nonlinear and redundancy because of the society、economic、science and so on. It is difficulty to prediction the complicated nonlinear set precisely by traditional process.

In this paper, the theory of prediction the household savings by SVM is that: firstly, build the sample of the historical data on it, secondly, on the kind of the data pre-processing, it contains data normalized and PCA dimensionality reduction process, then, using cross-validating to choose the best parameters c and g and using the beat parameters to train the training set, finally, forecast and analysis the test set. Specific forecast principle was showed in Fig.1.

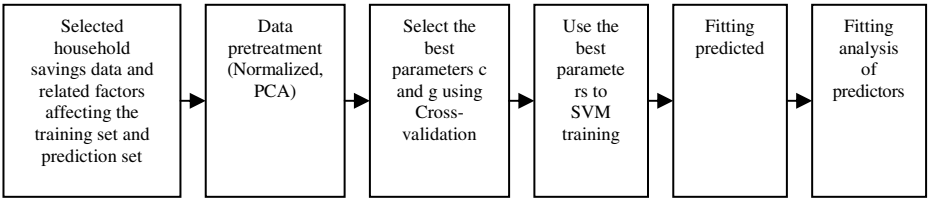

Fig. 1. The schematic of household savings prediction

Because of so much factors affected, and this lead to insure the influence function so difficulty, it is a typical kind of complex nonlinear system. In this paper, we chose the six norms as the major factor to affect the household savings, respectively, GDP, the equally income and pay in the urban residents, savings rate in one year, the consumer price index of urban residents, and the price indices of investment in fixed assets.

3 Prediction Model of SVM Household Savings

3.1 SVM

SVM prediction, searched out the nonlinear mapping function $\varphi(x)$:$R^d \rightarrow F$, and mapped to the output space based on incoming data ,than, do linear estimation at the high dimension characteristic space by

$$f(x) = (w \cdot \varphi(x)) + b \quad w \in F \tag{1}$$

b is a polarization and (w.) is a inner product operation, we can get Eq.2 with minimize generalization function by w and b.

$$R(w) = \frac{1}{2}\|w\|^2 + C\sum_{i=1}^{n} J^{\varepsilon}(y_i, d_i) \tag{2}$$

C is a punish coefficient, show the punishment about right and wrong, much more c much more punish. ε is insensitive loss function, d_i is the true output for SVM.

It is so difficult to figure out Eq.2 directly because the feature space dimension is higher and target function is not differentiable. So, introduction the point product function and using the Wolfe dual to solve this problem, is that:

$$\begin{aligned} &\min(\frac{1}{2}\|w\|^2 + C\sum_{i=1}^{n}\xi_i^2 + \hat{\xi}_i^2) \\ &st.\ W^T\varphi(x_i) + b - y_i \le \varepsilon + \hat{\xi}_i \quad i = 1,2...\ n \\ &y_i - (W^T\varphi(x_i) + b - y_i \le \varepsilon + \hat{\xi}_i \quad i = 1,2...\ n \\ &\hat{\xi}_i, \xi_i, i = 1,2...\ n \end{aligned} \tag{3}$$

There into, $\xi_i and\ \hat{\xi}_i$ mean slack variable, this is in order to consider some sample can't be classified by hyper plane accurately, and introduce the Lagrange multiplier method can achieve value vector.

$$w = \sum_{i=1}^{n}(a_i - a_i^*)\varphi(x_i) \tag{4}$$

There into, a_i and a_i^* mean the Lagrange multiplier, and they must content the condition as:

$$\sum_{i=1}^{n} a_i = \sum_{i=1}^{n} a_i^* \qquad 0 \le a, a \le ci = 1,2... n \tag{5}$$

Achieve $f(x)$ from (1) and (4) :

$$f(x) = \sum_{i=1}^{n} (a_i - a_i^*)(\varphi(x_i) \cdot \varphi(x)) + b$$

$$= \sum_{i=1}^{n} (a_i - a_i^*) K(x_i, x) + b \tag{6}$$

In the calculation of f(x) process, needn't w and definite data of $\varphi(x)$, we only need to figure out a_i , a_i^* and $K(x_i, x)$,this can avoid the dimensionality curse of the high dimensional data efficaciously. Choose the kernel function plays an important role in accuracy of the SVM model forecast. The moment SVM kernel function including polynomial function, RBF function and Sigmoid functioning this paper, use the SVM of RBF in the regression forecasting.

3.2 Prediction Model of Cross Validation SVM Household Savings

According to the basic principle of SVM, choose the RBF as the kernel function, penalty function c, kernel function g and insensitive loss parameter p are the major influencing factor in the SVM forecast accuracy. Do SVM model parameters optimization by traditional exhaustion or gradient descent lead the effect is poorer and time-consuming. In this paper, cross-validation (CV, Cross Validation) and SVM model parameter optimization.

3.2.1 CV Algorithm to Optimize the SVM Parameters

CV is a kind way of statistic analysis to checking the property of analyzer, the basic idea is that: sectionalize the raw data in a sense, a part of this as a train set, and others as a validation set. The method is that: train the grader by using the train set firstly, and than, testing the model by validation set, at least, put the classification accuracy as the performance index of evaluating classifiers.

In this paper, ensure the parameter by k-cv.

3.2.2 Sure and Choose the Influence Factors of Savings Change

The factor of influence the household savings is too much, in the paper, based on the summary a variety of material, choose the GDP, the equally income and pay in the urban residents, savings rate in one year, the consumer price index of urban residents and the price indices of investment in fixed assets as the mainly factor.

3.2.3 The Prediction Process of SVM Savings

1) Data is normalized

2) PCA dimensionality reduction process, proceeding PCA dimensionality reduction process for training set and testing set and simplify the complexity of the raw data.

3) Programming with the Matlab, sure related parameters of K-CV, in this paper, use the Libsvm-3.1 of Matlab.

4) Use K-CV to search the good parameter of SVM prediction model.

5) If reach algorithm termination conditions, than, get the best SVM household savings prediction model.

6) Get the household savings model with upper step, and forecast and precision evaluation the training set.

4 Simulation Research

4.1 Data Sources

In this paper, choose the household savings deposit(Y) from 1999 to 2009 to proceed the forecast verification experiment, the major influencing factor are the GDP(X1,a hundred million),the equally income (X2,yuan)and pay(X3,yuan) in the urban residents, savings rate in one year （X_4, /%） ,the consumer price index of urban residents(last year equal to 100)(X5,yuan),the price indices of investment in fixed assets(last year equal to 100)(X6,yuan).Based on “China Statistical Yearbook”, get the original set of this index, as table 1.

Table 1. Household savings and index factor form 1999 to 2009

Year	Y	X_1	X_2	X_3	X_4	X_5	X_6
2009	260771.7	340506.9	17175	12265	2.25	99.3	97.6
2008	217885.4	314045.4	15780.76	11242.9	2.25	105.9	108.9
2007	172534.2	265810.3	13785.81	9997.47	4.14	104.8	103.9
2006	161587.3	216314.4	11759.45	8696.55	2.52	101.5	101.5
2005	141051.0	184937.4	10493	7942.88	2.52	101.8	101.6
2004	119555.4	159878.3	9421.6	7182.1	2.25	103.9	105.6
2003	103617.3	135822.8	8472.2	6510.94	1.98	101.2	102.2
2002	86910.6	120332.7	7702.8	6029.88	1.98	99.2	100.2
2001	73762.4	109655.2	6859.6	5309.01	2.25	100.7	100.4
2000	64332.4	99214.6	6280	4998	2.25	100.4	101.1
1999	59621.8	89677.1	5854	4615.91	3.78	98.6	99.6

4.2 Built the SVM Prediction Model

In this paper, use Matlab(2011b) combine with Libsvm-3.1 realize build the SVM prediction model.Choose the household savings from 1999 to 2005 fourteen sets as the training specimen; choose the savings from 2006 to 2009 five sets as the tasting specimen. in this arctic, choose K-CV to sure the parameter, adjust c and g

continually, at least, choose the smallest c= 5.278 and g= 0.57435 as the best parameter, best mse= 0.00019164 and achieve SVM prediction model. The results of specific parameter selection are in Fig. 2 and Fig.3.

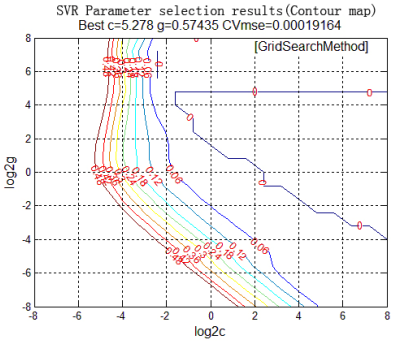

Fig. 2. Contour Map Parameters

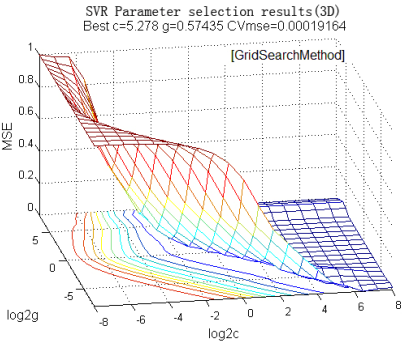

Fig. 3. 3D View Parameters

According to the forecast model, fitting training the household savings for 1991 to 2004, the result for it shows in Fig. 4, and the result for test set shows in Fig. 5.

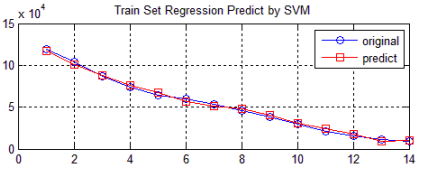

Fig. 4. Training Fitting Rendering

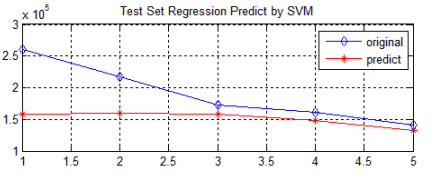

Fig. 5. Testing Fitting Rendering

4.3 Results Analysis

Table 2. Branch Predictor of SVM Model

Year	Actual Value	Predictive Value	Absolute Error	Relative Error
2009	260771.7	157886.0281	-2375.878926	-1.99%
2008	217885.4	160241.2201	-2483.136805	-2.40%
2007	172534.2	158523.1631	811.6767602	0.93%
2006	161587.3	147548.3125	2210.130281	3.00%

According to the table 2, the model studied by SVM can forecast the household savings control the relative error within 3 percent. We can forecast the impact on the household savings with the change of the impact factor fleetly. It is a feasible and effective way to forecast the household savings, can be provided by department.

5 Conclusions

Household savings is a complicated nonlinear time series data, it is related to the equally income and pay and savings rate in one year, it is hard to build the accurate mathematical model. SVM is suitable for the nonlinear time series modeling and prediction very much, and can reflect the change of the savings. In this paper, the experiments are performed with household savings in our country over the recent years; the result was that, the branch predictor of SVM can provide the dependable theoretical ground for national financial decisions.

Acknowledgments. This work was supported by the Technology Support Programs of Huai'an under grant HAG2011041 and the Education Teaching and Research of Huaiyin Institute of Technology under grant JYC201108.

References

1. Shi, F., Wang, X.-C., Yu, L.: 30 Cases Analysis of MATLAB Neural Network, pp. 112–113. University Press, Beijing (2010)
2. Chen, Y.-Y., Xiong, Q.-F.: The SVM application tutorial. China Meteorological Press, Beijing (2011)
3. Zhao, J.-W., Liu, S.-B., Kong, F.-R.: Application of SVM with Genetic Algorithms Optimizing Kernel Parameters. Linear Motor Model 18, 3547–3553 (2006)
4. Zhou, Y., Chen, Q.-Y.: Study on Network Traffic Prediction Based on Improved Back Propagation Wavelet Neural Network. Computer Simulation 27, 187–191 (2010)
5. Zhang, Y., Yin, T.-F.: Study on Tax Forecasting Based on Principal Component Analysis and Support Vector Machine. Computer Simulation 28, 358–360 (2011)

Simulation about Battery Equalization Charging Based on the Fuzzy Control

Yao Xiao

Department of Vehicle Engineering
Shandong Transport Vocational College, Weifang, China
yaoxiao1201@126.com

Abstract. Electric vehicles have developed rapidly for its advantages of energy saving and environment protection, while the problem of equalization circuit of batteries should be reckoned with. In order to resolving the lag of voltage equilibrium, the strategy aiming at battery state of charge is designed, and model of the charge equalization strategy is established and simulated, The feasibility of the strategy is proved.

Keywords: EV, Battery, Equalizing Charge.

1 Introduction

In order to meet the power requirements, electric vehicles usually use the energy supply methods as follow: battery monomer series and two or more batteries connected in parallel. Because of the differences of batteries, some battery cells will be over-charged and over voltage when charging, which lead to the decrease the thermo stability of batteries and the loss of service lifespan. It also increases the use and maintenance costs of EV. However, the strategy of battery equalizing charge can solve the above shortage effectively [1]. In this paper, with the purpose of eliminating the problems above, the control scheme of fuzzy equalization charging was designed.

2 Analysis of Equalizing Charge Technology

At present, many control methods of equalizing charge technology are put forward. Take some for example; cutout and shunt equalization, internal friction and energy feedback equalization, static and dynamic equalization [2]; all the methods have their acuter particular application.

The detection and control methods showed above can be classified into three categories: voltage balancing, battery SOC equilibrium and battery capacity equalization [3]. Voltage balance and SOC equilibrium are service of battery capacity; they have corresponding relationship in a certain range. Now the voltage balance method is widely used, however, because of the temperature, charging current, charging voltage and other factors, this method has the certain lag, can not reflect the real-time storage of the battery. So this method will cause the battery overcharge or

D. Jin and S. Lin (Eds.): Advances in Mechanical and Electronic Engineering, LNEE 177, pp. 329–333.
springerlink.com

undercharge, and at the same time the accuracy of the voltage detection is to be improved. Because of the detection accuracy problem in battery capacity, this method is seldom used.

With the depth of research in SOC algorithm and battery model [4], SOC estimation accuracy is improved, so SOC equilibrium could reflect the battery real state. Along the development of science, measure elements used for battery quantity are researched and produced. During this paper we defines SOC of a battery as research target, using the electric energy dynamic equalization schemes, in which can we realize the dynamic detection of the battery status and improve the efficiency of battery charging.

3 Design of Equalizing Charge System

In this strategy the widely-used power lithium battery is chosen as the equalizing object, the model of lithium battery was established. There are mainly three parameter circuit models: Rint model, Thevenin model and PNGV model [5]. The Rint model shown in figure.1 was selected because of its facility and the effect temperature brought to battery capacity was ignored.

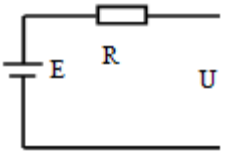

Fig. 1. Rint Model

Where, R was the cell internal resistance; U was the battery terminal voltage; E was the cell electromotive force.

At the beginning of charge, the open-circuit voltage method was used to calculate battery SOC and the current integral method was applied in the process of charging, so as to solve real-time and lag problem of voltage detection.

$$f(SOC) = k_1 * U + k_2 \tag{1}$$

$$SOC = SOC_0 + \frac{1}{Q_n}\int_0^T \eta I dT \tag{2}$$

In the above, k_1、k_2 are constants; Q_n is the battery rated capacity; I is the charging current; η is the charging efficiency.

On improving batteries' stability and life, the equalization circuit should be controlled easily and contains fewer elements so as to reduce the heat output and volume of elements. On the basis of field observation, the energy transfer and without loss equalization circuit is chosen as follow:

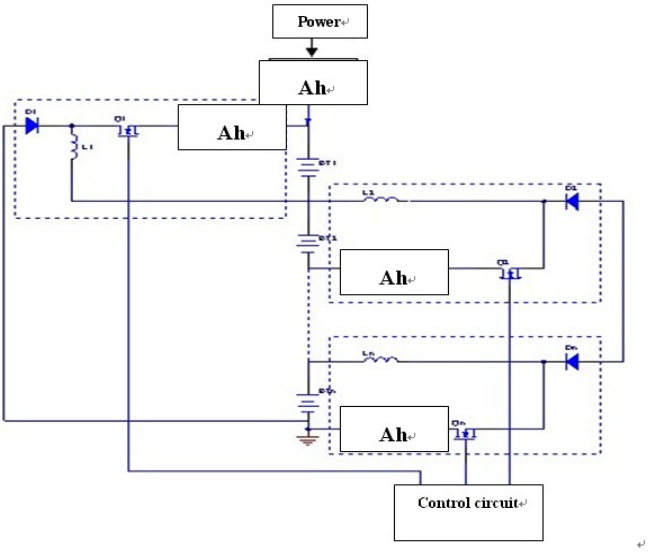

Fig. 2. The equalization circuit

In this, the equalization branch circuit is composed by one inductor one unilateral diode and one field-effect tube. Under the control of each field-effect tube, every cell's SOC could be adjusted through the charging current control. The branch circuit functions as a regulator through the charging process and has a simple structure. the charging generator which has various charging modes can be used as the outside power.

4 The Research of Control Strategy of Equalizing Charge

Due to the multi-variance non-linear and time varying factors, the fuzzy control technology is selected as the controller of the circuit. The fuzzy controller [6] has the advantages of simple model good time varying and so on, and is suited in non-linear system control.

Each cell's SOC should be gotten timely and sent to the fuzzy controller to equalize every battery cell, the SOC minimum and SOC D-value are chosen as the controller's input, and the controlled voltage is chosen as the output.

Generally each cell should not be over-charged and has a good state while SOC is between 0.2 to 0.8, so SOC minimum's and SOC D-value's domain of discourse are set to [0,1] and [0,0.8], their fuzzy subsets are {lower, low, mid, high, higher} and {zero, small, mid, big}, while the output's domain of discourse is [0,10],the fuzzy subset is { ZO、PS、PM、PB}.According to above subsets and experience, the fuzzy rules could be set as table 1:

Table 1. The Fuzzy Control Rules

SOC \ U_{out}	Lower	Low	Mid	High	Higher
Zero	ZO	ZO	ZO	ZO	ZO
Small	PS	PS	PS	PS	PS
Mid	PM	PM	PM	PM	PM
Big	PB	PB	PB	PB	PB

5 Simulation of the Equalizing Charge Circuit Model

The equalizing charge model shown in figure.3 is established using Matlab/Simulink based the above strategy. During simulation, the DC power supplies is selected as the outside power, and voltage is set to 8.4V, the maximum current allowed getting through the equalizing branch is set to 5A, a couple of lithium batteries are the equalizing objects whose rated voltage is 3.7V and terminal voltages are 3.0V and 2.8V,. Through simulation the result is shown in figure.4:

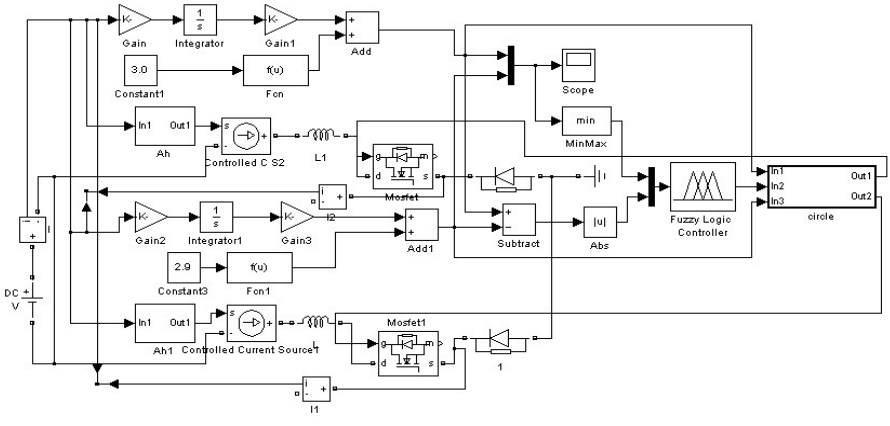

Fig. 3. The equalizing charge model

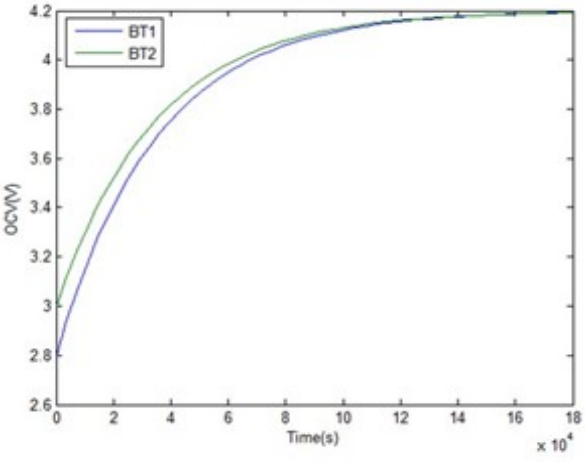

Fig. 4. The result of Simulation

As shown in figure.4, the both cells' SOC are 0.37 and 0.48, the value of disequilibrium reaches 11%, which would lead to the second cell being charged fully earlier than the other without equalizing controller. Under the control of fuzzy equalizing charge strategy, the current charging the second cell is bypassed while the other cells' current is turn up, and finally being charged to saturation.

6 Conclusions

In this paper, under the research of the fuzzy control technique we found that we can effectively reduce the battery pack no-balanced degree by regulating the monomer battery charging electric current and battery SOC state. At the same time, if we take battery SOC as research target, voltage balance of lag can be avoided, the battery can charge in a good state, in this way we can prolong the service life of the battery.

References

1. Wu, K.: The Study of Charge Equalization of Series-connected Batteries System. J. Hefei University of Technology (2006) (in Chinese)
2. Hu, X.: Power battery technology and application. Chemical Industry Press, Beijing (2009) (in Chinese)
3. Moore, S.W., Schneider, P.J.: A Review of Cell Equalization Methods for Lithium I on and Lithium Polymer Battery Systems. In: SAE 2001 (2001)
4. Lin, C.-T., Wang, J.-P., Chen, Q.-S.: Methods for state of charge estimation of EV batteries and their application. J. Battery Bimonthly 34, 376–38 (2004) (in Chinese)
5. Lee, Y.-S., Cheng, M.-W.: Intelligent Control Battery Equalization for Series Connected Lithium-Ion Battery strings. J. IEEE (2005) (in Chinese)
6. Lu, H.: The Key Technology of Charge Management System for Storage Batteries Group. Shanghai Jiao Tong University (2007)

Research of HRV and PRV under Electronic Synchronous Acquisition System

Aihua Zhang[1], Songsong Sun[2], and Jinhui Bi[2]

[1] College of Electrical and Information Engineering,
Lanzhou University of Technology, Lanzhou, 730050, China
[2] College of Computer and Communication,
Lanzhou University of Technology, Lanzhou, 730050, China
lutzhangah@163.com

Abstract. In order to discuss the unity of heart rate variability (HRV) and pulse rate variability (PRV) and explore the relationship between HRV/PRV and the autonomic nervous. R-R intervals and P-P intervals were obtained from ECG and pulse signals of 17 healthy volunteers by synchronous acquisition system. HRV and PRV were analyzed offline by spectral analysis. And PRV derived from pulse wave corresponds well to traditional HRV derived from ECG. The results indicate that PRV and HRV had the same features which synchronous acquisition ECG and pulse wave, and the PRV may replace HRV to estimate the excitement of autonomic nervous.

Keywords: VDT fatigue, heart rate variability, pulse rate variability, synchronous acquisition autonomic nerve, correlation.

1 Introduction

Under normal circumstances, the sympathetic nerve and parasympathetic nerve control the balance of the body's physiological activities. If this balance is broken, it will bring out a variety of dysfunction. With the development of the society, high pressure, emotional distress, fatigue and irregular life can lead to visceral dysfunction. This could be called vegetative nerve functional disturbance and affect the people's normal life seriously.

The same as electrocardiogram (ECG) and pulse signals, HRV and PRV signals can reflect the physiological changes of the human body. Compared with previous literature, we found that HRV can indicate the state of both parasympathetic and sympathetic functions in diagnosed patients whom had heart diseases, coronary disease, hypertension, diabetes or vegetative nerve functional disturbance [1-5]. We also found that pulse wave had similar function to estimate those diseases. Pulse parameters and the autonomic nervous function parameters may be used as the indexes in diagnosis and syndrome differentiation in depression [6-7]. As we all know, ECG and pulse wave are closely related. From Eduardo Gil's study, we found that although some small differences between the time-varying spectral indices extracted from HRV and PRV existed, PRV could be used as an acceptable surrogate of HRV during non-stationary conditions [8].

D. Jin and S. Lin (Eds.): Advances in Mechanical and Electronic Engineering, LNEE 177, pp. 335–338.
springerlink.com

Therefore, we analyzed the level of agreement between HRV and PRV signals in VDT fatigue experiment and further tested the expanding application of PRV in autonomic nerves function.

2 Methods

Seventeen volunteers (20~25 years age, healthy and familiar with the computer operation) underwent VDT fatigue experiments. The whole experiment was going on 1.5 hours and ECG and pulse signals of these volunteers were obtained synchronously in the experiments. Before and after phases were divided and 3 minutes signals were selected and analyzed in each experiment phases [9]. ECG and pulse signals after preprocessing were shown in Fig. 1.

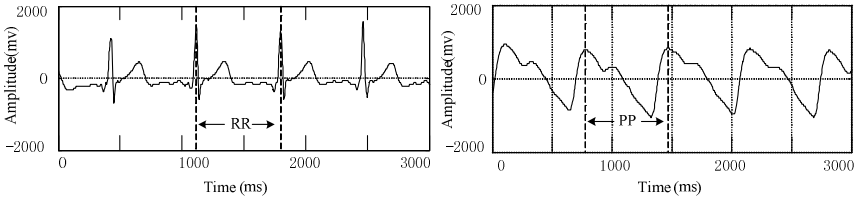

Fig. 1. Pre-processed ECG and pulse wave signal

Beats from ECG and pulses from pulse wave were detected to generate heart and pulse rate time series, and R-R intervals and P-P intervals could be extracted from those series. The software extracts R-R intervals and P-P intervals, constructs time series and subsequently performs spectral analysis using AR model of spectral estimated [10]. This technique decided the overall variability of a signal into its composing frequencies and provided insight into what extent a frequency contributed to the overall variability of the signal. The power spectrum of HRV and PRV have shown that they consist of three peaks: the very low frequency (VLF) band (<0.04 Hz), the low-frequency band (0.04~0.15 Hz) and the high-frequency band (0.15~0.4 Hz). The VLF fluctuations are thought to be mediated primarily by the sympathetic system, the low-frequency fluctuations by both the sympathetic and parasympathetic systems and the high-frequency fluctuations are under parasympathetic control [11].

The association between HRV and PRV was analyzed using Pearson's correlation coefficient. The closer the level of the correlation is to 1, the more related between HRV and PRV signals.

Finally, to assess *t*-test of HRV and PRV, the *p* value of less than 0.05 was considered statistically significant.

3 Results

After a 1.5h VDT fatigue experiment, the physiological parameters changed, and most of the volunteers had the specific features being fatigue such like eyes dry, swollen, blurred vision. Compared early experiment results with later phases, the results are shown in Table 1.

Table 1. HRV and PRV features data of before and after experiment

Feature	Before experiment		After experiment	
	HRV	PRV	HRV	PRV
VLF	25.934±105.38	24.488±107.39	18.696±142.80	21.721±109.45
LF	35.9084±124.63	36.0531±127.86	35.591±138.43	35.5488±181.61
HF	40.5725±203.22	40.2408±194.23	43.1117±185.50	43.5967±136.30
LF/HF	0.37083±0.0032	0.37892±0.0043	0.38821±0.0041	0.38023±0.0031
M(ms)	839.843±22523	841.089±24093	876.245±11638	873.877±11948
SDNN	31.0191±17.02	50.1023±14.001	29.8235±30.29	42.6984±31.067
ρ	>0.98		>0.98	

After the VDT experiment, the analysis result revealed that the mean difference between HRV and PRV of 2% in the VLF, LF and HF band and the mean of PP and RR interval were basically the same, besides, each features correlation of HRV and PRV signal were higher than 0.98, no matter early or later experiment. Comparing with early experiment, HRV and PRV changed significantly, the value of VLF decreased more than 10%, the least change was LF band that only below 1%, the most increase feature is HF band (6%), and the smallest was SDNN which was just only 3% in later experiment.

From Table 1, the *t*-test reliability results showed that under the same experimental condition the *p*-value was more than 0.98 and *p*-value was less than 0.05, under different experimental conditions. It suggested that the HRV and PRV changed significantly through the fatigue experiment, but under the same experimental condition each features of HRV and PRV were almost the same.

4 Conclusion

The present study provides merits to use synchronous acquisition to collect ECG and pulse signals, and research of relationship between HRV/PRV and autonomic nerve. PRV derived from pulse signal showed a high correlation and level of agreement with traditional HRV obtained with ECG. Furthermore, both HRV and PRV showed a moderate to high t test reproducibility.

According to the results of VDT fatigue experiment, high similarity was observed between the patterns of response of the HRV and PRV. Both of the two features had high correlation for low-frequency (0.04~0.15Hz) and high-frequency (0.15~0.4Hz). However, during experiment the power in the low-frequency band was extend to the high-frequency, so the power in the high-frequency is increased. Finally, the *t* test reliably of HRV and PRV measurements are comparable.

In conclusion, through the electronic synchronous acquisition system shows that under VDT fatigue, HRV and PRV are change significantly in the different phase, but in the same phase the change is not significant. Those results indicate that the sympathetic system functional depression and parasympathetic system functional excitement. It also shows that the VDT fatigue can influence the autonomic nerves activity. Through the synchronous acquisition found the use of PRV in autonomic nerve activity and future investigations should be explored to determine whether its use can be extrapolated to clinical conditions.

References

1. Fengming, H., Qinghua, Z.: Correlative study of heart rate variability and autonomic nervous function in patients with anxiety neurosis. China J. Prim. Med. Pharm. 17, 2628–2629 (2010)
2. Uehara, A., Kurata, C., Sugi, T.: Diabetic cardiac autonomic dysfunction: parasympathetic versus sympathetic. Annals of Nuclear Medicine 13, 95–100 (1999)
3. Muroni, P., Roberto, C., Barbarossa, I.: Emotional responses to pleasant and unpleasant oral flavour stimuli. Chemistry 4, 65–71 (2011)
4. Lijun, Z., Ping, C.: Analysis of Heart Rate Variability in patients with Hypertension or Concurrent Hypertension and Diabetes. Practical Journal of Cardiac Cerebral Pneumal and Vascular 19, 1628–1629 (2011)
5. Steven, O., Vera, B., Andrej, O.: Heart Rate Variability and Sensorimotor Polyneuropathy in Type Diabetes. Diabetes Care 2, 1652 (2012)
6. Haiyong, Z., Yihong, Q., Sijun, H., Yisheng, Z.: Detrended Fluctuation Analysis of Pulse Rate Variability Signals of Coronary Disease Patients. Space Medicine & Medical Engineering 20, 455–457 (2007)
7. Ling, J., Yi, S., Xiuwen, Z., Xinyi, Z.: Exploratory research on pulse parameters assessment on autonomic nervous function of depression. Chinese Journal of Information on TCM 04, 10–11 (2011)
8. Eduardo, G., Michele, O., Raquel, B.: Time-varying spectral analysis for comparison of HRV and PPG variability during tilt table test, vol. 8, pp. 2579–2582 (2010)
9. AiHua, Z., Zhiyue, Z., Hua, Y.: A Method of Estimating Visual Fatigue Based on the Features of ECG and Pulse Waveform. Computer Engineering 07, 279–281 (2011)
10. Lymant, R., Micheal, T.: An Introduction to Statistical Methods and Data Analysis. Science Press (2003)
11. Akselrod, S., Gordon, D., Ubel, F.: Power spectrum analysis of heart rate fluctuation: a quantitative probe of beat-to-beat cardiovascular control. Science 213, 220–222 (1981)

Design of Smart Home Control Terminal Based on ZigBee and Electronic Technology

LiGuo Tian, Meng Li, ZhiLiang Chen, and BeiBei Guan

Tianjin Key Laboratory of Information Sensing & Intelligent Control,
Tianjin University of Technology and Education,
Tianjin, 300222,
China
{tlg1234,limeng-3260711}@163.com,
czl_tj@sina.com,
bei199022@126.com

Abstract. With the improvement of people's living standard and the development of the embedded technology, communication technology and network technology, the living environment of smart home has become a kind of development trend for the future home life. In view of the growing demand of smart home system and the widespread use of the embedded technology, it proposed a kind of smart home control terminal based on the ZigBee technology. The control terminal using STM32F103VC microprocessor as control core, combined with ZigBee technology and sensor technology, realized to control the environmental temperature, illuminance, switches of household appliances, shut of doors and windows wirelessly and intelligently. The result shows that, the intelligent control terminal is simple and reliable, it works well.

Keywords: Smart Home, ZigBee Technology, Terminal Node, STM32F103VC.

1 Introduction

Along with the rapid development of the digital information technology and network technology, as well as the continuous improvement of material living standards, people's life style and habits have changed, the traditional houses are no longer satisfied, and smart home will certainly be the development direction of modern residence in the future. The smart home can not only provides users with safe, healthy and comfortable living environment, but also the user can locally or remotely monitor their own home furnishing state and control household appliances [1]. Based on the analysis of smart home system composition and function, the paper proposed a kind of smart home control terminal node based on the ZigBee technology [2], and designed the hardware and software system. After tested, the terminal node is stable and reliable, and realized the security, energy-saving, intelligent, comfortable and high-efficient living environment of the smart home.

D. Jin and S. Lin (Eds.): Advances in Mechanical and Electronic Engineering, LNEE 177, pp. 339–344.
springerlink.com

2 Wireless ZigBee Technology

ZigBee is a kind of wireless network technology which has the characteristic of short distance, low-power dissipation, low data rate, low cost and low complexity, has been widely used in industrial control, car automation, home and building automation, medical equipment control and other fields. ZigBee is a group of communication technology developed for the networking, security and application software based on the IEEE 802.15.4 Wireless standards, it has its own wireless communication standard, and can realize coordination communication among thousands of tiny nodes. These nodes requires very little energy, to transfer data from one node to another node through the radio wave by the way of relay, and the communication efficiency is very high [3].

3 Overall Design of the System

3.1 Design Objective and Principle of the System

The fundamental objective of the smart home is to provide people with a comfortable, safe, convenient and high-efficient living environment. Before designing the system, it is necessary to scheme the whole system. The smart home control terminal node based on ZigBee technology proposed in the article is a simple smart home system, and can be used in the ordinary families, so the following principles should be abided by:

(1) Simple and practical;
(2) Low price;
(3) Operation is stable, reliable, and durable;
(4) With scalability.

3.2 Overall Design of the System

Based on the application of the embedded technology in smart home control system, the paper uses a newest embedded chip STM32F103VC as the microprocessor, combined with ZigBee technology, the sensor technology and so on, to collect temperature and humidity, illumination and other environmental parameters under the circumstance of the smart home, as well as control the common household appliances wirelessly. The hardware system of the smart home control terminal node Based on ZigBee uses the STM32F103VC microprocessor as the main control core, collocated with ZigBee wireless communication module CC2530, temperature and humidity sensor module, 4.3 inch LCD touch screen display module, SD card data storage module. The software system is realized through the transplantation of the embedded operating system μC/OS andμCGUI, the system structural diagram as shown in Fig.1.

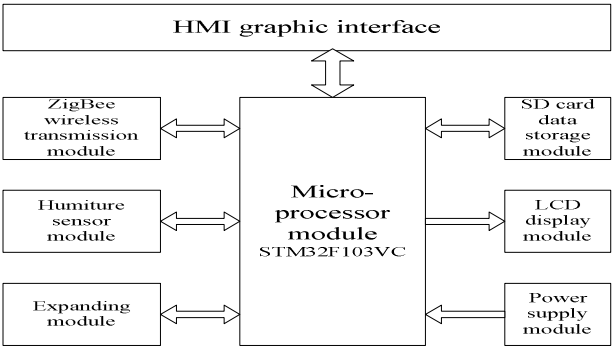

Fig. 1. The structural diagram of the system

4 The Hardware Realization

In the system of the intelligent control terminal node, the hardware system is the key and foundation, and could directly affect the stability, control and feedback accuracy and energy conservation of the whole system.

4.1 STM32F103VC Microprocessor Module

The processor uses the Cortex-M3 kernel made by ARM Company, which meets embedded domain requirements, such as high integration, low power consumption, real-time application, competitive price and so on[4]. Operating frequency of STM32F103xx series 32-bit flash micro-controller is 72MHz, which has on-chip integration of high-speed memory and enriched and enhanced peripheral and I/O connected by APB bus, and also be provided with two 12-bit ADC, one 12-bit double-channel DAC and 11 16-bit timers. All the equipment provide a standard communication interface without additional components, so as to reduce the system cost and provide handheld and general types of application with a low price, low power, high performance microcontroller solution.

4.2 ZigBee Wireless RF Communication Modules

The ZigBee wireless transmission module is mainly used to transmit the data or commands among the intelligent control terminal node and the other sensor nodes or household appliances control nodes. The chip which is used for 2.4GHz free-license ISM band adopts the second generation of TI ZigBee/IEEE 802.15.4 RF on-chip system CC2530. Operating frequency of CC2530 is 32MHz; it has 8K bytes of static RAM in which 4K bytes space is ultra low power consumption SRAM. Interrupt controller can provide service for a total of 18 interrupt sources, each of them is given an interrupt priority.

4.3 Humiture Sensor Module

The SHT71 is a highly integrated humiture sensor, which integrates temperature sensing, humidity sensing, signal conversion, A/D conversion and heater, the output directly is a digital signal. SHT71 has strong anti-interference ability, high cost performance, ultra low power consumption, and all qualifications meet the design requirements.

4.4 SD Card Data Storage Module

The Chinese translation of SD card (Secure Digital Memory Card) is secure digital card, which is a new generation of memory device based on semiconductor flash memory device with high memory capacity, fast data transfer rates, great flexibility and good movement security. Thus SD card collocated in the system is used to save the data at regular time; it is convenient to inquire the data in future. The connection layout between the SD card module and STM32F103VC is shown in Fig.2.

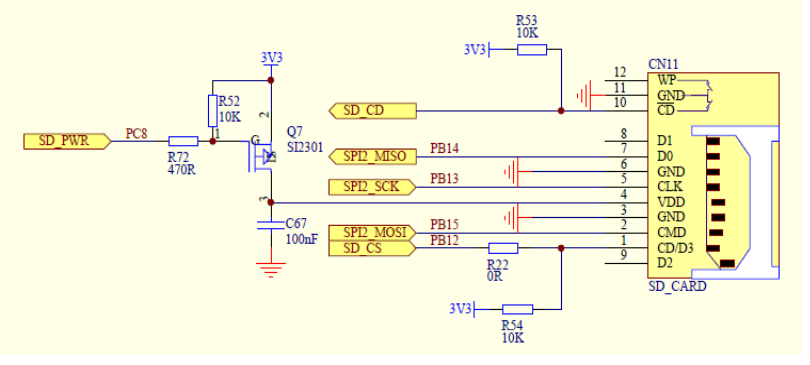

Fig. 2. The connection layout between the SD card module and STM32F103VC

4.5 Display Module

The Display module selects 4.3 inch TFT color LCD touch screen, which has features of low power consumption, ultrahigh brightness and simulation of I/O control. Display module is configured ADS7843 touch controller, supports one SD card (SPI mode) and one SPI DATA FLASH. HCI graphics interface is programmed through software, which is used to display some parameters, such as the current time, date, temperature, humidity, the opening and closure of household appliances.

4.6 Power Supply Module

The supply voltage is normal 5V. After AMS1117 regulated, 3.3V voltage will supply each chip. AMS1117 is a positive low-voltage drop voltage regulator; the voltage drop under 1A current is 1.2V. Its circuit principle diagram is shown in figure 3: D1 is a power light, when there is a power supply input D1 will be lightened, P2 is a power input interface.

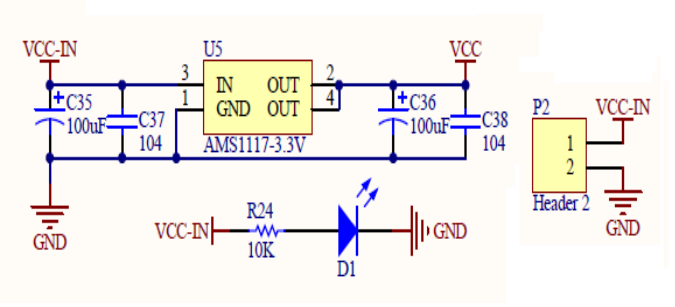

Fig. 3. The AMS1117 schematic diagram

5 The Software Realization

5.1 The Embedded Operation System µC/OS

Considering the multiple events and untime during the course of software design, soµC/OS embedded operating system is transplanted to realize the multi-task event processing [5]. Aiming at the function of the control terminal nodes to establish Task quantity, priority and buffer size in the µC/OS-II system. Idle Task which has the lowest priority is mainly running as the system is free to maintain the normal operation of the system. Task1 is the highest level of task; mainly respond interrupt and timing function. All the Tasks proceed orderly under the scheduling system, a higher priority task can interrupt the lower priority task, and a task corresponds to a process, and if the task is finished process is over, until the mission was again called. The flow chart of the main function is shown in Fig.4.

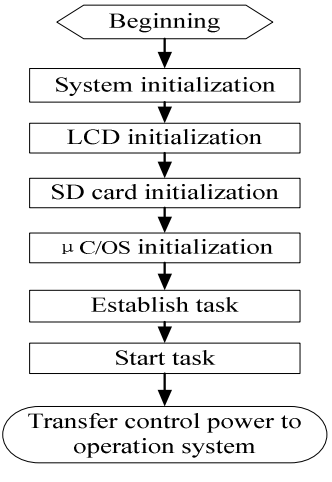

Fig. 4. The structure chart of the software architecture

5.2 The μC/GUI Graphic Interface

The μC/GUI is a kind of graphics support system in the application of embedded system [6]. It is designed for any LCD graphics display applications to provide with graphical user interface which is high efficient and independent to the processor and LCD controller, it is suitable for a single task or multi-task system environment, and also suitable for any size of real or virtual display on any LCD controller and CPU. Its design framework is modular, composed of different layers in various modules. A LCD drive layer contains all of the specific LCD graphics operations. μC/GUI can be running in any CPU, because it is compiled by the standard C code. μC / GUI can adapt to most of color or black and white LCD.

6 Conclusion

Along with improvement of the quality and the pace of life, people's work and life are becoming more and more informationized. The information-based society has changed people's life-style and work habits; it becomes an inevitable trend of social development to intelligentize home system. The smart home control terminal node based on ZigBee proposed by the paper is able to provide people with comfort, smart and safe living environment, and the node which has the advantages of simple structure, convenient control, energy saving and environmental protection and powerful expanding capability is suitable for general household, and has higher practical value.

Acknowledgments. The authors thank all the people who had given helps to them in the work. This work is supported by Key Project of Tianjin Science and Technology Support Programme under Grant 09ZCKFGX02100, Tianjin University Two-five Science and Technology Project under Grant SW20080006.

References

1. Chen, R., Wang, X.J., Chen, Q.: Development Opportunity and Challenge of Smart Home in the Internet of Things Era. Intelligent Building 15, 1–8 (2010)
2. Sun, Y., Shang, W.L., Cao, Y.: Research on the Project of Embedded Smart Home System Design Based on ZigBee. Computer Technology and Knowledge 7(36), 9494–9495 (2011)
3. Li, W.Z., Duan, Z.Y.: Introduction to ZigBee Wireless Network Technology and Practice. Beijing Aerospace University Press, Beijing (2007)
4. Wang, Y.H., Xu, W., Hao, L.P.: STM32 Series ARM Cortex-M3 Microcontroller Principles and Practice. Beijing Aerospace University Press, Beijing (2008)
5. Shao, B.B.: Embedded Real-time Operating SystemμC/OS-II, 2nd edn. Beijing University of Aeronautics and Astronautics Press, Beijing (2003)
6. μC / GUI Graphical User Interface with Graphic Library Manual Rev. 0. Micrium Technologies Corporation, U.S.A (2006)

Algorithm of Iterative Learning Control Based on the Sliding Mode Variable Structure Control

Hao Xiao-hong and Zhao Jing

School of Electric Engineering and Information Engineering,
Lanzhou University of Technology,
730050 Lanzhou, China
741570987@qq.com

Abstract. Iterative learning control is a kind of precise mathematical model without depending on the dynamic system, by repeating the same task execution to reduce error and make the system output as far as possible. The method of the value approach ideal sliding mode variable structure control has good robustness. The algorithm of sliding mode control was introduced as iterative learning control, and fuzzy control reduce sliding mode control was caused by the jitter, the simulation results showed that with the increase of iterations number, the error decreased gradually and was stabilized, and a better tracking effect could be gotten.

Keywords: iterative learning control, sliding mode variable structure control, fuzzy control.

1 Introduction

Iterative learning control (ILC) adopts the 'learning in the repeat' strategies, and it has the memory system and empirical correction mechanism. More specifically, through the controlling attempt about the controlled system, new control signal can be created with correcting undesirability control signal by output track and given deviation of the track, and the tracking performance of the system can be improved [1]. Therefore, iterative learning control was widely used in the controlled system with repetitive movements such like the industrial robots and soaking pit furnace temperature control system.

Sliding mode control (SMC) is the main theory and method of the variable structure control (VSC). In 1960s, the former Soviet union scholars Emelyanov, Utkin and Itkin first proposed the sliding mode control, so far, it has been fully improved and developed [2]. Sliding mode control system has not degeneration to the outside interference and parameters disturbance after entering the sliding mode motion in certain conditions. So this kind of control method has simple algorithm, good anti-jamming performance and easy online realization, which is suitable for uncertain nonlinear multivariable control object [3].

D. Jin and S. Lin (Eds.): Advances in Mechanical and Electronic Engineering, LNEE 177, pp. 345–350.
springerlink.com

1 The Design of Fuzzy Sliding Mode Controller Iteration

The remarkable characteristics of iterative learning control algorithm is simple, high control accuracy, and can be given with arbitrary precision tracking. But one of the main problems is robust problem. This is caused by due to the objective existence of uncertainties, and sliding mode control is good at solving the robust problem. The simple sliding mode control easily causes jitter, so fuzzy control and sliding mode control are combined to get soften control signal, reduce or avoid the general sliding mode control chattering phenomena [4]. The new method designed combining with these three methods can effectively improve the performance of the system.

1.1 The Design of Sliding Mode Controller

Set the controlled object for

$$x^{(n)} = f(\boldsymbol{x},t) + g(\boldsymbol{x},t)u(t) \tag{3}$$

And the error of the system tracking

$$\boldsymbol{e} = \boldsymbol{x}_d - \boldsymbol{x} = \left[e \ \dot{e} \cdots e^{(n-1)} \right]^T \tag{4}$$

The switch function is

$$s(\boldsymbol{x},t) = \boldsymbol{C}\boldsymbol{e} = c_1 e + c_2 \dot{e} + \cdots + e^{(n-1)} \tag{5}$$

Among them $\boldsymbol{C} = [c_1 c_2 \cdots c_{n-1} 1]$。 By taking $\dot{s} = 0$, the following function can be gotten.

$$\dot{s}(\boldsymbol{x},t) = c_1 \dot{e} + c_2 \ddot{e} + \cdots + e^{(n)} = c_1 \dot{e} + c_2 \ddot{e} + \cdots + c_{n-1} e^{(n-1)} + x_d^{(n)} - x^{(n)} \tag{6}$$
$$= \sum_{i=1}^{n-1} c_i e^{(i)} + x_d^{(n)} - f(\boldsymbol{x},t) - g(\boldsymbol{x},t)u(t) = 0$$

The equivalent controller is

$$u_{eq} = \frac{1}{g(\boldsymbol{x},t)} \left(\sum_{i=1}^{n-1} c_i e^{(i)} + x_d^{(n)} - f(\boldsymbol{x},t) \right) \tag{7}$$

To meet the condition of the sliding mode as $s(\boldsymbol{x},t) \cdot \dot{s}(\boldsymbol{x},t) \le -\eta |s|$ Among them $\eta > 0$, and switch control must be used. The switching controller can be designed as

$$u_{sw} = \frac{1}{g(\boldsymbol{x},t)}\eta \operatorname{sgn}(s) \tag{8}$$

Among them $\eta \geq D$。The Sliding mode controller is

$$u = u_{eq} + u_{sw} \tag{9}$$

The qualitative proof is shown as

$$\dot{s}(\boldsymbol{x},t) = \sum_{i=1}^{n-1} c_i e^{(i)} + x_d^{(n)} - f(\boldsymbol{x},t) - g(\boldsymbol{x},t)u(t) - d(t) \tag{10}$$

Take formulas (7) ~ (9) into formula (10) , the following formula can be gotten.

$$s\dot{s} = s \cdot (-\eta \cdot \operatorname{sgn}(s)) - s \cdot d(t) = -\eta|s| - sd(t) \leq 0 \quad . \tag{11}$$

1.2 The Design of Fuzzy Controller

According to the principle of sliding mode control, if the sliding mode controller is proposed by equivalent sliding mode control and switch control two components, its control rules is

$$\text{If } s(t) \text{ is ZO then } u \text{ is } u_{\text{eq}} \tag{12}$$

$$\text{If } s(t) \text{ is NZ then u is } u_{\text{eq}} + u_{\text{sw}} \tag{13}$$

Among them, NZ and ZO which are the fuzzy sets can be set "zero" and "nonzero", respectively.The fuzzy rule formula (12) shows that the fuzzy controller is the equivalent control ueq when the switch function s (t) is zero. The fuzzy rules formula (13) shows that fuzzy controller is switching control usw when the switch function s (t) is nonzero.Using the defuzzification fuzzy method, the fuzzy controller can be designed as

$$u = \frac{\mu_{\text{ZO}}(s)u_{\text{eq}} + \mu_{\text{NZ}}(s)(u_{\text{eq}} + u_{\text{sw}})}{\mu_{\text{ZO}}(s) + \mu_{\text{NZ}}(s)} = u_{\text{eq}} + \mu_{\text{NZ}}(s)u_{\text{sw}} \tag{14}$$

$$\mu_{\text{ZO}}(s) + \mu_{\text{NZ}}(s) = 1 \tag{15}$$

When $\mu_{NZ}(s)=1$, $u=u_{eq}+u_{sw}$. At this time it is the traditional equivalent sliding mode control. When $\mu_{NZ}(s)\neq 1$, the chattering eliminated can be realized through the membership function $\mu_{NZ}(s)$.

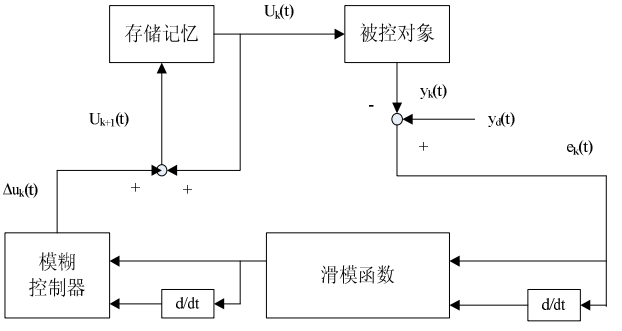

Fig. 1. The structure of fuzzy sliding mode iterative learning control

2 The Simulation Experiment

Set the transfer function for the controlled object is

$$G(s)=\frac{133}{s(s+25)} \tag{16}$$

Change the formula (16) into state equation

$$\dot{x}=Ax+Bu \quad . \tag{17}$$

In formula (17), $x=[x_1 \quad x_2], A=\begin{bmatrix}0 & 1\\ 0 & -25\end{bmatrix}, B=\begin{bmatrix}0\\ 133\end{bmatrix}$. The desired trajectory is $y_d=0.5\sin(\pi x)$, assuming the initial condition of this system is zero. Figure 2 showed the tracking error for the first, fifth, tenth iterative learning. As is shown in the figures, with the increase of iterations times, error was more and more small, constantly tending to zero, namely the system constantly converged in the operation.

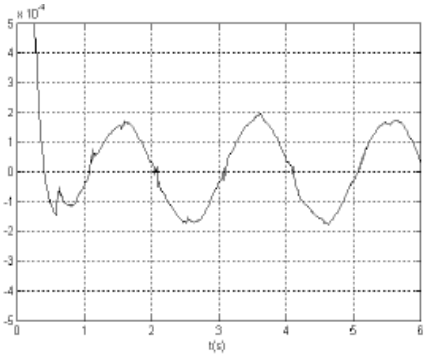

(a) Tracking error of the first time iterative learning

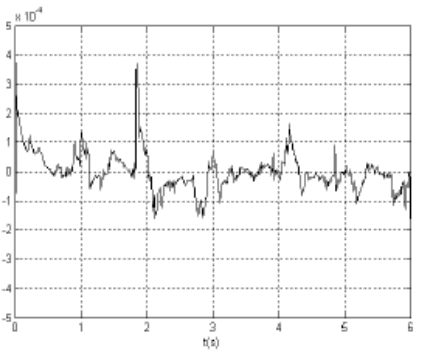

(b) Tracking error of the fifth time iterative learning

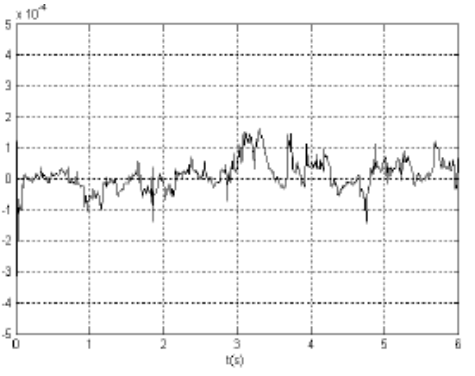

(c)Tracking error of the tenth time iterative learning

Fig. 2. System tracking error

3 Conclusions

ILC convergence speed is the key factor whether iterative learning control algorithm can realize. This paper sped up the convergence rate of the ILC by using the response speed characteristics of the sliding mode control, and alleviated the sliding mode control chattering by fuzzy control. Through the simulation, it can be seen that, with the increase of iterations times, error reduced gradually and verified the feasibility and validity of this method.

References

1. Xuan, S.M., Jian, H.B.: Iterative learning control, p. 2. National Defense Industry Press, Beijing (1999)
2. Fan, Z.C., Jing, H.: Sliding mode variable structure of intelligent control theory and application, p. 2. Science Press, Beijing (2005)
3. Ming, H.Y.: Variable structure control theory and application, p. 1. Science Press, Beijing (2003)
4. Kun, L.J.: Sliding mode variable structure control MATLAB simulation, p. 109. Tsinghua University Press, Beijing (2005)

An Identification Method of Bridge Structural Damage Based on Fourier Transform and Neural Network in Electronic Information Engineering

Xiao-jun Lu[1] and Ping Zhang[2]

[1] School of Transportation, Wuhan University of Technology, Wuhan, China
[2] Wuhan Zhenghua Architectural Design CO., LTD, Wuhan, China
lxjzp@126.com, 47079389@qq.com

Abstract. In the bridge health monitoring and evaluation systems, the modal parameter can only access needed accuracy after times of experiments. The paper proposed a kind of bridge structure damage diagnosis method based on Fourier transform and artificial neural network in electronic information technology in electronic information engineering. It firstly standardizes original disturbance data. Then, the random noise and Gaussian noise were injected into original data and discrete Fourier transform was used to analyze data with noise. Finally, the back-propagation BP neural network was used to determine these damage points. The numerical example based on experiments shows that the proposed method can effectively identify structural damage of the bridges.

Keywords: bridge structure, damage identification, Fourier transform, neural network.

1 Introduction

In the bridge health monitoring and evaluation system, the modal parameters of structure are of great important. It consists of a serial unique data, which is equal to the fingerprint of special structure. Each structure has its inherent modal parameters, such as natural frequency, model shape and damping. If the structure was damaged, the fingerprint of it will also change. Therefore, the modal analysis method can be used to identify damage in theory [1-3]. The essence of modal analysis is a kind of coordinate transformation, the aim of which is to place response vector in original physical coordinate system into the so-called modal coordinate system for description. Each base vector of the coordinate system is just a feature vector of vibration system. The benefit of using this coordinate system is that orthogonal properties of eigenvectors enable each coordinate of response vector is independent of each other without coupling.

The modal parameter identification methods can be divided into two categories, namely frequency domain identification and time domain identification. The frequency domain identification methods develop early. It transforms measured time domain data to frequency domain with FFT and is identified with power spectral density (PSD). As the physical concept of frequency domain method is clear and not

D. Jin and S. Lin (Eds.): Advances in Mechanical and Electronic Engineering, LNEE 177, pp. 351–356.
springerlink.com

easy to miss modal or generate false modal, so the reliability is higher and widely used in modal analysis. The time domain identification directly uses data in time domain for identification. It can avoid error of frequency domain method caused by FFT, such as frequency decomposition, leakage and aliasing, so it can access to more accurate result in general [4-6]. For small and simple structure, whether time domain or frequency domain analysis method can achieve satisfactory result in modal parameter identification. To big scale complex structure as bridge, the modal parameter can only access needed accuracy after times of experiments. Therefore, there is no clear identification method be applicable to all types of structure. It should be select reasonably according to actual situation. Based on Fourier transform and BP neural network, the paper proposed a kind of bridge structure damage diagnosis method. The paper is organized as follows: section 2 introduces basic theory of Fourier transform and neural network; section 3 gives diagnosis method; section 4 analyzes specific diagnosis example and section 5 concludes our work.

2 Fast Fourier Transform and Neural Network

2.1 Basic Theory of Fast Fourier Transform

FFT begins from fast DFT algorithm using periodic and symmetric of WN factor by J. W. Cooley and J. W. Tukey in 1965. In the later decades, FFT algorithm has been further developed. The commonly used algorithm is radix-2 algorithm and split-base algorithm. Firstly the Fourier transform of two-dimensional continuous function was introduced. Set $f(x, y)$ is function of two independent variable x and y, which meet the condition of $\int_{-\infty}^{+\infty}\int_{-\infty}^{+\infty}|f(x,y)|dxdy < 0$. Define (1) as Fourier transform of $f(x, y)$ and (2) as inverse Fourier transform.

$$F(u,v) = \int_{-\infty}^{+\infty}\int_{-\infty}^{+\infty} f(x,y)e^{-j2\pi(ux+vy)}dxdy . \tag{1}$$

$$f(x,y) = \int_{-\infty}^{+\infty}\int_{-\infty}^{+\infty} F(u,v)e^{j2\pi(ux+vy)}dxdy . \tag{2}$$

The amplitude spectrum, phase spectrum and energy spectrum of Fourier transform are:

$$|F(u,v)| = \left[R^2(u,v) + I^2(u,v)\right]^{1/2} . \tag{3}$$

$$\varphi(u,v) = \arctan\left[I(u,v)/R(u,v)\right]. \tag{4}$$

$$E(u,v) = R^2(u,v) + I^2(u,v) . \tag{5}$$

Where, $R(u,v)$ and $I(u,v)$ are real and imaginary parts of Fourier respectively.

After sampling, the continuous signal $f(x, y)$ becomes two-dimensional signal $f(m, n)$, where $0 \le m \le M-1$ and $0 \le n \le N-1$. Accordingly, the two-dimensional Fourier transform is defined as:

$$F(p,q) = \sum_{m=0}^{M} \sum_{n=0}^{N} f(m,n) e^{-j(2\pi/M)pm - j(2\pi/N)qn} . \tag{6}$$

The definition of discrete Fourier inverse transform is:

$$F(m,n) = \sum_{m=0}^{M} \sum_{n=0}^{N} f(p,q) e^{j(2\pi/M)pm - j(2\pi/N)qn} . \tag{7}$$

2.2 Artificial Neural Network

Artificial neural network is an adaptive non-linear dynamic system constituted by large amount of neurons with rich and perfect connections. The neuron is the basic unit of the neural network, which usually shows a multi-input and single-output non-linear device. BP neural network is a kind of multilayer feedforward neural network. From self-learning with several samples, establish non-linear mapping relationship between network output variable and input variable. Basic BP network is made up of input layer, hidden layer and output layer. The units in same layer are not connected.

The input layer and output layer have L and N neurons corresponding to network input variable I_l and output variable O_n. The hidden layer has M (M=2L+1) neurons. The input variable I_l is allocated to the m-th neuron based on (8) as its input D_m.

$$D_m = \sum_{l=0}^{L} \omega_{lm}^{1} I_l . \tag{8}$$

Where, ω_{lm}^{1} is the weight coefficient from unit 1 in first layer to the n-th unit in second unit. The output Cm of m-th unit is function of its input D_m, namely $C_m = f(D_m)$. The transfer function of neuron usually selects sigmoid function, namely:

$$f(x) = 1/(1+e^{-x}) . \tag{9}$$

Similarly, we can define the input G_n and output O_n of the n-th unit in the third layer are $G_n = \sum_{m=0}^{M} \omega_{mn}^{2} C_n$ and $O_n = F(G_n)$.

We can know from sigmoid function that the value range of output O_n is (0, 1). The expected output of sample should be normalized. After network training with a certain number of samples, the optimal weight coefficient can be determined so that the second residual error between output value and expected value is the minimum. The process is completed with BP algorithm.

3 Diagnostic Method Based on Fourier Transform and Neural Network

Firstly, the collected actual data $D = \{x_i : 1 \le i \le N\}$ was z-score standardized with the following formula. This method is the standardization of data with mean and standard deviation of original data. The original value of D was standardized to F with z-score.

$$E(x) = \frac{1}{n}\sum_{i=1}^{n} x_i \ . \tag{10}$$

$$D(x) = \sqrt{\frac{1}{n-1}\sum_{i=1}^{n}(x_i - E(x))^2} \ . \tag{11}$$

$$F = \left\{ y_i = \frac{x_i - E(x)}{D(x)}, 1 \le i \le N \right\}. \tag{12}$$

Then, the standardized data $F = \{y_i : 1 \le i \le N\}$ was divided into s sequences F_1, F_2, …, F_s $F_j = \{y_{ji} : 1 \le j \le s, 1 \le i \le t\}, N = s \times t$, the length of which is t. Select $s/2$ sequences randomly and inject noise data to these sequences with different SNR.

Clearly, the original with various noise data in time domain is chaotic, so it is difficult to extract fault mode from time domain. On this basis, we transform the data sequence from time domain to frequency domain with FFT.

After the noise data was injected, these data sequence was divided into two parts, namely $G_1 = \left\{ F_i, 1 \le i \le \left| \frac{s}{2} \right| \right\}$ and $G_2 = \left\{ F_i, \left| \frac{s}{2} \right| + 1 \le i \le s \right\}$, where G_1 is used for training coefficient of neural network and G_2 is fault classification sample data.

4 Computation Example

The proposed diagnosis above was used to actual bridge modal analysis so as to determine the diagnostic capability of the algorithm. Some bridge is located between site *a* of Area *A* and site *b* of Area *B*. There is another bridge in 6km downstream. The main bridge uses double tower double cable floating system cable-stayed bridge, the length of which is 718m and cross-bridge 179m +360 m +179 m.

Select 7th interference sensor in Fig 1 as measuring point so as to obtain 400 groups of interference data. The odd number of 400 groups was injected into noise data. Fourier transform was used to decompose data according to different fields and computed coefficients. The former 300 groups of data were used as training samples of neural network and later 100 groups as test sample to verify algorithm accuracy. The layout of 26 interference sensors is shown in Fig. 1. The fault recognition rate after been injected random noise and Gaussian noise with different SNR is shown in Table 1 and Fig. 2.

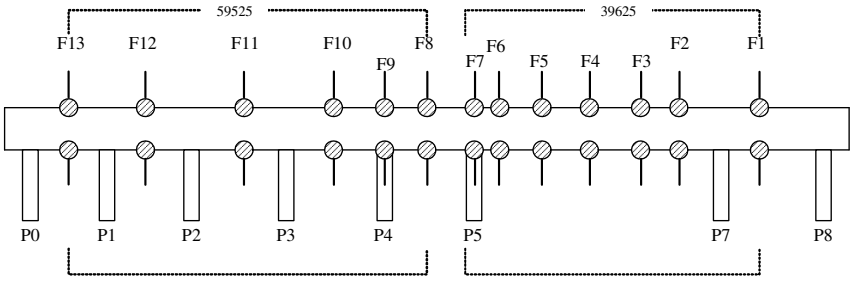

Fig. 1. Layout of interference sensors

Table 1. Fault recognition rate

Noise type	SNR					
	0.5	1	2	3	4	5
Gaussian noise	85.0%	82.0%	71.0%	65.0%	65.0%	63.0%
Random noise	96.0%	91.0%	81.0%	79.0%	75.0%	70.0%

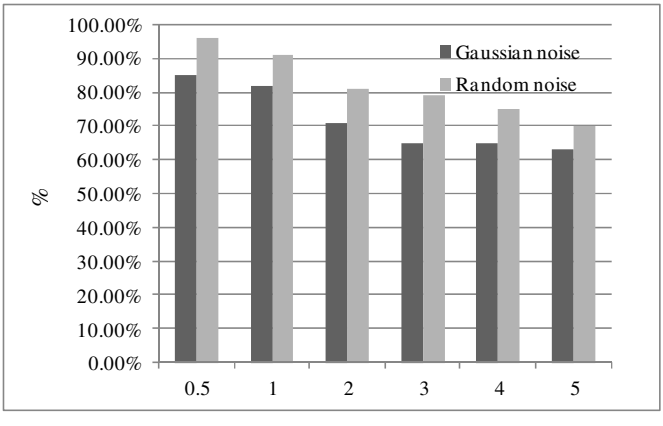

Fig. 2. Fault recognition rate comparison

From Table 1 and Fig. 2, we can see that the structural damage diagnosis on bridge measured data based on the method is feasible, which can achieve ideal recognition results.

5 Conclusion

To simple structural object, the time domain and frequency domain methods can all achieve ideal result. In the modal parameter identification of large scale complex structural objects, we can only ensure accuracy from times of experiments. A kind of bridge structure damage diagnosis method based on Fourier transform and artificial

neural network in eletronic information techonology was presented in the paper, which firstly injects random noise and Gaussian noise into original data. Then, the back-propagation BP neural network was used to determine these damage points. The numerical example based on experiments shows that the proposed method can effectively identify structural damage of the bridges. Next, we will focus on improvement of transmit function of BP network, so as to improve diagnostic speed and accuracy.

References

1. Shi, Z.Y., Doebljng, S.W., Farrar, C.R.: Application of the strain energy damage detection method to plate like structures. Sound and Vibration 128, 825–844 (1998)
2. Cornwell, P., Law, S.S., Zhang, L.M.: Structural damage localization from modal strain energy change. Sound and Vibration 224, 359–374 (1999)
3. Wu, X., Ghaboussi, J., Garrett, J.H.: Use of Neural Networks in Detection of Structural Damage. Computers and Structures 42, 649–659 (1992)
4. Cui, F., Yuan, W., Shi, J.-J.: Damage Detection of Structures Based on Static Response. Journal of Tongji University (Natural Science) 28, 5–8 (2000)
5. Zhen, D.-L., Li, Z.-F., Hua, H.-X.: A Summary Review of Structural Initial Damage Identification Methods. Journal of Vibration and Shock 21, 1–6 (2002)
6. Wang, B.-S., Ding, H.-J., Ni, Y.-Q.: Influence of Modeling Errors on Input Vectors to Neural Networks for Damage Identification. China Civil Engineering Journal 33, 50–55 (2000)

A GPS and Electronic Chart Based Maritime Positioning System for Searching and Rescuing Drowning People

Dongdong Wang[1,*], Kai Liu[1], Yongjian Chen[2], Xiaofeng Ma[2], Wenxu Wang[2], and Yang Liu[2]

[1] School of Electronics and Information Engineering, Beihang Univ., Beijing 100191, China
[2] CCCC Water Transportation Consultants Co., Ltd., Beijing 100088, China
boywang2007@163.com, liuk@buaa.edu.cn,
{chenyongjian,maxiaofeng,wangwenxu,liuyang}@pdiwt.com.cn

Abstract. With the rapid development of ocean shipping industry in China and the increasing of shipwreck occurrence, the higher requirements for maritime search and rescue are proposed. However, the current maritime search and rescue, depending on life jacket and searching in a large area, causes low efficiency. To solve this problem, this paper designed an intelligent maritime search and rescue system. The system integrates global positioning system (GPS), geographic information system (GIS), database synchronization and wireless transmission technologies. Test results show that the system guarantees the precise positioning of drowning people effectively and provides a reliable basis for rescue ships to search and track drowning people.

Keywords: maritime search and rescue, maritime positioning system, wireless data transmission, electronic chart.

1 Introduction

With the tremendous growth of marine economy, Chinese ocean shipping industry made a great development [1]. By the end of 2010, the unified national vessel registration database of registered ship has reached 259,360 and 13,178 million tonnage. Water transportation has made tremendous development, which brought great pressure to the Marine.

There have been great advances in Chinese maritime emergency search and rescue capacity in the past five years [1]. However, there still a big gap between Chinese maritime and developed countries [2], in which the defects of search and rescue positioning system have seriously hampered the effective conduct of search and rescue work in China, for example, in the United States the average time to complete the rescue work is 3 hours [3], while in China is 10 hours. For the status quo of China, to achieve an all-weather rapid response and precise positioning system for drowning people has become the most important task for search and rescue work.

Refs [4] and [5] adopted mobile location technology to search and rescue work of small vessels and drowning people. To a certain extent, this approach can really

* Corresponding author.

D. Jin and S. Lin (Eds.): Advances in Mechanical and Electronic Engineering, LNEE 177, pp. 357–363.
springerlink.com

enhance the efficiency of search and rescue work. However, on one hand the mobile location technology is not yet perfect, especially on coastal sea due to the distance between base stations, the positioning accuracy of only the cell coverage radius; on the other hand, mobile phone base stations can only cover the coastal waters which limits the scope of application. Therefore, the approach cannot perfectly improve the efficiency of search and rescue work. Ref [6] applied the "internet of things" technology to marine search and rescue work, which is a good idea and if be implemented may be effectively improve the efficiency of search and rescue work. However, the system needs fixed relay nodes and evenly distributed in all channels, which will bring two issues: First, the vast waters of our country, how many nodes? Second, nodes work underwater, cannot use solar energy, how to provide energy for each node? So, for today, this is an unrealistic approach.

In this paper, a GPS and electronic chart based maritime positioning system for searching and rescuing drowning people is proposed, which makes up for the defects of above-mentioned marine rescue system, and develops a set of practical devices. The system integrates global positioning system (GPS), geographic information system (GIS), database synchronization and wireless transmission technology, to effectively guarantee the precise positioning of drowning people, and provide a reliable basis for rescue ship to search and track the drowning people. Test results show that the proposed system effectively reduces rescue time and improve the efficiency of the searching and rescuing drowning people.

The rest of this paper is organized as follows: Section 2 introduces the system, Section 3 describes in detail on system design, Section 4 describes system performance testing and Section 5 summarizes the paper.

2 Maritime Search and Rescue Positioning System

The proposed GPS and electronic chart based maritime positioning system for searching and rescuing drowning people mainly consists of the active for help terminal carried by drowning people, the receiving terminal and the search and rescue display device installed in the search and rescue ship; the land command and control center gets the real-time information of rescue progress and sends commands to the search and rescue ship through the maritime satellite or sea search and rescue network radio, as shown in Figure 1.

The system works as shown in Figure 1: When shipwreck Occurs, the crew fall into water, then the active for terminal automatically open; the active for help terminal positioning by GPS, and send for-help signal containing its own location information to the near rescue vessel or marine rescue center; rescue vessel receive s the for-help information through the information receiving terminal, then show its location on the rescue display device. By this system the search and rescue workers will find that drowning people quickly and improve the survival rate of drowning people rescue events.

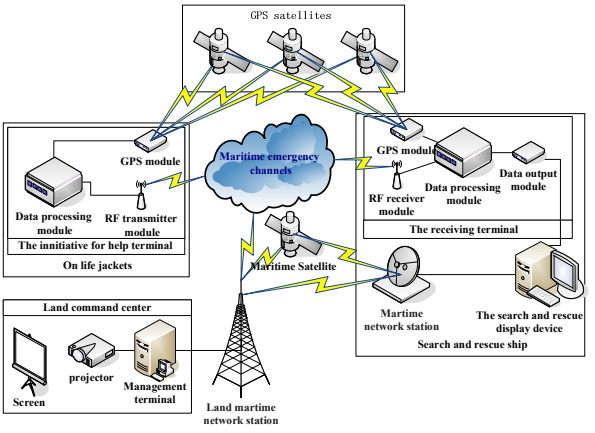

Fig. 1. Components of the proposed system

3 Maritime Search and Rescue Positioning System Design

The GPS and electronic chart based maritime positioning system mainly consists of active for help terminal, receiving terminal and search and rescue display device.

3.1 Active for Help Terminal

The terminal consists of GPS module, RF transmitter module, micro controller (MCU), lithium-ion battery, reed switch and LED indicator, as shown in Figure 2.

The workflow is shown in Figure 3.When reed switch conducted, the main system is powered; MCU begins to initialize the implementation, and supply power to GPS unit, then entering the running state; after powered, GPS unit calculates its location; when reach the sending time, MCU checks the positioning status of GPS, if GPS location is invalid, the location information stored in the MCU will be selected or the current location information will be selected, then MCU starts transmission program; MCU provides for-help data to RF modulation and then send data; after sent, system enters a low power state and waiting for the next send time.

3.2 Receiving Terminal

A terminal including three main parts: RF signal receiving module, MCU and data output module. The hardware structure of a receiving terminal is shown in figure 4.

The RF signal receiving module translates the received signal to original data; MCU, as the data processing unit, analyzes the original data and extracts the valid data; the data output module makes a data format conversion for the valid data and then outputs it.

3.3 Maritime Search and Rescue Display Device

The device marks the location, direction and speed of drowning people on the system charts accurately.

The hardware structure is shown in figure5. The external interfaces including a variety of interfaces, by which the device can get the position information both the active for help terminals and itself.

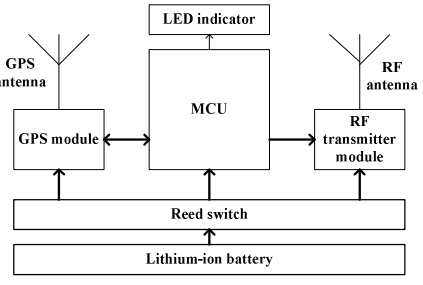

Fig. 1. Hardware structure of active for help terminal

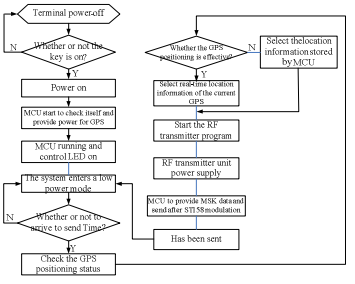

Fig. 3. Workflow of active for help terminal

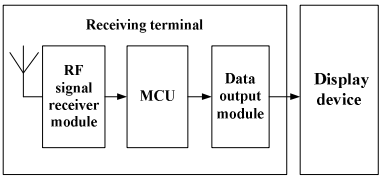

Fig. 4. Hardware structure of the receiving terminal

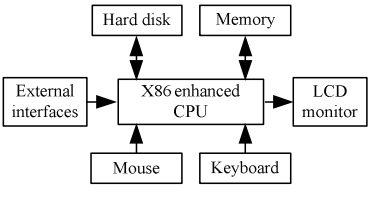

Fig. 5. Hardware structure of the display device

The design of positioning software is the core of the display device, which includes life safety system of drowning people and electronic chart platform.

(1) Life safety system for drowning people

The system integrates crew data, ship information, GPS, communication and navigation systems, GIS, Internet and other information; with one computer as a platform, displays the location, tracks and speed of drowning people in real-time.

(2) Electronic chart platform

The electronic chart depicts an overview of the total appearance of the coastal sea area; part of the harbor districts has been accurate to the ratio of 1:2000. In order to facilitate the ship safety navigation, the chart mainly marks navigation related channels, water depth, land names, isolated islands, reefs, beacons, submarine fiber optic cable and other elements. The elements of water quality, water depth, navigational obstructions, docks, anchorages, port area boundaries and port authorities are detailed in the areas near harbors.

4 Performance Test

4.1 Test Environment

Nine coast guard ships were used and tested in six waters of the Zhejiang and Hainan of China. The test environment is shown in Table 1.

Table 1. Coast guard ship and test environments

Coast Guard ship	Sea areas	Test environment			
		Weather	Electromagnetic interference	obstacles	The environment of active for help terminal
112	Ningbo	Sunny	without	4 islands	Shore water
1108	Ningbo	Sunny	without	2 islands	Shore water
1101	Wenzhou	Thick fog	Occasionally	without	Floating in the sea
1188	Wenzhou	Thick fog	someone call	1 island	Floating in the sea
1176	Wenzhou	Thick fog	Occasionally	without	Floating in the sea
1810	8-office	Sunny	without	without	On the kayak
1820	Sanya	Cloudy	without	without	On the kayak
1818	qinglan	Big Wave	without	without	On the kayak
183	Haikou	Cloudy	without	without	On the kayak

4.2 Hardware Test Results

The hardware test results of active for help terminal are shown in table 2, and the test results of maritime search and rescue display device are shown in table 3.

Table 2. The hardware test results of active for help terminal

group	Test items	Test results	
Physical test	Open method	Open automatically or manually	
	Carrying methods	Embedded in life jacket shoulder	
	Size	46×22×129mm	
	Weight	80g	
signal transmission test	Signaling frequency	Every 60 seconds	
	Transmit power	<6W	
	Channel frequency	156.800MHz	
	Frequency stability	±2ppm	
	Signal coverage	15-20n mile	
Battery test	Working time	≧12 hours	
	Standby time	6 Months	
Waterproof	IP67	Positioning test	5m

The physical test results of active for help terminal indicate that the terminal has small size, light weight, waterproof and easy to carry; the signal transmission performance test data shows that the output power of the terminal is high, the output

frequency is stable and the signal coverage is far; the battery performance test results show that the terminal battery has high capacity, long standby time and long working hours; the positioning performance of the terminal meets he indicators.

Table 3. The hardware test results of maritime search and rescue display device

Physical test	Size	459mm×170mm×410mm	
	Weight	11Kg	
	Built-in module	GPS/ CDMA/ distress signal receiver	
	External interfaces	USB 2.0/ RS232/ RS422/ RJ45/ GPS/ Antenna	
	Anti-electromagnetic interference	Field strength of 100 ~ 300MHz, microvolt 50dB	
display test	Start-up time	15 seconds (hot start)	45 seconds (cold start)
	Resolution	1280×1024	
	Refresh time	＜500 ms	

The physical performance test data indicates that the device is small in size, light weight, easy to install and easy to operate; high hardware configuration, powerful, rich of interface and strong expansibility; the number of receiving channels can be increased or decreased if necessary and the receiving function is fine, anti-electromagnetic interference, anti-static ability; good diffraction ability to reduce the interference of some islands on the signal. Positioning display system performance test results show that the device start-up time is short, the type of the received signal is rich, rapid renewal and high-resolution; Sea search and rescue network site tests show that the site keeps in touch with land command center very well.

4.3 Software Test Results

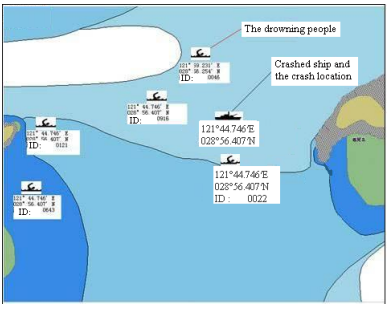

Fig. 6. The UI of life safety system

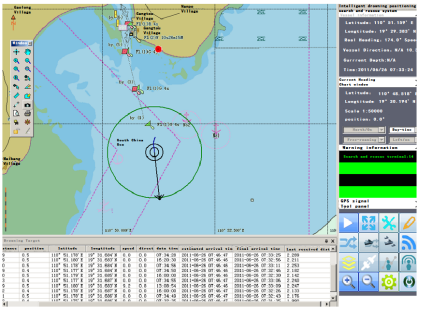

Fig. 7. The UI of electronic chart

The user interface (UI) of software life safety system for drowning people is shown in Figure 6. The test results show that the software can show the location, direction and speed of the crashed ship and drowning people vividly, comprehensively and in real-time, making the rescue work more effectively and minimizes the degree of casualties.

The UI of the electronic chart is shown in Figure 7. Test results show that the electronic chart display is smooth, rapid and seamless global roaming, zooming and rotation are supported. It provides a flexible user-drawn interface and supports a variety of professional model calculations, large-capacity moving targets management. The maximum track points and maximum route number is 200 thousand and 10 thousand, and tracks save time is 3 months.

5 Conclusions

A GPS and electronic chart based maritime positioning system for searching and rescuing drowning people is proposed in this paper, which can accurately show the location, direction and speed of both the drowning people and rescue ship. The system is an integrated application of GPS, GIS, database synchronization and wireless transmission technology, which consists of active for help terminal, receiving terminal and maritime display device. The active for help terminal, embedded in the life jacket of drowning people, can automatically send distress signal including its location information to search and rescue ship; receiving terminal and search and rescue display device, installed in the search and rescue ship, receive and display the position information of drowning people for search and rescue personnel in real time, ensuring the rapid implementation of search and rescue work. The test results show that the system is well-designed, low cost and has the advantages of far communication coverage, accurate positioning, high display performance, easy to use and steady running, which effectively improves the efficiency of search and rescue work for drowning people.

Acknowledgments. This work is supported by the National Key Technology R&D Program of China under Grant 2009BAG18B02.

References

1. The editorial department: The achievements in the eleventh five-year plan of maritime(4): Achievements base on digital. J. China Maritime Safety (1), 17 (2011)
2. Cheng, M.Y.: Comparison and reference of domestic and foreign salvage. J. World Shipping (12), 41–45 (2011)
3. Wang, H.: The Analysis of Chinese maritime search and rescue situation. J. Tianjin Navigation (3), 59–61 (2010)
4. Zheng, H.Y.: About the application of modern mobile communication positioning techniques in maritime search and rescue. J. China Maritime Safety (4), 44–46 (2007)
5. Wang, H.X., Yu, J.H.: About the application of mobile positioning techniques in maritime search and rescue. J. Marine Technology (S2), 37–38 (2008)
6. Pan, X.D.: Application of internet of thing in searching and rescuing drowning life. J. Chinese Shipping (7), 38–39 (2010)

Electronic Multimedia Retrieval Systems: Architecture, Features and Novel Directions

Carmelo Pino and Roberto Di Salvo

Department of Electrical, Electronics and Computer Engineering,
Catania University, viale Doria 6, Catania, Italy
{carmelo.pino,roberto.disalvo}@dieei.unict.it

Abstract. Internet growth and the development of web technologies, transformed the Web from a purely research network to an essential every day tool. In particular, the strong demand and availability of multimedia resources combined to the intrinsic semantic gap, favoured the evolution of content based multimedia retrieval systems. The request of flexibility that is required from the multimedia retrieval users and the semantic gap have been the spring for the evolution of the new generation of media retrieval system. This paper aims at illustrating the architecture and features of electronic multimedia retrieval by pointing out how these systems are provided with a suitable semantic layer to improve the system performance, where annotation, relevance feedback and semantics driven object recognition increase the precision of the multimedia retrieval. How the clustering of the multimedia materials may be used to increase the recall and to support the reuse of multimedia material for developing new artefacts is also discussed, thus envisaging novel research directions.

Keywords: electronic multimedia retrieval, image processing, semantic web, experience reuse, clustering.

1 Introduction

MultiMedia retrieval (MMR) aims at extracting multimedia content related to descriptors or metadata, thus supporting advanced search functions. These systems were made by extraction algorithms of multimedia items matching the Low Level Features (LLF) indicated in the user query [1].

However, the users needs are today the ones of retrieving contents from a multimedia archive at the semantic level. This requires novel techniques to extract relevant materials from machine-level audio-visual feature descriptors by using semantic-level descriptors. Such techniques give rise to a semantic layer, where the media retrieval systems my be done by words or by Query By Example interfaces (QBE). Relevance Feedback (RFB) is also provided to allow the users to refine their queries on the basis of the relevance of the retrieved material.

Since the design of an MMR system has to take into account the user directives, its implementation is directed toward the design of an explicit semantic layer that consists of semantic mapping methods interacting with the LLFs that represent the

D. Jin and S. Lin (Eds.): Advances in Mechanical and Electronic Engineering, LNEE 177, pp. 365–372.
springerlink.com

media data, to create a bridge between the LLFs of the stored items with the *High Level Features* (HLFs) that represent the high level media concepts.

There are different techniques to design a semantic layer of an MMR system, and different methodologies for the resources description. Resources description and the LLF mapping are mediated by standard schema like MPEG-7 or by ontologies that are, today, an essential support to describe and design semantic layers in any framework. Thus, aim of the paper is the one of presenting the main techniques used to design a semantic layer, the methods to describe the media contents, and the new challenges to model domain ontology mediated MMR systems. In particular, sect.2 outlines the characteristics of a modern multimedia retrieval system provided with a semantic layer dealing with the domain features. Section 3 illustrates the main techniques that increase the recall and the precision of an MMR system and envisages some future improvements of the current systems.

2 Semantic MMR Systems: Architecture and Main Features

The aim of the MMRs is to understand the semantic information contained into a media, by identifying the meaning (a car, a child, etc..). of the elements present into the media objects (e.g. a red object in the lower, a pink object with specific texture in determined position of the image, etc..). Fig.1 shows how this can be obtained by means of two examples (one for videos and the other for images). Both videos and images are first segmented, then each segmented object is mapped to high level concepts (or HLFs) in automatic or assisted way, and finally it is processed to extract its LLFs. Data extracted from the media must be saved in a structure in order to preserve information about objects, its low level representation and semantic mapping.

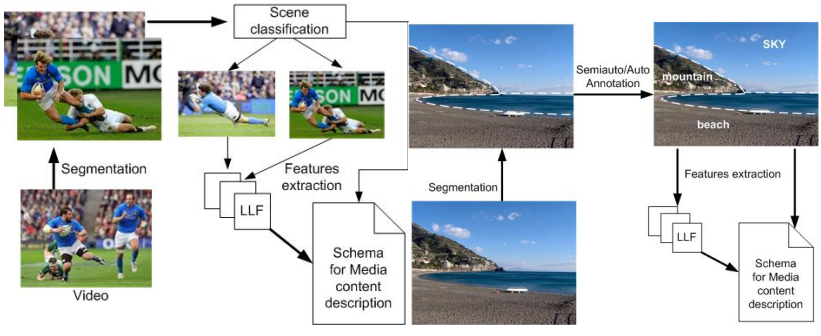

Fig. 1. Concept mapping for video (left) and for images (right)

The current standard de facto in multimedia contents description is the MPEG-7 [2], known as Multimedia Content Description Interface. It supports multimedia content description from several points of view, including media information, creation information, structure, usage information, textual annotations, media semantic, and low-level visual and audio features. Therefore, MPEG-7 description is associated with

the contents to allow the user to efficiently search the relevant material. There are many applications and domains which use MPEG-7 standard: a) Digital library: Image/video catalogue, musical dictionary, b) Multimedia directory services: e.g. yellow pages, c) Broadcast media selection: Radio channel, TV channel, d) Multimedia editing: Personalized electronic news service, media authoring.

The use of contents description metadata represents a way to unify contents and description in a unique media object. Fig.2 illustrates how we may structure an MMR system to store semantic information at the end of the concept mapping phase and to get relevant data from the description schema in the retrieval phase. This architecture is generalized in Fig.3, where we show the main functions of a electronic multimedia retrieval system [5]. The central part deals with the algorithms to implement the LLF extraction. The user interface allows the user to formulate a query by providing a suitable example. The semantic Layer works using MPEG-7 to map the LLF to HLF and vice-versa. Fig.3 shows also that annotations may be associated to the media, thus increasing the precision of the retrieval at the semantic level.

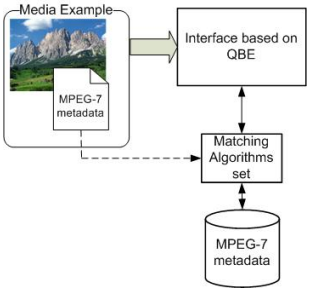

Fig. 2. Retrieval process using media object with standardized contents description schema following MPEG-7 metadata

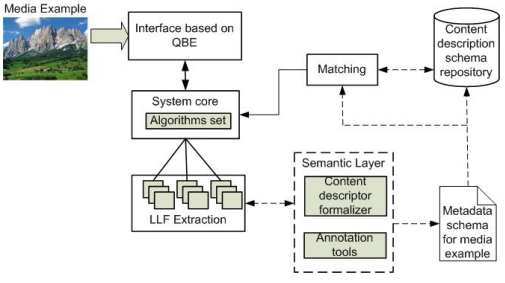

Fig. 3. A general semantic multimedia framework

Let us note that MPEG-7 is based on XML schemas. Its syntax enables some interchanges across applications over the web, but it does not support the required metadata interoperability. Consequently, Semantic Web technologies, such as the ones based on RDF and OWL, have been taken into account to translate MPEG-7 in standard format. Such technologies deal with ontologies [6], Machine learning [7], probabilistic techniques [8]. Ontologies are the most promising techniques to support the complete definition of a semantic layer and to help the entire process of data retrieval [29].

In fig 4 an example of personalized domain ontology is sketched. The ontologies may be expressed using OWL or Multimedia Web Ontology Language (MOWL) [31] that has been designed to facilitate semantic interactions with multimedia contents. It supports perceptual modeling of concepts using expected media properties. MOWL supports a probabilistic reasoning framework based on Bayesian Network. Fig.5 shows how a modern semantic layer consists of ontologies that define

the application domain concept cooperating with others that define the content media description, e.g., in the MPEG-7 the domain knowledge is integrated to the contents domain in the form of domain ontologies to achieve semantic interoperability.

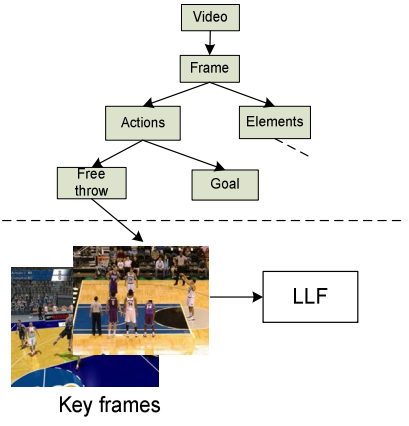

Fig. 4. Domain ontologies in basket video retrieval

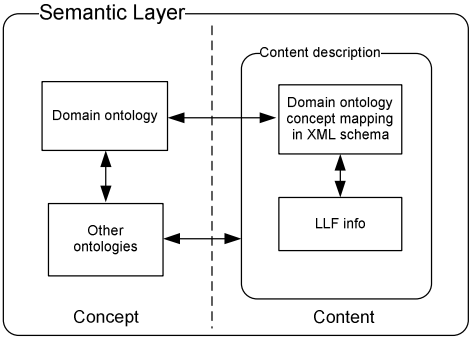

Fig. 5. Semantic layer where the concept (expressed with ontologies) are separated from the media Content (expressed with MPEG-/ or other). Domain ontologies are mapped with concept described in XML schema into content description schema.

3 Techniques to Improve Semantic Based MMR

The main techniques to improve MMR are as follows: a) annotation and relevance feedback, b) ontology and object recognition, d) ontology integration, and e) MOWL.

3.1 Annotation, Linked MM Data and Relevance Feedback

An overview of the annotation tools for video and image retrieval is given in [11], [12]. Also, projects have been carried out for the annotation and retrieval of multimedia material such as RUSHES (www.rushes-project.eu/default.aspx?page=home) i.e., an MM engine for the retrieval of annotated multimedia semantic units to reuse of experience to produce new MM materials. This is obtained according to the approach first proposed in [13] to let design concepts to emerge from linked data. In particular, storing the links between any MM materials existing in either a centralized or a distributed archive and the influential ones (e.g., the ones identified by the relevance feedback issued by the user), it is possible to interrelate different design stories., e.g., the designs of new MM assets from previous raw MM materials, also known as "rushes". In [14] an effective unsupervised clustering technique has been proposed to favor the extraction of similar semantic units. Such a clustering technique may be used to support either single users or communities of designers [15]. A first example following this trend is the framework named CALIMERA (Conference Advanced Level Information ManagemEnt and RetrievAl)

dealing with the management and retrieval of the multimedia information generated within the scientific conferences [10]. Its MM data store is structured to facilitate the retrieval of relevant data from metadata formats such as MPEG-7, RDF and OWL taking advantage from the annotations semi-automatically produced by the system. Clustering techniques for facilitating the reuse of experience are not present neither in this system or in the other current MMR frameworks. Thus, clustering techniques for similarity analysis should be integrated in the current and future MMR systems such as the ones proposed for video retrieval in [16] aiming at increasing precision or the ones based on the Self Organizing Maps proposed in [17] and [18] aiming at increasing recall. An integration of such approaches would guarantee that MM data belonging to the same cluster or to close clusters are similar between them and fits the query issued by the users. Massive archive of MM linked data may be clustered by using a parallel implementation of the mentioned clustering techniques over a GRID or CLOUD infrastructure as proposed in [19].

3.2 Semantic Enrichment for Object or Scene Recognition

Ontology may create the envisaged bridge from to LLF and HLF as pointed out in [20], where an ontology mediated retrieval system is proposed to combine logic-based retrieval with multimedia feature-based similarity retrieval. This approach could be used to extract MM materials to manage static and dynamic control systems. For example, the traffic control could be facilitated by an MMR system if it is able to automatically extract the current congested situations or dangerous people behaviors. In this case the MM store should be formed by real time images taken from cameras as shown in [21] and [22], whereas the ontological description of the traffic system given in [23] should be powered by a (feature-based) multimedia retrieval component to extract the images relevant for the query.

This would open a novel interesting scenario of MMR applications where a system manager may describe in advance the relevant situations that the Online MMR (OMMR) system should signal to prevent or limit dangerous consequences. The alert images extracted by OMMR should help the manager in better controlling the system. Semantic information may be derived also from the features of the media object (images in this case), e.g., [24], where an approach to find semantic meaning in visual object class is proposed accordingly to the Gestalt law of proximity. The approach of tagging the images implicitly is typical of the MM recognition systems, e.g. face recognition algorithms [25], which are able to derive either general or specific properties from images for either off-line retrieval or real time control.

Let us note now that an ontology that contains visual information can facilitate also the annotation process in a broad domain. Conversely, visual information may identify requirements that a visual ontology has to meet. Based on these requirements, an ontology based annotation approach is proposed in [26] which investigate how annotations may be created automatically from two existing knowledge corpora (WordNet and MPEG-7) by creating links between visual and general concepts. In this example we can see how the mapping between LLF and HLF is made using MPEG-7 as a container of metadata and HL concept. The problem of joint modeling text and image components of MM documents is addressed in [27].

3.4 Integrating Media and Domain Ontologies

As illustrated in [10], the integration between domain and processing ontologies adapts the processing workflow for the media contents retrieval taking into account the constraints defined by the users for the specific domain, whereas the media ontology and the domain-processing ontology are responsible of the definition of the system interfaces. Fig. 6 shows how an ontology may be obtained by merging domain, media and processing ontologies. The three ontologies related to: pre-processing, elaboration and performance criteria are merged in order to obtain an ontology that include all the concept and constraints.

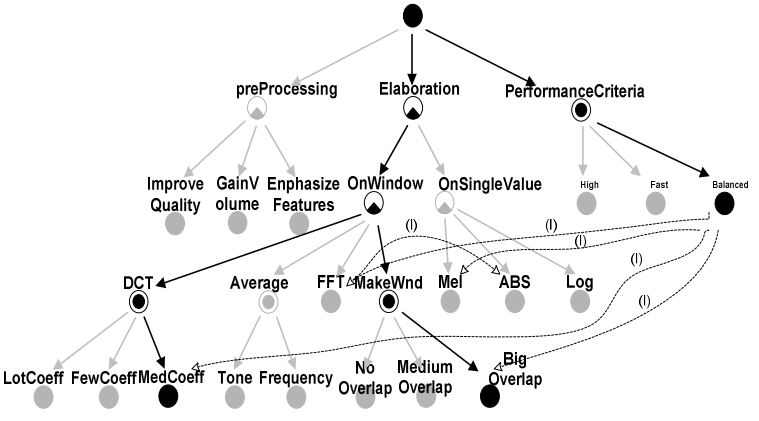

Fig. 6. MMR ontology driven system from merging media, domain and processing ontologies

4 Conclusions

Semantic based MMR architectures and features have been discussed to show that they improve the MMR systems that link images and textual descriptions without semantics aids such as the cross-modal systems, or others that refer to a detailed description of the metadata using MPEG-7. Thus, we expect that in a near future each resource may be identified by MPEG-7 contents descriptor using a specific RDF or MOWL schema to enrich MMR systems with semantics based techniques that improve precision of the retrieval process. Annotations, relevance feedback and object recognition may further improve the precision of the semantic MMR systems.

Also, merging several ontologies may provide the users with a wider vocabulary to retrieve the relevant data, as illustrated by the MMR system proposed in [30], where we can see one of the first approaches to tackle the retrieval of indexed multimedia keeping the semantics all over the steps of the process. The designed architecture and the implemented system allows to take advantage of the information sources with different levels of semantic richness. The architecture of this system uses not only the semantics of the indexed contents of some information sources, but also a domain semantics. This work summaries the results of a project carried out by two companies of the area of Car Design and Engineering.

Advanced user interfaces to better support query formulation and result visualization are also expected to provide the users with MMR systems that possess a semantic level more and more full-bodied. As well as clustering methods should be included in current MMR systems to enhance their performance in terms of recall. Moreover, the reuse of MM materials to produce novel MMs may be facilitated by structuring the MM archive as illustrated in [33]. This is for further study.

References

1. Salembier, P., Smith, J.R.: MPEG-7 multimedia description schemes. IEEE Transactions on Circuits and Systems for Video Technology 11, 748–759
2. Möller, R., Neumann, B.: Ontology-based reasoning techniques for multimedia interpretation and retrieval. Springer, London (2008)
3. Tong, S., Chang, E.: Support Vector Machine Active Learning for Image Retrieval. In: Proceedings of the Ninth ACM International Conference on Multimedia. ACM (2001)
4. Naphide, H.R., Huang, T.S.: A probabilistic framework for semantic video indexing filtering and retrieval. IEEE Transactions on Multimedia 3(1), 141–151 (2001)
5. Garcia, R., Celma, Ò.: Semantic Integration and Retrieval of Multimedia metadata. In: 5th Int. Workshop on Knowledge Markup and Semantic Annotation (2005)
6. Giordano, D., Kavasidis, I., Pino, C., Spampinato, C.: A Semantic-Based and Adaptive Architecture for Automatic Multimedia Retrieval Composition. In: 9th International Workshop on Content-Based Multimedia Indexing (CBMI), pp. 181–186 (2011)
7. Zhang, R., et al.: A Probabilistic Semantic Model for Image Annotation and Multi-Modal Image Retrieval. In: Tenth IEEE Int. Conf. on Computer Vision, vol. 1(X), pp. 846–851 (2005)
8. Yang, Y., Nie, F., Xu, D., Luo, J., Zhuang, Y., Pan, Y.: A Multimedia Retrieval Framework Based on Semi-Supervised Ranking and Relevance Feedback. IEEE Trans. Pattern Anal. Mach. Intell. (2011)
9. Tous, R., Delgado, J.: Semantic-Driven Multimedia Retrieval with the MPEG Query Format. Multimedia Tools and Applications 49(1), 213–233 (2010)
10. Sokhn, M., Mugellini, E., Khaled, O.A., Serhrouchni, A.: End-to-End Adaptive Framework for Multimedia Information Retrieval. In: Masip-Bruin, X., Verchere, D., Tsaoussidis, V., Yannuzzi, M. (eds.) WWIC 2011. LNCS, vol. 6649, pp. 197–206. Springer, Heidelberg (2011)
11. Dasiopoulou, S., Giannakidou, E., Litos, G., Malasioti, P., Kompatsiaris, Y.: A Survey of Semantic Image and Video Annotation Tools. In: Paliouras, G., Spyropoulos, C.D., Tsatsaronis, G. (eds.) Multimedia Information Extraction. LNCS, vol. 6050, pp. 196–239. Springer, Heidelberg (2011)
12. Badii, A., et al.: Semi-automatic annotation and retrieval of visual content using the topic map technology. In: VIS 2008 WSEAS Conferences, Pittsburgh (2008)
13. Faro, A., Giordano, D.: Concept Formation from Design Cases: Why Reusing Experience and Why Not. Knowledge Based Systems Journal 11(7), 437–448 (1998)
14. Faro, A., Giordano, D.: StoryNet: an Evolving Network of Cases to Learn Information Systems Design. IEE Proceedings Software 145(4), 119–127 (1998)
15. Giordano, D.: Evolution of interactive graphical representations into a design language: a distributed cognition account. International Journal of Human-Computer Studies 57(4), 317–345 (2002)

16. Memar, S., Suriani Affendey, L., Mustapha, N., Shyamala, C., Doraisamy Mohammadreza, E.: An integrated semantic-based approach in concept based video retrieval. Multimedia Tools and Applications, 1–19 (2011)
17. Faro, A., Giordano, D., Maiorana, F.: Discovering complex regularities: from tree to semi-lattice classifications. Int. Journal of Computational Intelligence 2(1), 34–39 (2005)
18. Faro, A., Giordano, D.: Discovering genes-diseases associations from specialized literature using the grid. IEEE Transactions on Information Technology in Biomedicine 13(4), 554–560 (2009)
19. Faro, A., Giordano, D., Maiorana, F.: Mining massive datasets by an unsupervised parallel clustering on a GRID: Novel algorithms and case study. Future Generation Computer Systems 27(6), 711–724 (2011)
20. Straccia, U., Visco, G.: An Ontology Mediated Multimedia Information Retrieval System. 40th IEEE International Symposium on Multiple-Valued Logic (ISMVL), 319–324 (2010)
21. Faro, A., Giordano, D., Spampinato, C.: Integrating location tracking, traffic monitoring and semantics in a layered ITS architecture. IEE Int. Transport Systems, IET Journal 5(3), 197–206 (2011)
22. Faro, A., Giordano, D., Spampinato, C.: Evaluation of the traffic parameters in a metropolitan area by fusing visual perceptions and CNN processing of webcam based images. IEEE Transactions on Neural Networks 19(6), 1108–1129 (2007)
23. Faro, A., Giordano, D., Musarra, A.: Ontology based intelligent mobility systems. In: IEEE Proc. Int. Conf. on Systems, Man and Cybernetics, vol. 5, pp. 4288–4293. IEEE, Washington, D.C. (2003)
24. Ahmad, N., Youngeun, A., Park, J.: An intrinsic semantic framework for recognizing image objects. Multimedia Tools and Applications, 1–16 (2011)
25. Faro, A., Giordano, D., Spampinato, C.: An Automated Tool for Face Recognition Using Visual Attention and Active Shape Models Analysis. In: 28th Annual International Conference of the IEEE Engineering in Medicine and Biology Society, EMBC 2006, pp. 4848–4852. IEEE (2006)
26. Hollink, L., Worring, M.: Building a Visual Ontology for Video Retrieval. In: Proceedings of the 13th Annual ACM International Conference on Multimedia (2005)
27. Rasiwasia, N., Costa Pereira, J., Coviello, E., Doyle, G., Lanckriet Gert, R.G., Levy, R., Vasconcelos, N.: A New Approach to Cross-Modal Multimedia Retrieval. In: Proceedings of the International Conference on Multimedia (2010)
28. Faro, A., Giordano, D., Pino, C., Spampinato, C.: Visual attention for implicit relevance feedback in a content based image retrieval. In: Proc. of the 2010 Symposium on Eye-Tracking Research and Applications, ETRA 2010, pp. 73–76. ACM (2010)
29. Lux, M., Klieber, W., Becker, J., Tochtermann, K., Mayer, H., Neuschmied, H., Haas, W.: XML and MPEG-7 for Interactive Annotation and Retrieval using Semantic Meta-data. J-Jucs 8, 965–984 (2002)
30. Marcos, G., et al.: A Semantic Web based approach to multimedia retrieval. In: Proceedings of the fourth International Workshop on Content-Based Multimedia Indexing (CBMI 2005), Riga, Latvia (2005)
31. Ghosh, H., Chaudhury, S., Kashyap, K., Maiti, B.: Ontology Specification and Integration for Multimedia Applications. In: Ontologies: A Handbook of Principles, Concepts and Applications in Information Systems, ch. 9. Springer (2007)
32. Pereira, F., Vetro, A., Sikora, T.: Multimedia retrieval and delivery: Essential metadata challenges and standards. Proc. IEEE 96(4), 721–744 (2008)
33. Faro, A., Giordano, D.: Design memories as evolutionary systems: socio-technical architecture and genetics. In: IEEE Proc. Int. Conf. on Systems, Man and Cybernetics, vol. 5, pp. 4288–4293. IEEE, Washington, D.C. (2003)

Research of EDM(Electrical Discharge Machining) Process Simulation Based on Grey Neural Network

Zhongyuan Lin[1], Yong Liu[1], and Litang Zhang[2]

[1] School of Mechanical Engineering&Automation, Xihua University, Chengdu, China
[2] Baoji University of Arts and Sciences, Baoji, China
lin303436@live.cn, liuyongletter@yahoo.com.cn,
langziboy1984816@163.com

Abstract. In order to solve the problem of parameter selection in EDM process, EDM process is simulated by using of the grey neural network and the experimental data on the accuracy of the model is verified. The result shows that the model by using of the grey neural network reflects the process characteristics of the machine itself. Difference between predicted and measured values is smaller and consistent with the actual production of electrical discharge machining process simulation. It is proved that the modeling by the grey neural network and using it to test is a feasible method to research the EDM process.

Keywords: EDM, neural network, grey system theory, process simulation.

1 Introduction

Electrical discharge machining technology is a completely different with the traditional processing techniques, it has been widely used in precision stamping die, complicated cavity dies, irregular hole, deep eyelet and the other special field of parts processing. EDM processing is not influenced by the hardness and strength of the workpiece material, although its processing speed is slow, but can greatly improve the shape of the workpiece, dimensional accuracy and reduce the surface roughness. However, the EDM process is a very complex and transient micro-physical processes, it is a complex stochastic process affected by the multi-parameter, difficult to establish an appropriate mechanism model to solve the problem of model selection of process parameters. In recent years, many scholars have made a lot of research. Tarng Y S used three-layer feedforward BP network to simulate annealing algorithm, realizing from processing parameters to processing results of the nonlinear mapping[1]. This paper applies the neural network and grey system theory with the characteristics of simple in modeling, fast convergence, high precision of the model, self-organization and adaptability based on the experimental data make a more accurate technological rule, fitting precision and prediction accuracy of EDM. In the situation of quite incomprehension on EDM process, the study has provided for the solution and means.

D. Jin and S. Lin (Eds.): Advances in Mechanical and Electronic Engineering, LNEE 177, pp. 373–379.
springerlink.com

2 EDM Experimental Design

2.1 Experimental Environment

Processing machine: Taizhou fangzheng DK7130 CNC EDM machine
Controller: Fangzheng NC standard controller BH80A
Workpiece material: 45 # steel
Electrode materials：two red copper bars, 45×20mm
Working fluid: EDM special working liquid

2.2 Determining the Test Variables

Influencing factors of EDM process are diverse and complex, therefore it is not scientific and not easy to do with limited processing in the testing time to take account of various factors. So in the study of changing the electrical parameters about the variation of processability, several of the major factors is studied on the influence law of the electrode wear, processing speed, surface roughness. We choose the pulse width, pulse interval, peak voltage and peak current as the parameters, to find out the effect of the main factors in EDM, and provide the data to support the follow-up of simulation, to provide the feasibility with using the grey neural network to simulate electrical discharge machining.

2.3 Drafted Experimental Scheme

In DK7130 as the experimental platform, we conducted 16 trials of positive and negative polarity through orthogonal experiment. In order to express the experimental data within a table, the code of positive polarity is set to 1, negative polarity to -1. Our specific research of EDM in 4 factors of pulse width, pulse interval, peak voltage, peak current as well as four levels of each factor under given conditions, measuring the electrode wear, processing speed and surface roughness, expressed by $L_{16}(4^4)$. The partial electrical parameters of the machine of the pulse width are 1～999us, pulse interval between 10 to 990us, 1～75A peaks current, 1～9 unit voltage. The part of experimental results are given in Table1.

3 EDM Process Simulation Based on the Grey Neural Network

3.1 A Summary of Grey Neural Network

Artificial neural network (ANN) is a complex network system composed of a large number of neurons connected with each other to simulate the human brain neural processing information, process parallel information and non-linear conversion[2]. A grey system theory is a new subject founded by Professor Deng Julong in the 1980s[3].It is a kind of new method to research the problem that it has not enough data and lack of information, namely we extract valuable information from the research object that part of the information is clear and partial information not clear in order to achieve the correct description of the system. Grey system theory holds that

there must be contacted and has some of the hidden rules within the system, although the system present very complex and disorganized data. So these characteristics provide basic theory for studying on EDM process based on grey neural network.

This paper chooses a jury system in series with artificial neural network, using experimental data which has been processed by jury system as the output, it also takes as the input data for subordinate neural network and is used in simulation with a BP neural network. The Grey neural network is an artificial organic combination and mutual complementation of grey model with a weak ability of nonlinear processing but simply in modeling and neural network with the capacity to efficiently integrate information. It is advantageous to establish grey neural network with grey model and neural network.

Table 1. Part of Experimental Result

No.	Pol-arity	Pulse Width t_i A /us	Pulse Interval t_0 B/us	Peak Voltage $\breve{u}_i$ C/u-nit	Peak Current $\breve{i}_e$ D/*A*	Experimental Results		
						Electrode Wear θ/%	Processing Speed v_w mm^3/min	Surface Roughness R_a /*um*
1	-1	20	30	1	2	0.4	10.41	2.43
2	-1	20	70	3	7	1.1	32.68	4.11
…	…	…	…	…	…	…	…	…
31	1	240	150	3	15	2	28.52	2.05
32	1	240	220	1	10	1	35.91	2.36

3.2 Process Simulation

3.2.1 Grey System Model

The central part of grey system theory and its processing method are grey dynamic model GM (h, n), its main purpose is to get grey function and grey differential equation. In the original model GM (h, n), the letter G stands for grey, M stands for model; (h, n) represents respectively nth order equation and n variables. The modeling mechanism of grey model: first the original data are processed based on grey generation theory; then the difference between actual value and model value is refined, setting up a grey differential equation model and analyzing the convergence in correlation degree; finally the data from GM model are inversely processed.

Set electrode loss, processing speed and surface roughness sequence for $x_1^{(0)}$,$x_2^{(0)}$,$x_3^{(0)}$;set pulse width, pulse interval, peak voltage and peak current sequence for $x_4^{(0)}$,$x_5^{(0)}$,$x_6^{(0)}$,$x_7^{(0)}$. It is the grey model of electrode wear that the model based on grey system theory combines with data of $x_1^{(0)}$, $x_4^{(0)}$,$x_5^{(0)}$,$x_6^{(0)}$,$x_7^{(0)}$; the grey model of processing speed and surface roughness is respectively $x_2^{(0)}$, $x_4^{(0)}$,$x_5^{(0)}$,$x_6^{(0)}$,$x_7^{(0)}$and $x_3^{(0)}$, $x_4^{(0)}$,$x_5^{(0)}$,$x_6^{(0)}$,$x_7^{(0)}$.

Suppose there is a sequence data $x^{(0)}$:

$$x^{(0)} = \left(x_1^{(0)}, x_2^{(0)}, \cdots, x_n^{(0)} \right) \tag{1}$$

We can get a monotonic growth curve by accumulative processing Eq.1, to improve the sequence of data regularity and weaken volatility. So get Eq.2:

$$x^{(1)} = \left(x_1^{(1)}, x_2^{(1)}, \cdots, x_n^{(1)} \right) \tag{2}$$

among them $x_i^{(1)} = \sum_{k=1}^{i} x_k^{(0)}$ (i=1,2,3,…,n).

Established model GM (h, n):

$$\frac{d^n\left(x_1^{(1)}\right)}{dt^n} + a_1 \frac{d^{n-1}\left(x_1^{(1)}\right)}{dt^{n-1}} + \cdots + a_n x_1^{(1)} = b_1 x_2^{(1)} + b_2 x_3^{(1)} + \cdots + b_{n-1} x_n^{(1)} \tag{3}$$

$$\hat{a} = \left[a_1, a_2 \cdots, a_n \vdots b_1, b_2 \cdots b_{n-1} \right]^T \tag{4}$$

Finally use the least square method to solve the coefficient vector $\hat{a}$, the solution of differential Eq.3 is the model.

Use the above method to deal with the experimental data in table 1, get a nonnegative sequences to seek the law of between data. In the model, experimental data with symmetry originated from orthogonal experiment, reflect overall all aspects in EDM of information. The electrode wear and processing speed experiment changes greatly in the negative polar environment, so choose negative polarity data modeling; the surface roughness experiment of the request is compared commonly high, therefore choose positive polarity data modeling.

3.2.2 Learning Algorithm and Construction of BP Neural Network

BP neural network is a multilayer feed-forward and back propagation neural network, its learning methods is the application of reverse transmission to readjust the threshold value and power value, making the error square sum of network to meet the requirement. General BP network consists of three layers, namely input layer, hidden layer and output layer, as shown in Figure 1. The output of each layer are input to the next level, connection weights between the two layers transfer weakened or enhanced information[4].

The concrete process of BP algorithm is to identify the input of input layer and the output of hidden layer at first, second determine the output in output layer and systematic error function, final ascertain the correction value of the threshold value and connection weights in hidden layer and output layer[5]. The prediction data from grey system model is used in BP neural network modeling, that prediction data used as input vector in the network and the actual data used as objective vector. The former 14 groups of data sequence used for modeling and the latter 2 groups used for prediction data. The difficulty of BP network construction design is to determine the hidden layer. It can be determined by empirical formula $m = \sqrt{n+l} + \alpha$, m represents the number of hidden nodes, n is the input nodes and l is the output nodes, α stands for adjustment constant and its value range in 1 ~ 10. Eleven form is appropriate value by experiment, a network construction with 1-11-1 is used.

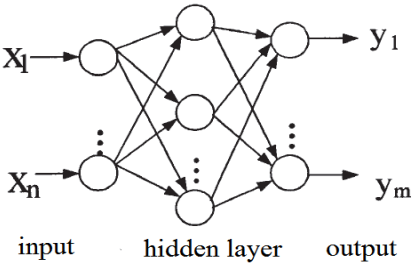

Fig. 1. The model of BP neural network

3.2.3 Analysis of Simulation Results

Through the modeling, the training accuracy has reached 0.001 when training pace gets to 37 steps in the electrode wear simulation of using Matlab software. The results show that the error curve of electrode wear of the maximum absolute error is 6.742%, the minimum is 0.001% and the mean absolute error is 1.105% in the Fig.2 Error Curve of Electrode Loss. Comparison experimental data with simulation of electrode wear, the absolute error from sample 1 and sample 2 after the grey neural network model prediction respectively is 6.9% and 13.2%.

Using the same steps in the processing speed simulation, the training accuracy has reached 0.001 when training pace gets to 32 steps. The maximum and the minimum absolute error respectively are 3.038% and 0.001%, the mean absolute error is 0.685% in the Fig.2 Error Curve of Processing Speed. With two sets of experimental data predict, sample 1 and sample 2 absolute prediction error of the model are 6.385%, 3.613%. When training pace gets to 59 steps, the accuracy has reached 0.001 in the surface roughness in the simulation experiment. The minimum and maximum absolute errors are 2.528% and 0.000015627% through Fig.3 Error Curve of Surface Roughness, the mean absolute error is 0.4378%. Comparison of the actual data and forecast data, the absolute prediction error of the sample 1 and sample 2 in the grey neural network model is 3.469%, 7.35%.

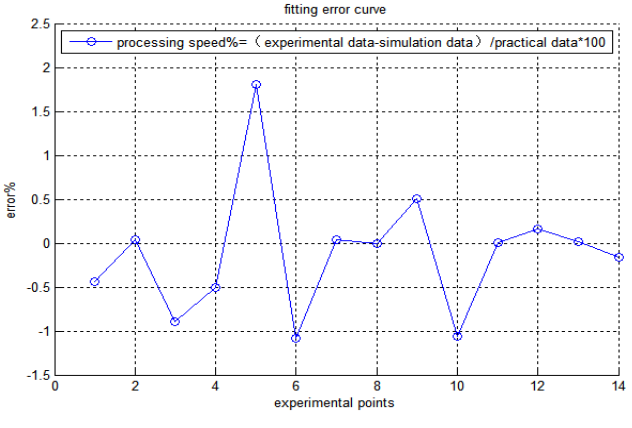

Fig. 2. Error Curve of Processing Speed

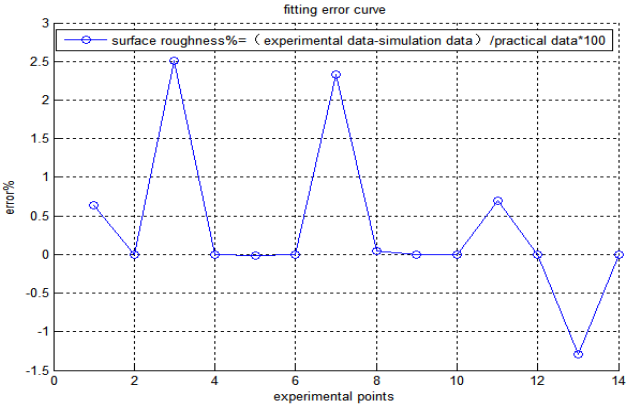

Fig. 3. Error Curve of Surface Roughness

Since the experimental system has randomness, error and other factors, so the actual data and forecasting data error is actually inevitable, but it can't deny the simulation is not correct. The experimental results show that the established model to meet the requirements of the generalization ability, can be mapped out the law of the machining process.

4 Conclusion

(1) By using the neural network technology and grey theory established EMD model, this model has modeling simple, high precision, less computation model, strong generalization ability and other characteristics, can accurately simulate the law of machine electrode wear, processing speed and surface roughness.

(2) In grey neural network modeling and simulation, if we can improve the learning samples and to be perfect, using of the network re-learning function to continue training model, so the prediction accuracy is enable further improved.

(3) The method used in this paper is universally suitable to another of the EDM machine tool research. As long as having process sample data on the machine, through the study of gray neural network, it can set up the model of the machining process.

References

1. Tarng, Y.S.: Determination of Optimal Cutting Parameters in Wire Electrical Discharge Machining. The International Journal of Machine Tools & Manufacture 35(12), 1693–1701 (1995)
2. Lou, L., Li, M., Peng, Y.: ANN Based Modelting for EDM Process. China Mechanical Engineering 12(4), 408–411 (2001)
3. Deng, J.: Grey theoretical basis. Huazhong University of Science & Technology Press (2002) (in press)

4. Yang, H., Zhou, P.: Artificial Neural Network Model of EDM Process. Machinery Design & Manufacture (1), 128–129 (2010)
5. Cao, F., Yang, D.: The Study of High Efficiency and Intelligent Optimization System in EDM Sinking process. Journal of Materials Processing Technology (149), 83–87 (2004)

Phenolphthalein Alkalinity Testing Research Based on Computer Vision Technology and Electronic Technology

Shengxian Cao, Dachang Huang, Yanhong Wang, and Guoying Li

School of Automation Engineering, Northeast Dianli University, Jilin, Jilin 132012
csxlb_jl@163.com

Abstract. Alkalinity is an important measurement index that maintains the safe and stable operation of industrial cyclic water. At present, the electronic measurement of alkalinity is mainly by the visual colorimetric method and potential titration method. These methods with complex operation and low automation fail to meet the monitoring need of cyclic water at industrial field. Therefore, an automatic electronic measurement device for alkalinity is designed in this paper. The device is based on visual colorimetric theory, using LabVIEW as system development software, using computer vision technology to obtain the change of solution color in alkalinity titration process, thus automatically determining titration end and gain alkalinity by Electronic Image processing methods. It is proved in the practice that Phenolphthalein alkalinity is measured quite accurately and fast by this device.

Keywords: Alkalinity, Electronic Electronic Image processing, Curvature.

1 Introduction

The alkalinity of water is the amount of substance of in per unit volume water which occurs reacting with strong acid, which is a measurement of buffering ability in water to acid[1]. In the circulating cooling water system, alkalinity determines the tendency of water fouling and corrosion to some extent, so the assay determination of alkalinity is one of the important base items in water quality detection[2].

Alkalinity measurement methods mainly include visual colorimetric and potentiometric titration. visual colorimetric principle is simple and convenient, which is suit to control test and routine analysis, but the measurement accuracy is low and manual operation may produce some artificial error[3]. Potentiometric titration indicates the titration end by the jump of electrode potential, which has high accuracy. Even if water is muddy and comes with color, it is not affect the judge of titration end. But it has long titration process, cumbersome and time-consuming operation, complex data handling. It is difficult to meet online tracking[4].

As computer vision and Electronic Image processing technology get more mature and perfect, image technology is increasingly used testing field, chemical analysis equipment based on Electronic Image processing techniques has also become an important research direction. Xueting Hu [5]proposes a new judge method of blue absorption titration end based on image recognition technology. Jichen Shen and Xueqing Wang [6]etc. propose detection method of quantitative analysis by collecting image information of sample solution on the basis of the principle that color values in

D. Jin and S. Lin (Eds.): Advances in Mechanical and Electronic Engineering, LNEE 177, pp. 381–386.
springerlink.com

colored substance in solution and its concentration is proportional. Yunfeng Yuan[7]collects the image information of pH test paper to detect liquor pH value using camera and uses machine vision to simulate artificial vision. In alkalinity measure, E. da Nobrega Gaiao etc.[8] propose alkalinity titration analysis methods based on digital image, which drops hydrochloric acid and chromogenic reagent by hand using routine burette and injected test solution into image detector, then judging titration end on basis of image RGB value, computing amount of hydrochloric acid was added dropwise and water quality alkalinity by hand.

This paper designs a suit of automatic alkalinity measuring device by Electronic Image processing technology. It uses computer vision instead of human vision, combines image detecting techniques with discrete curve to compute curvature and automatic identification titration end, realize automatic measurement of alkalinity.

2 Device Design

This device hardware main include computer, peristaltic pump, digital image sensor (camera), shadowless stabilivolt and so on. It is shown in figure 1:

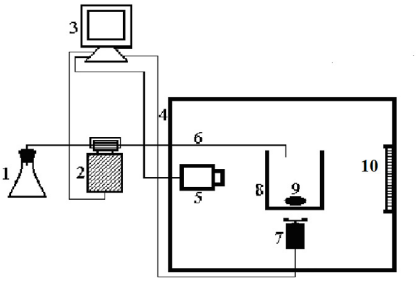

1、Titrating solution container 2、Constant dosing pump 3、Computer 4、Darkroom 5、Camera(CCD) 6、Titration tub 7、Magnetic stirrer 8、Etermination of optical glass pool 9、Magnetic rotor 10、Shadowless stabilivolt light source

Fig. 1. Schematic diagram of alkalinity measuring device

Peristaltic pump: Baoding Lange Constant pump BQ50-1J owns RS485 communication function, whose start, stop, speed and steering can be controlled by computer.

CCD camera: Philips SPC900NC realizes image obtain, store, transmission, dispose and recurrence, using CCD image sensor transforms optical signal into digital signals. Compared to common CMOS camera, it has steady performance, high sensitivity, low noise, fast response speed and small image distortion.

Shadowless stabilivolt light source: Daheng image series background light, it conducts LED around expansion board and arranged with high density, through the special design, it can issue uniform and stable light. Light irradiation from behind colored solution, provides stable solution color information for camera.

Darkroom: using self-made opaque metal box, to exclude external light on solution of image interference.

3 Alkalinity Measurement

3.1 Image Measurement Priceple

RGB color space is the most basic and most commonly used in Electronic Image processing, because the existing image acquisition devices initially collect the color information by RGB values, color display device also eventually used RGB values. All other color spaces used in Electronic Image processing are converted from the RGB color space. The results of the work if you need to show up, you need converting back to RGB color space[9]. RGB is ideal for color image, but applications have more restrictions on color description. Modern theories of color vision view that RGB color space is not an intuitive sense[10], from RGB values, it is difficult to know the value represented by the color of the cognitive attributes, The HSI model from psychological perception is more acceptable than the RGB. H(hue) is Color boost dominant wavelength, S(saturation) equivalent to the purity of the color stimulus, orthogonal with bright colors. I(brilliance) is brightness of the color. HSI model can eliminate strength component effect from color information(hue and saturation) carried by color image, which makes HSI model become the ideal tool for developing Electronic Image processing methods based on color description.

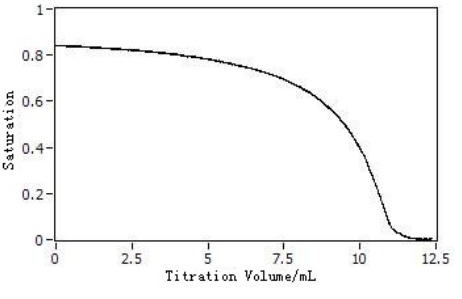

Fig. 2. Typical saturation curve

The device converts image information collected from RGB space to HSI color space, uses the image saturation value of solution reaction as a characteristic value, to judge titration end. With phenolphthalein as an indicator for measuring water phenolphthalein alkalinity, when the PH is greater than 8.3, solution is pink. The higher the PH value the darker the color. During the titration, with the ph value decreasing, the solution of its pink color faded, eventually becomes colorless. Figure 2 is solution image saturation curves collected by computer in the process from alkalinity titration to excessive process. In the initial titration, Solution pH value is higher, and solution color saturation value is close to 0.9(The maximum saturation value is 1), at this point, the solution showing pink and deep. During the titration, with the falling of solution pH value, saturation values continue to decline, solution of colors constantly changing light. When you reach the end point, the solution becomes colorless color, the color collected by camera is white background color of the light source through a colorless solution, and saturation is close to zero. Phenolphthalein alkalinity solution pink fade time is used as titration end, reacted in solution saturation

curve is the solution saturation to the rapid decline in the value of the turning point in stabilizing. When saturation value quickly dropped to close to the titration end, color from dark to light the process of rapid change. After saturation leveled that reach the titration end, solution color faded, saturation value gradually approaches zero. This paper calculates saturation of the curvature of the curve to find out the turning point to calculate the titration end.

Curve curvature shows the degree of curve curves. Curvature formula is as follows:

$$k = \left| \frac{y''}{\left(1 + y'^2\right)^{\frac{3}{2}}} \right| \tag{1}$$

$y = f(x)$, y' y'' is respectively the first derivative and second derivative, k is the curve curvature. In this paper, the saturation curve corresponding to the point of maximum curvature is the titration end.

3.2 Software Design

LabVIEW is a program development environment developed by United States national instruments company. Unlike other computer programming language based on text-based language, LabVIEW is a form of block diagram graphic programming language. The appliance uses LabVIEW as PC software development, through the camera real-time to collect solution image information, uses software for obtaining relevant regional image pixel RGB values, then by converting formula to convert RGB color values to HSI form, and then automatically extract the titration end on the basis of S curve. Finally, test solution alkalinity values according to the titration end point time to strike a titration acidity volume (concentration is known).

In this paper, saturation is stabilized as a basis for the judge to stop titration, its criterion is that maximum and minimum values of 100 saturation values continuously collected by the camera is less than 0.01, besides, Saturation is less than 0.2, because when the alkalinity of the solution is large, the initial titration of the saturation value of the solution changes very slowly.

Because the saturation curve that the device collected is a series of discrete points, each point differential coefficient uses backward difference derivative. (2) shows the saturation S is function about the titration volume v.(3) shows saturation relative to the v backward difference derivative. As the saturation value is subject to certain interference, two adjacent points difference alone derivative calculation of curvature of the curve to reflect changes in curvature of the curve. Therefore, to a point before the n-point before it proceeds to the average of the difference and as this difference in this paper. Processing methods such as equation (4) and (6) is the slope of the m-point. As the n value is too small, it is difficult to effectively reduce the interference caused by the error immediately, if n is too large, it is easy to lead to serious signal distortion. Experimental verification of this experiment uses n as 20.

$$S = f(v) \tag{2}$$

$$S' = \frac{f(v_{m+1}) - f(v_m)}{\Delta v} \tag{3}$$

$$S'_m = \frac{1}{n}[\frac{f(v_m)-f(v_{m-1})}{\Delta v}+\frac{f(v_{m-1})-f(v_{m-2})}{\Delta v}+\ldots+\frac{f(v_{m-n+1})-f(v_{m-n})}{\Delta v}] \quad (4)$$
$$= \frac{f(v_m)-f(v_{m-n})}{n\Delta v}$$

$$S''_m = \frac{S'_m - S'_{m-1}}{\Delta v} \quad (5)$$

$$k_m = \left| \frac{S''_m}{\left(1+S'^{2}_m\right)^{\frac{3}{2}}} \right| \quad (6)$$

The steps of calculation of curvature of the curve are as follows:

(1)Obtain saturation data $[S_1, S_2, ..., S_m]$;
(2)According to the type (4) and (5) to obtain each point value of first-order and second-order numerical
(3)According to the type (6), calculate the curvature at each point that value;
(4)Find the titration volume compare to the maximum curvature corresponding as titration end, calculate solution alkalinity according to titration acid concentration.

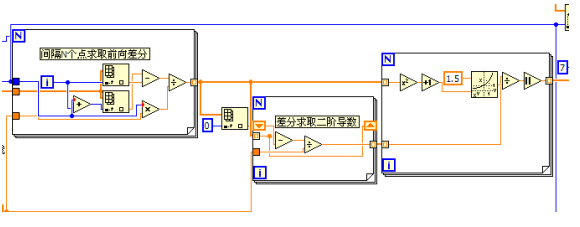

Fig. 4. Curvature calculation block diagram

Fig.4 is curvature calculation block diagram. Curvature of saturation curve is showed in Fig.5, the black curve is the saturation curve in Figure, red curve is the curvature. It is clear that curvature maximum value and turning point where saturation curve decline rapidly to get leveled is in a good correspondence.

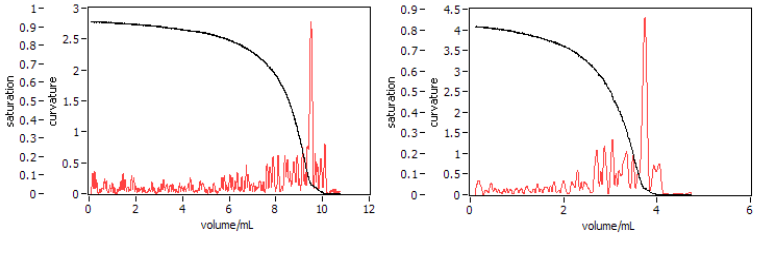

Fig. 5. Comparative experimental curvature

4 Conclusion

In this paper, the color saturation of the solution in phenolphthalein alkalinity titration is the object of study, titration end is determined by calculation of the maximum value of saturation curve curvature. The experiment shows this method, through this device measuring solution phenolphthalein alkalinity, has better measurement accuracy, high precision, good repeatability, and fast speed. This device can replace visual colorimetric for industrial cooling circulating water alkalinity automatic measurement, improve the automation standard of industrial water quality monitoring.

Acknowledgment. Project Subsidized by National Natural Science Foundation of China (No.50806010), Science and Technology Development Projects of Jilin Province (No. 20100432), Science and Technology Eleventh Five-Year Research Project of Department of Education of Jilin Province (2010. No.77), Doctoral Research Fund of Northeast Dianli University (BSJXM-200919).

References

1. Zheng, S.: Circulating cooling water quality and water treatment standard application guide. Chemical Industry Press, Beijing (2003) (in Chinese)
2. Wang, L., Ye, W., Dai, W.: Research on fast measuring methods of determining basicity calcium stiffiness and total hardness on cyclic cooling water. Science & Technology of Baotou Steel(Group) Corporation 31(6), 25–27 (2005)
3. Liu, H.: Measurement of Hardness and Alkalinity in Water Quality Analysis of Industrial Circulation Cooling Water. Metalurgical Power 2, 62–65 (2005)
4. Ma, D.C., Jiang, Q., Li, Y.W.: Application of mensurating alkalinity in water by automatic potentiometric titration. Chinese Journal of Health Laboratory Technology 17(10), 1797–1798 (2007)
5. Hu, X., Fan, Z., Long, W.: The New Method of Automatic Judgement for Titration End-Point of Methylene Blue Absorption Based on Image Recognition Technology. Foundry 9(4), 375–378 (2010)
6. Shen, J., Wan, X., Liu, B., Zhang, W.: Study on concentration detection of color solution based on image colorimetric analysis. Optical Instruments 30(2), 9–12 (2008)
7. Yuan, Y.: Study on the solution PH value tested experiment based on machine vision. Guangxi University, Nanning (2002) (in Chinese)
8. da Nobrega Gaiao, E., Lacerda Martins, V., da Silva Lyre, W., et al.: Digital image-based titrations. Analytica Chimica Acta 570(2), 283–290 (2006)
9. Gonzlez, R.C., Woods, R.E.: Digital Electronic Image processing. Electronics Industry Press, Beijing (2007)
10. Tao, L., Xu, G.: Color problem and application of machine vision. Chinese Science Bulletin 46(3), 178–190 (2001)

An Improved UKF Algorithm and Its Performance on Target Tracking Based on Electronic Technology

Yihuan Zhao[1], Weiheng Chen[1], and Jing Gao[1,2]

[1] Luoyang Optoelectronic Technology Development Center, 471009, Luoyang, China
[2] School of Electronics and Information Engineering, Beijing University of Aeronautics and Astronautics, Beijing 100191, China
zhaoyihuan@gmail.com

Abstract. In this paper, the principle of Unscented transformation is analyzed and an improved UKF (Unscented Kalman Filter) algorithm is proposed based on electronic technology. To simplify the computational complexity of the tracing system, identity matrix is introduced to the Unscented transformation, by which the complicated matrix calculation is replaced by simple numerical calculation for matrix square root solving. The new method called FMSRUKF (Fixed Matrix Square Root Unscented Kalman Filter) is an improved algorithm of UKF on target tracking based on Electronic Technology. Simulation results of variably accelerated motion target tracing under three dimensional coordinate shows that FMSRUKF achieves better precision and robustness.

Keywords: Unscented Transform, Tracking, UKF, FMSRUKF, Electronic Technology.

1 Introduction

A full description of the conditional posterior probability is needed to get the optimal solution of nonlinear filtering problem [1]. This precise description need too many parameters to be applied[2]. Nonlinear filtering problem has two kinds of suboptimal approximation solution. The first one is EKF (Extended Kalman Filter), Ignoring high order terms and using linear representations to approximate the nonlinear state. The other is UKF (Unscented Kalman Filter). Based on Unscented transformation, UKF use sampling to achieve a more accurate approximation distribution. It has the advantages of high precision, does not need to compute the Jacobean matrix etc.. In this paper, an improved UKF algorithm is proposed to simplify the Unscented transformation according to the characteristics of the system. The system accuracy and robustness can be improved by the new method.

2 System Mode

On discussion of moving target tracking, observation station and moving target is usually assumed in the same plane. The same method can be applied to three-dimensional target.

D. Jin and S. Lin (Eds.): Advances in Mechanical and Electronic Engineering, LNEE 177, pp. 387–391.
springerlink.com

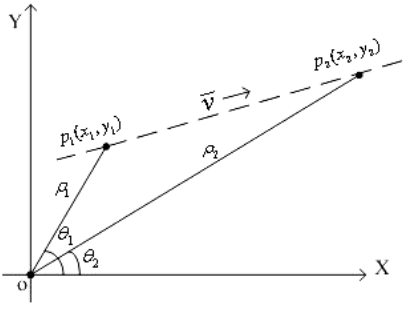

Fig. 1. A moving target plane is a two-dimensional coordinate system, with measuring station as origin. The motion velocity is vector $\overline{v}$. The target is located at point $p_1(x_1, y_1)$ at time t_1 ,and move to point $p_2(x_2, y_2)$ at the next time t_2. At time t_1, t_2, distance ρ_1, ρ_2 and angle θ_1, θ_2 can be measured, meeting the following conditions

$$\begin{cases} \rho = \sqrt{(x^2 + y^2)} \\ \theta = \arctan(y/x) \end{cases} \tag{1}$$

The coordinates of the target (x, y) at different time contains not only the location information at every moment, but also the velocity and acceleration. Equation (1) shows the nonlinear transformation relationship between measured values (ρ, θ) and corresponding coordinates (x, y). According to the continuous measurement (ρ, θ), all of the target movement state information can be mastered. As known, (ρ, θ) will be inevitably mixed with noise from direct measurement. Then, how to reduce the influence of noise to obtain more accurate information of target position becomes the main purpose of filtering algorithm.

3 Unscented Transformation and UKF Algorithm

Unscented transformation is a method that calculates the statistical characteristics of random variables after nonlinear transformation. For L-dimension random variable x, function y=f(x) is used to describe the nonlinear relationship. If $\overline{\boldsymbol{x}}$ and $\boldsymbol{P}_x$ was the mean and variance of x, matrix $\boldsymbol{\chi}$ can be built from 2L+1 vectors $\boldsymbol{\chi}_i$ (called Sigma Points).

$$\begin{cases} \boldsymbol{\chi}_0 = \overline{\boldsymbol{x}} \\ \boldsymbol{\chi}_i = \overline{\boldsymbol{x}} + (\sqrt{(L+\lambda)\boldsymbol{P}_x})_i & i = 1, 2, ..., L \\ \boldsymbol{\chi}_i = \overline{\boldsymbol{x}} - (\sqrt{(L+\lambda)\boldsymbol{P}_x})_{i-L} & i = L+1, L+2, ..., 2L \end{cases} \tag{2}$$

Where λ is a small scale parameter, and $\lambda = \alpha^2(L+k)-L$. Constant factor α determines the vectors' extended range around $\bar{x}$ and usually $10^{-4} \le \alpha \le 1$. Another scale parameter k is usually zero. $(\sqrt{(L+\lambda)\boldsymbol{P}_x})_i$ is the i[th] column of matrix's square root. The transformed vector points $\boldsymbol{Y}_i$ can be created with equation (3) from $\boldsymbol{\chi}_i$, using nonlinear function $f(\cdot)$.

$$\boldsymbol{Y}_i = f(\boldsymbol{\chi}_i),\ i = 0,1,...2L \tag{3}$$

The mean and covariance of weighted sample value is used to approximate the statistical characteristics $\bar{\boldsymbol{y}}$ and $\boldsymbol{P}_y$ of system output y.

$$\begin{cases} \bar{\boldsymbol{Y}} \approx \sum_{i=0}^{2L} w_i^m \boldsymbol{Y}_i \\ \boldsymbol{P}_y \approx \sum_{i=0}^{2L} w_i^c (\boldsymbol{Y}_i - \bar{\boldsymbol{Y}})(\boldsymbol{Y}_i - \bar{\boldsymbol{Y}})^T \end{cases} \tag{4}$$

Where

$$\begin{cases} w_0^m = \lambda/(L+\lambda) \\ w_0^c = \lambda/(L+\lambda) + (1-\alpha^2+\beta) \\ w_i^c = w_i^m = 1/[2(L+\lambda)], \quad i = 1,2,...,2L \end{cases} \tag{5}$$

and $\sum_{i=0}^{2L} w_i^m = 1$, $\sum_{i=0}^{2L} w_i^c = 1$. α is a factor as it is in equation (2). β contains priori information of the distribution of x, and $\beta = 2$ for Gauss distribution. UKF is a nonlinear process applying Unscented transformation to Kalman filter.

4 Improvement for UKF

UKF is based on Unscented transformation, which needs triangular decomposition of matrix. UKF computation period can be delayed because Gauss elimination process is executed at every filter iterator. An improved algorithm called FMSRUKF (Fixed Matrix Square Root UKF) is proposed to resolve this problem.

While $(L+\lambda)$ is a constant, $\boldsymbol{P}_x$ contains all the distribution information of $(L+\lambda)\boldsymbol{P}_x$. It is found from experiments that the diagonal elements of $\boldsymbol{P}_x$ draw the basic configuration of distribution information. An assured matrix $\sigma \boldsymbol{I}$ is introduced to UKF to replace $(L+\lambda)\boldsymbol{P}_x$. Factor σ is a constant calculated from diagonal elements of $\boldsymbol{P}_x$, and $\boldsymbol{I}$ is identity matrix.

If $\boldsymbol{I}_i$ was the i[th] column of $\boldsymbol{I}$, then $\boldsymbol{I}=[\boldsymbol{I}_1,\boldsymbol{I}_2,...,\boldsymbol{I}_L]$ $i=1,...,L$. $\boldsymbol{R}_i=(\sqrt{\sigma\boldsymbol{I}})_i$ is the i[th] column of matrix square root of $\sigma\boldsymbol{I}$. $\boldsymbol{R}_i=\sqrt{\sigma}\boldsymbol{I}_i$ $i=1,...,L$ because $\boldsymbol{I}$ is identity matrix. So matrix square root $\boldsymbol{R}_i$ can be calculated by $\sqrt{\sigma}$ instead of doing the triangular decomposition of matrix. Equation (2) is simplified as

$$\begin{cases}\boldsymbol{\chi}_0=\overline{\boldsymbol{x}} \\ \boldsymbol{\chi}_i=\overline{\boldsymbol{x}}+\sqrt{\sigma}\boldsymbol{I}_i & i=1,2,...,L \\ \boldsymbol{\chi}_i=\overline{\boldsymbol{x}}-\sqrt{\sigma}\boldsymbol{I}_{i-L} & i=L+1,L+2,...,2L\end{cases} \tag{6}$$

FMSRUKF can be built by UKF based on the above Sigma Points.

5 Experiment and Results Based on Electronic Technology

UKF, MAUKF[9] and FMSRUKF is applied in target tracking simulation experiment based on electronic technology to compare their performances.

If the initial position was $[x(t_0),y(t_0)]^T=[50,200]^T$ m, the initial velocity was $[v_x(t_0),v_y(t_0)]^T=[2,2]^T$ m/s, the initial acceleration was $[a_x,a_y]^T=[0.01,0.015]^T$ m/s^2, Distance measuring error was Gauss distribution with 0 mean and 0.1 variance, sampling interval was 1s, σ was 10^{-5} according to equation (13). The estimation errors for UKF, MAUKF and FMSRUKF are shown in Fig.2 and Fig.3.

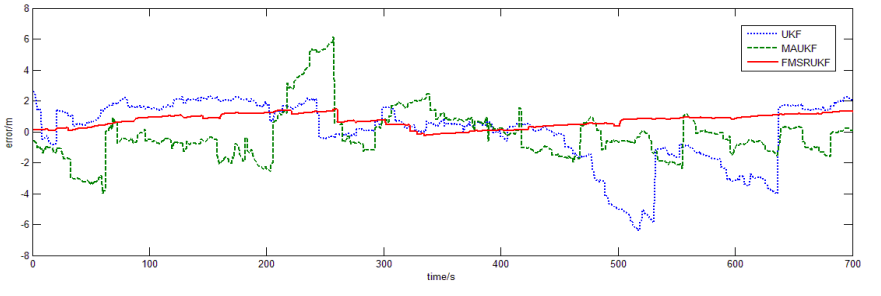

Fig. 2. Error comparison on x axial

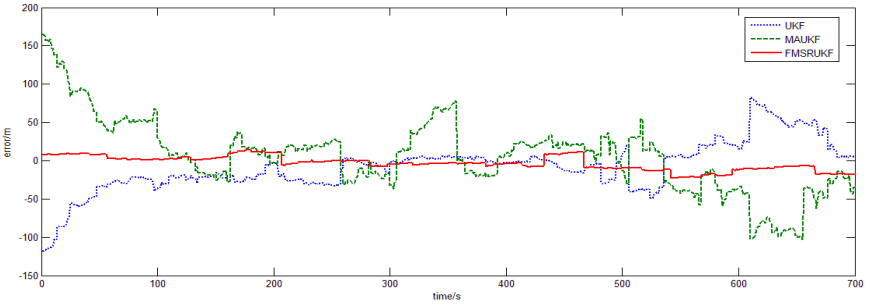

Fig. 3. Error comparison on Y axial

Fig.2 and Fig.3 shows that FMSRUKF works better than MAUKF and UKF when accuracy and robustness is compared.

6 Conclusion

FMSRUKF is an improved UKF via simplifying Unscented transformation based on electronic technology. It optimizes the filter calculation by eliminating the matrix decomposition process of calculating the matrix square root. Simulation shows that this method can improve the precision and robustness of tracking system.

References

1. Pan, Q., Yang, F., Ye, L., et al.: Survey of a kind of nonlinear filters – UKF. Control and Decision 20(5), 481–487 (2005) (in Chinese)
2. Kushner, H.J.: Dynamical equations for optimum nonlinear filtering. J. of Differential Equations 26(3), 179–190 (1967)
3. Maybeck, P.S.: Stochastic models estimation and control. Academic, New York (1982)
4. Julier, S.J., Uhlmann, J.K., Durrant Whyten, H.F.: A new approach for filtering nolinear system. In: Proc of the American Control Conf., Seattle, Washington, pp. 1628–1632 (1995)
5. Julier, S.J.: The spherical simplex Unscented transformation. In: American Control Conf., Denver, pp. 2430–2434 (2003)
6. Dimirovski, G.M., Xu, J.: UKF Design and Stability for Nonlinear Stochastic Systems with Correlated Noises. In: Georgi, M. (ed.) Proceedings of the 46th IEEE Conference on Decision and Control, pp. 6221–6231 (2007)
7. Wang, C., Liu, D.: Simulation analysis for hyperbola locating accuracy. Nuclear Electronics Detecion Technology 24(3), 288–291 (2004)
8. Sorenson, H.W.: Kalman filtering: Theory and application. IEEE Press, New York (1985)
9. Luo, Y., Zhong, H.: An improved UKF algorithm and its application in target tracking. Journal of Telemetry, Tracking and Command 29(1), 55–58 (2008)

The Design of RF Module Controller Based on SOPC

Xiujie Dong, Liang Zhang, Lian Yang, and Kai Fu

The School of Electronic Information, Zhongyuan University of Technology, China
xuxuzui19861217@163.com

Abstract. This artical proposes a design approach based on embeded system software core to control ISM RF module UTC-903SE. It is easy and fast by building UTC-903SE Controller IP Core and embeded processor Nios II Software Core. The article introduces the hardware and software design of the system. This system has the functions of sending and receiving data wirelessly and real-time. It provides convenient and faster way to acquisit data remotely for many situations.

Keywords: FPGA, SOPC, Nios, ISM, UTC-903SE.

1 Introduction

Along with the development of microelectronics industry nowdays, FPGA（Field Programmable Gate Array）is more popular for application such as programmable logic device.[1]

SOPC（System-on-a-Programmable-Chip）, firstly, it is SOC(System on a Chip), which builds overall system's main logic function on a chip. Secondly, it is programmable, and has flexible design method. It can scalable, extend, upgrade, and it has the function of software and hardware programmable on system.[2]

Along with the development of wireless communication technology, ISM band RF module frontend technology has become the key technology in communication and eletronic field, and has aroused wide public concern.[3]ISM Band, that is industry, science and medicine band, which has advantages such as unlimited using, cheap and so on.[4].

2 The Design of Program

This design use cyclone II series chips EP2C35F484C8N of ALTERA Company as the master chip. This chip has 3,326 configurable logic unit and 475 user pins,which not only meet the desire of this design,but also has large space for upgrade. ISM RF mdule use UTC-903SE of Hangzhou Weibu Technology Company.This module has UART series interface,which is easy for using and has broad application. The measured distance is 1800~2000 meters; FSK modulation; work at 430MHz~ 440MHz; suit for situation of multidrop.

This experiment use two same develop board(named A and B), which is used for sending and receiving data. This experiment method is reading real-time acquisition

D. Jin and S. Lin (Eds.): Advances in Mechanical and Electronic Engineering, LNEE 177, pp. 393–398.
springerlink.com

tempreture data by Board A and sending them out according to setted rate. The Board B receives and display them.

The overall block diagram of this program design is shown in figure 1.

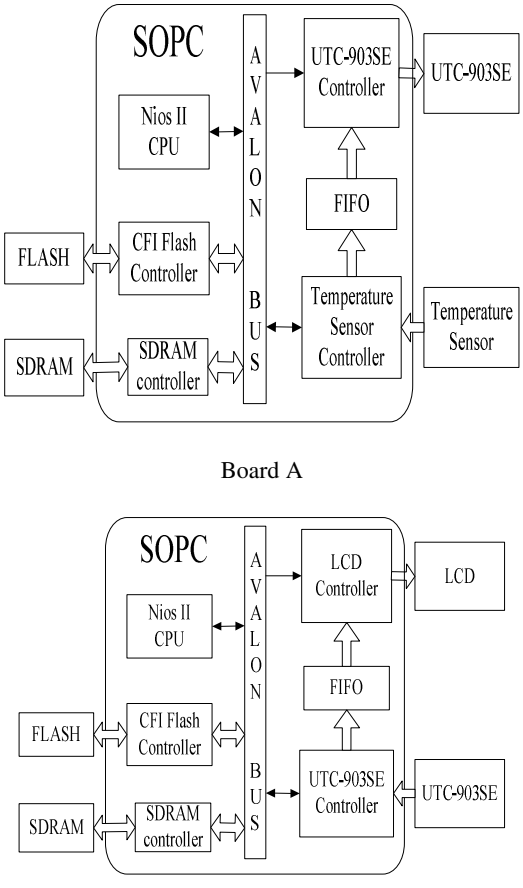

Fig. 1. The overall block diagram of this program

3 The Design of Hardware

3.1 Build SOPC

Building SOPC hardware system on the FPGA chip of two develop board, include FLASH Controller, SDRAM Controller, UTC-903SE Controller, Tempreture Sensor Controller and FIFO Controller.

The FLASH is used for store hardware configuration and application program. The SDRAM is used for data buffer. The UTC-903SE Controller is used for control the RF module sending and receiving data. The SOPC hardware system is builded as follows:

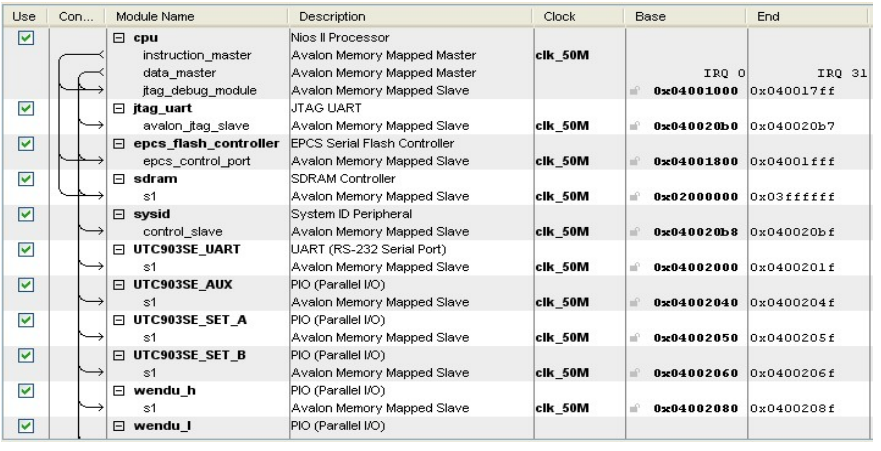

Fig. 2. The Diagram of SOPC

3.2 UTC-903C Module

UTC-903C module has seven pins, which is defined as follows：

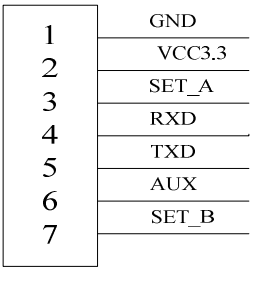

Fig. 3. Tthe diagram of UTC-903C module pins

The following table shows the description of these pins.

Table 1. The description of UTC-903C pins

Pin	Name	Direction	Description
1	GND		Ground
2	VCC		Supply power 2.1V-3.6V
3	SET_A	Input	select work mode
4	RXD	Input	Series interface input, TTL level
5	TXD	Output	Series interface output, TTL level
6	AUX	Output	Indicate work station
7	SET_B	Input	Select work mode

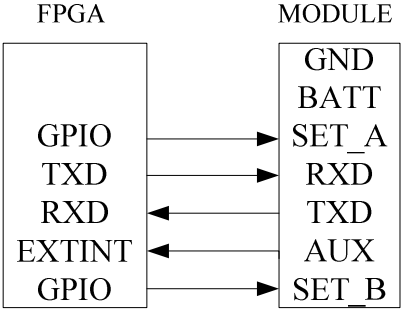

Fig. 4. The diagram of connection between master chip and module

4 The Design of Softwware

The design of software program of Nios II Processor use HAL (Hardware Abstration Layer) system library. HAL system library provides interactive device drive interface between application progam and basic hardware, which simplify the development of application program, and divide a clear boundary between application progam and basic hardware.

Then, improve reusability of application, which the chang of basic hardware will not infact application progam and realize the communication between system hardware and application program.HAI API(Application Program Interface) integrate ANSI C standard library, which make upper procedure access C function library like accessing system hardware and software.[5]

The flow diagram of program is shown as follows：

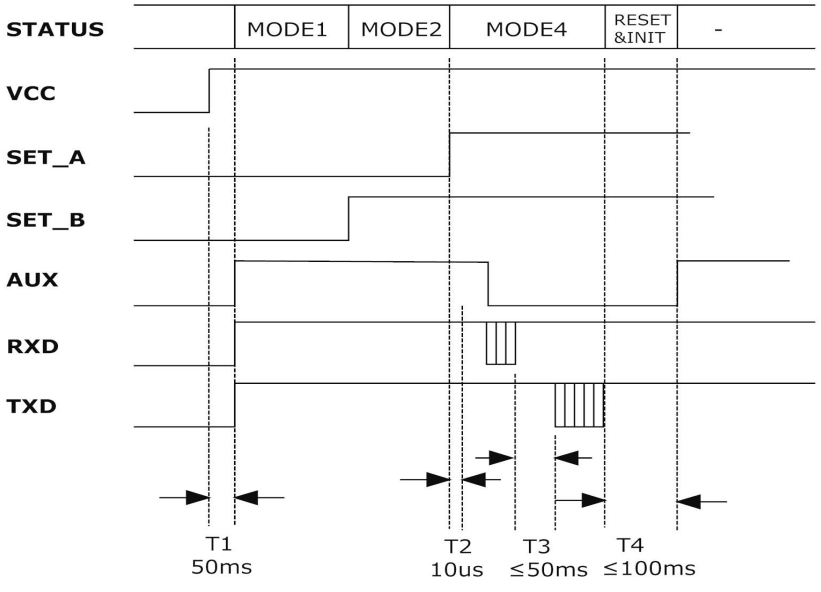

Fig. 5. The program flow diagram of UTC-903C module

```
Send Code：
  void main(void)
  {
      alt_u8 t[3];
      FILE *fp;
      while(1)
      {
          t[0]=IORD_ALTERA_AVALON_PIO_DATA(WENDU_H_BASE);
          t[1]=IORD_ALTERA_AVALON_PIO_DATA(WENDU_L_BASE);

          fp = fopen("/dev/UTC903SE_UART","r+");
          fwrite(t,3,1,fp);
          fclose(fp);
      }
  }
Receive Code：
  void main(void)
  {
      alt_u8 t[3];
      FILE *fp;
      while(1)
      {
          fp = fopen("/dev/UTC903SE","r+");
```

```
            fread(t,3,1,fp);
            fclose(fp);

            IOWR_ALTERA_AVALON_PIO_DATA(WENDU_H_BASE,t[1]);
            IOWR_ALTERA_AVALON_PIO_DATA(WENDU_L_BASE,t[2]);

            printf("t[0]=%x\n",t[1]);
            printf("t[1]=%x\n",t[2]);
        }
    }
```

5 The Result of Experiment

After restart of system, first of all, Board A send out the acquisitng tempreture data. Then, UTC-903SE module of Board B receive data and display them on computer by series interface.

After test, the tempreture data display on computer is right, and if change the tempreture and distance, the data received is right and right displayed. It indicate that the system meet the desire of desgn.

6 Conclusion

This paper introduce a program design of RF module controller based on combination of SOPC Builder and Nios II software and hardware of FPGA.

This design method is easy, fast and strong portability, wide applicability. The result of experiment indicate that this design program of RF module is easy for development and the function is right,which can send and receive data wireless.

References

1. Chen, W., Shi, H., Chen, L.: High Speed Communication Interface Base on SOPC. J. Electronic Measure Technology 33(7), 11–124 (2010)
2. Wang, P.: Design for Embedded System Based on FPGA. Journal of Xiangfan University 31(8), 42–44 (2010)
3. Zong, X., Liu, W.: Design of wireless temperature and humidity acquisition system. Hebei Journal of Industrial Science and Technology 27(6), 500–502 (2010)
4. Huang, Y.: A New Design Method about Low-Noise Amplifier at ISM Band. J. Electronic Technology Application 5, 60–62 (2010)
5. Shi, H., Wu, G.: TFT-LCD Graphic Display Design Based on Nios II. J. Microcomputer and Its Application 29(18), 3–43 (2010)

Study of Circulating Cooling Water Fouling Based on Electronic Technology and Multi-parameter Detection

Cao Shengxian[1] and Sun Yu[2]

[1] School of Automated Institute, Northeast Dianli University, Jilin 132012, Jilin, China
[2] School of Chemical Engineering, Northeast Dianli University, Jilin 132012, Jilin, China
csxlb_jl@163.com

Abstract. Scale sample of the iron content is an important symbol of the extent of corrosion to determine the circulating cooling water installations. In order to satisfy the projected need fouling features, the experimental design for dynamic closed loop cooling water system simulation of scale-like generation based on electronic technology and multi-parameter detection, and take dynamic water samples which iron content in real time during the simulation, microbial number 、 pH 、 dissolved oxygen, corrosion rate etc. In the precise analysis, JY/T015-1996 plasma emission spectroscopy measured in scale sample of iron ions, copper ions, organic matter content. The results show that the water has high iron, high-scale sample of the iron detection value indicates that the extent of corrosion is also relatively high; In addition, the copper ion content in the scale sample of high-lead content of organic matter, both a negative correlation.

Keywords: cooling water, multi-parameter detection, influencing factors, corrosion.

Introduction

Circulating cooling water in industrial production has been widely used. Recycled water quality deterioration, the circulating water system corrosion, scaling, biological contamination as three prominent issue[1]. Therefore, thermal equipment in the event of fouling and corrosion, thermal equipment would seriously jeopardize the safety, economic operation, in view of this, the dirt component analysis, to generate understanding of the law and take a variety of water quality parameters on the dirt has an important impact on the formation of the significance. Scale sample analysis methods commonly used in chemical analysis are manual[2], chemical analysis instruments[3-4], the surface images observed[5]and other methods. Currently used manual methods of chemical analysis. These methods can be more accurate detection of scale-like elements, but the scale-like ingredients and recycled water quality indices associated with the study is very rare. The author dirt dynamic simulation to generate cooling water, and record changes in water quality, and the final scale-like component analysis did association studies.

D. Jin and S. Lin (Eds.): Advances in Mechanical and Electronic Engineering, LNEE 177, pp. 399–404.
springerlink.com

1 Material and Method

1.1 Experimental Setup and Operation with Electronic Technology

This test system is a closed loop cooling water system to simulate water temperature 60 degrees heat exchanger system to 16mm diameter, 12mm diameter cold-drawn tubes of carbon steel tubes as analog to Jilin City Riverside gate at the water samples taken , the 3-micron membrane filtration as a cooling water to 1.3m /s velocity to the dynamic simulation of the actual operating conditions of the water-cooler heat exchanger, flow state. In order to ensure a constant cooling water inlet temperature is 22 degrees Celsius

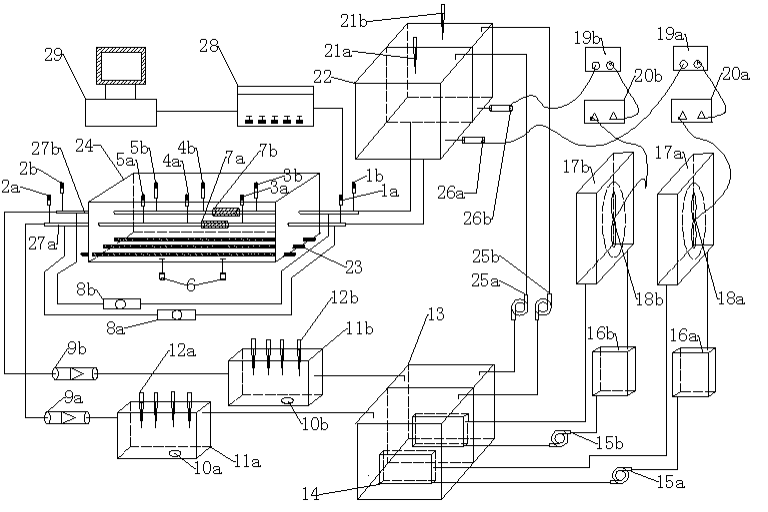

1 - inlet temperature; 2-- outlet temperature; 3,4,5 - tubes of the wall temperature; 6-- water bath temperature; 7-- corrosion rate detection sensor; 8-- differential pressure meter; 9-- electromagnetic flowmeter; 10 - experimental water sampling port; 11 - water quality testing pool; 12 - water quality (pH, conductivity, dissolved oxygen, ORP) instruments electrode probe; 13 - under the water tank; 14 - plate heat exchanger; 15 - circulating pump (air) ; 16 - air-cooled radiator; 17 - air-cooled heat sink; 18 - air-cooled motor; 19-PID automatic controller; 20 - drive; 21 - turbidity test probe; 22 - on the water tank; 23 - electric heating rod; 24 - thermostat water bath; 25 - cooling water circulation pump; 26 - on the water temperature; 27 - analog tubes; 28 - data acquisition front-end; 29 - industrial Computer

Fig. 1. Dynamic simulation of cooling water diagram of experimental apparatus

1.2 Analysis Method

The three groups simulation experiments, the use of iron ions during the simulation DL/T502.25-2006 analysis; scale sample analysis using JY/T 015-1996 measured plasma emission spectrometry method of scale-like iron ion content, copper content ,

organic matter content. Off-line detection of iron ions with the trend shown in Figure 2; SRB use of GB/T 14643.5-2009 methods; iron bacteria using GB/T14643.6-1993 methods; silica using GB/T16633-1996 methods; solid suspension objects using GB/T 1441 5-9 3 methods; pH, dissolved oxygen meter line monitoring. Scale-like precision in the analysis, the iron, the percentage content of non-other for the first group (53%), the second group (61%), and the third group (56%), this data, we can see the second group the highest degree of corrosion, corrosion of the first group the least.

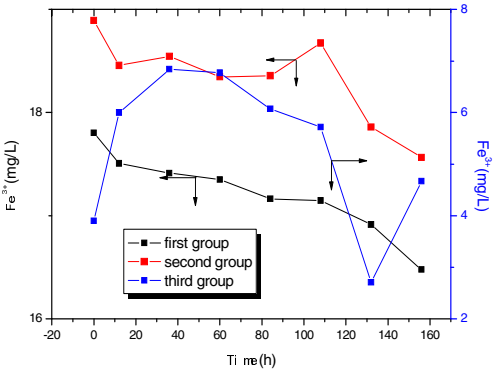

Fig. 2. Trends iron ions in water

2 Results and Discussion

2.1 The Impact of Dissolved Oxygen

When the cooling water flow over the surface of carbon steel pipe, because the water contains dissolved oxygen, both the initial contact with the wall surface of iron oxide grain boundary defects are the nucleation sites, the highest content of dissolved oxygen at this time, and thus oxidation the fastest rate; dissolved oxygen trends shown in Figure 3. And oxygen corrosion, others such as electrochemical corrosion, acid corrosion, microbial corrosion also occur simultaneously, among which oxygen corrosion, electrochemical corrosion of the other main, dissolved oxygen can not only lead to uniform corrosion, but also because the oxygen concentration difference will lead to localized corrosion (microbiological and electrochemical corrosion).

When carbon and dissolved oxygen in water contact, due to the uneven surface of the metal and water conductivity, carbon steel surface in the formation of many corrosion micro-cell, micro cell cathode reduction reaction occurred, anodic oxidation occurred eventually generate Fe_2O_3. Adequate supply of oxygen at this time, mostly the product of mainly FeO and other oxides[6], so the water is not high iron content.

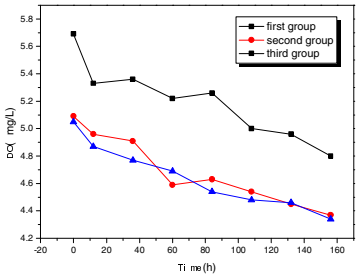

Fig. 3. Dissolved oxygen trends

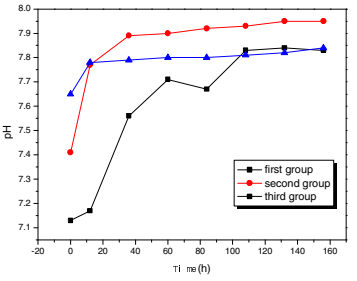

Fig. 4. pH trends

2.2 pH Effects

Trend-line detection of pH changes shown in Figure 4. effect of pH on corrosion: pH effects on metal corrosion rate often depends on the solubility of the metal oxide dependence on pH. Because the corrosion resistance of the metal oxide film on its surface is closely related to the performance. The most commonly used carbon steel as the material of the heat exchanger, carbon oxides dissolve in acidic aqueous solution and not soluble in alkaline aqueous solution, but when the pH value is high, the dissolved carbon to produce iron salts.

2.3 The Impact of Microbial

Meanwhile, the rugged metal surface, can lead to SRB (sulfate reducing bacteria) attachment, SRB in anaerobic environments sulfate respiration, which does not use oxygen and oxidation of organic compounds using sulfate ions of hydrogen or molecular hydrogen obtained energy, while producing sulfides, such as S^{2-}, S_xO^{3-} plasma generated easily with elemental iron precipitation, and further accelerated corrosion [8]:

$$H_2 + SO_4^{2-} \xrightarrow{SRB} S^{2-} + 4H_2O$$

$$2CH_3CHOHCOO^- + SO_4^{2-} \xrightarrow{SRB}$$

$$2CH_3COO^- + S^{2-} + 2CO_2 + 2H_2O$$

$$Fe^{2+} + S^{2-} \xrightarrow{SRB} FeS$$

Pitting corrosion pit deeper and deeper until the perforation scrapped. SRB on the sulfate ion migration, but also to create the necessary conditions for acid corrosion. Because of these factors on the O_2, H^+ consumption, water quality parameters of these very early changes in the rate. Therefore, in the cooling water running, constantly on the oxidation of dissolved oxygen and heat transfer equipment used by the propagation of microorganisms, dissolved oxygen levels are reduced. Scale analysis of the measured content of organic matter [the first group (4.1%), the second group (3.34%), and the third group (3.14%)]

2.4 Copper Ions with Electronic Technology

When the presence of Cu^{2+} in water, even at very low concentrations, but it is the anode reaction of the depolarizing agent, it contributes to the enhanced role of the anode, the cathode is relatively reduced, accelerating the corrosion scale formation; copper ions can be formed with the original elemental iron battery, loss of e-iron cathode, anode copper for the electron, and thus the formation of iron oxides; also [9] pointed out that elemental iron and iron oxide copper between a thin layer, the copper layer is sandwiched oxide and elemental iron, indicating that the initial oxidation of copper involved in the iron corrosion process, which accelerates the corrosion process for; Cu^{2+} is toxic microbial agents, inhibit microbial growth, which may slow the growth of microorganisms is the initial oxidation one of the reasons. In this regard, accurate analysis confirmed the data given in Table 1,

Table 1. Scale-like copper, organic matter content

	copper （%）	organic （%）
first group	0.06	4.1
Second group	0.06	3.34
third group	0.13	3.14

Figure 5 shows the water content of copper ions and negatively related to the total number of microorganisms.

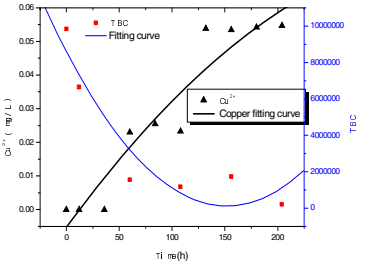

Fig. 5. Copper ions trends

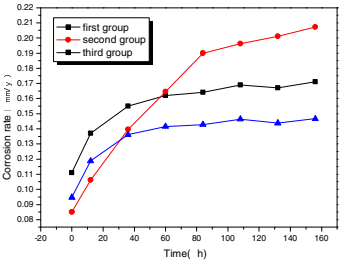

Fig. 6. Corrosion rate trends

2.5 On-Line Monitoring of Corrosion Rate with Electronic Technology

The corrosion rate of three trends (Figure 6), but also more intuitive to see that the rate of change of the second group was significantly higher than the other two groups. Observation of the first, third groups, the rate is higher than the second pre-group, but to end their run of less than the second group, and its corrosion rate corresponding to the end of the sort just and accurate analysis of scale samples from the iron content Sort consistent.

3 Conclusion

(1) High iron content in water, scale-like elements in the iron content is relatively high, the occurrence of corrosion large.

(2) pH low corrosion prone, prone to high levels of dissolved oxygen corrosion, the corrosion rate of contribution to the large.

(3) The presence of copper ions not only affects the corrosion, but also by affecting the propagation of microorganisms to influence the scale of organic matter content of samples.

(4) In addition, water and silica, the presence of suspended solids, but also directly or indirectly created corrosive conditions.

Acknowledgment. Project Subsidized by National Natural Science Foundation of China (No.50806010), Science and Technology Development Projects of Jilin Province (No. 20100432), Science and Technology Eleventh Five-Year Research Project of Department of Education of Jilin Province (2010. No.77), Doctoral Research Fund of Northeast Dianli University (BSJXM-200919).

References

[1] Feng, M., Lliu, G., Pan, T.: Cooling Water Treatment Technology. Journal of China Textile University (1999)
[2] SD 202.1-86, Scale and Products of Corrosion of Power Plant. Xian (1986)
[3] Ruiyuan, Z., Jian, Z., Feining, Y.: The Reason for the Failure Analysis of Medium Hardness Water Commonly Used in Water Treatment Formula Frocessing Copper Equipment. J. Water Treatment Technology (1996)
[4] Li, J.: Blast Furnace Cooling Water Circulation System Corrosion Problems. J. An. Gang. Technical (1994)
[5] Xie, J., Xie, S.: The Condenser Brass Corrosion Research (2006)
[6] Zhou, C., Ma, H.: High-temperature Oxidation of Iron. Journal of Dalian University of Technology (2010)
[7] Wang, Y.: Carbonated Mineral Water, Low-cost Iron Oxidation Process Water Chemistry Experiment. Jour. of China University of Geoscienoes (1995)
[8] Liu, Y., Liu, G., Zhan, G.: Sulfate-reducing Bacteria on the Electrochemical Corrosion Behavior of A3 Steel. J. Corrosion Science and Protection Technology (2003)
[9] Cheng, Y.: Researeh of Fouling Formation and Condensation Heat Transfer on Modification Heat Transfer Surface. D. Shandong (2009)

The Key Electronic Technology of Web-Based GMDSS Automatic Examination and Evaluation System

Tao Wang, Yuna Miao, and Qiang Zhang

Maritime College Shandong Jiaotong University Weihai, China
wtjd2000@yahoo.com.cn, miaoyn777@hotmail.com, 14209912@qq.com

Abstract. In consideration of the limit of artificial assessment of GMDSS electronic technology skills, with the development of standardized network GMDSS evaluation system, a Web-based GMDSS automatic examination and evaluation system is designed to realize the long-range automatic assessment. The system realizes the intelligent test paper combination based on genetic algorithm. It can make the statistical analysis of the normal distribution, record and playback the evaluation process and thus effectively improve the accuracy of evaluation.

Keywords: GMDSS, intelligent test paper design, automatic assessment.

1 Introduction

GMDSS (Global Maritime Distress and Safety System) is a well-developed communication system used in shipping industry to carry out distress salvage and safety communication. It is adopted by IMO (International Maritime Organization) to improve the existing maritime distress and safety communication to establish an effective search and rescue procedure, and it is also intended to further improve the existing routine communication at sea [1].To ensure the proper use of the marine equipment by the operators, all countries have established the certification and evaluation system, but most are still based on manual assessment and the evaluation result is not accurate enough due to the human factor.

Based on the GMDSS simulator, the key electronic technology involved in the development process includes: implementation of database connection pool and its management, input data validation, the generating algorithms of randomized assessment content, implementation of automatic scoring and the play back of evaluating process, etc. The present paper mainly focuses on database connection pool and the generating algorithms of evaluation contents.

2 Database Connection Pool and Its Management

In the development of JDBC-based database application, the management of database connection is a difficult point and also an important factor in determining the system's application performance. This mode solves the problems caused by frequent resource allocation and release. By applying this mode into database connection management

D. Jin and S. Lin (Eds.): Advances in Mechanical and Electronic Engineering, LNEE 177, pp. 405–408.
springerlink.com

and establishing a database connection pool, a cost-efficient connection allocation and usage strategy is offered. The core idea of the strategy is -- connection reuse [2].

Configuration Strategy. The GMDSS automatic evaluation system adopts the following configuration to implement design.

Adopt timer to check the status of each connection.

- First check whether the connection is closed. If so, delete it from the connection pool.
- If not closed, check if it is idle. If it is idle and exceeds the maximum idle time limit, then the connection is released to connection pool.
- If it is being used and exceeds maximum use time limit, then it is released to the connection pool.
- Check the number of connection in the connection pool, if less than the numbers in initialization, then new connections will be created.

Through the establishment of a database connection pool and a set of usage management strategies, an efficient and safe reuse of database connection is realized and the cost of frequent creation and closure of connection is avoided.

3 Genetic Algorithm of Intelligent Test Paper Generation

The so-called “intelligent test paper generation” means computer withdraw the test questions from database according to the generating parameters set up by the test designer and generate a test paper.[3,4,5] These parameters include test question number, degree of difficulty, scope of knowledge points, etc. The so-called “genetic algorithm” is a computing model simulating the natural biological evolution procedure[6,7,8]. Implementation steps

Step 1: Generate original species group randomly generate original species group according to the test type, full mark, degree of difficulty and time requirement.

Step 2: Calculate the proper value of individual

Step 3: If the termination condition is met, output the result and stop; otherwise, copy from the species group at a probability psi.

Step 4: Choose individuals to crossover at a probability of Pc to generate new species group

Step 5: Make the individual to mutate at a small probability Pmm to generate a new species group; return to step 2.

Mathematical model:

$$\left| \sum_{i=1}^{n} (A_{ijk} \times T_i) - B_{jk} \right| \leq d_{jk} \tag{1}$$

$$\sum_{i-1}^{n} T_i = f_s \tag{2}$$

Equation (1) stand for the number of test questions which is up to the requirement of test designer, in the meanwhile, the size of error is taken into account. Equation (2)

means the sum of each test question score should be equal to a given total score. When set nj as the number of component of index j , m as the sum of index and n as the total number of test question, then the number of equations can be obtained is n1+…+nm+1; that is to say, every index component meets the requirement of the model. In Equation (1) and (2), i means the number i test question, j means the number j index, k means the number k component; set Aijk value 0, 1, $\sum_{k-1}^{n_i} A_{ijk} = 1$, Aijk =1, which means the test question i has the component k property of index j; while Ti is the score of test question i, fs is the total score; Bjk is the scoring requirement of index j component k; djk is the allowable error of index j component k.

4 Test Quality Analysis and Normal Distribution Test[9]

- Test quality analysis involves two types of indicator

quantitative analysis indicator of the overall exam such as the normal distribution test, the test reliability indicator, the test validity indicator and so on; quality analysis indicator of test questions such as the degree of difficulty analysis, discrimination, etc. Using these indicators, a thorough evaluation can be made on the exam to further improve its quality. The present system collects detailed statistics and makes analysis on them. Here the main point of discussion is the normal distribution test of exam performance.

- Normal distribution test model

As the GMDSS automatic examination and assessment has a great number of testees, if W method is adopted, the testees have to draw lots and cause a big error, so in the system the method of moment is adopted. Here the mathematical three-level moment and four-level moment are used respectively to form the deviation and kurtosis, then a test is made to see if the testees performance is in appliance with the normal distribution. When the frequency distribution is normal, both coefficient of deviation and kurtosis are 0. Suppose that: 1) deviation coefficient equals to 0, then frequency distribution is symmetrical; 2) kurtosis coefficient equals to 0, then it is a mesokurtosis. The formula for kurtosis is as follows:

$$g_1 = \frac{n\sum(x-\bar{x})^2}{(n-1)(n-2)[\sum\frac{x-\bar{x}}{n-1}]^{\frac{3}{2}}} \tag{3}$$

If the result >0, the deviation is a positive deviation, otherwise, it is a negative deviation.The formula for kurtosis is as follows:

$$g_2 = \frac{n(n+1)\sum(x-\bar{x})^2}{(n-1)(n-2)(n-3)[\sum\frac{x-\bar{x}}{n-1}]^2} - \frac{3(n-1)^2}{(n-2)(n-3)} \tag{4}$$

If the result >0, it means the distribution curve is sharper than normal, while a negative value means the distribution curve is a little flat. In the formula, n means the number of testees, x means the raw scores of testees, $\bar{x}$ means the average score of testees.

First, with the raw score of testees, the system can calculate the average score. As average score is used several time in calculating deviation and kurtosis, it is the foundation of statistics. It can be obtained by adding all the raw scores of testees together and then divide it by the number of testees.

After the variance sum is obtained, it is very convenient to calculate the deviation and kurtosis. According to the formula of g1 and g2 , bring the variance sum $(\sum(x-\overline{x})^2)$ into formula, the coefficient of deviation and kurtosis can be figured out. According to the value and positive or negative condition ofg1 and g2 , one can tell if the test performance is a normal distribution or not.

5 Conclusion

For each assessment item in GMDSS evaluation system, make up some test questions according to maritime communication task and device operation requirement. Take the case of both training real devices and simulators into consideration. The using of the category regional random combination method to make up electronic technology assessment card improves the speed and efficiency, ensures the randomness and non-repetition of assessment content and enables all the questions to distribute evenly. The development of the system is important for GMDSS assessment and certification work. It makes it possible to compile the electronic technology assessment database, index, automatically combine assessment card and realize on-line automatic evaluation. It also improves the correctness, fairness and credibility of assessment paper combination, scoring and totaling of scores.

Acknowledgments. The present study is sponsored by Shandong Jiaotong University Science and Technology Research Foundation, the research period is from June, 2009 to December, 2010.

References

[1] Zhongchao, Z.: GMDSS Comprehensive Service, p. 17. Dalian Maritime University Press (1996) (in Chinese)
[2] The necessity of JSP database connection pool, http://web.lt263.com/html/2004-8-19/200481910331.html
[3] Yang, L.: Web-based Adaptive Test System. Huazhong Normal University, a master's degree theses (2002)
[4] Cheng, Q.: Online Examination System Design and Implementation. Beijing Institure of Technology, Master's degree thesis (2003)
[5] Chengqi, N.: Research on the Genetic Algorithm of Multi-constraint Objective Optimization Problems. Jiangxi Normal University, a master's degree thesis (2003)
[6] Rong, W.: Design and Implementation of Web-based Remote Examination System. Xi'an Jiaotong University, master's degree thesis (2001)
[7] Wanliang, W.: Artificial Intelligence and Its Applications. High Education Press, Beijing (2005)
[8] Zongben, X.: Bionics in Computational Intelligence: Theory and Algorithms. Science Press (2003)
[9] Yingcheng, L.: Design and Implementation of Examination System 's Normal Distribution. Chongqing Institure of Technologu Journal (2004)

Application of Power Electronic Technology in Optimizing the Operation of Thermal Power Plants

Wensheng Zhao, Tao Zhang, and Xuefeng Tang

North China Electric Power University, 071003 Baoding, China
452134234@qq.com, zhaowens@sina.com

Abstract. Rationally fixing operation optimization target values of thermal power units is the precondition and also forms the basis for effectuating performance evaluation and operation optimization. It therefore is vital for optimizing the operation of power plants. Actual states of operation of thermal power units can often not be correctly reflected by optimization target values determined with traditional methods. A way of operation optimization of thermal power units is proposed by applying power electronic technology for making full use of the large amount of historical data stored in power plants. The optimization target of thermal power units operation is found by applying power electronic technology mining algorithm. As a practical example optimal values for all modes of operation of a certain 300MW power set are found which may be used for guiding targets of fossil fired power plants can raise the power set's efficiency and reduce the emission of contaminants.

Keywords: data mining, power electronic technology, fuzzy association rules, operation optimization target, energy saving.

1 Introduction

With the development of information technology, power enterprises have accumulated a lot of historical data from the thermal power units of thermal system operating data to find the knowledge and means to improve system operation and optimize the production process. It is of great significance and value. Electricity production volume, high-dimensional and strong coupling is the essential features of production data. So traditional methods is difficult to find and summarize the knowledge implied in these data. In this paper, data mining techniques to introduce thermal power plant optimization process, the optimization target value method based on fuzzy association rules. Using data mining technology is a powerful data analysis and knowledge discovery capabilities, through the analysis of deep-seated historical data to determine the power plant operation to optimize the target to guide the operation. The optimization of data mining technique to determine the target value in the actual operation on the basis of the existing equipment. It can be achieved by operation adjustment . Compared with traditional method, it is reasonable accuracy and operability.

D. Jin and S. Lin (Eds.): Advances in Mechanical and Electronic Engineering, LNEE 177, pp. 409–413.
springerlink.com

2 The Data Mining Algorithm

Association rule mining in data mining is a very important research topic, and its focus on the association among the different data. In 1993 R.Agrawal was put forward based on the two phase frequency set theory of recursive method Boolean type algorithm for mining association rules---Apriori algorithm. It can be seen as a numeric association rules mining based and a special case. This paper will fuzzy association rules mining into power station optimization process, is put forward based on fuzzy association rules mining coal plants operation optimization method to determine the target, avoid the traditional numeric association rules mining border demarcation of excellent shortcomings. Specific mining algorithm are described below:

Affairs databases is showed as table 1:

Table 1.

	a_1	a_2	…	a_m
t_1	d_{11}	d_{12}	…	d_{1m}
t_2	d_{21}	d_{22}	…	d_{2m}
…	…	…	…	…
t_n	d_{n1}	d_{n2}	…	d_{nm}

Table 1 shows is that a typical affairs database D = {t_1, t_2,... , t_n}, including ti ($1 \le i \le n$) means that it is i-th in the database of D; Database attribute sets A = {a_1, a_2,... , a_m}, including attribute a_k ($1 \le k \le m$.) means that it is k-th attribute; $d_{i,k}$ for data item means that it is the k-th attribute value of the i-th affairs.

Introducing the concept of fuzzy sets a_k($1 \le k \le m$) attribute from A = {a_1, a_2,... , a_m}is divided into several fuzzy sets according toexpert knowledge:a_k={a_{k1},a_{k2},…,a_{kp}} (p>0), and its appropriate membership function is F_{ak} = {f_{ak1}, f_{ak2},... , f_{akp}}. Therefore, convert affairs databases in the table 1 into the dispersed database with fuzzy attribute, as is shown in the table 2:

Table 2.

	$a_{11}a_{12}a_{13}\ldots a_{1p}$	$a_{21}a_{22}a_{23}\ldots a_{2p}$	…	$a_{m1}a_{m2}\ldots a_{mp}$
t_1	d_{11}	d_{12}	…	d_{1m}
t_2	d_{21}	d_{22}	...	d_{2m}
…	…	…	…	…
t_n	d_{n1}	d_{n2}	…	d_{nm}

Calculating data items d_{ij} in the affair t_i , d_{ijh} is considered as membership of the fuzzy attribute a_{jh} (j stands for the j-th fuzzy attribute set, which is the first j column; h

stands for the h-th attribute of this attribute set) .And $d_{ijh}=f_{ajh}(d_{ij})$, the results is shown in the table 3:

Table 3. The calculation of the data membership

	$a_{11}a_{12}a_{13}\ldots a_{1p}$	$a_{21}a_{22}a_{23}\ldots a_{2p}$	…	$a_{m1}a_{m2}\ldots a_{mp}$
t_1	$d_{111}d_{112}\ldots d_{11p}$	$d_{121}d_{122}\ldots d_{12p}$	…	$d_{1m1}d_{1m2}\ldots d_{1mp}$
t_2	$d_{211}d_{212}\ldots d_{21p}$	$d_{221}d_{222}\ldots d_{22p}$	…	$d_{2m1}d_{2m2}\ldots d_{2mp}$
…	…	…	…	…
t_n	$d_{n11}d_{n12}\ldots d_{n1p}$	$d_{n21}d_{n22}\ldots d_{n2p}$	…	$d_{nm1}d_{nm2}\ldots d_{nmp}$

For a certain attribute a_{jh}, after adding this property membership in all affairs and divided by the total number of affairs, that is all the affairs of support for this attribute. For example: sup. $a_{11} = (d_{111} + d_{211} +... d_{n11}) / n$, namely to be support of the a_{11} for all affairs.

Behind of the steps is the same as Apriori mining association rules mining algorithm. Linking with frequent k-itemsets L_k ($k\geq1$), it leads to be candidate ($k + 1$)-itemsets C_{k+1}. After the calculation of support-S of every item set in the itemsets C_{k+1}. C_{k+1} should be sheared. Pruning includes deleting C_{k+1} itemsets for support that is less than the min_sup, deleting C_{k+1} containing the infrequent subset, deleting C_{k+1} itemsets including the same fuzzy attributes .

Repeating the above steps until the $L_{k+1} = \Phi$. And it lead to be all the frequent item sets. Then all frequent item sets used to generate all possible association rules. Still the rules are filtered by a standard of degree of confidence.

3 Applying Instance

Stable operating condition of historical data from the 300 MW thermal power unit is analyzed. Considered the power supplying minimum coal consumption as the goal of data mining, applying the fuzzy association rules mining algorithm for determining unit operation optimization target value of important parameters to guide optimizing operation. That is to say in each feature load interval choosing relevant with excellent performance index of the operation parameters interval as the parameters in the operating condition of the optimal interval, on condition that the units are operated stably. And the rules that determine the parameters of the optimal value are obtained. Then the experience of quantitative association rules effective certificate is used for consumption poor analysis and guiding optimizing operation.

By analyzing the unit historical operation data of nearly three months closely related with the power supply coal consumption rates, the data selection and data test were used to obtain 4136 groups operation data association which used to extract rules of extraction unit steady-state. Each sample includes each main steam pressure, main

steam temperature, the reheated steam temperature, the overheating desuperheated-water flow, and hot desuperheated-water flow, condenser water temperature and vacuum, exhaust temperature, excess air coefficient and so on. The characteristic parameters reflect the unit operation conditions and operating conditions. All attributes of data set are normalized to [0, 1]. Parameter attributes are blurred, and its membership functions are shown in the figure 1.Tthe triangular gradient and distribution are determined by the vector domain combining with actual the characteristics of the system. After basic data from data-set is blurred , it is considered as input vector of fuzzy association rules mining. Provided with the minimum support $S_{min} = 0.3$ and the minimum confidence $C_{min} = 0.75$, the use of fuzzy association rules mining determines unit operation optimization target value of important parameters to guide optimizing operation.

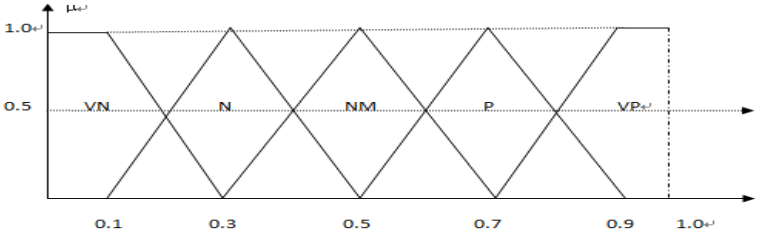

Fig. 1. Membership function

Taking under 100% load optimization target value of excess air ratio and exhaust gas temperature for example, it should be analyzed in detail. Blurring unit operation the unit loads of data for (298~300MW) stable operation of the working conditions of the recording as fuzzy association rules mining object. By means of fuzzy association rules mining, it abtains the following strong association rules:

<M_e, 1>, <b_g,0.20,0.30> ==> <a,0.30, 0.32>,

<T_g, 0.64, 0.68> (S=46%, C=81%)

M_e stands for load, b_g stands for the power supply coal consumption rate, a is excess air coefficient and T_g is exhaust gas temperature. Its support is 46%, and its confidence is 81%. Because it meets conditions of the minimum support and minimum confidence ($S \geq S_{min}$; and $C \geq C_{min}$), it is the strong association rules. This defuzzification interval is followed:

<M_e, 298, 300>, <b_g,326,330> ==> <a,1.290,1.296>,

<T_g, 145.6, 147.2>(S=46%,C=81%)

The above association rule indicates that under 100% load (298~300MW) and the power supply coal consumption is a little low (less than 328 g/kW•h) condition, the optimal value interval of excess air coefficient is 1.290 ~ 1.296, the optimal interval of exhaust gas temperature is 145.6~147.2℃. The operation optimization target should be selected in such optimal interval. And this paper takes the optimal interval center value

as a optimization target. So it obtains optimal value of the excess air coefficient is 1.293, the optimal value of exhaust gas temperature is 146.4℃ under 100% load excess.

According to the above steps, we can excavate important controlled and adjusted parameter in the 70%, 90%, 100% and other typical load condition by means of fuzzy association rules mining algorithm. We will obtain a group of the optimal operation value in different conditions.

4 Conclusion

Reasonably fixing operation optimization target values of fossil fired power sets is the precondition and also forms the basis for effectuating performance evaluation and operation optimization. Actual states of operation of power sets can often not be correctly coincident with optimization target values determined with traditional methods. The application can be largely restricted. Based on the large amount of historical data stored in power plants, the new method that application of power electronic technology determine the optimization operation target of the fossil fired power plant is proposed. By analyzing actual plant's operation data of a certain 300MW power set, we find operation optimization target values of important controllable parameters. And we makes use of operation optimization target values which is confirmed to be effective to guide operation. The conclusion of experiment indicates that based on power electronic technology of optimization target of operation method, it can raise the power set's efficiency and reduce the supplying electric of the coal consumption and the emission of contaminants. So it can guide optimal operation

References

[1] Agrawal, R., Imielinski, T., Swami, A.: Mining association rules between sets of items in large database. In: The 1993 ACM SIGMOD Conference, Washington DC, USA, pp. 246–257 (1993)

[2] Tzung-Pei, H., Chan-Sheng, K., Sheng-Chai, C.: A fuzzy data mining algorithm for quantitative values. In: Third International Conference on Knowledge-Based Intelligent Information Engineering System, Adelaide, Australia, pp. 480–483 (1999)

[3] Chen, N., Chen, A., Zhou, L.-X.: Efficient Algorithms for Mining Fuzzy Rules in Large Relationgal Databases 12(7) (2001)

[4] Park, J.S., Chen, M.S., Yu, P.S.: An Effective Hash Based Algorithm for Mining Association Rules. In: Proceedings of the 1995 ACM SIGMOD International Conference on Management of Data, San Jose, CA (1995)

[5] Rymon, R.: Search through systematic set enumeration. In: Proceeding of Third International Conference on Principles of Knowledge Representation and Reasoning, pp. 539–550 (1992)

[6] Houtsma, M., Swami, A.: Set-oriented mining of association rules. In: Proceeding of the 20th International Conference on Data Engineering, pp. 25–33 (1995)

Research and Implementation of 6LoWPAN Adaptation Layer Based on Electronic Technology

YouFen Hong[1], Hua Li[1,2], XingHang Xia[1], and XianRong Wang[1]

[1] College of Computer Science, Inner Mongolia University, Hohhot, China
[2] Center of Network and Information, Inner Mongolia University, Hohhot, China
cshongyoufen@imu.edu.cn

Abstract. With the rapid development of the electronic technology, the internet of things develops quickly and IP address exhausts gradually. IPv6 protocol finds another chance to go ahead. 6LoWPAN (IPv6 over Low-Power Wireless Personal Area Networks) is a kind of IPv6 protocol stack technology based on IEEE802.15.4 standard, and it can connect the wired network with wireless network seamlessly. This paper mainly analyzes the 6LoWPAN protocol stack and its adaptation layer protocol, designs and implements the adaptation layer's core functions which are fragmentation, reassembling, header compression and decompression. In addition, it puts forward a formal method about establishing CPN models of adaptation layer by CPN Tools, and designs test cases to test the implemented core functions. Test results show that the adaptation layer can make IPv6 packets transmit over IEEE802.15.4. This promotes the development of the electronic engineering.

Keywords: Electronic technology, The internet of things, 6LoWPAN adaptation layer, Core functions, CPN model, Conformance testing.

1 Introduction

The electronic technology develops quickly and is used widely. The internet of things has become a very important network and can be achieved by wireless embedded network. 6LoWPAN is a technology based on IPv6 and IEEE802.15.4, so it can combine wireless local area network with the Internet to realize related functions of the internet of things. IETF [1] (the Internet Engineering Task Force) establishes 6LoWPAN working group to specialize in the research work of IPv6 protocol stack based on IEEE802.15.4 standard. The task is to make and perfect 6LoWPAN related drafts, and ensure the correct communication between IPv6 protocol and IEEE802.15.4 standard.

IEEE802.15.4 standard is a kind of wireless RF technology [2] with low power consumption and low rate. It defines the MAC layer and PHY layer [3]. The size of a maximum physical layer packet for IEEE802.15.4 protocol is 127B, and the MTU (Maximum Transmission Unit) size for IPv6 packets is 1280B [4]. So a full IPv6 packet can not fit in an IEEE 802.15.4 frame, and an adaptation layer needs to be introduced between the two layers to make sure they can efficiently communicate. The core functions of 6LoWPAN adaptation layer include four modules which are

D. Jin and S. Lin (Eds.): Advances in Mechanical and Electronic Engineering, LNEE 177, pp. 415–421.
springerlink.com

fragmentation, reassembling, header compression and decompression [5]. The paper mainly analyzes and realizes the 6LoWPAN adaptation layer's core functions. Additionally, we use CPN Tools to establish formal models for the functions, and finish conformance testing according to the generated test sequence by CPN models.

2 6LoWPAN Adaptation Layer

2.1 6LoWPAN Protocol Stack

The main object of 6LoWPAN is to realize the communication between IEEE802.15.4 and IPv6, so as to make the wired network and wireless network connect seamlessly. As shown in figure 1, the 6LoWPAN adaptation layer is located between IPv6 layer and IEEE 802.15.4 MAC layer. When the payload of IPv6 packets exceeds the load capacity of IEEE 802.15.4 frame, the packets fragmented, reassembled, compressed and decompressed by the adaptation layer will transmit over IEEE 802.15.4 MAC layer correctly and effectively [5].

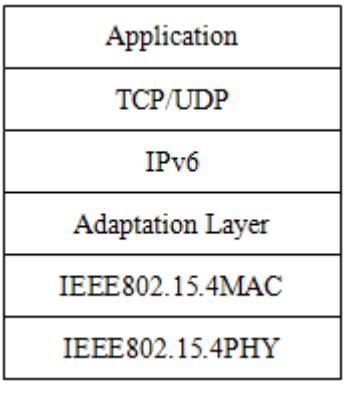

Fig. 1. 6LoWPAN Protocol Stack

2.2 Fragmentation and Reassembling

The MTU size for IPv6 packets is 1280B, which is far lager than the maximum size for IEEE802.15.4 frame, so the adaptation layer should have fragmentation and reassembling ability. When the adaptation layer is fragmenting the datagram, it needs to encapsulate a fragment header for every fragment. The first five bits of fragment headers indicate the fragment is the first fragment or subsequent fragments, shown in Figure 2. The difference between them is if they have the fragment offset [6]. The "datagram_size" field with 11 bits in fragment headers encodes the size of IPv6 packets, including IPv6 header and payload, and this field is same in all fragments, which is to make sure even recipients receive subsequent fragments firstly they can assign enough space to reassemble fragments. Beyond that, 11 bits can allow the fragmentation of packets with 2047 bytes mostly, so they are enough for packets

coming from IPv6 layer. The "datagram_tag" field shows the datagram that the fragments belong to, which eases the reassembling of fragments. When reassembling, fragment recipients assign corresponding space for packets according to the "datagram_size", reassemble the fragments which belong to the same packet according to the "datagram_tag", and then get original IPv6 packets.

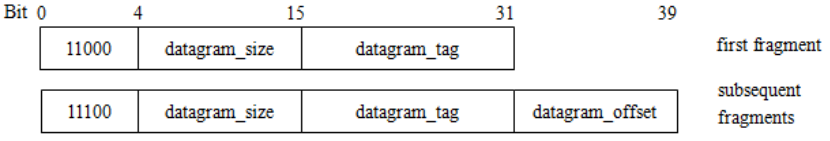

Fig. 2. Fragment Headers

2.3 Header Compression and Decompression

In order to avoid excessive fragmentation and reassembling, the adaptation layer has header compression and decompression abilities. Two kinds of header compression algorithms are proposed in 6LoWPAN drafts. They are stateless header compression [6] and context-based header compression [7]. We mainly analyze the stateless header compression. The header compression can compress those packets whose next header field is TCP, UDP or ICMPv6. Packets with the next header of UDP are considered in this paper. There are two header compression models are defined in 6LoWPAN documentations: HC1 model and HC2 model. They are used to compress IPv6 header and UDP header respectively. Figure 3 shows, when the dispatch value is 01000010, HC1 model will be used, and 40 octets of IPv6 header will be compressed to 2 octets. When the last bit of the byte after the dispatch value is 1, it means the next header of the packet needs to be compressed with HC2 model. HC2 header can be set some relevant options, and the uncompressed fields follow HC2 header immediately.

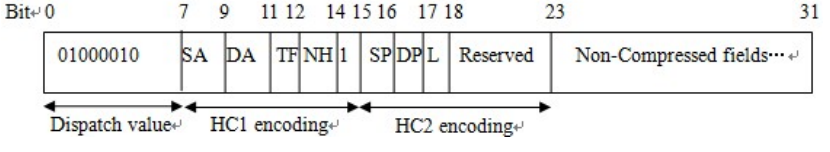

Fig. 3. HC1 Encoding and HC2 Encoding

Stateless IPv6 address includes an interface identifier (IID) and IPv6 address prefix. The IID of an IEEE 802.15.4 interface identifies the interface is unique in the local link. After a host sends a 6LoWPAN datagram, the MAC address of the host can be derived from the source address of the link layer, and the IID can be calculated from the MAC address [8], so the IID can be compressed. If the IPv6 address is a link local address, the prefix is FE80::/64 and can be compressed. The encodings of IPv6 source address and IPv6 destination address are SA and DA field, and both of them are set to be 11. If the IPv6 address can not be compressed, it must be carried in-line [9]. The version of IPv6 header is always 6 and must be elided to send. When both the

Traffic Class and the Flow Label are zero the TF field is set to be 1, otherwise they will be carried in-line. The Payload Length can be inferred from the "datagram_size" field in the fragment header, so it can be elided. The Hop Limit can not be compressed and must be carried in full.

When the Next Header field in the IPv6 header is UDP and the UDP header needs to be compressed, the NH field is set to be 01 and the last bit of HC1 header is 1. Both the source port and destination port are compressed to 4 bits, and the SP and DP field are set to be 1. The original port number with 16 bits is P added to short_port and the P is 61616(0xF0B0). The “short_port” is 4 bits and carried in-line [6]. The Length equals the Payload Length in IPv6 Header minus the length of extended headers, so it can be compressed and the L is 1. The Checksum cannot be compressed and carried in non-compressed fields. Five bits of the Reserved field are reserved for future use.

Decompression is an inverse process of header compression, so the original IPv6 packet can be get by decoding each field of HC1 header and HC2 header.

3 Adaptation Layer Formal Modeling

3.1 CPN and CPN Tools

CPN [10] (Color Petri Net) is a colored Petri net based on basic Petri nets. In addition, it is a formal modeling language and appropriate for describing the concurrent, asynchronous and distributed systems. CPN can make hierarchical models, do simulation and clearly describe dynamic behaviors for protocols. The CPN Tools developed by the Aarhus University in Denmark is a special tool for editing, simulating and analyzing colored Petri nets. CPN Tools can validate CPN models automatically according to its data types. Furthermore, this tool can generate and analyze the state space of CPN models, which is beneficial to analyze the reachability, boundedness, activity and so on. Test sequences generated automatically by CPN models can be used to design test cases to do conformance testing for protocols.

3.2 Adaptation Layer CPN Model

According to RFC4944 [6], we provide the CPN models of adaptation layer core functions. Due to the inverse characteristics, the paper only gives the CPN models of header compression and fragmentation. The CPN model of header compression, as shown in figure 4, describes the header compression process of IPv6 packet, including the IPv6 header compression and the UDP header compression. The compression of these two headers is realized by HC1 model and HC2 model respectively. Header compression is mainly the compression of the fields of IPv6 header and UDP header. The corresponding fields are used to construct the hc1 encoding and hc2 encoding. The payload is put after the compressed header to get the compressed IPv6 packet expressed by the color set of HCPACKET.

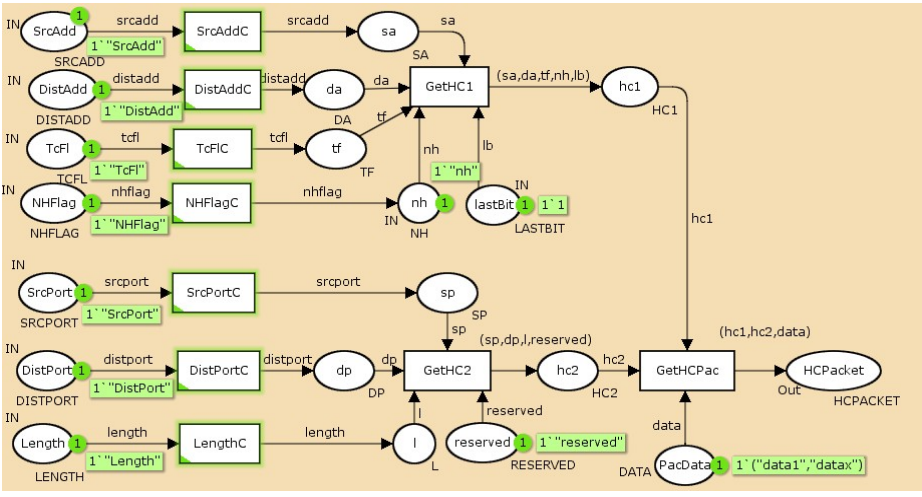

Fig. 4. Header Compression CPN Model

The CPN model of fragmentation function is shown in figure 5. It describes the fragmentation process for IPv6 packets. Fragment header includes the first fragment header and the subsequent fragment header. The latter has the offset field but the former does not. The offset field is designed to reassemble fragments. The receiver calculates the number of fragments by the payload of the IPv6 packet firstly, and then encapsulates the first fragment header or subsequent fragment header for datagram fragments. The fragment with the compressed header is the first fragment, and others are subsequent fragments, denoted by the color sets FIRSTFRAG and SEQFRAG in figure 5.

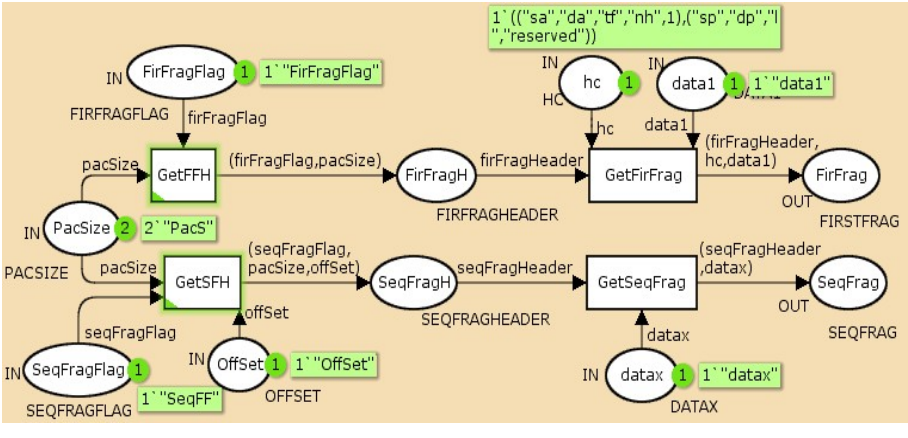

Fig. 5. Fragmentation CPN model

4 Implementation and Testing of Core Functions

As described in RFC4944, we can infer that when the length of the original IPv6 packets is larger than 81 octets, they need to be compressed. And compressed packets will be fragmented if the length of them is still larger than 81 octets. If the received fragment is the first fragment, it will be decompressed to be reassembled. This paper, according to the above processing scheme, header compression encodings, and the format of fragment headers, implements the core functions of adaptation layer for IPv6 header with the next header of UDP. We also design some effective test cases on the basis of CPN models to finish the conformance testing for adaptation layer. Test cases are mainly about compressing the fields in headers, encapsulating fragment header, extracting the length of the IPv6 packet from fragment header. Experiments show that when the size of IPv6 packets is larger than 81 octets, the sender can fragment and compress the header for the packet, and the receiver can decompress and reassemble the fragments. The test result is shown in figure 6 and 7.

```
Original IPv6 packet size: 208 octets.
Compressed IPv6 packet size: 175 octets     Fragments number: 3
c0 d0 00 00 42 db e0 02 ff 02 00 00 00 00 00 00 1f e6 8f 00 01 02 03 04 05 06 07
 08 09 0a 0b 0c 0d 0f 00 00 01 02 03 04 05 06 07 08 09 0a 0b 0c 0d 0f 00 00 01 0
2 03 04 05 06 07 08 09 0a 0b 0c 0d 0f 00 00 01 02 03 04 05 06 07 08

e0 d0 00 00 02 09 0a 0b 0c 0d 0f 00 00 01 02 03 04 05 06 07 08 09 0a 0b 0c 0d 0f
 00 00 01 02 03 04 05 06 07 08 09 0a 0b 0c 0d 0f 00 00 01 02 03 04 05 06 07 08 0
9 0a 0b 0c 0d 0f 00 00 01 02 03 04 05 06 07 08 09 0a 0b 0c 0d 0f 00 00

e0 d0 00 00 03 01 02 03 04 05 06 07 08 09 0a 0b 0c 0d 0f 00 00 01 02 03 04 05 06
 07 08 09 0a 0b 0c 0d 0f 00
```

Fig. 6. Compressed and Fragmented IPv6 Packet

```
Reassembled IPv6 packet size: 208 octets
60 00 00 00 00 a8 11 02 fe 80 00 00 00 00 00 00 76 2f 68 ff fe 55 37 97 ff 02 00
 00 00 00 00 00 31 33 00 ff fe 01 00 03 f0 b1 f0 bf 00 a8 e6 8f 00 01 02 03 04 0
5 06 07 08 09 0a 0b 0c 0d 0f 00 00 01 02 03 04 05 06 07 08 09 0a 0b 0c 0d 0f 00
00 01 02 03 04 05 06 07 08 09 0a 0b 0c 0d 0f 00 00 01 02 03 04 05 06 07 08 09 0a
 0b 0c 0d 0f 00 00 01 02 03 04 05 06 07 08 09 0a 0b 0c 0d 0f 00 00 01 02 03 04 0
5 06 07 08 09 0a 0b 0c 0d 0f 00 00 01 02 03 04 05 06 07 08 09 0a 0b 0c 0d 0f 00
00 01 02 03 04 05 06 07 08 09 0a 0b 0c 0d 0f 00 00 01 02 03 04 05 06 07 08 09 0a
 0b 0c 0d 0f 00 00 01 02 03 04 05 06 07 08 09 0a 0b 0c 0d 0f 00
```

Fig. 7. Decompressed and Reassembled Fragments

5 Conclusions

The adaptation layer connects IPv6 layer and the IEEE802.15.4 standard. The IEEE802.15.4 standard is an important technology of electronic engineering, so the adaptation layer benefits the research of electronic technology. This paper implements

the core functions which are fragmentation, reassembling, header compression and decompression for IPv6 packet. A formal modeling method for core functions is proposed and the CPN models are built. Finally, conformance testing has been finished according to CPN models. Test demonstrates that the core functions of the adaptation layer implemented in this paper makes IPv6 packets transmit over the IEEE802.15.4. The future work is to generate more effective test cases from the CPN models and use TTCN-3 language to do conformance testing for the adaptation layer.

Acknowledgement. This work was supported by National Natural Science Foundation of China (No. 61163011); Chun Hui Project of Education Department(NO.Z2007-1-01032); Natural Science Foundation of Inner Mongolia (NO.2011MS0912); Inner Mongolia University '211 Project' Innovative Talent Training Plan.

References

1. IETF. IPv6 over Low Power WPAN(6LoWPAN), `http://onsite.ietf.org/html.charters`
2. IEEE Computer Society. IEEE Std. 802.15.4 (2003)
3. Sun, L.L., Li, J.Z., Chen, Y.: Wireless Sensor Networks, pp. 109–112. Tsinghua University Press, Beijing (2005)
4. Deering, S., Hinden, R.: Internet Protocol, Version 6IPv6 Specification. RFC 2460 (1998)
5. Kushalnagar, N., Montenegro, G., Schumacher, C.: IPv6 over Low-Power Wireless Personal AreaNetworks(6LoWPANs): Overview, Assumptions, Problem Statement, and Goals. RFC4919 (2007)
6. Montenegro, G., Kushalnagar, N., Hui, J.: Transmission of IPv6 Packets over IEEE802.15.4 Networks. RFC4944 (2007)
7. Hui, J., Thubert, P.: Compression Format for IPv6 Datagrams in 6LoWPAN Networks. In: 6LoWPAN WG Meeting 74th IETF Meeting, San Francisco, California (2009)
8. Crawford, M.: Transmission of IPv6 Packets over Ethernet Networks. RFC2464 (1998)
9. Li, C.L.: Research of 6LoWPAN Technology and Implementation of Header Compression. Jilin University, Jilin (2011)
10. Jensen, K., Kristensen, L.M., Wells, L.: Colored Petri Nets and CPN Tools for Modeling and Validation of Concurrent Systems. International Journal on Software Tools for Technology Transfer (S1433-2779), 213–254 (2007)

Design for Water-Saving Irrigation Based on Electronic Technology Sensor and Wireless Data Transmission

Yan Sun[1], Yang Wu[1], Ling Chen[2], and Bing Yang[1]

[1] Engineering School, Anhui Agricultural University, Hefei, Anhui, China
[2] Foreign Languages School, Anhui Agricultural University, Hefei, Anhui, China
syxk119@sina.com

Abstract. In electronic engineering field , in order to achieve accurate, fast and reliable irrigation, this paper introduce a kind of automatic water-saving irrigation system based on electronic technology sensor and real-time online monitoring of wireless data transmission. Through a wireless network （TD-SCDMA） remote monitoring center connects the subordinate stage then constitutes a mater-slave system. The remote monitoring center gives the order to arouse the subordinate stage and the subordinate stage receives the order to collect datum and transmit them to the remote monitoring center, accordingly instruct irrigation. This article describes the system's working principles, hardware design and implementation methods from the hardware and software aspects. Practice shows that the system has stable performance, reliable data and establishes the foundation for further studying irrigation technology in electronic engineering field .

Keywords: electronic technology sensor, Data acquisition, Real-time monitoring, Water-saving irrigation.

1 Introduction

Accurate, rapid, reliable evaluation to the condition of crop moisture is the basic theory of effective, accurate irrigation. It is required accurate irrigation or custom-designed irrigation in the precise agriculture, hoping consider comprehensively every evaluation indicator which reflects actual water requirement. So far, different irrigation system has different moisture evaluation indicator which has its own distinguishing feature [1-3]. But most of them has somewhat imperfections and hasn't formed authoritative, standardized evaluation indicator or indicator system. It becomes a new challenge and hotspot of study to seek a more convenient way which shows the model of water-saving irrigation. In this sense, intelligent irrigation technology research of real-time monitoring crops based on electronic technology sensor has wide application prospects in the field of agricultural and water soil engineering.

2 Evaluation Indicator of Crop Water Requirement

Generally there are three kinds of evaluation index in the past. The first kind is taking the soil as object. Aiming at requirement of water-saving irrigation in precise agriculture, employing type of SWR-2 soil moisture sensor, Zhengjun Qiu and his

D. Jin and S. Lin (Eds.): Advances in Mechanical and Electronic Engineering, LNEE 177, pp. 423–428.
springerlink.com

colleagues have developed fast measuring instrument of soil moisture based on GSP and its instrument can generate chart of farmland of soil moisture [4]. Yihua Cai, Gang Liu and their colleagues developed the system of water soil collection based on the technology of wireless sensor network. And the technology has provides technical support for the application of WSN in the agriculture [5]. The advantage of taking soil as the object is relatively stable. But after all it is the indirect index of crop growth and it has the disadvantage of slow reflect and short precision.

The second kind is taking the environment as the object. For example, Jiabin Cai and his colleagues have mentioned the way of real-time estimation crop evapotraspiration on the basis of the real time weather forecast [6]. Yu Liu has developed the space features of major crops water irrigation in China based on the way of using standardized meteorological data and the GIS spatial analysis function [7]. So we can see that taking the environment as the object is mainly through the weather forecast to estimate crop evapotraspiration and use this way to direct crop irrigation. So though this way is simple and practical, its precision is relatively low.

The third kind is taking the crops themselves as the object. This index can be divided into morphological index and physiological index. Morphological index refers to crops and its morphologic character of relevant water sucking. Qinbing Zeng and his fraternity have confirmed that the change of the grapes' fruit size can be used to evaluate the growth of the grape and judge the condition of moisture loss of plant [8]. The way of its algorithms is complicated, so it is difficult to spread and apply in large area. Physiological index refers to some physiological characters of relevant moisture. Takahiro Sato and his fraternity utilized leaf water potential or stem potential and blade stomatic conductance crop index to analyze the condition of water shortage and then to guide irrigation[9]. But taking this method need insert resistance sensing needle into the stem of the plant, this will damage plant material and impact test accuracy more or less.

The indexes and methods mentioned above have been applied in different level successively. This study employed the method of non-contact sensor, seized the main factors, such as the canopy temperature, soil moisture content, the environment of crop growth etc. To construct the water requirement law of crop growth, providing the technical parameters and model for accurate irrigation.

3 System Working Principle and Hardware Design

3.1 System Working Principle

In the study, through detecting many kinds of parameters such as, the canopy temperature, the soil moisture, the air temperature and humidity etc. To realize the accurate automatic irrigation control of farmland. The sensors detect data online, using wireless data transmission. The sensors signal amplify circuit by signal regulation. Regulation is converted into digital signal by A/D converter and by encoding process, constitute transmission data frame, send/receive module by RF, and again bring about power amplification by power amplifier of RF; the collection of data on the spot is transferred in the remote monitoring center by using TD-SCDMA communication, and the computer in the remote monitoring center carry through data fusion for collected

data. So it can make water supplying plan, according guide irrigation through analyzing and processing the experiment data.

3.2 System Hardware Design

The system has three parts: sub-stations, TD-SCDMA net, the remote monitoring center respectively. Figure 1 is the general structure chart of the system. Among the three parts, the sub-station is made up with development platform of MiniARM embedded microcontroller and network node based on the ZigBee electronic technology sensor. MiniARM and the wireless sensor network node constitute the star type topology. In the system, sub-station realizes the data collection, data storage display, data communication, opening and closing water pump; TD-SCDMA net realizes the communication between the remote monitoring center and sub-station; the remote monitoring center is equipped with database and PC which can realize user management, sub-station management, data management, daily record management and intelligent decision-making, in addition, it can obtain weather information through Internet, then synthesize the weather information and environmental parameters, and automatically determine whether it need irrigation or when it is suitable etc. Accordingly achieve the purpose of intelligent irrigation.

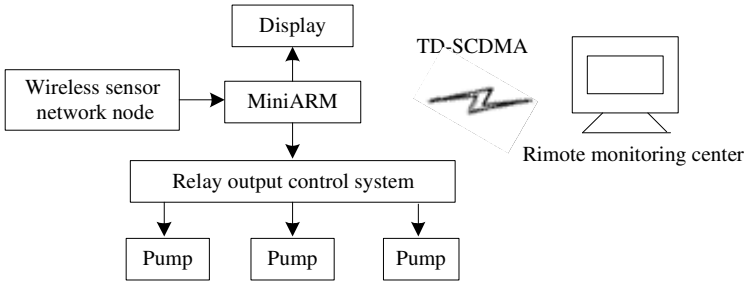

Fig. 1. Block diagram of the system

3.3 Design of the Electronic Technology Sensor Nodes

The system adopts British Jennic Company's JN5139-001-M02R1 module. The core chip of the module is JN5139 wireless microprocessor which is the 32-bit SCM including RF module, compatible IEEE802.15.4 ZigBee agreement.

The structural chart of electronic technology sensor node is shown in figure 2. Its mainly function is the collection of data of soil moisture, air humidity, temperature, crop canopy temperature; storage/display collected data; the transmission of wireless data; the function of voice prompt. The system uses the real voice. When testing parameters beyond the normal range, it can promptly and accurately remind users to regulate, thereby improve crop growth environment and its yields. In addition, the working power of the node adopts SA68D21DL supply. Users can install controller in the office or at home, which is not only against burglars, but can avoid the natural damage.

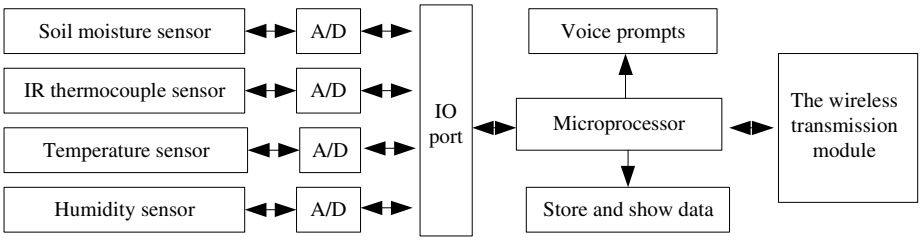

Fig. 2. Structural diagram of electronic technology sensor point

4 System Software Design

The system software is mainly software design of sub-station, including MinARM controlled system program and the wireless sensor node system program.

4.1 MiniARM Controlling System Program

The function of the MiniARM controlling system is to build wireless net, and send order to the sensor' node, then read the parameters transmitted by the sensor's node, again by set irrigation decision, to decide whether to irrigate. Its software diagram is shown in figure 3.

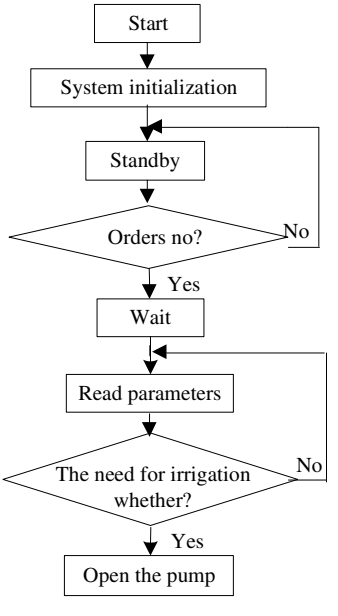

Fig. 3. Flow chart of the MiniARM controlling system

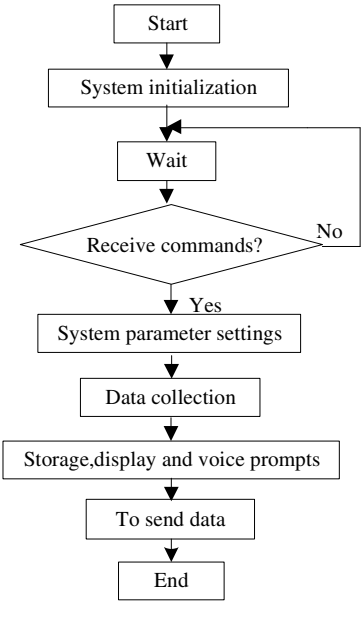

Fig. 4. Flow chart of the sensor point

4.2 Electronic Technology Sensor Node System Program

The electronic technique sensor node system program is made up with data collection subprogram, storage / display subprogram, voice prompt subprogram and MiniARM wireless communication subprogram. The software diagram is shown in figure 4. The function of the program is to real-time read the parameters measured by sensor and send the parameters in real time to guide the irrigation when sensor node receives order.

5 Remote Monitoring Center

Remote monitoring center design includes internet connection of Mobile TD-SCDMA, the monitoring center host-friendly interface display system. The software features of the system are broadly divided into five modules: Sub-station management, the user management, the data management, the log management, and intelligent decision-making. They are responsible for managing sub-station's working condition (data collection, processing, display, voice prompts, etc.); work of User's permissions distribution, user's add/remove, and user's password maintenance; operation of data's transmission, query, print and statistics; records of system's events; Fusion analysis the law of water requirement of crop, and guide irrigation.

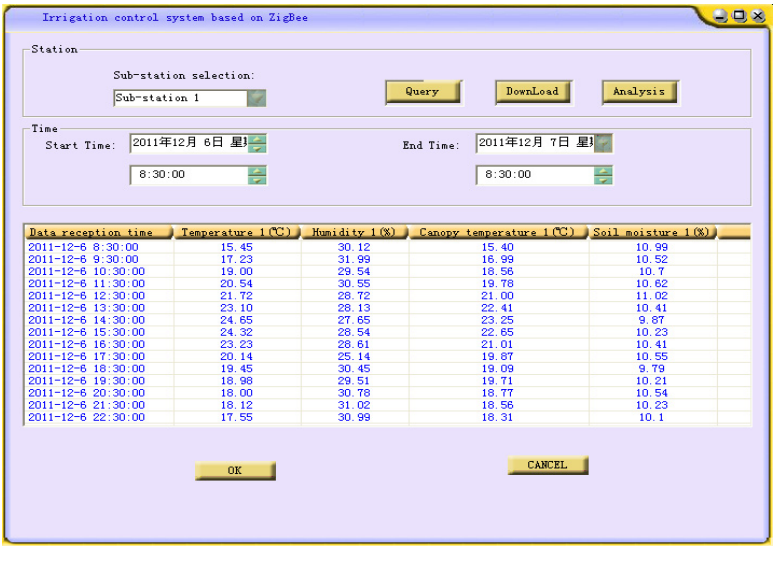

Fig. 5. Real-time inspecting interface of the sub-station 1

Later the system was tested for greenhouse wheat in experimental base in Anhui Agricultural University. Consider the number of wireless network configuration , we established a sub-station (including four electronic technology sensor nodes) to communicate with the remote monitoring center. Users can query, download and analyze data through a database. The page of real-time inspecting interface is shown in figure 5.

6 Conclusion

The intelligent irrigation system designed in this paper based on electronic technology sensor and automatic water-saving irrigation system of wireless data transmission is embedded systems technology, TD-SCDMA wireless WAN communication technology, the ZigBee LAN wireless communication technology, though it is point-to-point wireless intelligent control in small area, it meets the tendency to develop the intellectualized and networked agriculture, and has certain promotional value and application prospect. If it can optimize control strategy according to different requirement of crop growth, it will fully embody its superiority [10], and will carry forward its development electronic engineering field .

Acknowledgments. Supported by high school and Provincial level Natural Science Research Project in Anhui Province (KJ2011Z127).

Supported by Technology SME Technology innovation Fund of Ministry of Science (10C26213401639).

References

1. Kacira, B.S.: Noncontact and early detection of plant water stress using infrared thermometry and image processing. The Ohio State University (2000)
2. Annus, J.F., Van Herwaarden, A.F.: Increasing water use and water use efficiency in dry land wheat. Agronomy Journal 93(2), 290–298 (2001)
3. Goldhamer, D.A., Fereres, E.: Irrigation scheduling of almond trees with trunk diameter sensors. Irrigation Sci. 23, 11–19 (2004)
4. Luo, X., Zang, Y., Zhou, Z.: Research progress in farming information acquisition technique for precision agriculture. Transactions of the CSAE 22(1), 167–173 (2006)
5. Cai, Y., Liu, G., Li, L., Liu, H.: Design and test of nodes for farmland data acquisition based on wireless sensor network. Transactions of the CSAE 25(4), 176–178 (2009)
6. Cai, J., Liu, Y., Xu, D.: Real-time estimation of crop evaportranspiration and its validation by field experiments. Journal of Hydraulic Engineering 39(6), 674–679 (2008)
7. Liu, Y., Wang, L., Ni, G., Cong, Z.: Spatial distribution characteristics of irrigation water requirement for main crops in China. Transactions of the CSAE 25(12), 6–12 (2009)
8. Zeng, Q., Liu, C., Miao, Y., Wang, S., Huang, D.: Non-destructive measurement of diameter of overlapping grape fruit based on morphological image processing. Transactions of the CSAE 25(9), 356–360 (2009)
9. Takahiro Sato, O.S.A., Oweis, T.Y., Sakuratani, T.: Effect of supplemental irrigation on leaf stomata conductance of field-grown wheat in northern Syria. Agricultural Water Management 85, 105–112 (2006)
10. Fang, X., Zhou, Y., Cheng, W., Ding, C., Yang, X.: The design of wireless intelligent irrigation system based on Zigbee technology. Agriculture Mechanization Research 1, 114–118 (2009)

Research of Embedded Real-Time System Security Level Assessment Techniques with Electronic Technology

Wang Xuhui

Handan College, Handan 056005 China
ieee2010@foxmail.com

Abstract. This paper briefly describes the main ideas and implementation of technology strategy of Embedded real-time system security level assessment which is important part of mechanism to system flexibility based on embedded real-time system in electronic technology, designs the embedded real-time system security level assessment system based on pattern matching for the characteristics of embedded real-time systems. By building security level assessment system and simulation testing environment based on RT-Linux real-time operating system in electronic technology.

Keywords: security, Pattern matching, Embedded Operating System (EOS), Real-time System, RT-Linux.

1 Introduction

With the extensive application of real-time computer technology, embedded real-time systems are widely used in the field of industrial control and defense systems. How to ensure the reliability of real-time system in order to avoid disastrous consequence, currently is a very important area of embedded systems research, mechanism to system flexibility based on embedded real-time system came into being.

Embedded real-time systems usually arise in the implementation process some of the problems, such as some exception caused by malicious attacks of common suspicious or malicious code on the system. Moreover, the changes of system hardware state may also lead to system exception, such as equipment failure may make the system don't know what to do. Therefore, we can enhance the flexibility of real-time system itself and then improve the security and adaptability of the system. Embedded real-time system security level assessment techniques as a core part of Mechanism to System Flexibility is essential.

2 View of Embedded Real-Time System Security Level Assessment Strategy

Embedded real-time system security level assessment module is embedded real-time system core of mechanism to system flexibility, it can work out comprehensive assessment of collected information based on pattern matching method, then give the system's security level and action proposal which will be send to the module of explanation and implementation. The module will decompose the information after

D. Jin and S. Lin (Eds.): Advances in Mechanical and Electronic Engineering, LNEE 177, pp. 429–434.
springerlink.com

received them, then pass the decomposition information to the different module. After that, every module will start appropriate services according to the information received. Architecture of mechanism to system flexibility is shown in Figure 1:

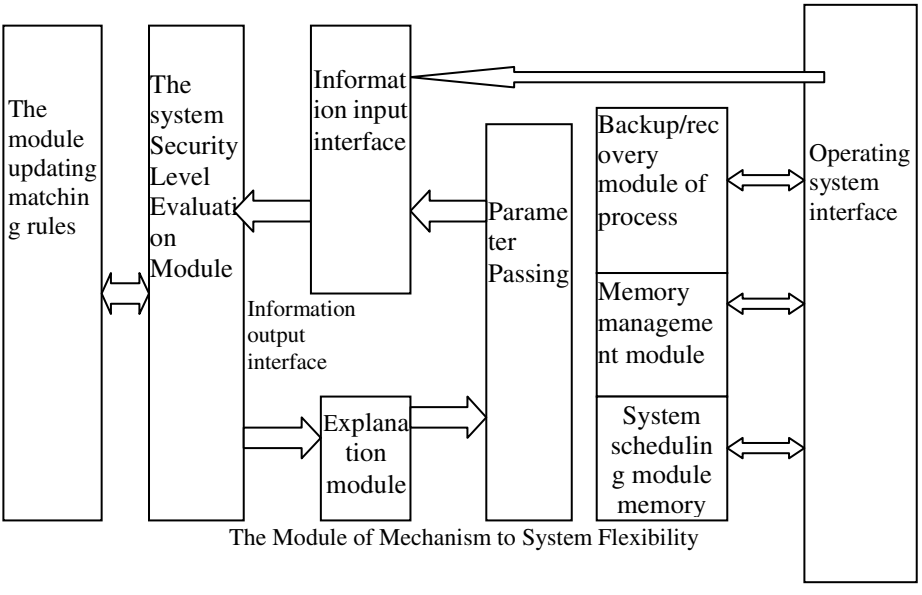

Fig. 1. Architecture of the Mechanism to System Flexibility

The Module of Mechanism to System Flexibility use pattern-matching principle, it collects the behavioral characteristics of various types of information, and then establishes Features Library related to them. If the input information that indicating the system behavior matches the records in the Features Library, then the system will give the corresponding system security rating. So the system security level evaluation can be realized. The input information is a formatted string that make up of process information, system information (including hardware information), it will be analyzed by pattern matching. After the information is inputted into system, the matching result will be getting by pattern matching, which will be output to the module of explanation and implementation. Parameters will be sending to distributed module of process security, memory management, and system scheduling though Parameter passing module, the distributed modules decide which coping strategies of mechanism to system flexibility will be use according to the data received.

3 Embedded Real-Time System Security Level Assessment Based on Pattern Matching

Pattern matching is to compare the collected information with the known pattern in the database of the system security level so as to give the current Security Level Status of the system. Security level assessment system receives a string consists of operating

system processes information, operating system information and embedded system hardware information through the information input interface, then compares it with the pattern in the database of the system security level.

Pattern matching function mainly consists of data structure definitions and Algorithm for matching rules. System uses the character string pattern matching that the data structure can be character string and two-dimensional character string array. Character string array can be use to define the string T and substring S. The collection of each string of security level that is patterns library of security level assessment exists as the form of two-dimensional array.

Pattern matching is the main tool of character string processing, which originated from the Markov algorithm. Its main function is to investigate whether the character string Contain the given string pattern or not, and to complete the given assignment or replacement operations.

Pattern matching is the location of substring, which is an important string operation. For two strings T (length of n) and S (length m), the process of finding substring S (also called pattern) in the string T is called pattern matching. The security level assessment system based on pattern matching has several strings, which can be classified into five security level sets, denoted by T1, T2, T3, T4 and T5 respectively, a level of security for each. T1 represents the highest level of security; T5 represents the lowest level of security. Each collection contains the strings of its security and there is more than one string in each security level. When pattern matching is successful, system security level can be got according to the matched string. Otherwise, the pattern of substring will be recorded in order to form a new string pattern of security level. Figure 2 shows this process:

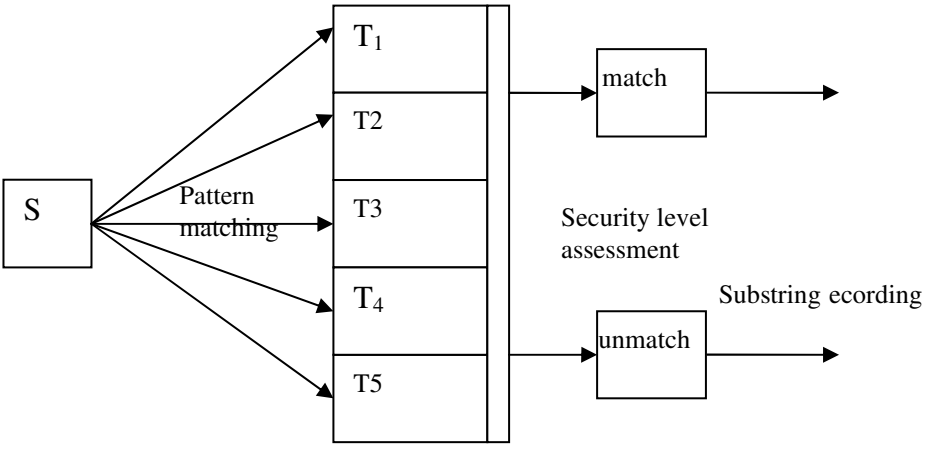

Fig. 2. Process of pattern matching

Pattern matching, just the information sub-string and each element of two-dimensional array can be compared and matched. If there is a pattern matched, the corresponding values of the array element will return to determine the current security level. If no matched pattern, the current information substring will be recorded. When a

certain amount of information sub-string is accumulated, through manual processing, the unmatched sub-string pattern can be processed to a new security level pattern string by using artificial intelligence algorithms.

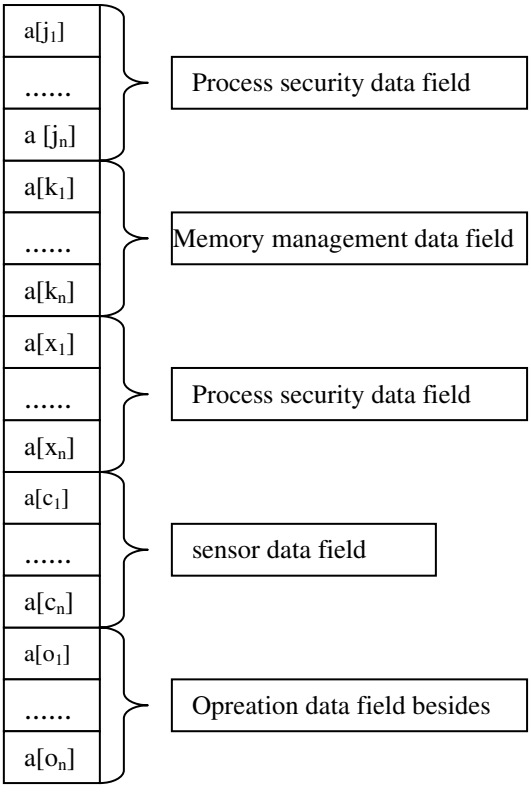

Fig. 3. Data structure definition of substring S (system state pattern)

System uses the string pattern matching. Character string array and two-dimensional character array are used as data structure. Using character string array to define the string T and substring S. Each collection of security level string that is the security level assessment pattern library is a two-dimensional array.

The Substring includes not only the data information from process security, System scheduling and Memory management, but also the status information of system hardware coming from the sensor and operating system status information which the distribution module cannot provide. Specific structure is shown in Figure 2.2.

Security level assessment pattern library stored information pattern of a variety of security level by using two-dimensional array data structure. Because the system has fixed five security levels, the row number of the two-dimensional array is 5. The pattern number of each security level is not fixed, so the column number of two-dimensional array is not fixed. After each pattern update, the column number of two-dimensional array is likely to increase, depending on the column number of the

longest row updated. The whole security level assessment pattern library is a two-dimensional array with unfixed number of column. To facilitate future pattern updates, the maximum column number of the two-dimensional array will not be limited. Specific structure is shown in Figure 4.

T_1 security level	a[b1]	.....	$a[b_n]$	.....	$a[b_m]$
T_2 security level	$a[c_1]$	.....	$a[c_n]$	.....	$a[c_p]$
T_3 security level	$a[d_1]$	.....	$a[d_n]$	.....	a[dq]
T_4 security level	$a[e_1]$	.....	$a[e_n]$	.....	$a[e_r]$
T_5 security level	$a[f_1]$	.....	$a[f_n]$	.....	$a[f_s]$

Fig. 4. Data structure definition of security level assessment pattern library

These unlatched system state pattern will be recorded after pattern matching for the pattern update. Pattern update is that, evaluating these unlatched system state patterns by using corresponding or artificial algorithm to get their proximity of each security level and then assigning it to the closest security level. To implement pattern update, there are two ways.

The first is to compare unmatched pattern with each pattern in every type of security level to obtain conformity information, and thus to determine the security level of the unlatched pattern, and to establish new patterns in the appropriate security level in order to achieve the purpose of pattern updating. For the case of the small number of patterns, this approach is simple and effective. But if a large number of patterns need to be processed, clearly this approach is inefficient, which can ensure maximum conformity yet.

The second is the use of pre-classified, which summarize the characteristics of each category and Compare them with patterns to get the degree of conformity. This process involves two steps: first step is to cluster the recorded system state pattern and analysis, within five categories, and to express the characteristics of each pattern type. Then the characteristics of each pattern type will be compared with each characteristics of five security level to find out the maximum conformity, therefore to furthermore determine the type of security level of new pattern. This process can be implemented by matrix operations. Following is a brief look at the second way.

After clustering five characteristics of pattern were generated, which compared with characteristics of pattern in the security level assessment pattern library to abstain corresponding degree of conformity, and then the pattern classification and update completed. The specific process is as follows:

1. The five cluster patterns and five security level patterns are stored into a one-dimensional array. Characteristics of five security level pattern are known, which is determined at the time of classification.

2. After operations 5 × 5 in conformity numerical matrix generated, the best conformity of five security level patterns and five cluster patterns can be obtained by matrix operation.

3. According to the conformity cluster patterns can be classified respectively, into the appropriate security level

4 Experimental Simulation and Performance Evaluation

Experiment emulation is based on RT-Linux real-time operation system. RT-Linux is open source and multi-tasking operating system, which has the characteristics of hard real-time. RT-Linux places a real-time kernel between the Linux kernel and hardware interrupts, regards standard Linux kernel as a process of the real-time kernel to manage together with user's process. The standard Linux kernel has the lowest priority; it can be interrupt by the real-time process, the normal Linux process still can run on Linux kernel. In this way, RT-Linux not only can use all services of Linux, but also can offer the real-time environment.

5 Conclusions

The embedded real-time system security issue has been hot in academic study circles. In order to improve the security and reliability of embedded real-time system, we can enhance the real-time system flexibility itself. The core problem of System Flexibility is system security level assessment, this paper deeply studies and discusses embedded real-time system security level assessment techniques according to current development status, designs and implements security level assessment System based on pattern matching. Simulation results show that the security level assessment system can effectively prevent the system from exception without affecting system performance and improve the capacity of flexible response in electronic technology.

References

1. Hwang, D.D., Schaumont, P., Tiri, K., Verbauwhede, I.: Securing embedded systems. IEEE Security & Privacy (2) (2006)
2. Zhao, G., Zhang, G., Yao, A.: Research of Mechanism to System Flexibility Based on Embedded Real-time System. In: 2010 International Conference on Advanced Measurement and Test, AMT 2010 (2010)
3. William Beckwith, R., Mark Vanfleet, W.: High Assurance Security/Safety For Deeply Embedded, Real-time Systems. In: 2006 Embedded Systems Conference (2006)
4. Oberthür, T.K.: Configurable Hybridkernel for Embedded Real-Time Systems. Embedded System Design (2007)
5. Kitani, T., Takamoto, Y., Yasumoto, K., Nakata, A., Higashino, T.: A flexible and high-reliable HW/SW codesign method for real-time embedded systems. In: 2004 IEEE First Symposium on Multi-Agent Security and Survivability (2004)
6. Zhang, G., Zhao, G., Yao, A., Liu, R.: Research of Mechanism to System Scheduling Flexibility Based on Embedded Real-time System. In: 2010 International Conference on Machine Vision and Human-Machine Interface, MVHI 2010 (2010)

The Critical Electronic Technology for Porting the μCOSII to ARM7TDMI Platform

Jianyong Lin[1] and Baohui Xie[2]

No.3663 North Zhongshan Rd, Putuo District, Shanghai 200062, China
[1] College Resources and Environmental Science, East China Normal University, China
[2] Honeywell Inc, Shanghai, China
13916079304@163.com

Abstract. Recently, the embedded system becomes increasingly complicated. With the development of electronic engineering, ARM plus RTOS has become one of main design methods. Porting the μCOSII to ARM7TDMI platform through the GPS receiving device was introduced particularly in the paper. The approach can provide the solution used in more complex real-time embedded system.

Keywords: embedded system, GPS (Global Positioning System), RTOS (Real Time Operating System), ARM (Advanced RISC Machine), ISR (Interrupt Service Routine).

1 Introduction

GPS as Critical electronic technology in semiconductor industry appeared in the 1970's, using to positioning, measuring the time and speed globally for all the directions and all the time. GPS is composed of satellite system in the air space, monitor system on the ground and GPS receiver which using wireless and computer technology plus data processing software. The GPS receiver is a little bit more complex system that can be divided into several modules: main control module which is responsible to the control and management works for application module; GPS module which is responsible to configure and control GPS receiver module; EXUI module which is responsible to manage the communication channel with outside device; DLINK module which is responsible to manage the data link related work; monitor module which is responsible to monitor the system status such as GPS receiver status, battery status, SD disk capacity and so on; File system module; USB communication module and hardware management module. And many modules and processing large amount of data, is suitable for industrial design, using the high performance PHILIPS2000 series MCU: LPC2214 which based on ARM7TDMI core, owned external memory bus. As for software, it is widely using in embedded system design where takes μCOSII as RTOS platform designed by Jean J.Labrosse, since open source and its highly reliability. μCOSII is a prompt multi-thread OS based on priority, scalable, highly stable and reliable. This paper using GPS receiver as an example demonstrates the critical technic during porting.

D. Jin and S. Lin (Eds.): Advances in Mechanical and Electronic Engineering, LNEE 177, pp. 435–441.
springerlink.com

2 Porting µC/OS-II to ARM7TDMI Platform

2.1 RTOS Kernel

RTOS is mainly used to manage the system resources, including task creation, scheduler, system ticker service, memory management, mailbox, processing and etc. All the system services are provided by µC/OS-II kernel. The kernel will be built together with application layer and driver layer into a whole real time system. During porting, the kernel is not changed, but the part related to MCU.

2.2 Source Code Related to MCU

This part is most important. Kernel is built together with application layer and driver layer into a whole as a real time system. It needs customize the same kernel to satisfy different hardware architectures, and it may need modify the source code according to specific MCU architecture. These source code are contained in three files: OS_CPU.H, OS_CPU_A.ASM, OS_CPU_C.C; and the development environment is ADS1.2.

2.3 Kernel Porting Architecture

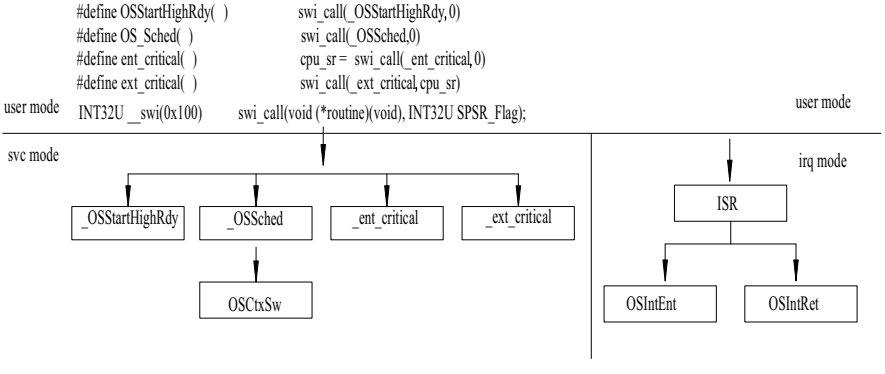

Fig. 1. Kernel Porting Architecture

Figure 1 demonstrates that using the SWI (software interrupt instruction) to switch the MCU mode from user mode to privilege mode, the SWI simulates the hardware interrupt that allows the context switch in ISR mode; furthermore, in privilege mode, it is very easy to operate the CPU internal registers. This paper, according to ADS1.2 pragma defined a special function that triggered by software interrupt instruction: INT32U __SWI(0X100) swi_call(void(*routine)(void),INT32U SPSR_Flag).This function can return a 32 bits unsigned integer and owns two parameters (the one is function pointer and another is unsigned integer). By this way, we can define other functions based on it, and through the function pointer, it is very easy to locate the handlers, and since it isolates the interface and implementation, it is very convenient for future maintenance.

2.4 OS_CPU.H：Mainly Including Constants, Macro and Type Definition Related to MCU:

2.4.1 System Type Definition
For ARM architecture, WORD is 32 bits, HALF-WORD is 16 bits and BYTE is 8bits.

2.4.2 Stack Grows Up Definition
According to ADS1.2 regulation, the growing-up direction of stack is full-decrease. In other word, adjust the SP pointer prior to push the data, and should pop the data then adjust the SP pointer;

2.4.3 Disable and Enable Interrupt Definition
This paper, save the current CPU status register (CPSR) to local variable and define OS_CRITICAL_METHOD=3, then using SWI ISR to implement the data exchange between CPU status register and local variable.

2.5 OS_CPU_A.ASM

2.5.1 void _OSStartHighRdy(void)
When finish RTOS initialization, this function will be invoked to start the task. It will load the task context with highest priority to CPU register and run this task. The system through the SWI macro OSStartHighRdy( ) to locate this function. Figure 2 shows the details:

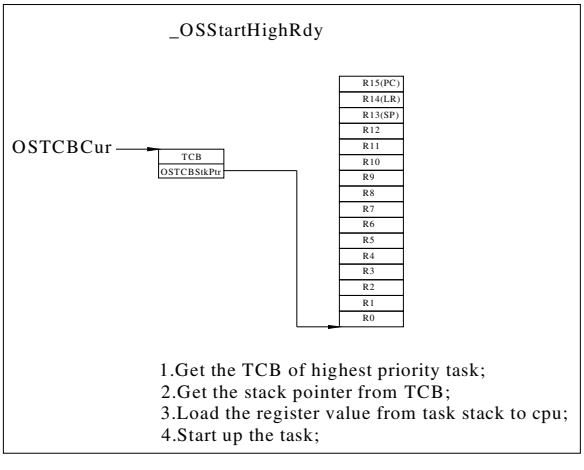

Fig. 2. void _OSStartHighRdy(void) implementation

2.5.2 void _OSSched(void)& void OSCtxSw (void)
These two functions are used to switch the context during task schedule, which is also using SWI links to interface OS_Sched( ) written in assembly language. When application invokes this function, _OSSched will push the context of current task to

SVC stack, and save the SP to a global variable gTaskSP; then will invoke function Sched( ) to determine the ready task with the highest priority, If it is a different task, then will invoke function OSCtxSw to finish the context switch, otherwise, it will return to the previous task. Refer Figure 3 for more detail.

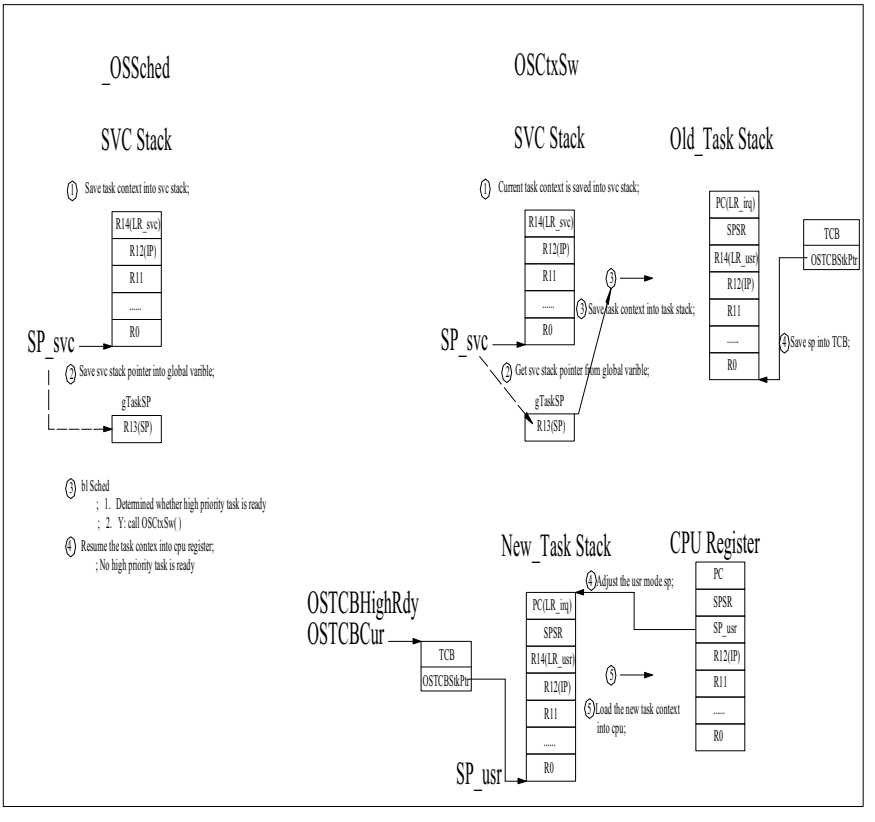

Fig. 3. void _OSSched(void)& void OSCtxSw (void) implementation

2.5.3 IRQ ISR

When CPU receives the interrupt signal, it needs interrupt preprocessing prior to enter ISR. When IRQ interrupt occurred,it will invoke HANDLER firstly, and save the current task context to IRQ stack, then function OSIntEnt will transfer the context from IRQ stack to task stack, and when exit ISR, function OSIntRet will load the context with the highest priority and ready task to IRQ stack, then macro HANDLE will load the context to CPU, refer Figure 4 for more detail.

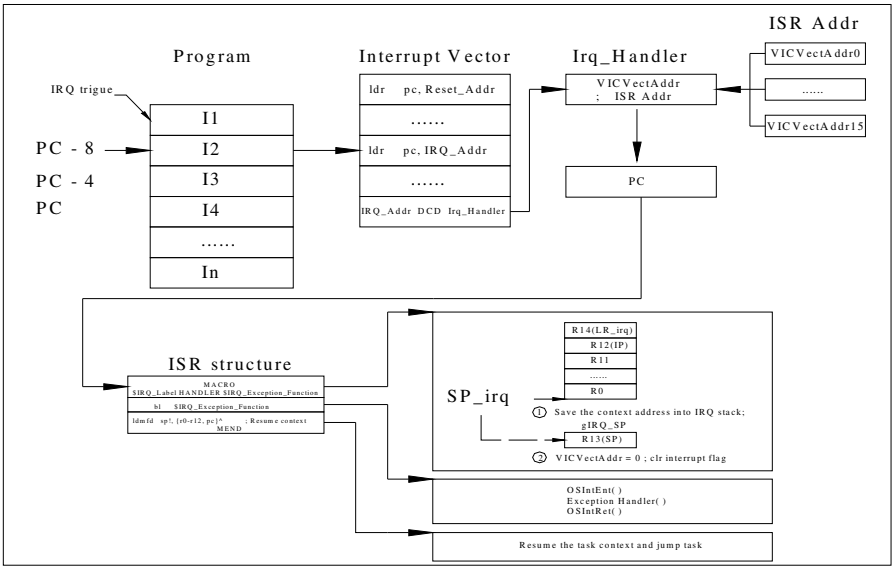

Fig. 4. IRQ Processing

2.5.4 void OSIntEnt(void)and void OSIntRet(void)

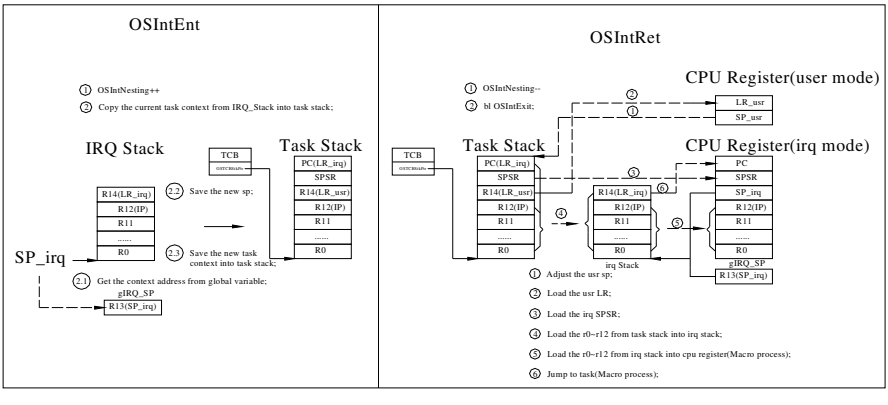

Fig. 5. void OSIntEnt(void) and OSIntRet(void) Implementation

These two functions are provided by RTOS to handle IRQ interrupt, used to protect the task context prior to enter ISR, and resume the ready and the highest priority task context, to implement the task schedule. According to IRQ handling procedure above, there is no need to implement the function of OSIntCtxSW. Refer to Figure 5 for more detail.

2.5.5 Timer0_Handler HANDLER bios_tmr0_ctrl(void)

The ticker ISR is used to provide the periodic tick for RTOS, it also should follow the IRQ processing procedure above, actually, in this paper, all the ISR should follow this context switch mode. Refer Figure 6 for more detail of function bios_tmr0_ctrl implementation:

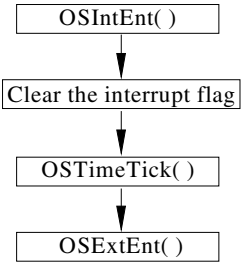

Fig. 6. void bios_tmr0_ctrl(void)Implementation

2.5.6 void _ent_critical(void) & void _ext_critical(void)

These two functions are used to protect the critical area, in this paper, using the method of OS_CRITICAL_METHOD=3. When invoke the macro OS_ENTER_CRITICL(), it will locate the function _ent_criticla through the SWI, and when CPU switches to user mode from SVC mode, it will load the CPSR of user mode to SPSR of SVC mode, then function _ent_criticla will load the SPSR of SVC mode to R0, at this point, can set the bits of I_BIT and F_BIT of SPSR to disable the interrupt, and when CPU returns to user mode, SPSR will load to CPSR and according to ATPCS(The Arm_Thumb Procedure Call Standard) principle, the R0 contained previous CPSR before disable interrupt returned to a local variable cpu_sr. Samly when invoke OS_EXIT_CRITICAL() to enable the interrupt, it should use the value of cpu_sr as the second parameter of function swi_call(_ext_critical,cpu_sr), and according to ATPCS(The Arm_Thumb Procedure Call Standard) principle, it will pass to SPSR via R1, and when exit SVC mode, it will resume the previous status and enable the interrupt. Refer Figure 7 for more detail.

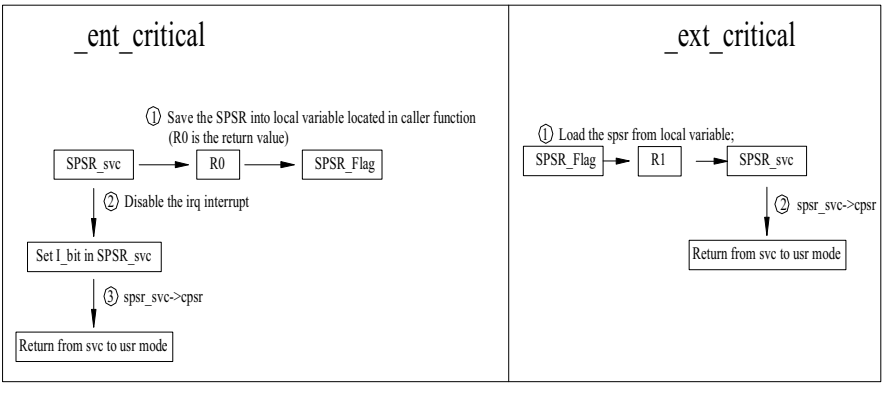

Fig. 7. void _ent_critical(void) & void _ext_critical(void) disable and enable interrupt

2.6 OS_CPU_C.C

2.6.1 void OSTaskStkInit(void)

This function is used to initialize the task stack during task creation, can be written by C language, since the full-decrease stack mode of ADS1.2, should decrease the SP pointer when push the datum. Refer the Figure 8, when task is just created, the parameter pdata of function OS_STK *OSTaskStkInit(void (*task)(void *pd) , void *pdata, OS_STK *ptos, INT16U opt) will pass to R0, R1-R12 will be initialized to zero, SPSR will be initialize to user mode and enable IRQ interrupt, R14 and PC will point to the start address of this task, and at the same will save the top address of SP to TCB. The RTOS can find the SP address via TCB and implement the appropriate operation.

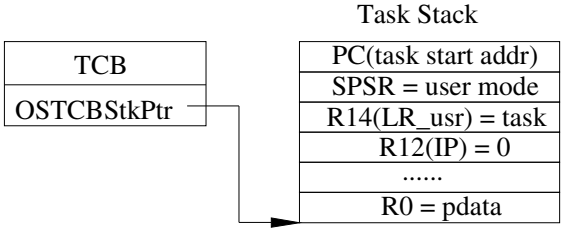

Fig. 8. void OSTaskStkInit(void)Initialize the stack

3 Conclusion

Several critical electronic technics when porting μC/OS-II to ARM7TDMI platform were demonstrated in this paper, and it provides the implementation of relevant functions. During the porting, SWI was used to define the function INT32U swi(0x100) swi_call(void(*routine)(void),INT32U SPSR_Flag) and the technic is the core. The technic is the entry to switch the MCU mode from user mode to privilege mode, and it is also the bridge between RTOS services and low level layer.We isolated the interface and the implementation through this bridge, which can reduce the modules coupling and improve the software maintainability. Currently, ARM plus RTOS is more and more popular for orienting to complex embedded system design in field of electronic engineering and is becoming the mainstream design. The approach in this paper can provide powerful tools.

References

1. Barry, R.: Using the freeRTOS Real Time Kernel. Real Time Engineers Ltd. (2010)
2. Jaggar (ed.): ARM Architectural Reference Manual. Prentice Hall, San Francisco (2009)
3. Lamie, E.L.: Real-Time Embedded Multithreading. CMP Books (2004)
4. Labrosse, J.J.: Embedded Real Time Operating System μC/OS-II. CRC Press (2003)
5. Phadke, A.G.: Synchronized phasor measurements a historical overview. In: 2002 Transmission and Distribution Conference and Exhibition, pp. 476–497. IEEE Press, Yokohama (2002)
6. Furber, S.: ARM System-on-Chip Architecture. CRC Press (2000)

Rapid Design of LED Spot Light Based on Normalized Cross Correlation Algorithm Used in Electronic Technology

YongJiang Di and PengJun Cao

School of Metallurgical and Materials Engineering, Chongqing University of Science and Technology, Chongqing, 401331, China
yjdee@163.com

Abstract. One spot light with full width at half maximum (FWHM) of 28° used in electronic technology and intelligent control was designed from a lambertian high power LED and a total inter reflection (TIR) lens. The rapid and accurate design of the spot light with specific light pattern was completed with the assistant of Monte Carlo Simulation, and was verified by normalized cross correlation (NCC) algorithm between the simulation patterns and the experimental measurements. The NCC of the spot light between the simulation and the measurements is large than 0.99 in the far-field region. The TIR efficiency of the LED spot light in the design is 93.5%.

Keywords: Optical modeling, electronic technology, normalized cross correlation algorithm, spot light.

1 Introduction

The LEDs (Light Emitting Diodes) are used everywhere, from indoor light, street light to vehicle head-light, and electronic advertising flat panel display. The LEDs have more advantage than traditional light source and have been regarded as the best potential light source for next-generation lighting. The LEDs can be controlled easily and digitized with lower power consumption, used in intelligent systems such as smart home lighting system. The accurate light patterns of optical system of LED with varies lens are needed to develop the wisdom and comfortable lighting for the rapid design.

The encapsulated LED with different radiation patterns in the far-field region can be obtained extensively. But most case where the LEDs are not direct used as illuminating lights – they are used as component of light products and the light are manipulated with other components such as reflect cup and lenses in a distance short than the far-field distance, and with different wanted light pattern lie on the purpose. So the far-field light patterns may not agreement with the practical light patterns, and the final light patterns are not always accurate with that one want. The Monte Carlo algorithm and normalized cross correlation algorithm widely used in electronic engineering and electronic image processing was adopted to design the LED spot light used in electronic technology.

D. Jin and S. Lin (Eds.): Advances in Mechanical and Electronic Engineering, LNEE 177, pp. 443–448.
springerlink.com

In this research, the lighting system with high power LED and a TIR lens was designed for spot light source with full width at half maximum (FWHM) of 28°. The lighting system was simulated by Monte Carlo ray tracing in various midfield and far-field distances. The one-dimensional intensity patterns were measured with a simple set-up in midfield and far-field distances. The NCC between the simulation patterns and the experimental measurements are used to verify the validity of the second order light design. The potential applications of the controllable lighting system with desired light pattern in electronic technology were discussed.

2 Optical Modeling Process and the Experimental Measurement

The power of high power white LED is 3W with approximately Lambertian light patterns. The establishing of LED geometric model was based on the above-mentioned LED and the configuration used in the simulation is shown in Fig. 1.

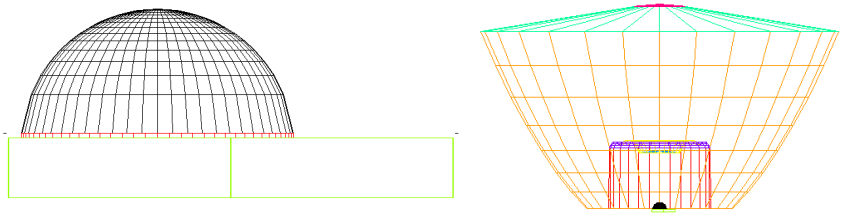

(a) (b)

Fig. 1. Geometric structure of high power LED (a) and controllable LED spot light system used in electronic technology (b)

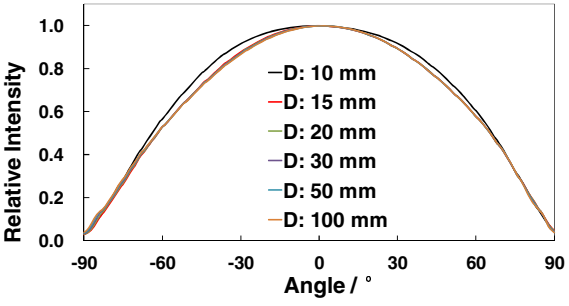

Fig. 2. Simulated angle radiation patterns of different distance of the high power LED

The lighting system was simulated with commercial software. The light ray was generated by Monte Carlo algorithm widely used in electronic engineering. The original ray number was 10 million. The dependence of one dimensional light patterns of simulated on the distance is shown in Fig. 2. It can be found that the change of light patterns with the distance is very small for the high power white LED for the

dimension of dome lens of LED is very close to that of the die and having a Lambertian light patterns. As the distance is larger than 10 times of the LED dimension, the light pattern is on the quasi far-field.

The experimental confirmation of the light patterns of the high power LED is measured by one set up shown in Fig. 3 (a). The origin point of the distance starting is the dome vertex of the two LED. The end point of the distance is that of the sink point of the power meter. 3 LEDs of each type was used for the measurement of the light patterns for the examination of the LED light uniformity. The distance of both the two types of LED light patterns is 1cm to 100 cm. 181 mini intensity absorbing surfaces equivalent to that of the power meter of the experiment with 1° angular difference for each two neighboring detected surfaces are set in the simulation shown in Fig.3 (b).

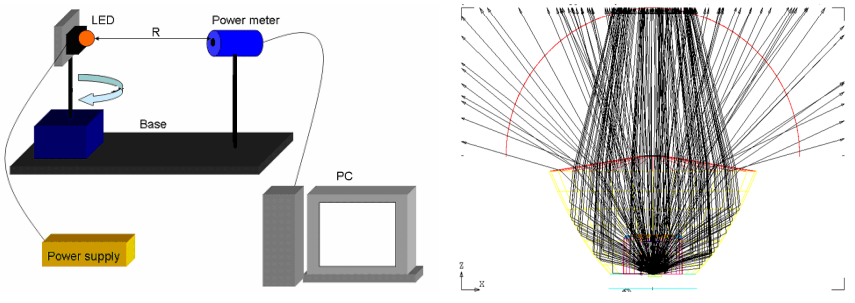

(b) (b)

Fig. 3. (a) Schematic of experimental set-up of the LEDs' one-dimensional intensity patterns measurement; (a) Diagram used in the simulation of the angular intensity distribution of the spot light source produced by Monte Carlo algorithm.

The similarity between the optical radiation patterns of the simulated and the measured was evaluated by the normalized cross correlation (NCC) algorithm. NCC is frequently used to merit the similarity between two images in electronic image processing. The NCC of the radiation pattern I_e at distance D with respect to the radiation pattern of reference I_s is

$$NCC = \frac{\sum_n \left[I(\theta_n)_e - \bar{I}\right]\left[I(\theta_n)_s - \bar{I}_s\right]}{\sqrt{\sum_n \left[I(\theta_n)_e - \bar{I}_e\right]^2 \sum_n \left[I(\theta_n)_s - \bar{I}_s\right]^2}}. \quad (1)$$

Where θ_n is the n-th view angle, e.g. the angle displacement of the detector shown in Fig. 2. $\bar{I}_s$ and $\bar{I}$ are the mean value of I_s and I across the angular range. The LED spot light radiation patterns of simulated and experimental radiation pattern are shown in Fig.4 with the typical radiation patterns for the distance from 5cm to 120cm. The Fig. 5 shows NCC vs. distance for the radiation patterns of Fig. 4.

The optical efficiency in the simulation is evaluated for input power of 1 Watt. The projected light intensity is 0.93 and 0.86 Watt for the LED with and without TIR lens respectively, so the optical efficiency in the simulation is 93.5%.

3 Comparison of Simulation with Experiment Result

The NCC values and the normalized radiation patterns between the simulation and the experiment were used to promote the modeling veracity. With the NCC algorithm, the light model can be improved to more close to that of the practicality. The light model is modified to cater to the normalized measured value at each view angles.

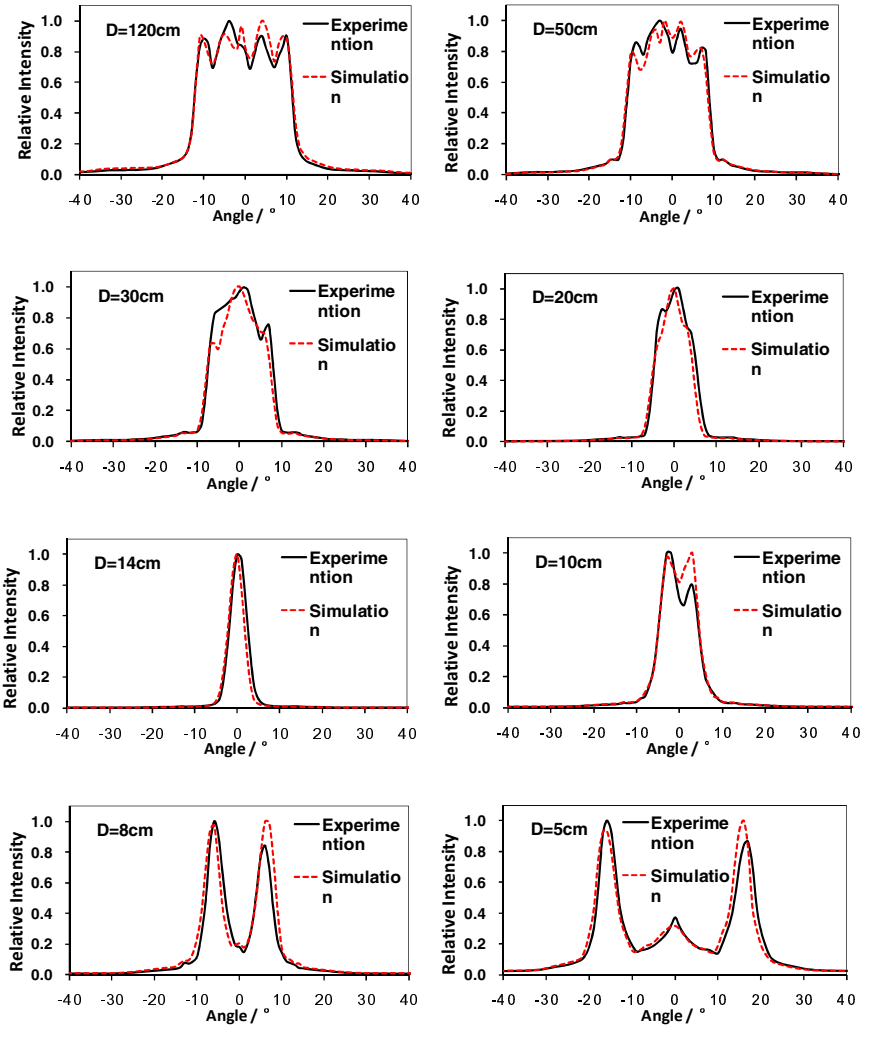

Fig. 4. Comparison of simulated and experimental pattern for different distance of the optical system with TIR lens.

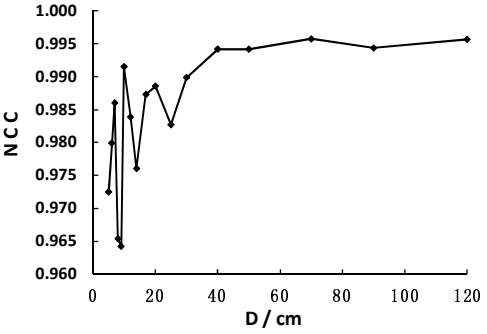

Fig. 5. NCC between the measurement and simulation of spot light system versus different distances.

One can see that the LED spot light radiation patterns of LED with TIR lens in midfield is different with the radiation patterns in far-field. When the distance is larger than 50cm, the optical radiation patterns keep almost unchanged with the increasing of the measurement distance. There are severe changes during the midfield when the measurement distance is short than 30cm. In the midfield region, the light pattern significantly varies from one distance to another due to the finite size of the LED structure for the LED can't be treated as a point light source. The discrepancy between the simulation and experiment decreases with the increasing of the distance. The unstable NCC data in the midfield may be come from the distance error and the instability during the rotation of the system. There is some discrepancy for experimental radiation pattern in the midfield for the strictly symmetrical is difficult to obtain during the rotation of the optical system in the experiment. The NCC is large than 0.99 for the far-field light radiation patterns. As the distance increases to the range in the far-field, the light pattern almost keep consistent with the distance at varies angular direction. The full width at half maximum (FWHM) in the far-filed is 28° with stable light patterns. The TIR lens has good efficiency. The TIR efficiency is 93.5% in the simulation. The LED spot light can be used in electronic technology and intelligent lighting control system for the stable and controlled light radiation patterns in the far-field. The variable and controlled light radiation patterns in midfield can also be used in smart lighting with the help of precise control system.

4 Summary

One high power LED spot light with FWHM of 28° with TIR lens used in electronic technology and intelligent lighting control system is designed by midfield and far-field simulation, and verified by normalized cross correlation algorithm. The light model was improved with the NCC between the simulation and the experiment. The NCC in the simulation of LED spot light is large than 0.99 in the far-field. The rapid design of precise LED spot light with any desired light pattern can be obtained with different LED and different TIR lens by the midfield and far-field light simulation. The variable optical radiation patterns can be obtained in midfield by accurate control,

and can be used in smart lighting system. The LED spot light can be used as light source in electronic advertising flat panel display and wisdom and comfortable lighting for the fast response and easy control.

Acknowledgments. This research is funded by Research Foundation of Chongqing University of Science & Technology with project No. of CK2010B28.

References

1. Chien, W.T., Sun, C.C., Moreno, I.: Precise optical model of multi-chip white LEDs. Optics Express 15, 7572–7577 (2007)
2. Sun, C.C., Lee, T.X., Ma, S.H., Lee, Y.L., Huang, S.M.: Precise optical modeling for LED lighting verified by cross correlation in the midfield region. Optics Letters 31, 2193–2195 (2006)
3. Sun, C.C., Chen, C.Y., He, H.Y., Chen, C.C., Chien, W.T., Lee, T.X., Yang, T.H.: Precise optical modeling for silicate-based white LEDs. Optics Express 16, 20060–20066 (2008)
4. Moreno, I., Sun, C.C., Ivanov, R.: A far-field condition for LED arrays. Applied Optics 48, 1190–1197 (2009)

An Improved TFIDF Algorithm in Electronic Information Feature Extraction Based on Document Position

Yong Zhuang

Zhejiang University, 310000 Hangzhou, China
catailers@gmail.com

Abstract. Feature extraction is an effective dimension reduction method in electronic document information feature representation. The term frequency–inverse document frequency (TFIDF) algorithm is a commonly used one for feature extraction. Analysis on TFIDF finds that it has shortcomings in term frequency computation. The feature that different position information of term in electronic document has different contribution on main content of document was used to design an improved TFIDF feature extraction algorithm based on electronic document position information, which was then applied in personnel information system. The accuracy of algorithm before and after improvement in different dimension was compared in prototype system. Experiment results show that the improved TFIDF algorithm is feasible and effective.

Keywords: electronic document position, feature extraction, TFIDF, data mining.

1 Introduction

With the increasing capacity of Web information, the information type also becomes increasingly heterogeneous. It is increasingly difficult for simple query or search can meet complex needs for users. It has become people's urgent requirements to quickly and efficiently find useful electronic resources and information on Internet. In the document characteristics representation, a good feature extraction algorithm can effectively decrease dimension number and then reduce system overhead and running time. Therefore, in the document data sort and organization process, it is necessary to design or select an effective feature extraction algorithm. The document feature extraction is also called key terms extraction, the essence of which is dimension reduction technique of high-dimensional data, namely to map high-dimensional data to lower dimension space with transformation. Main problem of dimension reduction is the transformation from high dimension to low dimension may mask original information. Thus, it is difficult to distinguish types with significant difference in the high-dimensional space may be mixed in the low-dimensional space. So, the key for transformation from high-dimension space to low-dimension is to seek for suitable map, so as to map target information in high-dimensional space into low-dimension space as actual as possible. The paper analyzes on traditional TFIDF algorithm and

D. Jin and S. Lin (Eds.): Advances in Mechanical and Electronic Engineering, LNEE 177, pp. 449–454.
springerlink.com

improves it based on special structure of document. A novel improved TFIDF feature extraction algorithm based on document position is proposed. The experimental result shows that accuracy of document feature extraction with improved algorithm has been improved. The paper is organized as follows: section 2 introduces related researches; section 2 gives improved document feature extraction algorithm; section 4 designs experiment prototype and analyzes on experiment result; section 5 concludes our work.

2 Related Works

The most widely used algorithms include inverse-document frequency weight evaluation, signal to noise ratio (SNR), TFIDF, mutual information (MI), and information gain (IG) [1, 2] on document feature extraction. Among them, the importance of assumption terms in inverse-document frequency weight evaluation method is proportional to frequency of terms within document, but inversely proportional to number of terms in document, called document frequency. The SNR assess importance of index terms from view of information theory. High frequency of term in document means it contains less information amount. Here is the formula of information amount:

$$I = -\log_2 p\,. \tag{1}$$

Where, p is frequency of term. The MI is a kind of term correlation and related application standard used for statistical model [3]. In the information theory, the formula of MI is:

$$I(x, y) = \log \frac{p(x \mid y)}{p(x)} = \log \frac{p(xy)}{p(x)p(y)}\,. \tag{2}$$

In case of document classification, $p(xy)$ is frequency of term x belong to type y in document; $p(y)$ is frequency of type y in document and $p(x)$ is frequency of term x in document.

The IG is always be used as entry selection criteria in machine learning [4], which also comes from information theory. For each term, the formula of IG is:

Information Gain (IG) in machine learning is often used as entries in the selection criteria [4]. Information gain is also derived from information theory, for each term, IG calculated as follows:

$$IG(t) = -\sum_{i=1}^{m} P(c_i)\log P(c_i) + P(t)\sum_{i=1}^{m} P(c_i \mid t)\log P(c_i \mid t) + p(\bar{t})\sum_{i=1}^{m} P(c_i \mid \bar{t})\log P_r(c_i \mid \bar{t})\,. \tag{3}$$

Where, $p(\bar{t})$ is the probability that term t does not appear; $P(c_i \mid t)$ is probability that term t appears and belongs to type c_i in document; $P(c_i \mid \bar{t})$ is the probability that term t does not appear but belongs to type c_i. The formula shows difference between information entropy, which is called information gain.

In the previous introduced algorithms, as the term frequency does not been considered and the situation that once appearance or more times of term not been took

into account, while TFIDF [5] algorithm not only take into account frequency, also combines with anti-document frequency. It has achieved significant result in many researches. The paper mainly analyzes on the algorithm and improves on it. Its computation formula is as following:

$$TFIDF(T_i, D_j) = TF(T_i, D_j) \times \log \frac{|D|}{|DF(T_i)|}. \quad (4)$$

Where, T_i is a particular term; D_j is the document where term located; $TFIDF(T_i, D_j)$ is the frequency of T_i in document D_j; $|D|$ is number of all document in the training set; $DF(T_i)$ is document number containing term T_i, namely value of $IDF(T_i, D_j)$; $TFIDF(T_i, D_j)$ is the weight of to be computed T_i in document D_j. The formula is based on the following intuition: (1) More time of term in the document means it has more representatives in the document. (2) More document of term means it has smaller distinction ability.

3 Analysis and Improvement on Document Feature Extraction Algorithm

3.1 TFIDF Algorithm Analysis

As to the formula of TFIDF, its main part is made up of term frequency (TF) and inverse document frequency (IDF). Although the formula considers two aspects of term frequency and document frequency, the formula is till simple and has not take into account some factors. Although some term has high frequency in the document, they have not contribution to document content, such as the, each, that, will and etc. These terms have no meaning on document topic description and should be deleted from keywords candidate set. Different position of term in document also means different contribution to content. For example, in a scientific literature, importance of keywords in the title must be greater than that in the content. In the TFIDF algorithm, however, the computation of term frequency does not distinguish weight, just compute number of terms and thinks that different position of term has same contribution to content. Therefore, the weight of term in different position should be adjusted and TFIDF algorithm can be improved as:

$$TFIDF(T_i, D_j) = \left[\lambda TF(T_i, D_j, B) + TF(T_i, D_j, Z)\right] \times \log \frac{|D|}{|DF(T_i)|}. \quad (5)$$

Where, λ is weight of term T_i appears in the title of document D_j; $TF(T_i, D_j, B)$ is the corresponding frequency. $TF(T_i, D_j, Z)$ shows frequency of term T_i in the body of document D_j, The meaning of other symbols are same as that in original TFIDF.

3.2 Value of λ

The paper divides document into two parts of title and body. Although the contribution of single term in tile and body has different contribution to document, the

two have some association after all. Main content of a document can be summer up with title and also be described in detail with body. But these parts describe same content. Based on these characteristics, we proposed an assumption that: although term in different position has different contribution to content of document, the sum of contribution of terms in different position to content of document is same. In other words, if the tile has only 5 terms in the document, while main body has 200 words, the contribution of 5 words in the title is equal to that of 200 words in the body. Based on the above assumption, we know that value of λ is related to total number of terms in title and that in body, which shows linear relationship. If the weight of term in body is 1 and that in title is λ, we can arrive at the relationship $\lambda \times N(D_j, B) = 1 \times N(D_j, Z)$. After mathematical transformation, the value of λ can be calculated by the following formula:

$$\lambda = \frac{N(D_j, B)}{N(D_j, Z)}. \tag{6}$$

Where, $N(D_j,B)$ is total term number in title of document D_j; $N(D_j,Z)$ is total term number in document D_j; λ is weight of term T_i in the title. Finally, the improved TFIDF algorithm is

$$TFIDF(T_i, D_j) = \left[\frac{N(D_j, B)}{N(D_j, Z)} \times TF(T_i, D_j, B) + TF(T_i, D_j, Z) \right] \times \log \frac{|D|}{|DF(T_i)|}. \tag{7}$$

4 Experimental System and Result Analysis

The paper designed personnel information system as prototype system. The system mainly collect access information from users based on their behaviors and then analyzes access information to obtain users' access characteristic. Finally, the personnel information system was established to record access character of each user. The system flow is shown in Fig. 1. In the input phase, record user behaviors to store access information into database. In the processing phase, main functional modules include pre-processing module, word segmentation module and improved TFIDF algorithm module. The pre-processing module mainly deal with snatched user access pages to filter some page markup language and transform page into text file with two parts of title and body. The word segmentation module is responsible for segment transformed text file and divides text into several words or phases. The final improved TFIDF algorithm module compute on weights of each word or phase and take word with highest weight $n(n=4)$ as keywords and then store them into personnel information system. In the output phase, the original information and processed information are merged to store into personnel information system.

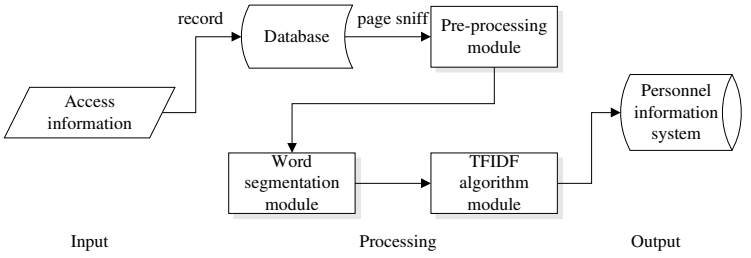

Fig. 1. Prototype system flow

4.1 Experimental Data Collection

The experiment platform of this paper is project items management platform-Trac in the lab. It provides a communication and management platform for project developers. The Trac platform manages development process of 8 projects in the experiment. Each group has its own blog, ticket and wiki system. There are thousands of blogs in the system of most groups. We randomly select 1010 blogs from each project group. After page markup language has been filtered, all blogs are transferred into text file with two parts of title and body finally. The so-called segmentation aims at divide complete text into several terms or phases. In the experiment, we used Pymmseg-cpp system, which is a high-performance word segmentation system programmed with Python. With this system, the text of collected 1010 blogs was conducted segmentation. The processed words are stores into MySQL database to convenient computation on value of TFIDF. Part of segmentation effect is shown in Table 1.

Table 1. Pymmseg-cpp segmentation

Document	*Position*	*Term*	*Num*
L_j	title	*trac*	1
L_j	title	*update*	1
L_j	title	*process*	1
L_j	body	*surfer*	1
L_j	body	*problem*	3
L_j	body	*project*	4
L_j	body	*update*	6

In the table, *document* is name of text file; *position* is the position of term in document; *term* is obtained word and *number* is frequency of word in related position.

4.2 Experimental Data Analysis

With the processed data, we can TFIDF value of each term in each document before and after improvement. Take the first 4 and first 6 words with largest TFIDF value in text file as keywords and then determine whether each group of keywords can

accurately express subject of each text, so as to compare accuracy of algorithms. The experiment result is shown in Table 2.

Table 2. Accuracy comparison of TFIDF before and after improvement

Algorithms	No4	P4/%	No6	P6/%
TFIDF	789	78.12	826	81.78
Improved TFIDF	812	80.40	855	84.65

The No4 and P4 in table show number and accuracy that first 4 words with biggest TFIDF as keyword respectively. The No6 and P6 just represent that of first 6 words.

From result in Table 2 we can know that accuracy of keywords extracted from improved TFIDF algorithm has certain increase under same situation. It validates the reasonableness of assumption to some extent. As mentioned above, the essence of document feature extraction is dimension reduction technique of high-dimensional data. From comparison between P6(81.78) of original TFIDF algorithm and P4(80.40) of improved algorithm, the accuracy of low-dimensional data after improvement is close to that of original high-dimensional data.

5 Conclusion

The paper improved on TFIDF algorithm based on implementation of personnel information system. It divides electronic document into two parts of title and main body. The character that different position of term in the electronic document has different contribution of main subject of document was used to add weight for term in different position in frequency computation. The accuracy before and after improvement in different dimension were also compared. The experimental result shows improved TFIDF algorithms not only improve accuracy, but achieve dimension reduction in the electronic document data mining.

References

1. Wang, M.-F., Liu, P.-Y., Zhu, Z.-F.: Feature selection method based on TFIDF. Computer Engineering and Design 28, 5795–5796 (2007)
2. Mnic, D., Geobelnik, M.: Feature selection for unbalanced class distribution and naïve Bayees. In: Proceedings of the 6th International Conference on Machine Learning, pp. 258–267 (1999)
3. Wiener, E., Pedersen, J.O., Weigend, A.S.: A neural network approach to topic spotting. In: Proceedings of the 4th Annual Symposium on Document Analysis and Information Retrieval, pp. 317–332 (1995)
4. Zhang, Y.-F., Peng, S.-M., Lv, J.: Improvement and Application of TFIDF Method Based on Document Classification. Computer Engineering 32, 76–78 (2006)
5. Xiong, Z.-Y., Li, G., Chen, X.-L., Chen, W.: Improvement and application to weighting terms based on document classification. Computer Engineering and Applications 44, 187–189 (2008)

Electronic RFID-Based Indoor Moving Objects: Modeling and Applications

Peiquan Jin, Lanlan Zhang, Lei Zhao, Huaishuai Wang, and Lihua Yue

School of Computer Science and Technology
University of Science and Technology of China
jpq@ustc.edu.cn

Abstract. With the development of electronic technologies, especially RFID sensors technologies, indoor space can be modeled with the help of deployment of RFID sensors. The fundmental issue in RFID-based indoor space is to create a framework to management indoor moving objects. In this paper, we focus on the modeling issue of RFID-based indoor space as well as indoor moving objects. We first present a conceptual framework to represent indoor space and indoor moving objects. Next, we analyze some potential application areas related with indoor moving objects. Modeling of indoor moving objects is much different from that of outdoor moving objects. For the latter, we usually assume that objects are moving in a free space, while indoor space is constrainted by doors, walls, elevators, and other factors. Therefore, we need develop new ways to describe indoor space and indoor moving objects. On the other hand, indoor applications are just in development, and a lot of issues are needed to be explored.

Keywords: indoor space, moving objects, model, applications.

1 Introduction

Moving objects data management has been widely studied in recent decade. Traditional moving objects data management is based on the GPS-enabled positioning technology [1, 2]. However, GPS signals will not work in indoor space. On the other hand, most of us spend most time in indoor space, such as in working department, in home, in supermarket, and so on. In order to develop location-based services for indoor environment, it is important and urgent to create effective ways to track and manage indoor moving objects [3].

In this paper, we concentrate on the modeling and applications of indoor moving objects management. Particularly, we aim at presenting a framework to model indoor space and indoor moving objects, which forms the foundation of indoor moving object management systems. Furthermore, we give some potential application areas of indoor moving objects. The main contributions of the paper can be summarized as follows:

(1) We analyze the semantics of indoor space and present a conceptual framework for indoor space and indoor model, in which the indoor space is defined as a set of

D. Jin and S. Lin (Eds.): Advances in Mechanical and Electronic Engineering, LNEE 177, pp. 455–461.
springerlink.com

rooms, doors and sensors, and indoor moving objects are modeled using a layered approach (Section 3).

(2) We present some potential application areas and analyze the challenges when applying indoor-moving-objects-based approach on them (Section 4).

2 Related Work

Indoor space has received much attention in recent years. Previous work related with indoor space focused on the modeling of indoor space. The indoor space models can be divided into three categories according to the different ways to describe indoor objects, which are the *object feature model*, the *geometric model* and the *symbolic model*. Among them, the object feature model mainly expresses the properties of indoor space and the relationship between operations and types. In the literature [6], the authors used the UML-based class model, CityUML/IndoorML, to describe the relationship among objects in indoor space. In [7], an ontology-based model named ONALIN was proposed for the navigation in the indoor space. The geometry model concerns about the geometric representation of indoor space, which is mainly used to visualize the indoor space. The 2D-3D hybrid model proposed in [8] supports the visualization of indoor space and the navigation in indoor space. The prismatic model in [9] can well analyze the topology of indoor space. A topology-based semantic model was presented in [10], in which the indoor space is represented as a single set of objects for the analysis of indoor space. The lattice-based semantic model [11] used lattice structure to represent the indoor space, which is mainly used for the navigation in indoor space.

Most of previous models used a graph-based technique to represent indoor space and indoor moving objects. Table 1 shows some graph-based models as well as their characteristics. As shown in Table 1, all the graph-based models take either rooms or doors as the nodes, and have some limitations on supporting various applications. For example, the deployment model [4,5] uses rooms as the nodes and sensors as the edges between rooms. It can effectively support indoor moving objects tracking and monitoring, but is not efficient when executing a KNN search on indoor moving objects.

3 Modeling of Indoor Moving Objects

3.1 Elements of Indoor Space

An indoor space consists of some cells (rooms). Rooms are connected by doors. When an object wants to pass from room A to room B, it has to pass by the door connecting those two rooms. We assume that some positioning sensors are deployed in indoor space. The typical sensors are RFID readers, hence in this paper we assume that RFID readers are used as the positioning devices and moving objects are equipped with RFID tags. Therefore, when a moving object is passing by a RFID reader, the reader will record the RFID tag identifier. A RFID reader has a limited range when sensing RFID tags. Such a range can be represented as a circle.

Figure1 shows an example of indoor space, in which there are seven rooms (r_1 to r_7) connected by nine doors (d_1 to d_9). There are also nine sensors deployed in Fig.1 (s_1 to s_9). When a moving object (mo_i) is passing by a sensor, the sensor will record its tag information and send to the server.

Generally, an indoor space consists of the following elements that are needed to be considered when modeling indoor space, as shown in Table 1.

Table 1. Elements of indoor space

Element	Description
Room	The basic geometric partitions of indoor space. A room usually has one or more doors, and rooms are not overlapped.
Door	A door connects a room to another one, or to outdoor space if it is the entrance gate of a building.
Sensor	In this paper, sensors refer to RFID readers. They are deployed on doors or in rooms to detect moving objects.
Static Objects	Static objects are located in rooms, such as a printer, a computer, or a FAX machine. Note we are not necessary to record all the static objects in the indoor space, but only need to concentrate on those objects of interests.

3.2 Modeling of Indoor Space

Definition 1. The indoor space *IS* is defined as a quadruple:

$$IS = (R, D, S, SO, connect, deploy, locate),$$

Where *R* is the set of rooms, *D* is the set of doors, *S* is the set of sensors, *SO* is the set of the static objects of interests, *connect* is the connecting relationships among rooms and doors, and *deploy* is the deployment information of all the sensors in the indoor space. ■

Definition 2. The connecting relationship among rooms in the indoor space *IS* is defined as *connect*(*IS*), which maps each door into two rooms and indicates that they are connected by the door:

$$connect(IS) = D \rightarrow R \times R,$$

Where *D* is the set of door and *R* is the set of rooms. ■

Definition 3. The deployment of sensors in the indoor space *IS* is defined as *deploy*(*IS*):

$$deploy(IS) = S \rightarrow \{D \mid R\},$$

Where *S* is the set of sensors, *D* is the set of door, and *R* is the set of rooms. ■

Definition 4. The locations of the static objects in the indoor space *IS* are defined as *locate*(*IS*):

$$locate(IS) = SO \rightarrow R,$$

Where *SO* is the set of static objects, *R* is the set of rooms. ■

3.3 Modeling of Indoor Moving Objects

In this section, we discuss the model for moving objects in indoor space. As the indoor space is basically static, we use the definition in Section 3 to represent the indoor space as a set of rooms, doors, static objects, and sensors, together with the deployment, connectivity, and location information about those entities. For moving objects, we use RFID tags as the identifiers of the moving objects, and record their trajectories through the detected data stream from sensors. Figure 2 shows the model.

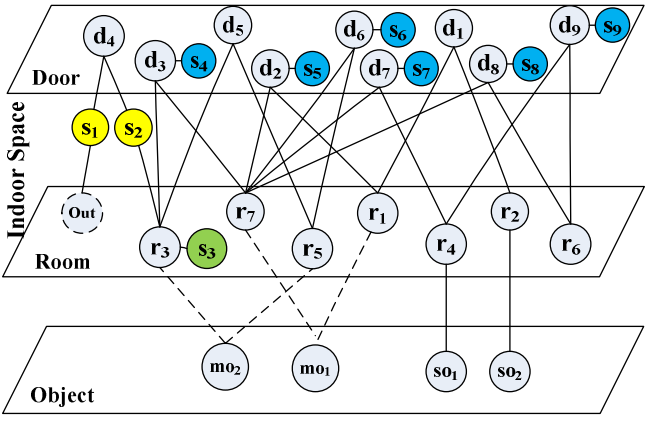

Fig. 2. Modeling indoor moving objects

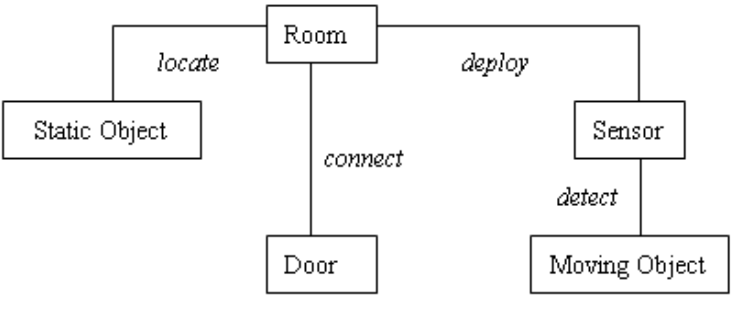

Fig. 3. The entities and relationships in the model

Figure 3 shows the entities and their relationships in the model. According to the model, the entities in indoor environment are classified into five types, i.e., rooms, doors, sensors, static objects, and moving objects. The rooms, doors, sensors and static objects form the indoor space, and those entities are basically kept unchanged. The moving objects typically are people moving in the indoor space, which we need an effective way to keep tracking of their locations, visiting durations, moving patterns, and other interested information. Those information about moving objects are useful in many application scenarios, such as custom analysis in shopping malls, abnormal object detection in subway station, and workers' performance analysis in factories.

The formal definition of the model is as follows.

Definition 5. The data structure of the indoor moving objects model is defined as follows:

$$IndoorMO\_Model = (MO, LDDM, IS),$$

Where *MO* is the set of moving objects in the indoor space *IS*, *LDDM* is a set of matrixes. A matrix *LDDM*(*i*) defines the distance between each two doors in the room *R*(*i*). ■

Definition 6. A moving object *MO*(*i*) in the model is identified by its RFID tag. We define each moving object as a trajectory recording each state when the object was detected by the sensors:

$$MO(i) = (tagID,\ \ attributes,\ \ trajectory),$$

where *attributes* are user-defined information to describe the moving object. *trajectory* is defined as follows:

$$trajectory = \{r \mid r =< tagID,\ \ sensorID,\ \ time >\},$$

and *tagID* is the RFID tag identifying the moving object, *sensorID* is the number of RFID reader, *time* is the time instant when the moving object was first detected by the sensor. ■

4 Applications of Indoor Moving Objects Management

In this section, we discuss some potential applications of indoor moving objects management. As people use most of their time in indoor environment, it is very important and valuable to develop user-oriented applications for indoor services.

4.1 Indoor Navigation

Navigation in indoor space is much different from that in outdoor space. While GPS signals are used in outdoor position locating and navigation, they are not available in indoor space, due to the special properties of GPS signals. The first important issue regarding the navigation in indoor space is the locating method. Generally, we can

represent the indoor space as a set of symbols and use symbolic method to determine the locations in indoor space. For example, each door in the indoor space can be initially assigned a location symbol, and those symbols are maintained in a database which is to be used in navigation.

Combined with some external facilities, it is possible to offer special indoor navigation services for some special persons and some special circumstances. For instance, blinded persons can use indoor navigation services in case that we can output the navigation voices via handy equipment such as mobile phones. It can be also used in emergent situations, e.g., finding ways-out when power off or indoor fire occurs.

4.2 Customer Analysis for Indoor Business Environment

According to traditional business analysis, we only use the buying history of customers as the data source. However, this way will not work if a customer did not buy similar merchants before. Indoor trajectories of customers provide some opportunities for us to conduct trajectory-based analysis for customer behaviors. For example, we can classify customers according to their staying duration in different locations in a shopping mall, and further find potential buyers for certain merchants. Moreover, we can realize personalized recommendation on the basis of the customers' trajectories in indoor sales environment as well as their buying history.

4.3 Tracking and Monitoring of Indoor Moving Objects

In many applications, we need to track and monitor the locations of indoor moving objects, such as tracking prisoners in jails, finding abnormal persons in subway system or airport, and so on. Tracking and monitoring indoor moving objects requires that we have a management platform to acquire, process, and maintain the information about indoor moving objects. With the emergent needs rising from public management and crisis management, tracking and monitoring of indoor moving objects will be a hot application area in the near future.

4.4 Indoor Social Network

Social network has been a hot topic in recent years, with the appearing of various social media such as Facebook, Twitter, and Flicker. One critical issue is to find online friends in an offline physical environment, e.g., to find my friends in an airport. Although current mobile phones usually offer some location services, they have low precision and efficiency when used in indoor environment. Some commercial tools such as Twitter and MSN support location-aware applications, but those techniques are only available in GPS or cell based location infrastructure. Besides, those techniques usually have a low precision when locating in indoor space. As people have more needs to find friends in indoor space than in outdoor space (we rarely want to find our friends when we are driving on road), it is urgent to develop social network services for indoor environment. Based on the indoor moving objects management framework, we can integrate with some social network platform and provide better services.

5 Conclusions

Indoor space has received much attention in recent years as most people work and live in indoor space. With the development of electronic technologies, especially RFID sensors technologies, indoor space can be modeled with the help of deployment of RFID sensors. In this paper, we present a conceptual framework for indoor space and indoor moving object. Compared with previous models, our model takes into account the relationships among rooms, doors, sensors and moving objects, and uses a layered approach to represent indoor space and indoor moving objects. We also make a survey on the applications of indoor moving objects management. With development of the indoor positioning techniques, such as wifi, Bluetooth, and RFID, location-based services for indoor space will be the next wave in moving objects data management.

References

1. Güting, R., Böhlen, M., et al.: A Foundation for Representing and Querying Moving Objects. TODS 25(1), 1–42 (2000)
2. Güting, R., Almeida, V., et al.: Modeling and Querying Moving Objects in Networks. The VLDB Journal 15(2), 165–190 (2006)
3. Jensen, C., Hua, L., Bin, Y.: Indoor—A New Data Management Frontier. IEEE Data Engineering Bulletin-Special Issue on Spatial and Spatio-temporal Databases 33(2), 12–17 (2010)
4. Jensen, C., Hua, L., Bin, Y.: Graph model based indoor tracking. In: Proc. of MDM, pp. 122–131. IEEE Computer Society, Los Alamitos (2009)
5. Zhang, J., Papadias, D., Mouratidis, K., Zhu, M.: Spatial Queries in the Presence of Obstacles. In: Bertino, E., Christodoulakis, S., Plexousakis, D., Christophides, V., Koubarakis, M., Böhm, K. (eds.) EDBT 2004. LNCS, vol. 2992, pp. 366–384. Springer, Heidelberg (2004)
6. Kolbe, T., Goger, G., Plumer, L.: CityGML: Interoperable Access to 3D City Models. In: Proc. of 1st Int. Symp. on Geo-Information for Disaster Management, pp. 883–899. Springer, Berlin (2005)
7. Dudas, P., Ghafourian, M.: ONALIN: Ontology and Algorithm for Indoor Routing. In: Proc. of MDM, pp. 720–725. IEEE Computer Society, Los Alamitos (2009)
8. Kim, H., Jun, C., Yi, H.: A SDBMS-based 2D-3D Hybrid Model for Indoor Routing. In: Proc. of MDM, pp. 726–730. IEEE Computer Society, Los Alamitos (2009)
9. Kim, J., Kang, H., et al.: Topology of the Prism Model for 3D Indoor Spatial Objects. In: Proc. of MDM, pp. 698–703. IEEE Computer Society, Los Alamitos (2009)
10. Lee, J.: A Spatial Access-oriented Implementation of a 3-D GIS Topological Data Model for Urban Entities. GeoInformatica 8(3), 237–264 (2004)
11. Becker, T., Nagel, C.: A Multilayered Space-Event Model for Navigation in Indoor Spaces. In: 3D Geo-Information Sciences, pp. 61–77. Springer, Berlin (2009)
12. Li, D., Lee, D.: A Topology-based Semantic Location Model for Indoor Applications. In: Proc. of ACM GIS. ACM, New York (2008)
13. Li, D., Lee, D.: A Lattice-based Semantic Location Model for Indoor Navigation. In: Proc. of MDM, pp. 17–24. IEEE Computer Society, Washington (2008)

All Phase FFT Analysis with Phase Measurement Applications in Electronic Measurement

Huichun Sun[1], Yonghui Zhang[1], Xiyuan Zhang[1], and Xiong Lin[2]

[1] College of Information Science & Technology, Hainan University, Haikou, China
[2] Hainan Power Grid Corporation Haikou Power Bureau, Haikou, China
zhyhemail@163.com

Abstract. At present, phase measurement method of power frequency three-phase power signal containing multiple harmonic, is generally based on the Hanning window FFT correction measurement methods. But their accuracy limited by the conventional FFT features is very difficult to guarantee. When the measured instantaneous phase is very small, the phase difference accuracy measured will be reduced; when the measured signal contains a large number of harmonic components, a larger measurement error will be made; when the cycle of the detected signal is instable, non-synchronous sampling will be produced so that the measurement accuracy will be affected. To solve the problems above, this paper analyzes the characteristic advantages of all phase FFT algorithm in the application of three-phase power phase measurement. The algorithm is an important electronic technology algorithm, which makes the measurement of small phase difference still maintaining high accuracy and makes the measurement results not affected by the harmonic component and non-synchronous sampling.

Keywords: All Phase FFT, Harmonic Analysis, Phase Invariance, Pseudo-fundamental Harmonic.

1 Introduction

For three-phase power signal measurement, the phase information of voltage and current is the important electronic measurement object in the testing and controlling power systems. How to measure the phase difference of power frequency fast and accurately has become an important research topic. Precise phase difference has important applications for calculating apparent power, effective power, and power factor etc in the electronic technology, but not easy to achieve it. At present, most of the phase instruments are based on hanning window FFT measurement methods such as ratio method, the energy center of gravity etc, but the accuracy of measurement is difficult to be guaranteed because it is restricted by the conventional FFT features and the noise. When the measured instantaneous phase is very small, the phase difference accuracy measured will be reduced; when the measured signal contains a large number of harmonic components, a larger measurement error will be made; when the cycle of the detected signal is instable, it will cause non-synchronous sampling. Non-synchronous sampling will produce a serious phenomenon of spectrum leakage,

D. Jin and S. Lin (Eds.): Advances in Mechanical and Electronic Engineering, LNEE 177, pp. 463–469.
springerlink.com

which introduces other disturbance frequencies. Although adding windows plays a role in preventing the spectrum leakage, the improvement of measurement accuracy is limited. In this paper, the all phase algorithm is a special FFT algorithm. Its nature is a data processing algorithm which deals with sampled data by all phase pretreatment method, and then makes the processed data done FFT transformation. Signal sequence is processed by all phase FFT transformation, in whose amplitude spectrum all phase FFT has the characteristics of suppressing spectral leakage, in whose phase spectrum all phase FFT has the characteristics of the phase invariance which means that the phase spectrum values around the main lines are constantly equal to the initial phase value of the center sampled data of the signal sequence[4][5].

2 Theoretical Analysis

2.1 Analysis of Basic Characteristics

The actual three-phase power signal is the linear superposition of the fundamental sinusoidal signal and multiple harmonics sinusoidal signal. As the system we are dealing with is a linear system, so we can take three-phase power signal equivalent to a sinusoidal signal.

The sinusoidal signal can be written as a linear combination of the exponential signal, so $x(n)$ can be seen as the linear combination of the exponential signal. In order to simplify the following derivation process, the three-phase power signal is taken equivalent to a single frequency complex exponential signal in this study. Firstly, the paper uses single frequency complex exponential signal as an object of study. Set up single frequency complex exponential signal as follows:

$$\phi(n) = e^{j(n\omega_0+\varphi_0)}, \ \omega_0 = \beta \cdot 2\pi/M \tag{1}$$

The formula of the frequency spectrum that single frequency complex exponential signal is processed through the conventional FFT transformation and all phase FFT transformation respectively will be derived in the following.

According to the formula of FFT transformation, the conventional FFT frequency spectrum of the single frequency complex exponential signal is directly obtained as follows:

$$\Phi_{FFT}(k) = \frac{1}{N}\frac{\sin[\pi(N\beta - Mk)/M]}{\sin[\pi(N\beta - Mk)/MN]} e^{j\left[\varphi_0 + \frac{N^2 - MNk - N\beta + Mk}{MN}\right]} \quad k = 0, 1, \cdots, N-1 \tag{2}$$

According to the process of data preprocessing of all phase FFT, preprocess the sampled data and get the formula of all phase data as follows[1]:

$$\phi_{ap} = \frac{1}{N}[N\phi(0), (N-1)\phi(1) + \phi(-N+1), \cdots, +\phi(N-1) + (N-1)\phi(-1)]^T \tag{3}$$

According to Eq.(3), the FFT frequency spectrum is as follows:

$$\Phi(k)_{apFFT} = \frac{\sin^2[\pi(N\beta - Mk)/M]}{\sin^2[\pi(N\beta - Mk)/MN]} \cdot \frac{e^{j\varphi_0}}{N^2} \quad k = 0,1,\cdots,N-1 \tag{4}$$

For the multi-frequency complex exponential signal, its formula of all phase FFT frequency spectrum is as follows:

$$\Phi'(k)_{apFFT} = \sum_{q=0}^{Q-1} \frac{\sin^2[\pi(N\beta_q - Mk)/M]}{\sin^2[\pi(N\beta_q - Mk)/MN]} \cdot \frac{e^{j\varphi_q}}{N^2} \quad k = 0,1,\cdots,N-1 \tag{5}$$

As follows are the five important conclusions derived from the formulas above:

- For single frequency complex exponential signal, all phase FFT amplitude spectrum is the square of the conventional FFT amplitude spectrum, which means that the attenuation degree of the main lines relative to the next lines increases. Therefore, all phase FFT has good side-lobe attenuation performance[1].
- Eq.(2) reveals that the phase value of each spectral line changes with a factor in the conventional FFT phase spectrum. Thus, compensation must be taken when using the conventional FFT algorithm to get a phase value. Eq.(4) reveals that in all phase FFT phase spectrum, the phase value of each spectral line is equivalent to the theoretical phase value of the center sampled data, and has nothing to do with the frequency deviation. This property is called the phase invariance of all phase FFT[1].
- Eq.(4) reveals that in all phase FFT phase spectrum, the phase value of each spectral line has nothing to do with non-synchronous sampling, and is equivalent to the theoretical phase value of the center sampled data.
- For mufti-frequency complex exponential signal, the phase value of each frequency component of the center sampled data will have an impact on phase values of all lines in all phase FFT phase spectrum. When the distance of each frequency component is greater than the spectrum leak range, it can be approximated that the center phase value for each frequency component is independent of each other in phase spectrum.

2.2 Analysis of Harmonic Suppression

All phase FFT harmonic analysis described the impact of harmonics on phase measurement. The actual signal is superimposed on some harmonics, and thus the harmonic analysis of all phase FFT algorithm is necessary in order to avoid measurement accuracy affected. For digital signal processing, if the signal source has not been effectively filtered by low-pass filter, the harmonic components in the signal source will not meet the sampling theorem and will produce frequency aliasing, so that the pseudo-fundamental components will be produced around the fundamental harmonic. However, these pseudo-fundamental components will affect the phase spectrum of the fundamental harmonic severely.

In the case of ideal sampling, the spectrum formula of the sampled signal is as follows[2]:

$$\hat{X}_a(j\omega) = \frac{1}{T}\sum_{k=-\infty}^{\infty} X_a(j\omega - jk\omega_s), \quad k = 0,1,2...\infty \tag{6}$$

Eq.(6) reveals that spectrum of the sampled signal is the periodization of the analog spectrum, and the cycle is a sampled digital frequency ω_s. If $\omega_s \le 2\omega_h$, the harmonic spectrum will overlap with the fundamental spectrum of other cycles and pseudo-fundamental harmonic $\omega_c^{'}$ may be produced. ω_h is the highest cut-off digital frequency of the harmonic.

The following will analyze the impact of harmonics on three-phase power signal. According to the characteristics of FFT, in order to make the spectral resolution equal to 1Hz, the sampled frequency must be equal to the transformed points N. The transformed points are generally N-th power of 2, such as 512, 1024 etc. For three-phase power signal, because its power frequency is equal to 50Hz, there is the following approximate relationship:

$$\omega_s \approx n\omega_c \tag{7}$$

Set up $\omega_h = m\omega_c$, $m = 1,2...\infty$. According to (6) (7), get the formulas as follows:

$$\begin{aligned} \omega_c^{'} &= |\omega_h - k\omega_s| \\ \omega_c^{'} &\approx |m - kn|\omega_c \end{aligned} \tag{8}$$

According to Eq.(8), if $m - kn = \pm 1$, some harmonics will produce pseudo-fundamental harmonic around the fundamental harmonic. Pseudo-fundamental harmonic has a great impact on all phase FFT algorithm, and reduces phase measurement accuracy.

For three-phase power signal, there are three ways to avoid the impact of harmonics: firstly increase the sampled frequency; secondly reduce the sampled resolution; thirdly increase the filter.

As follows is the first method. In the case of the same of the spectral resolution, the impact of the low-order harmonic can be effectively eliminated by means of increasing the sampled frequency. However, the impact of the high-order harmonic can be not completely avoided.

As follows is the second method. If the complexity of the design is constant, the impact of each order harmonic can be eliminated completely by changing the spectral resolution. sampled frequency and sampled points must be not integer times relationship. However, changing the spectral resolution will increase the effect of the fence.

As follows is the third method. The impact of every harmonic can be eliminated completely by means of increasing the filter.

3 Algorithm Simulation

3.1 Simulation of The Basic Characteristics

The theoretical analysis reveals that all phase FFT has excellent characteristics which helps to improve the accuracy of phase measurement. Now the basic features of all phase FFT and the conventional FFT are verified and compared by means of Matlab.

Set the single frequency complex exponential signal as follows:

$$x(n) = 5e^{j(n\beta_0 2\pi / M + 100\pi/180)} \tag{9}$$

Set β_0 equal to 50Hz. The conventional FFT frequency spectrum and the all phase FFT frequency spectrum is shown in figure 1 in the case of synchronous sampling.

Set β_0 equal to 51.3Hz. The conventional FFT frequency spectrum and the all phase FFT frequency spectrum is shown in figure 1 in the case of non-synchronous sampling.

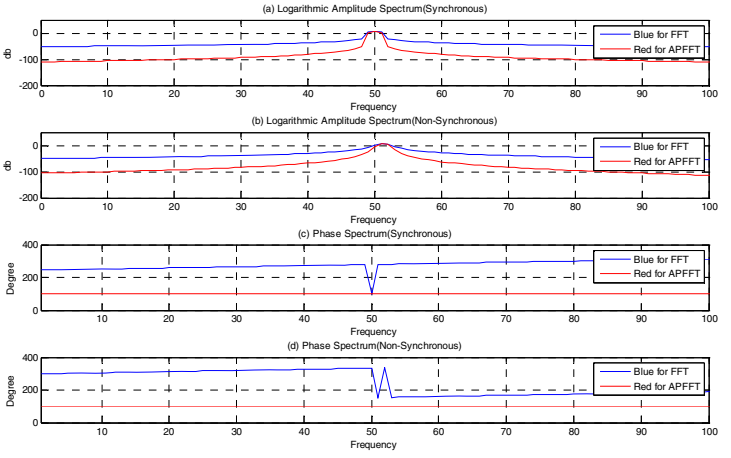

Fig. 1. Spectrum of single frequency complex exponential signal, and the spectral resolution is equal to1Hz

For APFFT, non-synchronous sampling will not affect the phase spectrum. The amplitude of the phase spectrum is always the phase value of the center sampled data of the signal. The amplitude spectrum also has good side-lobe attenuation performance. For FFT, the phase spectrum is related to non-synchronous sampling and the spectral resolution.

3.2 Simulation of Harmonic Suppression

Three-phase power signal is a composite sinusoidal signal from the fundamental harmonic and multiple harmonics. Composite sinusoidal signal is a multi-frequency

complex exponential signal. Characteristics of all phase FFT harmonic suppression are verified by means of Matlab for the simulation of composite sinusoidal signal.

As follows is a composite sinusoidal signal. The signal amplitude, frequency and phase information is in the table below. Now the signal sequence is analyzed respectively by the conventional FFT and all phase FFT.

$$x(n) = A_1 \times cos(\,2\pi n f_1/M + ph_1 \times \pi/180\,) + A_2 \times cos(\,2\pi n f_2/M + ph_2 \times \pi/180\,) + A_3 \times cos(\,2\pi n f_3/M + ph_3 \times \pi/180\,) + A_4 \times cos(\,2\pi n f_4/M + ph_4 \times \pi/180\,) + A_5 \times cos(\,2\pi n f_5/M + ph_5 \times \pi/180\,) + A_6 \times cos(\,2\pi n f_6/M + ph_6 \times \pi/180\,)$$

Table 1. The information of composite sinusoidal signal

Element	The first frequency components	The second frequency components	The third frequency components	The fourth frequency components	The fifth frequency components	The sixth frequency components
Amplitude(A)	3.34	0.67	0.044	0.0045	0.00022	0.0000037
Frequency(f)	51.3	101.1	154.7	203.3	556.2	1080.7
Phase(ph)	32.367	102.457	192.765	232.387	122.059	82.743

Set sampled frequency M equal to 768Hz, transformed points N equal to 512. The spectral resolution F is 1.5Hz. The amplitude spectrum and phase spectrum of the sequence is shown in figure 2.

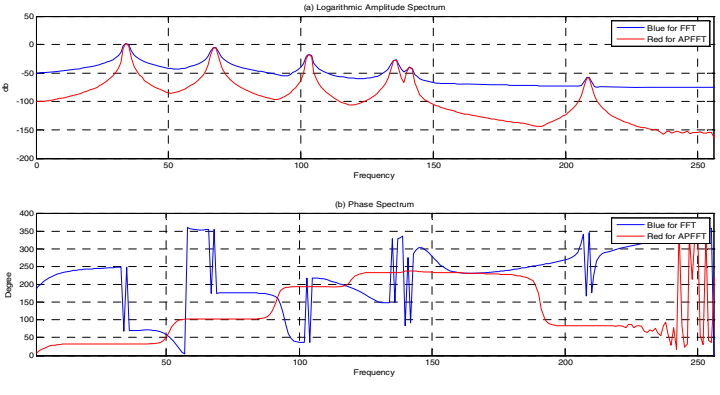

Fig. 2. Spectrum of multi-frequency complex exponential signal, and sampled frequency M is equal to 768Hz

The figure above reveals: When sampled frequency is equal to 768Hz, only the first five frequency components meet the sampling theorem. However, frequency aliasing does not appears around the fundamental harmonic. When an integer multiple of the

sampled frequency is not equal to sampled points, the impact of every harmonic can be eliminated completely. The spectral resolution is not equal to 1Hz, so the equivalent widths of the fundamental phase spectrum deviates to the left.

4 Conclusion

From the perspective of theory and simulation, the paper analyzes and compares with the characteristics of all phase FFT algorithm and the conventional FFT algorithm. All phase FFT phase measurement algorithm has three basic characteristics: Firstly, the algorithm has the characteristics of phase invariance. Regardless of size of the instantaneous phase value, phase value can be high-precision detected; Secondly, the phase measurement accuracy of the algorithm has nothing to do with the cycle stability of the measured signal; Thirdly, the phase measurement accuracy of the algorithm has nothing to do with the spectral resolution. In this paper, the analysis of theory and simulation reveals the characteristics of the harmonic suppression of all phase FFT algorithm. If there is not an integer multiple of the relationship between sampled frequency and sampled points, around the fundamental harmonic the pseudo-fundamental harmonics will be avoided producing by high-order harmonics, which reduces the phase measurement accuracy. In conclusion, all phase FFT algorithm in phase detection applications of the three-phase power is an ideal electronic technology algorithm, the algorithm has features of high precision, anti-interference, and easy to implement.

Acknowledgments. This paper supported by Colleges and Universities Scientific Research Projects of Education Department of Hainan Province [Hjkj2011-08], Youth Foundation of Hainan University[qnjj1023] and 211 Project Central Special Fund of Hainan University.

References

1. Wang, Z., Huang, X.: Digital signal spectral analysis of all-phase and filtering technique, pp. 30–32. Electronic Industry in Press (February 2009)
2. Ding, Y., Gao, X.: Digital Signal Processing. Xidian University Press (December 2006)
3. Zhou, K., Deng, C.: MATLAB and its application. Peiking University Press (March 2007)
4. Wang, L.: Research of high-precision digital phase measurement system. Master Thesis Suzhou University (April 2006)
5. Tang, Q., Lu, D.: Based on FFT algorithm in power system harmonic measurement. Design and Implementation (2008)
6. Zhang, Y., Zhang, X., Chen, X.: Phase Measurement of Three-phase Power Based on All-phase FFT. In: 2010 2nd International Conference on Signal Processing Systems (ICSPS), vol. (7), pp. 580–583 (2010)
7. Zhang, Y., Zhang, X., Chen, X.: Phase Measurement of Three-phase Power Based on Labview. In: 2010 International Conference on Intelligent Systems Design and Engineering Applications (ISDEA 2010), vol. (10), pp. 61–64 (2010)

An Internet-Based Netlab Combines Both Real and Virtual Experiments in Electronic Engineering

Kai Yang, Kai Li, Huan Zhang, and Shanan Zhu

College of Electrical Engineering Zhejiang University
Hangzhou 310027, China
kaiyoung@126.com

Abstract. This paper describes a C/S model-based network laboratory which combines both real and virtual experiments, the real experiments are based on physical equipments, while the virtual ones on simulation models. There are three experimental modes: the synchronization experimental mode, the asynchronous experimental mode and the virtual simulation mode. Experiments for six courses including circuit theory, analog electronic technique, digital electronic technique, micro-electronics, MCU and DSP have been implemented and they are being used in our school. The netlab enables the experimenters to design their own circuit and get simulation result simultaneously. Teachers may design some new components and add them into the platform.

Keywords: real and virtual experiment, electrical and electronic, C/S model, netlab.

1 Introduction

Experiment education is of great importance to the students who are major in engineering, it not only provides them with the chances to operate the experimental equipments by their hands, but also helps them to have a deeper understanding of the application of theoretical knowledge. However thanks to the high cost of the room space and the equipments, as well as the number limitation of users, the conventional laboratory can't meet the increasing demand for the engineering experiments. With the popularization of PC and the development of the internet, laboratory online which is a new way of experimental education becomes more and more popular because of its convenience, thus nowadays there are various types of network laboratories. Reference[1] presents a remote control laboratory online about operating a robot arm; Reference[2] describes an experimental system of digital circuit networks and three emulators; Reference[3] describes a microprocessor test box for experiment online; In reference [4] and [5], matlab is used to build a virtual lab for signal processing and electromagnetic simulation. There are more other experimental applications just like the above ones, however these virtual experiments are generally based on simulation model, by excluding the outside-interference and the other uncertainties, they are short of experimental authenticity.

D. Jin and S. Lin (Eds.): Advances in Mechanical and Electronic Engineering, LNEE 177, pp. 471–477.
springerlink.com

The electrical and engineering netlab of Zhejiang University combines both remote network laboratory which is based on physical equipments and virtual laboratory which is based on simulation models. The netlab is first domestic comprehensive network laboratory, which takes advantage of both real and virtual experiments. It is flexible when doing experiments in the netlab, the experimenters can choose to do the virtual experiments if the physical equipment is being used by other people. After obtaining the data from both real experiments and virtual ones, the experimenters can compare them to find out the differences between the theoretical value and the actual value.

2 System Design

The electrical and engineering netlab of Zhejiang University uses C/S model framework, it consists of three parts: the client side, the server side and the experiment side. The experimenters can login the netlab by installing a client package. Figure 1 is the system architecture of the netlab.

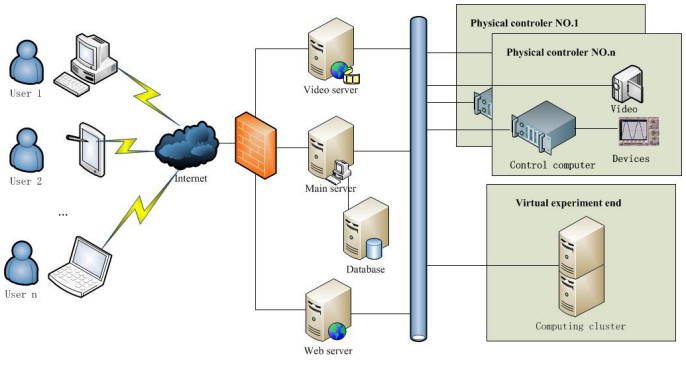

Fig. 1. System architecture

2.1 The Client Side

The client side is an .exe installation package, which is programmed by C++, the users can download it from the internet and install it, by inputting the admitted user's name and the correct password they can login the netlab. The client side contains the user's information management module and the physical experiment modules for different courses which is based on MFC framework. Most of the real experiments have their corresponding virtual experimental modules, the modules are based on FLEX. Experimenters can access to the virtual experimental platform by clicking the linking button which is embedded in the real experimental platform.

2.2 The Server Side

The server side contains the main server, the database sever, the video server and the web server. The main server is responsible for experimental data transmission. The main server program is divided into the real experimental part and virtual experimental part, the former is written by Java language, the latter is written by Python and based on the the Twisted [6] framework. The database server uses Oracle Database [7], it manages the information of the experimenter, such as the login management and authority control, it also stores the experimental data. The web server includes different experimental modules, it use the Apache Tomcat open-source software, meanwhile it handles the request from users. The video server provides video support for the physical experiments (such as the dynamic process monitoring of the inverted experiment and the blowing pendulum experiment), so that users can have a real progress of the experiment .

2.3 The Experiment Side

The experiment side consists of two functional blocks : real experimental controller and virtual experimental computing cluster. The real experimental controller program is installed on the controller computer, mainly responsible for the controller-side operating and monitoring. A data sampling card is used to send control signal and sample experimental data. Dozens of relays will change their status to be on or off according to the control signals to conduct different experimental circuit. The monitoring program can automatically check the running status of the sever. If an error is monitored, the server will restart automatically, as well as the controller program. This design is an important guarantee to make the netlab open all day long without people taking care of it. The virtual experimental terminus includes a group of server computing nodes, each node shares the simulation tasks with a master node to balance the load.

3 System Implementation

As the principle and the implement of the physical experiment and virtual experiment are quit different, the combination is mainly presented in the client side. The users login the netlab through a united client, he can choose to do real experiments or virtual experiments. If the user chooses to do the real experiment, the client computer will send commands which are coded into a data packet to the control computer. The commands will change the state of the relays to be on or off, to control the experimental equipments . The real experiment has two work modes: the synchronous experimental mode and the asynchronous experimental mode. The former mode has better experimental effect while the latter mode has better experimental efficiency. We take advantage of them both to meet different kind of experimenter's need. If the experimenter chooses the virtual experiment, the client computer will connect to the virtual platform which is stored in the web server, just like the real platform, all different kinds of experiments can be chosen.

3.1 Synchronization Experimental Mode

Synchronization experimental mode is to create a virtual link connection between the client and controller, the controller can directly interact with the client. Simplified the process shown in Figure 2:

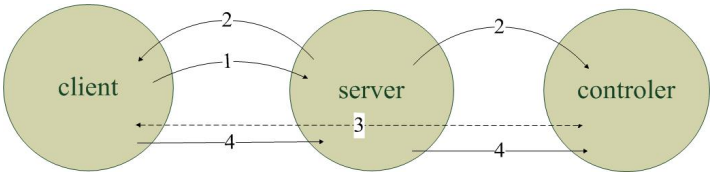

Fig. 2. Synchronization experiment process

Step 1 **:** the user should register the experiments on the server and complete the experimental design on the client computer,and then the server will put the experiment requests into the queue.

Step 2: when it comes the turn for the experimenter, the server will notify the him. Then the server will build a bi-directional channel (experimental virtual link) for sending signals.

Step 3: the client is directly to send experimental command to the controller, and the controller can also respond in real-time back with the experimental data.

Step 4: when experimenters send the stop command to the server or exceed the maximum experimental time, the experiment will be stopped. The server then automatically start the next experiment in the queue.

There are two ways to do synchronization experiments, one way is waiting in a queue online until the server notifies the experimenter. The other way is making an appointment for a certain time, at that time the experimenter can directly start the his experiment without waiting.

Synchronous experimental model allows the experimenter to modify the experimental design and the parameters during the process of experiment. The experiment effect is better especially with a variety of auxiliary equipments, such as videos, sound devices *etc.* The system sets a maximum time to prevent some experimenters from maliciously occupying the experimental equipments.

3.2 Asynchronous Experimental Mode

Asynchronous experimental mode means there is no virtual link connection between the client and controller, the experimenter doesn't need an appointment. What the experimenter has to do is to send the experimental design and parameters to the sever, and the server will automatically complete the experiment. The simplified process shown in Figure3:

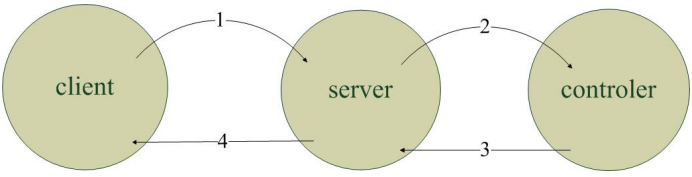

Fig. 3. Asynchronous experiment process

Step 1: the experimenter completes experimental design on the client, and sends the parameters data packet to the server.

Step 2: when the device is idle, the server will send the data packet to the controller, the experiment will be automatically done in accordance to the parameters.

Step 3: after the completion of the experiment, the real experimental data will be sent back to the server.

Step 4: the server gets the experimental data, if the experimenter is online, the server will send the experimental data to the experimenter, and he can see the result on the client.

In asynchronous experimental mode, the laboratory equipments are always in a running state, we can make full use of them, the efficiency is much better than that in the synchronous experimental mode. Especially the Circuit experiments, it only takes several milliseconds for a user to do one experiment, so hundreds of users can share the same set of equipment mostly at the same time without too much time delay.

3.3 Virtual Simulation Mode

Virtual simulation mode is based on Modelica [8]. Modelica is a program language based on mathematical equations, it uses mathematical equations to describe the characteristics of the physical component. We use Modelica to build physical component models. There is an open source *Modelica standard library* contains physical component models in electric and electronic, mechanical, control, electromagnetic fields and other areas. The electric and electronic library contains most of the basic component used in electrical and electronic disciplines, such as resistors, capacitors, inductors, diodes, transistors, and so on. The standard library also allows us to add new models designed by ourselves. The virtual experiment takes advantage of the Modelica Standard Library as well as the custom model library. The experimenter use the component which is listed on the left side of the experiment operational interface to design the experimental scenarios(see the Figure 6), then the scenarios are converted into an XML data packet, and the packet is transported through the communications interface to a computing node.

The simulation process begins as follow. Firstly, the XML description is converted into a Modelica description, and then through the open-source Modelica compiler (OMC), Modelica description is compiled to an executable file, which will be executed to get the simulation results, then the experimenter will see the results on the client interface. The simplified process shown in Figure 4:

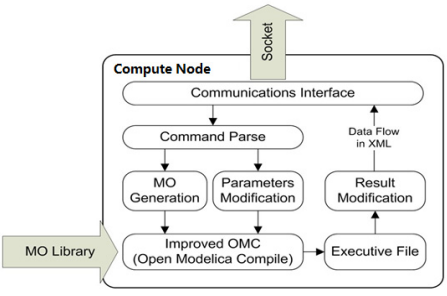

Fig. 4. Virtual simulation process

4 Experiment Example

Six courses including circuit theory, analog electronic technique, digital electronic technique, micro electronics, MCU and DSP have been implemented in the nelab. The operational methods are similar for both real and virtual experiments. First, choose the components to design a circuit and send it to the server. Second, the server examine the circuit by comparing with the correct one. Third, if the design is correct, then experimental scenario will be run, and get the final results. Fig. 5 and Fig. 6 show the results of a typical analog experiment, which converts the square wave into the triangular wave.

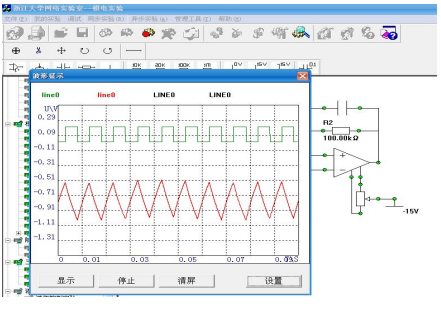

Fig. 5. Experimental result from real experiment

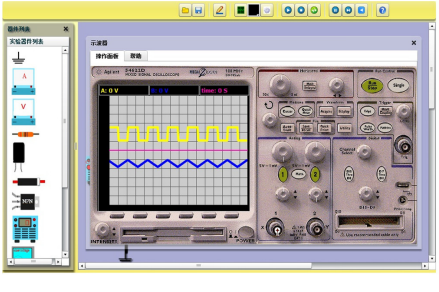

Fig. 6. Experimental result from the virtual simulation

From Fig. 5 and Fig. 6 we find that the waveform of the virtual experiment is relatively more uniform and smooth. While see the physical waveform, we find the value of some wave peak are bigger than the other's, because of some interference.

5 Conclusion

Zhejiang University Network Laboratory [9] has been used for experimental teaching. It opens to students of Zhejiang University remote college, who are major in electrical and engineering since 2005. Every year thousands of students from more than one hundred learning centers share the resource of the netlab. The combined netlab will soon be used in experimental teaching, comparing the real result with the virtual result which will help experimenters understand the experiments more deeply. The netlab will bring more convenience to more users. A network laboratory based on B/S model is being under construction. Users can login directly to the netlab through the PCs or the pads and other terminals. The new netlab will include an integrated experimental information management system, intelligent marking system and other extensional functions. What's more, the user even can ask the teacher for help online during an experiment. We expect the continuous development of network laboratory will make a greater contribution to the remote education in China.

References

1. Wu, M., She, J.H., Zeng, G.X., et al.: Internet-based teaching and experiment system for control engineer course. IEEE Transactions on Industrial Electronics 55(6), 2386–2396 (2008)
2. Donzellini, G., Ponta, D.: A simulation environment for e-learning in digital design. IEEE Transactions on Industrial Electronics 54(6), 3078–3086 (2007)
3. Bahring, H., Keller, J., Schiffman, W.: Remote operation and control of computer engineering laboratory experiments. In: Proc. WCAE: 33rd International Symposium on Computer Architecture (2006)
4. Sturm, B.L., Gibson, J.D.: Signals and systems using MATLAB:An integrated suite of applications for exploring and teaching media signal processing. In: Proc. 35th Frontiers in Education Conf.
5. de Magistris, M.: A MATLAB-based virtual laboratory for teaching introductory quasi-stationary electro-magnetics. IEEE Trans. Educ. 48(1), 81–88 (2005)
6. Alves, G.R., Gericota, M.G., Silva, J.B.: Large and Small Scale Networks of Remote Labs: A Survey. Advances on Remote Laboratories and E-learning Experiences. Univ. Deusto, Bilbao (2007)
7. Duan, B., Hosseini, H.M., Ling, K.V., Gay, R.K.L.: An Architecture for Online Lab E-learning System. Journal of Distant Education Technologies 4(2) (April-June 2006)
8. Engelson, V., Larsson, H., Fritzson, P.: A design simulation visualization environment for object-oriented mechanical and multi-domain models in Modelica. In: Proceedings of IEEE International Conference on Information Visualization, pp. 188–193 (1999)
9. Zhang, S., Zhu, S., Lin, Q.: NETLAB−An Internet based laboratory for electrical engineering education. Journal of Zhejiang University Science 6A(5), 393–398 (2005)

"Exploration-Internalization Mode" with Electronic Equipments in Self-study Center

Xianzhi Tian

Wuchang University of Technology, Wuhan, China
Julia030712@163.com

Abstract. In modern colleges, more and more reforms are on improving autonomous abilities of learners. And many of them are trying their best to improve learners from two aspects, the first one is on the professional qualities of learners and the next one is on the non-professional qualities of learners. Both of them are mainly used to improve the abilities of learners to improve their capabilities on dealing with modern social abilities. With the development of modern information, the training course will be influenced by modern information technology in a certain degree. And guiders rest upon information technology in a degree too. In the paper, the author has investigated the "exploration-internalization" mode from two aspects, not only from learners but also from the effectiveness of electronic equipments. All of the investigations are based on information technology and electronic equipments with some program control system. Therefore, it is a combination of different elements to urge the improvement of "exploration-internalization" mode.

Keywords: autonomous abilities, "exploration-internalization" mode, electronic equipments, program control system.

1 Introduction

About one century, many researchers put their focus on technology improvement. The detail purposes of them are different, but the common ones are on improving absorption efficiency of learners, and thus improving abilities of learners in society. In the paper, the author has used "exploration-internalization" mode. The mode is also used mainly from two aspects, one is on "exploration", which is from the angle of guiders. And the next one is on "internalization", which is from the angle of learners. The main task of guiders are on "exploring" the invisible abilities of learners. And the main task of learners are on "internalization" of their own abilities. But the "internalization" is through "exploration" mode. The two aspects are closely connected with each other. It is not easy for the author to separate "exploration" and "internalization" wholly. They are closely connected with each other.

From the theory of "exploration-internalization" mode, it is ideal and it is easy to be operated by guiders. But in reality, it is a long way to put the theory into practice. In the condition of modern information technology, guiders can get some enlightenments from web. But at the same time, information technology also requires higher guiding methods to realize the real aim of the mode. As for different courses,

D. Jin and S. Lin (Eds.): Advances in Mechanical and Electronic Engineering, LNEE 177, pp. 479–482.
springerlink.com

different guiding methods will be used properly, which is very important for real realization of "exploration-internalization" mode. In the paper, the author will study the topic from two aspects, one is on how to realize "exploration" and the next one is on how to realize "internalization". And the study is mainly focused on self-study center with electronic equipment for the improvement of autonomous learning abilities of learners.

2 Brief Investigation of "Exploration" Measures in Self-study Center with Electronic Equipments

As for "exploration measures",different people have different views on how to explore some invisible abilities of learners. In self-study center, learners are easy to indulge themselves in web news, web games and some other items not related with learning and their ideal learning plan will be abandoned due to their wasting their time on the above items. If learners waste time in self-study center, the original training aims of guiders will be in no use. Thus their autonomous learning abilities will not be improved and self-study center will only have bad impacts on learners.

As the application of "exploration-internalization" mode has been applied in learning course for one year, the author has invested 25 guiders to get the main measures to explore invisible abilities of learners. And the following measures can be found in the reform of guiding mode.

Table 1. Investigation of "exploration" measures in self-study center

Main measures	Case-guiding method	Discussion guiding method	Group-cooperation guiding method	Question-designed guiding method	Task-driven guiding method	Autonomous guiding method
rate	35%	62%	43%	65%	75%	36%
Comment of learners	Good	Very good	Very good	Should be improved	Very good	Should be improved

From the investigation, we can see that "discussion on guiding method""question-designed guiding method""task-driven guiding method" are welcomed by many learners. And a large parts of learners approved to promote them in further guiding course. And at the same time, some learners had given good suggestions on improving them. As for any other guiding methods, learners think that they must be improved for driving learning enthusiasm of learners. It is a long way to realize real realization of guiding reform. At the same time, with the development of modern information technology, different methods must be coincided with its developments. Therefore,the element of information technology must be taken into consideration during guiding reform. This one can be used during guiding course. At the same time, many kinds of learning and guiding resources can also be got from some webs through information technology. During the reform of guiding methods,, task-given point is the center one for realizing guiding ains. As for this one, learners should plan their learning course by the guide of guiders, which is the most important one for the improvement of autonomous learning abilities of learners.

During the realization of guiding aims, "exploration" measures can be seen from different angles. There are several points to be mentioned here as follows:

"Exploration" Measures-task driven method

Task-driven method is the main method for the "exploration" measures to improve absorption efficiency of learners. In fact, " exploration" measure is the main responsibility of guiders. How does a teacher explore the inner ability of learners? How does a teacher improve his/her absorption efficiency of learners? All of those questions should be taken into consideration by guiders. During the guiding course, guiders have to teach learners with different creative ideas. The most difficult points on exploring measures is focusing on digging out the effective guiding methods based on modern information technology. In fact, in recent years, many guiders put up forward on guiding methods to drive the inner potential abilities of learners.

According to some scientific researches, the courses of "exploration" measures-task driven method is shown as follows:

Table 2. Simple table for "exploration" measures-task driven method

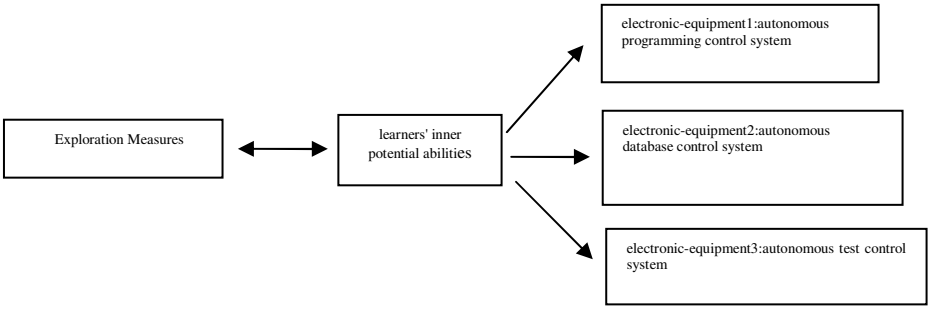

From the above table, it is easy to see that "exploration" measures-task driven method is to dig out the inner potential abilities of learners. It is mainly from three main electronic equipments, that is to say, autonomous programming control system, autonomous database control system and autonomous test control system. Among them.all systems are consistent with exploration measures. Whether the exploration measures are effective or not, the absorption efficiency of learners can be seen or not, they all depend on the operation of the three main systems. So the effectiveness of exploration measures will decide the inner potential abilities of learners. Therefore, it is necessary for guiders to have abilities to control the above three electronic equipments to dig out the inner potential abilities. Self-study center then becomes a good place for them to realize their abilities.

"Exploration" Measures in Self-study Center with Electronic Equipments

Generally speaking, different guiders have different measures to dig out the inner abilities of learners. But at the same time,different learners should be stimulated by different ways. So "exploration" measures are different. Generally speaking, there are several "exploration" measures as follows:

◆ **Task-driven measures**

As for this measure, learners should be given heavier tasks to drive their inner potential abilities. All tasks should be consistent with the learning basis of learners. So correct evaluation is very important for guiders. At the same time, task -checking is also very key for guiders. This measure is relatively boring and laborious for learners. But at the same time, learners must have patience in insisting on this measure. As for different tasks, progressive characteristic is necessary during realization of this measure. This measure should depend on the devices of information technology in self-study center based on web,especially on electronic-equipment2:autonomous database control system. In the database, scientific and meaningful tasks will be important for task-driven measures.In the center, so much heavy task will be given by web and checked by autonomous-learning style.

◆ **Guide-imitation measures**

As for this measure, the most important role in it is on guiders and learning environment. Sometimes, it is stimulated also from around learners. So we must take all factors into consideration. On the one hand, learners can develop themselves from the guide of guiders. On the other hand,,learners can imitate other excellent learners and got good influences from autonomous learning groups in self-study center. During this course, web source plays an important role. learners can not only get learning source from web, at the same time, they can also get learning methods and good learning modes from web.

◆ **Autonomous-learning and guiding measures**

This measure is combined with the above two measures. They can be mixed with each other during playing their own roles. In fact, this measure is the most important one during exploration of learners' inner potential abilities. It reflects the learning initiative of learners. And only by this measure, learners can reflect their learning motivation. This measure can be realized by electronic-equipment1:autonomous programming control system and electronic-equipment3:autonomous test control system.

In fact, the above ones are the basic main ones, there are also some other measures during learning course of learners.

3 Conclusion

In a word,with development of information technology, different measures on "Exploration-Internalization Mode" in Self-study Center with electronic equipments have been used to improve autonomous learning abilities of learners. And guiding reform must rely on information technology and will be improved with the efforts of guiders,especially guiders.

References

1. Allwright, D.M.: Autonomy in Language Pedagogy, CRILE Working Paper 6, Center for Research in Education, University of Lancaster, pp. 112–119 (1990)
2. Aoki, N., Smith, R.: Learner autonomy in cultural context: The case of Japan. In: Abstract for paper presented at the 11th World Congress of Applied Linguistics, Jyvaskyla, Finland (August 1996)

A Calibration Method of the Stereo Vision Measurement System for Electronic Productions

Qin Jia[1,2], and XueFei Liu[1]

[1] Environmental Management College of China, Qinhuangdao, China
[2] Institute of Electrical Engineering Yanshan University, Qinhuangdao, China
hb_jq2003@yahoo.com.cn, lxf2000@126.com

Abstract. To calibrate the camera parameters of stereo vision measurement system in industrial production, this paper analyzes the principle of camera calibration and gives full consideration of the impact of lens radial distortion and tangential distortion and proposes a solution algorithm. A camera calibration method adapting to the size of the work-piece measurement is proposed, and the camera calibration step is given. This method can complete the internal and external parameters calibrating of the cameras only one time, and the experimental result shows that this method can satisfy the calibration accuracy.

Keywords: Stereo vision, camera calibration, distortion model.

1 Introduction

The higher accuracy and speed measurement of the work-piece is often required in industrial production. Binocular stereo vision detection technology is ideally suited for this task. The camera calibration is necessary because the geometrical information of the object is extracted from two different viewpoints images in binocular stereo vision measurement system. The purpose of camera calibration is to determine the corresponding relationship between the camera coordinate and the world coordinate.

The camera calibration techniques can be divided into two types: traditional calibration and self-calibration. The traditional calibration technique requires high precision calibration object and accurate installation and expensive equipment. The self-calibration technique is independent of calibration reference and only uses the constraints of camera motion or the surrounding to calibrate, but the precision of the method is low and unstable because some parameters of the method are obtained by estimating. Many researchers have proposed many improved calibration methods [1-4]. Zhengyou Zhang proposed a two-dimensional target calibration method [5], this method only requires taking more than two different orientation images of the same calibration target, and then the internal and external parameters of the camera can be gotten. The method is a more flexible algorithm between traditional calibration and self-calibration. In this paper, the parameters of the cameras are gotten by the calibration algorithm of Zhang, and the lens distortion parameters are calculated with a new lens distortion model and data fitting function.

D. Jin and S. Lin (Eds.): Advances in Mechanical and Electronic Engineering, LNEE 177, pp. 483–488.
springerlink.com

2 Analysis of Calibration Principle

In the computer vision, the camera imaging model used pinhole model commonly [6]. The coordinate related to the three-dimensional object imaging include the world coordinate X_W, Y_W, Z_W, the camera coordinate X_C, Y_C, Z_C, the image plane coordinate x, y and the computer image coordinate u, v, Shown in Fig.1. Getting the internal and external parameters of the camera using a group of corresponding points which the world coordinates and the image plane coordinates are known is defined as camera calibration.

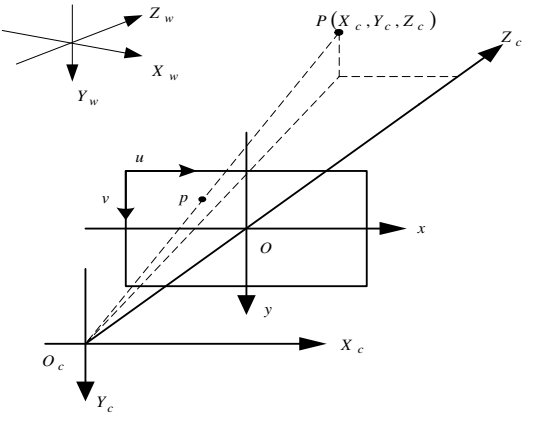

Fig. 1. Camera coordinates and world coordinates

The coordinate conversion of a space point P to its image point p is achieved through the conversion between the four coordinate systems. At first the coordinate $P(X_c, Y_c, Z_c)$ can be gotten by rotating and translating the point $P(X_w, Y_w, Z_w)$, then the image plane coordinate (x, y) can be gotten by triangular or geometric transforming, finally the computer image coordinate (u, v) of the point p can be obtained by conversion of metric units and pixel units. The coordinate matrix of the world coordinate and image coordinate is shown in Eq. (1).

In Eq. (1), R is the 3×3 rotation orthogonal matrix, and $R=E$ in the ideal state, T is the translation scale of the camera in the three axial orientations.

In Eq. (2), $f_x = f / dx$, $f_y = f / dy$ is the effective focal length of the horizontal direction and vertical direction respectively, dx, dy is the width and height of the image pixel respectively, γ is the slant coefficient, the (u_0, v_0) is the main point coordinate of the computer image coordinate. The K is the internal parameter matrix of the camera. The R and T are the external parameter matrix. Let $H = K[R \quad T]$, then the matrix H is known as homography matrix.

$$Z_C\begin{bmatrix} u \\ v \\ 1 \end{bmatrix} = \begin{bmatrix} 1/dx & y/dx & u_0 \\ 0 & 1/dy & v_0 \\ 0 & 0 & 1 \end{bmatrix}\begin{bmatrix} x \\ y \\ 1 \end{bmatrix} = \begin{bmatrix} f/dx & f\gamma/dx & u_0 \\ 0 & f/dy & v_0 \\ 0 & 0 & 1 \end{bmatrix}\begin{bmatrix} 1 & 0 & 0 & 0 \\ 0 & 1 & 0 & 0 \\ 0 & 0 & 1 & 0 \end{bmatrix}\begin{bmatrix} R & T \\ 0 & 1 \end{bmatrix}\begin{bmatrix} X_W \\ Y_W \\ Z_W \\ 1 \end{bmatrix} = K\begin{bmatrix} R & T \end{bmatrix}\begin{bmatrix} X_W \\ Y_W \\ Z_W \\ 1 \end{bmatrix} \quad (1)$$

$$T = \begin{bmatrix} T_X & T_Y & T_Z \end{bmatrix}^T, \qquad K = \begin{bmatrix} f_x & \gamma f_x & u_0 \\ 0 & f_y & v_0 \\ 0 & 0 & 1 \end{bmatrix} \quad (2)$$

There is deformation in lens generally, the main deformation is radial, and there is a slight tangential deformation. The results of the internal and external parameters are not accurate because the distortion isn't taken into account in the above process. The results can't be taken as the final camera parameters, but they can be used as the initial value of the non-linear optimization in the back process. The distortion model and data fitting function is proposed ,the distortion model is as following [7].

$$\begin{aligned} X_i &= \left(1 + k_1 r^2 + k_2 r^4 + k_3 r^6\right) x_i + 2p_1 x_i y_i + p_2 (r^2 + 2x_i^2) \\ Y_i &= \left(1 + k_1 r^2 + k_2 r^4 + k_3 r^6\right) y_i + 2p_2 x_i y_i + p_1 \left(r^2 + 2y_i^2\right) \end{aligned} \quad (3)$$

In Eq. (3), $r^2 = x_i^2 + y_i^2$, (x_i, y_i) is the actual coordinate of the target corners, (X_i, Y_i) is the standardized coordinate of the target corners, k_1, k_2, k_3 are radial deformation coefficients, and p_1, p_2 are the tangential deformation coefficients. Extracting the corner coordinates of the target image and calculating the corresponding corner coordinates using the distortion model and taking the two sets of coordinate values into the data fitting objective function , then the values of the corresponding distortion parameters can be calculated ultimately. The data fitting function is as following.

$$\min F = \sum_{i=1}^{N} (X_i - x_i)^2 + \sum_{i=1}^{N} (Y_i - y_i)^2 \quad (4)$$

It can be seen from Eq. (4) that the data fit better and the obtained parameters are more accurate if the value of the function is smaller. The parameters which make the objective function minimum are gotten finally through iterating the optimization algorithm. This method simplifies the calculation and reduces the solution difficulty.

3 Calibrating Process

The calibration consists of two parts. The one is calibrating two cameras respectively to get the internal parameters using the single-camera calibration method, the other is getting the position relationship between the two cameras by a set of calibration points in same world coordinate, and it can be achieved by capturing the same target of the public areas in one time. The specific steps are as follows.

1) Print and make the black and white plane calibration target;

2) Capture the calibration target from different orientations according to the different view field of the two cameras respectively to get the multiple sets of images;

3) Make Wiener filter for the images to suppress noise and reduce blurred edges;

4) Extract the image coordinates of the corners using Harris algorithm for each set of image, and make the image coordinates correspond the three-dimensional coordinates;

5) Solve the linear equations to get the approximate solution of the internal and external parameters by matching the image coordinates and the world coordinates of the calibration points;

6) Use the above described method to make nonlinear optimization to get the exact solution of the internal parameters and the distortion coefficient;

7) Place the calibration target in a public view area of the two cameras to take an image of the target respectively, then extract the reference points and calculate the homography matrix H of the two images and the target using the above method respectively. The external parameters of the target can be calculated after getting the H because internal parameters of the cameras have been pre-calibration;

8) The external parameters of the two cameras are represented as R_1, t_1 and R_2, t_2 respectively, R_1, t_1 is the relative position of the left camera and world coordinate, R_2, t_2 is the relative position of the right camera and world coordinate. For a point P, let the non-homogeneous coordinates of the world coordinate and the left camera coordinate and the right camera coordinate are X_w, X_{c1} , X_{c2} respectively, then

$$X_{c1} = R_1 X_w + t_1 \qquad X_{c2} = R_2 X_w + t_2 \tag{5}$$

After eliminating X_w

$$X_{c1} = R_1 R_2^{-1} X_{c2} + t_1 - R_2^{-1} t_2 \tag{6}$$

The geometric relationship between the two cameras can be described as

$$R = R_1 R_2^{-1} \qquad t = t_1 - R_2^{-1} t_2 \tag{7}$$

The R and t of the two cameras can be calculated by R_1, t_1 and R_2, t_2 .

According to the above process, the two cameras are determined in the world coordinate established by the same calibration target.

4 Experimental Results and Analysis

Two CV-M4+CL CCD cameras whose resolution is 380 × 1030 and Computar lens whose focal length is 12 mm are used in the experiment. The calibration target is black and white calibration plate and is fixed to a glass, the size of each grid of the target is 30 mm× 30 mm, the total corners is 25 × 4 = 100. The distance of the target and the camera is 600mm in calibrating. Fig.2 and Fig.3 shows several calibration images of the left and right cameras respectively, Fig.4 shows an image while the left

and the right camera calibrate at the same time. The internal and external parameters of the two cameras can obtained using the above mentioned calibration method. The obtained results are shown in Table 1.

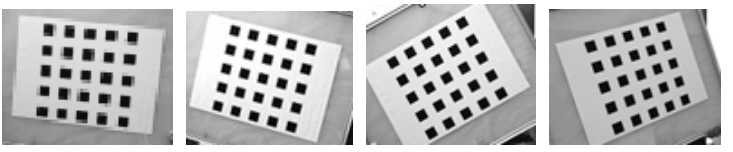

Fig. 2. Calibration images of left camera

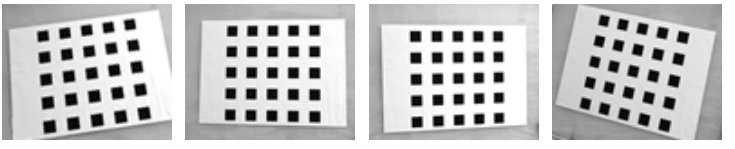

Fig. 3. Calibration images of right camera

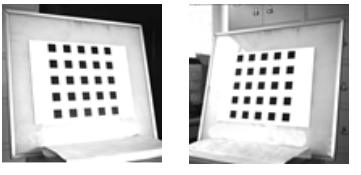

Fig. 4. Calibration images of left and right cameras taking at the same time

Table 1. Result of dual cameras calibration

	Left camera			Right camera		
f_x	1 891.17			1 879.52		
f_y	1 886.12			1 874.01		
γ	-3.746 046			-3.608 298		
u_0	678.263			680.923		
v_0	497.744			501.716		
k_1	-0.028 121			-0.043 518		
k_2	0.010 934			0.013 212		
k_3	-0.012 336			-0.024 573		
p_1	-0.003 214			0.017 763		
p_2	-0.007 532			-0.002 469		
R	0.901 56	-0.010 21	0.053 13	0.987 56	0.016 39	-0.056 67
	0.013 76	-0.981 52	-0.031 79	-0.009 10	-0.982 13	-0.021 56
	0.092 54	0.076 53	-0.921 77	-0.043 43	0.087 44	-0.955 38
t	-121.503	-109.716	1 140.66	-92.783	-127.391	1 309.41

The values f_x / f_y of the left and right camera are 1.0015 and 1.0016 respectively, and very close to 1. It's visible that the pixel of the captured image is square. The value X , Y , Z of each camera is 0.02 º, 0.02 º and 0 º respectively, and very close to zero, it's visible that the image axis almost is not slant. It can be seen from the result that the effective focal length and the main point coordinates and the distortion coefficients of the same type of camera are somewhat different, it shows that that the production and installation of the camera lens has errors.

5 Conclusions

Based on the analysis of the binocular stereo camera calibration method of Zhang, this paper studies the lens radial distortion and tangential distortion and a solving algorithm is proposed. A flexible and accurate calibration method adapting to industrial measurement of work-piece size based on the project needs is proposed, the method can complete the calibration of the measurement system in one time. The experimental result shows that this method is not only quick and easy, but also can achieve satisfactory calibration accuracy.

Acknowledgment. This project is supported by the Scientific Research Foundation of Qinhuangdao City, China(No.201101A059).

References

1. Liang, L., Yin, D., Wang, C.: Design and Detection Methods for Accurate Camera Calibration Target. Journal of Xi'an Jiaotong University 45(4), 82–85 (2011)
2. Kannala, J., Brandt, S.S.: A Generic Camera Model and Calibration Method for Conventional, Wide-angle, and Fish-eye lenses. IEEE Transactions on Pattern Analysis and Machine Intelligence 28(8), 1335–1340 (2006)
3. Qu, X., Zhang, L.: Camera Calibration and 3D Reconstructi0n Based on a New Imaging Model. Chinese Journal of Scientific Instrument 32(8), 1830–1836 (2011)
4. Zeng, X., Lu, D.: A New Method of Camera Calibration Based on OpenCV and Tsai. Mechanical & Electrical Engineering Magazine 25(12), 49–52 (2008)
5. Zhang, Z.: A Flexible New Technique for Camera Calibration. IEEE Transactions on Pattern Analysis and Machine Intelligence 22(11), 1330–1334 (2000)
6. Bradski, G., Kaebler, A.: Learning OpenCV. SouthEast University Press, Nanjing (2009)
7. Gbson, S., Cook, J., Howard, T.: Accurate Camera Calibration for Off-line Video-based Augmented Reality. In: Proceedings of the IEEE and ACM International Symposium on Mixed and Augmented Reality, pp. 37–46 (2002)

A Geographic Information System Model for Evaluation of Electric Power Generation from Photovoltaic Installations

Ignacio J. Ramírez-Rosado[1] and Pedro J. Zorzano-Santamaría[2]

[1] Department of Electrical Engineering, University of Zaragoza, Edif.Torres Quevedo C/ María de Luna 3, 50018 Zaragoza, Spain
[2] Department of Electrical Engineering, University of La Rioja, Edif. Departamental, C/ Luis de Ulloa 20, 26004 Logroño, Spain
ijramire@unizar.es

Abstract. This paper presents a novel and useful GIS model for evaluation of electric power generation from the solar resource available in a given region, through the creation of a comprehensive geographical database in a Geographic Information System (GIS). A large amount of data from various sources (weather, reflectance, technologies, etc.) are subjected to detailed calculations which lead to the evaluation of specific local characteristics of power generation (during a typical period of time: typical month, typical year) at each point of the region under study. It has been applied to the Spanish region of La Rioja, divided into cells of GIS coverage of 5x5 meters, a resolution never used before (more than 1012 points studied). The model is applicable to any resolution and any area where reliable meteorological and geographical data can be collected.

Keywords: Power Generation, Renewable Resources, Geographic Information Systems, Photovoltaic Energy Production.

1 Introduction

The GIS model developed in this paper for evaluating solar energy resources in a geographical area uses, in each point of the study area, an average value of total radiation usable by a photovoltaic (PV) panel of any type of PV technology; the model also uses a large amount of data and detailed calculations what leads to precise evaluation of the electric power generation from PV installations that efficiently convert the solar resource into electricity.

A simple method for evaluating the solar resource is the interpolation of the average values of daily global irradiance (H), obtained from meteorological stations [1] near the study area (usually spaced a few tens of km in developed areas and several hundred km in developing areas). More sophisticated methodologies [2] utilize satellite images to characterize the cloud cover (usually for a resolution of 5 km). These methods are not efficient if we want to get a very fine resolution (few hundred meters or less). In these cases of high resolution, GIS modeling

D. Jin and S. Lin (Eds.): Advances in Mechanical and Electronic Engineering, LNEE 177, pp. 489–496.
springerlink.com

methodologies [3] are better used, because of the effects of: a) the terrain and its vegetation characteristics or shadow effects due to solar trigonometry, the slope and the reflective properties depending on the nature of the terrain; b) the geographical dispersion of the variables involved in the evaluation of the electricity from solar radiation. The combination of these effects influence irradiance values evaluated at certain locations more than the extension, to such locations, of solar radiation measures recorded in meteorological stations relatively close to these locations. Notice that local irradiation can be considered by spatial interpolation techniques of the irradiance values from these ground meteorological stations.

In our GIS model, we use the local average daytime temperature that greatly influences the conversion efficiency of radiation into electricity of different photovoltaic technologies, with a very fine resolution never used until now (resolution of 5x5 meters, that is, the GIS cell of the model of this paper has almost the size of a standard PV panel). Our model, with detailed calculations, is also well suited to assess (with higher resolution with respect to other models) electricity from solar resources.

Notice that the model defined in this paper, for the evaluation of electric energy generated by any type of PV technologies in a region, uses all the computing power of geometrical-statistical-geographical calculus that a Geographic Information System inherently provides, along with the ability to build, with any type of data (such as alphanumeric data, like position and name of weather stations; shape or cover data, like type of ground surface materials; tables of technical data of PV panel technologies, etc.) geo-referenced databases, that is, assigning to each specific magnitude (such as the value of solar irradiance, the value of surface reflectance, the value of a tilt angle of a PV panel, etc.), its geographical position, and using these features to spatially analyze the geographical variables stored (such as the global daily irradiance, the mean monthly ambient temperature, or the monthly converted electrical energy per unit area of a PV panel, etc.).

2 GIS Model

Any region of the Earth can be represented as a map in a GIS with associated geo-databases, such as the absolute position (latitude and longitude), or the height above sea level. Furthermore, sufficient details can be associated to include a geographical model of the terrain such as the height of buildings and other obstacles. Those obstacles provide (using the solar geometry associated with each point of study), a GIS cover with areas of shadow over the terrain, during the annual cycle of translation of the planet. The average ground slope at each point of study is calculated internally with the digital terrain model. Coordinate data identify the geographical location of meteorological stations and locate (at these points) the meteorological variables, including seasonal variations over a typical month or a typical average year. These pointed statistical magnitudes can be extended to the entire study area with spatial interpolation techniques (kriging and co-kriging spatial interpolation [4]).

Soil characteristics that influence the received irradiance are associated with each point of study in the GIS, such as the albedo of land, evaluated from the reflectance of surface materials, whether natural (rock, vegetation, surface water, etc.) or artificial

(building materials, roads, major infrastructure, etc.). Seasonal variations are also included if the reflectance of materials changes over an average year, as it is common in the vegetation or crops, snow days, etc.

On the other hand, as described below, during the process of calculating the electrical energy generation available from solar radiation at any point of the study area, we preferred to implement the precise relationships tailored to the local features, starting with general and theoretical calculations from the solar constant (i.e., extraterrestrial solar energy received per unit time in a unit area, outside the influence of the atmosphere and located at the mean Sun-Earth distance). Also, we calculate the correlation of these theoretical calculations with those statistically measured at meteorological stations installed in the area of study. The more historical data can be arranged and more densely ground stations located throughout the region studied, the more free of bias and adjusted to local weather patterns will be the results. The implemented methodology also leads to a more specific calculation to evaluate the electric energy generation obtained from the sun with a PV panel in a particular semiconductor, with arbitrary tilt and orientation angles (even if the panel is equipped with solar trackers with one or two axes), located at any point in the study area, and collecting solar energy directly (excluding local shadows, due to the obstacles imposed by the topography of the site and evaluated from the digital terrain model), and including the diffuse irradiance transmitted through local weather patterns or even the reflected one from the surrounding terrain.

Our calculation algorithm, corresponding to our model designed in the GIS, follows several steps [5]:

Solar Irradiance on a Horizontal Surface. Clearness Index. Since the meteorological data of global irradiance (H) of ground stations are measured by horizontal sensors, they should be related to the correspondent theoretical values (H_o "clear days global horizontal irradiance") as if they were measured outside Earth's atmosphere. These theoretical values H_o depend on intrinsic solar irradiance (or solar constant, G_s = 1.3655 kWm^{-2} [6]) and the Earth-Sun geometry: the distance and reference angles depend on the date of the year, the latitude and solar time (which corresponds to the longitude of the site in every moment of the day; this time period is the reference of hourly, daily, monthly or annual calculation).

Then, with the meteorological data at each point of the region where there are ground stations, we can define the average clearness index K_T (daily, monthly, seasonal, annual), as indicated in equation (1).

$$K_T = \frac{H}{H_o} \tag{1}$$

The spatial interpolation technique of kriging (co-kriging in mountainous areas, because it fits better in these areas with spatial interpolation [4]), extends these clearness indexes, K_T, as a grid, to the whole region studied. This grid, multiplied by the theoretical values H_o of each point of the area, provides the grid coverage, extended to the entire region under study, of global irradiance on a horizontal surface, H.

Solar Irradiance on Tilted or Tracking Surfaces. Beam, Diffuse and Reflected Irradiance. Solar radiation is received in the photovoltaic panel by direct impact of sun rays (beam or direct irradiance H_b, which vanishes when the shadow of an obstacle reaches the panel), by radiation transmitted through the atmosphere (diffuse irradiance H_d, present even with cloud cover) and global irradiance H reflected by the surrounding soil (which is reflected according to the surface albedo).

Different approaches ([7], [8], [9], [10], [11], [12]) are implemented within the GIS, based on available data, in order to determine (at each point of the study area) the direct hourly irradiance and diffuse hourly irradiance of an average day from global horizontal irradiance and clearness index, or with other implemented approaches ([13], [14]), from Linke turbidity index. In a simple isotropic model, we calculate over a horizontal surface the hourly global irradiance I_b, I_d and I, from daily values H_b, H_d and H. Furthermore, hourly global irradiance I is given in equation (2) from hourly direct I_b and hourly diffuse irradiance I_d.

$$I = I_b + I_d \tag{2}$$

Then, the hourly irradiance I_t of an average day, in the plane of a tilted PV panel, is:

$$I_t = I_b \frac{\cos\theta}{\cos\theta_z} + I_d \left(\frac{1+\cos\beta}{2}\right) + I\ \rho \left(\frac{1-\cos\beta}{2}\right) \tag{3}$$

θ is the incidence angle of the solar beams on the PV panel. θ_z is the azimuth. β is the tilted angle of the panel (all mentioned angles, in an hour of an average day). ρ is the albedo of the surrounding ground in a particular season (the albedo can have seasonal changes). With PV panels in solar tracking, solar trigonometry equations ([15]) determine the relationships among angles, hours and days in an average month or year. We compute the tilted irradiance I_t for all hours of the average day or all days of the average month and, summing them, we obtain the daily total (or monthly total) irradiance H_t.

Monthly Converted Electrical Energy per Unit Area of PV panel. Following Evans [16], the electrical energy per unit area (E_P) of photovoltaic panel, converted from solar energy intercepted by the active semiconductor layer of the panel, depends on the performance of the photoelectric conversion that occurs in the semiconductor η_P (that is, on the specific manufacturing technology, such as panels constructed of mono- or poly-crystalline silicon wafers or thin-film technologies like CdTe, $CuInSe_2$ or amorphous silicon, all of them with different module efficiencies η_R at reference temperature T_R, usually 25ºC), and depends on the average temperature reached by the panel T_P in the position of the PV installation (a geographical variable). Thus, E_P is given by equation (4).

$$E_P = \frac{E_{PV}}{S} = \eta_P\ H_t = \eta_R \left[1 - TC_P\left(T_P - T_R\right)\right] H_t \tag{4}$$

where TC_P is the temperature coefficient for module efficiency, in K^{-1}.

T_P is related to the mean monthly ambient temperature T_A on the site (a geographical variable magnitude), through Evans' formula by equation (5).

$$T_P = \frac{NOCT - 20}{800}\left(219 + 832\ K_t\right) + T_A \tag{5}$$

where *NOCT* is the Nominal Operating Cell Temperature that depend on the type of PV module considered, while K_t is the monthly clearness index on the location (K_t is a geographical variable).

We thus calculate GIS maps of the electrical energy E_P, obtained from the PV installation at any point in the region under study, of a particular type of PV panel and semiconductor conversion technology, with fixed-tilt or mobile installations with trackers of one or two axis.

3 Computing Results

The development of the computational model to evaluate the electrical energy generation from solar radiation in a specific area has been applied to the geographic space covered by the region of La Rioja, Spain. The construction of geo-referenced databases necessary for our model, has required GIS mapping of digital terrain model, weather (temperature and radiation) and the uses of the land (to establish the albedo or reflectance of the ground). The grid size of the GIS covers has been set to 5x5 meters.

We have collected and managed meteorological data from official stations available in La Rioja, a station belonging to the Spanish National Network (Agoncillo Airport), with over 60 years of data, and data from 10 stations of the Regional Government Network of La Rioja [17], most of them with over 10 years of meteorological data stored every 15 minutes every day. The list of meteorological stations is geo-referenced in Table 1. The computer model requires the creation of albedo's seasonal coverage in the area of analysis. That is, for each of the seasons we have obtained a reflectance index map (in per unit), showing the change that presents the reflectance of the surface or area of study, covered with natural materials (vegetation, farmland, water) or man-made ones (building materials, roofs, driveways).

Table 1. List of meteorological stations, geo-referenced (UTM 30T)

Station	X (m)	Y (m)	Z (m)
Logroño	543 408	4 700 460	408
San Román	544 789	4 675 898	1 094
Ezcaray	499 552	4 686 914	1 000
Villoslada	527 583	4 663 694	1 235
Ocón	563 272	4 682 107	1 105
Yerga	584 943	4 666 139	1 101
Ventrosa	512 665	4 669 180	1 565
Moncalvillo	531 525	4 686 160	1 495
Calahorra	582 843	4 683 014	350
Aguilar	585 428	4 646 588	752

We have included, in the GIS platform [18], a database of PV panel technologies with relevant technical information (Table 2) to construct maps of electrical energy generation produced from PV panels at each point of the study area. While performing the calculations we introduce the angle data associated with fixed-tilt panels or solar trackers with one or two axes.

Table 2. Technical data of PV panel technologies used in the GIS platform.

PV semiconductor type	η_R (%)	*NOCT* (ºC)	TC_P (ºC^{-1})
Mono-crystalline Silicon	13.0	45	0.40
Poly-crystalline Silicon	11.0	45	0.40
Amorphous Silicon	5.0	50	0.11
CdTe	7.0	46	0.24
CIS	7.5	47	0.46

One of the many results obtained are shown in Fig. 1, which gives the map of the region studied (grid of 5x5 meters), with coverage of daily electrical energy generation obtained per square meter of PV mono-crystalline silicon panels, with solar trackers of two axes. We used the annual solar resource available in La Rioja as starting information (daily average annual irradiance calculated by the GIS platform) from regional meteorological data. Furthermore, in Fig. 1, note microclimate effects (eastwards and westwards clearer spots).

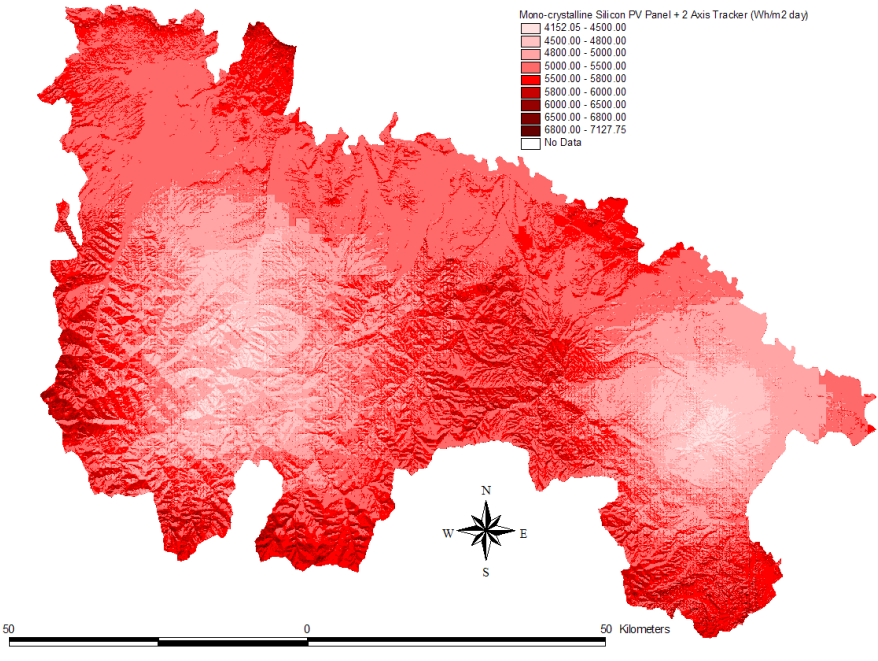

Fig. 1. Daily electrical energy generation (Wh/m^2) in La Rioja

Using the large amounts of obtained maps, we can compare the most efficient PV technologies at each site, taking into account not only the present solar resource, but also those local peculiarities (local microclimates, average temperatures, shadows of obstacles, albedos, etc.) in a particular point of the region under study. Thus, the GIS model of this paper is useful for selecting the geographical locations with the most suitable PV technology to achieve the highest amount of solar energy converted into electricity. Furthermore, such GIS model can be applied to choose the most suitable PV technology for a specific site (Mono- or Poly-crystalline Silicon, Amorphous Silicon, CdTe, CIS semiconductor type), or it can be applied to determine the most suitable solar tracking technology for the same specific site (one horizontal- or vertical-axis, two-axis solar trackers), and the most suitable tilt angles (oriented to the South, oriented eastwards or westwards).

4 Conclusions

This paper presents an novel and useful GIS model for evaluation of electric power generation from the solar resource available in a given geographical region, through the creation of comprehensive geographical database in a Geographical Information System (GIS). The model takes into account the geometry of the solar photovoltaic panels both fixed and mobile, including the influence of the shadows due to geographical constraints. Furthermore, such model considers the diffuse irradiance source and its influence to calculate the value of global irradiance, including the preeminence of the albedos associated with each point on the surface of the region under study. Unlike other models, our GIS model presents the spatial and temporal variability of the albedo at each point, with different spatial coverage per season (spring, summer, autumn and winter).

Since the model can be used at any resolution, is well suited to assess (with higher resolution with respect to other models) solar resources in rural areas where isolated photovoltaic applications are technically and economically feasible solutions mainly due to small power demands involved and difficult access to power distribution networks (due to significant economic costs associated with the installation of electric power lines needed to achieve these distribution networks). These rural areas are typically prevalent in countries where the solar resource is easily available, usually in subtropical climatic zone. In developed countries this type of isolated photovoltaic application can be used to facilitate the development of remote rural areas of high tourist potential.

In urban areas, the photovoltaic systems can be easily connected to power distribution networks, where they can dump clean electricity from renewable sources, and minimizing the consumption of electricity from conventional, non-renewable sources. Furthermore, it is also common in developed countries (for example, in Spain) the requirement of energy saving measures through the acquisition of solar energy for home consumption. Then, those requirements are mandatory when designing and constructing new buildings (whether houses, factories, or shopping centers, etc.). The model implemented in GIS, with a high resolution, provides a useful tool for proprietors, architects or development agencies, when evaluating the available solar power on sites where buildings will be located.

Acknowledgments. The authors would like to thank the "Ministerio de Ciencia e Innovación" of the Spanish Government for supporting this research under the Project ENE2009-14582-C02-02.

References

1. Schroedter-Homscheidt, M., et al.: The ESA - ENVISOLAR Project: Experience on the Commercial Use of Earth Observation Based Solar Surface Irradiance Measurements for Energy Business Purposes. In: Dunlop, E., Wald, L., Šúri, M. (eds.) Solar Energy Resource Management for Electricity Generation from Local Level to Global Scale, pp. 111–124. Nova Science Publishers, New York (2006)
2. Dumortier, D.: Use of Satellite Images to Produce Solar Radiation and Daylight Information: Experience from Three European Projects. In: Dunlop, E., Wald, L., Šúri, M. (eds.) Solar Energy Resource Management for Electricity Generation from Local Level to Global Scale, pp. 11–28. Nova Science Publishers, New York (2006)
3. Cebecauer, T., Huld, T., Šúri, M.: Using high-resolution digital elevation model for improved PV yield estimates. In: 22nd European Photovoltaic Solar Energy Conference, pp. 3553–3557. WIP Renewable Energies, Milano (2007)
4. D'Agostino, V., Zelenka, A.: Supplementing Solar Radiation Network Data by Co-Kriging with Satellite Images. International Journal of Climatology 12, 749–761 (1992)
5. Duffie, J.A., Beckman, W.A.: Solar Engineering of Thermal Processes. Wiley-Interscience, New York (2006)
6. Fröhlich, C.: Solar Irradiance Variability since 1978. Space Science Reviews, 1–13 (2006)
7. Iqbal, M.: An Introduction to Solar Radiation. Academic Press, Orlando (1983)
8. Liu, B.Y.H., Jordan, R.C.: The Interrelationship and Characteristic Distribution of Direct, Diffuse and Total Solar Radiation. Solar Energy 4(3), 1–19 (1960)
9. Collares Pereira, M., Rabl, A.: The Average Distribution of Solar Radiation Correlations between Diffuse and Hemispherical and between Daily and Hourly Insolation Values. Solar Energy 22(2), 155–164 (1979)
10. Erbs, D.G., Klein, S.A., Duffie, J.A.: Estimation of the Diffuse Radiation Fraction for Hourly, Daily and Monthly Average Global Radiation. Solar Energy 28(4), 293–304 (1982)
11. Hottel, H.C.: A Simple Model for Estimating the Transmittance of Direct Solar Radiation through Clean Atmospheres. Solar Energy 18(3), 129–134 (1976)
12. Klein, S.A., Theilacker, J.C.: An Algorithm for Calculating Monthly Average Radiation on Inclined Surfaces. Journal of Solar Energy Engineering 103, 29–33 (1981)
13. Kasten, F.: The Linke Turbidity Factor Based on Improved Values of the Integral Rayleigh Optical Thickness. Solar Energy 56, 239–244 (1996)
14. SoDa: Solar Radiation Data, `http://www.soda-is.com/eng/index.html`
15. Braun, J.E., Mitchell, J.C.: Solar Geometry for Fixed and Tracking Surfaces. Solar Energy 31(5), 439–444 (1983)
16. Evans, D.L.: Simplified Method for Predicting Photovoltaic Array Output. Solar Energy 27(6), 555–560 (1981)
17. de La Rioja, G.: Meteorología: Estaciones del Gobierno de La Rioja, `http://ias1.larioja.org/estaciones/estaciones/mapa/portada/index.jsp`
18. ArcGIS® v.9 Software, Environmental Systems Research Institute, Inc. (Esri), Redlands, California (2005)

Multi-objective Model for Optimal Integration of Dispersed Generation and Energy Storage Systems in Electric Power Distribution Networks Expansion

I.J. Ramírez-Rosado[1] and E. García-Garrido[2]

Electrical Engineering Department
[1] University of Zaragoza, Spain
[2] University of La Rioja, Spain
ignacio.ramirez@unizar.es

Abstract. This paper presents a multi-objective model for planning studies of power distribution systems. The methodology determines optimal economic costs, "pollution", reliability, and power losses in electric power distribution networks expansion for optimal integration of alternative dispersed generation sources and energy storage systems. The proposed optimal multi-objective planning model can be very useful in determining the most satisfactory selection of investments to meet new energetic, environmental and electric service quality targets from the point of view of new energy policies. This model was tested on a part of the electric power distribution system of La Rioja (Spain).

Keywords: dispersed generation, energy storage, electric power distribution networks, optimal planning.

Nomenclature

γ_s set of network nodes associated with future substations;

γ_a set of network nodes associated with future energy storage units;

γ_l set of proposed routes, between nodes, to build future feeders;

γ_{sc} set of proposed nodes associated with future conventional substations;

γ_{Ec} set of network nodes associated with existing conventional substations;

N_n set of proposed feeder sizes;

γ_{El} set of existing feeders, between nodes, in the existing distribution system;

γ_n set of the nodes of the distribution system;

γ_{sr} set of network nodes associated with renewable (non-conventional) substations;

$(If_{is})_{t,n}$ investment cost associated with a future substation in node i for a type of plant (t) (conventional, mini-hydraulic, wind turbine or photovoltaic plants) with a power size (n);

D. Jin and S. Lin (Eds.): Advances in Mechanical and Electronic Engineering, LNEE 177, pp. 497–504.
springerlink.com

$(If_i)_{p,e}$ investment cost associated with a future energy storage system in node *i* with a power size (*p*) and energy storage capacity (*e*);

$(If_{i,j})_N$ investment costs associated with a future feeder between nodes *i* and *j* with a feeder size N;

C_i energy supplied from a substation in node *i*;

$(Iv_{i,j})_N$ variable cost constant, associated with a future feeder between nodes (*i,j*) with a size *N*;

$(Iv_{i,j})_E$ variable cost constant, associated with an existing feeder between nodes (*i,j*);

Iv_{is} operational cost constant for a substation in node *i*;

$(F_{i,j})_h$ power flow, in kVA, through the route (*i,j*) in the period of time *h*;

D_h duration of the period of time *h*, *h* = 1, 2, 3;

$(Y_i)_{t,n}$=1 if a substation (type *t*, size *n*) is built in node *i*. Otherwise, this variable is equal to 0;

$(Y_i)_{p,e}$=1 if an energy storage system of power capacity *p* and energy storage capacity *e* is built in node *i*. Otherwise, this variable is equal to 0;

$(Y_{i,j})_N$ = 1 if a feeder of size *N* is built on the route $(i, j) \in \gamma_l$. Otherwise, this variable is equal to 0;

K_{ij} constant for the route (*i,j*) depending on the feeder resistance and the rated voltage;

$(F_{i,j})_{\max}$ peak power flow in kVA, on the route (*i, j*);

$(F_{i,j})_F$ average power flow, in kVA, through the route $(i, j) \in \gamma_l$;

$(F_{i,j})_E$ average power flow, in kVA, through the route $(i, j) \in \gamma_{El}$;

$T_{i,j}$ suitable constant that depends on the failure rate of the feeder on the route (*i,j*), the repair rate, and the power factor;

$H_{i\max}$ power size of the conventional substation in node *i*;

G_i peak power demand in node *i*;

H_{ri} power generated, in kVA, by a renewable (non-conventional) energy source in node *i* during the first period;

H_{b1i}, H_{b2i}; power stored, in kVA, by a storage unit in node *i* during the first and second periods respectively;

H_{b3i} power supplied, in kVA, by a storage unit in node *i* during the third period;

$H_{c1i}, H_{c2i}, H_{c3i}$; power supplied, in kVA, by a conventional substation in node *i* during the first, second and third periods, respectively;

t_v constant depending on the load demand curve ($0 \le t_v \le 1$);

$(S_{ij})_N$ power capacity limit associated with the route $(i, j) \in (\gamma_l \cup \gamma_{El})$ for feeder size N;

H_{rk} power generated by a renewable (non-conventional) energy source in node *k*;

$H_{k\max}$ power size of the renewable (non-conventional) substation in node *k*.

1 Introduction

If an electric power distribution network must be expanded for supplying electricity to new consumers, then such expansion should be optimal. This kind of optimization was traditionally carried out by pure economic criteria, but environmental concerns, the quality of the electric service, the integration of new technologies into lower voltage levels, etc. require taking into account new technical and social considerations [1,2,3]. Nevertheless, some of the new alternative dispersed generation sources (i.e., wind energy, biomass, photovoltaic generation, cogeneration, etc.) are not competitive yet in strictly economic terms but they offer other advantages [4,5,6,7]; thus it is interesting to study the economical, energetic and environmental aspects for the integration of these different types of small dispersed generation sources and energy storage systems in electric distribution networks.

This paper presents a multi-objective methodology with four optimization objectives for planning the expansion of an existing electric power distribution network, considering that such network can include (in the present or in the future) new dispersed generation sources and/or energy storage systems. These four optimization objectives are: minimization of the economic costs, both fixed and variable ones; minimization of the network energy losses; minimization of the "pollution"; and maximization of the reliability of the distribution network.

In dealing with such a complex problem, it is necessary to use meta-heuristic resolution methods. The genetic algorithms [3] have been selected for the multi-objective optimization of distribution network expansion. In summary, this paper presents a useful tool for the multi-objective planning of distribution networks expansions considering economic, technical and social criteria.

2 Multi-objective Planning Model

The problem to be solved is the optimal expansion of an existing distribution network. This problem is a multi-objective optimization one that leads to the minimization of several objective functions subject to various technical constraints. Thus the electric power distribution network expansion can be stated as:

$$\text{Min } [\, O_1(x, y), O_2(x, y), O_3(x, y), O_4(x, y)], \tag{1}$$

Subject to $(x, y) \in X = \{(x, y) \mid g_c(x, y) \{\geq,=,\leq\} 0,\ g_c \in C\}$ where $O_i(x, y)$ are the objective functions, $g_c(x, y)$ are the technical constraints and C is the set of the constraints.

In order to solve the multi-objective planning model, a multi-objective optimization methodology based on the optimization by goals is used. This methodology solves a mono-objective optimization of the economic cost function, and the other three objective functions are treated by additional mathematical constraints. Then, the multi-objective optimization model is solved using genetic algorithms. The multi-objective optimization methodology is stated as:

$$\text{Min } [\, O_1(x,y)] \tag{2}$$

Subject to $(x, y) \in X = \{(x, y) \mid g_c(x, y)\{\geq,=,\leq\}\ 0, \forall\ g_c \in C\}$; $(x, y) \in X = \{(x, y) \mid O_2(x, y) \leq \varepsilon_{ppl}\}$; $(x, y) \in X = \{(x, y) \mid O_3(x, y) \leq \varepsilon_{pe}\}$; $(x, y) \in X = \{(x, y) \mid O_4(x, y) \leq \varepsilon_{re}\}$ where ε_{ppl}, ε_{pe} and ε_{re} are parameters values defined by the planner from his/her experience and professional point of view. The variation of the parameter values suitably, successively and systematically leads to exploring the set of non-dominated solutions (Pareto frontier) of the multi-objective planning model.

In this case, the four objective functions are:

1.- $O_1(x,y)$, objective function of the economic costs (€). This includes the fixed costs of the future feeders, the future substations and the future energy storage units, as well as the variable costs of the future and existing feeders, and the operational costs (associated with energy conversion costs from conventional generation plants) of the future and existing conventional substations. It can be stated as:

$$\sum_{i \in \gamma_s} (If_{is})_{t,n} (Y_i)_{t,n} + \sum_{(i,j) \in \gamma_l} \sum_{N \in N_n} (If_{i,j})_N \ (Y_{i,j})_N + \sum_{i \in \gamma_a} (If_i)_{p,e} (Y_i)_{p,e} + \sum_{i \in \gamma_{sc}} Iv_{is} \ C_i + \sum_{(i,j) \in \gamma_l} (Iv_{i,j})_N \sum_{\mathrm{h}} (F_{i,j})_h^2 D_h + \sum_{i \in \gamma_{Ec}} Iv_{is} \ C_i + \sum_{(i,j) \in \gamma_{El}} (Iv_{i,j})_E \sum_{\mathrm{h}} (F_{i,j})_h^2 \ D_h \tag{3}$$

2.- $O_2(x,y)$, objective function of peak power losses of the feeders (kW). It can be stated as:

$$\sum_{(i,j) \in \gamma_l} K_{ij} (F_{i,j})^2_{\max} + \sum_{(i,j) \in \gamma_{El}} K_{ij} (F_{i,j})^2_{\max} \tag{4}$$

3.- $O_3(x,y)$, objective function of "pollutant energy" (kWh/year). The energy supplied by conventional substations is used in the "pollution" objective function, i.e.:

$$\sum_{i \in (\gamma_{sc} \cup \gamma_{Ec})} C_i \tag{5}$$

4.- $O_4(x,y)$, objective function of reliability (kWh/year). The non-supplied expected energy is considered as a reliability objective function of the distribution system. It can be stated (for radial distribution network) as:

$$\sum_{(i,j) \in \gamma_l} T_{i,j} (F_{i,j})_F + \sum_{(i,j) \in \gamma_{El}} T_{i,j} (F_{i,j})_E \tag{6}$$

As mentioned above, the four objective functions are minimized subject to the following technical constraints:

I.- Technical constraints associated with power balance conditions. These constraints are applied to three different periods.

- for the first period (h=1)

$$\left[H_{ri} + H_{c1i} - H_{b1i} + \sum_j ((F_{i,j})_1 - (F_{j,i})_1) - t_v \ G_i \right] = 0 \ \ \forall i \in \gamma_n \tag{7}$$

- for the second period (h=2)

$$\left[H_{c2i} - H_{b2i} + \sum_j ((F_{i,j})_2 - (F_{j,i})_2) - t_v G_i \right] = 0 \quad \forall i \in \gamma_n \tag{8}$$

- for the third period (h=3)

$$\left[H_{c3i} + H_{b3i} + \sum_j ((F_{i,j})_3 - (F_{j,i})_3) - G_i \right] = 0 \quad \forall i \in \gamma_n \tag{9}$$

H_{b1i}, H_{b2i} and H_{b3i} are selected to achieve a resulting load demand with a load factor equal to 1 in node i (by combining the supplied power from the energy storage unit with the initial power demand in such node);

II.- The energy balance in the nodes with storage systems must be observed, considering their efficiency. Thus,

$$\eta (H_{b1i} D_1 + H_{b2i} D_2) - H_{b3i} D_3 = 0 \tag{10}$$

where η is the efficiency.

III.- A multi-objective planning solution has associated a radial operation state.

IV.- The power capacity limits of the feeders must be observed in all the periods under study, as well as the ones of the substations.

$$(F_{i,j})_1, (F_{i,j})_2, (F_{i,j})_3 \le (S_{ij})_N \quad \forall i.j \in (\gamma_l \cup \gamma_{El}) \tag{11}$$

$$H_{c1i}, H_{c2i}, H_{c3i} \le H_{i\max} \quad \forall i \in (\gamma_{sc} \cup \gamma_{Ec}) \tag{12}$$

$$H_{rk} \le H_{k\max} \quad \forall k \in \gamma_{sr} \tag{13}$$

3 Computational Results

The expansion model and the proposed multi-objective optimization techniques have been successfully applied in the study of the optimal expansion of an existing 13.2 kV electric power distribution network of La Rioja (Spain). The data were provided by a Spanish electric utility. Fig. 1 shows the electrical representation of such existing power network as well as the proposed routes to build future feeders (with four proposed feeder sizes, LA30, LA 56, LA80, LA 110) and the proposed locations to build future dispersed generation sources and energy storage systems. Furthermore, the proposed future feeders can be selected as reserve feeders in order to improve the reliability of the power network. Furthermore, t_v= 0.5, power factor = 0.85, $D_1+D_2+D_3=D$, D_1= 0.35 D and D_3= $D/2$.

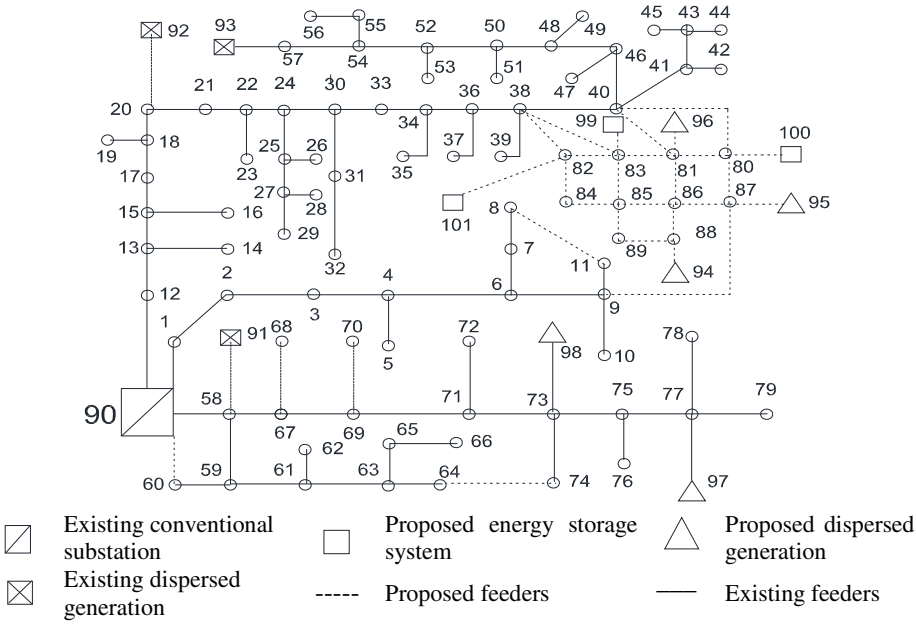

Fig. 1. Representation of the existing distribution network and proposed future routes, dispersed generation sources and energy storage systems

In the node 90 there is a conventional 12.5 MVA substation. The existing dispersed generation sources (mini-hydraulic) are in the nodes 91, 92 and 93 (220 kVA, 76 kVA and 115 kVA, respectively). The future dispersed generation sources are proposed to be built in the nodes 94, 95 (wind generators), 96, 97 (mini-hydraulic generators) and 98 (photovoltaic generators). The proposed sizes of these dispersed generation sources are 75, 100 and 150 kVA. The proposed power size and energy capacity of the energy storage systems (nodes 99, 100 and 101) are 50 kW and 600 kWh, respectively. Table 1 shows the power demand requirements (kVA) in the network nodes.

Table 1. Power demand requirements

Node	Load	Node	Load	Node	Load	Node	Load	Node	Load	Node	Load
2	*51.3*	*19*	*33.6*	*39*	*18.3*	*56*	*18.0*	*72*	*63.3*	*83*	*200*
3	*128.3*	*23*	*134.3*	*42*	*45.8*	*57*	*44.4*	*74*	*63.3*	*84*	*200*
5	*59.9*	*26*	*0.8*	*44*	*46.4*	*60*	*63.3*	*76*	*63.3*	*85*	*200*
8	*27.9*	*29*	*118.5*	*45*	*11.6*	*62*	*63.3*	*78*	*63.3*	*86*	*200*
10	*59.9*	*31*	*134.3*	*47*	*111.0*	*64*	*63.3*	*79*	*63.3*	*87*	*200*
11	*149.7*	*32*	*83.9*	*49*	*22.2*	*66*	*63.3*	*80*	*200*	*88*	*200*
14	*1.0*	*35*	*33.6*	*51*	*177.6*	*68*	*63.3*	*81*	*200*	*89*	*200*
16	*116.6*	*37*	*6.6*	*53*	*11.1*	*70*	*63.3*	*82*	*200*		

A total of 41 non-dominated solutions or plans were identified for the multi-objective problem. The optimal distribution network topologies were obtained, as well as the optimal values of the objective functions. Some results obtained are shown in Table 2.

Table 2. Resulted Plans

Plan Number	$O_1(x,y)$ x 10^3	$O_2(x,y)$	$O_3(x,y)$ x 10^3	$O_4(x,y)$ x 10^3	feeders	reserve feeders	dispersed generation sources	energy storage systems
1	*610.1*	*293.63*	*23183*	*86.0*	*92*	*0*	*3*	*0*
2	*1194.8*	*289.55*	*22401*	*81.1*	*96*	*0*	*7*	*0*
3	*1195.1*	*289.92*	*22401*	*81.5*	*96*	*0*	*7*	*0*
4	*1344.3*	*290.29*	*22336*	*81.8*	*96*	*0*	*7*	*0*
5	*1344.6*	*289.55*	*22206*	*80.7*	*97*	*0*	*8*	*0*
6	*1495.0*	*289.92*	*22184*	*81.1*	*97*	*0*	*8*	*0*
7	*1641.9*	*289.56*	*22076*	*80.1*	*97*	*0*	*8*	*0*
8	*1943.6*	*293.05*	*21945*	*79.8*	*97*	*0*	*8*	*0*
9	*2683.6*	*289.58*	*21620*	*78.0*	*92*	*0*	*8*	*0*
10	*612.5*	*289.66*	*23183*	*43.7*	*92*	*1*	*3*	*0*
11	*615.2*	*292.64*	*23183*	*43.0*	*92*	*1*	*3*	*0*
12	*617.0*	*289.66*	*23183*	*39.7*	*92*	*1*	*3*	*0*
13	*710.1*	*288.43*	*23183*	*29.8*	*92*	*3*	*3*	*0*
14	*791.3*	*289.66*	*23183*	*26.8*	*92*	*8*	*3*	*0*
15	*1181.5*	*259.90*	*23307*	*76.0*	*95*	*0*	*3*	*3*
16	*1196.3*	*258.52*	*23307*	*71.1*	*95*	*0*	*3*	*3*
17	*1376.1*	*293.15*	*22401*	*26.3*	*96*	*7*	*7*	*0*
18	*1201.1*	*289.92*	*22401*	*40.1*	*96*	*1*	*7*	*0*
19	*1202.6*	*285.95*	*22401*	*37.9*	*96*	*1*	*7*	*0*
20	*1294.5*	*285.74*	*22401*	*29.7*	*96*	*3*	*7*	*0*
21	*1379.6*	*285.95*	*22401*	*26.3*	*96*	*9*	*7*	*0*
22	*1947.1*	*287.82*	*21945*	*69.2*	*97*	*0*	*8*	*0*
23	*1949.6*	*293.05*	*21945*	*41.6*	*97*	*1*	*8*	*0*
24	*1950.4*	*286.38*	*21945*	*37.8*	*97*	*1*	*8*	*0*
25	*2043.9*	*289.64*	*21945*	*29.9*	*97*	*3*	*8*	*0*
26	*2140.5*	*295.09*	*21945*	*26.3*	*97*	*10*	*8*	*0*
27	*2837.7*	*285.82*	*21598*	*69.9*	*97*	*0*	*8*	*0*
28	*2841.2*	*290.81*	*21598*	*42.4*	*97*	*1*	*8*	*0*
29	*2842.4*	*286.85*	*21598*	*39.7*	*97*	*1*	*8*	*0*
30	*2960.4*	*286.79*	*21598*	*29.8*	*97*	*7*	*8*	*0*
31	*3020.2*	*286.98*	*21598*	*26.3*	*97*	*9*	*8*	*0*
32	*1920.2*	*259.08*	*22460*	*67.7*	*99*	*0*	*7*	*3*
33	*1897.4*	*259.96*	*22460*	*70.3*	*99*	*0*	*7*	*3*
34	*1561.2*	*274.71*	*22484*	*82.4*	*98*	*0*	*7*	*2*
35	*1378.9*	*277.40*	*22443*	*77.4*	*97*	*0*	*7*	*1*
36	*1477.9*	*259.08*	*22916*	*70.0*	*97*	*0*	*5*	*3*
37	*1475.2*	*259.97*	*22916*	*74.0*	*97*	*0*	*5*	*3*
38	*1903.4*	*259.96*	*22460*	*35.1*	*99*	*1*	*7*	*3*
39	*1902.7*	*264.17*	*22460*	*35.5*	*99*	*1*	*7*	*3*
40	*1483.9*	*259.08*	*22916*	*33.8*	*97*	*1*	*5*	*3*
41	*1459.0*	*262.25*	*22916*	*34.8*	*97*	*1*	*5*	*3*

These computer results, in terms of optimal economical costs, improvement of the power network losses, optimal reductions of pollution, and increase of the distribution system reliability, provide very useful information for the planners in order to select the optimal investments according to new energy policies and laws. From the computer results, the decrease in the “pollutant energy” has the largest impact on the economical costs of the distribution network due to the building of new renewable energy sources. The building of the larger feeder sizes and reserve feeders increase

the reliability of the electric power distribution network. Furthermore, the building of energy storage systems and new renewable energy sources reduces the peak power losses.

4 Conclusions

New energy trends suggest that there will be an increment in the use of alternative generation systems (and small energy storage systems) in lower voltage levels, impacting the primary electric power distribution networks. It is essential to study the integration of these new generation and storage systems into the distribution networks in order to achieve the environmental and the electric service quality targets from the point of view of the new energy policies. This paper presents a multi-objective planning model to study the impacts of these new systems on the expansion of existing distribution networks as well as an illustrative example of application to a electric power distribution network of the region of La Rioja (Spain). The optimal planning problem is a complex one due to the very large number of involved economical, technical and environmental factors. Therefore, optimal multi-objective planning models (similar to the one in this paper) can be very useful in determining the most satisfactory selection of investments to meet new technological, social and legislative trends in the field of the electric power distribution networks.

Acknowledgments. The authors would like to thank the "Ministerio de Ciencia e Innovación" of the Spanish Government for supporting this research under the Project ENE2009-14582-C02-02.

References

1. Barin, A., Pozzatti, L.F., Canha, L.N., Machado, R.Q., Abaide, A.R., Arend, G.: Multi-objective analysis of impacts of distributed generation placement on the operational characteristics of networks for distribution system planning. Electrical Power and Energy Systems 32, 1157–1164 (2010)
2. Lakshmi Devi, A., Subramanyam, B.: Optimal DG Unit Placement for Loss Reduction in radial distribution System- A case Study. (ARPN) Journal of Engineering and Applied Sciences 2(6) (2007)
3. Ramírez-Rosado, I.J., Bernal-Agustín, J.L.: Reliability and Costs Optimization for Distribution Networks Expansion Using and Evolutionary Algorithm. IEEE Transactions on Power Systems 16(1), 111–118 (2001)
4. Baker, P.P., de Mello, R.W.: Determining the Impact of Distributed Generation on Power Systems: Part 1- Radial Distribution Systems. In: Proceedings of the IEEE PES Summer Meeting, Seattle (USA), vol. 3, pp. 1645–1656 (2000)
5. Choi, J.-H., Kim, J.-C.: Network Reconfiguration at Power Distribution System with Dispersed Generations for Loss Reduction. In: Proceedings of the IEEE PES Winter Meeting, vol. 4, pp. 2363–2367 (2000)
6. Griffin, T., Tomsovic, K., Secrest, D., Law, A.: Placement of Dispersed Generations Systems for Reduced Losses. In: Proceedings of the 33rd Hawaii International Conference on Systems Sciences, Maui, Hawaii, pp. 1–9 (2000)
7. Daly, P.A., Morrison, J.: Understanding the Potential Benefits of Distributed Generation on Power Delivery Systems. In: Rural Electric Power Conference, A2-1–A2-13 (2001)

A Method of Remote Interactive Control in Electricity SCADA System Based on Internet

Guoling Liu*, Zhenyu Yang, and Wenfeng Jiang

School of Information, Shandong Polytechnical University, Jinan, China
maindollar@126.com

Abstract. Electricity SCADA system faces a series of complex requirements to be studied and analyzed carefully.This paper firstly investigates the importance of remote control interface on electricity SCADA system, then propose a new scheme for remote control based on Internet. This paper introduces the details of RCI status in SCADA system and general RCI structure. The remote control center's access process and software implement with IEC protocol is given. The web technology makes the system presenting data simply and being accessed at random location. Finally, this paper analyze the security in such a system based on Internet and discussed the security measures.

Keywords: SCADA, Remote Control, Web Application.

1 Introduction

The demands for remote engineering applications have been increased due to the advancements in information technology tools which benefits with friendly access, near real-time operation, visual access and efficient utilization of available bandwidth. The same techniques are used to demonstrate embedded control applications with an additional server to handle the programming of the micro controller remotely [1]. The browser-server architecture is used in these applications with the remote hardware. The hyper text markup language (HTML) pages are created for each control applications which accessed through the Internet.

Supervisory Control and Data Acquisition (SCADA) is a term used to describe the technology that enables a user to collect data from one or more distant facilities and send limited control instructions to those facilities [2]. Traditional SCADA systems are similar to DCS (Distributed Control Systems) in that they are both used in process control and monitoring. However, the predominant problems are distance of communication and data latency. With DCS systems, the field data gathering or control units are usually located within a more confined area (e.g. factory, refinery, and power plant) and the communications are usually done using high-speed communications medium such as a reliable and high speed local area network (LAN). Traditional SCADA systems are based on IEC (International Electrical Commission) 61970 and connected only in a private local area network. Now, web technology is

* Biographies: Guoling Liu, born in 1973, female, Jinan people of Shandong Province, association professor, Master's degree, research field in data collection and processing.

D. Jin and S. Lin (Eds.): Advances in Mechanical and Electronic Engineering, LNEE 177, pp. 505–510.
springerlink.com

commonly used in industry engineering applications. The trend in most systems is that they are connected through the Internet. Web services components provide more standard and open interfaces for the information sharing and interoperability among application systems of power enterprises.

With the expanding of electric power market, it is a difficult problem to ensure the high quality and safety of an electric power. As a main part of automation system in converter station, electricity SCADA system faces a series of complex requirements to be studied and analyzed carefully. This paper proposes a new method of remote control based on Internet in electricity SCADA system. The web technology makes the system presenting data simply and being accessed at random location. At last, this paper analyze the security in such a system based on Internet and discussed the security measures.

2 RCI Structure

2.1 RCI Status in Automation System

The demand for power keeps growing at a big scale and rapid speed never imagined in the past throughout the world. For strong demands for development with industry and resident daily life converter stations locate far away from the dispatch center. At the same time, demanding remote and convenient operations as well as obligations to reduce transmission loss have to be met.。

A SCADA system in a high voltage direct current(HVDC) is an industrial measurement and control system which includes a central host or several master terminal units(MTU) , one or more field data gathering and control units (remote terminal units or RTUs), and a collection of standard and/or custom software used to monitor and control the remote field data elements.

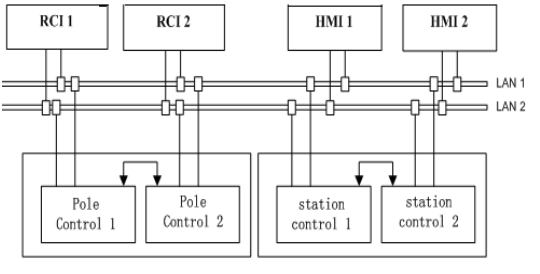

Fig. 1. RCI in electricity automation control system

The traditional automation system in HVDC Transmission Project includes 4 levels: equipment level, field level, Control & Protection level and SCADA level. RCI (Remote Control Interface) and HMI (Human Machine Interface) are located in the same level in parallel, that is, in SCADA level. The Control & Protection level and SCADA level in HVDC automation control system are showed in Fig. 1 [3] .

2.2 General Structure of RCI System

The RCI is the link between the Control & Protection systems in the HVDC converter stations and the dispatch center. It is in charge of exchanging telecontrol information between converter stations and the dispatch center. The RCI communicates with the Station Control and Pole Control via the station LAN, receives monitoring information (binary states, measured values) from the control stations, and sends control requests (binary commands and analog setpoints) to Station Control and Pole Control systems. Fig. 2 shows the overall structure of RCI system [4].

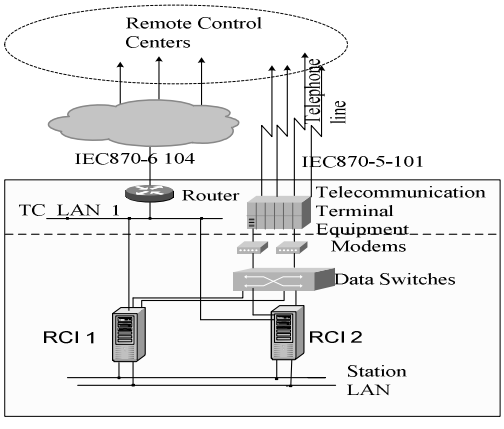

Fig. 2. The general structure of RCI system

Each of the links among the converter stations and the dispatch center consists of a high-speed network data link and two serial telecontrol links. The remote communication with the dispatch center is done by means of the following protocols: gh-speed/ network protocol and Serial telecontrol protocol.

For data exchange with the dispatch center via the serial telecontrol lines, the standard IEC 60870-5-101 is used. This standard describes an asynchronous and byte-oriented serial data transmission protocol.

Each RCI/Gateway unit has its individual IP address. The gateway computers in the dispatch center act as master stations, i.e. it has the responsibility to establish a connection to RCI A or B at the converter station. The gateway which is actually on duty, first tries to establish connection to one of the converter station's RCI. If this connection fails, it tries to connect to the other RCI. At any time, not more than one connection could be established. However, the control center has the responsibility to select RCI A or B unit for the connection. The stand-by gateway could not send any messages nor attempt to establish connections.

The monitoring information types used by the HVDC Control & Protection system are mapped as ASDU types, transmission modes and interrogation groups etc. When the RCI receives any ASDU type which is not supported, the ASDU would be discarded without causing any error. A negative confirmation is returned to the initiator.

3 Remote Control Center

With the development of industry electric power enterprises expands unceasingly. The maintenance in remote areas, safe operations and efficiency needs more convenient operating mode.

For remote access in random location and time it is necessary to introduce Internet technology and build the web server as remote control center. In remote control center applications should be developed for client or browser access by any way of logging on. Connection SCADA system to the Internet can bring a lot of advantages in terms of command and data viewing.

In MTU web server applications can be developed so as to convey commands to special MTU by IP address or domain. The remote control center with web server is showed in Fig. 3.

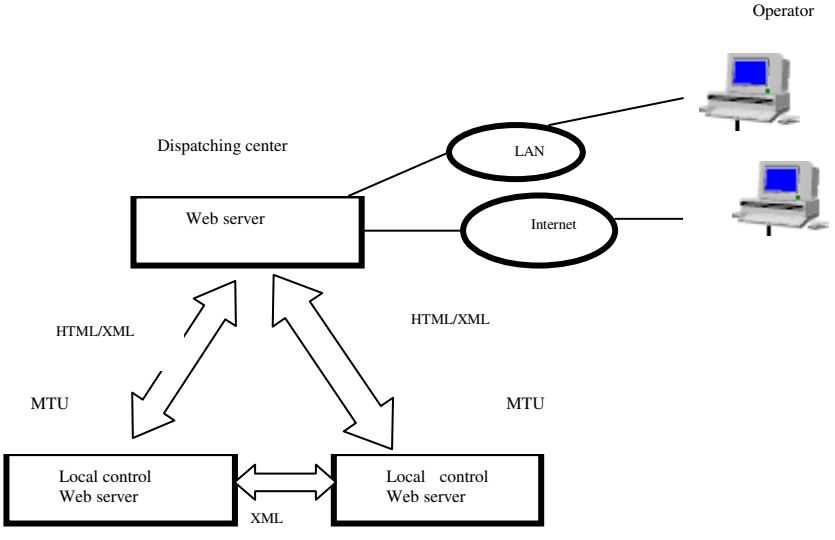

Fig. 3. The web access process based on Internet

4 Software Implement

4.1 IEC Protocol Module

Fig. 4 shows the most important parts of the RCI software structure as well as the data flow [5]. Each module in Fig. 4 is simply described as follows:

FE module: front end module, exchange data with Control & Protection systems through SCADA LAN, meanwhile ,exchange data with protocol server: IEC104 Server and IEC101 Server.

M/S control: the module to control master/slave, determine master or slave role of itself; Telecontrol Interface: in FE module, interface to IEC104 Server and IEC101

Server; Interface for FE: in IEC104 Server and IEC101 Server, interface to FE module; Interface for HMI: software interface to HMI, used to be provoked by HMI.

Process Data: store current value of points to be sent to dispatch center, the basic structure is as the following table 3.

Configure Data: database for configuration information, the basic structure is as following Table 4. The online and the offline section are linked together via the point identifier. Protocol Server: protocol stack. For each connection the server has its own server task.

4.2 Distributed Programming

RCI software system is a big scale distributed system, some modules of which may run in different machines. This needs distributed programming based on ICE middle ware technology [6]. The ICE (Internet Communications Engine)is an object-oriented middle ware that provides object-oriented Remote Procedure Call, grid computing, and Publish/subscribe functionality developed by ZeroC and dual-licensed under the GNU GPL and a proprietary license. It supports C++, Java, .NET-languages (such as C# or Visual Basic), Objective-C, Python, PHP, and Ruby on most major operating systems such as Linux, Solaris, Windows and Mac OS X. ICE client/browser and server have the logical internal structure shown in following Fig.4.

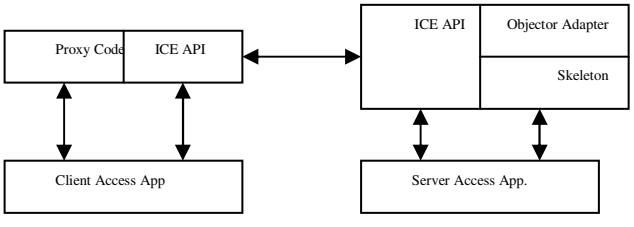

Fig. 4. The constitution structure of ICE

4.3 Security

Many operators hold back on connecting SCADA system to the Internet because the Internet is highly open and less safer. But there are so many advantages connecting SCADA systems through the Internet. Java and XML can improve the security and performance. In addition, we can adopt data mining technology to analyzing system logs so as to rule out the dangerous interference.

In SCADA system the threats could take place after an attacker gains user access rights and performs actions which look very legitimate, but in fact which can disrupt the control process. It is possible to detect such behavior by using data mining technology to analyze user actions in SCADA system logs. In data mining we can get security pattern from association rules. We can use security patterns to analyze the potential attacks against it and evaluate secure systems.

Package java.security provides the classes and interfaces for the security framework. Java security technology includes a large set of APIs, tools, and implementations of commonly used security algorithms, mechanisms, and protocols.

The guard interface represents a guard, which is an object that is used to protect access to another object. The Java security APIs spans a wide range of areas, including cryptography, public key infrastructure, secures communication, authentication, and access control. Java security technology provides the developer with a comprehensive security framework for writing applications, and also provides the user or administrator with a set of tools to securely manage applications.

5 Conclusions

Having analyzed the status of RCI system and the software development with IEC in a high voltage direct current transmission, a new method of connecting SCADA system to Internet is proposed. It has the guiding significance in the automation system in HVDC Transmission Project. Internet-based SCADA systems can improve interoperability and can be more cost effective. Internet-based SCADA system are highly open so that it is still less reliable and secure than traditional SCADA systems. Using Java and XML can improve Internet-based SCADA systems' performance, functionality, reliability and security. We believe our research work lays a new direction for research on remote interactive control in electricity SCADA systems.

References

1. Jagadeesh Chandra, A.P., Sudhaker Samuel, R.D.: Design of Man Machine Interface for Real-Time Online Control of DC Drives. Technological Developments in Education and Automation, 237–241 (January 2010), doi:10.1007/978-90-481-3656-8_44
2. Boyer, S.: SCADA: An Introduction Including What Not to SCADA. ISA Encyclopedia of Measurement and Control, EMC 37.01 (2001)
3. Zhang, Z.-B., Liu, G.-L., Geng, Z.-X.: Design and implement of remote control interface for high voltage direct current. In: Proceedings of the 3rd International Conference on Computer and Electrical Engineering, ICCEE 2010, Chengdu, China, November 16-18, vol. 10, pp. 364–367 (2010)
4. Coates, G.M., Hopkinson, K.M., Graham, S.R., Kurkowski, S.H.: A trust system architecture for SCADA network security. Power Delivery (January 2010), doi:10.1109/TPWRD.2009.2034830
5. Karlecik-Maier, F.: A new closed loop control method for HVDC transmission. IEEE Transactions on Power Delivery 11(4), 1955–1960 (1996)
6. Yang, X., Jin, Y.-X., Chen, Y.: Stability analysis of AC/DC power transmission system based on bifurcation theory. In: Proceedings of the 2010 Asia-Pacific Power and Energy Engineering Conference, APPEEC 2010, Chengdu, China, March 28-31 (2010), doi:10.1109/APPEEC.2010.5449291
7. Karawita, C., Annakkage, U.D.: A hybrid network model for small signal stability analysis of power systems. IEEE Transactions on Power Systems 25(1), 443–451 (2010)

The Design Based on Fuzzy PID Electro-hydraulic Servo Control

Hongying Wang and Jianjun Ma

Henan Polytechnic Institute,
Nanyang Henan, China
Ying09200@163.com

Abstract. The study based on the DC servo motor control system obtains the speed control system dynamic and static characteristicsa of the single loop with current positive feedback and voltage negative feedback and completes mathematical model and simulation, which provides a reliable theoretical basis for the practical application of speed control program.

Keywords: Servo moto, PID, performance index, feedback, response.

1 PID Control Algorithm

The rule of PID control is the most commonly used control rule in simulation control systems. The PID controller and the controlled objects are primary components in Control system.

The PID controller is Linear, the Controlling quantity is the subtraction of the given r(t) and the output y(t)

$$e(t) = r(t) - y(t) \tag{1}$$

The PID control equation is shown as follows:

$$u(t) = k_p \left[e(t) + \frac{1}{T_l} \int_0^l e(t)dt + \frac{T_D de(t)}{dt} \right] \tag{2}$$

With the development of computer technology, the digital PID controller replaces the original simulation PID controller, making the PID control more flexible. Position PID control algorithm and the incremental PID control algorithm are commonly used in digital PID controller.

The continuous PID control algorithm can not directly be used in computer control because Because computer control is the sample control,so the The continuous PID control algorithm has to be discreted.

The position PID algorithm uses a series of sampling time points kT instead of the continuous amount of time t in simulation PID algorithm, Its formula is as follows:

D. Jin and S. Lin (Eds.): Advances in Mechanical and Electronic Engineering, LNEE 177, pp. 511–516.
springerlink.com

$$\begin{cases} t \approx kT & (k = 0,1,2...) \\ \int_0^l e(t)dt \approx T\sum_{j=0}^{k} e(jT) = T\sum_{j=0}^{k} e(j) \\ \frac{de(t)}{dt} \approx \frac{e(kT) - e(k-1)T}{T} = \frac{e(k) - e(k-1)}{T} \end{cases} \tag{3}$$

Thediscrete PID expression is as follows:

$$\begin{aligned} u(k) &= k_p\left[e(k) + \frac{T}{T_l}\sum_{j=0}^{k} e(j) + \frac{T_D}{T}(e(k) - e(k-1))\right] \\ &= k_p e(k) + k_i\sum_{j=0}^{k} e(j)T + k_d\frac{e(k) - e(k-1)}{T} \end{aligned} \tag{4}$$

$$k_i = \frac{k_p}{T_l}; k_d = k_p t_{D;} \tag{5}$$

It can be derived from the formula (4) that the actuator is directly controlled by output in position PID control algorithm, and the output value and the actuator position directly correspond.The output u (k) is related to the past state in Position PID control algorithm, and there will have intensive computation in e (k)'s accumulation. Moreover, once a system malfunction, e (k)'s significant changes will cause significant change in output and the actuator ,this will lead to serious consequences. To solve this problem, you need to use the incremental PID control.

In cremental PID algorithm, the output is the controller incrementΔu (k), the equation by the recursive principle can be obtained as follows:

$$u(k-1) = k_p\left[e(k-1) + k_i\sum_{j=0}^{k-1} e(j) + k_d(e(k-1) - e(k-2))\right] \tag{6}$$

The cremental PID control formula is:

$$\begin{aligned} &\Delta u(k) = u(k) - u(k-1) \\ &\Delta u(k) = k_p\left[e(k) - e(k-1) + k_i e(k) + k_d(e(k) - 2e(k-1) + e(k-2))\right] \end{aligned} \tag{7}$$

From formula(6),it can be derived that incremental PID control algorithm just needs the first three diference to get the increment in the PID control algorithm, three parameters play a decisive role on the property of the controller. Generally speaking, their impact is as follows:

1.1 The Scale Factor Affects System Responsing Speed and Control Precision

The greater the value, the faster the system responsing speed, but too great will result in the system overshoot and oscillation, leading to system instability. Conversely, the

too small value will cause the system to respond slowly, leading to a longer adjusting time and poor precision, and finally affecting the property of system.

1.2 The Integral Factor Affects the Steady-State Deviation

The greater the value, the faster the integrale speed, and the faster the steady-state deviation elimination. But too great value will result in excessive overshoot, leading to poor property. When it is too small, the system integrale speed will reduce, the steady-state deviation elimination will be slower, transition time will be longer, leading to a longer time for getting a stable system, and also finally affecting system performance.

1.3 The Differential Coefficient Affects the System Dynamic Performance

Differential aspects of PID control reflects the changing trends of deviation signals, inhibiting these signals changes in all other directions, it can reduce the overshoot and increase the system stability. too large differential coefficient will adcance the responsing and make system adjusting longer, so then affecting the system performance.

2 Fuzzy Control Algorithm

2.1 Fuzzy Control Theory

Fuzzy control system is theoretically based on fuzzy math,the knowledge of fuzzy language form and fuzzy reasoning science, it uses a digital controller with a closed-loop structure which has a feedback channel controlled by computer.

In the Fuzzy control, charged object will be seen as a "black box", and the expert 's control experience to this "black box" is described as "fuzzy rules". then based on these "fuzzy rules",the machine will control the "black box" automatically.Therefore, the fuzzy control has given a processing method which is able to convert experts' natural language to computer identified mathematical functions just that digital signals, this mathod will make control more effective.

As it does not depend on the mathematical model ,but relying on the "fuzzy rules" that converted from experts' control experience, the fuzzy control is a typical intelligent control.

The specific steps of the fuzzy controller are: computer sampling to obtain the output of control object is compared with the input to get the system controlling amount ,that is the deviation e. The deviation e is blured to the fuzzy amount in the fuzzy representation of fuzzy language. the fuzzy linguistic variables of the Deviation e is called as a subset of E.

Based on fuzzy inference Synthesis rule R ,the controlling amount U is obtained by blurring of E and R .

$$U = ER \tag{8}$$

The resulting U is a fuzzy amount. In the control system, we need to clear the fuzzy quantity U to get a exact amount ,then convert the exact amount into a precise

analog value that imposed on the actuator to control the controlled object. In this way, data acquisition and controlling are running constantly to achieve the fuzzy control to the controlled object.

2.2 The Structure of Fuzzy Controller

The design of Fuzzy controller is derived from human control process. In the reality of industrial control process, the operator usually observe the output and its changes or the combination to determine the control amount. The fuzzy control determines the input amount to the controller on this basis. in the control system, the number of independent variables of Fuzzy controller is called system dimension. Single-input and single-output controller is generally designed as one-dimensional or two-dimensional, but occasionally three dimensional fuzzy controller .

(1) One-dimensional fuzzy controller

One-dimensional fuzzy controller is used to control the first-order objects, Selection bias e is its only input. the controlling amount U is the output . Its structure is shown in Figure 1.

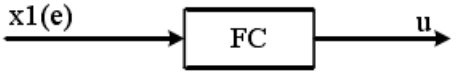

Fig. 1. Structure of one-dimensional fuzzy controller

(2) Two-dimensional fuzzy controller Two-dimensional fuzzy controller input has two components, namely, the deviation e and error change rate ec. Its control effect is better than one-dimensional fuzzy controller, because it can reflect the dynamic nature of the control process output, so the two-dimensional fuzzy controller is the most widely used applications. The frame structure shown in Figure 2.

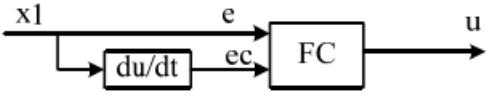

Fig. 2. Two-dimensional fuzzy controller structure

Two-dimensional fuzzy controller rules are as follows

$$\text{R1: if E is } A_1^1 \text{ and EC is } A_1^2 \text{ then U is B1}$$

$$\vdots$$

$$\text{Rn: if E is } A_n^1 \text{ and EC is } A_n^2 \text{ then U is Bn}$$

In the rules, A1. . . An, B1. . . Bn are the a subset of the input and output domain , two-dimensional fuzzy controller rule can be expressed as the following formula:

$$R_{(x,y)} = \bigcup_{i=1}^{n} (A_i^1 \times A_i^2) \times B \tag{9}$$

(3) Three-dimensional fuzzy controller Three-dimensional fuzzy controller has three input control components, namely bias e, the rate of change ec and the bias change rate of ec ecc. The block diagram shown in Figure 3.

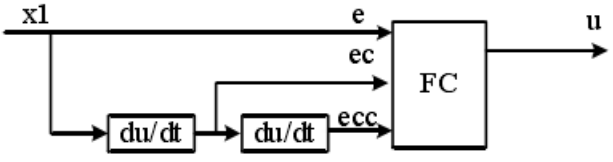

Fig. 3. Three-dimensional fuzzy controller structure

Theoretically, the higher the controller dimensionality, the more precise control. However, the number of control rules for the high-dimensional controller will increase, and this will lead to a huge increase in the amount of fuzzy inference operation. So,there cause the control rules are complex, the control time is too long.Therefore, except under special circumstances, generally,do not use high-dimensional controller. Two-dimensional fuzzy controller is the most widely used controller.

3 Fuzzy PID Servo Controller Design

PID controller is calibrated by the fuzzy controller In the fuzzy PID controller, in general, the controller input is the displacement bias e and bias change rate ec, PID controller output is the correction of the three parameters, respectively, Δk_i , Δk_p , Δk_d .Their linguistic variables are: E, EC, Δk_i , Δk_p , Δk_d .

Domain of system variables as follows:

The domain of input variables E, EC is: {-3, -2, -1,0,1,2,3}the domain of kp is: {-0.3, -0.2, -0.1,0,0.2,0.2,0.3}the domain of ki is: {-0.06,0.04,0.02,0,0.02,0.04,0.06} You should select "Positive big values (PB)", " Positive middle values (PM)", " Positive small values (PS)", "zero (Z)", "negative small values (NS)", "negative middle values (NM)", "negative big values (NB) "to describe the system variables. Therefore, the fuzzy subset of the system is as follows:{NB, NM, NS, Z, PS, PM, PB}. Membership function of each variable is a combination function which is formed by left z-shaped membership function, right s-shaped membership function and the middle of the triangle membership function.

References

1. Ling, J.L., Zhang, J.: The co-simulation interface and applied research based on AMESim and Matlab/Simulink. Machine Tool & Hydraulics (1), 148–149 (2008)
2. Bo, X.L., Gang, Y., Yun, F.X.: The electro-hydraulic position/force hybrid control simulation study based on AMEsim and Simulink. Machine Tool & Hydraulics (05), 205–207 (2007)
3. Dong, P., Wang, Q., Tao, Y.: The application of fuzzy PID control in aerosol automatic conference system. In: Proceeding of the Fourth World Conference on Intelligent Control and Automation, vol. (2), pp. 923–926 (2002)
4. Jing, N., Qing, X.Z., Zai, L.F.: Nonlinear modeling and SSA control of the electro-hydraulic servo system. China Mechanical Engineering (06), 2166–2169 (2008)
5. Lei, L., Yu, Y.F., Shun, W.: The application of fuzzy PID control on electro-hydraulic servo system. Chinese Hydraulics & Pneumatics (07), 52–54 (2009)
6. Gang, C., Yi, C., Bi, W.S.: The multi-sliding mode fuzzy control of the nonlinear electro-hydraulic servo system. Transactions of the Chinese Societh for Agricultural Machinery (10), 222–226 (2008)
7. Wang, Z.Y., Ming, Z.X., Feng, H.Y.: The adaptive fuzzy neural network control of electro-hydraulic servo system. China Mechanical Engineering (4), 681–684 (2004)
8. Fan, T.: The simulation and experimental study for for Fuzzy PID control of the electro-hydraulic servo system. Taiyuan University of Technology (2010)

Study of Sulfate Reducing Bacteria on Copper Pitting Corrosion Based on Electronic Technology

Shengxian Cao, Kaiyan Yuan, and Lingling Sun

School of Automation Engineering,
Northeast Dianli University, Jilin, Jilin 132012
csxlb_jl@163.com

Abstract. The corrosion behavior of H68 brass in sulfate-reducing bacteria was studied by open-circuit potential of electrode and the electrochemical impedance spectrometry. The corrosion characteristics and mechanisms of sulfate-reducing bacteria were analyzed by the cyclic potention dynamic polarization electrochemical techniques and scanning electron microscopy. The results show that the charge-transfer resistance of H68 brass presents the regular of rise, down and rise with the metabolic activity of sulfate-reducing bacteria. Metabolic activity of sulfate-reducing bacteria can decrease the solution pH value, which destroyed the CuO passivation layer of copper electrode surface, accelerated corrosion of copper electrode, promoted pitting corrosion of metal, and increased the sensitivity of pitting corrosion of copper electrode.

Keywords: sulfate-reducing bacteria, pitting corrosion, brass, electrochemical techniques, Electronic Technology.

1 Introduction

Technical equipment of modern industry and daily life has been widely used copper because of its excellent technology features and superior use features. But in the practical application of copper, they are easy to be affected by the surrounding environment corrosion damage. Metal corrosion is a very complex reaction, which occurs mainly in metal and dielectric interface. The metal corrosion process, which is the destruction of spontaneous, will reduce energy. In the corrosion process, metal and corrosive medium can form a thermodynamically unstable system [1-2]. As the metal corrosion process is complex, so it also has a variety of classifications. According to the damage form of the corrosion, the metal corrosion can be divided into comprehensive corrosion, localized corrosion and corrosion under stress, the danger of localized corrosion is much bigger than the overall corrosion; According to corrosive environments, metal corrosion and corrosion can be divided into the atmosphere corrosion, soil erosion, sea water corrosion and so on[3-4]; According to the corrosion process, corrosion can be divided into physical metal corrosion, chemical corrosion and electrochemical corrosion of these three kinds.

Maximum damage on the copper caused by corrosion is pitting corrosion. The damage caused by pitting corrosion is unrepaired. In the electric power, petroleum,

D. Jin and S. Lin (Eds.): Advances in Mechanical and Electronic Engineering, LNEE 177, pp. 517–522.
springerlink.com

chemical industry, brass microbial corrosion is everywhere[5]. Therefore, the study of microbial metal point erosion has the important meaning on the influence of the law, and action mechanism.

2 Experimental Materials and Methods

2.1 The Cultivation of SRB Bacteria

Sulfate-reducing bacteria (SRB) medium: Weigh dipotassium hydrogen phosphate 0.5g, ammonium chloride 1.0g, Sodium sulfate 0.5g, calcium chloride 0.1g, magnesium sulfate 2.0g, sodium lactate 3.5g, yeast extract 1.0g. These reagents dissolved in 1000mL desalted water, with sodium hydroxide or hydrochloric acid to adjust pH value to 7.2+0.2. The dissolved liquid placed in the pot steam autoclave sterilization 15min.

2.2 Electrode Samples

Copper electrode sample, which sample area is 1 cm2, test surface will be buffed by levigation sand paper 150 #, 500 #, 800 # step by step. Non-working surface are sealed with epoxy resin. Electrode working face are polished smooth, washed with dilute sulfuric acid, ethanol, deionized water in turn to clean and remove oxide, organic matter, etc. The electrode samples are placed into the oven drying stand for later use.

2.3 Experimental Methods

Adding microbial culture medium into the assembled three-electrode system, the electrolyte is the microbial growth medium. Installed working electrode, auxiliary electrode, and working electrodes were connected with the electrochemical workstation, through a data cable to connect it to the workstation with CHI660C chemical measurement software on your computer. Electrochemical workstation warmed up. At the first, the open circuit potential-time is measured. The specific data set are the sampling time 2000s, the sampling interval of 0.1s, high and low potential limit into 1V,-1V respectively. Secondly, it can measure AC impedance, the initial potential value is the open circuit potential values, high frequency is set to 100000Hz, low-frequency 0.005Hz, the amplitude of 0.005V, standing time 1200s, its sensitivity is set to automatic. Finally, the potentiodynamic polarization curves are measured, the initial potential is set to -1V, and the termination potential is set to 1.5V, sweep frequency is set to 0.5mv/s.

After setting parameters, it can measure the exchange electrode impedance. It can simulate proper equivalent circuit for impedance spectra by means of computer, analysis and calculate the electrochemical parameters. It carries out a preliminary analysis of microbial corrosion.

3 Experimental Results and Analysis

3.1 The Open-Circuit Potential of Electrode of Copper in Sulfate-Reducing Bacteria

Clean copper electrode is placed into the culture medium. At the beginning of three days, the culture medium of organic matter and other particles adsorbed on the copper electrode surface, and the open circuit potential continue to move negative, but the negative move small scale, indicating that the influence of sulfate-reducing bacteria on the open circuit potential of copper electrode is not obvious. In the bacteria medium, the open circuit potential is more negative than in sterile medium, indicating that sulfate-reducing bacteria could accelerate the corrosion of copper electrodes. When the copper electrode immersed to 5 days, the circuit potential appeared to move trend, it is because of microbial metabolism the copper electrode surface. The open-circuit potential of electrode of copper in sulfate-reducing bacteria is shown in Fig.1.

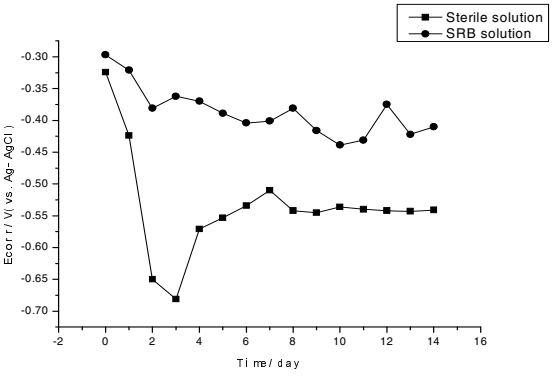

Fig. 1. The open-circuit potential of electrode of copper in sulfate-reducing bacteria

3.2 The Electrochemical Impedance Spectrometry of Electrode of Copper in Sulfate-Reducing Bacteria

AC impedance spectra of different immersion time of copper electrode in sterile medium and sulfate-reducing bacteria are shown in Fig.2. The data are fitted by using Zview software, the results are shown in Table 1.

As can be seen from the Table.1, with the increase of immersion time, the charge transfer resistance of the copper electrode in the sterile medium is increased first and then slightly decreased. This should be due to copper electrode is oxidized in a sterile medium, formed a layer of copper oxide film on copper electrode surface. The film hindered further corrosion of the metal. Due to the increase of soaking time, the charge transfer resistance of the copper electrode is slightly reduced, but little change.

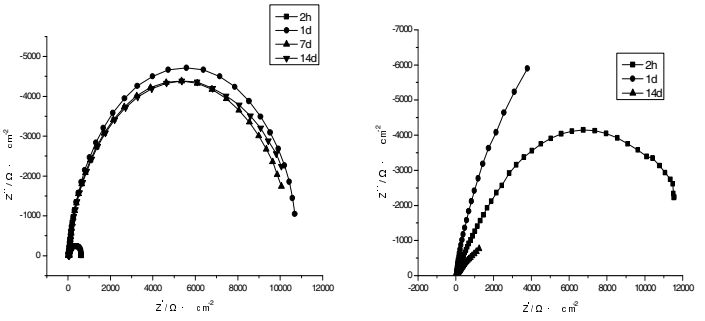

a) blank b) bacteria

Fig. 2. The electrochemical impedance spectrometry of electrode of copper in sterile medium and in sulfate-reducing bacteria

Table 1. The electrochemical parameters of copper in the medium at different times

immersion time		$R_s(\Omega)$	$R_t(K\Omega)$	Q1($F\cdot cm^{-2}$)	N1	$R_f(\Omega)$	Q2 ($F\cdot cm^{-2}$)	N2
2h	bacteria	27.11	13.33	3.48E-07	0.68			
	blank	29.46	7.42	0.00023	0.53			
1d	bacteria	7.32	51.37	0.00016	0.87	39.49	4.72E-12	0.35669
	blank	35.23	159.67	2.89E-06	0.69			
5d	bacteria	9.43	0.86	0.00013	0.50	17.68	6.36E-09	0.63532
	blank	39.27	134.23	0.00027	0.60			
7d	bacteria	13.32	0.51	2.06E-05	0.49	27.16	2.73E-10	0.51748
	blank	46.85	106.13	2.89E-05	0.57			
10d	bacteria	27.45	0.97	0.0016	0.81	228.8	1.58E-05	0.59895
	blank	48.14	131	1.67E-05	0.71			
12d	bacteria	25.46	141.4	0.0015	0.90	343.6	1.69E-05	0.62682
	blank	40.42	128.3	4.12E-05	0.75			
16d	bacteria	26.86	2.32	0.0018	0.86	496.3	2.27E-05	0.66745
	blank	37.72	121.3	9.40E-05	0.72			

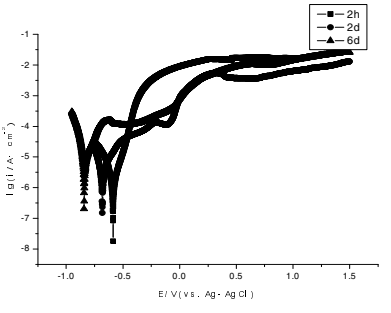

Fig. 3. The polarization curves of electrode of copper in sulfate-reducing bacteria

3.3 The Polarization Curves of Electrode of Copper in Sulfate-Reducing Bacteria

It can be seen from Fig 3 in the sulfate -reducing bacteria medium, the corrosion potential of copper electrode appeared to move to the negative direction. At the initial immersion time (2h), copper electrode shows typical active dissolution characteristics and on the copper electrode surface does not generate passivation layer or not generate a complete passivation layer. But two days later, the copper electrode surface automatically generates a complete passivation layer, and there is an obvious pitting potential at the-0.1V. Copper electrode enters into the passivation area at -0.6V or so after immersing 6 days. With increase of the current density, copper electrode occurs pitting corrosion at -0.15V, which is namely pitting potential.

4 Analysis of the Electrode Surface Corrosion

The scanned corrosion products by SEM morphology of copper electrode in sulfate-reducing bacteria medium for 14 days are shown in Fig4. The figure shows that sulfate-reducing bacteria metabolism on the copper electrode surface generated the uneven distribution and a porous membrane. After removing the corrosion products of copper electrodes surface, there are many different sizes corrosion pits on the copper electrode surface. May be the reason is that sulfate-reducing bacteria metabolism on the copper electrode surface generated the uneven distribution biofilm which changed the chemical nature of the copper electrode surface. Meanwhile sulfate-reducing bacteria adsorbed on the biofilm and formed a poor solubility micro-environment on the copper electrode surface. It accelerated corrosion of the metal membrane and prompted serious pitting of copper electrode.

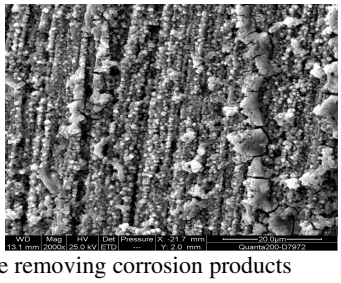

a) Before removing corrosion products

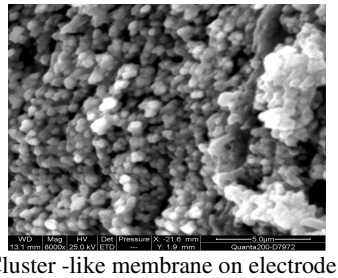

b) Cluster -like membrane on electrode surface

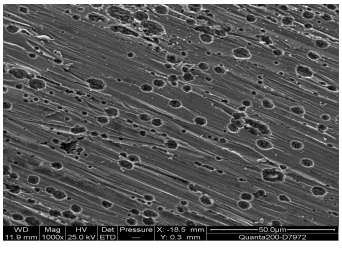

c) After removing corrosion products

Fig. 4. Copper electrode surface SEM scanning images

5 Conclusion

(1) The pH value of solution decreased at the metabolic activity of sulfate-reducing bacteria time, and formed a layer of biological membrane on the copper electrode surface. It changes the chemical properties of the copper electrode surface, accelerated corrosion of copper electrodes and promoted pitting corrosion of copper electrode occurrence.

(2) Sulfate-reducing bacteria can accelerate the copper electrode corrosion, and increase the sensitivity of copper electrode pitting corrosion.

(3) Copper electrodes' charge transfer resistance of in sterile medium is much larger than that in have bacterium medium. The charge transfer resistance of copper electrode in bacterium medium presents the regular of rise, down and rise.

Acknowledgment. Project Subsidized by National Natural Science Foundation of China (No. 51176028), Science and Technology Development Projects of Jilin Province (No. 20100432), Science and Technology Eleventh Five-Year Research Project of Department of Education of Jilin Province (2010. No.77), Doctoral Research Fund of Northeast Dianli University (BSJXM-200919).

References

1. Gong, M.: Theory of metal corrosion and corrosion control, pp. 3–5. Chemical Industry Press, Beijing (2009) (in Chinese)
2. Liu, Y., Zhang, P.: Principles of metal corrosion, p. 5. Aviation Industry Press, Beijing (1993) (in Chinese)
3. Chen, Z.: Corrosion and Protection of Taiwan overview of technology development. In: Third Cross-Strait Symposium on Corrosion and Protection of Materials, pp. 10–14. Corrosion and Control Chemical Industry Press (2002)
4. Shen, Y.: Green Chemistry, pp. 6–9. China Environmental Science Press (2004) (in Chinese)
5. Bansal, B., Muller-Steinhagen, H.: Crystallization Fouling in Plate Heat Exchangers. Journal of Heat Transfer 115, 584–591 (1993)

A New SAT-Solver Based Algorithm for the Electronic Engineering

Benzhai Hai[1,2] and Ruiyun Xie[3]

[1] School of Information Engineering
Wuhan University of Technology, Wuhan, China
[2] School of Computer Science &Technology
Henan Normal University, Xinxiang, China
[3] Dep. of Computer Science and Technology,
Henan Mechanical and Electrical Engineering College,
Xinxiang, China
haibenzhai@gmail.com

Abstract. Boolean satisfiability (SAT) solvers are used heavily in electronic engineering verification tools for checking satisfiability of Boolean formulas. Most state-of-the-art SAT solvers are based on the DPLL algorithm and require the input formula to be in conjunctive normal form (CNF). We represent the vhpform of a given NNF formula in the form of two graphs called vpgraph and hpgraph. The input formula is translated into a 2-dimensional format called vertical-horizontal path form (vhpform). In this form disjuncts (operands of ∨) are arranged orizontally and conjuncts (operands of ∧) are arranged vertically.The formula is satisfiable if and only if there exists a vertical path through this arrangement that does not contain two opposite literals (l and ¬l). The input formula is not required to be in CNF. This algorithm is very important both for the design of integrated circuit and the development of electronic engineering.

Keywords: SAT, NNF, DPLL, ELECTRONIC ENGINEERING.

1 Introduction

The Boolean satisfiability (SAT) problem decides whether a given Boolean formula is satisfiable or unsatisfiable. The SAT problem is of central importance in various areas of computer science, including theoretical computer science, electronic engineering verification, and artificial intelligence. The SAT problem is NP-complete [1] and no provably efficient algorithms are known for it. Most state-of-the-art SAT procedures are variations of the Davis-Putnam-Logemann-Loveland (DPLL) algorithm and require the input formula to be in conjunctive normal form (CNF). The design and implementation of SAT solvers becomes much easier if the input formulas are restricted to CNF. Given a truth assignment s to a subset of variables occurring in a formula, a Boolean constraint propagation (BCP) algorithm determines if s falsifies the given formula, else it provides the set of implied assignments (unit literals). Modern SAT solvers spend about 80%-90% of the total time during the BCP steps. For formulas in CNF, BCP can be carried out very efficiently using the two-watched literal scheme [2].

D. Jin and S. Lin (Eds.): Advances in Mechanical and Electronic Engineering, LNEE 177, pp. 523–527.
springerlink.com

Typical formulas generated by the industrial applications are not necessarily in CNF. We refer to these formulas as non-clausal formulas. In order to check the satisfiability of a non-clausal formula f using a CNF based SAT solver, f needs to be converted to CNF. This is done by introducing new variables [4, 3]. The result is a CNF formula f0 which is equi-satisfiable to f and is polynomial in the size of f. This is the most common way of converting f to a CNF formula. Conversion of a non-clausal formula to a CNF formula destroys the initial structure of the formula, which can be crucial for efficient satisfiability checking. The advantage of introducing new variables to convert f to f ' is that it can allow for an exponentially shorter proof than is possible by completely avoiding the introduction of new variables [5]. However, the translation from f to f ' also introduces a large number of new variables and clauses, which can potentially increase the overhead during the BCP steps and make the decision heuristics less effective. In order to reduce this overhead modern CNF SAT solvers use pre-processing techniques that try to eliminate certain variables and clauses [6]. The disadvantage with pre-processing is that it does not always lead to improvement in the SAT solver performance. It can also fail on large examples due to significant memory overhead.

We propose a new SAT solving framework based on a representation known as vertical-horizontal path form (vhpform) due to Peter Andrews [7, 8]. The vhpform is a two-dimensional representation of formulas in NNF. We represent the vhpform of a given NNF formula in the form of two graphs called vpgraph and hpgraph. The vpgraph encodes the disjunctive normal form and the hpgraph encodes the conjunctive normal form of a given NNF formula. The size of these graphs is linear in the size of the given formula.

2 Preliminaries

A Boolean formula is in negation normal form (NNF) iff it contains only the Boolean connectives "∧" (.AND.), "∨" (.OR.) and"¬" (.NOT.), and the scope of each occurrence of "¬ "is a Boolean variable. We also require that there is no structure sharing in a NNF formula, that is, output from a gate acts as input to at most one gate. A NNF formula is tree-like, while a circuit can be DAG-like.

Conversion of Boolean Circuits to NNF:

In our work Boolean circuits are converted to NNF formulas in two stages. The first stage re-writes other operators (such as xor, iff, implies, if-then-else) in terms of ∧,∨, ¬ operators. In order to avoid a blowup in the size of the resulting formula we allow sharing of sub-formulas. Thus, the first stage produces a formula containing ∧,∨, ¬ gates, possibly with structure sharing. The second stage gets rid of the structure sharing in order to obtain a NNF formula.

Vertical-Horizontal Path:

It is known that every propositional formula is equivalent to a formula in NNF. Furthermore, a negation normal form of a formula can be much shorter than any DNF or CNF of that formula. More specifically, we use a two-dimensional format of a nnf formula, called a vertical-horizontal path form (vhpform) as described in [9]. In this form disjunctions are written horizontally and conjunctions are written vertically. For example Fig. 1(a) shows the formula f= (((p ∨¬r) ∧¬q ∧r) ∨ (q ∧ (p ∨ ¬s) ∧¬p)) in vhpform.

Vertical path: A vertical path through a vhpform is a sequence of literals in the vhpform that results by choosing either the left or the right scope for each occurrence of ∨. For the vhpform in Fig. 1(a) the set of vertical paths is {<p, ¬q, r>,<¬r, ¬q, r >,< q, p, ¬p >,< q, ¬s , ¬p >}.

Horizontal path: A horizontal path through a vhpform is a sequence of literals in the vhpform that results by choosing either the left or the right scope for each occurrence of ∧. For the vhpform in Fig. 1(a) the set of horizontal paths is {<p, ¬r,q>, <p, ¬r, p,¬s>, <p, ¬r, ¬p>, <¬q,q>, ,<¬q, p,¬s>, <¬q, ¬p >, <r,q>, <q, p,¬s>,<r, ¬p>} The following are two important results regarding satisfiability of negation normal formulas from [2]. Let F be a formula in negation normal form and let σ be an assignment (σ can be a partial truth assignment).

Theorem 1. s satisfies F iff there exists a vertical path P in the vhpform of F such that s satisfies every literal in P.

Theorem 2. s falsifies F iff there exists a horizontal path P in the vhpform of F such that s falsifies every literal in P.

Example 1. The vhpform in Fig. 1 has a vertical path <p,¬q,r> whose every literal can be satisfied by an assignment s that sets q to true and p, r to false. It follows from Theorem 1 that s satisfies f. Thus, f is satisfiable. All literals in the vertical path <¬r, ¬q , r >cannot be satisfied simultaneously by any assignment (due to opposite literals r and ¬r).

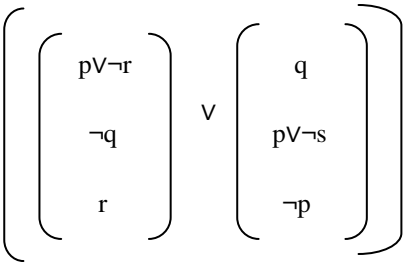

Fig. 1. The vhpform for the formula f=(((p ∨¬r) ∧¬q ∧r) ∨ (q ∧ (p ∨ ¬s) ∧¬p))

3 Graph Based Representations

3.1 Graphical Encoding of Vertical Paths (Vpgraph)

A graph containing all vertical paths present in the vhpform of a NNF formula is called a vpgraph. Given a NNF formula f, we define the vpgraph Gv(f) as a tuple (V,R,L,E,Lit), where V is the set of nodes corresponding to all occurrences of literals in f, $R \subseteq V$ is a set of root nodes, $L \subseteq V$ is a set of leaf nodes, $E \subseteq V \times V$ is the set of edges, and Lit(n) denotes the literal associated with node $n \in V$. A node $n \in R$ has no incoming edges and a node $n \in L$ has no outgoing edges.

The vpgraph containing all vertical paths in the vhpform of Fig. 2(a) is shown in Fig. 2(b). For the vpgraph in Fig. 2(b), we haveV ={1,2,3,4,5,6,7,8},R = {1,2,5}, L = {4,8}, E = {(1,3), (2,3), (3,4), (5,6), (5,7), (6,8), (7,8)} and for each $n \subseteq V$, Lit(n) is shown inside the node labeled n in Fig. 3.1(b). Each path in the vpgraph Gv(f), starting

from a root node and ending at a leaf node, corresponds to a vertical path in the vhpform of f. For example, path <1,3,4> in Fig.2(b) corresponds to the vertical path <p, ¬q, r>in Fig. 2(a) (obtained by replacing node n on path by Lit(n)).

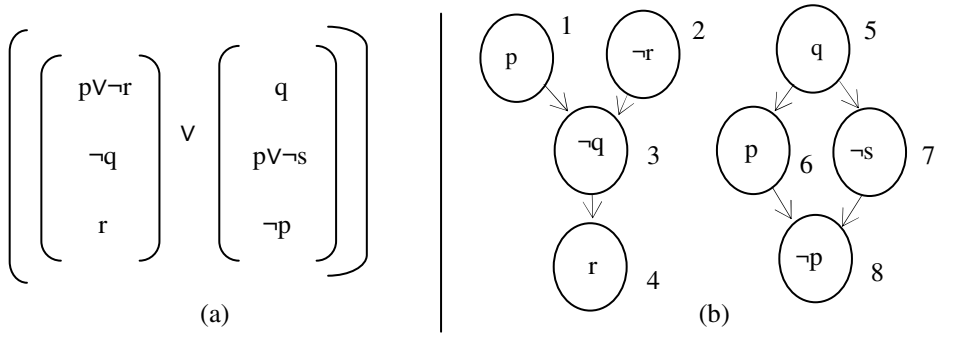

Fig. 2. (a) The vhpform for the formula f = (((p ∨¬r) ∧¬q ∧r) ∨ (q ∧ (p ∨ ¬s) ∧¬p))
(b) the corresponding vpgraph

3.2 Graphical Encoding of Horizontal Paths (Hpgraph)

A graph containing all horizontal paths present in the vhpform of a NNF formula is called a hpgraph. We use Gh(f) to denote the hpgraph of a formula f.The procedure for constructing a hpgraph is similar to the above procedure for constructing the vpgraph. The difference is that the hpgraph for f = f1∧f2 is obtained by taking the union of the hpgraphs for f1 and f2 and the hpgraph for f = f1∨f2 is obtained by concatenating the hpgraphs of f1 and f2.

The hpgraph containing all horizontal paths in the vhpform in Fig.3(a) is shown in Fig. 3(b). For the hpgraph in Fig. 3(b), we haveV ={1,2,3,4,5,6,7,8}, R={1,3,4}, L={5,7,8}, E ={(1,2), (2,5), (2,6), (2,8), (3,5), (3,6), (3,8), (4,5), (4,6), (4,8), (6,7)} and for each n∈V, Lit(n) is shown inside the node labeled n.

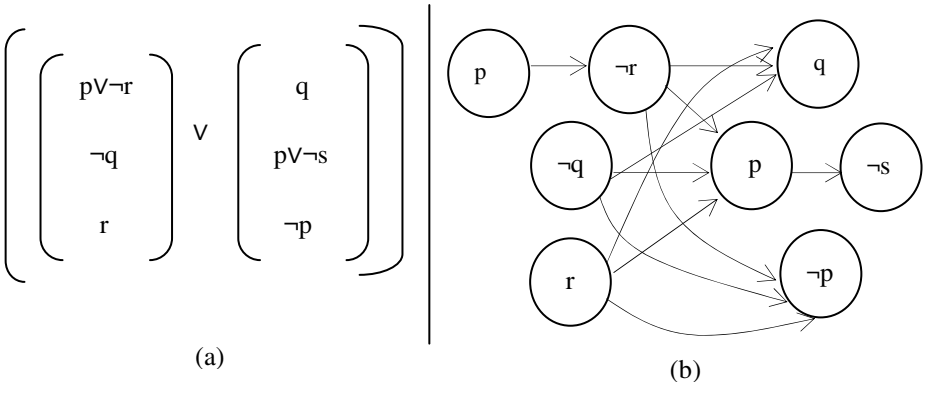

Fig. 3. (a) The vhpform for the formula f=(((p ∨¬r) ∧¬q ∧r) ∨ (q ∧ (p ∨ ¬s) ∧¬p)) (b) the corresponding hpgraph

It can be shown by induction that the vpgraph and hpgraph of a NNF formula are directed acyclic graphs (DAGs). One can also represent vpgraph and hpgraph as directed series-parallel graphs. Series-parallel graphs have been widely studied and many problems that are NP-complete for general graphs can be solved in linear time for series-parallel graphs [10].

When constructing an hpgraph/vpgraph from a NNF formula f each literal inf gets represented as a new node in the hpgraph and vpgraph of f. We assume that the node number corresponding to each literal l in f is the same in the hpgraph and the vpgraph of f. Thus, the set of nodes in the hpgraph and vpgraph are identical.

4 Conclusions

We presented a new SAT-solver based algorithm for the electronic engineering . The core of this algorithm is a two-dimensional representation of NNF formulas called vertical horizontal path form (vhpform). The vhpform of an NNF formula contains vertical and horizontal paths. A vertical path is like a cube (term) in the DNF representation of a given formula, while a horizontal path is like a clause in the CNF representation of a given formula. The vpgraph encodes all vertical paths and the hpgraph encodes all horizontal paths. Both vpgraph and hpgraph can be obtained in linear time in the size of the given NNF formula. The NNF of formula is usually more succinct than the (pre-processed) CNF of the circuit in terms of number of variables, so it is very useful for the improving of electronic engineering.

References

1. Cook, S.A.: The complexity of theorem-proving procedures. In: STOC, pp. 151–158 (1971)
2. Moskewicz, M.W., Madigan, C.F., Zhao, Y., Zhang, L., Malik, S.: Chaff: Engineering an efficient SAT solver. In: Design Automation Conference (DAC 2001), pp. 530–535 (June 2001)
3. David, A.: Plaisted and Steven Greenbaum. A structure-preserving clauseform translation. J. Symb. Comput. 2(3) (1986)
4. Tseitin, G.S.: On the complexity of derivation in propositional calculus. In: Studies in Constructive Mathematics and Mathematical Logic, pp. 115–125 (1968)
5. Järvisalo, M., Junttila, T., Niemelä, I.: Unrestricted vs restricted cut in a tableau method for boolean circuits. Annals of Mathematics and Artificial Intelligence 44(4), 373–399 (2005)
6. Eén, N., Biere, A.: Effective Preprocessing in SAT Through Variable and Clause Elimination. In: Bacchus, F., Walsh, T. (eds.) SAT 2005. LNCS, vol. 3569, pp. 61–75. Springer, Heidelberg (2005)
7. Andrews, P.B.: Theorem Proving via General Matings. J. ACM 28(2), 193–214 (1981)
8. Andrews, P.B.: An Introduction to Mathematical Logic and Type Theory: to Truth through Proof, 2nd edn. Kluwer Academic Publishers, Dordrecht (2002)
9. Davis, M., Putnam, H.: A computing procedure for quantification theory. J. ACM 7(3), 201–215 (1960)
10. Takamizawa, K., Nishizeki, T., Saito, N.: Linear-time computability ofcombinatorial problems on series-parallel graphs. J. ACM 29(3), 623–641 (1982)

Wavelet Transform Based Information Hiding and Applications in Electronic Engineering

Yanping Chu[1] and Xinhong Zhang[1,2,*]

[1] Computing Center, Henan University,
Kaifeng 475001, China
[2] Institute of Complex Intelligent Network System,
Henan University, Kaifeng 475001, China

Abstract. In the recent years, information hiding has been widely applied in electronic engineering field. The implementation of information hiding can be divided into two categories. One is space method; another one is transform domain method. In this paper, the information hiding is proposed based on wavelet transform domain method. It uses lifting Hara wavelet and combination with zero tree wavelet method to achieve information hiding.

Keywords: Wavelet transform, zero-tree, information hiding.

1 Introduction

Until recently, information hiding techniques received much less attention from the research community and from industry than cryptography. The main driving force is concern over copyright; as audio, video and other works become available in digital form, the ease with which perfect copies can be made may lead to large-scale unauthorized copying, and this is of great concern to the music, book, and software publishing industries. There has been significant recent research into digital `watermarks' (hidden copyright messages) and `fingerprints' (hidden serial numbers); the idea is that the latter can help to identify copyright violators, and the former to prosecute them.

In the foundation of wavelet multi-resolution analysis, we can make full use of some characteristics of the human visual model (HVS) and the auditory model (HAS). We can make the embedded vector information quantity, covert and robust to achieve a more perfect degree. Using wavelet transform for image processing, according that the human's eyes are not sensitive to high frequency components of the image characteristics, image portion of the high frequency component is used for carrying secret information and realizing information in the image of the implicit transfer, in order to meet the need of secret information. In the same time it can maintain a good visual effect.

The traditional research of wavelet transform is a real number domain transform. Even though analysis signal is a sequence of integers, the corresponding wavelet

* Corresponding author.

D. Jin and S. Lin (Eds.): Advances in Mechanical and Electronic Engineering, LNEE 177, pp. 529–534.
springerlink.com

transform coefficients is also real. Because the digital image is generally low with digit integer representation, the most commonly used is the 8. We very much hope that the image matrix of wavelet transform is an integer matrix. It is like an "integer to integer wavelet transform". An integer sequence mapping an integer to integer wavelet coefficients and the mapping is reversible. Having this property is called integer wavelet transform wavelet transform. There are several ways to get the integer wavelet transform. The simplest way is built upon the lifting scheme that is based on integer wavelet transform. Sweldens proved that the way based on the lifting scheme can realize the wavelet transform from integer set to integer set. Achieving the integer wavelet transform we can get integer transform results only when a decimal is for integral operation from the "prediction" and "update" process in the filter. The integral operation of wavelet coefficients is done a small change. The characteristics of decomposition are remained.

2 Band Selection Based on HVS

In the information hiding techniques, the position of information hiding embedding band is the important factors. It will affect the relationship between embedded information capacity and visibility. Embedding capacity increasing can bring the visual effect falling. According to the research of human visual system (HVS), we know that the human visual system has the characteristic which is more sensitive to image smoothing part and is less sensitive to small changes in the image texture. According to the human visual masking effect research, a larger volume of data can be hided in the image edge and texture. The image's flat portion is relatively sensitive to noise. By thinking of multi-resolution analysis, image flattening portion is corresponding with the low frequency sub-band of wavelet transform. It is to say that low frequency sub-band focused the most of the energy of image while the high frequency part corresponding to the image edge and texture, namely the details. Therefore, the low-frequency part of the image is the most important.

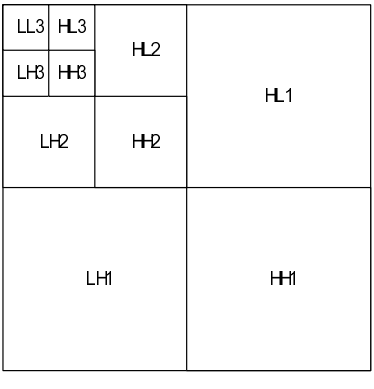

Fig. 1. Wavelet transform diagram

Loss compression, low pass filter and image scaling operations cannot cause too big effect for a portion of this data. Considering the robustness of watermarking, the watermark information should be embedded into the low frequency sub-band of the image frequency domain decomposition. But for the same reason, the change of the low frequency band of human visual impact is bigger. A lot of watermark was embedded into the low frequency and it was very difficult to guarantee no visibility of the image reconstruction after embedding information. If the hidden data was embedded into the high frequency part of image, we can hide information well by using the characteristics of high frequency coefficient. But such information was unable to withstand the loss compression, low pass filtering and so on some simple image processing. If can fully integrate the watermark embedding high, low frequency band characteristics, we may get a better information embedding method. Wavelet multi-resolution analysis provides a good choice for data embedding band. As shown in the figure 1.

As an example of that on an N×N image n scales wavelet decomposition: The low frequency component of LLn is the image of a low scale approximation. Most of energy in this image is concentrate on that. Let LHi, HLi, HHi (i=1, 2, 3…n) respectively, horizontal, vertical and diagonal edge, contour and texture. The features of wavelet have good spatial direction. They are in line with the characteristics of the human visual system (HVS). In order to balance among the robustness of watermark, embedding capacity and visual contradiction, combine of high, low frequency band characteristics, we can make the image decomposition.

3 Compression Based on Embedded Zero-Tree Wavelet Coding

Zero-tree is defined for a given threshold T. When the wavelet coefficient x and all of its descendants are the unimportant coefficient, that is less than the threshold T, it was said above nodes constitute a tree structure for zero tree. Image after wavelet transformation, the first of its coefficients are quantized treatment. In the successive approximation, the selection of threshold sequences Ti satisfy the iterative Ti = Ti-1/2. The initial threshold T0 must meet the conditions: For all wavelet coefficients x, x has $|x|<2T0$. All the process of successive approximation quantization needs to continue to divide from the middle of the last quantization threshold in order to be the current value. The main scanning (Dominant Pass), fine scanning (Refinement Pass) and symbol coding (Symbol Encode) are completed in three stages, in order that the requirements of target bit rate are reached.

The advantage of embedded zero tree coding is that all zero coefficient position in the zero tree structure can be remembered as soon as zero root position is remembered. So it can greatly improve the compression ratio. Because of this, the zero tree coding has become a part of new image coding international standards JPEG2000. By the practice, if according to a certain order of scanning, zero roots will more easily occur continuously. At the same time, if we can use a variety of encoding method to represent these consecutive zero roots, we can further improve the compression ratio and signal to noise ratio of image coding. By the structure of zero-tree, we can make full use of each sub image characteristics in the wavelet domain to effectively represent data.

4 Watermark Embedding and Extraction

A core issue of lossless information hiding algorithm based on the high frequency is to find a suitable watermark embedding position. Inoue proposed two kinds of watermark embedding methods. One is to embed the watermark into unimportant coefficient in wavelet domain, by using a small positive or negative to instead of unimportant coefficients in zero-tree to embed the watermark; the other is to embed the watermark into important coefficients in wavelet domain.

The particular way to embed the watermark in unimportant coefficients is: at the first, do Three-tier wavelet decomposition to original image ,then choose 3 sub-band group (LH3, LH2, LH1), (HL3, HL2, HL1), and (HH3, HH2, HH1) to constitute a zero tree. The lowest frequency sub-band (LL3) is invariant. Watermark embedding algorithm is as follows:

(l) Select any of a group of the 3 sub-band groups to embed watermark. Set the threshold T. T= Cmax. In which Cmax is the maximum of wavelet coefficient in selected sub-band group. And 0.01< <0.1

(2) In the threshold T, find the unimportant coefficient and construct the zero-tree. Let Z1, Z2, ..., ZN, representation of zero-tree, where N is the number of zero-tree.

(3) Code the watermark information which require to embed for two-value bit sequence W(k), k=1,2, ..., N.

(4) For k=1, 2, ..., N. if W (K) =0, Use the -M instead of all elements in zero-tree, and in the experiment, adjust according to distortion level after embed watermark in the image.

(5) Save the Z1, Z2, ..., ZN zero root positions. Then inverse the wavelet transform, access to the embedded watermark image.

In watermark detection, the first is to do wavelet decomposition on being detected image. Wavelet basis and decomposition of the series are the same as watermark embedding. Then do watermark detection according to the preserved ZTR position when the watermark embedded. The method is as follows:

(1) According to ZK zero root position, obtain the ZK parent coefficient and 4 sub coefficient values. Then calculate their average.

(2) If the average is less than 0, the watermark value is 0, or 1.

When embed the watermark in the unimportant coefficients, embedding area is mainly in the part of image which changes are relatively flat. Because the human visual system is very sensitive to the change of this part, the more strength the watermark embedding is increased, the more obvious the image distortion is.

5 Algorithm Steps

Combine the integer wavelet transform and embedded zero tree wavelet coding. Integrating the advantages of both can effectively improve the efficiency of operation and image information hiding rate. The specific algorithm combining these two methods is as follows:

Information embedding process:

1. Realizing Arnold random permutation to the watermark image of w, get random sequence w1. Scan the scrambled watermark for one-dimensional sequence.
2. Realizing 3 stage integer wavelet transforms to the carrier image and obtains the four forks tree structure of coefficient. Set a threshold value T, and search to get M zero trees of the threshold value. Z1, Z2, …, ZM.
3. Embedding information according to embedding method in the fifth part.

Information extraction process:

1. Realizing 3 stage integer wavelet transform to the image contain hidden information and obtain the four forks tree structure of coefficient.
2. Watermark extracting according to embedding method in the fifth part. Get the initial detection of watermark w2. Do error correction on initial detection watermark combining the sub coefficient of wavelet zero tree.
3. Ascend dimension the watermark information after the error correction and transform for two-dimensional, then get image w3.
4. Realizing Arnold random permutation to the watermark image of w3, restore getting the original image information.

6 Algorithm Analysis

This algorithm is mainly to combine integer wavelet transform and zero tree wavelet, in order to achieve the effect of information hiding. The algorithm fully set the features of integer wavelet transform and zero tree wavelet. Algorithm analysis as follows:

1. Realizing wavelet transform with integer wavelet transform. The wavelet transform was a real number operation ago. This improvement greatly reduces the amount of calculation and improves operational efficiency.
2. Giving full play to advantages of the zero tree wavelet as long as remember the ZTR position, can remember the all zero coefficient location in zero tree structure. It is more suitable for the wavelet coefficients of the organization.

Still need improvement:

Integer wavelet transform has many advantages. But through doing integer wavelet transform at the image, energy concentration is a lot worse than the first generation wavelet transform. Integer wavelet transform has a certain gap with general wavelet transform in focus on the energy characteristics and related characteristics. This is mainly reflects that through the integer wavelet transform, amplitude changes in each sub-band coefficient are little lot than they through the general wavelet transform. Basing on the above problems, we should further research distribution characteristics of each sub-band coefficient in the image which through integer wavelet transform. Combine with quantization threshold selection method in the zero tree coding. Design an adaptive to select a quantitative threshold scheme in order to solve the above problem.

7 Summary

In the recent years, information hiding has been widely applied in electronic engineering field. The implementation of information hiding can be divided into two categories. One is space method; another one is transform domain method. In this paper, the information hiding is proposed based on wavelet transform domain method. This paper mainly introduces information hiding algorithm base on the lifting wavelet and embedded zero tree wavelet coding method. In this paper, information hiding algorithm combines the integer wavelet transform and embedded zero tree wavelet.

Acknowledgment. This research is supported by the Medical Science Foundation of Henan Province grants No. 2011020114.

References

1. Shapiro, J.M.: Embedded image coding using zerotree of wavelet coefficients. IEEE Tran. on Signal Processing 41(2), 3445–3462 (1993)
2. Said, A., Pearlman, W.A.: A new, fast, and efficient image codec based on set partitioning in hierarchical trees. IEEE Trans. Circuits and Systems for Video Tech. 6, 243–250 (1996)
3. ISO/IEC, ISO/IEC 15444-1, Information technology-JPEG 2000 image coding system-Part 1: Core coding system [OL] (2000)
4. Adams, M.D., Kossentini, F.: Reversible integer-to-integer wavelet transforms for image compression: Performance evaluation and analysis. IEEE Transactions on Image Processing 9(6), 1010–1024 (2000)

Underwater Sensor Network Nodes Self-localization in Electronic Technology

Hua Zhang

316000 School of Electromechanical Engineering,
Zhejiang Ocean University,
Wenhua Road, Zhoushan,
Zhejiang Province No. 105, China
xiaoyaozhh@163.com

Abstract. The independent positioning mechanism can reduce the difficulty of modeling, it is more complex for wireless sensor networks which is a new application of electronic technology to use in the marine environment than in terrestrial environments. It was established of the relationship between the distance of beacon nodes and unknown nodes, and the Taylor series was used in a manner based on the traditional centroid algorithm idea on underwater sensor networks node distribution of two dimensional and three-dimensional respectively on linear approximation in this paper. Simulation results show that: it can achieve the node in the effective two-and three-dimensional positioning on using the linear approximation of the Taylor series and it can be realized by electronic technology.

Keywords: UWSN, Three-dimensional, Taylor series, Node self-localization.

In electronic technology, a new technology named wireless sensor network is being on studying all over the world. The accuracy of node localization are related to the effectiveness of the data collected of wireless sensor networks, and it is little affected by environmental factors although the position error increased of the independent of distance positioning performance. It may refer to the land environment research ideas studying on underwater sensor networkss including routing protocol, mac protocol, node location and coverage, etc[1-3]. It is the positioning of common concern mechanism that the positioning accuracy to satisfy most application requirements. The underwater sensor networkss is the extension of land-based Wireless sensor networks applications to the underwater. It was described the current application of underwater sensor networkss prospects and challenges, discussed short-range acoustic communication and mac protocols by Heidemann J, etc,[4,6]. Nodes of underwater sensor networkss are arranged by underwater robot on seabed showing as the two-dimensional distribution or in the sea showing as the three-dimensional distribution [5,8]. It was discussed on underwater sensor networkss nodes self-localization on two-dimensional and three-dimensional by using Taylor series linearization method to deal with the distance, achieve optimal control of the node self-localization in this paper.

D. Jin and S. Lin (Eds.): Advances in Mechanical and Electronic Engineering, LNEE 177, pp. 535–540.
springerlink.com

1 Distribution of Sensor Nodes on 2D and Its Mathematical Model

It had been discussed on the self-positioning in sensor networks issues from RANGE, AOA, etc, proved that the sensor network to locate and transfer data by Niculescu D [9,11]. Assuming the signal transmission model of sensor nodes is the spherical model, regardless of time of signal transmission between nodes, without considering the noise, the node distribution is uniform, good connectivity between nodes. The subjects were two-dimensional, nodes dispenser randomly, each beacon node communicate with each other to get through the location information, the node coordinate respectively $P_i(x_i, y_i), (i = 1, 2, \cdots, n)$, unknown node coordinates $X_j(x_j, y_j), (j = 1, 2, \cdots, m)$; for each unknown node real coordinates, estimated coordinates and centroid coordinates are not the same, set coordinates of an unknown node $X(x_{est}, y_{est})$ which communicate with beacons builds a centroid coordinates by centroid algorithm, error exists between them,

$$x_{est} = x_{av} + \Delta x; y_{est} = y_{av} + \Delta y \tag{1}$$

$\Delta x; \Delta y$ were denoted as the error between the true value and the node constructed by beacon nodes respectively, and $f(x, y)$ as the unknown node with the distance between the beacon nodes, as

$$f(x, y) = \sqrt{(x - x_i)^2 + (y - y_i)^2}; i = 1, 2, \cdots, n \tag{2}$$

The unknown node coordinates can be solved from the mathematical point of view, if the equation 2 that the two coordinates of beacon node and distance equations to meet the full rank case. In fact, it will be made the measured data in the coordinates and the distance there are certain errors, which is solved using the equation 2 bring some error, resulting in lower accuracy due to restrictions on the node itself, such as computing power, communication interference. The Taylor series of the distance equation Transformation is used because the Taylor series approximation of the real tangent method is used to solve equation. Multivariate Taylor series expansion is shown in the second line of equation 3, as Lagrange remainder.

$$f(x_{est} + \Delta x, y_{est} + \Delta y) = f(x_{est}, y_{est}) + (f_x^{'}, f_y^{'})_X \begin{pmatrix} \Delta x \\ \Delta y \end{pmatrix} + R; R = \frac{1}{2!}(\Delta x, \Delta y) \begin{pmatrix} f_{xx}^{''} & f_{xy}^{''} \\ f_{yx}^{''} & f_{yy}^{''} \end{pmatrix}_{X^*} \begin{pmatrix} \Delta x \\ \Delta y \end{pmatrix}, X^* = (x_{est} + \theta\Delta x, y_{est} + \theta\Delta y) \tag{3}$$

There is Taylor series high-end remainder and if the discarded higher order, there is the approximation error to a certain extent. Let's assume known the distance values between beacon nodes and unknown nodes in order to reduce the error of solving the coordinates, respectively $d_i, i = 1, 2, \cdots, n$, modify the equation 2, in order to further constrain the distance range of the unknown coordinates of the nodes. The modified equation is shown as follows,

$$f(x, y) = \sqrt{(x - x_i)^2 + (y - y_i)^2} - d_i; i = 1, 2, \cdots, n \tag{4}$$

The convenient function is described form $f(x,y)$, it is expanded in the Equation 4 with multiple Taylor series expansion in the real coordinates of unknown nodes $X\ (x_{est}, y_{est})$, seeking an order partial derivatives on equation 4, respectively

$$f_x^{'} = \frac{x - x_i}{f_{xy}}; f_y^{'} = \frac{y - y_i}{f_{xy}} \tag{5}$$

It is shown of unknown node's expansion on the Taylor series as follows on equation 6:

$$f(x,y) \approx f(x,y)\big|_{X_{est}} + \left(f_x^{'}, f_y^{'}\right)_{X_{est}} \begin{pmatrix} \Delta x \\ \Delta y \end{pmatrix} \tag{6}$$

The right side of the two of equation 6 is shown as follows respectively,

$$f(x,y)\big|_{X_{est}} = \sqrt{(x_{est} - x_i)^2 + (y_{est} - y_i)^2} - d_i \left(f_x^{'}, f_y^{'}\right)_{X_{est}} \begin{pmatrix} \Delta x \\ \Delta y \end{pmatrix} = f_x^{'} * \Delta x + f_y^{'} * \Delta y\big|_{X_{est}} = \frac{x_{est} - x_i}{f_{xyX}} \Delta x + \frac{y_{est} - y_i}{f_{xyX}} \Delta y \tag{7}$$

Among them, $f_{xyX} = \sqrt{(x_{est} - x_i)^2 + (y_{est} - y_i)^2}$, $\Delta x = x_{est} - x_{av}; \Delta y = y_{est} - y_{av}$

Therefore, the equation 7, $\frac{x_{est} - x_i}{f_{xyX}}; \frac{y_{est} - y_i}{f_{xyX}}$ can be obtained from the known information.

2 Distribution of Sensor Nodes of 3D and Its Mathematical Model

Sensor nodes are suspended at different depths in the ocean data acquisition in the three-dimensional of UWSN, and the sensor networks must be able to continue to work properly. It is hard to extend the existing node self-localization system and the algorithm to three-dimensional directly, not only topology but also more complex on spatial relationships of three-dimensional. It is one of the keys on the three-dimensional of underwater sensor networkss application on reasonable and effective in the self-localization [10]. A certain number of parameters setting as the same sensor nodes were arranged in three-dimensional space randomly, the nodes were uniformly distributed, the beacon nodes had their own information such as location, the same region a certain number of unknown nodes arranged, a three-dimensional Cartesian coordinate system to be set.

The coordinate of an unknown node was set as $X(x_{av}, y_{av}, z_{av})$, which the beacon nodes communicate with built a coordinate centroid $X\ (x_{est}, y_{est}, z_{est})$ by Centroid Algorithm coordinates, and error exists between them,

$$x_{est} = x_{av} + \Delta x; y_{est} = y_{av} + \Delta y; z_{est} = z_{av} + \Delta z \tag{8}$$

The distance between beacon nodes and unknown were shown as $d_i, i = 1, 2, \cdots, n$. The $f(x,y,z)$ was error distance between the beacon nodes and unknown nodes.

$$f(x,y,z) \approx f(x,y,z)\big|_{X_{est}} + \left(f_x^{'}, f_y^{'}, f_z^{'}\right)_{X_{est}} \begin{pmatrix} \Delta x \\ \Delta y \\ \Delta z \end{pmatrix} \tag{9}$$

The first expansion of equation 9 was shown in equation 10 of the first, the second one was shown in equation 10 of the second.

$$f(x,y,z)\big|_{X_{est}} = \sqrt{(x_{est}-x_i)^2+(y_{est}-y_i)^2+(z_{est}-z_i)^2}$$

$$(f_x^{'}, f_y^{'}, f_z^{'})_{X_{est}} \begin{pmatrix} \Delta x \\ \Delta y \\ \Delta z \end{pmatrix} = f_x^{'} * \Delta x + f_y^{'} * \Delta y + f_z^{'} * \Delta z \big|_{X_{est}} = \Delta x + \frac{y_{est}-y_i}{f_{xyzX}} \Delta y + \frac{z_{est}-z_i}{f_{xyzX}} \Delta z \tag{10}$$

In equation 10, $\frac{x_{est}-x_i}{f_{xyzX}}; \frac{y_{est}-y_i}{f_{xyzX}}; \frac{z_{est}-z_i}{f_{xyzX}}$, can be calculated by a numerical iteration.

3 Simulation and Analysis

The 30 beacon nodes and 10 unknown nodes were arranged in the space and the number of 45 individuals was taken. The simulation environment was set on frequency for 3G of computer in matlab7.0.1.

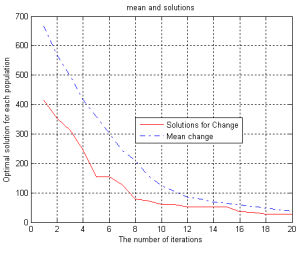

Fig. 1. Average and optimal solution of 2D

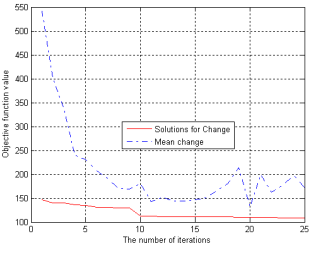

Fig. 2. Average and optimal solution of 3D

It showed each iteration of the average value and the optimal solution in the iterative process in figure 1. The blue line in figure 1 was represented the average curve, which was the average error in the population trend between the unknown nodes and beacon nodes in each generation. It can be observed from the graph, the average error has been reduced with the number of iterations increasing indicating that the positioning accuracy in the continuous improvement. The red one in figure 1 was represented the optimal solution in the iteration process trends., the optimal solution in the data was failed to reach the ideal of 0 in figures 1, which with the parameter setting and relevant, including the number of iterations, the probability of each operator, also with the degree of approximation curve. The three-dimensional model was more complex on model selection and mathematical treatment comparing with the two-dimensional, using a more ideal model presenting the nodes distribution in UWSN, seeing in equation 9. The design algorithm was almost the same processed as the two-dimensional case, focusing only on the genetic algorithm fitness function, the three variables must be used in select populations representing three-dimensional coordinates. It showed in figure 2 that each iteration of the average value and the optimal solution in the iterative process. The blue line in figure 2 was represented the

average curve, which was the average error in the population trend between the unknown nodes and beacon nodes in each generation. It can be observed from the graph, the average error had been reduced with the number of iterations increasing indicating that the positioning accuracy in the continuous improvement. The red one in figure 2 was represented the optimal solution in the iteration process trends.

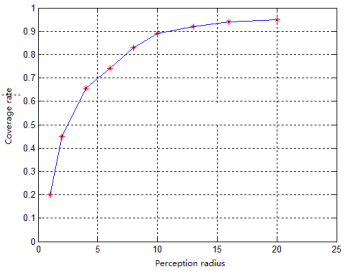

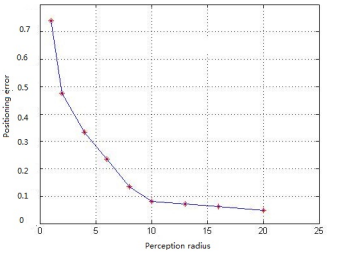

Fig. 3. Coverage rate with perception radius **Fig. 4.** Location error with perception radius

It showed that when the radius increases, the coverage will be perceived increases in figure 3 and that when the perception radius increases, the positioning error in the reduced in figure 4. That is because when the perception radius increases, the node can accept more than one beacon node information so that the coverage increases, and because of the existence of multiple beacon nodes make nodes more precise positioning. The three-dimensional distribution is much better than the two-dimensional distribution on average value of nodes self-localization and individuals in the optimal solution, but in the three-dimensional space of factors affect the localization parameters are much more complex than the two-dimensional space, including communication in the measurement of the distance between the nodes, the node's own location information, the effective radius of the node's communication node, the node surrounding noise, movement of the sea currents. They are able to locate through the algorithm from the simulation results point of view on two or three-dimensional distribution.

There is too many things to do on applying to the actual situation, it is used in the nodes self-localization by almost independent of the external environment impact for an ideal simulation environment, which also is the direction of further research.

Conclusion

The data acquisition location information is also the same essential of underwater sensor network as terrestrial wireless sensor networks in electronic engineering, when the sensing radius increases, coverage will become greater and positioning error in the reduced. It is far more complexity of the aquatic environment than the land environment. It was researched on the two-dimensional and three-dimensional model on nodes self-localization of underwater sensor network, and the results were shown by analysis and simulation that the algorithm can effectively locate the unknown node. We can easily catch that electronic engineering can be used in underwater sensor network.

Acknowledgements. This work is supported by Zhejiang Provincial Education Department(Y201119307).

References

[1] Cui, J.H., Kong, J., Gerla, M., Zhou, S.: The challenges of building scalable mobile underwater wireless sensor networks for aquatic applications. IEEE Network 20(3), 12 (2006)
[2] Bulusu, N., Heidemann, J., Estrin, D.: Density adaptive algorithms for beacon placement in Wireless sensor networks. In: Proceedings of IEEE ICDCS 2001, Phoenix, AZ (April 2001)
[3] Mao, G., Fidan, B., Anderson, B.: Wireless sensor network localization techniques. Computer Networks 51(10), 2529–2553 (2007)
[4] Chandrasekhar, V., Seah, W.K.G., Choo, Y.S., Ee, H.V. (eds.): Localization in underwater sensor networks: survey and challenges. ACM (2006)
[5] Sheng, X., Hu, Y.H.: Maximum likelihood multiple-source localization using acoustic energy measurements with wireless sensor networks. IEEE Transactions on Signal Processing 53(1), 44–53 (2005)
[6] Heidemann, J., Ye, W., Wills, J., Syed, A., Li, Y. (eds.): Research challenges and applications for underwater sensor networking. IEEE (2006)
[7] Cheng, W., Teymorian, A.Y., Ma, L., Cheng, X., Lu, X., Lu, Z. (eds.): Underwater localization in sparse 3d acoustic sensor networks. IEEE (2008)
[8] Teymorian, A.Y., Cheng, W., Ma, L., Cheng, X., Lu, X., Lu, Z.: 3d underwater sensor network localization. IEEE Transactions on Mobile Computing, 1610–1621 (2009)
[9] Niculescu, D.: Positioning in ad hoc sensor networks. IEEE Network 18(4), 24–29 (2004)
[10] Rice, J.: Telesonar signaling and Seaweb underwater wireless networks. Space and Naval Warfare Systems Center, San Diego (2001)
[11] Angeline Peter, J.: Using Selection to improve Particle Swarm Optimization. In: Proceedings of the IEEE Congress on Evolutionary Computation, ICEC, pp. 84–89 (1998)

Electronic Technology Structure Design on Web-Based GMDSS Automatic Examination and Evaluation System

Tao Wang, Yuna Miao, and Qiang Zhang

Maritime College
Shandong Jiaotong University Weihai, China
wtjd2000@yahoo.com.cn,
miaoyn777@hotmail.com,
14209912@qq.com

Abstract. Traditionally, GMDSS evaluation is carried out artificially. This paper aims to design a mode which can evaluate GMDSS exams automatically. A Web-based GMDSS automatic examination and evaluation system is designed to realize the long-range automatic assessment. On the basis of JSP electronic technology, the database connection pool electronic technology and combined C/S and B/S framework are adopted to realize the system.

Keywords: GMDSS, B/S, C/S, Evaluation system.

1 Introduction

Global Maritime Distress and Safety System (GMDSS) is an IMO-adopted modern communication system aimed at protecting the safety of life at sea. At present many countries have established GMDSS evaluation systems. To improve the objectivity and accuracy of the system and to eliminate the man-made influence, a Web-based GMDSS automatic examination and evaluation system is designed to realize the long-range automatic assessment [2].

2 Web Application Framework

The Web application of the GMDSS automatic evaluation system is accomplished on the basis of JSP electronic technology [3, 4], as shown in Fig. 1. First, create a life cycle event listener. Before Web application and sending any requests, initialize the database connection pool for use. Then, map the application requests to the controller Servlet. The controller deals with requests and assigns them to access controller (composed of many action classes) to achieve the action class and controls the access to resources. Finally, JSP obtains data and send them back to user.

D. Jin and S. Lin (Eds.): Advances in Mechanical and Electronic Engineering, LNEE 177, pp. 541–544.
springerlink.com

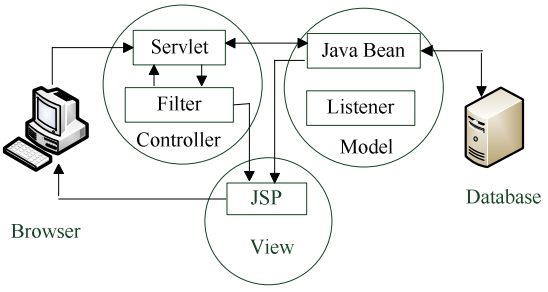

Fig. 1. Web application framework

The Web application framework is based on M/V/C layer. After the main requests of GMDSS skill evaluation system are analyzed, they are mapped to the proper component types [5].

- As database access is abstract, it is not necessary to understand the specific data mode or data engine, Java Bean can assume the role model and achieve the goal.
- An efficient and safe database connection is achieved by adopting a database connection pool. To access Java Bean, database must be initialized to prepare for the start of application, while life cycle event listener is just suitable for the component type used for this task.
- Only the identified users can access the appropriate resources, as the filters in the system can control the access and meet this requirement.
- The dealing of requests is accomplished by the powerful Java code, and Servlet is the most appropriate as controller.
- The display is easy to modify. This is what JSP is most good at and it can serve as visual role.

System Structure

- There are two prevailing application system structures right now, namely, the client/server mode (C/S) and the browser/server mode (B/S). The main advantage of C/S is that it is interactive and has a complete set of application program. It is powerful in management, statistical analysis and printing. It provides safe storing and withdrawing mode. For the same task, C/S mode is faster. And B/S mode is a new structure based on Web technology. It simplifies the workload of clients. The clients have no need to connect with database, thus it is simple to maintain and easy to operate as the clients only have to be familiar with the browser. According to the actual requirement of GMDSS automatic examination and assessment system, the system combines C/S and B/S, as shown in Fig. 2.

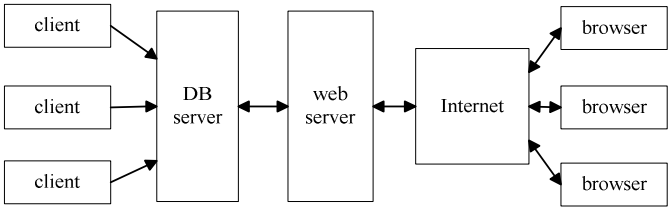

Fig. 2. Web-based GMDSS Automatic Examination and Evaluation System Structure System Framework

The GMDSS automatic electronic skill evaluation system mainly includes: log-in module, exam database design module, assessment content random generating module, evaluating module and the play back module, as shown in Fig. 3.

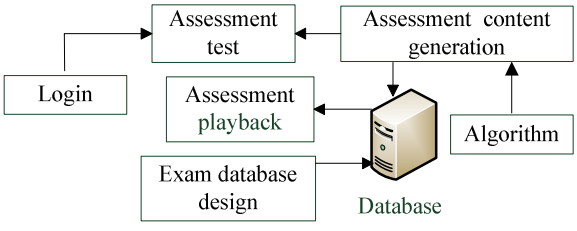

Fig. 3. GMDSS automatic evaluation system framework

Log-in module: The personnel being evaluated log in the system by input their candidate number and ID.

Exam database design module: Mainly accomplish the design of exam database, input answers and formulate the scoring criteria.

Assessment content random generating module: Based on classification and different areas, by use of the random algorithm, the module can randomly combine different assessment content and generate the test card.

Evaluation module: Make evaluation for the personnel being evaluated, including time control, automatic scoring and result display.

Play back module: Record the evaluation process and play back after that.

3 Database Connection Pool

In the development of JDBC-based database application, the management of database connection is a difficult point and also an important factor in determining the system's application performance. On a through analysis of database connection, an efficient connection management strategy is proposed. For the shared resources, a famous design mode is adopted, that is, resource pool. This mode solves the problems caused by frequent resource allocation and release. By applying this mode into database

connection management and establishing a database connection pool, a cost-efficient connection allocation and usage strategy is offered. The core idea of the strategy is -- connection reuse [6].

Establish a Static Connection Pool. The so-called static pool means that the connections in the pool are allocated when initializing and can't be closed arbitrarily. Java provides many container types to establish the connection pool, such as Vector, Stack and so on. In the system initialization, connections are created under configuration and placed into the connection pool, thus avoid the cost caused by arbitrary creation and closure of connection.

4 Conclusion

This paper designs the electronic technology structure of the GMDSS assessment system. The implement of the system will ensure the GMDSS training quality, improve trainees' electronic technical skills and ensure the smooth communication and operation safety at sea. It also reduces the chances of GMDSS false alert accidents and avoids the occurrence of ship detention owing to the improper use of GMDSS equipment.

Acknowledgments. The present study is sponsored by Shandong Jiaotong University Science and Technology Research Foundation, the research period is from June, 2009 to December, 2010.

References

[1] Zhongchao, Z.: GMDSS Comprehensive Service, p. 17. Dalian Maritime University Press (1996) (in Chinese)
[2] Defu, R., Xiaofei, W.: Web-based platform for seafarer assessment model. Navigation Technology (April 2008) (in Chinese)
[3] Zhihui, D.: JSP Programming Practice. Tsinghua University Press (2002) (in Chinese)
[4] Simon, B., Sam, D., Dan, J.: JSP Programming Guide, 3rd edn., 1st edn. Electronic Industry Press (August 2004); translated by Yan, B., Jianchun, C., Chuanfeng, W.
[5] Wenhua, Y.: Introduction to JSP Dynamic Web Page Practices. Science Press (2001) (in Chinese)
[6] The necessity of JSP database connection pool, http://web.lt263.com/html/2004-8-19/200481910331.html

Fast Collision Detection Algorithm in Electric Engineering Virtual Estate Roaming

Shengbing Che and Yan Liu

College of Computer Science and Information Technology,
Central South University of Forestry and Technology,
410004, Changsha, Hunan, China
cheshengbing727@163.com
290198176@qq.com

Abstract. The combination of electronic technology and virtual reality technology plays more and more role in real estate. Users can fully experience through electronic glove, electronic helmet and virtual roaming software. The projections of most building models in visual estate on the horizontal plane are rectangles. Based on the trait of building models, this article propose one way of fast collision detection algorithm for virtual estate roaming. This algorithm firstly divides the projection on the x_z plane of scene into grids; then obtains building models' minimum bounding rectangles aligned with x_z axis and the grid where rectangle is located; finally judges whether the rectangle and the projection on x_z plane of view point collide or not by their spatial relationship. This article proposes solutions for minority particular building models such as arched door.

Keywords: Electric Technology, irtual Estate, grids, Buding Model, Collision Detection.

1 Introduction

Recent years, virtual estate roaming plays more and more important role in property sales and urban Planning. To improve the reality of the virtual scene and prevent unreal cases such as observers going through the wall, collision detection in virtual scene roaming is very necessary. Usually,there are numbers of virtual objects which contain thousands of triangles in the virtual scene.If we traverse all the triangles and tetrahedrons to do collision detection in the scene every signal time observers roaming,the scene rendering would be very slow.

Collision detection algorithm commonly used in virtual roaming always simplify observer as asphere or viewpoint and then do collision detection by estimate the spatial relationship of the sphere or viewpoint with triangles in the virtual scene. All the algorithms mentioned in references [2-4] estimate spatial relationship between avatar(sphere or viewpoint) and triangles in scene.It still will take lots of time traversing triangles in the scene and estimating spatial relationship,although they take measure such as partitioning scene into grids to reduce testing triangles .It is unnecessary to do intersection test with triangles every roaming time, owing to the

D. Jin and S. Lin (Eds.): Advances in Mechanical and Electronic Engineering, LNEE 177, pp. 545–549.
springerlink.com

particularity of virtual building in virtual estate roaming scene. The virtual buildings whose projections on the horizontal plane are rectangles mostly and much more unify and similar with each other than virtual objects in other virtual roaming scene.So it is sufficient doing intersection test with the projection rectangle only once for most virtual buildings.

2 Introduction to the Algorithm

This article propose a kind of fast collision detection algorithm for virtual estate roaming, ensuring high rendering frame rate. For most virtual building models in estate roaming scene, their projections on the horizontal plane are rectangles. So the building models can be simplified as their minimum bounding rectangles aligned on x_z axis. The algorithm simplifies collision problem between observer and most building models to estimation of spatial relationship between building models' minimum bounding rectangles aligned on x_z axis and the position of view point. For most virtual building models in estate roaming scene, it is considered that collision occur when viewpoint ' projection on x_z plane locates in the rectangle. This algorithm firstly partitions the scene projection on the x_z plane into grids, then obtain building models' minimum bounding rectangles aligned on x_z axis and the grid where they located in. Finally this algorithm judges whether the rectangle and the viewpoint ' projection on x_z plane collided by their spatial relationship. This article also propose solution for minority special building models such as arched door.

The algorithm firstly partitions the scene projection on the x_z plane into *M*N* grids and store the index of each grid in array *array_grid[M][N][10]* whose first and second dimensions store the grid's indexes in the x and z direction, the third dimension stores indexes of projection rectangles located in the grid. Each model locates in one or several grids. Then the algorithm read virtual models and the flag value which identifies whether or not the model is a special one that cannot be simulated by projection matrix such as arced door. Then obtaint the model's maximum and minimum coordinate in x_z plane *(max_x,max_z)and (min_x,min_z)* and turn them into the scene coordinate *(max_x,max_z)and (min_x,min_z).*Then store them in array *array_rectangl[index][4]*, whose first dimension stores projection rectangle's index in this array, second dimension stroes projection rectangle's four coordinates. Stroe the frist dimension value of the array in array *array_grid*'s third dimension.

During roaming, the algorithm first find projection rectangles that located in the same grid with the viewpoint, then do intersection test between them. There is no collision occur if the viewpoint isn't in the current projection rectangle. Otherwise, judge the flag value mentioned above. If the value is *FLASE*(the model is not a special one and can be simulate by projection rectangle),the algorithm makes collision response. If the value is *TRUE*(the model is a special one that can not be simulate by projection rectangle)the algorithm do intersection test between the viewpoint and triangles of the model.

3 Algorithm's Details

3.1 Preprocessing for Collision Detection

The first thing we should do in the preprocessing stage is to obtain models' minimum bounding rectangle aligned with x_z axis. This kind of rectagles'four sides aligne on x and z axis respectively. Considering most buildings orientation(face south),this kind of bounding rectangle has good tightness. Since the rectangle can be described by its two coordinates at the top left r and the bottom right corne, it is sufficient to get the model's maximum and minimum coordinate in x_z plane *(max_x,max_z) and (min_x,min_z).*

The algorithm in this article obtain them in model-reading stage.The algorithm frist define the initial value for *min_x*, *min_z*, *max_x* and *max_z*; then transverse every vertex storing them in array *Vertex*; then compare *min_x* and *max_x* with *Vertex[vn][0]*, compare *min_z* and *max_z* with *Vertex[vn][3]*; finally update them.

The coordinate value of *(min_x, min_z)* and *(min_x,max_z)* obtained here referent to coordinate system used to create the model. So they should turn into scene coordinate-*(x_min,z_min)*and*(x_min,x_max)* according to model's poison and display scale in the model-reading stage.These two couple coordinate value are stored in array *array_rectangle[M][4]* whose first dimension stores the two couple coordinate 's(or projection rectangle's) index in this array, second dimension stroes the four value of the two couple coordinate.

To avoid compare the viewpoint with all the elements in array *array_rectangle*, the algorithm in this article partition the scene's projection on the x_y plane into *M*N* grids by step of *SCALE*. Each projection rectangle of models locate in one or several grids. Suppose the width of the scene is *SCENCE_WIDTH* and the height of the scene is *SCENCE_HEIGHT*, then the value of *M* and *N* euqals to the up-round value of *SCENCE_WIDTH/SACLE* and *SCENCE_HEIGHT/SCALE*. The index of each grid is stored in array *array_grid[M][N][10]* whose first and second dimensions store the grid's indexes in the x and z direction,the third dimension stores indexes of projection rectangles located in the grid. The algorithm set the value of *SCALE* small enough to insure that there are 10 projection rectangle in each grid at most, which can accelerate the comparison speed.

3.2 The Collision Detection Algorithm of Viewpoint and Bounding Rectangle

The algorihtm detect the collision of viewpoint and bounding rectangle by the spatial relationship between the viewpoint and bounding rectangle. If the viewpoint is in the bounding rectangle, they are colliding. Otherwise, they are not colliding.

If the spactial relationship is judged between current viewpoint and rectangle, there will be no result until collision. To avoid the lag of collision detection, the algorithm obtain the poison of the next viewpoint *point_next* based on the step and direction of roaming as well as the position of current viewpoint first. Then estimate the spatial relationship between the coordinate of *point_next (x_next,z_next)* and the projection rectangle's left-up coordinate *(x_min,z_min)*,right-bottom coordinate *(x_max,z_max)* that identity the rectangle. When $x\_min \leqq x\_next \leqq x\_min$ *and* $x\_max \leqq z\_next \leqq z\_max$, the next viewpoint is colliding with the bounding rectangle.

This algorithm calculate the index (*m* and *n*) of the grid where next viewpoint *point_next* locates as follow:

```
m=ceil(x_next/SCALE);   //ceil() is rounded up function
n=ceil(z_next/SCALE);
```

Then the algorithm find indexes of bounding rectangles that locate in the grid stored in array elements *array_grid[m][n][]*. In the first dimension of *array_grid[m][n][]* stores the gird's index m on the direction of x axis,in the second dimension stores the grid's index n on the direction of z axis, in the third dimension stores the bounding rectangles 'indexes in the array *array_rectangle* .The bounding rectangle mentioned above are those ones that locate in the grid whose index in array *array_grid* is m and n. Then we can get the rectangles left-up coordinate*(x_min,z_min)* and right-bottom coordinate *(x_max,z_max)* stored in *array_rectangle[index][4]*. Fianlly the algroithm compare them with the coordinate of next viewpoint *point_next*.

3.3 The Collision Detection Algorithm of Viewpoint and Triangle

For most building models, we can judge whether the viewpoint and building collide with each other by the algorithm mentioned above. But for some particular building such as arched door,this collision detection algorithm may appear error. Such as the next viewpoint *point_next* is not colliding with the building even if *point_next*'s projection on x_z plane is in the bounding rectangle In this case, the algorithm do intersection test between the viewpoint and triangles of the model.

To estimate the spatial relationship between viewpoint and the triangle, we should estimate the spatial relationship between next viewpoint *point_next* and the the plane where the triangle locate.The spatial relationship includes such case as: viewpoin is at the front of the plane; viewpoint is on the plane; viewpoint is at the back of the plane. In the first case, the viewpoint is not colliding with the triangle.In the third case, the viewpoin has collided with the rectangle already. In the second case that viewpoint is on the plane, we should estimate whether the point is in the triangle or not.

If the sum of the three included angles constituted by point_next and the three vertexes of the triangle equals to 360°, point_next is in the triangle. So if the sum is greater than or equal to 360°,the next viewpoint point_next is colliding with the triangle, then the algorithm response to the collision.

4 Experimental Results and Conclusion

This article develop the virtual estate roaming system including 106 virtual objects structured by 7582 triangles, and take the fast collision detection algorithm in the system. The frame rate of the scene is 65 frame/s based the algorithm in literature[4],while it is 86 frame/s based the algorithm in this article. This algorithm reduce the time complexity, improve the efficiency of collision detection in virtual estate roaming system,optimize the system performance in some extent. The full use of electronic equipment such as electronic glove and electronic helmet can make users feel more real. The use of electornic technology prove the reality of the reaction of collision.

References

1. Zou, Y.-S., Ding, G.-F., Xu, M.-H., He, Y.: Survey on real-time collision detection algorithms. Application Research of Computers 25(1), 9–12 (2008)
2. Gao, L.-N., Ma, Y.-H.: A Solution for Collision Detection in Virtual Ramble. Computer Simulation 23(2), 189–191 (2006)
3. Zhang, Y.-W., Qing, D., Guo, F.-D.: Fast Collision Detection Algorithm Based on Vector in Virtual Roaming Environment. Computer Engineering 37(21), 270–272 (2011)
4. Chang, M., Luo, Z., Li, D., Ji, J.-W.: Fast collision detection algorithm for virtual environment walkthrough. Journal of Huazhong University of Science and Technology (Nature Science Edition) 36(11), 7–10 (2006)
5. Zhou, L., Su, H.-G.: Research on general file formats and algorithms of 3-D models and their implementation with OpenGL. Computer Engineering and Design 30(2), 433–436 (2009)
6. Govindaraju, N.K., Lin, M.C., Manocha, D.: Quick-CULLIDE: Fast Inter-and Intra-Object Collision Culling Using Graphics Hardware. In: Proceedings of the 2005 IEEE Conference on Virtual Reality, pp. 59–66 (2005)
7. Ning, T., Guo, C., Zhang, S.: Optimization of collision detection method using hybrid bounding box. Computer Engineering and Applications 47(1), 1–3 (2011)
8. Zhao, W., Tan, R.-P., Li, Y.: Real Time Collision Detection Algorithm in Complex Virtual Environment. Journal of System Simulation 22(1), 125–129 (2010)

Reconfigurations of the Real Agri-foods Supply Chain with a Subcontractor to Accommodate Electronic Technology

Fethi Boudahri, Mohammed Bennekrouf, Fayçal Belkaid, and Sari Zaki

Department of Electrical Enginneering,
Manufacturing Enginneering Loboratery of Tlemcen
Fathi_boudahri@yahoo.fr

Abstract. The supply chain of agricultural products has received a great deal of attention lately due to issues related to public health. Something that has become apparent is that in the near future the design and operation of agricultural supply chains will be subject to more stringent regulations and closer monitoring, in particular those for products destined for human consumption (agri-foods)to follow the rhythm of electronic technology. This work is concerned with the planning of a real agri-food supply chain for poultry products (chicken and turkey-cock meat) with a subcontractor in the city of Tlemcen (Algeria). More precisely, the aim of this work is coordi-nation of decisions for location, allocation and transportation of products toachieve an efficient and green logistic network design and distribution planning. LINGO optimization solver (Version12) has been used to get the solution to the problem.

Keywords: clustering based location-routing, agri-food supply chains, optimization.

1 Introduction

The term agri-food supply chains (ASC) are formed by the organizations responsible for production (farmers), distribution, processing, and marketing of agricultural products to the final consumers [1]. What differentiates ASC from other supply chains is the importance played by factors such as food quality and safety [2]. Other relevant characteristics of agri-foods include their limited shelf life, their demand and price variability, which makes the underlying supply chain more complex and harder to manage than other supply chains. This work is an extension of other work. In this paper, we will solve the problem where there is the over-command from customers (for example in the bank holidays or season celebration). For solving these critical situations, we make of contracts with subcontractors to cover the lack of under command our slaughterhouses already localized.

This work is organized as follows. First, the problem is described. Then, the mathematical model is presented. Computational results are presented in section 3. The last section concludes the paper and provides some directions for future research.

D. Jin and S. Lin (Eds.): Advances in Mechanical and Electronic Engineering, LNEE 177, pp. 551–556.
springerlink.com

2 Problem Descriptions

Our problem is to determine the centroid of the cluster customers (set of retailers), and location / allocation between the slaughterhouses and the clusters. A cluster of customers includes customers in the closest distance with a condition that the amount of demands from different customers of this customer clusters (sets of retailers) is less than the capacity of the truck transport used. We used two types of transport trucks; one capacity of 400 units, other 800 units. it was assumed that the volume or weight of the turkey-cock is 5 times larger than chicken. Once the customer clusters are defined with their positions and capabilities, it remains for us to locate the different slaughterhouses and allocate the customer clusters to slaughterhouse, in such a way that capacity of vehicles (truck transport) and slaughterhouses are respected.

2.1 Model Parameters

i : Index for slaughterhouse; i∈ I, j : Index for customer clusters; j ∈ J
k : Index for customers; k ∈ K, l : Index for products; l ∈L
m : Index for products; m ∈M, I = {1,……..r} for Set of slaughterhouse;
J = {1,……..t} for Set of customer clusters; K = {1,……..s} for Set of customers;
L = {1,……..p} for Set of products; M={1,……..q} for Set of subtractors;
xi , yi : Geometric position of the slaughterhouse i;
x'j , y'j : Geometric position of the customer cluster j;
x k , yk :Geometric position of the customer k;
nj :Number of customers assigned to customer cluster j;
Qj: Capacity of a vehicle that travels to the customer cluster j;
Dclk: Demand of customer k for product l;
Dcclj: The demand for a product l by the customer cluster j;
Vlij: volume of product l at customer cluster j delivers by slaughterhouse i;
V`lmj: volume of product l at customer cluster j delivers by subtractor m;
FCi: Fixed cost for establishing a slaughterhouse i;
Dij: Distance from slaughterhouse i to the centroid of customer cluster j;
β:Cost of transporting one unit per km at cluster j delivers by slaughterhouse i;
β`:Cost of transporting one unit per kilometres at customer cluster j delivers by subtractor m;
Qli : Capacity of Slaughterhouse i for product l;.

2.2 Model Parameters

Yjk = 1, if the customer k is assigned to customer cluster j, = 0, otherwise;
Z ij = 1, if the customer cluster j is allocated to slaughterhouse i, = 0, otherwise;
X i = 1, if the slaughterhouse i is open, = 0 otherwise;

3 Problem Descriptions

The mathematical model formulated for the minimization of Total Cost (TC) transportation in the city of Tlemcen (Algeria) in order to cover the entire order requested. Since the problem is highly complex, it cannot be solved in a single stage.

For this purpose, the entire problem (objective criterion) is decomposed into two problems; each problem is solved in a sequential manner, while accounting for dependence between them. The objective criterion is decomposed into the following sub problems:

(1) Capacitated Centered Clustering Problem (CCCP) [3]. [problem 1].
(2) Location- Allocation Problem [4]. [problem 2].

3.1 Capacitated Centered Clustering Problem (CCCP)

In a first stage, the problem of grouping the retailers into clusters is formulated as a capacitated centered clustering problem. The originality and eciency of this approach come from the fact that it limits dissimilarity among the formed groups since these clusters are centered at the "average" of their points' coordinates.

The mathematical model of CCCP is given as follows:

$$\text{Min } Z1 = \sum_{k\in K}\sum_{j\in J}\left\|\left(x_k - x_j^{'}\right) + \left(y_k - y_j^{'}\right)\right\|^2 Y_{jk} \tag{1}$$

Subject to:

$$\sum_{j\in J} Y_{jk} = 1, \forall\, k \in K \tag{1.1}$$

$$\sum_{k\in K} Y_{jk} = n_j, \forall\, j \in J \tag{1.2}$$

$$\sum_{k\in K} x_i Y_{jk} \le n_j x_j^{'}, \forall\, j \in J \tag{1.3}$$

$$\sum_{k\in K} y_i Y_{jk} \le n_j y_j^{'}, \forall\, j \in J \tag{1.4}$$

$$\sum_{j\in J} Dc_{lk}\, Y_{jk} \le Q_j \quad \forall\, l \in L \tag{1.5}$$

$$(x_k, y_k), \left(x_j^{'}, y_j^{'}\right) \in R^2, n_j \in N, Y_{jk} \in \{0,1\}, \tag{1.6}$$

The problem (1) aims at de**fin**ing the set of **customer's** clusters by minimizing the total distance between these customers and the centre of the clusters.

Constraint (1.1) impose that each customer is allocated to exactly one customer cluster. Constraint (1.2) gives the number of customers in each cluster. Constraints (1.3), (1.4) locate the centroid of customer cluster.

Constraint (1.5) imposes that a customer cluster must be less than the capacity of truck transportation and constraint (1.6) defines the decision variables, and the upper limits to the number of individuals per group.

3.2 Location- Allocation Problem

The objective of the problem (2) is to minimize the cost function composed of fixed and variable costs. The fixed costs are linked to the opening of slaughter-houses and include investment costs for the land, the land tax and the slaughter units. The variable costs include the economical as well as the ecological transportation costs.

$$Min\ Z2 = \sum_{i=1}^{r} FC_i X_i + \sum_{l=1}^{p} \sum_{i=1}^{r} \sum_{j=1}^{t} \mathrm{V}_{lij}(\beta * D_{ij} + \alpha_i) Z_{ij}$$

$$+ \sum_{l=1}^{p} \sum_{i=1}^{q} \sum_{j=1}^{t} \mathrm{V}'_{lmj}\ (\beta' * D_{ij} + \alpha'_i) \quad .. \tag{2}$$

Subject to:

$$\sum_{i \in I} Z_{ij} = 1, \qquad \forall\, j \in J \tag{2.1}$$

$$\sum_{i \in I} \mathrm{V}_{lij} * Z_{ij} = \mathrm{Dcc}_{lj}, \forall\, l \in L, \forall\, j \in J \tag{2.2}$$

$$\sum_{j \in J} \mathrm{V}'_{lmj} + \sum_{j \in J} \mathrm{V}_{lij} \leq Q_{li}\, X_i, \forall\, l \in L, \forall\, i \in I \tag{2.3}$$

$$\sum_{i \in I} X_i = n, \tag{2.4}$$

$$Z_{ij} \in \{0,1\} \tag{2.5}$$

$$X_i \in \{0,1\} \tag{2.6}$$

Constraint (2.1) assumes that each customer cluster j (sets of retailers) is assigned to exactly one slaughterhouse i. Constraint (2.2) indicates that the volume shipped of product l from the slaughterhouse i to the customers cluster j is equal to amount requested. Constraint (2.3) indicates number of slaughterhouse i open. Constraint (2.4) assume that the volume shipped from the slaughterhouse i is less than or equal to the capacity of the slaughterhouse i for the product l. Constraints (2.5) and (2.6) are integrity constraints.

4 Experimental Results

The model is applied to the problem. LINGO 12 has been used to solve the three programs and to obtain exact solutions by using Branch and Bound with default parameters of the solver.The inputs to the phase 1 or CCCP are the coordinates of locations of customer's k (xk, yk), The input data can be taken from the small sized benchmark problems. For this, we used AutoCAD software to position the different customer (see appendix Table).

Table 1. Result of Problem 1

J	(x'_j, y'_j)	n_j	Affect	Dcc_{lj}	
CC1	(24110.14,18008.24)	05	C64,C66,C67,C68,C70	195	22
CC2	(21565.55,13367.35)	11	C16,C17,C18,C28,C29,C31,C33,C34,C38,C48,C75	250	29
CC3	(23438.47,14718.72)	08	C3,C6,C8,,C9,C53,C62,C95,C99	235	33
CC4	(22040,14041.28)	06	C1,C21,C35,C39,C78,C89	245	27
CC5	close	/	/	/	/
CC6	(22825.65,14040.49)	19	C4,C12,C13,C51,C52,C86,C90,C91,C92,C93,C94,C96,C101,C102,C103,C107,C109,C110,C111	510	58
CC7	(22071.15,14095.02)	12	C5,C11,C22,C40,C50,C72,C73,C87,C88,C100,C106,C108	460	64
CC8	(21520.81,17290.96)	7	C24,C55,C56,C57,C59,C69,76	220	29
CC9	(22081.88,15479.50)	6	C14,C43,C54,C65,C71,C98	245	31
CC10	(21358.30,14228.66)	6	C10,C37,C47,C49,C77,C105	255	29
CC11	(22977.17,13730.13)	11	C2,C7,C19,C23,C27,C63,C83,C84,C85,C97,C104	465	67
CC12	close	/	/	/	
CC13	(20517.71,13275.33)	13	C5,C20,C25,C26,C30,C32,C36,C41,C42,C44,C45,C46,C74,C79,C80,C81,C82	465	51
CC14	(23605.37,18148.45)	03	C58,C60,C61	75	7

Table 2. Result of Problem 2

slaughterhouses	Location(Xi)	Allocation (Zij)	Product1	Product2
S1	Open	CC2, CC6, CC9, CC11	250, 460, 255, 465	29,64,29,51
S2	Close	/	/	/
S3	Open	CC5	510	58
S4	Close	/	/	/
S5	Open	CC4,CC10	245,465	27,67
S6	Close	/	/	/
S7	Open	CC1,CC3,CC7,CC8,CC12	195,235,220,245,75	22,33,29,31,7

After solving phase 1 with the objective of minimization of total cost (Z1), we can get the centroid of each customer clusters with their coordinates (x'j, y'j), total number of customers assigned to each customer cluster (nj). These results (output phase1) are configured in the following table 1.capitalized. The font sizes are given in Table 1.

The output of phase 1 along with the coordinates of locations of slaughterhouse (xi, yi), fixed cost for establishing a slaughterhouse i (FCi), capacity of a slaughterhouse i (Qi) and the distance from slaughterhouse i to centroid of each customer clusters j(sets of retailers) (Dij) will become the input to the Phase 2 and it has been assumed that the number of slaughterhouses is equal to the integer part of total number of customer clusters.

After solving phase 2 with the objective of minimization of total cost (Z2), we can get location of slaughterhouses needed to cover the total demands of customer cluster j and allocated slaughterhouses i to customer cluster j, in such a way that capacity of vehicles and slaughterhouses are respected. These results (output phase2) are presented in the table 2.

5 Conclusion

In recent years, many companies (production or service) are trying to reactivate their logistics networks for welcome to electronic technology. The objective of this work is to reform the distribution network of multi poultry products (chicken and turkey-cock) in city of Tlemcen, because of different retailers claim on the market instability of the poultry's meat (prices, lags behind the delivery ...). For this, we have built a mathematical model that consists of two problems.

The first problem is to group retailers into clusters provided that the demand on poultry products for each customer which belongs to a cluster is satisfied. The second is to locate slaughterhouses and affect sets of retailers (clusters) to slaughterhouses locate.

For solve this model, we decomposed the problem into two sub problems; sub problem is solved sequentially by LINGO optimization solver (Version12).

A perspective to this work would be to involve another echelon to this a real agri_foods supply chain with the farmers' locations. This would lead to greater size instances of this problem which is NP-Hard. That would require the development of some heuristics and metaheuristics to solve it.

References

1. Aramyan, C., Ondersteijn, O., Van Kooten, O., Lansink, A.: Performance indicators in agri-food production chains. In: Quantifying the Agri-Food Supply Chain, ch. 5, pp. 49–66. Springer, Heidelberg (2006)
2. Ahumada, O., et al.: Application of planning models in the agri-food supply chain. European Journal of Operational Reseearch 195, 1–20 (2009)
3. Chaves, A.A., Antonio, L.: Clustering search algorithm for the capacitated centered clustering problem. Computers & Operations Research 37, 552–558 (2010)
4. Pirard, F.: 'une démarche hybride d'aide à la décision pour la reconfiguration et la planification stratégique des réseaux logistiques des entreprises multi site, thése de doctorat (September 2005)

Modular Program of Fault Detection Module with Medical Electronic Technology

Wangping Xiong[1], Qinglong Shu[2,*], and Xian Zhou[1]

[1] School of Computer,
Jiang Xi University of Traditional Chinese Medicine,
NanChang, JiangXi, China
[2] School of Basic Medicine Sciences,
Jiang Xi University of Traditional Chinese Medicine,
NanChang, JiangXi, China
xiaoxiongxwp@126.com

Abstract. The use of the status of the fault detection of medical electronic technology and engineering colleges laboratory electronic equipment, and build a set of medical electronic engineering from the traditional fault detection module and the combination of intelligent fault detection module fault detection scheme.The program gives the specific structure of each module and the specific way of implementation of the program, given instance.

Keywords: Electronic Technology, Fault detection, Modular testing program.

1 Introduction

With the rapid progress of science and technology, electronic equipment in the general experience with analog, digital, intelligent and virtual four stages of development, the complexity and integration has become increasingly high. In order to guarantee the stability, reliability and security of electronic equipment, maturing intelligent fault detection technology has been partially replaced by the face of the complex structure of the device or difficult to fault, there are some limitations of the traditional fault detection technology will become the development trend of the field of electronic engineering testing, but in the future for quite a long time, the traditional fault detection techniques can not be completely intelligent fault detection technology replaced, mainly because there are two, one the traditional fault detection techniques is the basis of the detection of all electronic engineering, and second only in difficult, high-precision, large and complex equipment testing requirements, the use of expensive, complex intelligent testing instruments to more practical value. The face of the status of the use of engineering colleges Practice teaching a variety of electronic equipment to mix and match the above two points, coupled with the limitations of traditional detection techniques, the contradiction between the three was particularly prominent. To this end, the author of the long-term practice, in-depth study and exploration, refining summarize a set of engineering colleges class laboratories, and with a similar situation in other industries in electrical engineering fault detection scheme.

* Corresponding author.

D. Jin and S. Lin (Eds.): Advances in Mechanical and Electronic Engineering, LNEE 177, pp. 557–562.
springerlink.com

The traditional fault detection techniques is related things in the field of rational, theoretical knowledge and operational logic to determine the integrated use of practical experience.The existence of fault resolution is not high; false alarm rate, CND and RTOK of a disproportionately large; inadequate sources of information; no reasoning mechanism, scalability and poor fault detection of defects, but because of their practical implementation of a long time, have a mature theoryand the classical method; ready various levels, various types of fault detection device; through artificial directly and flexibly to varying degrees of equipment fault diagnosis and testing, is still suitable for engineering colleges class laboratory accounted for a higher proportion of small and medium-sizedordinary electronic equipment fault detection, as well as logical thinking and practice on students hands-on ability.

Advantages of these two kinds of detection techniques are insufficient, of engineering colleges laboratory various types of equipment under the existing conditions, the detection process can be optimized, modular testing program can be used in device testing work.the organic combination of traditional detection technologies and intelligent detection technology into two modules, based on the measured object and detection purposes, targeted to select the module suitable for solving the corresponding problem.This modular testing program is in line with the status and practice of teaching needs of today's university laboratory, but also through the module between the advantages of complementary electronic engineering detection technology to make full use of.

2 The Modular Program

Traditional fault detection module consists of classic detection methods of the traditional electronic measuring instruments and electronic equipment.

2.1 Traditional Electronic Measuring Instruments

Traditional electronic measuring instruments designed to measure one or several electrical parameters, can be used for a variety of electronic measuring general electronic equipment.Main can be summarized into the following six categories:

1) Signal Generator: used to measure the desired waveform signal.Such as low-frequency, high frequency signal source; function signal generator and RF signal generator.
2) Signal analysis instrument: used to the power of observation, analysis and record a variety of changes, including the analysis of the time domain, frequency domain, digital domain. Such as oscilloscopes, dynamic signal analyzers, spectrum analyzers and logic analyzers, etc.
3) 3)The frequency and phase measurement instruments: used to measure the signal frequency, time interval and phase. Such as frequency meter, the wavelength of the table, and the phase meter.
4) Network characteristics of measuring instruments: used to measure the electrical network characteristics. Such as the frequency characteristics tester (Sweep), impedance testers and network analyzers.

5) Electronic component test instrument: used to measure a variety of electronic components, electrical parameters, or display its characteristic curve. Such as transistor curve tracers, impedance analyzer.
6) Other aids: used to tie in with the equipment to fully play its role. Such as amplifiers, attenuators, detectors, filters, and a variety of AC and DC power supply, etc..

2.2 Classical Detection Methods for Electronic Equipment

The classic detection method of the electronic equipment is the most effectiveness, practicality, regularity, the versatility of the fault detection method, time-tested mainly grouped into the following five kinds:

1) Parameter measurement: the use of the various types of test instruments to equipment failure circuit of parameters (AVΩ, and various component parameters) for quantitative detection method. This law applies to the specific fault in the search for the fault level circuit components.
2) Signal tracing method (signal injection method and waveform observation method in combination): from faulty equipment on the circuit input test signal (requires optional sine wave or square wave) with an oscilloscope step detection (tracing)circuit signal is normal or not.This method is suitable for multi-stage amplifier with the same signal, but this method should pay attention to the judge the measured signal is indeed the result of the role of test signals, rather than a reflection of the other parasitic oscillation or interference signals.
3) Short-circuit bypass method: short-circuit method is the need to suspected faulty circuit in a two or a few temporarily with a lead pick up, to avoid influence from the other unit circuit to determine the fault exists in the unknown circuit. This method is suitable for multi-stage balanced amplifier circuit.Bypass rule is the appropriate capacity and voltage capacitor to bypass certain parts of the circuits of faulty equipment inspection, to determine the fault location method according to the reaction of the failure phenomena of AC bypass. This law applies to power supply noise and parasitic oscillation parts in the equipment circuit.
4) Split test method: It is reasonably have been implicated in the circuit and fault, part by part separated, effective method to determine the range of failures. This law applies to closed-loop fault detection circuitry.
5) interference method: use a multimeter test pen or small electronic circuit used tools, and quickly click on the input of the amplifier from the final stage of forward-level step by step, point to a certain level of input, output has no soundthis one may be a problem.This method is suitable for the scene was not a signal generator, test video, audio, power amplifier and high-frequency signal amplification circuit.

In addition to the seven major classical detection methods, there are a number of colleagues have mentioned other tests, but these methods there are some defects, it is best to minimize the use of.

2.3 Intelligent Fault Detection Module Structure

Constitute the intelligent fault detection system of the detection module consists of a stand-alone mode and intelligent fault detection method.

Intelligent detection technology is developed on the basis of a combination of computers and artificial intelligence in engineering practice is mainly composed of the computer as the main intelligent detection system. System structure can be divided into a stand-alone mode, three kinds of distribution mode and network mode.

The distribution model is linked to the industrial LAN monitoring node for each monitoring site, decentralized control and centralized operation, administration and testing, the detection task Collaboration and resource sharing mode, this mode is suitable for the detection of large and complex equipment.The network model is the condition monitoring, diagnostic technology, network technology combination of the three remote detection system (RMDS), this model applies to the cross-regional monitoring and diagnosis of large and complex equipment.

Stand-alone mode to complete the full functionality of the system is composed by a computer and associated interface and the necessary peripherals.Redundant technology for multi-machine can be used to improve system reliability.This structure features a single, practical small-scale system is suitable for simple detection of objects, the dominant intelligent fault detection system, so as of today's engineering colleges Laboratory intelligent fault detection systemthe best choice.

3 The Modular Program of Practical

The actual operation of the program can be divided into three kinds:

1) The fault is not difficult, complexity is not high maintenance time is not tight, small and medium-sized ordinary electronic equipment, fault detection can be traditional fault detection module is the classic detection methods of the traditional electronic measurement instruments and electronic equipment.
2) small and medium-sized general equipment failure is difficult (hidden, indirect and soft failure), time to repair is urgent, the number of faulty equipment; high, fine, sharp equipment; large and complex equipment, etc. should be intelligent fault detection technology modulestand-alone mode detection systems and intelligent fault detection method for fault detection.
3) When the device is in the mixing of the above two situations exist, it should be beyond the confines of even more complex when the flexible approach, based on actual need or use the most efficient and accurate means of detection; or cross-use, joint use of a variety of differentdetection methods in order to ultimately achieve the fast, accurate, stable eliminating the purposes of all the failures of the equipment.

4 Detected Instance of Electronic Engineering

4.1 Based on Fault Tree Quantitative Analysis of the Basic Principles

Most universities in Engineering Laboratory is still based on small and medium-sized general equipment for practical teaching for the main and basic, this causes the damaged equipment is often in a large number and require a short time to repair the state.Based on the above, the modular program for rapid detection of the prominent functional fault tree rules more desirable to solve such problems.

1) To construct a reasonable fault tree

The fault tree construction process shown in Figure 1.

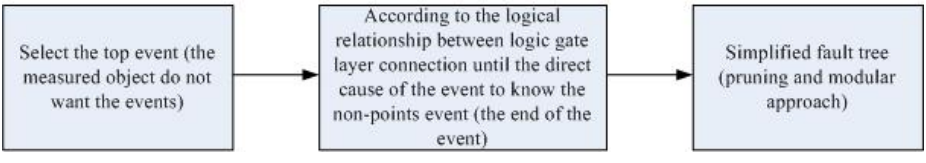

Fig. 1. Electronic engineering fault tree build process

2) To determine the failure probability of the end of the event

Event failure probability is given mostly by experience or by parts run failure, demand failure, component testing and maintenance and other aspects of model analysis.

3) Determine the probability of occurrence of each minimal cut sets.

Cut the end of the event set refers to the equipment set.The minimal cut set cut centrally contained in the end of the event will not remove any cut-set a.The solution of the minimal cut sets typically used downlink method (Fussel-vesely algorithm) according to the logic "and" door the cutset capacity, without the number of cut sets."Or" logic gate plus the number of cut sets, does not increase the number of events the nature of the end of the cut set.Experience "and" door put under the door all the input events line is arranged in an encounter "or" door, until you can not break down all replaced by the end of the event date.Income cut-set and then by pairwise comparison, according to the minimum cut-set defined, remove the non-minimal cut sets, the rest is the fault tree are all minimal cut sets.

4.2 Search for Sources of Failure Based on Analysis of the Importance

A minimal cut sets represent a failure mode equipment, detect faults, one by one to detect the minimal cut sets of failure modes, fault tree analysis of complex equipment to search for sources of failure, but a large number of failure modes need to detect thisthe actual work is sometimes difficult to achieve. This can be used to solve the important degrees of the minimal cut sets of fault tree analysis to simplify. The specific method is: calculate the minimal cut sets importance, were analyzed and compared in magnitude, may not detect small values of the importance of minimal cut

set failure mode, while important to the failure modes that must be detected by descending order of importance of value for testing, can improve the hit rate of fault detection, fault detection greatly reduced the workload.

With the continuous development of future high-tech electronic equipment, electronic engineering, fault detection technology requirements are also bound to. Its development is bound with the fault-tolerant control, combining the reliability of redundant control, autonomous control, and redundancy management system design. The next generation of detection systems will be modular, serialization and standardization of equipment. The traditional fault detection techniques based on comprehensive utilization of intelligent fault detection technology, construct efficient and intelligent fault detection platform will be the development trend of the fault detection of electronic engineering technology.

Acknowledgements. This research was supported by the National Natural Science Foundation of China (No. 81001680)

References

1. Fang, Y., Xiao, J.: Electronic device Intelligent Fault Diagnosis Technology and Development. J. Application Research of Computers 14(6), 48–51 (2004)
2. Shi, F., Zhou, S.: Electronic equipment fault diagnosis Principles and Practice. J. Jiangxi Science 23(1), 69–71 (2007)
3. Perepletchikov, M., Ryan, C.: The Impact of Software Development Strategies on Project and Structural Software Attributes in SOA. In: Meersman, R., Tari, Z. (eds.) OTM-WS 2005. LNCS, vol. 3762, pp. 442–451. Springer, Heidelberg (2005)
4. Morita, I.: Toward realization of Service-Oriented Architecture. J. Fujitsu Scientific and Technical Journal 42(3), 307–315 (2006)
5. Lai, Y.P., Chang, C.C.: A Simple Forward Secure Blind Signature Scheme Based on Master Keys and Blind Signatures. In: Proceedings of the 19th International Conference on Advanced Information Networking and Applications, pp. 139–144 (2005)
6. Han, J., Kambr, M.: Data Mining Concepts and Techniques. Higher Education Press (2001)
7. Su, W.: Application and standardization of data mining tools. J. Computer Engineering 30(8), 40–42 (2008)
8. Wang, C.: Principle and the use of electronic measuring instruments. J. Financial Electronic 14(2), 18–21 (2009)

Research of Hybrid Genetic Algorithm Based on Elite Choice and Adaptive Genetic for Electronic Technology

Li Kang and Guo-Liang Liu

Department of Electrical Engineering and Automation,
Luoyang Institute of Science and Technology, Luoyang, 471023, Peoples R. China
{kangli20112012,liuguoliang}@163.com

Abstract. With the development of electronic technology and the quick popularization of electronic image processing, elite adaptive hybrid genetic algorithm has become an important platform for image processing. Aiming at deficiencies in global search and convergence speed of traditional basic genetic algorithm in the field of electronic technology, a new elite adaptive hybrid genetic algorithm based on elite choice and adaptive genetic is proposed in this paper. This algorithm combined adaptive thinking with elite selection algorithm; fathers and multiple sub-groups will be composed of family, select the family of outstanding individuals into the genetic groups. Simulation of the elite adaptive hybrid genetic algorithm in electronic image processing, and analyze its performance.

Keywords: Maintaining Optima Saving, Adaptive Genetic Algorithm, Hybrid Genetic Algorithm, Elite Choice, Electronic Technology.

1 Introduction

Hybrid genetic algorithm plays an important role in areas such as computational intelligence, artificial life, electronic technology, and image processing, but basic genetic algorithm still produces many shortcomings and defects in the theory and application of technology, mainly due to its falling into local optimal solution and slow convergence speed easily. Genetic algorithm is evolutionary algorithms produce the most widely used and it is one of the research direction and field, it is benefit from biotechnology industry natural selection and genetic mechanisms for natural random genetic algorithms [1]. They are the essence of the search for groups which to have breached the next search of an heuristic that domain, the whole solution to the information collected from space, and search for a distributed[2].

At the same time, the genetic algorithms as a new technology in the field of electronic engineering and electronic technology, there are many local needs to research and development and fulfillment in the basic algorithm to inherit in speed and the optimal solution has conflicted, to local capacity for early age is attractive in such a shortcoming [3], applications research shows that carry genetic algorithm with the question of integration that knowledge is a unique algorithms, it may produce better solution of performance [4].

D. Jin and S. Lin (Eds.): Advances in Mechanical and Electronic Engineering, LNEE 177, pp. 563–567.
springerlink.com

Aim at the shortage of basic algorithm in the field of electronic technology [5]. Genetic heredity make improvements to basic algorithm to select mix genetic and mixed algorithms had considerably improved the basic genetic algorithm.

2 Elite Adaptive Hybrid Genetic Algorithm

2.1 Basic Genetic Algorithm

Different coding methods and genetic operator have different algorithm, but these genetic heredity algorithms have a common feature of life, genetic and evolutionary process of choosing a range of mechanisms that to do the best [6].Solution to the search procedures based on this are in common, Goldberg unified basic algorithm genetic to Simple Genetic Algorithms.

The basic and the most commonly used selection operators is proportion selection operators proportion selection operators [7]. It is refers to the individual which was chosen to the next generation of the group and genetic probability and the individual fitness is proportional to the size. Basic crossover operator is the single point crossover operator in each pair matched each individual, random set a loci of position after two individuals for crossing the gene behind the intersection in the probability of P_d set to exchange, thus produce two new individual basic a mutation operator, it is a common variation operation with binary string coding for the chromosomes, to each of the individual genetic loci that, in accordance with the mutation probability value for the variation of P_n point, has been designated as variation point 0 to 1.

2.2 Elitist Selection Genetic Algorithm in the Field of Electronic Technology

Basic algorithm in the genetic heredity and evolutionary in nature and mechanism and carry on a group, the operator finally got the best solution or to approximate solutions, the genetic operator on a group, and can not ensure that the performance is always better than fathers, so the process will appear again, or even a temporary setback; it will delay the algorithm to speed. To ensure their performance is not under elder, the elite chosen from the basic algorithm to select the genetic key algorithm improved in two points.

Basic algorithm father has just inherited a bigger group of elite two genetic algorithm that a father's blood out of more of theirs (their numbers can be configured), if the father of a genetic ns was younger, the family would have the NS plus two members. Inheritance in the basic algorithm for all their into a genetic groups, although it remains the diversity, but a lot of bad genes is also entering the group of elite; genetic algorithms are selected from each family elite into two groups, which is inherited from the NS plus two members select the two groups of individuals to genetic.

To produce a number of their fathers, that the sample of the group chose genetic diversity; elite group to ensure their performance is higher in the fathers, the group was always close to the best solution.

2.3 Adaptive Genetic Algorithm

Basic algorithm, the incidence of genetic disorders p_d, p_n genetic parameters with populations evolutionary process, continued to be equal value of research shows that

the use of genetic parameter to control the genetic evolution, can easily lead to an early age, lower algorithm search for efficiency, according to population, the situation to evolve in genetic parameter p_d and p_n, helping to improve the performance of genetic algorithm.

This definition of the population degree of ripeness is :

$$\eta = \frac{\overline{f_{\max}}}{f_{\max}} \tag{1}$$

$f_{\max}$ is the greatest value to the degrees of individual, the greater than the average for the individual to the average value. the regulations is with $0<\eta<1$, the closer to a show of degree of ripeness, in addition, elements take on greater than the group of individuals to adapt to the average, and has less adverse impact of the individual, the definition more reasonable, calculated amount is very small.

The definition of p_d and p_n could be defined as:

$$\begin{cases} P_d = 1 \Big/ \exp(k_1.\eta) \\ P_n = 1 - \exp(-k_2.\eta) \end{cases} \tag{2}$$

Here $k_1>0$, $k_2>0$, $k_1$and k_2 value can be set according to the practical problems. Speed through the above to deal with, when populations tend to convergence, p_d will reduce the probability, the range of p_n will increase the probability, and can keep the population of the diversity and avoid premature. When populations cross probability of an individual, p_d will increase, the range of p_n will reduce the probability, and thus, populations tend to increase the convergence algorithm.

2.4 Elite Adaptive Hybrid Genetic Algorithm in the Field of Electronic Technology

The elite genetic algorithms and adaptive genetic algorithm in the proper way of combined to form the elite and to blend into a genetic algorithm this algorithm, the process has pledged their individual which is bound not to inherit fathers, so the basic algorithm to select the proportion of that process has no sense, so mixed algorithms to remove the steps and to reduce the amount of genetic process. The flowchart of elite adaptive hybrid genetic algorithm shows in figure 1.

3 Implementation of New Algorithm in Electronic Image Processing

To verify the elite which can adaptive unique algorithms capability in electronic image processing, the performance of implementing a test of the greatest value problem is:

$$f(x) = \exp[-2\ln 2(\frac{x-0.1}{0.8})^2]\sin^6[5\pi(x^{3/4} - 0.05)] \tag{3}$$

This function ($t \in [0, 1]$) exists within the scope of the five great value points, and five great value point uniform with different sizes. This function can be a very good at test

genetic algorithm, it is proposed to global search capability. The maximum position t^*= 0.079, maximum function f_{max}=0.989.The key control parameters of basic genetic algorithm are: population size N as 20, p_n=0.08, p_d =0.59, select the operation scale operator. select the use of genetic algorithm to use eq(2) adaptive by the rules, p_d and p_n to adaptive parameter separate arguments to k_1 =2, k_2=0.2 ;elite genetic algorithm, the fathers of their number Q_s=10 adaptative and the outstanding genetic algorithm to the other argument with the basic algorithm, the same genetic heredity to mix and blend of the method parameters prescribed by the same parameter value in the distance less than$\theta \leq 10^{-4}$ .It will can not evolution each algorithm simulation 200 each algorithm, the convergence speed of various algorithms to compare as shown in table 1. Comparison of convergence speed shown as in figure.2

Table 1. Convergence speed of various algorithms to compare

Various Algorithms	Convergence speed
Simple GA	146.32
Adaptive GA	106.41
Elite GA	28.62
Mixed GA	12.38

By the results of the basic algorithm for the improvement of inheritance, it is very large extent of the algorithm to converge speed, especially a genetic algorithm, and its performance than before to mix with all the algorithms for the genetic test function as a result of the mixed blood are the basic algorithm shortens to 90% above the algebra.

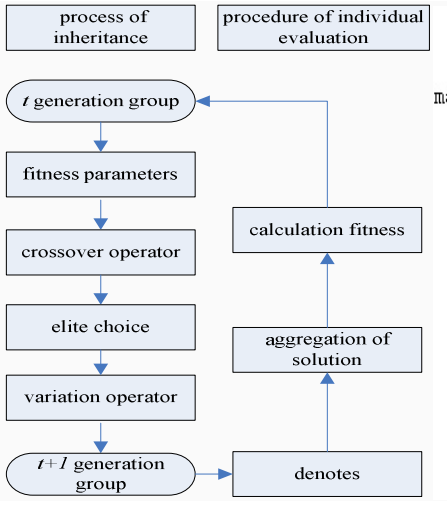

Fig. 1. The Flowchart of Elite adaptive hybrid genetic algorithm

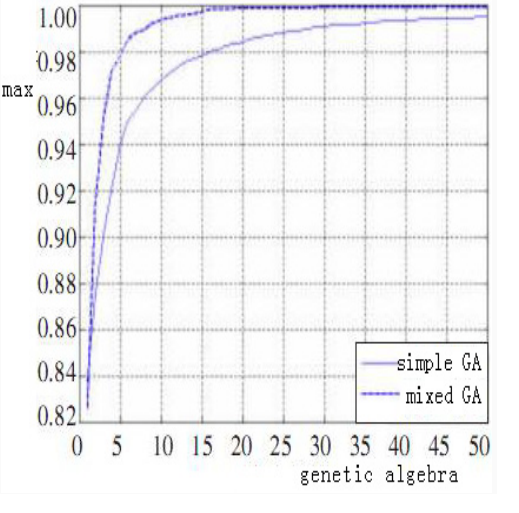

Fig. 2. Comparison of convergence speed

4 Conclusion

This paper puts forward the new hybrid genetic algorithm based on elite choice and adaptive genetic with the fundamental algorithm made reasonable progress in the field of electronic technology. The new elite mixed adaptive hybrid genetic algorithm to ensure that the samples of diversity, at the same time greatly accelerate the convergence speed, using a multi-peak function to verify the performance of the hybrid algorithm.

References

1. Hwang, S.-F., He, R.-S.: Improving real-parameter genetic algorithm with simulated annealing for engineering problems. Advances in Engineering Software 37(6), 406–418 (2006)
2. Vermeulen-Jourdan, L., Dhaenens, C., Talbi, E.-G.: Clustering Nominal and Numerical Data: A New Distance Concept for a Hybrid Genetic Algorithm. In: Gottlieb, J., Raidl, G.R. (eds.) EvoCOP 2004. LNCS, vol. 3004, pp. 220–229. Springer, Heidelberg (2004)
3. Eshelman, L., Schaffer, J.: Real-coded genetic algorithms and interval schemata. Foundations of Genetic Algorithm 2 20(2), 187–202 (1993)
4. Dorado, J., Santos, A.: Hybrid two-Population Genetic Algorithm. Fuzzy Days, 464–470 (2001)
5. Herrera, F.: Hybrid cross over operators for real-coded genetic algorithms: an experimental study. Soft Compute 13(1), 112–118 (2004)
6. Bagheri, E., DeJong, D.H.: Function optimization by means of a parallel approach to fuzzified genetic algorithm. In: Proceedings of the 11th IEEE Symposium on Computers and Communications, vol. 6(26-29), pp. 675–680 (2006)
7. Lee, K.Y., Mohamed, P.S.: A real-code genetic algorithm involving a hybrid crossover method for power plant control system design. In: Proceedings of 2002 Congress on Evolutionary Computation, vol. 2(12-17), pp. 1069–1074 (2002)

Grey Model to the Forecast of Demand for Power Applying Electronic Technology of Matlab

ChunRong Ding[1] and Jing Yi[2]

[1] School of Information and Computer Science,
Anhui Agricultural University, Hefei, China, 230036
dcr@ahau.edu.cn
[2] North China Electric Power University, Beijing, China, 102206
yijing_bj@126.com

Abstract. Electronic technology has developed into an advanced stage, which can be applied to many fields. Matlab, a high-level programming language, is a most developed kind of electronic technology, which is widely used in forecast. Grey model is effectively used in the forecast of demand for power is particularly effective. Based on the application of the grey model, we used Matlab to come to the results. We used grey model to forecast the annual power consumption from 2001 to 2010 based on the initial data of the annual power consumption and then verified the accuracy and the reliability of grey model.

Keywords: Matlab, Electronic technology, Grey model, Forecast of demand for power.

1 Introduction

With the continuous development of the information age, electronic technology has been playing an increasing important role in the economic and social development currently. In recent years, the development of computer technology has exceeded its own field, and worked closer and closer with other applied sciences, becoming an effective solution to practical problems[1]. Matlab is second to none in the applied science and technology soft wares[2]. Matlab has developed into current Matlab7.1 version since the Mathworks Co. launched the first commercial version in 1984, which has obtained remarkable progress.

Based on the analysis of the grey model, we used Matlab to come to the results. We also used grey model to forecast the annual power consumption from 2001 to 2010 based on the initial data of the annual power consumption and then verify the accuracy and the reliability of grey model.

2 Basic Theory of Matlab

Matlab (MATrix LABoratory), a combination of numerical calculation, symbolic calculation and graphical visualization, can be mainly applied to engineering

D. Jin and S. Lin (Eds.): Advances in Mechanical and Electronic Engineering, LNEE 177, pp. 569–574.
springerlink.com

calculation, signal processing, image processing, financial modeling and other fields[3]. Matlab consists of the main program and a variety of optional toolboxes, of which the main program contains hundreds of core internal functions and the toolbox can be divided into two categories: functional and discipline[4].

Functional toolbox is mainly used for the extended symbolic calculation, graphical simulation and real-time interaction. Disciplinary toolbox is for professional use including the package of statistical tools and information processing toolbox[5]. The basic data unit of Matlab is a matrix, and almost all operations are based on the matrix. While in the process of forecasting via grey model, there is a tremendous need of matrix calculations, and grey model just fits it.

3 The Principle and the Error Verification of Grey Model

3.1 Modeling Principle

GM (1,1), a model of a first order differential with only single variable , is the most commonly used grey model. The modeling principle is[6]:

Setting the initial sequence $x^{(0)}$:

$$x^{(0)} = \left[x^{(0)}(1), x^{(0)}(2)..., x^{(0)}(n) \right] \tag{1}$$

Using the1-AGO to generate first-order accumulated sequence to weaken the randomness and volatility of the original sequence:

$$x^{(1)} = \left[x^{(1)}(1), x^{(1)}(2)\ldots, x^{(1)}(n) \right] \tag{2}$$

$$x^{(1)}(k) = \sum_{i=1}^{k} x^{(0)}(i) \qquad (k = 1, 2\ldots, n) \tag{3}$$

Sequence $x^{(1)}(k)$ abides the exponential growth law, while the solution of the equation is exactly that of the law, thus the sequence $x^{(1)}(1)$ satisfies the following first-order linear differential model:

$$\frac{dx^{(1)}}{dt} + ax^{(1)} = u \quad \text{and } a, u \text{ are undetermined coefficients.} \tag{4}$$

According to the definition of derivative, (3) can be displayed in discrete form, and the differential can be written as:

$$\begin{aligned} \frac{\triangle x^{(1)}}{\triangle t} &= \frac{x^{(1)}(k+1) - x^{(1)}(k)}{k+1-k} = x^{(1)}(k+1) - x^{(1)}(k) \\ &= \alpha^{(1)} \left[x^{(1)}(k+1) \right] = x^{(0)}(k+1) \end{aligned} \tag{5}$$

The equation can be written as:

$$\alpha^{(1)}\left[x^{(1)}(k+1)\right]+\frac{1}{2}a\left[x^{(1)}(k+1)+x^{(1)}(k)\right]=u \tag{6}$$

Thus:

$$\begin{aligned}
&k=1, x^{(0)}(2)+\frac{1}{2}a\left[x^{(1)}(1)+x^{(1)}(2)\right]=u\\
&k=2, x^{(0)}(3)+\frac{1}{2}a\left[x^{(1)}(2)+x^{(1)}(3)\right]=u\\
&\vdots\\
&k=n-1, x^{(0)}(n)+\frac{1}{2}a\left[x^{(1)}(n)+x^{(1)}(n-1)\right]=u
\end{aligned} \tag{7}$$

These results can be simply noted as a matrix: $Y_n = BA$ (8)

$$\text{Among: } Y_n=\begin{Bmatrix} x^{(0)}(2)\\ x^{(0)}(3)\\ \vdots\\ x^{(0)}(n)\end{Bmatrix} A=\begin{pmatrix} a\\ u\end{pmatrix} B=\begin{Bmatrix} -\frac{1}{2}\left[x^{(1)}(1)+x^{(1)}(2)\right] & 1\\ -\frac{1}{2}\left[x^{(1)}(1)+x^{(1)}(2)\right] & 1\\ \vdots & \\ -\frac{1}{2}\left[x^{(1)}(n-1)+x^{(1)}(2)\right] & 1\end{Bmatrix} \tag{9}$$

3.2 Model Verification and Analysis of the Errors

After modeling, we should conduct an analysis of the model's accuracy. We selected the posteriori differential test. The results of the test are shown in the Table 1:

Table 1. Posteriori differential test of grey model

Statistics	Average residual errors	The original series, the mean square errors S_1	Residual error mean square errors S_2	Variance ratio C	Small-error probability P
Value	-1041.4822	5128.09	1075.5719	0.2097	1

From Table1, we can see that the accuracy of grey model is P=1>0.95, C=0.2097<0.35, and it levels in A. Thus we can use the model to forecast the power consumption.

4 Empirical Example

According to the principles of grey model ahead, we use the GM (1,1) to forecast the power demand, and we selected the data of power consumption from 2001 to 2010 for verification. We got the results via Matlab as: $\alpha = -0.1109,\ \ \mu = 13363$

Thus the grey model can be written as:

$$x^{(0)}(k+1) = 65814.05(e^{0.1109} - 1)e^{0.1109k}(k = 0,1,2,\cdots) \tag{10}$$

The initial data and forecast value are shown in Table 2:

Table 2. The initial data and forecast value under grey model

The Year	Initial data	Forecast value	Relative errors
2001	14633.5	17557	0.1997
2002	16331.5	19617	0.2011
2003	19031.6	21918	0.1517
2004	21971.4	24490	0.1146
2005	24940.4	27363	0.0971
2006	28588	30574	0.0694
2007	32711.8	34161	0.0443
2008	34541.4	38170	0.1050
2009	36595.15	42648	0.1654
2010	41923	47652	0.1367

The fitting Figure is shown in the Figure 1:

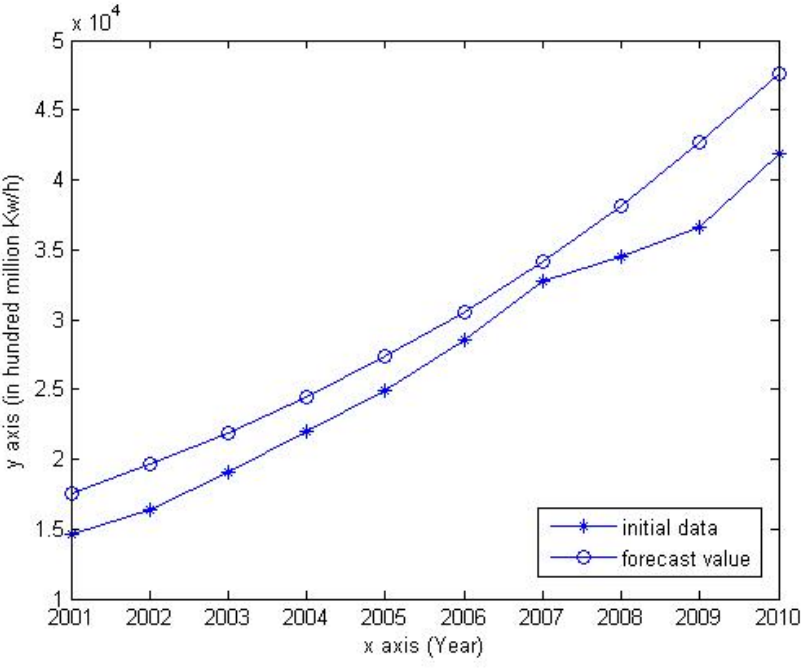

Fig. 1. Fitting of initial data and forecast value

5 Conclusions

Electronic technology has developed into an advanced stage, which can be applied to many fields. As an advanced kind of electronic technology, Matlab has a good operating environment, fruitful resource of functions, and its programming is far more efficient than other high-level program languages. Grey forecast model is widely used in various fields effectively. Grey model can conduct a large number of matrix calculations with certain complexity and difficulty. When be applied to Matlab, grey model can be realized much more convenient and effective. The development of computer application technology plays an indispensable role in solving the practical problems in the process of economic and social development, which is supposed to be vigorously promoted.

Acknowledgements. First I will express our deep gratitude for the support of the fund for outstanding young talents of university 2011, that is "Study on the data miming methods for the incomplete information system (Fund: 2011SQRL047)".

Thank you for my partners and my assistants. Because of their joined work, I can successfully finish the paper.

Last but not least, I'd like to thank my families and all my friends, for their encouragement and support.

References

[1] Mao, H.-S., et al.: Computer application technology. Tsinghua University Press (2006)
[2] Zhang, X.-D., et al.: Co-simulation technology based on Matlab/Fluent. Computer Engineering 20 (2010)
[3] Computational Mathematics Department of Tongji University, Modern numerical calculation. Beijing Posts and Telecom Press (2009)
[4] Zhang, X.-M., Ni, H.-X.: The fundamentals and Applications of Matlab. China Electric Power Press, Beijing (2009)
[5] Li, G.-N., Ruan, X.-Q.: Economic forecasting, decision-making and Matlab implementations (2007)
[6] Niu, D.-X., et al.: Electric Load Forecasting Technology and Application. China Electric Power Press, Beijing (2002)

The Research on Improved Iterative Control Algorithm for Maximum Entropy Model in Electronic Technology

Wei Yongqin, Guo Yinjing, Wu Na, and Zhang Rui

College of Information and Electrical Engineering,
Shan Dong University Science and Technology
Qianwan Port Road Number 579,
Qingdao Economic and Technological Development Zone
ieee2010@foxmail.com

Abstract. In the distributed processing, where common labeled data may be not available for designing classifier ensemble, however, an ensemble solution is necessary, traditional fixed decision aggregation could not account for class prior mismatch or classifier dependencies in electronic technology. Previous transductive learning strategies have several drawbacks, e.g., feasibility of the constraints was not guaranteed and heuristic learning was applied. We overcome these problems by developing improved iterative scaling (IIS) algorithm for optimal solution. This method is shown to achieve improved decision accuracy over the earlier approaches in electronic technology.

Keywords: distributed processing, maximum entropy (ME), iterative scaling (IS), optimal solution, electronic technology.

1 Introduction

In many distributed classification problems, the function which combines local classifier features is learned in an advanced method. And these methods require elicitation of teaching across the classifier ensemble [1] [3], and some important data may be not exist, traditional methods can't solve this problem. Some transductive learning strategies were proposed [2] [3]. And there, decisions on test samples were chosen aiming to satisfy constraints measured by each local classifier. These approaches were shown to reliably correct for class prior mismatch and to robustly account for classifier dependencies. But there are two main limitations of those works. First, feasibility of the constraints was not guaranteed. Second, heuristic learning was applied. Here we overcome these problems via an improved iterative scaling for aggregation in distributed classification.

According to the viewpoint on statistical learning, we want to get a probability assignment to satisfy whatever information is available. Intuitively that if we have little or no information about an event, we should choose a broad probability distribution to all possible events; on the other hand, when available information is sufficient to give high likelihood to a particular event's occurrence, there should be a sharp probability to indicate it. The great advantage given by information theory is that we can construct a unique, unambiguous criterion to represent the "amount of uncertainty" by a probability distribution, i.e., Shannon entropy [3]:

D. Jin and S. Lin (Eds.): Advances in Mechanical and Electronic Engineering, LNEE 177, pp. 575–580.
springerlink.com

$$H(X) = -\sum P(x)\log P(x) \tag{1}$$

P(x) is the probability mass function when random variable X takes output x. When we consider continuous random variables, Shannon entropy can be extended to differential entropy, defined as

$$H(X) = -\int_{-\infty}^{\infty} f(x)\log f(x)dx \tag{2}$$

Where f(x) is a probability density function.

The entropy function agrees with our common sense in that higher entropy indicates more uncertainty, while lower entropy indicates less uncertainty. The maximum entropy distribution has an important property that no possibility is ignored; it assigns positive probability to every event that is not absolutely excluded by the given information. Some well-known distributions are maximum entropy distribution when given appropriate moment constraints. For example, if we have no information to set up constraints, then the uniform distribution is maximum entropy distribution. So the standard approach to find a unique distribution satisfying given constraints is to invoke the principle of maximum entropy [6].

There are many good calculation models, and some constraints are ruled in them [3] [4] [5]. However, infeasibility of constraints could still be a problem in practice, moreover, even in the feasible case, there is no unique feasible solutions which are not guaranteed to possess any special properties. To make test set as accurate as possible, we believe we should seek the minimal use of the extra support necessary to achieve the constraints. The algorithm is stated as follows:

2 Algorithm Statement

To capture the learning principle mathematically, we now define:

$$\max_{\{P_u,\{P_e[c|\underline{x}]\},\{P[\underline{x}^{(j)},c^{(j)}]\}\}} H(C,\underline{X}) = -\sum_{\underline{x}\in x_{test}} \frac{P_u}{N_{test}} \sum_c P_e[c\mid \underline{x}]\log\Big(\sum_{\underline{x}\in x_{test}} \frac{P_u}{N_{test}} P_e[c\mid \underline{x}]\Big) - \sum_j \sum_{(\underline{x}^{(j)},c^{(j)})\in x_j} P[\underline{x}^{(j)},c^{(j)}]\log P[\underline{x}^{(j)},c^{(j)}] \tag{3}$$

Subject to

$$\begin{aligned} &P_{ME}[\hat{C}_j = \hat{c}\mid C=c, \underline{x}\in x_r^{(j)}] = P_{GT}^{(j)}[\hat{C}_j = \hat{c}\mid C=c] \quad \forall j,\forall c,\forall \hat{c} \\ &P_u + \sum_j \sum_{(\underline{x}^{(j)},c^{(j)})\in x} P[\underline{x}^{(j)},c^{(j)}] = 1 \\ &\sum_c P_e[C=c\mid \underline{x}] = 1 \qquad\qquad \forall \underline{x}\in x_{test} \end{aligned} \tag{4}$$

And $1 - P_u = P_o$

We propose an algorithm seeking to find the minimum value $P_o = P_o^*$ and the constraints are still feasible. When test set support is sufficient by itself to meet the

constraints, $P_o^* = 0$; otherwise $P_o^* > 0$. And next, we introduce Lagrange Multiplier ß to set the level $1 - P_u$.

The Lagrangian cost function corresponding to (3) and (4) is:

$$\begin{aligned} L_{ME}(\beta) = & -\sum_{\underline{x} \in X_{test}} \frac{P_u}{N_{test}} \sum_c P_e[c|\underline{x}] \log P_e[c|\underline{x}] - P_u \log \frac{P_u}{N_{test}} \\ & - \sum_j \sum_{(\tilde{\underline{x}}^{(j)}, \tilde{c}^{(j)}) \in \tilde{S}_j} P[\tilde{\underline{x}}^{(j)}, \tilde{c}^{(j)}] \log P[\tilde{\underline{x}}^{(j)}, \tilde{c}^{(j)}] \\ & + \sum_{j,\hat{c},c} \gamma[\hat{C}_j = \hat{c}, C = c] \begin{pmatrix} N_{ME}[\hat{C}_j = \hat{c}, C = c | \underline{x} \varepsilon x_r^{(j)}] - \\ P_{GT}^{(j)}[\hat{C}_j = \hat{c} | C = c] N_{ME}[C = c | \underline{x} \varepsilon x_r^{(j)}] \end{pmatrix} \\ & + \alpha(P_u + \sum_j \sum_{(\tilde{\underline{x}}^{(j)}, \tilde{c}^{(j)}) \in \tilde{S}_j} P[\tilde{\underline{x}}^{(j)}, \tilde{c}^{(j)}] - 1) \\ & + \sum_{\underline{x} \in X_{test}} \theta(\underline{x}) (\sum_c P[c|\underline{x}] - 1) \\ & + \beta(1 - P_u) \end{aligned} \tag{5}$$

Here, $\{\gamma[\hat{C}_j = \hat{c}, C = c], \forall j, c, \hat{c}\}$ are the Lagrangian multipliers associated with the local classifier constraints, which need to be learned. The Lagrangian multipliers α and $\theta(\underline{x})$, $\forall \underline{x} \varepsilon X_{test}$ will be automatically chosen to satisfy the pmf sum constraints. The Lagrangian multiplier β is treated as an "external" parameter and chosen to set the value of $1 - P_u$ as previously discussed. The improved iterative scaling (IIS) algorithm for minimizing $L_{ME}(\beta)$ consists of alternating i) optimization of P_u, $\{P_e[c|\underline{x}]\}$, and $\{P[\tilde{\underline{x}}^{(j)}, \tilde{c}^{(j)}]\}$ given $\{\gamma[\hat{C}_j = \hat{c}, C = c]\}$ held fixed, followed by ii) updata of $\{\gamma[\hat{C}_j = \hat{c}, C = c]\}$ given the other parameters fixed. In step ii), we update single Lagrangian multipliers, rather than a batch algorithm where all Lagrangian multipliers are updated in parallel. We believe there are no difficulties inherent to a batch version-we simply chose a sequential algorithm.

For fixed $\{\gamma[\hat{C}_j = \hat{c}, C = c]\}$, the globally optimal values for the remaining parameters, determined by taking partial derivatives of $L_{ME}(\beta)$ and setting to zero, are found to be:

$$P_e[c|\underline{x}] = \frac{\exp(\sum_{j=1}^{M} \sum_{\hat{c}=1}^{K} \gamma[\hat{C}_j = \hat{c}, C = c](P_j[\hat{C}_j = \hat{c} | \underline{x}^{(j)}] - P_{GT}^{(j)}[\hat{C}_j = \hat{c} | C = c]))}{\sum_{c'=1}^{K} \exp(\sum_{j=1}^{M} \sum_{\hat{c}=1}^{K} \gamma[\hat{C}_j = \hat{c}, C = c](P_j[\hat{C}_j = \hat{c} | \underline{x}^{(j)}] - P_{GT}^{(j)}[\hat{C}_j = \hat{c} | C = c]))} \tag{6}$$

$$\forall c, \underline{x} \varepsilon X_{test},$$

$$P[\tilde{\underline{x}}^{(j)}, \tilde{c}^{(j)}] = \frac{1}{Z(\underline{\gamma})} \exp(\sum_{\hat{c}=1}^{K} \gamma[\hat{C}_j = \hat{c}, C = \tilde{c}^{(j)}] \begin{pmatrix} P_j[\hat{C}_j = \hat{c} | \underline{x}^{(j)}] - \\ P_{GT}^{(j)}[\hat{C}_j = \hat{c} | C = \tilde{c}^{(j)}] \end{pmatrix}) \tag{7}$$

$$\tilde{\underline{x}}^{(j)}, \tilde{c}^{(j)} \in \tilde{x}_j, j = 1, ..., M,$$

3 Experimental Results and Analysis

We evaluated on data sets from the China central machine learning repository in Table 1 and we followed the experimental protocol from [3].

To simulate a distributed classification environment we used five local classifiers, each a classifier working on a randomly selected subset of features.

Table 1. Data sets used for the experiments

Data	No. of Class	No. of Feature	Feature subspace size
Blood cancer	4	18	[15,14,15,16,17]
Bone disease	9	21	[15,16,15,17,18]
Liver Disorder	2	6	[5,4,5,4,5]
Diabetes	2	7	[6,3,4,5,6]
Nephropathy	2	60	[52,54,56,58,59]
Heart	2	32	[28,27,29,30,31]

From table 1, we can know that every disease has its own classes and continuous features. All features in the data sets are continuous-valued and were modeled by Gaussian densities. We performed five replications of two-fold cross-validation for all data sets. For each replication, the data set was randomly divided into two equal-sized sets. In the first fold, one set was used as training and a subset of the other was used for testing, with these roles reversed in the second fold. We averaged test error rates over all replications and folds, for a given fold, only a subset was used for testing in order to introduce a controlled level of prior mismatch between the training and testing sets. This was accomplished as follows. The original test set priors and training set priors are very similar since they are based on a random, equal-sized split of the whole dataset. To introduce more prior mismatch and to test the robustness of the various combining schemes to incorrect local class priors, we performed resampling on the test data. For example, suppose in the original test set there are two classes with priors as $[\alpha, 1-\alpha]$. The new test set is then obtained by sampling with replacement from the original test set (to create a data set of size equal to the original test set size), based on these new priors. Note that sampling with replacement does introduce significant sample duplication in some cases. For example, on Diabetes, for test class prior distribution [0.2 0.8] (used in Table 2) with 92 unique samples from class 2 and 365 test samples to be drawn, all samples from class 2 are likely to have a duplicate in the resampled test data. Sampling with replacement was used because of the small sizes of some of the data sets – sampling without replacement would have severely constrained the test set prior distributions that could have been achieved on these small data sets. Table 2 shows the class priors chosen for the test set, for different datasets, averaged over the ten experimental trials. We quantified the mismatch between test set priors ($P_{test}(C=c)$) and local training set priors $(P_{trn}^{(j)}[C=c])$ by the sum of cross entropies: $M=\sum_{j=1}^{M}\sum_{c=1}^{K}P_{trn}^{(j)}[C=c]\log(\frac{P_{trn}^{(j)}[C=c]}{P_{test}[C=c]})$.

Table 2. Average test class priors and mismatch values for different data

Data	Class Priors on the Total Data Set	Mismatch	Pre-set Class Priors on the Test Set
Blood cancer	[0.23 0.26 0.23 0.25]	0.96	[0.1 0.4 0.11 0.39]
		2.73	[0.04 0.46 0.05 0.45]
		missing	[0 0.5 0.05 0.45]
Bone disease	[0.13 0.13 0.13 0.13 0.13 0.13 0.13]	0.066	[0.13 0.13 0.12 0.17 0.15 0.15 0.1]
		1.41	[0.05 0.08 0.27 0.05 0.24 0.26 0.05]
		2.40	[0.03 0.24 0.03 0.04 0.3 0.05 0.31]
		missing	[0.03 0.24 0.03 0.04 0.33 0.05 0.31]
Liver discover	[0.32 0.56]	0.34	[0.6 0.4]
		1.79	[0.8 0.2]
		3.56	[0.9 0.1]
		missing	[1 0]
Diabetes	[0.67 0.33]	0.74	[0.4 0.6]
		1.43	[0.3 0.7]
		2.57	[0.2 0.8]
		missing	[1 0]
Nephropathy	[0.47 0.53]	0.32	[0.3 0.7]
		0.89	[0.2 0.8]
		2.28	[0.1 0.9]
		missing	[0 1]
Heart	[0.36 0.64]	0.21	[0.5 0.5]
		1.24	[0.1 0.9]
		2.25	[0.05 0.95]
		missing	[0 1]

When there are no examples from one of the classes in the test batch , an extreme case of prior mismatch is that this class has a zero test set prior probability , we refer to this case as the missing class case, In"missing class" experiments , we find that the missing class case is interesting for several reasons. First, it represents an extreme case of prior mismatch and thus a severe test of the robustness of a method to prior mismatch. Second, in an application scenario it may be important to recognize that one of the classes is wholly not present in the testing data. This may provide valuable actionable information. Next, we compared the results obtained for IIS using local training support and training support derived from the constraints. Measured error rate on the test set and the joint entropy on the test training supports. The IIS algorithm allocated probability mass between the training sets and test set without any constraint by letting $\beta = 0$.

4 Conclusions

We calculated and analyzed various asymptotic properties of the improved iterative control algorithm for maximum entropy probability. First, the algorithm solves a convex optimization problem with linear constraints [7], therefore, a unique solution at each β for which the constraints are feasible.Sencond, IIS algorithm descends in the Lagrangian cost function for a given β. If the problem is infeasible at a given β, convergence of the algorithm is not guaranteed. When $\beta = 0$, there is no constraint on P_u—this solution thus achieves highest entropy $H(C,X)$, compared to solutions at other β values. Third, From experiment data, we can see the classification performance of EIIS is better than naive Bayes and with much lower joint entropy, and we also see the phenomenon of lower error rates in the high mismatch cases on some data sets, especially for the EIIS method in electronic technology.

Acknowledgments. We thank Pro.Guo yinjing for stimulating discussions and for encouragement to complete the manuscript, this work was supported by National Natural Science Fouddation of China grant No.61071087.

References

1. Darroch, J., Ratcliff, D.: Genralized Iterative Scaling for Log-linear Models. Annals of Mathematical Statistics 43(5), 1470–1480 (1972)
2. Della Pietra, S.A., Della Pietra, V.J., Lafferty, J.: Inducing Features of Random Fields. IEEE Transactions on Pattern Analysis and Machine Intelligence 19, 380–393 (1997)
3. Miller, D.J., Pal, S.: Transductive Methods for the Distributed Ensemble Classification Problem. Neural Computation 19(3), 856–884 (2007)
4. Basak, J., Kothari, R.: A Classification Paradigm for Distributed Vertically Partitioned data. Neural Computation, 1525–1544 (2004)
5. D'Costa, A., Ramachandran, V., Sayeed, A.M.: Dsitributed Classification of Gaussian Space-Time Sources in Wireless Sensor Networks. IEEE Journal on Selected Areas in Communications 22(6), 1026–1036 (2004)
6. Jaynes, E.T.: Papers on Probability, Statistics and Statistical Physics, 1st edn. Springer (1989)
7. Collins, M., Schapire, R.E., Singer, Y.: Logistic Regression, Adaboost and Bregman Distances. Machine Learning, 158–169 (2000)
8. Boyd, S., Vandenberghe, L.: Convex Optimization, p. 137. Cambridge University Press (2004)

Application of Least Square Support Vector Machine in Electronic Engineering Based on Principal Component Analysis

Yuansheng Huang and Hongsong Ma

North China Electric Power University, 071003, Baoding, China
a6531472@126.com

Abstract. Electronic engineering can be further broken down into electrical measuring, adjusting and electronic technology. This paper starts from the electrical measurement technique and presents a least square support vector machine model in electronic engineering based on principal component analysis. Principal component analysis can extract main components of the input variables data which have impact on the power load, and to a certain extent, it reduces the dimension of the input variables while eliminates the original input variables redundant information, making the extracted integrated factor represent the original variables better. At the same time selecting least squares support vector machine as load forecasting model that can better achieve the nonlinear curve fitting to improve the forecast accuracy, and improve generalization performance. Use the model as a grid short-term load forecasting model, and make a case analysis compared to other methods. The experimental result shows that the model has good predictive results, and it can be applied to electronic engineering of other regions and power price forecasting field.

Keywords: load forecasting, principal component analysis, least squares support vector machine.

1 Introduction

Short-term load forecasting is playing an important role in developing plans for the purchase of electricity and arranging the way to run. Accurate predictions can improve the security and economy of grid operation, thereby improving the power quality and realizing automation of power system operation. So the short-term load and f electronic engineering orecasting requires the highest possible prediction accuracy [1].

Based on the analysis of the associated literature, this paper presents a least squares support vector machine load forecast model based on principal component analysis, using principal component analysis to pre-process data, and extracting the trained samples of SVM from data to reduce input variables and make input variables more representative. Then use LS-SVM model for short-term load forecasting to improve the training speed and prediction accuracy.

D. Jin and S. Lin (Eds.): Advances in Mechanical and Electronic Engineering, LNEE 177, pp. 581–586.
springerlink.com

2 Principal Component Analysis

Principal component analysis takes a dimensionality reduction method to identify a few integrated factor to represent the original number of variables, making these factors reflect the amount of information of the original variables as much as possible, and correlation between them is very low, greatly improving the prediction performance of SVM.

Let indicators of n samples in the k values, the aim is to present a $Y = \begin{pmatrix} Y_1 & Y_2 & \cdots & Y_k \end{pmatrix}^T$, so as to meet the following three conditions:

$$Y_k = a_{k1}X_1 + a_{k2}X_2 + \cdots a_{kk}X_k \quad . \tag{1}$$

Covariance matrix of Y is a diagonal matrix; the variance of Y is as large as possible.

Then, selecting the indicators which make the largest contribution to variance achieves the goals of principal component analysis.

Through mathematical derivation, principal component analysis to extract comprehensive factor set out below:

Assume R as covariance matrix of input samples $\mathrm{x} = \begin{pmatrix} \mathrm{x}_1 & \mathrm{x}_2 & \cdots & \mathrm{x}_k \end{pmatrix}^T$, it has the pair of eigenvalues and eigenvectors $(\lambda_1,\mathrm{e}_1), (\lambda_2,\mathrm{e}_2), \cdots, (\lambda_k,\mathrm{e}_k)$, the i-th principal component is:

$$\mathrm{Y_i} = \mathrm{e_i^T X} \quad . \tag{3}$$

Here, $\mathrm{Var(Y_i)} = \mathrm{e_i^T} \sum \mathrm{e_i} = \lambda_\mathrm{i}, (\mathrm{i} = 1, 2, \cdots, \mathrm{k})$.

As can be seen from the above formula, the characteristic value reflects the proportion of new information contained in the associated principal components. According to this article, the cumulative contribution of principal components determines the network input indicators. The total contribution rate of the i-th principal component is defined as:

$$\beta_\mathrm{i} = \frac{\sum_{\mathrm{p}=1}^{\mathrm{i}} \lambda_\mathrm{k}}{\sum_{\mathrm{p}=1}^{\mathrm{k}} \lambda_\mathrm{k}} \quad . \tag{4}$$

3 Least Squares Support Vector Machine

The main idea of SVM is a nonlinear mapping with the input vectors mapped to the high-dimensional feature space H, based on structural risk minimization principle to construct the optimal decision function, and clever use of original space nuclear function to replace the dot product of high-dimensional feature space [2][3].

The loss function of least squares supports vector machine method replaces the traditional quadratic programming method with least-squares linear system. When

Standard support vector machine and least squares support vector machine use the principle of structural risk, they select different loss functions in the target optimization, and they are error ξ_i (slack variables allowed wrong points) and two-norm of error ξ_i .Assume training sample as $\{(X_i, y_i)\}_{i=1}^{N}$, in which $X_i \in R^n$ is n-dimensional training sample input, and $y_i \in R$ is the output of the training sample [4].

$$\min_{\omega,e} : J(\omega, e) = \frac{1}{2}\omega^{\mathrm{T}}\omega + C\sum_{i=1}^{N}\xi_i^2 \quad . \tag{5}$$

Constraints：

$$y_k = w^T\varphi(x_k) + b + e_k \quad . \tag{6}$$

Where: $\varphi(\bullet) : R^n \to R^{n_h}$ is the kernel space mapping function; weight vector $w \in R^{n_h}$ (original space); error variable $e_k \in R$ is the deviation. According to (5), define the Lagrangian function:

$$L(w,b,e;a) = J(w,e) - \sum_{k=1}^{N} a_k\{w^T\varphi(x_k) + b + e_k - y_k\} \quad . \tag{7}$$

Lagrange multiplier $\alpha_k \in R$. On the type of optimization, make the partial derivatives of L for w, b, e_k , a_k equal to zero, eliminating the variable w, e to get the following matrix: equation:

$$\begin{bmatrix} 0 & I^T \\ I & \Omega + \dfrac{1}{\mathrm{C}}I \end{bmatrix}\begin{bmatrix} b \\ a \end{bmatrix} = \begin{bmatrix} 0 \\ y \end{bmatrix} \quad . \tag{8}$$

Where: $x = [x_1 x_2 ... x_N]$, $y = [y_1 y_2 ... y_N]$, $I = [1...1]$, $a = [a_1 ... a_N]$, $\Omega_{kl} = \psi(x_k, x_l) = \varphi(x_k)^T\varphi(x_l)$, $k, l = 1, ..., N$ 。 According to mercer conditions, there are mapping function φ and nuclear function $\psi(\bullet, \bullet)$:

$$\psi(x_k, x_l) = \varphi(x_k)^T\varphi(x_l) \quad . \tag{9}$$

Least squares support vector machine function is estimated as follows:

$$y(x) = \sum_{k=1}^{N} a_k \psi(x, x_k) + b \quad . \tag{10}$$

4 Analysis

This paper selects load data of a regional grid from May to October in 2009 as training samples and test samples. According to the preceding literature related analysis, this paper select input variable indicators of sample data, including a load value at the moment a week ago, a load value at the moment a day before, two days before and three days, a load value a quarter of an hour before, two quarter of an hour before and three quarters of an hour before, the type of week, temperature and humidity and so on. There are ten indicators. At the same time, the paper also uses the classical SVM algorithm and BP neural network for load forecasting, and compares results.

Using SPSS software to analyze normalized data and extract comprehensive factor. The results are as the following table:

Table 1. The initial explained variance of factor

Component	Initial Eigenvalues		
	Total	Variance (%)	Cumulative (%)
1	3.960	39.602	39.602
2	1.620	16.201	55.804
3	1.184	11.840	67.644
4	1.045	10.448	78.091
5	0.896	8.958	87.050
6	0.652	6.518	93.568
7	0.511	5.107	98.674
8	0.121	1.208	99.882
9	0.011	0.106	99.987
10	0.001	0.013	100.000

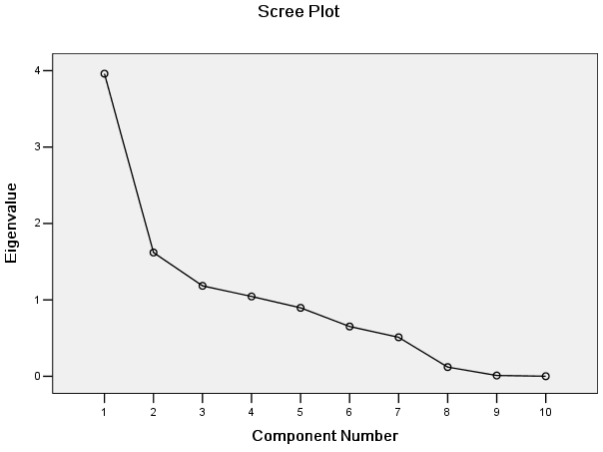

Fig. 1. Gravel figure of principal component extracted factor

Based on the above analysis of the total explained variance and gravel figure, when five principal components factor are extracted, the cumulative explained variance contribution rate has reached 87.05%, so the five principal components extracted from the original input variables can replace 87.05% of the information, reducing dimensions and eliminating the correlation between variables, so as to reduce training time of load forecast model. Regard extracted five principal components as the input variables of the next step, and calculate load forecasts with least squares support vector machine. Specific predictions are shown as below:

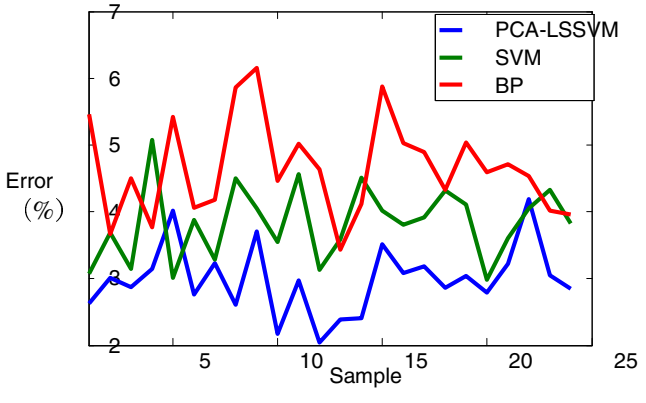

Fig. 2. Error comparison of load forecasting models

As can be seen from Figure 2, PCA-LSSVM model has obvious advantages in improving forecasting precision. It is more accurate than neural networks under the conditions of small sample-sized and non-linear volatile short-term load forecasting.

According to Matlab calculations, PCA-LSSVM, SVM and BP models relative errors were 2.99,3.84 and 4.65. PCA-LSSVM model's forecasting error was significantly lower than SVM and BP neural network, and its accuracy has been greatly improved.

5 Summary

Electronic engineering can be further broken down into electrical measuring, adjusting and electronic technology. This paper starts from the electrical measurement technique and presents a principal component analysis based on support vector machine model, using the principal component analysis to extract the principal components of historical data and eliminate a lot of noise and redundancy, then data extraction from the processed LSSVM training samples, to improve the training speed and prediction accuracy. Finally, the model is applied to electronic engineering, and has better generalization performance and prediction accuracy compared to SVM and BP neural network.

References

1. Cherkassky, V., Ma, Y.: Practical Selection of SVM Parameters and Noise Estimation for SVM Regression. IEEE Trans. on Neural Networks 17, 113–126 (2004)
2. Sklar B.: Digital Communications-Fundamentals and Applications 2nd edn. Pearson Education, London (2006)
3. Dong-xiao, N., Shu-hua, C., Jian-chang, L., Lei, Z.: Power Load Forecasting Technology and Its Application, 2nd edn. China Electric Power Press, Beijing (2009)
4. Bo, L., Ling, W., Hui-jin, Y.: An Effective PSO-based Memetic Algorithm for Flow Shop Scheduling. IEEE Trans. on Systems, Man and Cybernetics Part B 37, 18–27 (2007)
5. Dong-xiao, N., Zhi-hong, G., Mian, M.: Study on Forecasting Approach to Short-term Load of SVM Based on Data Mining. In: Proceedings of the CSEE, Beijing, vol. 26, pp. 6–12 (2006)
6. Hong-chun, S.: Electrical Engineering Signal Processing, 1st edn. Science Press, Beijing (2009)

Research on Exactly SEIF-SLAM and Its Application in Electronic Engineering

Xiaohua Wang and Ping Li

College of Electronic and Information, Xi'an Polytechnic University, Xi'an, China
w_xiaohua@126.com

Abstract. In historical electronic engineering, information cannot be fully utilized for information confusion because of small weight particle removed in resample and single iteration of particle filter algorithm. A SLAM algorithm based on exactly sparse extended information filter combing particle filter is brought forward, Information matrix of exactly sparse extended information filter maintain robot position historical information, particles containing historical information are obtained by Gibbs sample, Particles set describe the posterior distribution of robot position well, and the accuracy of state estimation SLAM algorithm is improved. The simulation results indicate that the method is valid.

Keywords: simultaneous localization and map building (SALM), exactly sparse extended information filter, particle filter, Gibbs sample.

1 Introduction

As a mobile robot could navigate in unknown environment autonomously with the help of SLAM, therefore, how to fuse new observed information to the previous becomes a problem to be solved in electronic engineering. Nowadays, the improved SLAM is often proposed from a perspective of the choice of Important Function or re-sampling to deal with the particle "exhausted" phenomenon in Particle Filter (PF). The re-sampling methods include Important Sampling (IS), residual re-sampling, minimum variance sampling, Polynomial re-sampling, hierarchical re-sampling, etc[1]. The selection of Important Functions contains Unscented Kalman Filter(UKF)[2], Auxiliary Particle Filter(APF)[3], Regular Particle Filter(RPF)[4], Marginal Particle Filter(MPF), Auxiliary Marginal Particle(AMP)[5] , etc.

Extended Information Filter (EIF) increases the computational complexity. The Sparse Extended Information Filter (SEIF) [6] is consistent with its local distribution. Exactly Sparse Extended Information Filter (ESEIF) is a theory based on robot re-location and has proved to be consistent globally [7].

In the traditional or improved SLAM-PF, there exists a problem called particle "forgotten" phenomenon. With the application of the algorithm of the ESEIF to PF framework, this paper proposes the ESEIF-PF SLAM which can keep the historical information of relative variations of a robot's poses. And all the known relative variations related to the robot's state form the conditional probability distribution of SLAM posterior probability. By using the Gibbs sampling, new samples occur from

D. Jin and S. Lin (Eds.): Advances in Mechanical and Electronic Engineering, LNEE 177, pp. 587–592.
springerlink.com

the SLAM complete posterior distribution. Thus the particle set can describe the real posterior distribution in detail and improve the accuracy of the state estimation of the SLAM.

2 SLAM Based on ESEIF

2.1 Description of ESEIF-SLAM [8]

In SLAM, a map consists of feature vectors. After the combination of the robot poses with environmental map, the problem is how to decide a density distribution of the posterior probability. At k o'clock, the distribution of the joined posterior probability can be explained in the form of Gaussian distribution.

$$\begin{aligned} p\left(X_{r(k)}, M \mid Z^{k}, u^{k}\right) &= N\left(\begin{bmatrix} \mu_{x_{r(k)}} \\ \mu_{M} \end{bmatrix}, \begin{bmatrix} \Sigma_{x_{r(k)}x_{r(k)}} & \Sigma_{x_{r(k)}M} \\ \Sigma_{Mx_{r(k)}} & \Sigma_{MM} \end{bmatrix}\right) \\ &= N^{-1}\left(\begin{bmatrix} \eta_{x_{r(k)}} \\ \eta_{M} \end{bmatrix}, \begin{bmatrix} \Delta_{x_{r(k)}x_{r(k)}} & \Delta_{x_{r(k)}M} \\ \Delta_{Mx_{r(k)}} & \Delta_{MM} \end{bmatrix}\right) \end{aligned} \tag{1}$$

$\eta_k = \Delta_k \mu_k$, $\Delta_k = \Sigma_k^{-1}$ are the information vector and information matrix separately. Each element districted in $\Delta_{x_{r(k)}x_{r(k)}}$ and Δ_{MM} restrains a state vector. $\Delta_{x_{r(k)}M}$ and $\Delta_{Mx_{r(k)}}$ indicate the relevance between robot pose estimation and characteristic position estimation.

2.2 Motion Prediction

Based on EIF-SLAM, the process of motion prediction becomes more complex than EKF-SLAM. Firstly, the predicted robot pose $\hat{X}_{r(k)}$ can be obtained relying on the kinematics model of a mobile robot, and $\left[X_{r(k-1)}, M\right]^T$ turns into an augmented vector $\left[X_{r(k)}, X_{r(k-1)}, M\right]^T$. Then the information filter of the posterior probability can be conveyed by (2). Secondly, the marginal probability $\left[X_{r(k)}, X_{r(k-1)}, M\right]^T$ and the state-posterior probability $p(X_{r(k)}, M \mid Z_{1k-1}, u_{0k})$ can be easily gained by (3).

$$p\left(X_{r(k)}, X_{r(k-1)}, M \mid Z^{k-1}, u^{k}\right) = N^{-1}(\hat{\eta}_k, \hat{\Delta}_k) \tag{2}$$

$$\begin{aligned} p(X_{r(k)}, M \mid Z_{1:k-1}, u_{0:k}) &= \int p(X_{r(k)}, X_{r(k-1)}, M \mid Z_{1:k-1}, u_{0:k}) dX_{r(k-1)} \\ &= N^{-1}(\bar{\eta}_k, \bar{\Delta}_k) \end{aligned} \tag{3}$$

2.3 Exact Sparsification and Observation Update

In the process of motion prediction, the marginalization component gives rise to a fully populated information matrix. Thus, it's urgent to make the information matrix

sparse. The observed feature points Z_n are divided into $Z_n=[Z_\alpha Z_\beta]$. Z_α is used to update state vectors according to the rule of observation update.

$$p(X_{r(k)}, M \mid Z_{1:k}, u_{0:k}) \propto p(X_{r(k)}, M \mid \{Z_{1:k-1}, Z_\alpha\}, u_{0:k}) \tag{4}$$

Then referring to the method of the calculation course of the marginal probability, the information related to feature points is acquired by removing the robot's poses from state vectors. Finally, Z_β is applied to re-locate the robot poses as illustrated in (5). G is the Jacobi matrix, $\bar{\mu}_{m_\beta}$ implies the prediction value of M_β.

$$\begin{aligned} X_k &= g(M_\beta, Z_\beta, w_k) \\ &= g(\bar{\mu}_{m_\beta}, Z_\beta) + G(M - \bar{\mu}_k) + w_k \end{aligned} \tag{5}$$

3 SLAM Based on ESEIF-PF

3.1 The Expression of SLAM Conditional Probability

The posterior possibility $p(X_{r(1:k)}, M \mid Z_{1:k}, u_{0:k-1})$, combined poses of a robot and its environmental map based on SLAM-PF, can be decomposed into $p(X_{r(1:k)} \mid Z_{1:k}, u_{0:k-1})$ and $p(M \mid X_{r(1:k)}, Z_{1:k}, u_{0:k-1})$. Besides, $X_{r(k)}$ and the prior state $X_{r(k-1)}$ are respectively independent. Path estimation $p(X_{r(1:k)} \mid Z_{1:k}, u_{0:k-1})$ of the robot can be given by

$$p(X_{r(1:k)} \mid Z_{1:k}, u_{0:k-1}) = p(X_{r(k)} \mid X_{r(k-1)}, Z_{1:k}, u_{0:k-1}) \cdots p(X_{r(1)} \mid X_{r(0)}, Z_{1:k}, u_{0:k-1}) \tag{6}$$

3.2 Gibbs Sampling

Gibbs Sampling [9] is an iterative sampling approach based upon conditional distribution. From the joint-probability distribution within two stochastic variables or more, a sampling sequence can be obtained to approximate the joint-probability distribution. Besides, the Gibbs Sampling can take turns to take a sample. According to the formula of Gibbs Sampling in SLAM, a sample of the robot paths will be easily obtained. And just do for N times; N path samples will be got.

3.3 SLAM Based on SEIF-PF

The detailed implement process of SLAM based on SEIF-PF is followed,

Step 1: Particles Initialization

Step 2: Particle Prediction. According to the control vector u_k and the robot motion model, the robot pose distribution can be predicted, or $\bar{\eta}_k$ and $\bar{\Delta}_k$ corresponding to each particle can be calculated.

Step 3: Data Association. Adopting the method of maximization applied to observing the data association, the observed information and the estimation map can be associated with each other.

Step 4: Particle Update. The exactly sparse process and observation update can be carried out relying on the observation information corresponding to each particle. With the application of equation (4), (5), (6), η_k and Δ_k will be received, or updating the prior distribution and obtaining the proposed distribution.

Step 5: Estimation of the Robot Path. With $X^i_{r(k)}$ gotten, the weight can be made out. If $1\Big/\sum_{i=1}^{N}(w_k^i)^2$ is less than the given threshold, Gibbs Sampling will be applied to acquire the posterior probability distribution $p(X_{r(1:k)}|Z_{1:k},u_{0:k-1})=\sum_{i=1}^{N}w_k^i\delta(X_{r(1:k)}-X^i_{r(1:k)})$.

Step 6: Map Estimation Update. Relying on the associated observation information, the associated feature-estimation values will be updated. And the relevance of the information vector and the information will be computed. Then that observation information without any relevance with the features will be as new features and added to the map.

4 Experiments and Analysis

4.1 Experimental Model

The robot motion model regarded to control command is adopted. $u_k=[v_k,\Delta\theta_k]^T$ denote control variables, $(v_k,\Delta\theta_k)$ respectively imply a robot's linear velocity and deflection angle, ΔT is the period of motion, L indicates the distance between wheels of the robot.

$$X_{r(k+1)}=f(X_{r(k)},u_k,w_k)=\begin{bmatrix} x_{r(k)}+v_k\Delta T\cos(\theta_k+\Delta\theta_k) \\ y_{r(k)}+v_k\Delta T\sin(\theta_k+\Delta\theta_k) \\ \theta_k+\dfrac{v_k\Delta T\sin\Delta\theta_k}{L}\end{bmatrix}+w_k \quad . \tag{7}$$

Model of observation can be conveyed by

$$Z^r_{l(k)}=\begin{bmatrix}\sqrt{(x_l^r-x_{r(k)})^2+(y_l^r-y_{r(k)})^2} \\ \arctan\dfrac{y_l^r-y_{r(k)}}{x_l^r-x_{r(k)}}-\theta_r\end{bmatrix}+v_k \quad . \tag{8}$$

4.2 Experimental Results and Analysis

The SLAM for a robot based on ESEIF-PF is tested in the MATLAB environment where the number of particles is set 200.

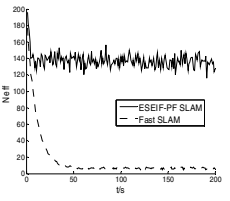

Fig. 1. Variation of particles

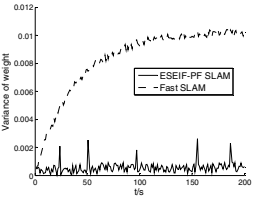

Fig. 2. Variance of weight

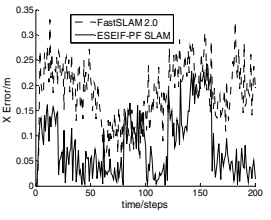

Fig. 3. (a) Position errors in X

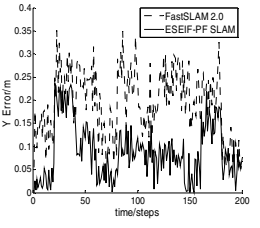

Fig. 3. (b) Position errors in Y

Fig.1 display a variation diagram of valid particles with time based on the above two algorithms. It can be seen that the increase of valid particles with time embodies an exponentially decreasing tendency in the algorithm of FastSLAM2.0. While the number of valid particles keeps stable in a large amount, and it varies around 140 accounting for 70%.Fig.2 display a variation diagram of variance of weight with time. It's obvious that the variance of weight in ESEIF-PF SLAM is far less than that in FastSLAM2.0. It has proved that it will have better particle diversity based on the ESEIF-PF SLAM. In contrast, the particle "exhausted" phenomenon is really serious in FastSLAM2.0.Fig.3 displays the comparison of position errors.

In order to further illustrate the performance of the algorithm, this paper separately compares average errors of pose estimates in X and Y direction based on ESEIF-PF SLAM and FastSLAM2.0. From Fig.3, it's easy to find the ESEIF-SLAM with higher estimation precision than the FastSLAM2.0.

5 Conclusions

This paper has proposed the ESEIF-PF SLAM combined Exactly Sparse Extended Information Filter and Particle Filter based on SLAM applied in electronic engineering. The information matrix and information vectors are used to keep and store the history information of particles. Gibbs Sampling is applied to contradict the "forgotten" phenomenon when only using the temporary information in single iterative process, meanwhile keep the diversity of particles, decrease the degradation phenomenon and the particle set can better describe the posterior probability distribution. Moreover, the paper has improved the estimation precision of states.

References

[1] Yu, H., Wang, Y.: A Review on Mobile Robot Location and Map-building Algorithms Based on Particle Filters. Robot 29(3), 281–289 (2007)
[2] Sanjeev, A.P., Maskell, S., Gordon, N.: A tutorial on Particle filters for on-line non-linear/non-gaussian Bayesian tracking. IEEE Trans. Signal Proeeeding, 174–188 (2002)
[3] Pit, M., Shephard, N.: Filtering via simulation: Auxiliary Particle fllters. Journal of the American Statistical Association 94(446), 590–599 (1999)
[4] Musso, C., Oudjane, N., LeGland, F.: Improving Regularised Particle filters. In: Sequential Monte Carlo Methods in Practice, Gordon, pp. 234–247. Springer, NewYork (2001)
[5] Martinez-Cantin, R., Freitas, N., Castellanos, J.A.: Analysis of Particle Methods for Simultaneous Robot Localization and Mapping and a New Algorithm: Marginal-SLAM. In: IEEE International Conference on Robotics and Automation, Roma, pp. 2415–2420 (2007)
[6] Walter, M., Eustice, R., Leonard, J.J.: A Provably Consistent Method for Imposing Sparsity in Feature-Based SLAM Information Filters. In: Proceedings of ISRR 2005, pp. 214–234 (September 2005)
[7] Frese, U.: A proof for the approximate sparsity of SLAM information matrices. In: Proceedings of the ICRA, Barcelona, Spain, pp. 331–337 (April 2005)
[8] Waltef, M.R., Eustice, R.M., Leonard, J.: Exactly sparse extended Information filters for Feature- based SLAM. International Journal of Robotics Research 26(4), 335–359 (2007)
[9] Zhang, H., Liu, Y., Fan, X.-P., Qu, Z.: Mobile robot simultaneous location and mapping based on particle filtering with fixed-lag Gibbs sampling. Application Research of Computers 25(11), 23–28 (2008)

Investigation on SEIF Based on SLAM in Electronic Engineering

Xiaohua Wang, Fan Wang, and Ping Li

College of Electronic and Information, Xi'an Polytechnic University, Xi'an, China
xiangpingfly100@163.com

Abstract. In traditional PF commonly used in electronic engineering, only the present information is used in a single interactive process and the information standing for the small weight of particles will be removed, leading to the problem that the information cannot be made full advantage of. This paper presents a joint SLAM algorithm combined Sparse Extended Information Filter (SEIF) and Particle Filter (PF) aiming to solve the problem occurring in the traditional particle filter algorithms. Information matrixes can keep all history information of poses related to a robot. With the application of Gibbs sampling, new particle set will be re-obtained resulting that posterior distribution can be described better and the state estimation precision is improved. A large amount of Monte-Carlo simulation experiments have proved that the algorithm proposed in this paper has improved the robot's location precision by approximately 80% over the FastSLAM2.0.

Keywords: SLAM, Sparse Extended Information Filter (SEIF), particle filter, Gibbs sampling.

0 Introduction

Particle Filter(PF) has a better adaptability in the real robot's system of both nonlinear and non-Gaussian processes. In electronic engineering, the Simultaneous localization and mapping(SLAM) based on PF in robotics[1,2] is an important research area. Unscented Particle Filter (UPF), combining Unscented Kalman Filter instead of Extended Kalman Filter (EKF) and PF in SLAM, has a further better filtering effect, while its biggest problem is how to choose a proper control parameter[3]. Some researchers increase the number of Taylor remainders in EKF to improve the estimation accuracy of particle filters[4]. In [5], one approach to alleviate this situation is the use of iteration in UPF. Those particles with high likelihood value are used to improve estimation accuracy in Auxiliary Particle Filter(APF)[6], and Regular Particle Filter (RPF) relies on re-sampling from consistently approximate distribution[7], both of which are appropriate for weak process-noise system. Marginal Particle Filter (MPF) and Auxiliary Marginal Particle Filter(AMPF)[8] choose to sacrifice high computational complexity to overcome its drawback of the particle degeneracy phenomenon.

This paper proposes an improved SEIF-PF SLAM algorithm which can keep the historical information of relative variations of a robot's poses by its corresponding

D. Jin and S. Lin (Eds.): Advances in Mechanical and Electronic Engineering, LNEE 177, pp. 593–598.
springerlink.com

information matrix and information vectors in electronic image processing. Besides, all the known relative variations related to the robot's poses form the conditional probability distribution of SLAM posterior probability. With the help of Gibbs sampling, new samples occur from the SLAM complete posterior distribution to make sure that the particle set gained from above can describe the real posterior distribution better and improve the accuracy of the estimation of the SLAM algorithm.

1 Theory of SEIF-SLAM

1.1 The Theory Basis of SEIF-SLAM

In a robot's navigation task, its behavioral dynamic system is mainly designed to contain heading to a goal point coordinately and avoiding obstacles. At a direction of the goal point, an attractor is generated:

$$\dot{\phi} = f_{\phi t}(\phi, d_t) = -\lambda_{tar}(\phi - \phi_{tar})(e^{-c_1 d_t} + c_2) \tag{1}$$

Where,ϕ_{tar} indicate the angle between a goal point and the robot, λ_{tar} indicate the strength of the attractor and is positive, C_1 defines the decay of the strength of the repellor with the increasing distance to the goal point, the global minimum strength of the attractor is denoted by C_2.

1.2 Pose Estimation

The process of robot's pose estimation in SEIF-SLAM becomes more complex than EKF-SLAM because of calculating the marginal probability. First of all, it will be considered how to get the predicted robot pose $\hat{X}_{r(k)}$, and the state vector $\left[X_{r(k-1)}, M\right]^T$. The posterior probability based on pose estimation can be expressed by

$$p\left(X_{r(k)}, X_{r(k-1)}, M \mid Z^{k-1}, u^k\right) = N^{-1}(\hat{\eta}_k, \hat{\Delta}_k) \tag{2}$$

Then, the problem, which is commonly referred to the following (3), is how to calculate the $\overline{\eta}_k$ and $\overline{\Delta}_k$ in the marginal probability.

$$\begin{aligned}
\overline{\eta}_k &= \hat{\eta}_k^2 - \hat{\Delta}_k^{21}(\hat{\Delta}_k^{11})^{-1}\hat{\eta}_k^1 \\
&= \begin{bmatrix} Q^{-1}(f(\mu_{x_{r(k-1)}}, u_k) + Q^{-1}F\Omega \\ \eta_M - \Delta_{M x_{r(k-1)}}\Omega \end{bmatrix} \\
\Omega &= (\Delta x_{r(k-1)} x_{r(k-1)} + F^T Q^{-1} F)^{-1}\left\{\eta_{x_{r(k-1)}} - F^T Q^{-1}(f(\mu_{x_{r(k-1)}}, u_k) - F\mu_{x_{r(k-1)}})\right\}
\end{aligned} \tag{3}$$

$$\begin{aligned}
\overline{\Delta}_k &= \hat{\Delta}_k^{22} - \hat{\Delta}_k^{21}(\hat{\Delta}_k^{11})^{-1}\hat{\Delta}_k^{12} \\
&= \begin{bmatrix} (Q + F\Delta^{-1}_{x_{r(k-1)}x_{r(k-1)}}F^T)^{-1} & Q^{-1}F\Phi\Delta_{x_{r(k-1)}M} \\ \Delta_{M x_{r(k-1)}}\Phi F^T Q^{-1} & \Delta_{MM} - \Delta_{M x_{r(k-1)}}\Phi\Delta_{x_{r(k-1)}M} \end{bmatrix} \\
\Phi &= (\Delta x_{r(k-1)} x_{r(k-1)} + F^T Q^{-1} F)^{-1}
\end{aligned}$$

Q denotes the covariance matrix used to control noises, $f(\mu_{x_{r(k-1)}}, u_k)$ represents a robot's pose estimation value after movement, $\mu_{x_{r(k-1)}}$ defines an expected value of the state vector at the $k-1$ moment, and F indicates the Jacobian matrix.

1.3 Sparse Information Matrix [10]

In the process of a robot's motion prediction, the marginalization component gives rise to a fully populated information matrix. Thus there is a demand to make the related information matrix sparse. If the total number of active feature points and passive ones observed is out of the upper limit of that in the map, those features with the weakest correlation will be removed by sparse rules to make the information matrix sparse.

1.4 Update the Observed Data

According to the observed value coming from sensors and the observation equation of the system, the information matrix and vectors will be updated. At the same time, the state estimation is also updated.

$$\begin{aligned} \Delta_k &= \overline{\Delta}_k + H^T R^{-1} H \\ \eta_k &= \overline{\eta}_k + H^T R^{-1}(Z_k - h(\overline{\mu}_k) + H\overline{\mu}_k) \end{aligned} \tag{4}$$

R, $\overline{\mu}_k$, H denote the covariance of observation noise, the expected value of state vector and the observation Jacobian matrix separately. Observation update is linear, and therefore it can make the execution in constant time[11].

2 SLAM Associated with SEIF-PF

2.1 The Expression of SLAM Conditional Probability

With the combination of the robot poses and its environmental map based on SLAM-PF, the joint posterior possibility $p(X_{r(1:k)}, M | Z_{1:k}, u_{0:k-1})$ can be separated into two sections, or $p(X_{r(1:k)} | Z_{1:k}, u_{0:k-1})$ and $p(M | X_{r(1:k)}, Z_{1:k}, u_{0:k-1})$. The state transferred probability $p(X_{r(k)} | X_{r(k-1)}, u_k)$ of the robot is the direct embodiment of Markov characteristics. Besides, the condition $X_{r(k)}$ and the prior state $X_{r(k-1)}$ are non-interference. The path estimation, or $p(X_{r(1:k)} | Z_{1:k}, u_{0:k-1})$, can be given by the following equation

$$p(X_{r(1:k)} | Z_{1:k}, u_{0:k-1}) = p(X_{r(k)} | X_{r(k-1)}, Z_{1:k}, u_{0:k-1}) \cdots p(X_{r(1)} | X_{r(0)}, Z_{1:k}, u_{0:k-1}) \tag{5}$$

$p(X_{r(k)} | X_{r(k-1)}, Z_{1:k}, u_{0:k-1}) \cdots p(X_{r(1)} | X_{r(0)}, Z_{1:k}, u_{0:k-1})$ are the conditional probabilities of the joint posterior probabilities.

2.2 Gibbs Sampling

Relying on the conditional distribution, Gibbs sampling[12] is also an iterative sampling approach. In the joint-probability distribution filled with two stochastic variables or much more ones, a sampling sequence can be obtained to approximate the joint-probability distribution. In addition, the Gibbs Sampling can take turns to sample referring to other given values.

2.3 SLAM Based on SEIF-PF

The executive process of SLAM relying on SEIF-PF is just as the following:

Step 1: Estimate poses of particles. According to the control vector and the robot motion model, the robot pose distribution at k o'clock can be estimated.

Step 2: Data Association. By using the method of maximization to observe the data association, the observed data and the estimated map can be confused. With the application of the observation model, the information vector and information matrix will be received according to particle observation information.

Step 3: Estimate the Robot Path and update the map. With the pose vectors gotten by taking samples from the proposed distribution, the weight $w_k^i = \frac{p(X^i_{r(bk)} \| Z_{1k}, u_{0k-1})}{q(X^i_{r(bk)} \| Z_{1k}, u_{0k-1})}$ of particles can be made out. If the reciprocal value of the sum of the weight is less than the threshold given in advance, Gibbs Sampling will be used to obtain the posterior probability distribution of the robot paths at the k moment. Then according to the equation (4), the relevance of the information vector and the information corresponding to each feature point will be calculated. Then that observed information without any relevance with the features will be as new features and confused.

3 Experimental Simulation and Analysis

In MATLAB platform, the motion model and observation model in reference [13] are applied to experimental simulation. The particle number is 200.

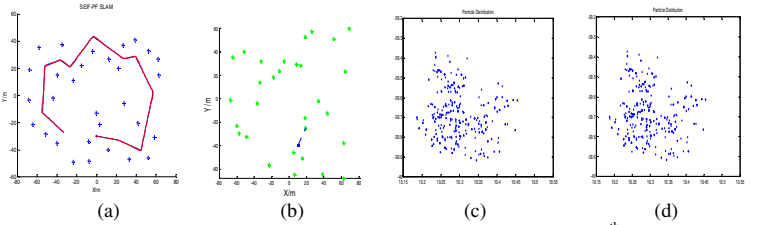

(a) (b) (c) (d)

(a)Reference path and estimated position (b) Particle estimation at the 15th step
(c) Particle distribution of FastSLAM2.0 (d) Particle distribution of SEIF-PF SLAM

Fig. 1. Simulation of SEIF-PF SLAM

In Fig.1 (a), "+", "--", "—"separately express the estimated position of feature points, the reference trajectory and the estimated path. In Fig.1 (b), it displays the particle estimation of the robot poses of the ESEIF-PF at its 15th step. In Fig.1(c), it's the particle distribution with the application of FastSLAM2.0. Fig.1 (d) is related to the particle distribution of SEIF-PF SLAM. It's obvious that the particle distribution is more uniform than ever. In Fig.1, the coordinates of X and Y, the unit of which is meter(m), separately represent the location of the robot or the particle

To further illustrate the performance of the algorithm, the mean errors of pose estimation in X, Y direction between this paper's proposed algorithm and the FastSLAM2.0, are compared. Fig.2 displays the result of Monte-Carlo simulations for 50 times. It can be seen that the estimation precision of the algorithm put forward by this paper is significantly prior to FastSLAM algorithm.

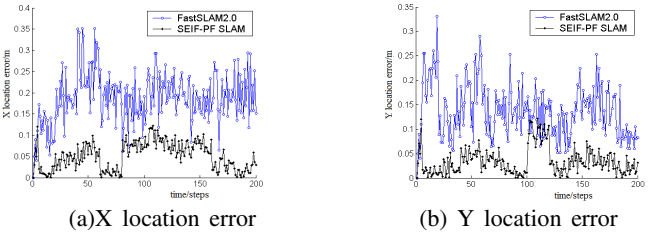

(a)X location error (b) Y location error

Fig. 2. Error comparisons of the two algorithms

4 Conclusions

This paper has proposed SEIF-PF SLAM in robotics applied in electronic engineering. The information matrix is used to memory the history information of the robot's poses. Gibbs Sampling is applied to gain a new particle set which can better describe the real posterior probability distribution. In the simulation experiments, owing to the algorithm proposed in this paper, the gained particles are evenly distributed and more various than ever. Moreover, the particle set can better describe the posterior probability distribution of the robot's states and the estimation precision of states has been improved.

References

[1] Montemerlo, M., Thrun, S., Loller, D., Wegbreit, B.: FastSLAM2.0:An improved particle filtering algorithm for simultaneous localization and mapping that provably converges. In: Proceeding of the International Joint Conference on Artificial Intelligence, IJCAI, Acapulco, Mexico, pp. 1151–1156 (2003)

[2] Li, M.-H., Hong, B.-R., Luo, R.-H.: Improved Rao-Blackwellized particle filters for mobile robot simultaneous localization and mapping. Journal of Jilin University (Engineering and Technology Edition) 7(2), 401–406 (2007)

[3] Kim, C., Sakthivel, R., Chung, W.K.: A robust algorithm for the simultaneous localization and mapping Problem. In: IEEE International Conference on Robotics and Automation, pp. 2439–2445. IEEE Press, Piseataway (2007)
[4] Palam, S.A., Maskell, S., Gordon, N.: A tutorial on Particle filters for on-line non-linear/non-Gaussian Bayesian tracking. IEEE Transactions on Signal Processing 24(5), 174–188 (2002)
[5] Shojaie, K., Ahmadi, K., Shahri, A.M.: Effects of Iteration in Kalman Filters Family for Improvement of Estimation Accuracy in SLAM. In: IEEE/ASME International Conference on Advanced Intelligent Mechatronics, ETH Zurich, Switzerland, pp. 441–453 (2007)
[6] Pit, M., Shephard, N.: Filtering via simulation: Auxiliary Particle filters. Journal of the American Statistical Association 94(446), 590–599 (1999)
[7] Musso, C., Oudjane, N., Legland, F.: Improving Regularised Particle filters. In: Sequential Monte Carlo Methods in Practicle, Gordon. Springer, NewYork (2001)
[8] Martinez-Cantin, R., De Freitas, N., Castellanos, J.A.: Analysis of Particle Methods for Simultaneous Robot Localization and Mapping and a New Algorithm: Marginal-SLAM. In: IEEE International Conference on Robotics and Automation, Roma, Italy, pp. 2415–2420 (2007)
[9] Thrum, S., Kolle, D., Ghahmarani, Z., Durrant-Whyte, H.: SLAM updates require constant time. School of Computer Science. Carnegie Mellon University, Pittsburgh, Technical Report (2002)
[10] Thrun, Y., Liu, S., Koller, D., Ng, A.Y., et al.: Simultaneous Localization and Mapping with Sparse Extended Information Filters. The International Journal of Robotics Research 23(7-8), 693–716 (2004)
[11] Waltr, M., Eustice, R., Leonard, J.: A provably consistent method for imposing sparsity in feature-based SLAM information filters. In: Proceedings of ISRR, Orlando, Florida, U.S., pp. 214–234 (2005)
[12] Zhang, H., Liu, Y.-L., Fan, X.-P., et al.: Mobile robot simultaneous localization and mapping based on particle filtering with fixed-lag Gibbs sampling. Application Research of Computers 25(11), 2293–2296 (2008)
[13] Wang, X.-H., Fu, W.-P.: Data association method of SLAM based on improved minimal connected dominating set. Journal of Computer Applications 30(9), 2294–2296 (2010)
[14] Lauer, M., Lange, S., Riedmiler, M.: Modeling moving objects in a dynamically changing robot application. In: Advances in Artificial Intelligence, Koblenz, Germay, pp. 291–303 (2005)
[15] Sun, Y.J.: Iterative relief for feature weighting: Algorithms, theories, and applications. IEEE Transactions on Pattern Analysis and Machine Intelligence 29(6), 1035–1051 (2007)

Reliability Test of Timesten Memory Database for Online Charging System in Electronic Commerce

Jun Sun* and Huazhu Song

College of Computer Science and Technology, Wuhan Univeristy of Technology, 430070 Wuhan, Hubei, China
sunj@whut.edu.cn

Abstract. In electronic commerce, the reliability of online charging system is very important for transactions. In this paper, the reliability of Timesten memory database in online charging system is investigated. First, an extremely condition is designed for verifying the reliability of memory database. In this condition, while replication is working and a larger batch of data is being copied from active unit to standby unit, active unit is shut down due to some technology problem, e.g. loss of power, the fault of electronic technology and etc. Then, a special java program is coded for this test. The test results indicate there is the non-consistency of data between active unit and standby unit when the active unit is shut down, but the data still can be replicated normally after the replication is restarted and the consistency of data between different servers can also be kept. It means memory database in online charging system has high reliability so it can be used safely in electronic commerce.

Keywords: memory database, replication, reliability, online charging system, electronic commerce.

1 Introduction

The online charging system (OCS) in electronic commerce can provide online real-time control, data service for prepaid operation, and real-time charging for value-added service. OCS can provide better real-time environment and tolerance ability than other systems because it adopts some unique technologies, especially memory database. In fact memory database can provide OCS more excellent performance than other databases.

The memory database is a kind of database management system that directly operates the data in the memory. This innovation can increase the performance of database dramatically, because the speed of reading and writing data in memory is several orders of magnitude higher than that in disk, and meanwhile, the memory database also abandons the traditional method of disk data management, the system structure of database is redesigned by based on all of operated data is stored and operated in the memory; it also improves the algorithm of data cache and parallel operation, so the speed of data processing in an memory database is about 10 times faster than that in traditional database. But, the memory database requires larger

* Corresponding author: Jun Sun, Address: LuoShi Road 122, Hongshan District, Wuhan, 430070, China, Email: sunj@whut.edu.cn.

D. Jin and S. Lin (Eds.): Advances in Mechanical and Electronic Engineering, LNEE 177, pp. 599–604.
springerlink.com

memory than other databases because the real-time transaction only communicates with real-time memory database in OCS,

However, as a kind of memory-resident relational database, all data operation of memory database, such as increasing records, deleting records and modifying records, is executed in memory. This unique characteristic also increases the risk of data loss while it increases the performance of database, for example, the data in the memory will not be existed after power off or releasing memory. But for enterprises, especially telecommunicated enterprises, stability and reliability of database is very important, the loss of data is not permitted.

Whether power off, electronic technology fault will lead to the loss of data in memory database is very important for memory database's application in OCS. In this paper, we will design a test to investigate the reliability of replication of memory database, and Timesten memory database will be selected to build OCS.

2 Online Charging System Based on Memory Database

2.1 Replication

Replication, which is the process of maintaining copies of data in multiple databases[9], is a very important mechanism of Timesten database to keep its efficiency, stability and reliability. In fact, replication keeps the consistency of data between different servers because it can synchronize the data between different servers. Replication also can carry the full copy, incremental copy and incremental copy of data, just like physical database can carry the full backup, incremental backup, differential backup of data.

However, replication must be bidirectional in online charging system for retaining the data consistency between different servers. In fact, as the system need to be updated, the standby unit is updated firstly, and then system switches between standby unit and active unit, standby unit begin to process the transaction, this mechanism lets the database in the standby unit provide data for the transaction and lets transaction update the data in the standby unit immediately. Once the active unit has been updated, the transaction data need be copied from the standby unit to active unit. So, at least two servers are necessary for the system to carry bidirectional duplication in online charging system.

Replication also has an important job that is keep consistency of data between different servers. The active unit usually is not permitted to shut down in online charging system; this provides the stability of the system and continuity of the transaction. However, once the active unit is shut down, some hardware faults happen in most cases, how to keep the transaction going on. In fact, even though this case happens, online charging system can switch to standby unit to keep the transaction going on, as to the data of active unit.

Timesten memory database can store and recover the data of database in active unit. Once the active unit is repaired, the replication will be used to synchronize the data between active unit and standby unit. This mechanism keeps the data consistency between active unit and standby unit in memory database. To realize this mechanism, memory database use the checkpoint file and transaction log file to recover data. In memory database, these files are stored in the hard disk. Check point file includes an

image file of memory database, transaction log file records any change of memory database. So, once the databases need to be recovered, Timesten database will recover the database by combining the checkpoint file and transaction log file. Even if the database is closed and data in memory lost, memory data can also be recovered by checkpoint file and transaction log file when it is restarted.

2.2 The Deploying of Timesten Memory Database in OCS

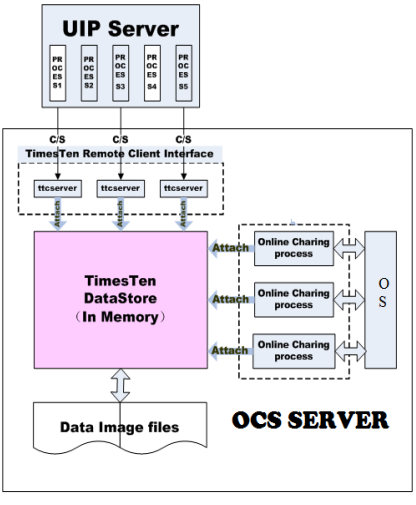

Fig. 1. The deploy scheme of Timesten memory database in OCS

For improving the database performance, memory database and real-time charging unit is deployed in the same host machine (Fig.1)[8], online charging processes exchange data with memory database by the method of memory attached; this assures the real time characteristics of data transfer. Processes in User Interface Process (UIP) visit TimesTen by the method of client/server. UIP has two versions, one is JAVA version, which uses the TimesTen's diver program, and another is .NET version, which uses itself driver program.

Active and standby unit in Online charging servers deploy a Timesten database respectively, as the TimesTen database is updated in active unit, replication will synchronize the database in standby unit to keep the data consistency between active unit and standby unit. So, once the active unit has some problem or need to be updated, system can do master-slave switch, then the old standby unit becomes new active unit and the old active unit becomes the new standby unit, this mechanism will provide the stability of OCS

2.3 The Strategy of Master-Slave Switch in OCS

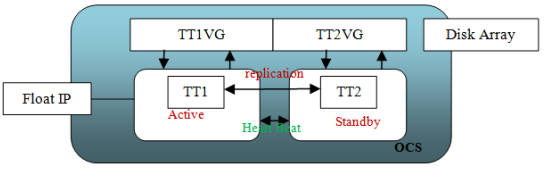

Fig. 2. The Configuration of Timesten Memory database in OCS

Fig.2 is the simplify master/ slave model of online charging unit in TimesTen memory database. In software layer, replication is used as synchronization method between memory databases; in hardware layer, OCU communicates with other servers by Gigabit-Ethernet. But for providing the stable and effective data synchronization in a same server, a rapider

communication method must be selected. In our system, Heart Beat mechanism is used to keep the data's consistency between active unit and standby unit in OCS.

In Heart Beat mechanism, Timesten memory database in active unit and standby unit communicate by its independent IP address respectively. However, the system doesn't assign TT1 by the IP(IP1) of active unit, it only defines a float IP and assigns this IP to the TT1, if active unit has some problem, the master-slave switch must be carried, the float IP will be assigned to the standby unit TT2, lastly, float IP will be selected the IP which is used by the OCU sever.

By this method, whether OCU server is in active unit or standby unit, its float IP is a same one, it let the whole OCU server look like transparent.

3 Reliability Test of Replication

In online charging system, the data synchronization between active unit and standby unit is realized by replication, so the reliability of replication assures the data consistency between active unit and standby unit. In this section, a test is designed for verifying the reliability of replication.

3.1 Assumption

Table 1. The structure of test table

Name	Data Type
Test2	A Number

Table 2. The Environment table for reliability test of replication

Roler	IP address	Operating System	Name of Data source	Synchonized Object	Object Owner
Active Unit	192.168.80.129	Windows server 2003	Masterds	Table test2	administrator
Standby Unit	192.168.80.140	Windows server 2000	subscriberds	Table test2	administrator

A factitious extremely condition is designed to verify the reliability of replication in memory database. In this case, a great amount of data is changed as well as the replication is working for synchronization, the active unit is shut down at this time, it means the replication in active unit is closed but it does not finish its job. Will this condition lead to the non-consistency of data between active unit and standby unit?(data is added into active unit, but it is not added into standby unit.)

3.2 Reliability Test of Deplication

Step 1: Firstly, test whether replication is opened successfully and clear Table test2(Tabe.1) in the two sides;

Step 2: Execute small Java program in the active unit to insert a batch of 300000 rows data, (the code is omitted here)

Step 3: Open windows command and execute connect.class program

>Java connect

Step 4: In executing process, power off the virtual unit to simulate the case which active unit has problem, that means replication will be forced to stop and data replication also stops.

Step 5: Look for the synchronized data in subsriberds data source in standby unit by the following command.

Command>select * from test2;

Result will be

```
< 21463, <NULL>, <NULL> >
21463 rows found.
Execution time (SQLExecute + Fetch Loop) = 7.643503 seconds.
Command>
```

We can find 21453 rows data are replicated to standby unit successfully as the replication of active unit is still working.

Step 6: Now restart active unit and check how many data are inserted by program before we shutdown active unit.

```
< 22200, <NULL>, <NULL> >
22200 rows found.
Command>
```

In fact, 22000 rows data are inserted in active unit, it means there are loss of data in replication process because the active unit is shut down

Step 7: Restart the replication of active unit, then check the data in standby unit

Execute the following command in active unit

Command>call ttrepstart();

Execute the following command in standby unit

Command>select * from test2;

Now, we can find there are 22200 rows data in table test2 in the standby unit,

This is consistent with active unit.

3.3 The Analysis of Test Result about Reliability of Replication

Although replication doesn't succeed to copy data from active unit to standby unit computer completely when the active unit computer is shut down, the unfinished synchronization job also will be restarted again once replication is restarted, so the data synchronization between active and standby unit will be finished in a short time and this process is without loss of data.

This indicates although the power off interrupts the replication process, the system will update the data and synchronize the data by replication according the log file once the replication is restarted until the data between active unit and standby unit is consistent. That process proves the reliability of replication.

4 Summaries

In the paper, the reliability of Timesten memory database in OCS is investigated. For verifying the reliability of memory database, first, an extremely condition is designed,

which is used to simulate the case that the system lost power or has some electronic technology fault. Then, a special java program is coded for this test. The results indicate there is the non-consistency of data between active unit and standby unit, but the data still can be replicated normally after the replication is restarted and the consistency of data between different servers can also be kept. It means memory database in online charging system has high reliability in electronic commerce.

References

1. Jiang, Z.P.: Store Management of Memory Database. Master thesis, Huazhong University of Science and Technology, Wuhan (2008) (in Chinese)
2. Li, W., Zhang, X.W., Li, G.: Research and implementaion of main memory database in telecom billing system. Journal of Zhengzhou University of Light Industry (Natural Science) 23, 42–44 (2008) (in Chinese)
3. Hu, Q.X.: The Design and Analytics for Online Charge System Base on 3G. Master Thesis, Shanghai Jiao Tong University, Shanghai (2010) (in Chinese)
4. Wang, C.: Research about Several Key Technology of Memory Database. Master Thesis, Zhejiang University, Hangzhou (2003) (in Chinese)
5. Ge, J.J.: The Researching of Transaction Scheduling and Data Recovery in Real-time Main Memory Database System. Qingdao University, Qingdao (2007) (in Chinese)
6. Cha, D.Y.: Research and Implementation of Embedded Real-time Memory Database. University of Electronic Science and Technology of China, Chengdu (2009) (in Chinese)
7. Wu, B.: Design and implementation of Real-Time Memory Database. Zhejiang University, Hangzhou (2005) (in Chinese)
8. Oracle Corporation. Oracle TimesTen Memory Database Operation Guide Release 7.0., USA (2007)
9. Oracle Corporation. Oracle TimesTen Memory Database Replication guide Release 7.0., USA (2007)

Secure Multi-party Computation – An Important Theory in Electronic Technology

Xiaomei Wang[1], An Wang[2], and Shengqin Bian[3]

[1] School of Computer and Communication Engineering,
University of Science and Technology, Beijing 100083, China
[2] Institute for Advanced Study, Tsinghua University, Beijing 100084, China
[3] School of Computer and Communication Engineering,
University of Science and Technology, Beijing 100083, China
{wangxiaomei,xiaobian}@ustb.edu.cn,
wanganl@tsinghua.edu.cn,

Abstract. Secure multi-party computation (SMC) is a key point in the field of information security and also widely used in electronic technology. The application of SMC plays an important role in many special electronic technologies such as electronic voting, electronic auction, secret sharing and threshold signature. Participant of the secure multi-party computation may leak and analyze the middle computation result or the private data, how much it will cost for a participant during the assault is depending on how much private data are leaked. This paper proposed the concept of conditionality anti-assault, under this model, even the participant is vicious, and the protocol itself is still secure.

Keywords: electronic technology, secure multi-party computation, conditionality resisting attack.

1 Introduction

Security is always an import topic in many technologies that have been widely used, recent years, more and more electronic technologies start to put secure theory into their deployment, electronic voting, electronic auction, etc. are examples already widely used technologies, these kinds of technology cannot be deployed without considering the security, many security protocols can be combined into the electronic technology, secure multi-party computation is one of them. The concept of secure multi-party computation was first brought forward by Yao in his paper [1] in 1982, and he proposed the definition of secure multi-party computation for the first time and provided a resolution for the millionaire puzzle. Subsequently, Goldreich, Micali and Wigderson put forward a protocol of secure multi-party computation that can compute arbitrary functions based on the cryptography security in their paper [2] in 1988. Then, in 1998, Goldreich pointed out that for particular problems we need use particular solutions to achieve high efficiency. This idea finally introduced the technology of secure multi-party computation to many fields including the Computational Geometry, the statistical analysis, and the data mining and so on, which can be referred to from papers [4-6].

D. Jin and S. Lin (Eds.): Advances in Mechanical and Electronic Engineering, LNEE 177, pp. 605–608.
springerlink.com

Du from Purdue University US pointed out some secure double-party computation problems that are worth of researching in his paper [7], like proper value of matrix, Characteristic vector, analysis of variance and so on, he also pointed out that it's significant meaningful to extend the secure double-party computation to secure multi-party computation, and spread the protocols under the half-honest model to the protocols under vicious model, but no solution was provided for these problems in his paper.

2 Model of Secure Multi-party Computation

Normally, the models of secure multi-party computation are separated into two kinds: half-honest model and vicious model.

Half-honest Model: If all participants are honest or half-honest, we can call this model a half-honest model, the assailants in this model are always passive.

Vicious Model: Models that have vicious participant will be called vicious model. The participant in this model is always active.

Participant in half-honest model can giveaway, analyze and deduce the intermediate computing result or private data, the cost of the participant during the assault process are evaluated by how much original private data are leaked out, if the assailant can analyze or deduce out the information he want by the intermediate result without leaking out his own private data, then his cost for the assault is minimum. If the assailant has to giveaway his own original private data to get the information he want, then the cost is maximum.

Alice has $n \times N$ matrix A, Bob has $N \times m$ matrix B, and the secure matrix product protocol assures that they can compute out $A \cdot B$ together without giveaway their private information to each other. According to following steps, after computation finishes, Alice will have matrix V_a while Bob will have matrix V_b, and satisfying the formula

$$V_a + V_b = A \cdot B \,. \tag{1}$$

Step1. Alice and Bob will negotiate to create an $N \times N$ reversible matrix M, vertically decompose matrix M into two $N/2 \times N$ matrixes: M_{left} and M_{right}, horizontally decompose M^{-1} into two $N \times N/2$ matrixes: $M_{inv\text{-}top}$ and $M_{inv\text{-}bottom}$.

Step2. Alice computes A_1 via $A \cdot M_{left}$, and computes A_2 via $A \cdot M_{right}$, and sends A_1 to Bob.

Step3. Bob computes B_1 via $M_{inv\text{-}top} \cdot B$, and computes B_2 via $M_{inv\text{-}bottom} \cdot B$, and sends B_2 to Alice.

Step4. Alice gets V_a which is equal to $A_2 \cdot B_2$, Bob gets V_b which is equal to $A_1 \cdot B_1$, the protocol ends.

Alice computes A' via $A \times M$, converting matrix A to A' (accordingly converting B to B'), then when the A' is leaked to Bob, he cannot get all information of A by this, which means the protocol is secure.

3 Contribution of This Paper

According to the partition of current models of secure multi-party computation, a new model is proposed.

Conditionality Anti-Assault Model: Under half-honest model, if participant don't want to pay the maximal cost and don't want to participate the cooperation assault, we call this model conditionality anti-assault model.

First, let's introduce an attribute of a matrix.

Polar decomposition: Any n rank reversible matrix S can be decomposed to the product of one n rank orthogonal matrix P and one n rank positive definite matrix Q, this decomposition uniquely exists.

The private information of Alice is one n rank reversible matrix S, Bob knows the matrix computation result as PMQ, in which P and Q are polar decomposition of the reversible matrix S, Carol's private information is n rank reversible matrix M, under conditionality anti-assault model, it's impossible for Alice and Bob to compute together the Carol's private information M.

To prove this, we suppose that if Alice and Bob can compute out matrix M. After computation, Alice will have matrix V_a, Bob will have matrix V_b and $V_a + V_b$ is equal to $P^{-1} \cdot (PMQ) \cdot (Q)^{-1}$ which is equal to M, since Alice and Bob are computing together, they will exchange the information of V_a and V_b to each other to get matrix M. Besides, for n rank reversible matrix M, Bob can get one n rank orthogonal matrix A_1 and one n rank positive definite matrix A_2 through polar decomposition, which can present a unique formula:

$$M = A_1 \cdot A_2 \tag{2}$$

In above we suppose PMQ is equal to B, P, M and Q are all reversible matrix, so PMQ is also reversible, which means B is also reversible, so Bob can get orthogonal matrix C_1 and positive definite matrix C_2, to present

$$B = C_1 \cdot C_2. \tag{3}$$

Now we have

$$P \cdot M \cdot Q = P \cdot A_1 . A_2 \cdot Q = (PA_1) \cdot (A_2 Q) = B = C_1 C_2 . \tag{4}$$

So we can get that PA_1 is equal to C_1, A_2Q is equal to C_2.
So P is equal to $(C_1)^{-1} \cdot (A_1)^{-1}$, and Q is equal to $(A_2)^{-1} \cdot (C_2)^{-1}$.

At all events, Alice will not cooperate with Bob, because even he can get private information of Carol, his private information will become unsecure, so we call the assault above conditionality anti-assault. Besides, in above demonstration we used polar decomposition, if we use QR decomposition or UL decomposition, we can both setup conditionality anti-assault model.

4 Future Expectation

If participant of the protocol try to work together to filch others' private information, it will be important to be able to resist (n-1) participant's union under a half honest model with n participant having no dependable third party. The conditionality anti-assault model proposed can be used to determine the security of a secure multi-party computation protocol. If a protocol is designed to be able to restrict the communication of (n-1) participant's information, then it can resist (n-1) participant's joint assault. The SMC will definitely play an important role in more and more electronic technologies, and what's more, the SMC is not the only one theory that closely related with electronic technology, many more secure theories will be combined into the electronic technology.

References

1. Yao, A.: Protocol for Secure Computations. In: Proceedings of the 23rd Annual IEEE Symposium on Foundation of Computer Science, pp. 160–164. IEEE Computer Society Press, Los Alamitos (1982)
2. Goldreich, O., Micali, S., Wigderson, A.: How to play any mental game. In: Proceeding STOC 1987 Proceedings of the Nineteenth Annual ACM Symposium on Theory of Computing, New York, pp. 218–229 (1987)
3. Goldreich, O.: Secure Multi-party Computation, working draft (2000), `http://www.wisdom.weizmann.ac.il/~oded/pp.html`
4. Atallah, M.J., Du, W.: Secure Multi-party Computational Geometry. In: Dehne, F., Sack, J.-R., Tamassia, R. (eds.) WADS 2001. LNCS, vol. 2125, pp. 165–179. Springer, Heidelberg (2001)
5. Du, W., Atallah, M.J.: Privacy-Preserving Cooperative Statistical Analysis. In: 2001 ACSAC: Annual Computer Security Applications Conference, New Orleans, Louisiana, USA, December 10-14, pp. 102–110 (2001)
6. Vaidya, J., Clifton, C.: Privacy preserving association rule mining in vertically partitioned data. In: The Eighth ACM SIGKDD International Conference on Knowledge Discovery and Data Mining, Edmonton, Canada, pp. 639–644 (2002)
7. Du, W.: A study of several specific secure two-party computation problems [Ph.D. dissertation]. Purdue University, USA (2000)

Granular Deleting in Multi Level Security Models – An Electronic Engineering Approach

Dirk Thorleuchter[1], Gerhard Weck[2], and Dirk Van den Poel[3]

[1] Fraunhofer INT, Appelsgarten 2, D-53879 Euskirchen, Germany
[2] Infodas GmbH, Rhonestraße 2, D-50765 Köln, Germany
[3] Ghent University, B-9000 Gent, Tweekerkenstraat 2, Belgium
Dirk.Thorleuchter@int.fraunhofer.de,
dirk.vandenpoel@ugent.be
http://www.crm.UGent.be

Abstract. Data protection and information security can be assured by using a multi-level-security (MLS) access control model. However, a workflow between persons with different security levels is complicated by the fact that the exchange of information is only allowed in one direction: from persons that are assigned to a specific security level to person that are assigned to the same security level or to a higher security level (write up). Literature show solution approaches by using a MLS model with increased granularity. This enables distributing parts of documents to subjects of lower security levels without causing a security compromise. However, it does not consider an important aspect of workflows: the deleting of information. Thus, this work uses electronic engineering enlarges the introduced MLS model with increased granularity by integrating a deleting feature. This enables an improved workflow between persons with different security levels.

Keywords: Multi-level-security, Security, Modeling, Usability, Operating System, Electronic Engineering

1 Introduction

Today, many operation systems that are based on multi-level-security (MLS) are known [1]. As known from the use of these multi-level-security (MLS) models, a workflow among users (subjects) with different security levels is not permitted, because it is in contrast to the well-known 'no write down' and 'no read up' rules [2, 3, 4]. These rules say that a subject has to write information in a document (an object) that is assigned to an equal or a higher security level than the subject itself [5, 6]. Further, a subject can access to information from objects that are assigned to an equal or to a lower security level than the subject itself [7, 8]. This leads to two interesting aspects: a subject of lower security level could not read a text written by a subject of higher security level. Further, a subject of higher security level could not write information within a text written by a subject of lower security level. It could be clearly seen that a workflow between those two subjects is not supported by existing MLS operation systems [9, 10, 11].

D. Jin and S. Lin (Eds.): Advances in Mechanical and Electronic Engineering, LNEE 177, pp. 609–614.
springerlink.com

To enable such a workflow, an increased granularity view on the data is nessesary. Such an MLS model is introduced in [12]. It is realized by storing information in objects of different security levels within one document. Thus, a document is defined as a set of objects. It is shown that this MLS model increase the usability by enabling a workflow among subjects. Further, it is shown that this model enables several knowledge extraction and text mining operations [13-22] on the data to extract relevant features e.g. an automatic assignment of textual patterns to security levels.

However, a disadvantage of this MLS model as well as of all further MLS models can be seen. They do not consider granular deleting operations. An object only can be deleted in total. Deleting parts of the object content causes a security compromise [23].

Granular deleting helps to increase the usability of workflows among subjects. In this paper, the existing granular MLS model is extended by implementing a granular deleting operation on the model. An example for the use of the electronic engineering based extended MLS model as well as conclusions and an outlook are given.

2 A New Extended MLS Model

This new MLS model based on the Bell LaPadula model and it extends the high granular MLS model from [2, 19]. Here, we present a formal description of the new model.

Let an object $O\{i,j\}$ be defined as in Bell LaPadula model that consists of data, files, programs, subjects etc. The definition of a frame object O^{sup}_i as a list of objects is taken over from [12] where $n \in N$ equals the number of frame objects in a multi-level-security system, $m_i \in N$ be the number of objects in O^{sup}_i, $i \in \{1,..,n\}$, and $j \in \{1,.., m_i\}$. Then, [12] formulize a frame object as

$$O^{sup}_i \equiv [O\{i,1\}, .., O\{i,m_i\}] \tag{1}$$

As defined in [2, 12], C is the classification category (security level) and $C^{O\{i,j\}}$ is the corresponding classification category of an object. Further, K is the compartment information, P is the power set, and $PK^{O\{i,j\}}$ represents all needs-to-know categories of an object as calculated by the power set of all object specific compartment information. In contrast to [12], we define the deleting category of an object $Del^{O\{i,j\}} \in \{true, false\}$ as a boolean variable. Then, object categories can be formulized as

$$(C^{O\{i,j\}}, PK^{O\{i,j\}}, Del^{O\{i,j\}}) \tag{2}$$

We define a subject $S\{k\}$ as a process, programs in execution with subject categories $(C^{S\{k\}}, PK^{S\{k\}})$. This definition is not in contrast to the standard definition from Bell LaPadua because deleting of subjects is not a relevant feature in a workflow. We define $p \in N$ as the number of subjects in a multi-level-security system and we define $k \in \{1, ..., p\}$. Then, reading of object $O\{i,j\}$ by subject $S\{k\}$ is allowed if and only if

$$C^{S\{k\}} \geq C^{O\{i,j\}}$$
$$\text{and}$$
$$PK^{O\{i,j\}} \subseteq PK^{S\{k\}} \tag{3}$$
$$\text{and}$$
$$Del^{O\{i,j\}} = \text{false}$$

In [12], an object $O\{i,j\} \equiv [data\{i,j,1\}, .., data\{i,j,q_{i,j}\}]$ is defined as a list of data units (e.g. line, sentence, text phrase, etc.). Further, $q_{i,j} \in N$ is defined as the number of data units in an object $O\{i,j\}$ and $l \in \{1, .., q_{i,j}\}$ is defined as the position where a subject $S\{k\}$ insert content. Then, a writing split $O_w\{i,j,l\}$ on position l of an object $O\{i,j\}$ is defined as a list of three objects: $O_w\{i,j,l\} \equiv [O1\{i,j\}, O2\{i,j\}, O3\{i,j\}]$ with $O1\{i,j\} \equiv [data\{i,j,1\}, ..., data\_\{i,j,l\text{-}1\}]$ and $O3\{i,j\} \equiv [data\{i,j,l\}, \ldots, data\{i,j,q_{i,j}\}]$. Additionally, $O2\{i,j\} \in \varnothing$ is defined as a new and empty object. Writing of object $O\{i,j\}$ by subject $S\{k\}$ is allowed if and only if

$$C^{O1\{i,j\}} = C^{O3\{i,j\}} = C^{O\{i,j\}}.$$
$$\text{and}$$
$$PK^{O1\{i,j\}} = PK^{O3\{i,j\}} = PK^{O\{i,j\}}$$
$$\text{and}$$
$$Del^{O1\{i,j\}} = Del^{O3\{i,j\}} = Del^{O\{i,j\}} \tag{4}$$
$$\text{and}$$
$$C^{O2\{i,j\}} \equiv C^{S\{k\}}$$
$$\text{and}$$
$$PK^{O2\{i,j\}} \equiv PK^{S\{k\}}$$
$$\text{and}$$
$$Del^{O2\{i,j\}} \equiv \text{false}$$
$$\text{and}$$
$$O^{sup}_i \equiv [O\{i,1\}, \ldots, O_w\{i,j,l\}, \ldots, O\{i,m_i\}]$$

Let $[data\{i,j, h_1\}, ..., data\{i,j, h_2\}] \subseteq O\{i,j\}$ be a list of data units that should be deleted from object $O\{i,j\}$ by subject $S\{k\}$. Let $h_1 \in \{1, \ldots, q_{i,j}\}$ be the start position and let $h_2 \in \{1, \ldots, q_{i,j}\}$ be the end position, respectively. Let a deleting split $O_{del}\{i,j, h_1, h_2\}$ from position h_1 to position h_2 of an object $O\{i,j\}$ be a list of three objects. $O_{del}\{i,j, h_1, h_2\} \equiv [O1\{i,j\}, O2\{i,j\}, O3\{i,j\}]$ with $O1\{i,j\} \equiv [data\{i,j,1\}, ..., data\_\{i,j,h_1\text{-}1\}]$ and $O2\{i,j\} \equiv [data\{i,j, h_1\}, ..., data\_\{i,j,h_2\}]$ and $O3\{i,j\} \equiv [data\{i,j, h_2\text{+}1\}, \ldots, data\{i,j,q_{i,j}\}]$. Let deleting from object $O\{i,j\}$ by subject $S\{k\}$ be allowed if and only if

$$C^{O1\{i,j\}} = C^{O2\{i,j\}} = C^{O3\{i,j\}} = C^{O\{i,j\}}$$

and

$$PK^{O1\{i,j\}} = PK^{O2\{i,j\}} = PK^{O3\{i,j\}} = PK^{O\{i,j\}}$$

and

$$Del^{O1\{i,j\}}\ Del^{O3\{i,j\}} = Del^{O\{i,j\}} \tag{5}$$

and

$$Del^{O2\{i,j\}} \equiv true$$

and

$$O^{sup}{}_i \equiv [O\{i,1\}, \ldots, O_{del}\{i,j, h_l, h_2\}\ , \ldots, O\{i,m_i\}]$$

An example for the use of this extended formal approach is given: Let the sentence: 'The efficiency is 40 percent for a single cycle and 60 percent for combined cycle operations.' be stored in an object. Deleting a text pattern '40 percent for a single cycle and' is not possible in standard approach [2, 12, 24] because an object only can be deleted in total. Using the extended formal approach a new frame object is created that consists of two new objects labelled as not deleted: 'The efficiency is' and '60 percent for combined cycle operations'. It consists of one object labelled as deleted: '40 percent for a single cycle and'. A user can read in objects only if they are not deleted.

3 Conclusion and Outlook

This work shows a formal approach created with electronic engineering that theoretically enables subjects to delete objects without causing a security compromise. The default value for the object category 'deleting' is false. Deleting a textual pattern within a document means that a new object is created that contains the pattern. The object category 'deleting' is set to true for this new object while the deleting value of the other objects remain false. Thus, reading of deleted textual pattern is not possible. The new object itself remains in the MLS e.g. for possible restoring purposes. This new approach can be used to improve workflows among subjects without causing a security compromise. Future work should focus on realizing this new model in form of an operating system to evaluate the performance of this improvement. Further work should focus on a formulization for restoring information for this approach.

References

1. Pfleeger, P., Pfleeger, S.L.: Security in computing. Prentice Hall, Old Tappan (2003)
2. Bell, D.E., LaPadula, L.J.: Secure Computer Systems: Mathematical Foundations. Mitre Corp., Bedford (1973)

3. Biba, K.J.: Integrity Considerations for Secure Computer Systems. Mitre Corp., Bedford (1977)
4. Gericke, W., Thorleuchter, D., Weck, G., Reilaender, F., Loss, D.: Vertrauliche Verarbeitung staatlich eingestufter Information - die Informationstechnologie im Geheimschutz. Informatik Spektrum 32(2), 102–109 (2009)
5. McLean, J.: A comment on the Basic Security Theorem of Bell and LaPadula. Inf. Process. Lett. 20(2), 67–70 (1985)
6. Feiertag, R.J., Levitt, K.N., Robinson, L.: Providing multilevel security of a system design. In: Sixth Symposium on Operating System Principles, pp. 57–65. ACM, New York (1977)
7. Obiedkov, S., Kourie, D.G., Erloff, J.H.P.: Buildung access control models with attribute exploration. Comput. Secur. 28(1-2), 2–7 (2009)
8. Saltzer, J.H., Schroeder, M.D.: The protection of information in computer systems. Proc. IEEE 63(9), 1278–1308 (1975)
9. Li, E.Y., Du, T.C., Wong, J.W.: Access control in collaborative commerce. Decis. Support Syst. 43(2), 675–685 (2007)
10. Holeman, S., Manimaron, G., Davis, J., Chakrabarti, A.: Differentally secure multicasting and its implementation methods. Computer Security 21(8), 736–749 (2002)
11. Lindgreen, R., Herschberg, I.S.: On the validity of the Bell-LaPadula model. Comput. Secur. 13(4), 317–333 (1994)
12. Thorleuchter, D., Van den Poel, D.: High Granular Multi-Level-Security Model for Improved Usability. In: 2nd International Conference on System Science, Engineering Design and Manufacturing Informatization, pp. 191–194. IEEE Press, New York (2011)
13. Thorleuchter, D., Van den Poel, D., Prinzie, A.: Analyzing existing customers' websites to improve the customer acquisition process as well as the profitability prediction in B-to-B marketing. Expert Syst. Appl. 39(3), 2597–2605 (2012)
14. Thorleuchter, D., Herberz, S., Van den Poel, D.: Mining Social Behavior Ideas of Przewalski Horses. In: Wu, Y. (ed.) Advances in Computer, Communication, Control and Automation. LNEE, vol. 121, pp. 649–656. Springer, Heidelberg (2011)
15. Thorleuchter, D., Van den Poel, D.: Companies Website Optimising concerning Consumer's searching for new Products. In: International Conference on Uncertainty Reasoning and Knowledge Engineering, pp. 40–43. IEEE Press, New York (2011)
16. Thorleuchter, D., Van den Poel, D.: Semantic Technology Classification. In: International Conference on Uncertainty Reasoning and Knowledge Engineering, pp. 36–39. IEEE Press, New York (2011)
17. Thorleuchter, D., Van den Poel, D., Prinzie, A.: Extracting Consumers Needs for New Products. In: 3rd International Conference on Knowledge Discovery and Data Mining, pp. 440–443. IEEE Computer Society, Los Alamitos (2010)
18. Thorleuchter, D., Van den Poel, D., Prinzie, A.: Mining Innovative Ideas to Support new Product Research and Development. In: Locarek-Junge, H., Weihs, C. (eds.) Classification as a Tool for Research, pp. 587–594. Springer, Berlin (2010)
19. Thorleuchter, D., Van den Poel, D.: Extraction of Ideas from Microsystems Technology. In: Jin, D., Lin, S. (eds.) Advances in CSIE, Vol. 1. Advances in Intelligent and Soft Computing, vol. 168, pp. 563–568. Springer, Heidelberg (2012)
20. Thorleuchter, D., Weck, G., Van den Poel, D.: Usability Based Modeling for Advanced IT-Security - An Electronic Engineering Approach. In: Jin, D., Lin, S. (eds.) Advances in Mechanical and Electronic Engineering. LNEE, vol. 177, pp. 615–619. Springer, Heidelberg (2012)

21. Thorleuchter, D., Van den Poel, D.: Rapid Scenario Generation with Generic Systems. In: Management Sciences and Information Technology. Lecture Notes in Information Technology. IERI, Delaware (in press, 2012)
22. Thorleuchter, D., Van den Poel, D.: Using Webcrawling of Publicly-Available Websites to Assess E-Commerce Relationships. In: Service Research and Innovation Institute (SRII 2012). IEEE Computer Society, Washington (in press, 2012)
23. Bell, D.E., LaPadula, L.J.: Secure Computer System: Unified Exposition and Multics Interpretation. Mitre Corp., Bedford (1976)
24. Landwehr, C.E.: Formal models for computer security. Comput. Surv. 13(3), 247–278 (1981)

Usability Based Modeling for Advanced IT-Security – An Electronic Engineering Approach

Dirk Thorleuchter[1], Gerhard Weck[2], and Dirk Van den Poel[3]

[1] Fraunhofer INT, Appelsgarten 2, D-53879 Euskirchen, Germany
[2] Infodas GmbH, Rhonestraße 2, D-50765 Köln, Germany
[3] Ghent University, B-9000 Gent, Tweekerkenstraat 2, Belgium
Dirk.Thorleuchter@int.fraunhofer.de,
dirk.vandenpoel@ugent.be
http://www.crm.UGent.be

Abstract. We introduce usability based modeling as new approach to enable an advanced IT-security in electronic engineering. Operating systems based on multi-level-security (MLS) are modeled. These systems contain IT-security as an inherent feature however they also consists of many restrictions for users. Modeling increases the usability of these systems by preserving their high degree of security. This enables operating systems in future that are both, useful and secure. The new approach is in contrast to standard approaches in IT-security that have the aim to increase security in state of the art operation systems that are useful for general purposes but of low security. In a case study, three use cases are selected as starting point for usability based modeling on MLS. Usability gaps are identified and the current landscape of technological research and development is scanned to identify possibly solution approaches. After an evaluation, some approaches are presented that are able to bridge the identified usability gaps.

Keywords: Multi-level-security, Security, Modeling, Usability, Operating System, Electronic Engineering.

1 Introduction

IT-security means protecting information from unauthorized access, use, disclosure, disruption, modification, or destruction [1]. Today, the use of heterogenic operating systems connected in a complex and intricate way and available at every time (24 hours a day) leads to new challenges in IT-security. The appearance of new kinds of (successful processed) security attacks can be monitored permanently [1]. Thus, state of the art operation systems are not protected against these new external attacks yet. Further, these systems are not protected against internal attacks as occurred e.g. by unwitting user behavior [1].

Beside state of the art operating systems, further operating systems are known that are based on multi-level-security (MLS) [2]. MLS describes the capability of an operating system to process information with different sensitivities without causing a security compromise [3, 4, 5]. The MLS architecture prevents the system from

D. Jin and S. Lin (Eds.): Advances in Mechanical and Electronic Engineering, LNEE 177, pp. 615–619.
springerlink.com

external security attacks and it also prevents the users of the system from obtaining access to information for which they lack authorization [6, 7, 8]. Unfortunately, many security restrictions have to be fulfilled by these operating systems [9, 10]. As a result, a decreased or low usability of these operating systems can be seen [11, 12]. This is in contrast to state of the art operating systems with high usability. This also is the reason why these systems are rarely applied in commercial environments [2, 13]. Exceptions are the use of these systems in military or in financial domains.

This paper presents a new usability modeling approach for MLS operating systems to increase usability without decreasing IT-security in electronic engineering. That leads to advances in IT-security and in far future, to operating systems that are both, useful and secure.

2 Methodology

We present an approach that is in contrast to the standard approach in IT-security. There, research focuses on increasing security in state of the art operation systems [1] e.g. to enlarge operating systems that are useful for general purposes with new security features. This is normally done by building a model of an operating system and by creating IT-security scenarios. Then, the operating system is modeled based on these scenarios to identify week points in the model.

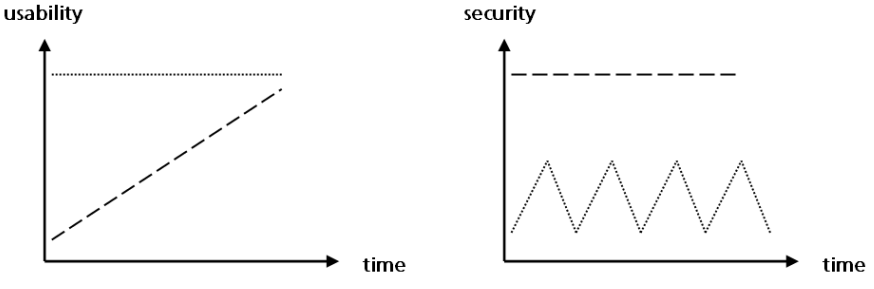

Fig. 1. The two ways of modeling and its effect on usability and security: a) Security based modeling of a state of the art operating system to increase security (…….) b) Usability based modeling of a MLS operating system to increase usability (_ _ _ _ _)

The results of this security based modeling can be evaluated in two dimensions (see Fig. 1). The first dimension is the usability of the operation system. The evaluation results in a high value for the usability dimension over time. This is because a state of the art operating system is useful for general purposes and it fulfils the needs of the users.

The second dimension is the security. A state of the art operating system is not secure because only known security bugs can be fixed by modeling. Fixing security bugs increases security at present time. However, many security bugs in the operating system and its applications are unknown yet. By use of new kinds of security attacks as described in Sect. 1, one easily can access to the operating system and to the information without authorization. The occurrence of these new security attacks leads

to a decreased security for the operating system at that time and a new security based modeling is necessary to fix the new security bug again. Further, unwitting user behavior also decreases security of these systems permanently. Thus in future, a state of the art operating system will be useful however it will be not secure regardless whether security modeling is successful processed or not.

This paper introduces a new methodology based on an alternative modeling way. An operating system is modeled that is based on MLS. The system contains IT-security inherently and it remains secure regardless whether a new kind of security attack appears or regardless whether unwitting user behavior occurs. It continuously gets high result values for the security dimension over the time (see Fig. 1). Unfortunately, these operating systems have to fulfill many usability restrictions to ensure security. That leads directly to a low usability at present time. To increase usability, a methodology is used as depicted in Fig. 2. Usability scenarios (use cases) are provided. Then, the operating system is modeled based on these scenarios (usability modeling). As a result, week points (usability gaps) in the model concerning usability can be seen.

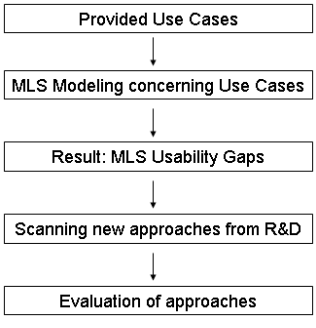

Fig. 2. The processing of this usability based modeling approach: After providing use cases, a MLS is modeled to identify its usability gaps. A scanning for new approaches appeared from technological research and development (R&D) leads – after an evaluation – to the identification of new solutions to bridge the usability gaps.

The identified usability gaps can be bridged by considering current knowledge from technological research and development. There, new approaches probably can be identified that can be used to improve usability. While research and development in information technology normally is not done for improving usability of MLS systems, newly appeared approaches for other domains have to be identified and evaluated for their use in a MLS domain. This increases the value of its usability dimension step by step. If a usability gap can not be bridged at present time then the usability value remains constant till a new solution approach will be available. Implementing solution approaches that decrease security are not allowed by the MLS operation system. Thus, by implementing solution approaches, usability is not in contradiction to security and an operating system can be realized in future that is both, useful and secure.

3 Case Study, Conclusion, and Outlook

In a case study [14, 15], several use case are selected. An example for a use case is the transfer of sensitive data to an unsecured network. Further examples are the workflow of users with different security levels and the assignment of new information to security levels. Existing usability gaps are identified by processing usability based modeling. After a scanning process, new problem solution approaches are identified from technological research and development. They are evaluated to select these approaches that are able to bridge the identified usability gaps.

Examples for these evaluated results are the integration of a high level security gateway and a fourth generation firewall to prevent usability gaps occurring by transferring sensitive data between subjects of different security levels [15].

A further evaluated approach is homomorphic encryption that enables processing of encrypted data without decrypting them before. This allows a workflow of users with different security levels by ensuring the confidentiality of the processed data. Thus, it bridges the corresponding usability gap. Further, a result of the case study is that the use of semantic text mining approaches [16-25] is able to support an automatic assignment of information to security levels. This bridges the usability gap that a human based assignment of new information to security levels is time consuming.

This work shows that usability based modeling of operating systems based on MLS leads to the identification of usability gaps. To bridge these gaps, possible new solutions approaches from technological research and development are identified. The identified approaches normally are created for a different purpose e.g. research on homomorphic encryption focuses on ensuring the confidentiality in cloud computing. Thus, they have to be evaluated to show whether they are able to bridge the identified usability gaps in MLS or not. Approaches that bridge a usability gap lead to an increase in MLS usability. Approaches that cannot be used to bridge a usability gap do not decrease usability. Thus, over a long period of time, the MLS usability will increase steadily. In future, this methodology might solve IT-security problems by providing an operating system that is both, useful and secure.

Although this case study shows that some usability problem can be solved, many further usability problems are still unsolved. Future work should focus on monitoring the technological landscape to identify newly appeared approaches from research and development to solve further usability problems.

References

1. Bidgoli, H. (ed.): Security – Threats, Vulnerabilities, Prevention, Detection, and Management, vol. 3. John Wiley and Sons, Bakersfield (2006)
2. Pfleeger, P., Pfleeger, S.L.: Security in computing. Prentice Hall, Old Tappan (2003)
3. Bell, D.E., LaPadula, L.J.: Secure Computer Systems: Mathematical Foundations. Mitre Corp., Bedford (1973)
4. Bell, D.E., LaPadula, L.J.: Secure Computer System: Unified Exposition and Multics Interpretation. Mitre Corp., Bedford (1976)
5. Biba, K.J.: Integrity Considerations for Secure Computer Systems. Mitre Corp., Bedford (1977)
6. Feiertag, R.J., Levitt, K.N., Robinson, L.: Providing multilevel security of a system design. In: Sixth Symposium on Operating System Principles, pp. 57–65. ACM, New York (1977)

7. Landwehr, C.E.: Formal models for computer security. Comput. Surv. 13(3), 247–278 (1981)
8. Lindgreen, R., Herschberg, I.S.: On the validity of the Bell-LaPadula model. Comput. Secur. 13(4), 317–333 (1994)
9. McLean, J.: A comment on the Basic Security Theorem of Bell and LaPadula. Inf. Process. Lett. 20(2), 67–70 (1985)
10. Obiedkov, S., Kourie, D.G., Erloff, J.H.P.: Buildung access control models with attribute exploration. Comput. Secur. 28(1-2), 2–7 (2009)
11. Saltzer, J.H., Schroeder, M.D.: The protection of information in computer systems. Proc. IEEE 63(9), 1278–1308 (1975)
12. Li, E.Y., Du, T.C., Wong, J.W.: Access control in collaborative commerce. Decis. Support Syst. 43(2), 675–685 (2007)
13. Holeman, S., Manimaron, G., Davis, J., Chakrabarti, A.: Differentally secure multicasting and its implementation methods. Computer Security 21(8), 736–749 (2002)
14. Thorleuchter, D., Van den Poel, D.: High Granular Multi-Level-Security Model for Improved Usability. In: 2nd International Conference on System Science, Engineering Design and Manufacturing Informatization, pp. 191–194. IEEE Press, New York (2011)
15. Gericke, W., Thorleuchter, D., Weck, G., Reilaender, F., Loss, D.: Vertrauliche Verarbeitung staatlich eingestufter Information - die Informationstechnologie im Geheimschutz. Informatik Spektrum 32(2), 102–109 (2009)
16. Thorleuchter, D., Van den Poel, D., Prinzie, A.: Analyzing existing customers' websites to improve the customer acquisition process as well as the profitability prediction in B-to-B marketing. Expert Syst. Appl. 39(3), 2597–2605 (2012)
17. Thorleuchter, D., Herberz, S., Van den Poel, D.: Mining Social Behavior Ideas of Przewalski Horses. In: Wu, Y. (ed.) Advances in Computer, Communication, Control and Automation. LNEE, vol. 121, pp. 649–656. Springer, Heidelberg (2011)
18. Thorleuchter, D., Van den Poel, D.: Companies Website Optimising concerning Consumer's searching for new Products. In: International Conference on Uncertainty Reasoning and Knowledge Engineering, pp. 40–43. IEEE Press, New York (2011)
19. Thorleuchter, D., Van den Poel, D.: Semantic Technology Classification. In: International Conference on Uncertainty Reasoning and Knowledge Engineering, pp. 36–39. IEEE Press, New York (2011)
20. Thorleuchter, D., Van den Poel, D., Prinzie, A.: Extracting Consumers Needs for New Products. In: 3rd International Conference on Knowledge Discovery and Data Mining, pp. 440–443. IEEE Computer Society, Los Alamitos (2010)
21. Thorleuchter, D., Van den Poel, D., Prinzie, A.: Mining Innovative Ideas to Support new Product Research and Development. In: Locarek-Junge, H., Weihs, C. (eds.) Classification as a Tool for Research, pp. 587–594. Springer, Berlin (2010)
22. Thorleuchter, D., Van den Poel, D.: Extraction of Ideas from Microsystems Technology. In: Jin, D., Lin, S. (eds.) Advances in CSIE, Vol. 1. AISC, vol. 168, pp. 563–568. Springer, Heidelberg (2012)
23. Thorleuchter, D., Weck, G., Van den Poel, D.: Granular Deleting in Multi Level Security Models - An Electronic Engineering Approach. In: Jin, D., Lin, S. (eds.) Advances in Mechanical and Electronic Engineering. LNEE, vol. 177, pp. 609–614. Springer, Heidelberg (2012)
24. Thorleuchter, D., Van den Poel, D.: Rapid Scenario Generation with Generic Systems. In: Management Sciences and Information Technology. Lecture Notes in Information Technology. IERI, Delaware (in press, 2012)
25. Thorleuchter, D., Van den Poel, D.: Using Webcrawling of Publicly-Available Websites to Assess E-Commerce Relationships. In: Service Research and Innovation Institute (SRII 2012). IEEE Computer Society, Washington (in press, 2012)

Using Electronic Technology and Computational Intelligence to Predict Properties of Dangerous Hydrocarbon

Jinyong Cheng[1] and Xiaoyun Sun[2]

[1] Shandong Provincial Key Laboratory of Fine Chemicals,
School of Information, Shandong Polytechnic University,
Jinan, 250353, China
[2] College of Chemistry, Chemical Engineering and Materials Science,
Shandong Normal University,
Jinan 250914, China
cjy@spu.edu.cn

Abstract. Electronic technology and computational intelligence method is used to estimate physical and chemical properties of dangerous hydrocarbon chemicals in this paper. The upper flammable limit (UFL) and lower flammable limit (LFL) are very important properties of dangerous hydrocarbon chemicals. Genetic algorithm (GA) is applied to select the most statistically effective molecular descriptors for evaluating this property. The squared correlation coefficient, root mean square error and average absolute deviation over the main dataset using GA and SVM method are 0.9712, 0.3199 and 3.4066%, respectively. The obtained results indicate that the method is powerful for prediction of FDD of dangerous hydrocarbon chemicals.

Keywords: Electronic technology, Support vector machine, Genetic algorithm, Quantitative Structure-Property Relationship, Flammability dangerous degree.

1 Introduction

Flammability characteristics of dangerous hydrocarbon chemicals are demanded to design safe handling, transportation, and storage, so there is a need to carry out comprehensive research [1]. The upper flammable limit (UFL) is the point above which the mixture is too rich in fuel to ignite. The range between these two limits is the explosive range. Many methods have been developed to respectively estimate the LFL and UFL of dangerous hydrocarbon chemicals [2], [3], [4]. As a rule, the lower the LFL value is, the upper the UFL value is, the flammable danger is higher. Therefore, flammability dangerous degree (FDD) of dangerous hydrocarbon chemicals should be determined by the LFL and UFL more scientifically. The definition formula is FDD=(UFL-LFL)/LFL. The FDD value is higher, the flammability danger is higher. FDD can provide valid guidance for prevention and control of chemical accidents. Then, accurate knowledge of FDD is important for determining the potential for fire and explosion hazards. To prevent from fire and explosion of dangerous hydrocarbon chemicals, knowledge about FDD is critical.

D. Jin and S. Lin (Eds.): Advances in Mechanical and Electronic Engineering, LNEE 177, pp. 621–626.
springerlink.com

However, to our knowledge, FDD, an important flammability characteristic, has not been reported in the literature.

Recently, a quantitative structure property relationship approach (QSPR) has been extensively applied to predict the flammability characteristics of diverse sets of dangerous chemicals [5]. In QSPR studies, variable selection method is a key technology to build accurate and robust models. There are many variable selection methods including ant colony algorithm, principal component analysis and genetic algorithm, etc. Genetic algorithm (GA) is used to select best subset variables with respect to an objective function. Application of the genetic algorithm for subset variable selection was presented by Leardi et al. for the first time [6]. At present, many different technologies, such as partial least squares (PLS), multiple linear regression (MLR), and different types of artificial neural network (ANN), have been widely used in the QSPR modeling, which can be applied for inspection of linear and nonlinear relation between interested property and molecular descriptors, respectively. Meanwhile, the neural networks also suffer some disadvantages inherent to its architecture, such as overtraining, over fitting, network optimization, and reproducibility of results. Due to these reasons above, a more accurate and informative modeling technique which can be effectively used in QSPR analysis is desirably needed. Support vector machine (SVM) is recently developed from the machine learning community by Vapnik and co-workers. In recent years, SVM is gaining popularity due to many attractive features and promising empirical performance. It has also been extended to solve regression problems, and has shown great performance in QSPR studies due to its remarkable ability to interpret the nonlinear relationships between molecular structure and properties.

Electronic technology and computational intelligence method is used to estimate physical and chemical properties of dangerous hydrocarbon chemicals in this paper. In the work, the aim is to predict FDD of dangerous hydrocarbon chemicals from their molecular structures by using GA-SVM method. Predictive power and validity of the model is checked by several techniques.

2 Materials and Methods

2.1 Data Set and Determination of Molecular Descriptors

The predictive power and validity of a model depend on the quality of the dataset used for its development. There are many compilations for properties of dangerous hydrocarbon chemicals. But, of them, IPCS INCHEM offers quick and easy electronic access to thousands of searchable full-text documents on chemical risks and the sound management of chemicals. More importantly, IPCS INCHEM is produced through cooperation between the International Programme on Chemical Safety (IPCS) and the Canadian Centre for Occupational Health and Safety (CCOHS) which ensures reliability of data. Therefore, the LFL and UFL data of 30 dangerous hydrocarbon chemicals were collected in this database and used for this study. The values of FDD were obtained according to the equation (1). These dangerous hydrocarbon chemicals were selected in this study because of their wide application in food, medicine, and

textile and so on, where safety concerns are escalated due to dangerous hydrocarbon chemicals processes.

Molecular descriptors must be calculated from the chemical structure. Therefore, all structures of dangerous hydrocarbon chemicals were drawn and optimized with the HyperChem 8.0 program. The pre-optimizations of all molecules were performed adopting MM+ molecular mechanics force field. Further optimizations were done using the semi-empirical AM1 method. The molecular structures were optimized using the polak-ribiere algorithm until the root mean square gradient was 0.01kcal/mol. After optimization, more than 1000 molecular descriptors of each molecule were calculated using Dragon software developed by the Milano Chemometrics and QSAR research group.

2.2 Genetic Algorithm- Support Vector Machine Coupled Approach

In QSPR studies, one important step is to find the most statistically effective molecular descriptors of desired property from more than 1000 molecular descriptors, and then, to establish the optimum quantitative equation between desired property and the most statistically effective molecular descriptors. For this problem, genetic algorithm is a generally accepted method to select best subset variables with respect to desired property.

Before performing GA technique, the dataset should be divided into two new collections: training set and test set. Training set is used to generate optimum model and test set is used to check validity of the obtained model. The process of division of dataset into two new collections is usually randomly performed. The division was randomly done.

In order to obtain the most statistically effective molecular descriptors of desired property, the program is started with one descriptor at the starting point. After running the program, we can obtain the best multivariate linear model. Then, the number of desired variables should be increased to two, three, five, and so on, and all calculations for them are repeated. The fitness function is the first rule to determine if one descriptor is selected. The calculation must be stopped when the fitness function does not improve significantly of the best-obtained model with increasing in the number of variables, because the best multivariate linear model has been achieved and the optimum subset of descriptors which yield to the best multivariate linear model has been obtained. All molecular descriptors are sorted in accordance with the effect of every molecular descriptor on the desired property.

3 Results and Discussion

GA-SVM method was used to develop the possible nonlinear model to research the relation between the selected descriptors and FDD. In order to obtain support vector machines (SVM) learning results and generalization ability, four SVM parameters (ε=0.01, γ=0.016746, C=831.7465, n=7) were optimized and had got the best combinations after several hundreds of experiments running.

Table 1. Dangerous hydrocarbon chemical data set with the calculated based on reported value and predicted (GA-MLR) flammability dangerous degree

No	hydrocarbons	Cas	FDD(calc)	FDD(pred)
1	1-NONADECENE	18435-45-5	11.3333	11.3684
2	1-OCTADECENE	112-88-9	11.6667	11.2991
3	1-OCTENE	111-66-0	7.5000	7.4623
4	1-PROPENE	115-07-1	4.5000	4.537
5	1-TETRADECENE	1120-36-1	10.2500	10.6685
6	1-UNDECENE	821-95-4	9.6000	9.5655
7	2-BUTENE, (Z)-	590-18-1	5.0625	5.0251
8	2-PENTENE, (E)-	646-04-8	5.2667	5.467
9	3-HEPTENE, (E)-	14686-14-7	6.0909	6.4689
10	3-HEXENE, (E)-	13269-52-8	6.5000	6.2407
11	4-OCTENE, (E)-	14850-23-8	6.6667	6.9409
12	3-ETHYLHEPTANE	15869-80-4	5.7500	6.0306
13	HEXANE, 2,2,5,5-TETRAMETHYL-	1071-81-4	4.8571	4.8216
14	HEXANE, 2,2,5-TRIMETHYL-	3522-94-9	5.5000	5.537
15	HEXANE, 3-ETHYL-	619-99-8	5.4444	5.6807
16	HEXANE,2,4,4-TRIMETHYL-	16747-30-1	5.5000	5.2776
17	PENTANE, 3-ETHYL-	617-78-7	6.0000	5.503
18	1,2-BUTADIENE	590-19-2	5.0000	4.9988
19	1,2-PENTADIENE	591-95-7	7.2000	7.1628
20	1,3-BUTADIENE	106-99-0	4.7500	4.7146
21	1,4-PENTADIENE	591-93-5	7.1875	7.2247
22	1,5-CYCLOOCTADIENE	111-78-4	7.6000	7.4147
23	1,5-HEXADIENE	592-42-7	7.3846	7.5039
24	1,5-HEXADIENE, 2,5-DIMETHYL-	627-58-7	7.0000	6.7763
25	2,3-PENTADIENE	591-96-8	6.5625	6.5266
26	1-DECENE	872-05-9	9.3636	8.996
27	1-HEXENE	592-41-6	5.5833	6.7776
28	2-HEXENE, (E)-	4050-45-7	6.2581	5.985
29	HEPTANE, 3,3,5-TRIMETHYL-	7154-80-5	5.1857	5.5967
30	1,2-HEXADIENE	592-44-9	7.3846	7.6772

Table 1 shows the predicted values for FDD using GA-SVM method. The predicted results are in agreement with the calculated results based on reported values. This fully demonstrates that GA-SVM model is accurate in prediction of FDD of dangerous hydrocarbon chemicals. Fig. 1 shows the plot of the predicted FDD values by GA-SVM method versus the calculated values based on reported values for both the training and test sets. As shown, the accuracy of the predicted FDD over the training set and the test set is almost equal. The case fully illustrates the higher accuracy using GA-SVM method.

The validity of the proposed GA-SVM model is proved. The main statistical parameters of the obtained GA-SVM model are shown in Table 2. As shown in Table 2, the squared correlation coefficient, root mean square error and average absolute deviation of the model over the main dataset are 0.8881, 0.4445 and 4.8980%,

respectively. The results show that the obtained model is valid to predict FDD of dangerous hydrocarbon chemicals. Also, the residuals of the predicted values of the FDD against the calculated values for the model were listed in Fig. 2. As most of the calculated residuals are distributed on both sides of the zero line, one may conclude that there is no systematic error in the development of the present model.

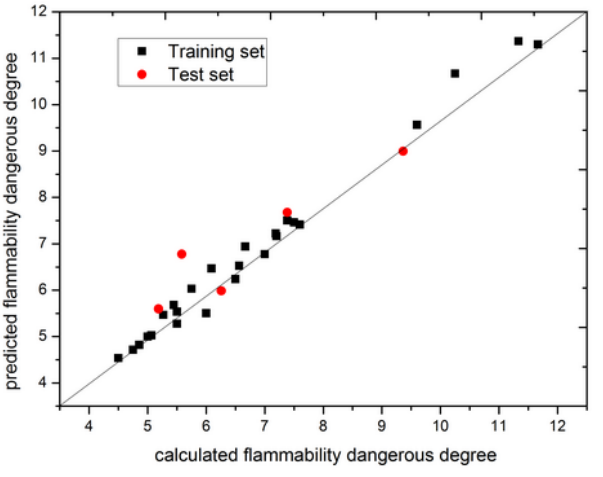

Fig. 1. Plot of predicted versus calculated values of flammability dangerous degree using GA-SVM method

Table 2. Statistical parameters of the GA-SVM model

Statistical parameter	value
Training set	
R2	0.9876
Average absolute deviation	2.4251%
Root mean square error	0.2172
n	25
Test set	
R2	0.8324
Average absolute deviation	8.3137%
Root mean square error	0.6149
N	5
Training set + Test set	
R2	0.9712
Average absolute deviation	3.4066%
Root mean square error	0.3199
n	30

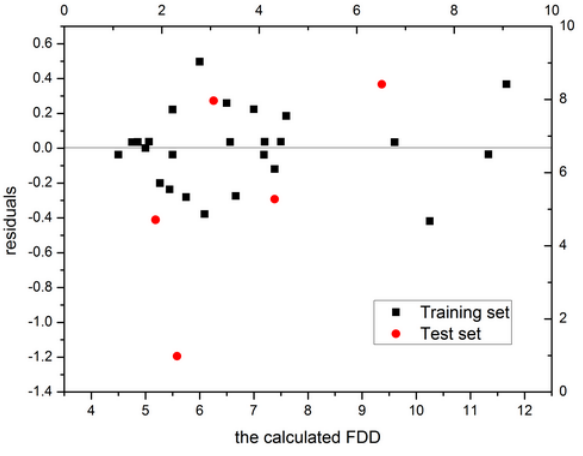

Fig. 2. Plot of the residuals versus the calculated FDD values for the GA-SVM model

4 Conclusion

Flammability danger degree is an important characteristic of flammable dangerous hydrocarbon chemicals. A GA-SVM method was presented for the prediction of FDD of flammable dangerous hydrocarbon chemicals. Based on the results and discussion presented, R^2, RMSE and AAD were employed to check predictive power and validity of the model. The result shows the obtained model can be used to predict the flammability danger degree of flammable dangerous hydrocarbon chemicals.

Acknowledgement. This work is supported by A Project of Shandong Province Higher Educational Science and Technology Program(J10LG20), China, and by Natural Science Foundation of Shandong Province (ZR2011FQ038), China, and by grant 2011WSB11001 of the Shandong medical health science and technology development programs to Shao-qing Wang.

References

1. Juan, A.L.: Neural network particle swarm method to predict flammability limits in air of organic compounds. Thermochimica Acta 512, 150–156 (2011)
2. Seaton, W.H.: Group contribution method for predicting the lower and upper flammable limits of vapors in air. J. Hazard. Mater. 27, 169–185 (2005)
3. Shebeko, Y.N., Fan, W., Bolodian, I.A., Navzenya, V.Y.: An analytical evaluation of flammability limits of gaseous mixtures of combustible-oxidizer-diluent. Fire Saf. J. 37, 549–568 (2002)
4. Kondo, S., Urano, Y., Tokuhashi, K., Takahashi, A., Tanaka, K.: Prediction of flammability of gases by using F-number analysis. J. Hazard. Mater. A 82, 113–128 (2001)
5. Aboozar, K., Hamid, M.: Quantitative Structure Property Relationship for Flash Points of Alcohols. Ind. Eng. Chem. Res. 50, 11337–11342 (2011)
6. Leardi, R., Boggia, R., Terrile, M.: Genetic algorithms as a strategy for feature selection. J. Chemometr. 6, 267–281 (1992)

Key Technologies Research of Transfer Rate Test in Electronic Information Exchange Platform

Ai-min Wang[1], Xiao Li[1], and Qiang Song[2]

[1] School Computer and Information Engineering of Anyang Normal University, Anyang, China
[2] Mechanical Engineering Department of Anyang Institute of Technology, Anyang, China
songqiang01@126.com

Abstract. This paper studies the key technology of improving the transmission function and stability of electronic information exchange platform, relevant technology of realizing function improvement in JAVA, the impact of polling interval of IIP engine upon system transmission rate and relevant technology of improving performance of IIP, and the relation between sending sliced data of varying size and the data transmission rate and so on. The whole technology that has applied to the development and test of Large-scale E-administration system has made good application effect.

Keywords: electronic information exchange platform, data rate test, XML, JDBC, performance improvement Document.

1 Introduction

With the growing popularity of network technology, the development of e-government has become the core of the development strategy of country information and has been the important means of promoting the reform of government affairs system and enhancing managerial effectiveness for governments at all levels. The structure of data exchange platform of e-government includes information layer, data exchange layer and application layer. And data exchange layer is the most important distributed electronic information exchange platform (IIP) among the above three modules in e-government, which includes many data exchange services such as perfect data exchange protocol, supporting data pulling and data pushing, data routing, data validation and data management and so on. Data exchange is the fundamental function of electronic information exchange platform, which realizes data transmission in safety on platform between authorized users. This platform should support the presentation of isomeric data and data exchange between isomeric application systems, and the exchange between structured data (such as data in relational database) and unstructured data (such as graphic files), and the data transmission mode of one-to-one and one-to-many, and provide the mechanism of resume broken transfer and perfect security mechanism.

It is the efficiency and the transmission rate of data exchange function that is an important technological index measuring the e-administration system. Remarkably, the further improvement of platform relies on the guidance of test results such as stability, rate, concurrency and so on. Therefore, it is the electronic information exchange platform that is the main target of performance test and stability test.

D. Jin and S. Lin (Eds.): Advances in Mechanical and Electronic Engineering, LNEE 177, pp. 627–631.
springerlink.com

This paper studies the key technology of transmission performance and stability of electronic information exchange platform. And its overall performance has already been applied to the development and test of a large-scale e-administration system with satisfactory results.

2 Study Method of Performance Test

Testing the performance depends on specific performance target of the system being tested and determines whether applications satisfy these requirements. It is important to eliminate variables as much as possible, for example, the error in code may lead to the performance problems or even cover them. It need to compare different performance test results precisely. If adjustment process has changed the realization of components, the function of applications should be tested again. After the application passes the functionality test, can its performance be tested. Besides the application changes, other things such as the hardware, the amount of network communication, software configurations, system services can be changed unexpectedly also, so it is also important to control the changes of applications.

1. Measure performance. Adjusting its performance correctly needs to record each test result correctly and comprehensively and also maintain them. The record work of test includes: first, precise system configuration, especially the differences from the previous. Second, original data and the results computed by performance monitoring tools. These records can not only indicate whether applications achieve performance goals, but also help to identify the potential causes of future performance problems. It can not distinguish whether different results are caused by changes in the test or changes in the application unless running a series of identical performance test in each test. That making performance test operations run automatically as much as possible is helpful to eliminate the differences made by operators. Some other benign factors can also effect performance test results, for example, running time before applications being tested, and the consumptive time before or during the test results being recorded by the test case, which is not the result data by tests but the necessary consumption of running programs and can affect the final test data greatly. That is just like the differences between the performance of cold car-engines and heat car-engines. Applications having run long time are different to applications just start at the beginning because of factors such as memory fragments.

2. Set benchmark performance. Run one test to establish benchmark after setting performance goals. The more similarity certification environment has with production environment, the larger satisfying possibility of performance arranged by applications will be. Therefore, a practical certification environment seems to be much important at the beginning. The benchmark performance can also be set by traditional methods or use performance index of existing programs that have similar functions. For example, the benchmark of large-scale system with data transmission function is that it can run normally more than 72 hours under continuous data transmission.

3. Pressure test. Pressure test is one special form of the performance tests which is similar to destructive tests of other engineering fields. The purpose of pressure test is to make applications fail. It reduces its performance by adding load to be processed until

applications fail because of resource saturation or making mistakes. Pressure test is helpful to reveal small mistakes which will be found when deploying applications. Pressure test should start on each area of applications early in stages of development as this type of mistake is always caused by design defects. It should better restore these small mistakes rather than restore them until symptoms appear after neglecting them.

4. Solve performance problem. It is time to solve the problems showed in the results after performance test results come out. It always put the performance problems down to more than one factor when analyzing the problems showed up. Therefore, finding the solution for worse performance is quite similar to carrying out scientific experiments. Scientific experiment traditionally follows a process including six steps: observation, initial assumption, forecast, testing, controlling and conclusion. The conclusion is composed of hypothesis supported by the best evidence aggregation accumulated in that process. It can solve the performance problems following the same process. Certainly there are many aids helping to analyzing performance problems, such as Optimize Suite for Java of Borland Company, which has a obvious effect in analyzing the problems of occupying memory.

5. Test the flow. We should test systematic function of the whole platform after the function of the whole data exchange platform–-including the function of data exchange, transmission control of data and routing or forwarding of data, has been performed. The major technological index that need be tested is: maximum normal work-time of system, average rate of transmitting different types of data, impact that the system configuration has on the performance of transmission rate such as the size of the sector when transmitting different sizes of data and Whether there is defect or bug when checking the function of the system while testing the performance.

3 XML Technology and Their Application in Testing the Rate

3.1 XML

XML (Extensible Markup Language) is a general language norm established by W3C organization in Feb,1998, which is a simplified subset of SGML and a set of rules of defining semantic tags which divide the document into several parts and markup them. It is a meta-markup language which defines syntax language concerned with specific field and tag language of structured semantic. XML is a major representation technology of information in e-administration. XML technology mainly centered in XML Parser and the Parser API related with XML include DOM and SAX. Interpreting XML files is the beginning of processing XML files. The interpreter gets XML files and checks whether they are well structured and effective. XML interpreter generally has two types: standard interpreter checking the files are well structured and certification interpreter checking whether the files correspond with DTD.

3.2 Application of XML in Test

The test results produced by the test need to be recorded for several times just like testing rate and then compute the average of them. That recording the results

dynamically is a problem to be solved. If establishing a file alone, there may be thousands of the number of records in a test after reading and writing the document which will consume large amount of time of CPU when results come out and that will affect the true test data instead.

The test results recorded by XML documents can solve the problems above. When accessing XML documents with DOM, DOM can help access the information in XML documents using hierarchic object model. DOM generates one node-tree based on the structure and information of XML documents by which we can access personal information. The text information in XML documents convert into a group of nodes. No matter what the types of information in XML documents are, such as the table data, a column of items or just the document, DOM creates a node-tree when we creating a document object of XML documents. DOM forces us to use tree model like Swing Tree Model to access the information in XML documents of our own. We should just record each result into DOM tree and write the whole tree into XML document when the final result comes out.

4 Performance Test of IIP

4.1 JDBC

JDBC is API providing JAVA code with accessing all kinds of database management system using SQL. JDBC has a driver manager which manages and controls various drivers related to different databases. JDBC is a kind of bottom API, which means that it can directly call SQL instructions with easier realization than other database interconnection. Meantime, it is also basic for building advanced API and other database tools. The architecture of JDBC is shown in figure 1:

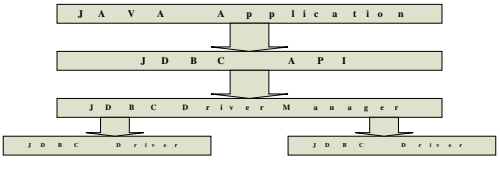

Fig. 1. Architecture of JDBC

Driver Manager class is the management level of JDBC which play role between the user and the application. It follows available drivers and establishes connections between the database and corresponding driver.

4.2 Stability Testing

The task need testing after the single-data edition of IIP has been developed includes: maximum time of getting the system work properly, getting the transmission rate of the tested computer in JBuilder and getting average time spent in a transmission in JBuilder. It is, as it were, stable of data exchange system of IIP operating at full load

more than 72 hours in actual network environment, so it can set the decidable stability index up to 72 hours in JBuilder temporarily (the stability test need be tested for several times). The purpose of the test is stability and therefore the lower tier X-Linker is not included which means it requires IIP to write a functional unit simulating the transmission of information layer instead of X-Linker as this test is not in actual network environment. This function has been performed by false router. Test cases should transmitting data continually in order to make IIP work constantly. This can be implemented using the method of "passing the buck".

Using false router . There are not only modules of data sending, but also Hook functions triggered after the realization of receiving data in the test case. IIP directly sends the data to its own path of data reception and triggers the Hook function of its own after it has been sent to exclusive path of thread polling by test cases. It is called one transmission from sending the data to triggering its own Hook function. Testing data demands that the output should be XML and should record the arrival time of data, consumptive time of the process, the size of data and this transmission rate.

5 Conclusion

Based on the technology stated above, we've achieved good application results in testing the function of information exchange and the performance proceeding from development demand of e-administration electronic information exchange platform.

Test results have great help in improving system performance, so the performance of platform will have great improving space. There is available improvement in system implementation and system development on developing language. Therefore the later improvement work is necessary besides the implementation of the function of electronic information exchange platform. And the performance of IIP also has large improvement space.

References

1. Mengqiang, X.: Programming base in JAVA. Renmin Postal Publishing House (2006)
2. Wang, A., et al.: Reflection Reference Manual on.NET, p. 3. Tsinghua University Press (2003)

Research for the Square Corner Detection Algorithm Based on Electronic Measurement Engineering

GuoLing Lv[1], ZhenJie Hou[2], and HongYu Zhao[3]

[1] College of Computer and Information Engineering,
Inner Mongolia Agricultural University, Hohhot, 010018, China
[2] College of Information Science and Engineering,
Changzhou University, Changzhou, 213164, China
[3] Computer College, Beijing University of Technology, Beijing, 100124, China
lv_guoling@126.com

Abstract. Camera calibration technology has been widely applied to electronic measurement engineering. According to the calibration needs manual confirmation corner time-consuming and the problem which possibly exists in setting error, this paper presents a square corner detection algorithm of black-and-white checkerboard for automatic dual-rotating template which can obtain feature points which needed for the calibration of black-and-white chessboard. The algorithm combines with black-and-white detecting operator (BW) thinking, through the construction of double operator template, regulate parameter and template for self-adaption according to the results of detection, detect corners on a black-and-white checkerboard iteratively, and achieve the forecast effect at last. The algorithm not only practical, but also enhance the detection accuracy of effective corner in checkerboard and noise inhibiting ability.

Keywords: electronic measurement engineering, 3D reconstruction, calibrate, black-and-white checkerboard, square corner detection.

1 Introduction

3D reconstruction is one of the key problems in electronic measurement engineering, the 3D reconstruction is split into two parts by whether to solve the camera parameters, one is based on calibrated [1] reconstruction technique and the other is based on uncalibrated [2]. Based on uncalibrated reconstruction techniques has strong instantaneity because of it needs estimate the scene prior information, but the algorithm is complex and difficult to achieve the ideal effect of reconstruct. The reconstruction technique based on camera calibration accurately solves the intrinsic and extrinsic parameters of the camera so that it can restore the 3-D scene information of the two-dimensional image, therefore the reconstruction technique is an important module of 3D reconstruction system and the precision of its calibration results and the stability of its algorithm directly affects the performance of the whole system. The square corner information on black-and-white checkerboard is usually part of camera calibration in 3D reconstruction, the traditional square corner detection is commonly the method of confirming the square corner information manually but the square

D. Jin and S. Lin (Eds.): Advances in Mechanical and Electronic Engineering, LNEE 177, pp. 633–638.
springerlink.com

corner detection on black-and-white checkerboard will be influenced by the background, noise of image etc in general. A method of square corner detection for identifying the square corner on black-and-white checkerboard was presented in Literature [3], but may often confuse the chessboard under the complex background.

This paper presents a square corner detection algorithm of black-and-white checkerboard for non-manual dual-rotating template based on BW [3]. The algorithm constructs "+" operator template, then regulate template and parameters for self-adaption according to the results of its square corner detection, and detects square corner on the black-and-white checkerboard repeatedly. The algorithm has advantages such as high efficiency, anti-noise ability, strong self-adaptability and anti-interference ability under the actual background etc, and can be applied to camera in an aberrant case of corner detection.

2 The Square Corner Detection Algorithm for Black-and-White Checkerboard

2.1 BW Operator

With black-and-white checkerboard pixels as the center if the gray value varies with the accumulation exists more differences between pixel along the direction of d_1、d_4 and pixel along the direction of d_2、d_3, it can be think this feature points is the square corner on black-and-white checkerboard, this is the thought of BW operator [3], as shown in Fig. 1 below.

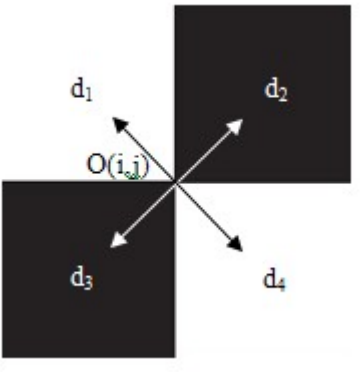

Fig. 1. Map of square corner on the checkerboard

2.2 The Square Corner Detection Algorithm for Dual-Rotating Template

In order to reduce the burden of practical application operation, the algorithm of Harris square corner detection should be adopted in corner detection at first, and then detect the square corner which has been acquired for second by though adopt the algorithm that proposed in this paper. In practical application, the algorithm in this

paper constructs template which as shown in type (1) and type (2), according to the thought of BW operator.

$$c_1(i,j) = \left| \sum (I_1 + I_4) - \sum (I_2 + I_3) \right| \tag{1}$$

$$c_2(i,j) = \left| \sum (I_1 - I_4) + \sum (I_2 - I_3) \right| \tag{2}$$

Where I_i (i=1, 2, 3, 4) express the pixel grayscale value which is traverse along the direction of d_i with O(i, j) as the center. Based on type (1) and type (2) to build such as type (3) and type (4) shows multi-order matrix which will do filter detection on image.

$$\begin{bmatrix} 0 & & 1 & & 0 \\ & & \vdots & & \\ -1 & \cdots & 0 & \cdots & -1 \\ & & \vdots & & \\ 0 & & 1 & & 0 \end{bmatrix} \tag{3}$$

$$\begin{bmatrix} 0 & & 1 & & 0 \\ & & \vdots & & \\ 1 & \cdots & 0 & \cdots & -1 \\ & & \vdots & & \\ 0 & & -1 & & 0 \end{bmatrix} \tag{4}$$

When detection algorithm can't get ideal effect, it will detect the square corner again by though rotate the template matrix.

Concrete realization of this algorithm is as follows:

(1)The first, detect image for Harris square corner [4-6];

(2)The square corner which has been acquired by steps (1) construct template such as type (3) and type (4), according to the operation of type (1) and type (2);

(3)Do filter detection on image;

(4)To determine whether exceed the times of iteration, if it has been exceeded skip to steps (5); Are the detection results judgment for the prediction results, rotate template as type(3) and type (4) if not, return steps(4); If the outcome is for the prediction turned to steps (6);

(5)The algorithm is failure, please acknowledge the square corner for manual;

(6)The nearby square corner will deal with merging, find its position of center for replacement.

2.3 The Square Corner Detection Algorithm for Manual

The traditional camera calibration acquire the square corner on black-and-white checkerboard though manual operation usually, its procedures as follows: first acknowledge 4 points on checkerboard by manual operation, then construct the grid

(grid size confirmed in advance), and correction at last ,as shown in Fig. 2.This method is still need to calibrate template, and the precision which template has been calibrated can affect calibration results, and the efficiency of the algorithm is low, more time-consuming when dealing with multiple image.

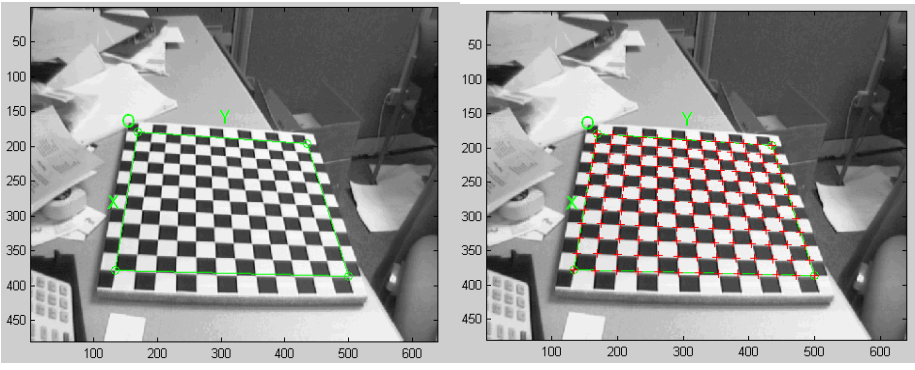

Fig. 2. Acquire the square corner on black-and-white checkerboard for manual

3 The Experimental Results and Analysis

This paper uses homemade black-and-white checkerboard for experiment. Black-and-white checkerboard make up of 13*14 square, the resolution of the images for 632 * 471. The square corner detection algorithm of black-and-white checkerboard for dual-rotating template use matlab7.0 programming achieve under by the Windows XP workbench according to its principle and process, and experiment for contrast. Fig. 3 is corner detection for Harris of the experimental result, phenomenon of shift position of corner (or leaving false corner) have been existed. Though test, the algorithm in this paper operate stable and extract square corner accurately, furthermore it can remove leaving false corners successfully, as shown in Fig. 4 shows meet the requirements of experiments.

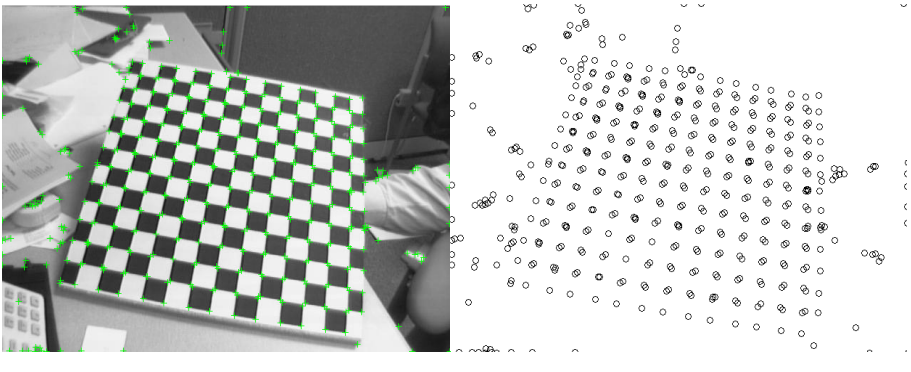

Fig. 3. Square corner obtained in Harris corner detection

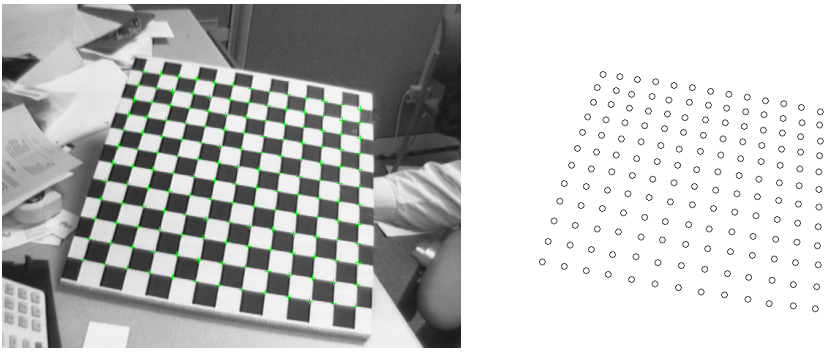

Fig. 4. Square corner obtained in the improved algorithm

On the original algorithm and the improved algorithm of square corner extracting, statistics the situation of square corner which has been acquired, as shown in Table 1.

Table 1. Comparison of square corner

black-and-white checkerboard image	The number of square corner	The number of square corner with shift	The number of leaving false corner
The original algorithm	320	24	69
The improved algorithm	156	16	0

4 Conclusions

The algorithm combined with the thought of BW operator, it ideally detected square corner on black-and-white board which need for calibration. The results of experiment show that this algorithm make researchers did not set information of square corner checkerboard for manual tediously, and that run with high efficiency, operate easily, own strong reliability, in addition the algorithm is able to remove leaving false corners, so it has strong practical significance in electronic measurement engineering.

Acknowledgment. Thanks go to the members of the Research Group for help and encouragement. The paper supported by the National Natural Science Foundation of China (61063021).

References

1. Zhang, Z.J.: A flexible new technique for camera calibration. IEEE Transactions on Pattern Analysis and Machine Intelligence 22(11), 11330–11334 (2000)
2. Zhao, H.Y., Li, Y.H., Hou, Z.J.: Research of hierarchical reconstruction based on robust vanishing point. Microcomputer & Its Applications 30(9), 31–35 (2011)

3. Liu, Y., Wang, F.L., Chang, Y.J., Zhe Lv, J.: Black and White X2Corner Detection Algorithm. Journal of Northeastern University (Natural Science) 28(3), 249–252 (2002)
4. Miroslav, T., Mark, H.: Fast comer detection. Image and Vision Computing 16(1), 75–87 (1998)
5. Li, Y., JiaXiong Pang, J.: Sub-pixel Edge Detection Based on Spline Interpolation of D2 and LOG Operator. Journal of HuaZhong University of Science and Technology 28(3), 77–79 (2000)
6. Zou, N., Liu, J., ManLi Zhou, J.: Zernike Moment-Based Edge Detection. Journal of HuaZhong University of Science and Technology 27(5), 1–8 (1999)

Study on Control of Micro-source with Non-linear Load with Power Electronic Technology

QunHai Huo[1,*], TongZhen Wei[1], and JiangBo Wang[2]

[1] Institute of Electrical Engineering,
The Chinese Academy of Sciences,
Beijing, 100190, China
[2] Power Electronics Department,
China Electric Power Research Institute,
Beijing 100192, China
huoqunhai@163.com

Abstract. The micro-source in micro-grid may be very close distance to the load, and the power output is directly affected by the non-linear load. The harmonic problem caused by the non-linear load of energy-storage micro-source is studied in this paper. The control system is designed using the Modified Sliding Mode Variable Structure Control (MSMVSC) with power electronic technology. The result showed that the voltage loop using the modified sliding mode algorithm can effectively improve harmonic problems.

Keywords: Micro-grid, Micro-source, Non-linear load, the Modified Sliding Mode Variable Structure, Power Electronic Technology.

1 Introduction

Recently the more application technologies of Distributed Generation (DG) include Micro-turbine power generation [1]-[3], Fuel cell power generation [4],[5], Photovoltaic power generation [6], [7], Wind Power [8], [9], Biomass power generation and so on. Micro-source below 500KW is the main development trend of new DG [10]. One of characteristics for Micro-grid is small inertia, so the micro-grid in general is equipped with a distributed storage devices which is used for voltage support of micro-grid [11]-[14].

The micro-source in micro-grid may be very close to the load in distance, there is no long transmission line, and there is no limit to the stability of the transmission line, but the entire system was pure resistive and very rapid changes in output, and the power output is directly affected by the non-linear load.

The harmonic problem caused by the non-linear load of energy-storage micro-source is studied in this paper. The control system is designed using MSMVSC [15]. The result showed that system performance had been significantly improved.

* Corresponding author: TongZhen Wei (e-mail: tzwei@mail.iee.ac.cn)

D. Jin and S. Lin (Eds.): Advances in Mechanical and Electronic Engineering, LNEE 177, pp. 639–644.
springerlink.com

2 Topology of Energy Storage Micro-source

Main power supply topology is shown in Fig. 1. Batteries are used to provide power, and the voltage increased from 480V up to 720V. This equipment is used for main power supply device in micro-grid, and the other micro-sources are connected to it.

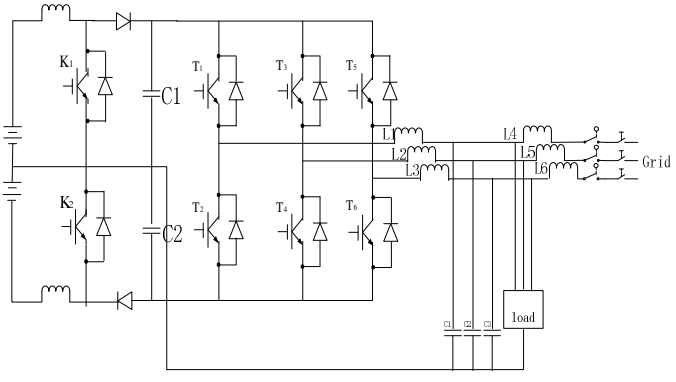

Fig. 1. Topology of Energy Storage micro-source

3 Theoretical Derivation

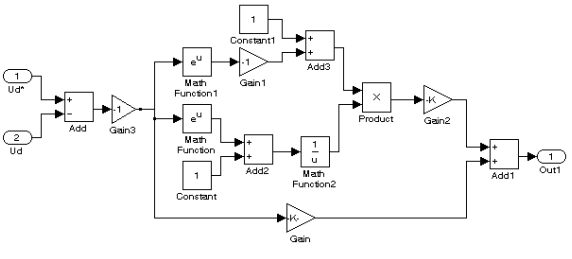

Fig. 2. Index sliding mode controller

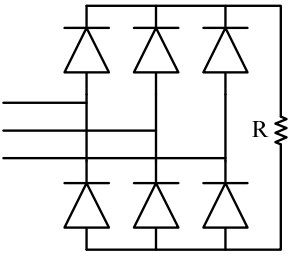

Fig. 3. Uncontrolled rectifier with resistive load

Choosing the sliding model:

$$S = U_d * - U_d \tag{1}$$

U_d is d-axis load voltage through park transformation, $U_d *$ is reference voltage.

By using the exponential rate reaching law technology, a modified sliding mode controller was designed as Fig 2:

$$\frac{dS}{dt} = -K * \frac{1 - e^{-S}}{1 + e^{-S}} - K' * S \quad K' = 1/K > 0 \tag{2}$$

4 The Simulation and Discussion

In this paper, the simulation model is built by SimpowerSystems of matlab, and the situation of load balance is simulated using MSMVSC firstly. Then the three situations

of non-linear load are simulated: (1) Uncontrolled rectifier with resistive load (Fig. 3). It is simulated using PI control firstly, and the corresponding voltage and current waveforms showed in Fig. 6 and Fig. 7. It is simulated using MSMVSC later, and the corresponding voltage and current waveforms showed in Fig. 10- Fig. 13. (2) Uncontrolled rectifier with resistive load and capacitance in parallel (Fig. 4). Current waveforms showed in Figure 14. (3) Uncontrolled rectifier with resistive load, capacitance and inductance in parallel (Fig. 5). Voltage and current waveforms showed in Fig. 15 and Fig. 16. The main purpose of the simulation was to test load characteristics of different power factor.

Simulation parameters: on the balanced load, three-phase loads are 10 ohms; on the non-linear load, resistive load is 10 ohms. Bus voltage is 720V, and the bus capacitor C1, C2 is 4500uF. The simulation results are shown in Fig. 6- Fig. 16.

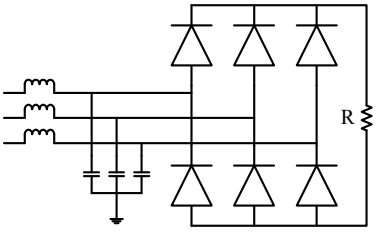

Fig. 4. Uncontrolled rectifier with resistive load and capacitance in parallel

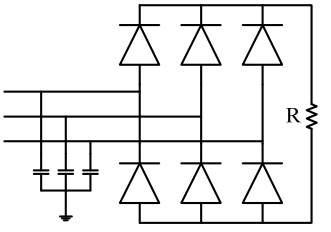

Fig. 5. Uncontrolled rectifier with resistive load, capacitance and inductance in parallel

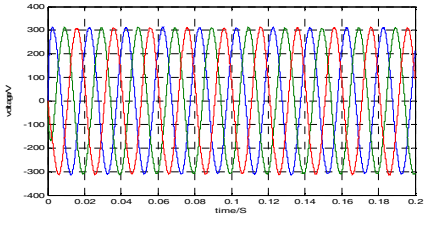

Fig. 6. Voltage waveform of three phases under balanced load

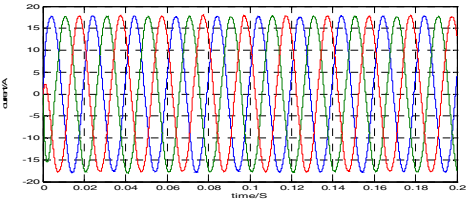

Fig. 7. Current waveform of three phases under balanced load

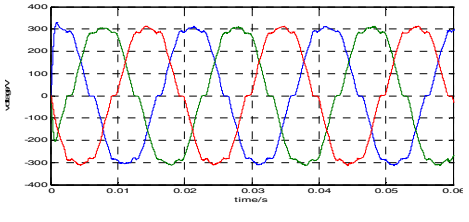

Fig. 8. Voltage waveform of PI control with uncontrolled rectifier with resistive load

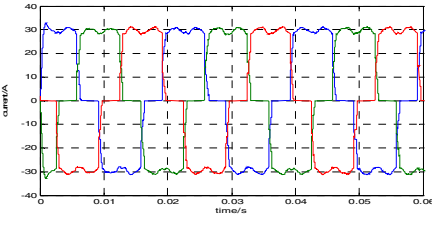

Fig. 9. Current waveform of PI control with uncontrolled rectifier with resistive load

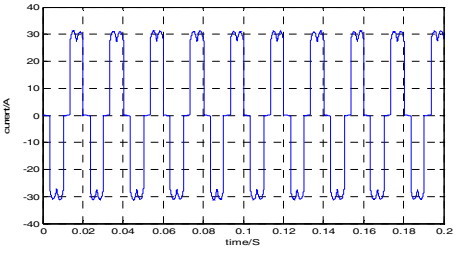

Fig. 10. Current waveform of phase A with uncontrolled rectifier with resistive load

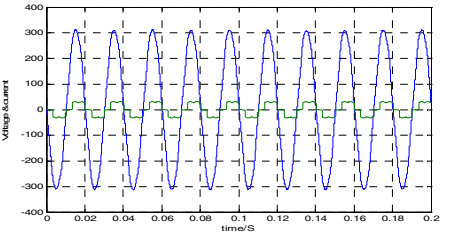

Fig. 11. Voltage and current waveform of phase A with uncontrolled rectifier with resistive load

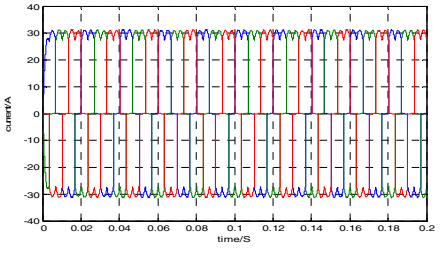

Fig. 12. Current waveform of three phases with uncontrolled rectifier with resistive load

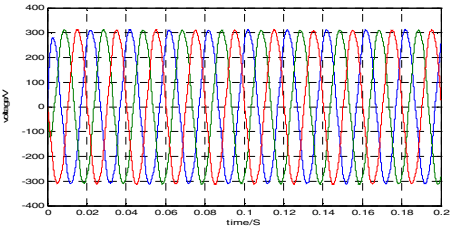

Fig. 13. Voltage waveform of three phases with uncontrolled rectifier with resistive load

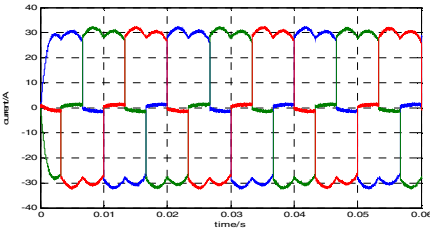

Fig. 14. Current waveform of three phases with uncontrolled rectifier with resistive load parallel connected capacitance

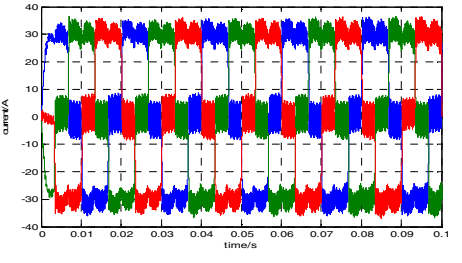

Fig. 15. Current waveform of three phases with uncontrolled rectifier with resistive load, capacitance and inductance in parallel

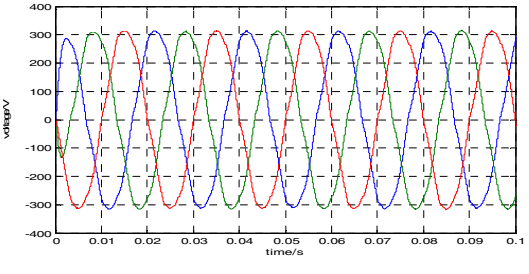

Fig. 16. Current waveform of three phases with uncontrolled rectifier with resistive load, capacitance and inductance in parallel

In DC circumstances, PI control can achieve non-static error control, but for 3 times, 5 times and so on low harmonic control is bad. Through Figure 8 can also see that the output waveform contains a large number of low harmonics. The sliding mode of the MSMVSC is constant, that is, the system has a better robustness and is not sensitive to the system change and external interference. Therefore, the MSMVSC can achieve a better control effect for non-linear load.

Three cases have the same output voltage waveform, but current waveform has more obvious differences. When the system is connected with uncontrolled rectifier with resistive load and capacitance in parallel (Fig. 14), the entire load-side showed capacitive, and current lags behind voltage. When the system is connected with uncontrolled rectifier with resistive load, capacitance and inductance in parallel (Fig. 15), the current ripple exacerbated, but output voltage waveform is still very good (Fig. 16), it proved that the MSMVSC has a good control effect.

Choosing the appropriate algorithm, micro-source can work with balanced load and non-linear load. Fig.10 can be seen that the load current is the standard U-shaped wave, and it can reflect the load characteristics. Fig.11 can be seen that the application of sliding mode control strategy could improve the output voltage for the standard smooth sine wave, control results is satisfying. Fig.12 and Fig.13 are the waveforms of the three-phase voltage and current, the modified sliding mode control is used, micro-source can work in the smoothing. The voltage loop using the modified sliding mode algorithm can effectively improve harmonic problems caused by the non-linear load.

Acknowledgments. This work has been financed by the National Natural Science Foundation of China under award number 50807052,51107134.

References

1. Ming, G., Onifri, M., Lin, Z., Ma, J.: Experimental studies on a CCHP system based on a micro-turbine. In: 2011 Second International Conference on Mechanic Automation and Control Engineering (MACE), pp. 2159–2162 (2011)
2. Kish, G.J., Lehn, P.W.: A micro-turbine model for system studies incorporating validated thermodynamic data. In: 2011 IEEE Power and Energy Society General Meeting, pp. 1–6 (2011)
3. Tong, J., Yu, T.: Nonlinear PID control design for improving stability of microturbine systems. Electric Utility Deregulation and Restructuring and Power Technologies, 2515–2518 (2008)
4. Jain, S., Agarwal, V.: An Integrated Hybrid Power Supply for Distributed Generation Applications Fed by Nonconventional Energy Sources. IEEE Transaction on Energy Conversion 23(2), 622–631 (2008)
5. Sedghisigarchi, K., Feliachi, A.: Impact of fuel cells on load-frequency control in power distribution systems. IEEE Transaction on Energy Conversion 21(1), 250–256 (2006)
6. Femia, N., Lisi, G., Petrone, G., Spagnuolo, G., Vitelli, M.: Distributed Maximum Power Point Tracking of Photovoltaic Arrays: Novel Approach and System Analysis. IEEE Transactions on Industrial Electronics 55(7), 2610–2621 (2008)

7. Wongsaichua, W., Lee, W.-J., Oraintara, S., Kwan, C., Zhang, F.: Integrated high-speed intelligent utility tie unit for disbursed/renewable generation facilities. IEEE Transactions on Industry Applications 41(2), 507–513 (2005)
8. Hamlyn, A., Cheung, H., Wang, L., Yang, C., Cheung, R.: Adaptive Interfacing Control Strategy for Electricity Generations from Wind Power to Distribution Grids. In: 2007 Large Engineering Systems Conference on Power Engineering, pp. 78–83 (2007)
9. Ochoa, L.F., Padilha-Feltrin, A.F., Harrison, G.P.: Time-Series-Based Maximization of Distributed Wind Power Generation Integration. IEEE Transaction on Energy Conversion 23(3), 968–974 (2008)
10. Fazanehrafat, A., Javadian, S.A.M., Bathaee, S.M.T., Haghifam, M.-R.: Maintaining The Recloser-Fuse Coordination in Distribution Systems in Presence of DG by Determining DG's Size. In: IET 9th International Conference on Developments in Power System Protection, DPSP 2008, pp. 132–137 (2008)
11. Louie, H., Strunz, K.: Superconducting Magnetic Energy Storage (SMES) for Energy Cache Control in Modular Distributed Hydrogen-Electric Energy Systems. IEEE Transactions on Applied Superconductivity, Part 2 17(2), 2361–2364 (2007)
12. Borowy, B.S., Casey, L.F., Davis, G.H., Rajda, J., Schauder, C.D.: Advanced Semiconductor Impact on Distributed Generation, Energy Storage and the Utility Grid. In: Power Engineering Society General Meeting, pp. 1–8 (2007)
13. Laaksonen, H., Saari, P., Komulainen, R.: Voltage and frequency control of inverter based weak LV network microgrid. In: 2005 International Conference on Future Power Systems, pp. 2–6 (2005)
14. Choi, S.S., Tseng, K.J., Vilathgamuwa, D.M., Nguyen, T.D.: Energy storage systems in distributed generation schemes. In: Power and Energy Society General Meeting - Conversion and Delivery of Electrical Energy in the 21st Century, pp. 1–8 (2008)
15. Gao, W.: Variable structure control theory foundation. Science and Technology of China Press, Beijing (1990)

Design of Building Energy Consumption Acquisition Unit Based on ARM Processor

GuoSheng Ma[1] and XiaoBo Xia[2]

[1] Electronic Engineering Institute, Hefei, 230037, China
gsmaw@sina.com
[2] Anhui Antai Sci. & Tech. Corp. Hefei, 230088, China
xxb@rishi.cn

Abstract. In building energy consumption monitoring system, data acquisition unit is an important device. Building energy consumption acquisition unit mainly achieves to collect data of various meters within its monitoring area. This paper introduces a design of building energy consumption acquisition unit based on ARM11 processor and Windows CE. The design achieves data transmission between unit and data center over GPRS or Internet. This design also includes a Wi-Fi module, a large memory SD card and a USB interface.

Keywords: Energy Consumption Monitoring, Data acquisition, ARM, Windows CE.

1 Introduction

With the rapid growth of the economy, energy needs in all sectors has been increasing sharply in China. According to the National Bureau of Statistics of China, from 2005 to 2009, the total energy consumption in China are respectively 2246820, 2462701.5, 2655830, 2850000 and 3066470 thousand tons of standard coal, as shown in Figure 1. Although both the central and local governments had promoted hard efforts, the total energy consumption kept increasing progressively with years under great energy needs. Thus, China is facing a grim situation in the energy-saving emission reduction work.

According to statistics, the total area of government office buildings and large public buildings accounts for less than 4% of the total area of urban construction. In contrast, the electricity consumption accounts for about 22% of the total electricity consumption in urban construction, and the annual electricity consumption per square meter is 10 to 20 times higher than that in residential buildings, which is

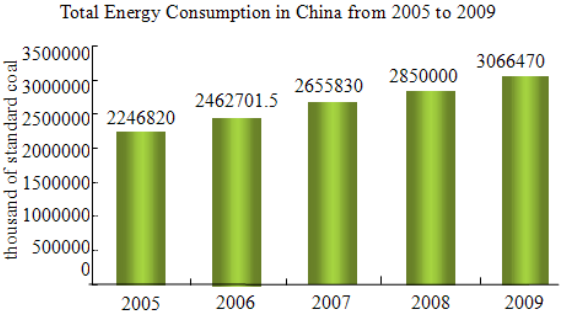

Fig. 1. Total energy consumption in China from 2005 to 2009[1]

D. Jin and S. Lin (Eds.): Advances in Mechanical and Electronic Engineering, LNEE 177, pp. 645–650.
springerlink.com

1.5 to 2 times as high as that in similar constructions in developed countries. The energy conservation in government office buildings and large public buildings not only associates with the goal of reducing 20% energy consumption per unit of GDP by the end of the National Eleventh Five-Year Plan period, but also acts as a powerful demonstration of energy-saving emission reduction work[2].

The energy consumption acquisition unit is one of the key devices in the building energy consumption monitoring system. This paper introduces a design of building energy consumption acquisition unit based on S3C6410 ARM11 processor and Windows CE 6.0 operating system. This device not only satisfies the requirements in basic functions of data acquisition and monitoring, but also adds a Wi-Fi module, a large memory SD card and a USB 2.0 interface.

2 The Building Energy Consumption Monitoring System

The building energy consumption monitoring system supply online monitoring and dynamic analysis service through installing energy consumption devices on buildings and collecting data over long-distance transmission [3].

This system consists of data acquisition subsystems and data centers. The data acquisition subsystem consists of smart meters and building energy consumption acquisition units. Data center receives and storages the data uploaded by monitored buildings.

3 The Design Requirements of Building Energy Consumption Acquisition Unit

According to *Technical Guide Rules for Transmission*, a building energy consumption acquisition unit should satisfy the following requirements [3]:

1) Acquisition interface: at least one RS-485 interface;
2) Acquisition rate: maximum rate should be at least 9600bps;
3) Acquisition protocols: support DL/T645-1997, CJ/T188-2004, GB/T19582-2008, each interface could be configured with one protocol respectively;
4) Number of metering devices supported: at least 32;
5) Acquisition periodicity : acquire data periodically or on the command from data centers, periodicity could be set from 10 minutes to 1 hour;
6) Memory capacity: at least 16MB;
7) Uploading interface: at least one wired or wireless interface;
8) Uploading periodicity: real time at acquisition;
9) Data centers supported: at least 2;
10) Configuration/maintenance interface: equipped with local configuration/ maintenance interface;
11) Network functions: receive commands, upload malfunctions, encrypt data, resume broken downloads and analysis DNS;
12) Power: less than 10W.

4 Hardware Structure Design

According to design acquirements, the hardware structure of the building energy consumption acquisition unit is shown as Figure 2.

4.1 ARM Processor

The system uses SAMSUNG high performance processor Samsung S3C6410A, run at 533 MHz. It adopts ARM1176JZF-S core, which includes separate 16KB Instruction and 16KB data caches, 16KB Instruction and 16KB Data TCM, and adopts the de-facto standard AMBA bus architecture. The S3C6410X also includes many hardware peripherals to meet various special requirements. The supply voltage for logic core is 1.2V, and various power-down modes are available such as Idle, Stop and Sleep mode [4].

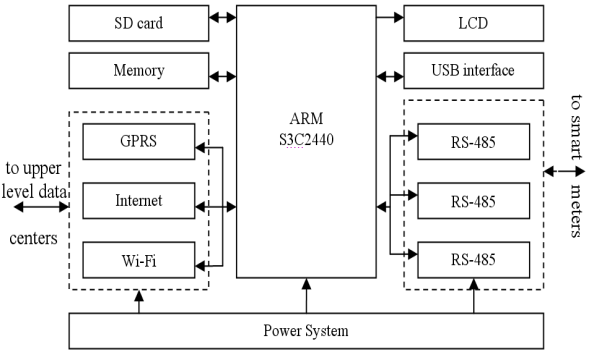

Fig. 2. Hardware structure of building energy consumption acquisition unit

4.2 Serial Communication Interface

The system provides RS-485 interfaces and RS-232 interfaces for serial communication. There are three RS-485 interfaces for energy consumption acquisition. All of them support DL/T645-1997, CJ/T188-2004 and GB/T19582-2008 protocols, with each interface configured with one protocol. The RS-232 interface is provided to support GPRS module.

4.3 USB Interface

The S3C6410A processor provides two USB interfaces; one is distributed to Wi-Fi module, and the other can be used for a USB mouse or keyboard, which facilitates the operation under Windows CE operating system.

4.4 Memory Subsystem

The memory subsystem contains SDRAM, FLASH ROM and SD card memorizers. It adopts two pieces of K4X51163PG-FGC6 SDRAM (64M) chips and one piece of K9F2G080B NAND FLASH ROM (256M) chip. Besides, to provide the unit with a large memory for energy consumption data, it is also equipped with a 4GB SD card.

5 Software Structure Design

The software of the building energy consumption acquisition unit is based on Windows CE operating system. The software is developed using Visual Studio 2005.

According to *Technical Guide Rules for Transmission,* the software structure is designed to include presentation layer, application layer, information resource and data layer, network layer, standard specification system and security system. The application layer includes Data Acquisition Subsystem, Data Process Subsystem, Data Uploading Subsystem, Data Display Subsystem, Database Management Subsystem and System Configuration Subsystem.

5.1 Data Acquisition Subsystem

This subsystem acquires energy consumption data from energy meters within its monitoring area through RS-485 interfaces. Acquisition unit inquires data meter by meter, and meters answer in turns. And it supports such communication protocols: MODBUS-RTU, DL/T645-1997, CJ/T188-2004, and GB/T19582-2008.

5.1.1 Data Acquisition Target

According to *Technical Guide Rules for Acquisition*, data acquisition target includes building basic information acquisition target and energy consumption acquisition target.

Building basic information acquisition target is differentiated into two parts: basic items and appended items. Basic items include building name, building area and heating area, etc., while appended items vary by building types.

Energy consumption acquisition target includes categorized energy consumption data and itemized energy consumption data. Categorized energy consumption data include electric energy consumption, water consumption, gas consumption, heat consumption and other power consumption. Itemized energy consumption data, taking electric energy as an example, is differentiated into four items: illumination-and-socket power, air-condition power, motive-power power and special power [5].

5.1.2 Data Acquisition Method

The acquisition unit supports manual data entry and automatical data acquisition. Thereinto, automatic acquisition adopts polling mechanisim, as the acqusition unit polls each of the smart meters in a round-robin fashion. Besides, automatic acquisition can be configured with acquisition frequency, from once per quarter to once per hour. Acquisition is in accordance with *CJ-T188-2004 Technical requirements of utility meters data transmission* [6].

5.2 Data Process Subsystem

According to *Technical Guide Rules for Acquisition,* acquisition unit should verify the validity of the data and make some calculation. Thereinto, the calculation, take electronic power as an example, includes summation of electronic power, electronic power per unit area and differentiated electronic power per unit area, etc.

5.3 Data Uploading Subsystem

According to *Technical Guide Rules for Acquisition,* acquisition should be able to display building basic information, energy consumption monitoring condition, categories and items of energy consumption data, original readings from all branches and summations by stage (hour, day, month and year), as well as the comparisons with reference buildings. Display can be in form of pie chart, bar chart, line graph and table, etc.

Based on LCD touch-screen and Windows CE 6.0 operating system, this subsystem is designed with a simple and beautiful display interface and an easy-to-use control interface. Take bar chart as an example: when viewing monthly statistics of some year, you can drag leftward or rightward to view other months' statistics, and you can drag upward or downward to view other years' statistics. Also you can click on one month to view detail information of this month, and double click on one month to view daily statistics of this month. One screenshot of the Data Display Subsystem is shown as Figure 3.

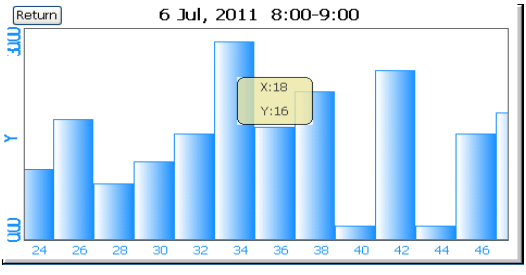

Fig. 3. A screenshot of Data Display Subsystem (bar chart), click on some bar will show detail in a textbox, and then the textbox will fade away.

5.4 Database Management Subsystem

The database is implemented using Microsoft® SQL Server™ 2005 Compact Edition. SQL Server Compact Edition shares a common programming model with the other SQL Server editions, enabling developers to transfer skills and knowledge quickly and easily. Besides, it occupies 5MB memory and 2MB disk, uses indexes to balance its optimizer for speed and efficiency, and provides single data file with password protection and 128-bit file level encryption [7].

The acquisition unit includes a database, in which there are two tables, building information table and energy consumption table. The building information table storages the base information of the buildings located within its monitoring area, including the name, the function, the age, the area and the type of the building. The energy consumption table storages the energy consumption data that differentiated by categories and items.

Considering that the ARM processor in this acquisition unit is of a relatively lower running-frequency while the data size is quite large, the acquired energy consumption data is not stored in only one database file, but is stored differentiating years and categories, thus to improve query efficiency.

6 Conclusion

This paper introduces a design of building energy consumption acquisition unit based on S3C6410 ARM11 processor and Windows CE 6.0 operating system. This design entirely satisfies the national criteria; support DL/T645-1997, CJ/T188-2004 and GB/T19582-2008 communication protocols; acquire data from all kinds of energy meters through RS-485 interfaces; equipped with GPRS, Ethernet and Wi-Fi network communication modules to communicate with data centers; equipped with a large memory SD card; provide a USB interface and control interface based on Windows CE 6.0 operating system.

References

1. National Bureau of Statistics of China. National Statistics Database [DB] (2010)
2. Ministry of Housing and Urban-Rural Development of the People's Republic of China, Software Development Instruction in Building Energy Consumption Monitoring System for Government Office Buildings and Large Public Buildings (2009)
3. Ministry of Housing and Urban-Rural Development of the People's Republic of China, Technical Guide Rules for Transmission of Itemized Energy Consumption Data in Building Energy Consumption Monitoring System for Government Office Buildings and Large Public Buildings (2009)
4. USER'S MANUAL of S3C6410X RISC Microprocessor. Samsung Electronics Co., Ltd. (2008)
5. Ministry of Housing and Urban-Rural Development of the People's Republic of China, Technical Guide Rules for Acquisition of Itemized Energy Consumption Data in Building Energy Consumption Monitoring System for Government Office Buildings and Large Public Buildings (2009)
6. CJ-T188-2004 Technical Requirements of Utility Meters Data Transmission (2004)
7. SQL Server Compact 3.5 Features Datasheet (2006)

Customizing Google Maps for Ubiquitous Real Time Mobility Information Systems

Alfio Costanzo and Alberto Faro

Department of Electrical, Electronics and Computer Engineering,
Catania University, viale Doria 6, Catania, Italy
alfioc87@hotmail.it, afaro@dieei.unict.it

Abstract. Current information systems available for mobile users generally lack of real time information to help users to choose the best paths to destination taking into account current traffic conditions. For these reasons, the paper aims at illustrating a mobility information system that allows both driving and walking people to know the best paths to destination depending on the traffic data collected by a suitable sensing infrastructure. The services are provided to both PCs and user mobiles that, as pointed in many market studies, are the future versions of the current GPS based navigation systems. The basic location service consists of a minimum path finder provided by a program written in Prolog. How customizing Google Maps to display the best paths by a familiar Google Maps based interface is also widely illustrated.

Keywords: Mobile computing, Real time information systems, Ubiquitous information systems, Google Maps.

1 Introduction

Current mobility information systems available for mobile users generally lack of real time information on the traffic network that help users to choose the best routes to destination or to postpone a travel due to traffic congestions or bad weather conditions. In principle, two main issues obstacle the implementation of such a system: a) the cost of the sensing infrastructure, and b) the different architectures of the navigation systems, also called navigators in the paper, available on the market since they are based on non standard databases and proprietary graphical interfaces.

In [1] we have shown that the travel time of each road segment may be estimated in real time with a satisfactory accuracy by fusing measurements on car speed and density coming from sensors (e.g., cameras, magnetic loops, etc.) and perceptions issued by policemen or authorized people working on the territory (e.g., taxi and bus drivers). In particular, how using cheaper webcams for both mobility and security has been shown in detail in [2]. Also, traffic information from *floating car data* techniques may be used for the roads that are not monitored by the mentioned *in situ technologies,* or cannot be controlled by any people. In this case the cars are located dynamically by triangulating the signals continuously emitted by their wi-fi or cellular phones or by GPS based techniques [3]. Therefore, a monitoring structure of the road network may be obtained more and more at reasonable costs.

D. Jin and S. Lin (Eds.): Advances in Mechanical and Electronic Engineering, LNEE 177, pp. 651–659.
springerlink.com

This motivates the development of navigators that show the best path to destination by taking into account the current traffic conditions. Let us note that this information may change substantially the car circulation in a city since it would decrease the traffic flows, the average travel times of the cars from source to destination and improve gas mileage as pointed out by the sheets of the most popular navigators, i.e., Tom Tom and Garmin.

For these reasons, in this paper we aim at illustrating a mobility information system able to assist both driving and walking people by a customized Google Maps interface that supports real time intelligent city applications to be used on smart phones that, as pointed in many market studies, e.g. [4], are the future versions of the navigators.

The use of JQMobile [5] allows us to deliver Google Maps based information on any user devices (PC, cellular phone or PDA) without changing the format of the interface. Also, a server based on Ruby on Rails [6] (RoR) is adopted to collect the real time information coming from the sensing system and to compute the best source-destination path for providing the mobile users with real time information that help their mobility and logistics activities. The choice of the RoR is due to the fact that it follows the Models-Views-Controllers (MVC) paradigm [7] that, as discussed in [8], favors the implementation of the mentioned location services as a set of use scenarios (or use cases) immediately understandable by the users according to the user centered design principles, e.g., [9], [10], [11], [12]. Let us note that this approach favors also the implementation of cognitively sound interfaces that effectively support activities in which the users should decide in few time [13], [14].Sect.2 will present the general architecture of the system. Sect.3 will show: a) how the Google Maps APIs may be used to built, in a semi-automated way, the urban graph of the city as a set of geographically referenced intersections, b) how to find the adjacent intersections of each intersection, and c) how to describe each pair of adjacent intersections by a street segment featured by distance and the current travel time. Finally, in sect.4 we briefly outline the program adopted to compute the minimum path from source to destination and will show how the responses are displayed on the user mobiles by means of a Google Maps based JQMobile interface.

2 Creating the Urban Road Graph in the Google Maps Format

The road graph is the main graphical support to provide the mobile users with location based services (LBSs); in fact, these services generally are GPS based navigation systems that provide the users with geo-referenced information to achieve the desired destination points though the road network.

The most diffused navigation systems (i.e., the ones based on Google Maps and the GPS navigators, such as Tom Tom and Garmin) are provided with static maps, where the traffic ways of the roads cannot be modified, travel times are based on average values, the intersections are always of the same type, traffic lights are not taken into account, neither special events such as storms, strikes, works in progress, accidents are considered to suggest alternative paths to destination. Navigators with dynamical maps could be developed if one uses typical GIS tools such as AutocadMap [15] or ArcInfo [16] that allow the designer to build maps where the mentioned basic properties of the roads may be modified to report timely the traffic

changes. However, such GIS tools consist of complex software routines conceived to plan and control the territory by using powerful PCs, and consequently not suitable for mobile applications featured by simple user devices.

For this reason, in the paper we propose that real time LBSs will be based on dynamical maps obtained by a set of geo-referenced waypoints, i.e., the road intersections, superimposed to the relevant Google Maps so that it will be possible to display on the user mobiles the best paths to destination by interconnecting the waypoints by polylines that take into account the current traffic conditions monitored by the sensing infrastructure. This will give rise to an ubiquitous mobility information system whose location based services will be based on real time data and will be provided by familiar Google Maps interfaces.

To determine the set of intersections of the road network, it is necessary to identify: a) their geographical coordinates, i.e. the latitude *lat* and the longitude *lng*, and the roads involved in each intersection, i.e., the vector *intersection*(i, first_road, second_road, *lat*, *lng*) and b) the array R(i, j, street_segment_name, distance, travel time), whose general element represents the road segment, if any, connecting the adjacent intersections i and j featured by a length (or distance) and a travel time.

As known, the intersections between two roads can be identified in Google Maps by using the API *at*(*first_road*, *second_road*) as shown in fig.1. However, such API does not work for every country. Thus, the first step of our method is to illustrate how this task can be accomplished by a novel function, called ***get_intersection***, obtained by using the Google MAPS API *get_directions* with the *walking* option to go from the *first_road* to the *second_road*. Indeed, the result of this API is a path whose first point is the sought intersection if the *second_road* is indicated in its info window. Fig.2 shows how *get_intersection* finds, following the proposed method, the right position of the intersection starting from the names of the streets issued by the user.

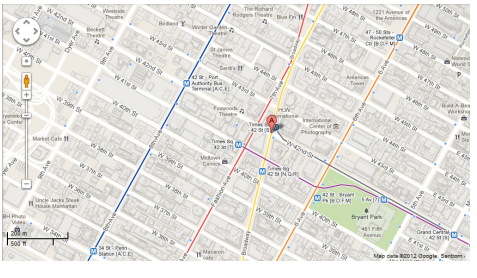

Fig. 1. The map obtained by entering the query: *"broadway* ***at*** *42nd, new york, ny"*, where in bold we point out the API ***at*** used by Google Maps the respond to the user query

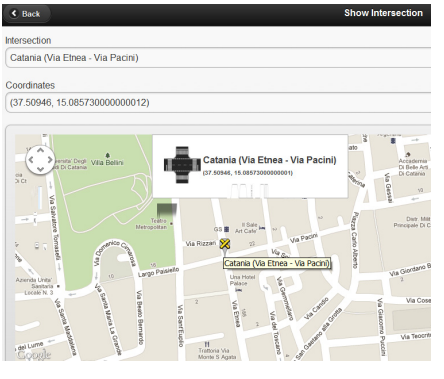

Fig. 2. Intersection found by our *get_intersection* on the basis of the two street names. The icon is inserted automatically with its geo-coordinates.

To avoid to repeat manually this operation, for each intersection we have developed another novel function, called ***get_all_intersections*(from_road, to_road)**, that identifies the intersections of the roads in the interval [from_road, to_road] with all the other roads, thus filling the relevant part of the vector *intersection*(i, first_road, second_road, *lat*, *lng*). Let us note that, thanks to the form given to this search, the function *get_all_intersections* may be executed in parallel by a Grid or Cloud of PCs, where each PC is responsible to find the intersections between a set of roads with all the others. This feature is very important since *get_all_intersections* is synchronized for every road pair with the response of the API *get_direction* that is obtained by Google Maps within a not negligible delay, typically some hundreds of milliseconds.

Fig.3 shows how *get_all_intersections* works in practice: for each road it searches the intersection, if any, with all the others. The existing intersections are identified by a pair of coordinates different from zero and stored in both an XML file and in a proper MySQL table.

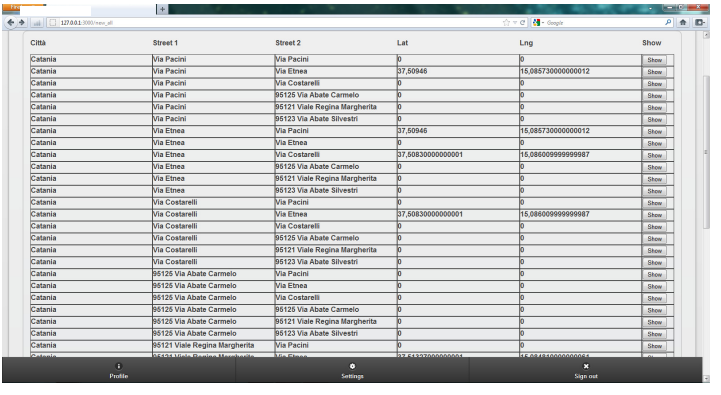

Fig. 3. The function *get_all_intersections* at working

Of course, the intersections of several road pairs could be excluded a-priori, i.e., without using *get_all_intersecions* since they belong to distant neighborhoods, as well as when searching for the intersection between two roads r_1 and r_2 one could store the intersections between the roads belonging to the path connecting the roads r_1 and r_2, thus avoiding of executing the search for such road pair. Optimization rules to decrease the *get_all_intersections* processing time are for further works.

Fig.4 shows all the found intersections displayed in only one shot by a set of small red circles. However, not all the intersections are identified by *get_all_intersections*, e. g., because the name of one of the roads is not indicated in the Google Maps, or because the suggested walking direction from r_1 to r_2 does not pass though any intersection between r_1 and r_2 nevertheless the existence of such an intersection. For this reason, we have provided the users with a *icon_insertion* function that allows them to insert manually the icons into the intersections that have not been found by *get_all_intersections*. If the user decides to store the intersection, the function will fill the corresponding entry of the vector *intersection* by computing the relevant geo-coordinates, as shown in fig.5.

To find the values of the the array R, we have to fill any entry (i, j) whose intersections i and j are connected according to *get_direction* with a path of only one step; the distance is the one bindicated by *get_direction*, whereas the travel time related to the entry (i, j) will be computed by the RoR server according to the method proposed in [1] taking into account the current traffic values. In our framework this is obtained by another function called ***get_all_adjacent_intersections(i_a, i_b)*** that finds the values of the array R by executing its horizontal slices [i_a, i_b] on several PCs working in parallel, thus decreasing considerably the processing time of the procedure. Also the array R is stored in an XML file and proper table of the RoR server. Let us note that the travel times featuring the relevant entries (i, j) of the array R are periodically updated by the server so that R would represent as accurately as possible the current traffic conditions.

Fig. 4. Displaying all the intersection identified automatically by the function *get_all_intersections*

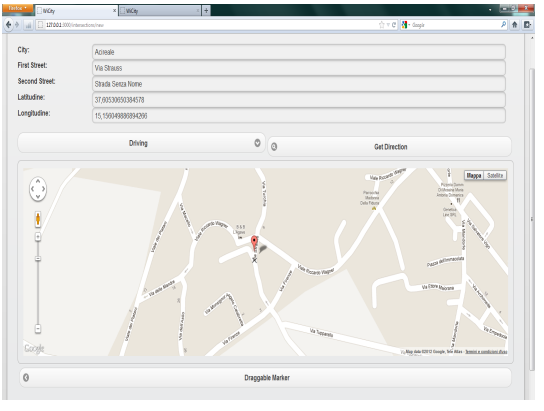

Fig. 5. Inserting the icons by using the function offered by the system allows the user to insert the intersections not found by the function *get_all_intersecions*

3 Minimum Path Finder and User Mobile Interface

In our implementation we have used a rule based algorithm written in Prolog [17] to compute the minimum path from a source to a destination node of the graph representing the road network. The description of such a program is outside the scope of the paper and may be found in [18], where we have clarified that it has been chosen since its time performance is similar to the procedural ones, but its functionalities may be extended more easy than the procedural ones, e.g., [19], [20], to support a great variety of user decisions. Here, it is enough to say that, as illustrated in fig.6, the Prolog program behaves as black box that receives at its input the source and destination nodes issued by the user and returns as output the sequence of intersections that allows the mobile user to go from the source to the destination in a minimum time depending on the travel times of the road segments stored in the traffic network represented by the array R.

To display the suggested sequence of intersections on the user devices by using the same interface of Google Maps we have developed an RoR version based on JQMobile that is able to show the same *view* on either the PCs and mobiles.

In particular, the RoR server displays the path in the Google Maps framework by imposing that the Google Maps API *getdirections* interconnects an initial point to a final one by passing through the intersections computed by the mentioned Prolog program that have to be considered by *getdirections* as mandatory *waypoints*. Since the set of the waypoints consists of adjacent intersections, the path obtained by *getdirections* is exactly the minimum one from the time or distance point view depending on if the intersections passed to *getdirections* are obtained by the Prolog program taking into account the travel time or the distance dimension of the array R.

Let us note that besides the minimun path to a fixed destination, the Prolog program is able to show also the destination services that are nearest to the user, i.e., the ones located within a circle, whose radius is set by the user, around the current user position. Thus, the RoR server first dispay the nearest services and then it will display the best path to the destination chosen by the user. Fig.7 illustrates how such path is displayed on the mobile. It looks like the one provided by Google Maps even if it is displayed by a method that differs from the one followed by Google Maps. Of course, the waypoints don't coincide necessarily with the ones provided by Google Maps.

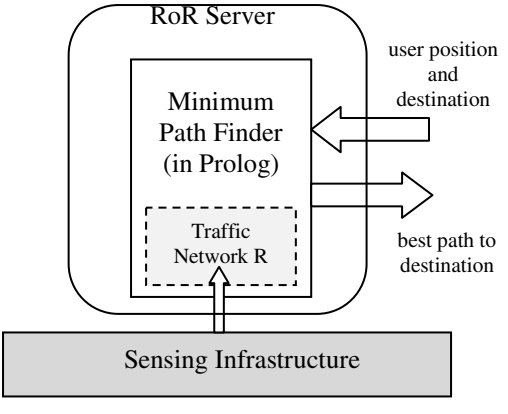

Fig. 6. RoR server, sensing infrastructure and Prolog Program the produces the best path on the basis of the user inputs and on the current values of the traffic network represented by the array R

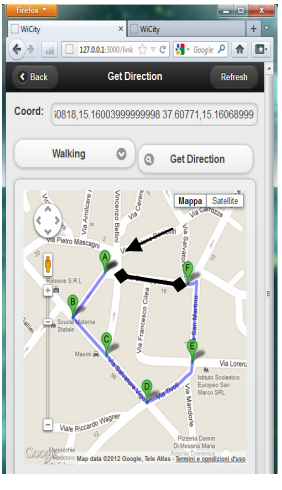

Fig. 7. Minimum path from A to F obtained by the proposed method that takes into account the current situation: roads in black is temporary closed, road with arrow is a one way street

Finally let us note that the user position is obtained by either a GPS of the user device (i.e., PC or mobile) or by the geo-coordinates of the Access Point to which the PC or the mobile is connected. Since such coordinates generally don't coincide with

the ones of an intersection of the road network, we have to further extend our approach by imposing that the array R will be augmented by further four entries connecting the source and destination addresses to the intersections delimiting the road segments in which they are located. The computation of the geo-coordinates of such entries may be obtained by identifying the entries of the array R whose intersections are respectively adjacent to the source and destination node. The distances between the source/destination nodes and the adjacent intersections can be derived by the API *get_direction,* whereas the travel time should be estimated by using the formulas described in [1].

4 Concluding Remarks

The paper has shown how customizing the Google Maps makes possible to develop GPS navigation systems on mobiles taking into account real time conditions and providing the users with a basic service to help their mobility and logistics activities. The navigator is displayed by a familiar Google Maps interface controlled by JQMobile graphical commands.

Let us note that the Prolog algorithm, used to compute the minimum path, is able to find both the minimum walking and driving paths and that both such paths usually differ from the ones suggested by Google Maps. The former is due to the possible presence of events that don't allow the users to follow some roads, whereas the second is mainly due to the current traffic conditions. Since, in some cities, also the people walking conditions may influence the choice of the path to reach by walking the destination, we plan to include this aspect in future studies.

Also, we plan to use urban ontologies [21], [22] to describe the objects used in the information system by a standard RDF vocabulary [23] so that it will possible to apply the approach to all the cities at the only condition that these cities will transform the relevant urban data into standard RDF descriptions.

The scenario based approach used to design the software and the mentioned ontologies will favor the software reuse to develop novel services similar to the ones offered by the proposed software, as suggested in [24]. Finally, the use of fast and robust image processing techniques based on denoising techniques [25], fast clustering [26] and effective statistical methods [27] will allow us to monitor more and more the traffic network by not expensive webcams, thus improving the estimation of the travel time and the effectiveness of the offered LBSs.

References

1. Faro, A., Giordano, D., Spampinato, C.: Evaluation of the Traffic Parameters in a Metropolitan Area by Fusing Visual Perceptions and CNN Processing of Webcam Images. IEEE Transactions on Neural Networks 19(6) (2008)
2. Faro, A., Giordano, D., Spampinato, C.: Adaptive background modeling integrated with luminosity sensors and occlusion processing for reliable vehicle detection. IEEE Transactions on Intelligent Transportation Systems 12(4), 1398–1411 (2011)
3. Leduc, G.: Road Traffic Data: Collection Methods and Applications, Working Papers on Energy, Transport and Climate Change, N.1, JRC European Commission, 47967 - 2008

4. Telematics Reserach Group (TRG), Preview portable navigation: the future is bright for connectivity (2010), http://www.telematicsresearch.com/press_data/pdfs/PortableNavigation.pdf
5. David, M.: Developing Websites with jQuery Mobile. Focal Press (2011)
6. Hartl, M.: Ruby on Rails 3. Addison Wesley (2011)
7. Dubberly Design Office, The Model-View-Controller Pattern in a Rails-Based Web Server (2011), http://www.dubberly.com/wp-content/uploads/2011/04/DDO_Article_MVC_Pattern.pdf
8. Faro, A., Spampinato, C.: Implementing ITS 3.0 Applications by Integrating Ruby on Rails, Sesame and Protegè Technologies. In: Signal-Proc. of the Seventh International Conference on Image Technology and Internet-Based Systems (SITIS), pp. 62–68. IEEE (2011)
9. Faro, A., Giordano, D.: StoryNet : an Evolving Network of Cases to Learn Information Systems Design. IEE Proceedings Software 127, 119–127 (1998)
10. Mansar, S.L., Marir, F., Reijers, H.A.: Case-Based Reasoning as a Technique for Knowledge Management in Business Process Redesign. Electronic Journal on Knowledge Management 1(2), 113–124 (2003)
11. Jacobson, I., Ng, P-W.: Aspect-oriented software development with use cases. Addison Wesley (2004)
12. Faro, A., Giordano, D.: Concept Formation from Design Cases: Why Reusing Experience and Why Not. Knowledge Based Systems Journal 11(7), 437–448 (1998)
13. Giordano, D.: Evolution of interactive graphical representations into a design language: a distributed cognition account. International Journal of Human-Computer Studies 57(4), 317–345 (2002)
14. Faro, A., Giordano, D.: Ontology, esthetics and creativity at the crossroads in Information System design. Knowledge Based Systems 13(7) (2000)
15. AutoDesk, AutoCAD and Autodesk Map 3D Software: A Comparison (2011), http://www.autodesk.com/autodeskmap
16. Ormsby, T., et al.: , Getting to Know ArcGIS Desktop: Basics of ArcView, ArcEditor, and ArcInfo, Second Edition Updated for ArcGIS 9.3 ESRI (2008)
17. Bratko, I.: PROLOG Programming for Artificial Intelligence. Addison-Wesley Educational Publishers Inc. (2011)
18. Faro, A., Giordano, D., Spampinato, C.: Integrating Location Tracking, Traffic Monitoring and Semantics in a Layered ITS Architecture. Intelligent Transport Systems, IET 5(3) (2011)
19. Zhan, F.B., Noon, C.E.: Shortest Path Algorithms: An Evaluation Using Real Road Networks. Transportation Science 32(1), 65–73 (2008)
20. Sneyers, J., et al.: Dijkstra's algorithm with Fibonacci heaps: An executable description. In: Proc. 20th ACM Workshop on Logic Programming (WLP 2006). ACM Press (2006)
21. Zhai, J., Jiang, J., Yu, Y., Li, J.: Ontology-based Integrated Information Platform for Digital City. In: IEEE Proc. of Wireless Communications, Networking and Mobile Comp., WiCOM 2008 (2008)
22. Faro, A., Giordano, D., Musarra, A.: Ontology based intelligent mobility systems. In: IEEE Proc. International Conference on Systems, Man and Cybernetics, vol. 5, pp. 4288–4293. IEEE (2003)
23. Powers, S.: Practical RDF. O'Reilly Media (2003)
24. Faro, A., Giordano, D.: Design memories as evolutionary systems: socio-technical architecture and genetics. In: Faro, A., Giordano, D. (eds.) IEEE Proc. International Conference on Systems Man and Cybernetics, pp. 4334–4339 (2003)

25. Cannavò, F., Nunnari, G., Giordano, D., Spampinato, C.: Variational Method for Image Denoising by Distributed Genetic Algorithms on GRID Environment. In: Proc. Int. Workshops on Enabling Technologies: Infrastructure for Collaborative Enterprises, WETICE 2006. IEEE (2006)
26. Faro, A., Giordano, D., Maiorana, F.: Mining massive datasets by an unsupervised parallel clustering on a GRID: Novel algorithms and case study. Future Generation Computer Systems 27(6), 711–724 (2011)
27. Crisafi, A., Giordano, D., Spampinato, C.: GRIPLAB 1.0: Grid Image Processing Laboratory for Distributed Machine Vision Applications. In: Proc. Int. Workshop on Enabling Technologies: Infrastructure for Collaborative Enterprises, WETICE 2008. IEEE (2008)

Study of Maximum Power Point Tracking (MPPT) Method Based on Adaptive Control Theory

Xiuling Wang[1], Haocheng Wang[2], and Rongsheng Meng[2]

[1] College of Information Engineering,
Inner Mongolia University of Technology,
Inner Mongolia, 010051, China
[2] Inner Mongolia Branch Company,
Beijing Jingneng New Energy Co., Ltd.,
Inner Mongolia, 010070, China
wxltt3756@yahoo.com.cn

Abstract. The output power of photovoltaic cell array was affected by light intensity and temperature changes, so the maximum power point tracking (MPPT) technology is used in photovoltaic systems widely. This paper presents an adaptive duty cycle interference Observation MPPT method for photovoltaic power systems and its simulation. The results show that: under the control of the improved method, which can track the maximum power point of photovoltaic array steadily and effectively, in the same time, in the case of sunlight intensity, ambient temperature and other system parameter perturbations, it can find new work points quickly and keep the system steadily. The method shows good dynamic characteristics.

Keywords: PV model, adaptive control, MPPT, simulation.

1 Introduction

In a photovoltaic system, the output characteristics of photovoltaic array are nonlinear characteristics. The output related to internal characteristics of photovoltaic cells, the environment, such as light intensity, load and temperature and other factors. A certain light intensity and ambient temperature, the photovoltaic cells can work in a different output voltage, but only in one output voltage, the output power of photovoltaic cells achieve the maximum, then the operating point of the photovoltaic cells achieve the highest point of the output power curve, called the maximum power point (MPP). Therefore, for a photovoltaic power generation system, we should find the optimal state of the photovoltaic cells, to maximize the conversion of light energy into electrical energy, improve the efficiency of the system. Use a control method in real time and adjust the operating point of the photovoltaic cells, make the photovoltaic system to work in near the maximum power point, which technology known as the maximum power point tracking (MPPT) technology [1].

The adaptive control theory was put forward in control engineering. In a complex control process, and the control object is unknown or poorly understood, adaptive control reflects its unique superiority.

D. Jin and S. Lin (Eds.): Advances in Mechanical and Electronic Engineering, LNEE 177, pp. 661–665.
springerlink.com

2 The Output Characteristics of Photovoltaic Cell

Typical photovoltaic cell (power P-voltage V) characteristic curve was shown in Fig. 1. The characteristics of the PV are nonlinear, and its output was affected by the light intensity, ambient temperature and load effects. In a certain light intensity and ambient temperature, the photovoltaic cells can work in a different output voltage, but only in one output voltage, output power of photovoltaic cells achieve the maximum, that is achieve the maximum power point (MPP) [2].

Therefore, in the photovoltaic power generation system, to improve the efficiency of system, an important way is to adjust the operating point of the photovoltaic cells in real-time.

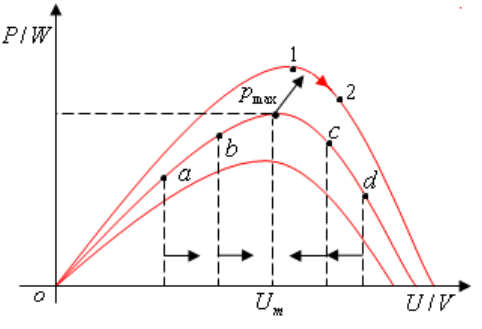

Fig. 1. P-V characteristics of photovoltaic cell

3 MPPT Method Based on Adaptive Control Thought

3.1 The Traditional Perturbation and Observation Method

A traditional perturbation and observation method principles are as follows [3]: PV system controller changes the output of the photovoltaic array in each control cycle with a smaller step size (the step size is stationary, which can be increased and reduced, and the control object can be PV array output voltage or current, the process known as "interference"), then, we contrast output power before and after of interference. $\Delta p > 0$, which show that the direction of the reference voltage adjustment is correct, we can continue to interference by the original direction. $\Delta p < 0$, which show the reference voltage adjustment in the wrong direction, and we need to change direction of interference. When a given reference voltage increases, the output power increases, the operating point is located in the left side of the MPP in Fig. 1, we need to continue to increase the reference voltage; if the output power decreases, the operating point is located in the right side of the MPP need to reduce the reference voltage. When a given reference voltage decreases, the output power decreases, which shows the operating point is located at the left side, we need to increase the reference voltage, if the output power increases, the operating point is

located in the right side of the $p_{\max}$, we need to continue to reduce the reference voltage. In this way, the actual operating point of the PV array will be able to gradually close to the MPP and eventually reach steady state in the vicinity of a smaller range of reciprocating.

The method uses a modular control loop, which is simple and easy to implement, and less demanding sensor accuracy. But its response is slow, and it applies to the occasions of sunshine intensity change slow. In the steady-state case, it may lead to a slight oscillation of MPP in the vicinity of the actual operating point, so there will be amount of power loss. That is, the traditional perturbation and observation method can not consideration to accuracy and response speed.

3.2 MPPT Method Based on Adaptive Control Theory

The MPPT method based on adaptive theory keeps the idea of a traditional perturbation and observation method. The difference is the size of the perturbation depending on the system operating point, and it reflects the adaptive theory. Adaptive method can find MPP accuracy, stability and quickly. After finding the MPP, it can ensure the system works at MPP or very close to MPP. In theory, it can be infinite approach the MPP [4].

Adding a on-line step size regulator α, $\alpha(k+1) = M\dfrac{|dp|}{\alpha(k)}$. Of which: $\alpha(k)$ is adjustment step size of the interference voltage, and changes between 0 and 1; $dp = p(k) - p(k-1)$ is size of power change; M is constant, to determine the sensitivity of adaptive.

When environmental factors such as the PV array temperature, sunlight intensity changes suddenly, traditional perturbation and observation method thinks that the reason that lead to output power change is the output voltage (or current) increase or decrease an adjustment step, which may cause the controller away from the MPP. The step size regulatorα can solve this problem. When $|dp|/\alpha(k)$ is smaller, which shows changes of output power is mainly due to the step adjustment, and changes of $\alpha(k+1)$ is smaller than $a(k)$. When $|dp|/\alpha(k)$ is larger, which shows the change of power is mainly caused by external factors, such as PV array surface temperature, sunlight intensity. In this case, if the MPP drifts by big margin, the step size $\alpha(k+1)$, increase, which can fast-track to the new MPP [5].

Introducing a parameter e, to judge the $|dp|$. In theory, we can always find the MPP of photovoltaic arrays. At the MPP, $dp = 0$ is established. In the actual operation, almost no point makes $dp = 0$. So, traditional perturbation and observation method often led to the running of the oscillation of the system operating point near the MPP, resulting in some power loss. Introducing a parameter e (its size can be set according to the different accuracy requirements), to judge the $|dp|$. When $|dp| < e$, the system thinks that have found the MPP. When the MPP is found, disturbances stops, which ensure the system works in the vicinity of MPP. The process is shown in Fig. 2 [6].

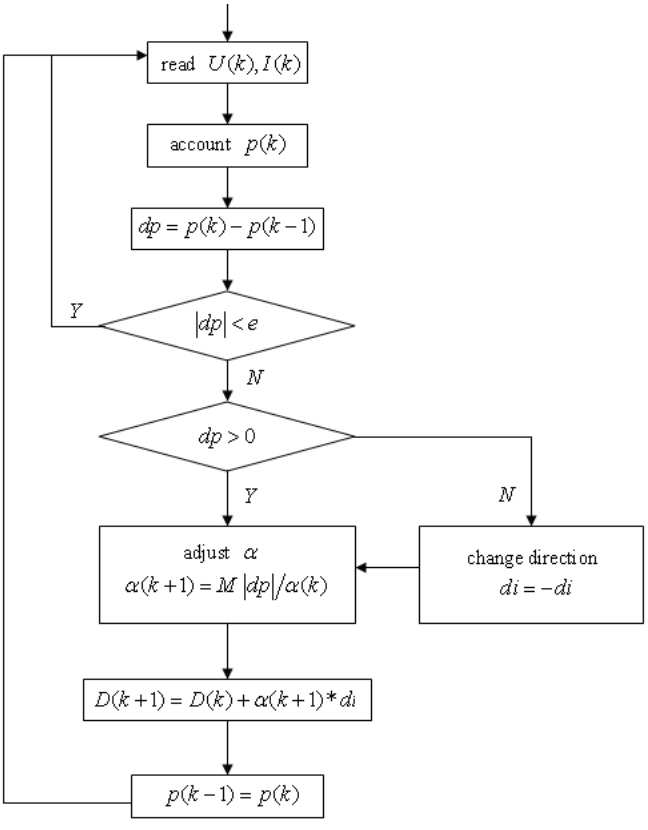

Fig. 2. Flow chart of adaptive control

4 Simulation and Analysis

Setting simulation conditions: the sunshine intensity increase from $800W/m^2$ to $1000W/m^2$, the temperature of PV array drops from $T = 56^oC$ to 25^oC, the load resistance R=5Ω, step size $\Delta U = 0.01V$ and $\Delta U = 0.05V$, simulation time 1S, the parameters e =0.001, M =1/2500. We get the waveform is shown in Fig. 3. From which we found that the waveform has not only the tracking speed, but also a very rapidly response factors for external environment changes, and it almost no steady state error. So we conclude that the adaptive disturbance observation method applied to photovoltaic arrays MPPT is feasible. It has good dynamic and steady-state performance.

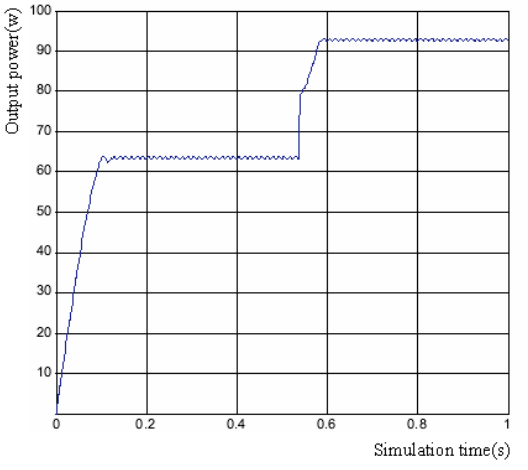

Fig. 3. MPPT simulation waveforms (step size $\Delta U = 0.05V$)

Acknowledgments. The authors gratefully acknowledge the support of College of Information Engineering of Inner Mongolia University of Technology. The paper has been supported by the Natural Science Foundation of Inner Mongolia University of Technology (ZS201006) and the Natural Science Foundation of Inner Mongolia (2011MS0721).

References

1. Dorofte, C., Borup, U., Blaabjerg, F.: A Combined Two-Method MPPT Control Scheme for Grid-Connected Photovoltaic System. Power Electronics and Applications, 1–10 (2005)
2. Luque, A., Hegedus, S.: Handbook of Photovoltaic Science and Engineering, pp. 80–100. Wiley, Hoboken (2002)
3. Simoes, M.G., Franceschetti, N.N., Friedhofer, M.: A fuzzy logic based photovoltaic peak power tracking control. In: Proceedings of IEEE International Symposium Industrial Electronics, pp. 300–305 (1998)
4. Mutoh, N., Ohno, M., Inoue, T.: A Method for MPPT Control While Searching for Parameters Corresponding to Weather Conditions for PV Generation Systems. Industrial Electronics, 1055–1065 (2006)
5. Walker, G.: Evaluating MPPT converter topologies using a MATLAB PV model. J. Electr. Electron. Eng. 21(1), 49–56 (2001)
6. Zhang, C.: Research on MPPT and Anti-islanding of Grid-Connected Photovoltaic Power Generation System, PhD thesis, pp.36–48. Zhejiang University (2006)

Author Index